Modeling and Assessment of Urban Energy Systems

Thèse N° 9389

Présentée le 6 mai 2019

à la Faculté de l'environnement naturel, architectural et construit
Laboratoire d'énergie solaire et physique du bâtiment
Programme doctoral en energie

pour l'obtention du grade de Docteur ès Sciences

par

Amarasinghage Tharindu Dasun PERERA

Acceptée sur proposition du jury

Prof. M. Paolone, président du jury
Prof. J.-L. Scartezzini, Prof. S. V. Moussavi Nik, directeurs de thèse
Prof. M. Patel, rapporteur
Dr T. Hong, rapporteur
Prof. F. Maréchal, rapporteur

2019

ÉCOLE POLYTECHNIQUE
FÉDÉRALE DE LAUSANNE

Abstract

Improving the energy sustainability of our cities involves the integration of multiple renewable energy technologies into existing energy infrastructure, stretching the capabilities of traditional energy systems to the limit. To consider the transition take place in distributed energy system sector, complex cyber physical interactions need to be adequately modelled, which is not possible with currently used white box models. Furthermore, the volatility of climate conditions and frequent extreme climate events due to climate change as well as climate phenomena at urban scale make it essential to improve the robustness and resilience of energy systems. Again, white box models do not allow sufficient flexibility in the modelling approach. To address these limitations, thesis seeks to optimize distributed energy system design with the help of grey- and black-box techniques.

A grey box model based on fuzzy logic is introduced to consider the dispatch strategy when designing electrical hubs. The grey box model shows better performance when optimizing electrical hubs. It has been shown that the method can achieve a renewable energy integration level of up to 80%. However, the grey box model fails to handle complex energy flows within the energy system. Therefore, a black-box method based on reinforcement learning is introduced to consider complex energy systems catering multi-energy services. Reinforcement learning based on a fully connected neural network (FNN), outperforms the grey box model by improving the objective function values by 60%. A convolution neural network improves the objective function values further (by up to 20% compared to FNN). The results reveal that black box models are competent when conducting optimization for complex energy systems. Distributed optimization is introduced to move from a single energy system to an energy internet consisting of several interacting energy systems. The energy internet is optimized considering fully cooperative and non-cooperative scenarios. The optimization algorithm shows a good capability to reach the Epsilon-Nash equilibrium when conducting the optimization. Finally, supervised and transfer learning methods have been introduced when conducting energy system optimization at the regional and national scale, which reduced the computation time by 84%.

Stochastic and robust programing methods are introduced to improve the climate flexibility of energy systems. A hybrid stochastic-robust optimization algorithm is developed by extending the novel approach to consider both climate uncertainty and extreme events. A regional climate model provides climate scenarios for the stochastic optimization. The results of the study show that renewable energy technologies such as solar PV and wind can be used to cater 50% of the annual energy demand while guaranteeing a robust operation of the energy system during extreme climate events. The model is then further extended by integrating computational models for urban energy simulation considering urban climate. Results of the analysis show that a performance gap of up to 40 % can be observed when neglecting the influences of urban climate in the design of urban energy systems. In the final part of this thesis, a multi-criterion decision making technique is introduced into the energy system optimization model. This helps decision makers to weight a number of conflicting objectives and to consider impacts at the urban scale.

Key words: Urban Energy Systems, Machine Learning, Distributed Optimization, Urban Physics, Climate Change, Multi-criterion Decision Making, Energy Sustainability

Résumé

Pour rendre nos villes plus durables du point de vue énergétique, diverses énergies renouvelables sont intégrées à l'infrastructure existante, se heurtant aux limites de cette dernière avec des pertes d'énergie majeures à la clé. L'optimisation des systèmes énergétiques décentralisés demande la modélisation d'interactions matériels et informatiques complexes, impossible avec l'approche en boîte blanche utilisée communément. Par ailleurs, la volatilité des conditions climatiques et la haute probabilité d'événements climatiques plus fréquents et plus extrêmes tout comme des phénomènes climatiques urbains nécessitent une grande solidité et une résilience des systèmes énergétiques. La modélisation en boîte blanche ne permet pas une flexibilité suffisante là non plus. Cette thèse cherche par conséquent à optimiser la conception de systèmes énergétiques à l'aide d'une modélisation en boîte grise et en boîte noire.

Un modèle informatique en boîte grise, fondé sur la logique floue est introduit afin de prendre en compte la stratégie d'acheminement lors de la conception d'une Pélectrique. Il a été démontré qu'ainsi jusqu'à 80% d'énergie renouvelable peuvent être intégrés. Or la modélisation en boîte grise n'est pas en mesure de traiter des flux d'énergie complexes à l'intérieur du système énergétique. Dès lors, une méthode de modélisation en boîte noire fondée sur l'apprentissage par renforcement est introduite afin de permettre la prise en compte de systèmes énergétiques complexes intégrant des services multi-énergétiques. L'apprentissage par renforcement fondé sur un réseau neuronal entièrement connecté surpasse le modèle à boîte grise, améliorant les valeurs de fonction objectif de 60%. Un réseau neuronal convolutif les améliore encore de 20 %. Ces résultats démontrent la compétence de modèles en boîte noire dans le cadre d'optimisation de systèmes énergétiques complexes.

L'optimisation distribuée est introduite pour le passage d'un système unique à un internet énergétique consistant de plusieurs systèmes interconnectés. Ce dernier est optimisé pour des scénarios coopératifs et non coopératifs. L'algorithme d'optimisation démontre une excellente capacité d'atteindre l'équilibre Epsilon-Nash. Enfin, des méthodes d'apprentissage supervisé et de transfert sont introduits pour l'optimisation à l'échelle régionale ou nationale, diminuant le temps de calcul de 84%.

Des méthodes de programmation stochastiques et robustes sont utilisées afin d'améliorer la flexibilité de systèmes énergétiques par rapport au climat. Un algorithme hybride d'optimisation est ajouté pour la prise en compte de l'incertitude climatique et d'événements climatiques extrêmes. Un modèle climatique régional fournit des scénarios pour l'optimisation stochastique. Les résultats montrent que les énergies renouvelables telles que le pv et l'énergie éolienne peuvent fournir jusqu'à 50% des besoins annuels grâce à cette approche, tout en garantissant une opération robuste. Le modèle est étendu encore par l'intégration de modèles informatiques d'énergie urbaine en tenant compte du climat urbain. Une analyse démontre un écart de performance de près de 40 % si l'impact du climat urbain est négligé dans la conception d'un système énergétique urbain. Finalement, une approche multi-critère de prise de décision est introduite dans le modèle, permettant aux décideurs de pondérer des objectifs contradictoires et de considérer leurs impacts à l'échelle urbaine.

Mots clé: systèmes énergétiques urbains, apprentissage automatique, optimisation distribuée, physique urbaine, changement climatique, décisions multi-critères, durabilité énergétique

Acknowledgement

First, I would like to thank Professor Jean-Louis Scartezzini for his encouragement, advice, and for the freedom he gave me to explore my research interests with a great generosity. I particularly thank him for his great support during a critical period in my studies, where several of my manuscripts got rejected one after the other. The multi-disciplinary environment he created within the Solar Energy and Building Physics Laboratory is amazing and helped me a lot, not only to broaden the scope of my research but also expanded my scientific connections and built up networks of collaborations. I also thank him for financial support during my one week stay in the Lawrence Berkeley National Lab (LBNL) (in addition to the support provided to attend many conferences and summer/winter schools).

Second, I thank my co-supervisor Professor Vahid Nik, currently at the University of Lund in Sweden, for many fruitful discussions and helpful suggestions during my research. He was a close colleague for me than a supervisor. He moved away from his role as a professor or co-supervisor in certain instances and supported me throughout this work as a collaborator. I also thank him for having many wonderful meetings and useful discussions together during my research and introducing several experts to me which helped to expand my collaboration network. It was really a pleasant experience to work with him.

I thank Dr. Tianzhen Hong for hosting me at LBNL and providing me guidance during the stay. I would like to thank Professor Mario Paolone, Professor Francois Marechal and Professor Martin K. Patel and Dr. Tianzhen Hong for accepting the invitation to be in the jury panel.

I greatly appreciate the financial support of the Swiss Innovation Agency Innosuisse for this thesis, as a part of the Swiss Competence Center for Energy Research SCCER FEEB&D. I am really grateful to all the members of SCCER-FEEB&D for their support. I particularly thank Dr. Dasaraden Mauree for his support, help and coordinating my work within the SCCER–FEEB&D. I am also grateful to Dr. Nahid Mohajeri for her support during the initial stages of my PhD in Switzerland, her encouragement, and for many fruitful discussions and helpful suggestions. Many of which have been led to support scientific collaboration and broadening the research frontier. This includes joint teaching courses and joint supervising master students. I thank Dr. Silvia Coccolo for providing interesting insights about the promising areas that my work can be extended. I also thank Mrs. Barbara Smith for her continuous support to improve my English language and writing skills. All my journal papers usually go through her and besides just correcting the language she provide detail explanation of each mistake I made which was really helpful. The support from Marlène was also very helpful when

going through documentation work. The common lunches, dinners, and trips we had together with all the Lezards were really refreshing. I am grateful to all of them for the companionship. I must thank Yujie for many interesting discussions we had together. I am really grateful to Isabelle Dustin for taking care of me during last four years as a perfect land lord.

I greatly appreciate the support from Mr. Udaranga Wickramasinghe, PhD student at EPFL, throughout this work as a close friend and a co-worker. Udaranga encourage me to use GPU programing which helped me a lot when optimizing energy systems considering uncertainty. His deep understanding about machine learning techniques and flexibility in programing helped me to handle the challenging task of introducing reinforcement learning into the energy system optimization process. I should also mention the support from Dr. Nadeesh Madusanka whom I share research ideas frequently. I also thank Professor Rahula Attalage, Professor Kapila Perera and Professor Ajith de Alwis from University of Moratuwa for the guidance they provided me as an undergraduate and Master student at University of Moratuwa, Sri Lanka. Furthermore I should extend my gratitude to the Sri Lankan families in Lausanne, families of Bandara Ayya, Menaka ayya, Walter ayya and Dias ayya for inviting me regularly for various events. Furthermore, I would especially acknowledge Dr. Isabelle Dustin being so kind and caring as my land lord.

Finally, my deep appreciation and thanks go to my parents, my brother, and mother in law for their love and great support before and during my PhD studies. I am really grateful to Surani for all the support, encouragement and the unconditional love. At last but not least, I would respectfully acknowledge all the taxpayers of Sri Lanka and Switzerland for their commitment towards free education.

Lausanne, 10th February 2019

Table of Contents

List of Figures

List of Tables

Nomenclature

The notations used for the deterministic model discussed in Chapter 2-5 and 8-10

Sets:

t ϵ T set of all hours in the year
FϵƑ set of objective functions
NϵƝ set of decision space variables related to system design
dϵƊ set of decision space variables related to control system (D : W U L)
w ϵW set of decision space variable related to fuzzy controller ($W \subset D$)
l ϵ L set of all decision space variables related to secondary level controller (L⊂D)
s ϵ S set of system components

Objective functions used: (FϵƑ)

LEC Levelized Energy Cost ($/kWh)
GI_{EG} Grid Integration level considering exports
GI_{IG} Grid Integration level considering imports
GI_{IEG} Grid Integration level considering both imports and exports

Decision space variable: (dϵƊ)

N^{SPV} Number of SPV Panels
$N^{TY\text{-}SPV}$ Type of SPV Panel
N^{W} Number of wind turbines
$N^{TY\text{-}}W$ Type of wind turbine
N^{Bat} Number of battery banks
k Type of ICG
w_{ij} weight matrix for fuzzy rules
Lim_{BC} limit cost for battery charge ($)
Lim_{BD} limit cost for battery discharge ($)
Lim_{GTB} limit cost for battery charge from grid ($)
Lim_{BTG} limit cost for battery discharge to grid ($)
SOC_{min} minimum state of charge
$SOC_{Min,G}$ minimum state of charge when discharging to grid
SOC_{Set} maximum state of charged to be reached when charging from grid

Other variables used in the model:

CRF Capital Recovery Factor
DOD Depth of Discharge
FAC Fixed Annual Cash-flow ($)
FAC^{GI} cash flow for grid integration ($)
ICC Initial Capital Cost ($)
θ_t^{SPV} SPV cell temperature (°C)
η_t^{PV} Efficiency of SPV panels
FC_t^{ICG} Fuel consumption of the ICG (l/year)
FC_t^{CHP} Fuel consumption of the CHP (l/year)
G_t^{β} Global tilted solar irradiation on SPV panel (kWh/m^2)
$G_t^{b,\beta}$ Beam radiation (kWh/m^2)
$G_t^{r,\beta}$ Reflected solar radiation (kWh/m^2)
H_0 Extraterrestrial solar radiation (kWh/m^2)
LPS_t Loss of power supply (kWh)
MT Clearness index
$P_t^{Bat-Max}$ Maximum power flow from the battery (kW)
P_t^{EG} Units exported to the grid (kWh)
P_t^{ELD} Electricity demand of the micro grid at time step t (kWh)
P_t^{ICG} Power generation by ICG (kWh)
$P_{\max}^{ICG}$ Maximum power output of ICGs (kW)
$P_{\min}^{ICG}$ Minimum power output of ICGs (kW)
P_t^{IG} Units imported from the grid (kWh)
P_t^{RE} Power generated using renewables (kW)
P_t^{SPV} Power generated from SPV panels (kW)
P_t^{W} Power generated from wind turbines (kW)
x^k_t Inputs to the fuzzy controller
y_t Operating load factor of ICG
OM^F_s Fixed operation and maintenance cost ($)
OM^V_s Variable operation and maintenance cost ($)
R^l l^{th} implication rule for the fuzzy controller

Input Parameters for the model:

Θ, θz, β angle of incidence for an arbitrarily inclined surface oriented toward the equator, zenith angle and tilt angle of SPV panel (rad)
β tilt angel of SPV panels (rad)
θ_a Ambient temperature (°C)
$\eta_{W\text{-}losses}$ General power losses in wind turbine
AM Air Mass
A_{SPV} collector area of one SPV panel (m^2)
ELD_t Electricity Load Demand (kWh)
GC_t^{EG} COE for selling electricity to MUG ($)
GC_t^{IG} COE for purchasing electricity from MUG ($)
P_R Rated power of the turbine (kW)
v_{CI} Cut-in wind speed of the turbine (ms^{-1})
v_{CO} Cut-off wind speed of the turbine (ms^{-1})
v_R Rated wind speed of the turbine (ms^{-1})
v_t Wind speed at hub level of wind turbine (ms^{-1})

Constraints used:

EG_{Lim} Maximal units sold to the grid (kWh)

IG_{Lim} maximum units purchased from the grid (kWh)
LOLP Loss of Load Probability

Other acronyms used

ESP Energy Service Provider
GI Grid Interactions
$ICO2_s$ lifecycle CO2 emission of system components
ICG Internal Combustion Generator
SPV Solar PV
SOC State of charge of battery bank
t time step
TCO2 Total CO2 emission
OM Operation and maintenance cost
WRE Waste of Renewable Energy
GC Grid Cost for electricity

The notations used for the stochastic model discussed in Chapter 6 and 7

Sets:

c ϵ C set of system components
dϵD set of decision space variables related to control system (D : W U L)
FϵF set of objective functions
h ϵ H set of year of the project
l ϵ L set of all decision space variables related to secondary level controller (L⊂D)
NϵN set of decision space variables related to system design
p ϵ P Set of criteria
s ϵΩ set of scenarios
t ϵ T set of all hours in the year
w ϵW set of decision space variable related to fuzzy controller ($W \subset D$)

Optimization Scenarios

DE Deterministic model with extreme weather data
SO Stochastic optimization
SRO Stochastic Robust Optimization

Objective functions used:

Flexibility Flexibility of the system (FϵF)
GI Grid Integration level (FϵF)
NPV Net Present Value (FϵF)

Constraints used:

LOLP Loss of Load Probability
LOLP-Ex Loss of Load probability at extreme events
$P^{TG\text{-}Lim}$ Maximal units sold to the grid (kWh)

Decision space variable: (dϵD**)**

System components

k Type of ICG (NϵN)
N^{SPV} Number of Panels (NϵN)
$N^{TY\text{-}SPV}$ Type of SPV Panel (NϵN)
N^{W} Number of wind turbines (NϵN)
$N^{TY\text{-}W}$ Type of wind turbine (NϵN)
N^{Bat} Number of battery banks (NϵN)

Dispatch strategy

Lim_{BC} limit cost for battery charge (l ϵ L) ($)
Lim_{BD} limit cost for battery discharge (l ϵ L) ($)
Lim_{GTB} limit cost for battery charge from grid (l ϵ L) ($)
Lim_{BTG} limit cost for battery discharge to grid (l ϵ L) ($)
SOC_{min} minimum state of charge (l ϵ L) ($)
$SOC_{Min,G}$ minimum state of charge when discharging to grid (l ϵ L)
SOC_{Set} maximum state of charged to be reached when charging from grid (l ϵ L)
w_{ij} weight matrix for fuzzy rules (w ϵW)

Other variables used in the model:

$\eta_{t,s}^{PV}$ Efficiency of SPV panels
d time period that the extreme climate condition is expected to prevail (hours)
CRF Capital Recovery Factor
DOD Depth of Discharge
FAC Fixed Annual Cash-flow ($)
FAC^{GI} cash flow for grid integration ($)
FIPD fuzzy representation for Impact of the Performance Degradation
$G_{t,s}^{\beta}$ Global tilted solar irradiation on SPV panel (kWh/m^2)
ICC Initial Capital Cost ($)
IPD impact of the performance degradation
$LPS_{t,s}$ Loss of power supply (kWh)
OM Operation and maintenance cost ($)
$P_{t,s}^{Bat-Max}$ Maximum power flow from the battery (kW)
$P_{t,s}^{EG}$ Units exported to the grid (kWh)
$P_{t,s}^{ELD}$ Electricity demand of the micro grid at time step t (kWh)
$P_{t,s}^{IG}$ Units imported from the grid (kWh)
P_{t}^{RE} Power generated using renewables (kW)
$P_{t,s}^{SPV}$ Power generated from SPV panels (kW)
$P_{t,s}^{W}$ Power generated from wind turbines (kW)
PC_p performance change for pth criterion
PD Performance Degradation
PRI real interest rate
R_P reference value for the performance indicator
$R_{CPU/GPU}$ ratio of CPU time to GPU time

Input Parameters for the model:

β tilt angel of SPV panels (rad)
$\eta_{\text{Wind-losses}}$ General power losses in wind turbine
η_{Sys}^{SPV} General power losses in SPV panels
A_{SPV} collector area of one SPV panel (m^2)
$ELD_{t,s}$ Electricity Load Demand (kWh)
$GCT_{t,s}$ COE for selling electricity to MUG ($)
$GCF_{t,s}$ COE for purchasing electricity from MUG ($)
P_R Rated power of the turbine (kW)
v_{CI} Cut-in wind speed of the turbine (ms^{-1})
v_{CO} Cut-off wind speed of the turbine (ms^{-1})
v_R Rated wind speed of the turbine (ms^{-1})
v_t Wind speed at hub level of wind turbine (ms^{-1})
Wp weight for the performance indicator p
WRE Waste of Renewable Energy
$P^{FG\text{-}Lim}$ maximum units purchased from the grid (kWh)

Other acronyms used

$\mathbb{E}[x]$	Expected value for x
CPU	Central Processing Unit
COE	Cost of electricity ($)
GC	Grid Cost for electricity ($)
GPU	Graphics Processing Unit
GI	Grid Interactions (kWh)
ICG	Internal Combustion Generator
MTG	Main distribution grid
NI	Net interactions with grid
SOC	State of charge of battery bank
SPV	Solar PV
T_{Opt}	Time taken for optimization (seconds)
T_{Sim}	Time taken for simulation (seconds)
T_{Tot}	Total time taken for simulation and optimization (seconds)
TDY	typical downscaled year
TMY	typical meteorological year
TOU	Time of use
V2G	Vehicle to Grid
VRE	Variable Renewable Energy

1 Introduction

Readers are encouraged to read the following book chapter and journal paper for further information

A. T. D. Perera, Silvia Coccolo, Pietro Florio, Vahid M. Nik, Dasaraden Mauree and Jean-Louis Scartezzini, Linking Neighborhoods into Sustainable Energy Systems, Teodora-Emilia Motoasca (eds.), Avinash Kumar Agarwal (eds.), and Hilde Breesch (eds.), Energy Sustainability in Built and Urban Environments, Springer-Nature Publishers

Dasaraden Mauree, Silvia Coccolo, A.T.D. Perera, Vahid M. Nik, Emanuele Naboni, Jean-Louis Scartezzini Addressing sustainability and resilience of urban areas to bridge the gap between the well-being of urban dwellers and the urban energy system infrastructure (manuscript under review in Renewable and Sustainable Energy Reviews)

1.1. Energy sustainability of ever expanding cities

Energy sustainability of cities is a target that needs to be achieved by improving both demand side and generation. However, it is more complicated than simply improving the energy efficiency and sustainability of a single sector because there are complex interactions between different sectors. A wide community of researchers aims to make 100 % renewable energy systems a reality [1–5] in order to improve the sustainability of energy sector. Replacing dispatchable energy sources driven by fossil fuel by distributed solar PV (SPV), wind and biomass/bio energy sources is a major challenge in this context. Mismatch in time of peak demand and generation due to the stochastic nature of wind speed and solar radiation makes the renewable energy integration process difficult [6,7]. A number of recent studies have focused on this aspect by addressing technical issues [8–11]. Battery banks, H2/fuel-cells, etc. can be used to store electricity when renewable energy resources are ample and cater the electricity demand when renewable energy is scarce. Improving the architecture of energy systems by integrating energy storage and conversion technologies helps improving the contribution of renewable energy technologies [12]. Multiple energy sources, conversion methods and storage devices will however complicate the energy flow within the system, especially when catering the demand of multiple energy services.

1.2. Ever increasing complexity of the energy system super-structure and the challenges in the design process

Power generation by using fossil fuels based on the Rankine cycle, the Bryton Cycle or internal combustion generators are mature technologies. Concurrent generation of heat and electricity by using fossil fuel resources with a vapor power cycle and a gas power cycle have been amply discussed in the literature. However, this should not undermine recent efforts to develop thermodynamic cycles such as the Organic Rankine Cycle, the Kalina cycle, etc. which are live examples for improvements in energy conversion methods [13,14]. Classical decentralized power systems tend to follow a simple strategy when catering the varying demand (load factor of the device is adjusted to cater the changes in demand) [15]. This strategy can be extended in order to improve the efficiency when combining several dispatchable energy sources where an energy economic dispatch strategy can be used to derive the optimum operating point of each dispatchable energy source [16]. The dispatch of conventional power systems considering energy -economic and environmental aspects is a rich area of study.

When considering renewable energy integration, a number of studies have focused on the use of geothermal, biomass and bioenergy to replace fossil fuel resources. However, a notable change in

energy system architecture cannot be observed in these instances although improvements in energy conversion technologies are reported (except for hybrid power cycles). Integrating solar energy into an energy system is more difficult when compared to biomass and geothermal from the optimization perspective due to its stochastic nature [17]. A number of studies have focused on solar thermal power generation assisting concentric solar collectors where classical power generation methods can be used [18]. At the same time, recent studies have focused on using solar thermal energy with energy storage [19]. Phase change materials have been suggested to store energy using latent heat [20]. In addition, use of solar thermal energy combined with biomass and geothermal energy has also been discussed [21]. Both the aforementioned methods can be used to harness solar energy with minimum impact on the grid. In general, these techniques can be categorized as use of non-dispatchable thermal energy source to generate electricity with the support of an energy storage and dispatchable energy source where improvement in system architecture is witnessed to integrate renewable energy.

Similar to renewable based thermal energy, grid integrated Solar PV (SPV) systems and wind farms have been amply discussed. Hybrid energy systems combining SPV panels, wind turbines, energy storage/s and dispatchable energy sources are also getting popular [22]. These systems have been used for a number of applications considering both the grid-connected and the stand-alone mode of operation. A number of system configurations have been proposed when moving from electricity supply to providing multi energy services [12]. Depending upon the energy services provided by the system, multiple energy storages can be used (though not more than one energy storage per energy service), which will absorb the fluctuations of non-dispatchable energy sources. In addition, there are instances where cascade storages are used (more than one storage is used to store energy per one energy service). A few energy storage technologies, such as battery banks, H2 storage, compressed air, pump water storage, super capacitors can be used considering techno-economical aspects. Similarly, several PCMs have been used in cascade thermal storages. The superstructure of the energy systems can be further extended considering non dispatchable energy storage such as electric vehicle and buildings as thermal storage, which will make the superstructure more complicated [23,24]. In addition, elasticity of demand can be considered. Access to renewable energy technologies and the potential of these renewable energy technologies, seasonal variation of these energy sources as well as the capacity factor of the energy system can be used to simplify the superstructure, which will make the design and the real-time control of the system achievable.

1.3. Practices in the present state of the art and its limitations

Energy systems are getting more and more complicated as they are expected to cater multiple

energy services connected to multiple energy sources, conversion methods, storage devices and grids [25,26]. There exists more than one way to cater the demand in most of the instances; especially for instances where non-dispatchable energy sources are integrated (as explained before). Furthermore, future forecasts for renewable energy generation demand for multiple energy services and real time price of multi energy services in the grid need to be considered, which makes it difficult to determine the optimum control strategy for an energy system. Hence, it is important identify the best technique that can be adopted in this regard.

The choice of a given energy management system for a particular time step will influence the performance of the system in the next few time steps. For example, the decision to discharge a battery bank at time step *t* will result in a loss in renewable energy storage or a load mismatch in catering multi energy services in time step *t+n*. Hence, it is important to understand the influence of the dispatch strategy in system sizing. On the other hand, the dispatch strategy depends on the system configuration. These aspects are coupled.. A simplified dispatch strategy is therefore used in system configuration optimization, which will evaluate the critical aspects of energy management important for system sizing as shown in Fig. 1.1.

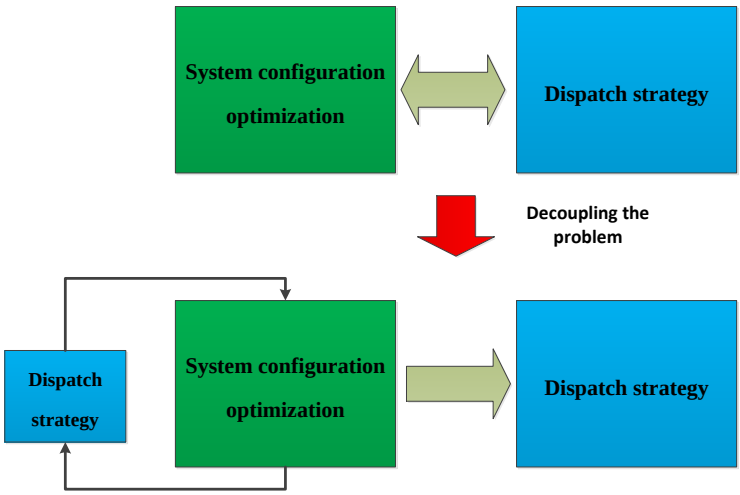

Fig. 1. 1*:* Interrelationship of system configuration and dispatch strategy

For the sake of simplicity, optimization methods used in the present state of the art can be classified into two categories. The first type is based on design optimization combining rule based dispatch strategies; the second method is based on design optimization with a selected day-hour dispatch strategy [27,28]. The former is used in design problems where energy flow within the system is simple. It is assumed that the system can operate in a finite number of states and the state transition is optimized considering the changes in input parameters considering it as a Markov Decision Process (MDP). This can be conducted as a single level or bi-level optimization problem

[27,28]. The main advantage of this method is simplicity. However, when multiple energy sources with multiple energy conversion techniques are considered to cater multiple energy services, operating states grow exponentially. This leads to instances where the operation strategy needs to be simplified extensively, thereby not replicating the real-time operation of the energy system in the operation. This specific weakness makes it difficult to use this method in urban energy system design.

The second method is the selected day-hour approach. A bi-level optimization algorithm is used to design the energy system [29–31]. The primary algorithm focuses on optimizing the dispatch strategy and the secondary algorithm focuses on optimizing the system configuration. Initially, a few representative time slots will be selected and the performance of the system is optimized for the selected time slots instead of 8760 time steps. Both mono and multi objective optimization have been conducted considering aspects such as lifecycle cost, environmental impact etc. Ralph Evins [29] extended the bi-level optimization algorithm to consider 8760 time steps, not to be limited to a few selected days and hours. However, the computational time increases by up to three days when using this method. According to Murray et-al [32] and Paolo et-al [33], the computational time required for a bi-level optimization algorithm can be reduced by using a MILP for both system design and operation strategy while considering 8760 time steps, which allows considering seasonal storage. According to Murray et-al [32], future forecast for non-dispatchable renewable energy sources, grid conditions which can be used with model predictive control (MPC) scheme to assist the energy system optimization process. Paul et-al [34] incorporated MPC into the dispatch strategy in the energy system optimization process. However, they limited the scope to selected days and hours without considering 8760 time steps. Furthermore, uncertainty in renewable energy generation, demand and grid conditions are not considered in their work and the time horizon for the forecast is for short term storage.

When considering the recent literature, we understand that the complexity of the models used to optimize energy systems has increased significantly in order to accommodate the growing complexity of energy systems. White box models have become competent in efficiently modeling energy conversion processes within energy systems. However, such a high level of proficiency has not been exhibited in two respects i.e. handling the uncertainty and data driven models. For example, there is no satisfying way to convert climate relevant uncertainty into energy system relevant information while accommodating it in the optimization process. As a result, the vulnerability of energy systems to extreme climate events becomes higher. On the other hand, electric vehicles, smart buildings and P2P trading demand the energy system to be sensitive to the

information flow requiring data driven approaches to be incorporated into the design process not to be limited to white box models [35]. Such a change in the urban energy system modeling approach is essential in the energy system design process in order to speed up the energy transition.

When integrating non-dispatchable renewable energy technologies such as solar PV and wind in distributed energy systems, their energy interactions plays a vital role. The exchange of information among the distributed energy systems is essential for their smooth functioning. The concept of an energy internet has emerged in order to allow higher interactions among distributed energy systems through a multi-energy network [36,37]. However, the recent literature on energy system design uses a similar approach for single energy systems and multiple energy system scenarios (energy internet). Either each energy system is optimized separately or the entire energy internet is optimized in a single step as shown in Fig. 1.2. Although material, energy and cash flows among the energy systems can be accounted in this way, it is time consuming to accommodate information flow by using the white box methods as practiced at present. As a result, there is a research gap with regard to incorporating information flow among the energy hubs, which is essential for the operation of each energy hub while interacting with others. Consideration of information flow in the design phase allows energy internets to accommodate higher fractions of renewable energy technologies while maintaining their autonomy [35,38]. Hence, data driven approaches based on grey and black box methods should be looked on as possible alternatives to the currently used white box models.

Chapter 2 of this thesis assesses the capability of grey box models when designing distributed energy systems. Following the introduction of the grey box model used to optimize energy hubs, a comprehensive assessment is conducted to evaluate the potential of incorporating non-dispatchable renewable energy technologies for a single energy hub when using grey box models. Chapter 3 further extends the grey box model to a black box model where machine learning is introduced to design distributed energy systems. Reinforcement learning is introduced to consider complex operation of energy systems while incorporating the forecast for renewable energy potential, grid conditions and demand. Chapter 4 extends the scope further, moving from a single distributed energy system to an energy internet where several energy systems interact with each other in order to cater the energy demand of a wider area. Distributed computing is introduced in this study for the first time to design energy internets. A comprehensive assessment is conducted on the design of an energy internet considering three operating modes: 1) grid optimization followed by energy system optimization, 2) fully cooperative scenario and 3) non-cooperative scenario. Renewable energy integration, lifecycle cost, system configuration etc. of each energy system as well as the energy

internet are discussed in detail for three scenarios.

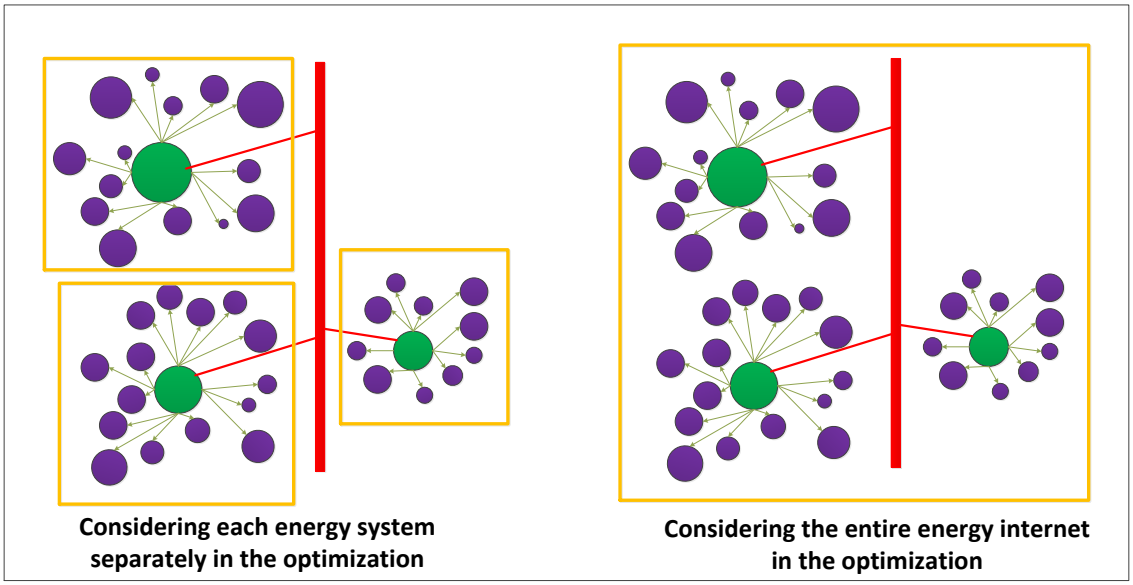

Fig. 1. 2: present approaches used to design energy internet.

Energy system optimization conducted using white box models often requires starting from the initial conditions whenever there is a notable change in demand or renewable energy potential. Hence at the regional or national scale top down statistical models need to be used , although these do not have a higher accuracy when compared to the bottom up models. One of the main advantages of data driven models is their capability to quickly adapt to the changes in the external environment. Chapter 5 of this thesis presents the capability of using a transfer learning technique in order to adapt the computational models developed in Chapters 2 and 4, which enables design of distributed energy systems at regional and national scale.

1.4. Uncertainties, vulnerability and resilience

A number of different uncertainties need to be considered when designing distributed energy systems. According to George et-al, [39] the uncertainties in demand, renewable energy potential and market prices can have a notable impact on both design and operation of distributed energy systems. Assessing both the short-term and long-term impact of uncertainties becomes a broad area of study. Considering both scope and relevance to the urban context, this thesis limits its scope to an analysis of the impact of climate uncertainty on the design process of distributed energy systems. Towards this end, possible methods to incorporate the climate uncertainty and extreme climate events are discussed in Chapter 7 and 8. The computational models developed in Chapters 2 and 3 are extended further to design climate resilient urban energy infrastructure. The deterministic model introduced in Chapters 2-5 is extended to a stochastic model in Chapter 6.

According to Panteli & Mancerella [40], converting climate relevant data into energy system relevant

data requires a large pool of scenarios to be simulated. Several recent studies have focused on optimizing the design of distributed energy systems considering climate uncertainty. However, these studies either limit the impact assessment to selected time steps or significantly reduce the number of scenarios when conducting the optimization process. Furthermore, none of the recent studies have considered the impact of extreme climate conditions on the energy system. Towards addressing these limitations in the present state of art, Chapter 6 tries to develop a computational platform that combines an energy system optimization model with a regional climate model (Fig. 1.3). Several climate scenarios are developed in order to represent both climate uncertainty and extreme events. Graphical Processor Unit (GPU) computing is introduced in order to consider a larger pool of scenarios (above 5000) through large scale parallelization. Finally, Chapter 6 introduces a hybrid stochastic-robust optimization algorithm that can consider both climate uncertainty and extreme events. Promising pathways for climate adaptation in the energy sector are discussed especially from the distributed energy system perspective.

Flexibility of the energy system is important for climate adaptation. Although this has been widely discussed from an operation perspective, it has not been discussed in detail from a design perspective, which is equally important. Therefore, Chapter 7 proposes to redefine the flexibility concept considering the design of the energy system. A novel method is proposed to compute the capability of energy systems to withstand performance degradation due to climate uncertainty. Subsequently, the flexibility level of several energy system designs is evaluated.

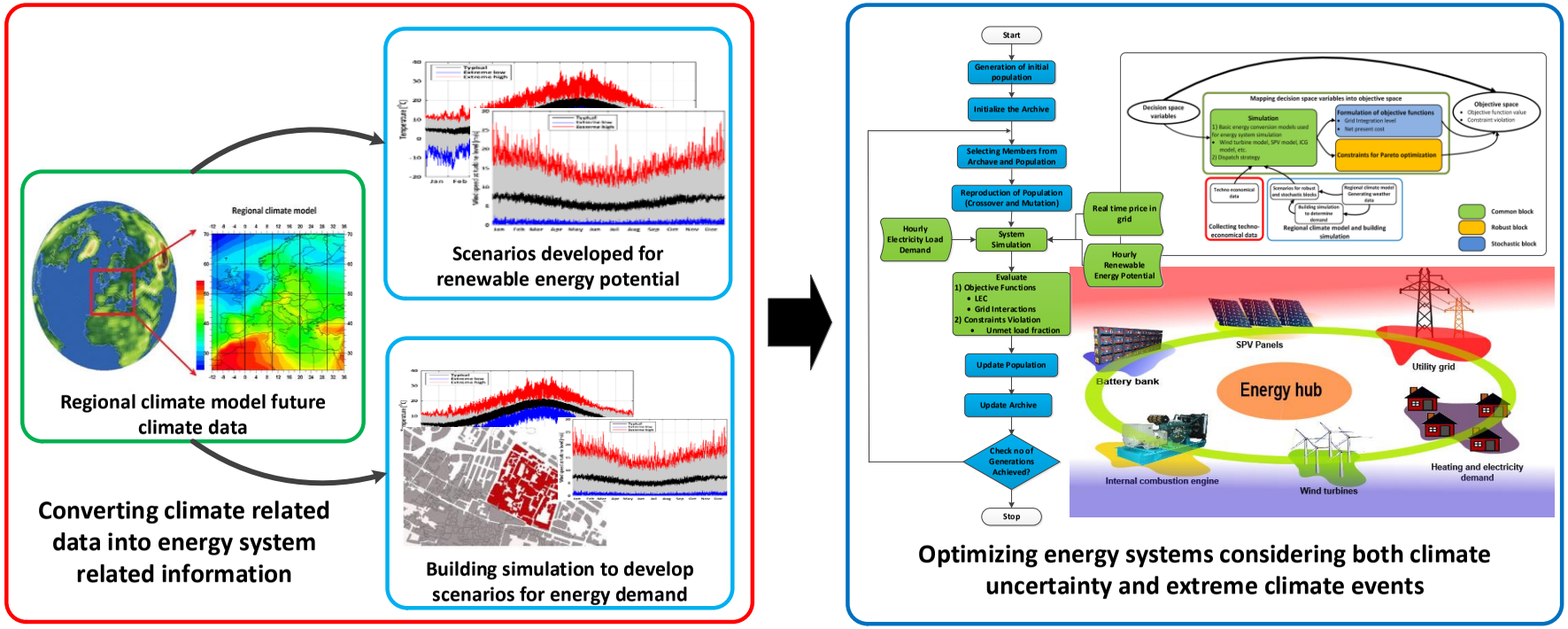

Fig. 1. 3: Outline of the computational model developed combining regional climate model and energy system optimization mode to 1)integrate climate scenarios based on regional climate model to support energy system optimization, 2)introduce novel optimization algorithm to consider climate uncertainty and resilience 3) benchmark the performance of the novel computational algorithm to design climate resilient energy systems.

1.5. Extending the design process to the urban scale and the assessment of energy systems

Regional climate models discussed in Section 1.4 can only present the climate effects at the meso-scale. Such meso-scale models fail to present phenomena such as the urban heat islanding effect, the cooling pool effect etc., which play a major role in the energy system design process. Hence, bringing urban physics into the energy system design is important during the design process of urban energy systems. Chapter 8 extends the urban energy system design process to consider the urban climate. An urban climate model is coupled with an urban simulation model and an energy system optimization model (introduced in Chapters 2 and 3) in order to consider the influences of urban physics. Such a coupling notably extends the scope of the energy system model developed in Chapter 2, 3 and 5. The impacts of urban climate on the energy demand under different urban densities are investigated in Chapter 8 with the focus on understanding the influences of urban climate on the energy system. Subsequently, Chapter 9 analyzes the efficiency of different urban forms from the perspective of energy autonomy and the renewable energy integration level extending the model developed in Chapter 8. An energy system is optimized for different urban archetypes in order to perform this task. Subsequently, more efficient urban forms are derived considering the climate conditions of Dubai (United Arab Emirates) and Hemberg (Switzerland), which present contrasting climatic conditions.

Urban energy planning is a broad subject. According to Manfren et-al [41] it consists of five major phases. This process starts from collecting basic data, preprocessing them, and finally designing the energy system. Once the energy system has been designed, it is important to go through the post processing phase evaluating aspects related to energy efficiency, economy and environmental impact. Finally, this should be followed by an impact assessment considering a life cycle assessment and local DG planning. Combining the design phase and the post processing phase is always challenging, especially when trying to come up with a final system design. Chapters 2 to 9 demonstrate various efforts made in order to render the design process more efficient. Similarly, efforts were made to conduct post processing. Unfortunately, these cannot be all accommodated into the thesis. Chapter 10 presents a comprehensive method that connects energy system design with post processing (1.4). Decision making and Pareto analysis play a vital role in the post processing path. Multiple criterions need to be considered simultaneously in the assessment process. Hence, multi-criterion decision making plays a major role in this regard and must be part of design optimization. Different methods based on Fuzzy TOPSIS, Analytical Hierarchical Process etc can be used. Chapter 10 presents a comprehensive way to combine Pareto analysis and multi-criterion decision making to complete the post processing phase.

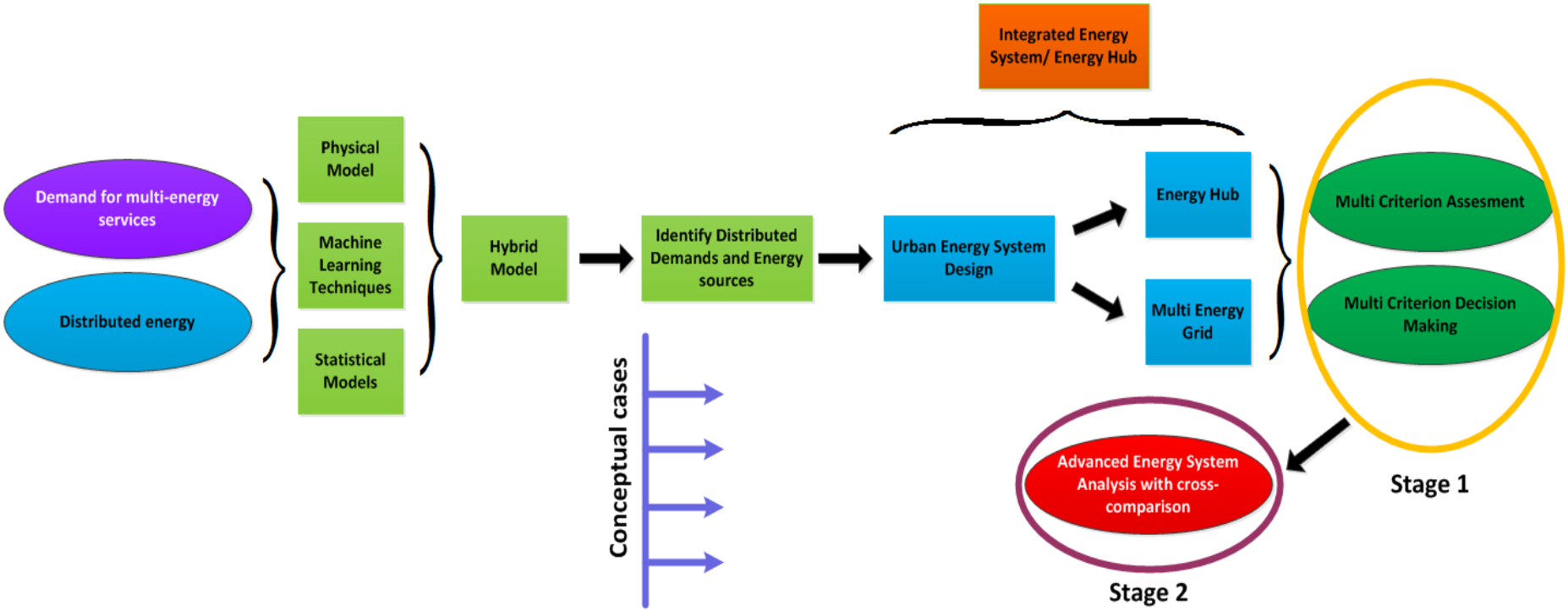

Fig. 1. 4: Steps to be followed in urban energy planning

1.6 Addressing different climate conditions

The climate condition of a city is having a notable impact on the energy system. It influences both renewable energy generation and demand profile. Hence, it is important to demonstrate the applicability of a computational model for different climate conditions. The computational model developed in this thesis is used to design energy systems considering contrasting climate conditions. For example, the case studies for Chapter 2 and Chapter 10 are conducted in Hambanthota, a coastal city in Sri Lanka with tropical climate conditions. The case study in chapters 3, 4, 6 and 7 are applied for Sweden considering Nordic climate conditions. The city of Nablus in Palestine is considered for Chapter 8. Nablus is located in the northern part of the West Bank and has Mediterranean climate conditions. Chapter 9 is based on two case studies conducted in Dubai, United Arab Emirates and Hemberg, Switzerland. These two cities present totally contrasting climate conditions. Dubai has a tropical desert climate while Hemberg has a moderate alpine climate conditions. Although not included as separate chapters, a number of case studies are conducted for Junction-Geneva, Cartigny-Geneva and Ecublens-Lausanne in Switzerland. These studies are published in conference and journal proceeding papers included in the beginning of Chapter 10. The computational model is now in the process of being tested for 16 European capitals considering different climate conditions. The cities considered in the thesis and the climate conditions are tabulated in Table 1.1.

1.6. Conclusions

This chapter presents the organization of the thesis. In brief, Chapters 2 to 4 introduce a novel computational model to design distributed energy systems and an energy internet. Chapter 5 presents promising approaches to conduct an optimization of a large number of energy systems at regional or national scale with the support of supervised and transfer learning techniques. Chapters 6 and 7 are devoted to considering uncertainties in the energy system optimization and promising ways to quantify the flexibility of energy systems to adapt to changes in the external environment. Chapters 8 and 9 are devoted to understanding the influence of urban physics on energy system design. The energy system design model developed in Chapters 2 to 3 is extended by coupling building simulation and an urban climate model to perform this task. Finally, Chapter 10 presents a promising way to assess urban energy systems by linking Pareto analysis with decision making.

Table 1.1: Climate conditions of the cities considered in the thesis

Climate conditions	Cities considered (Coordinates)	Country	Chapters	Koppen-Geiger climate classification
Tropical-coastal Climate	Hambantota (6° N, 81° E)	Sri Lanka	Chapter 2	AF-Equatorial fully humid
Nordic Climate	Lund (55° N, 13° E)	Sweden	Chapter 3,4,5	Cfb
Mediterranean Climate	Nablus (32° N, 35° E)	Palestine	Chapter 8	Csa-climate Temperate, dry summer, hot summer
Tropical desert climate	Dubai (25° N-55° E)	United Arab Emirates	Chapter 9	Bwh-Tropical, subtropical, desert Climate
Moderate alpine climate	Junction-Geneva (46° N, 6° E) Cartigny-Geneva Ecublens-Lausanne Hemberg-St. Gallen	Switzerland	Chapter 2,3,9 and 10	Cfb-warm temperate, fully humid, warm summer

2 Energy hub model and the assessment of renewable energy integration by using grey box models

A paradigm change in energy system design tools, energy market, and energy policy is required to attain the target levels in renewable energy integration and in minimizing pollutant emissions in power generation. Integrating non-dispatchable renewable energy sources such as solar and wind energy is vital in this context. Distributed generation has been identified as a promising method to integrate Solar PV (SPV) and wind energy into grid in recent literature. A comprehensive mathematical model for a multi energy hub is presented in this chapter. Following that, a novel dispatch strategy is introduced (based on grey-box models) in this chapter to address the limitations in the existing methods in optimizing grid-integrated Energy hubs considering real time pricing of the electricity grid and curtailments in grid integration. Multi-objective optimization is conducted for the system design considering grid integration level and Levelized Energy Cost (LEC) as objective functions to evaluate the potential of Energy hubs to integrate SPV and wind energy.

This chapter is based on (preprint version):

A.T.D. Perera, V. M. Nik, D. Mauree, and J.-L. Scartezzini, “Electrical hubs: An effective way to integrate non-dispatchable renewable energy sources with minimum impact to the grid,” 2017 (190), pp. 232–248, Applied Energy.

Author contribution for the journal paper:

In this article, ATD, designed the research with the support of VMN, DM and JLS. ATD conducted the analysis and prepared the first draft of the manuscript. VMN, DM and JLS supported in revising and finalizing the Manuscript.

Readers are encouraged to read following conference proceedings for further information

1. A.T.D. Perera, V.M. Nik, Dasaraden Mauree, J-L Scartezzini Optimum design and control of grid integrated electrical hubs considering lifecycle cost and emission, IEEE EnergyCon 2016, Leuven, Belgium
2. A.T.D. Perera, V.M. Nik, Dasaraden Mauree, J-L Scartezzini Sensitivity analysis of the dispatch strategy in designing grid integrated electrical hubs, IEEE EnergyCon 2016, Leuven, Belgium

2.1. Introduction

Integrating renewable energy technologies into the electricity grid is gradually getting popular due to rapid depletion of fossil fuel resources and global concerns on greenhouse gases emissions and nuclear energy. Several countries have their own goals with different time lines in this regard. For example, Germany has a goal to cover 50% of the generation system using renewable energy by 2030 [1], while in Finland it is 38% by 2020 [2]. Switzerland is expected to phase-out nuclear energy by 2035 by increasing the energy efficiency and the share of renewable energy sources. In Sri Lanka, it is expected to increase the share of non-conventional renewables, such as SPV and wind energy, up to 20% by the end of 2020. Recent studies highlight that distributed generation using solar PV (SPV) and wind energy is promising to foster the renewable energy penetration in the market [3], [4].

Energy systems fully driven using renewable energy sources is a dream that wider community of researchers try to make a reality [5]–[9]. Replacing dispatchable energy sources driven by fossil fuel through distributed SPV, wind and biomass/bio energy sources is the major challenge in this context. Mismatch in time of peak demand and generation due to stochastic nature of wind speed and solar radiation as well as of electricity demand makes the renewable energy integration process difficult [10], [11]. Integration of dispatchable energy sources, energy storage and converting into hybrid renewable energy systems is a cost effective approach in increasing the reliability during the renewable energy integration process. Further, this helps to amalgamate energy sources with higher seasonal variation in energy potential [12], [13] with less impact to the grid. More importantly, this is the starting point of minimizing the contribution of dispatchable energy sources based on fossil fuels, which makes existing energy systems more eco-friendly and sustainable [10], [14]. However, optimum design of such energy systems is a challenging task.

Several research groups have focused on optimizing grid-integrated hybrid energy systems which Fathima and Palanisamy [15] provide a review of the major recent works. Two different approaches can be used in this context to optimize the system design and dispatch simultaneous:

Energy system is expected to operate in finite set of states (finite state machines) in which operating conditions for the dispatchable energy sources and storage is defined. Subsequently, state transfer function is optimized along with the energy system (sizing problem) based on the objective functions considered [16]–[19].

Optimum operating conditions for dispatchable energy sources and storage is obtained for each time step considering these as decision space variables [20]–[24]. This can be further classified into

two groups, depending whether dispatching is optimized as time depended small scale problems or globally as a unique large size problem as explained in Ref. [25].

Both these methods are coming with their strengths and weaknesses. The first method can consider non-linear models (considering valve point effect, etc.) easily for energy conversion processes without simplification and present performance of the system (for 8760 time steps) with less computational time. However, the number of possible states that the system could operate increases exponentially with the complexity of the energy flow within the system (especially for poly-generation with multiple dispatchable energy sources and storages). Second method is more suitable when considering complex energy systems with multiple dispatchable sources and storage. However, the computational time and resources required become extremely high when using this method. According to Evins [22] optimization time can reach up to seven days when considering second method while Pruitt et al [24] report that there are limitations in handling a time horizon due to the increase of decision space variables. Further, simple linearization of objective functions can influence the results of the optimization problem significantly [26]. Hence, designing energy systems with simple energy flow such as hybrid energy systems and grid tied hybrid energy systems tends to use the first method while the second method is used for poly-generation [20]–[24]. The first part of the chapter introduces the computational model used in this thesis to formulate objective functions for the energy system optimization. Subsequently, a novel optimization algorithm to design grid integrated energy hubs [22], [27], [28] is introduced by extending the first method based on finite states.

The second part of the chapter presents a detailed assessment on the potential of energy hubs to integrate SPV and wind energy with a minimum impact to the grid. Integrating higher fractions of non-dispatchable renewable energy technologies while operating at higher autonomy levels (minimum grid interactions) is a difficult task [44], [45]. According to Ueckerd et-al [46] direct integration of higher fractions of non-dispatchable renewable energy sources above 30% is beyond the reach due to the limitations in the grid. A quantitative and qualitative analysis about the potential of integrated energy systems (such as energy hubs) to extend the SPV and wind energy integration (with minimum impact to the grid) is missing in literature besides its timely importance. This moves beyond design optimization where detailed assessment of the energy hub is required. To achieve this objective, Pareto optimization is conducted in this study considering Levelized Energy Cost (LEC) and Grid Interaction (GI) level (extending the definitions in Ref. [44], [45]) as objective functions. System configuration and variables of the dispatch strategy are considered as decision space variables to be optimized. Sensitivity of the mode of grid interactions (importing and exporting

electricity from the grid), the price of electricity and the curtailments in the grid and role of ICG and energy storage on SPV and wind energy integration are taken as the aspects to be assessed.

The chapter is arranged in the following manner: the computational model used to formulate energy system optimization is introduced in the first part (followed by a novel optimization algorithm based on fuzzy logic) ; the second part is devoted to evaluate the potential of energy hubs to increase the SPV and wind energy contribution with a minimum impact to the electricity distribution grid considering the recent and future changes in the grid. Section 2.2 presents the designing process of energy hubs, system configuration of the energy hub and the overview of the computational model. Section 2.3 presents the computational model used to assess energy as well as cash flow and the formation of objective functions considered for the optimization. Section 2.4 illustrates the simulation process with a detailed description of the dispatch strategy. Section 2.5 illustrates the optimization algorithm used, decision space variables and the combination of objective functions used for Pareto optimization. Finally, the role of energy hubs in integrating SPV and wind energy is discussed in Section 2.6.

2.2. Overview of the problem

This section provides an overview about the concept of energy hub within the framework of distributed generation under Section 2.2.1 and system configuration considered for the energy hub in Section 2.2.2. A detailed overview about the novel computational model developed to design energy hubs is also discussed in this section (2.2.3) mapping it into different parts of the chapter. The approach introduced in Chapter 2 is further extended in Chapter 3 concerning the operation strategy. Main parts of the computational model and interconnection among components is illustrated in Section 2.2.3.

2.2.1. Distributed generation to energy hubs

It is a challenging task to use distributed renewable energy sources in order to deliver the distributed demand. This needs to be achieved through several steps as demonstrated in Fig. 2.1. Distributed demand should be identified: building performance simulation tools, such as EnergyPlus [47] or CitySim [48], can be used to calculate the distributed demand. Clustering the demand helps to locate “demand centers” where the distributed energy systems will be located [49]. Simultaneously, it is important to assess the potential of renewable energy sources qualitatively to identify the promising renewable energy technologies. Afterwards, basic data for the selected energy technologies need to be collected.

Designing distributed energy systems consists of two processes i.e., designing the energy systems and designing the grid. This study only focuses on the energy system, therefore operation and maintenance of the utility grid is not considered. The method which is introduced in this study can be used to assess the potential of renewable energy integration in virtual power plants, smart micro-grids, grid-tied hybrid energy systems with minor modifications in boundary conditions, and the computational model [50]–[52] which are similar in operation.

2.2.2. System configuration of an energy hub

The energy hub, considered in this thesis consists of non-dispatchable energy sources: solar PV panels, solar thermal panels and wind turbines, as well as dispatchable energy sources; internal combustion generator (ICG) (Fig. 2.2 (a)), combined heat and generator (CHP). Moreover, a battery bank and a thermal storage are used as the energy storage. The energy hub interacts with the main utility grid (which is called as the grid hereafter) whenever it is required to cater the demand. Grid curtailments are considered for both import and export electricity to and from the energy hub and real time price is considered from the Energy Service Provider when interacting with the grid both electrical and thermal grid. For the sake of clarity, the chapter 2 limits its scope to the electrical part (Fig. 2.2 (b)) of the multi energy hub introduced on Fig. 2.2 (a). Chapter 3 extends its scope from an electrical hub to a multi energy hub.

2.2.3. Overview of the developed design tool

Design optimization of energy hubs consists of several interconnected steps as shown in Fig. 2.3. Energy System design process starts with collecting basic techno-economic data, renewable energy potentials, demand profile and information related to the grid. Main objective of the computational model is to optimize the design and control strategy based on the objective functions considered. Variables related to the system and dispatch strategy are considered in the optimization algorithm. The first part of the computational model is used to calculate the energy flow and cash flow of the system (Fig. 2.3). A computational model is developed to present the energy conversion process and cash flow in each system component towards achieving this objective (Section 2.3.4). A generalized model is presented in this Chapter covering both heat and electricity parts. However, electricity part is only considered in the dispatch strategy of Chapter 2 (multi-energy dispatch is discussed in Chapter 3). Sizing and selection of the system components affect the energy flow considerably and need to be considered in modelling; this makes the optimization block to be sandwiched between two blocks (i.e. Collecting Data and Mathematical Model). Mathematical model will present the energy conversion process of each system device. Computational model for wind turbines and SPV

panels will produce a time series of hourly power generated using the computational model which is transferred to the Simulation block as shown in Fig. 2.3. Similarly, mathematical models for energy storage and ICG are used in evaluating the energy flow being coupled with the dispatch strategy.

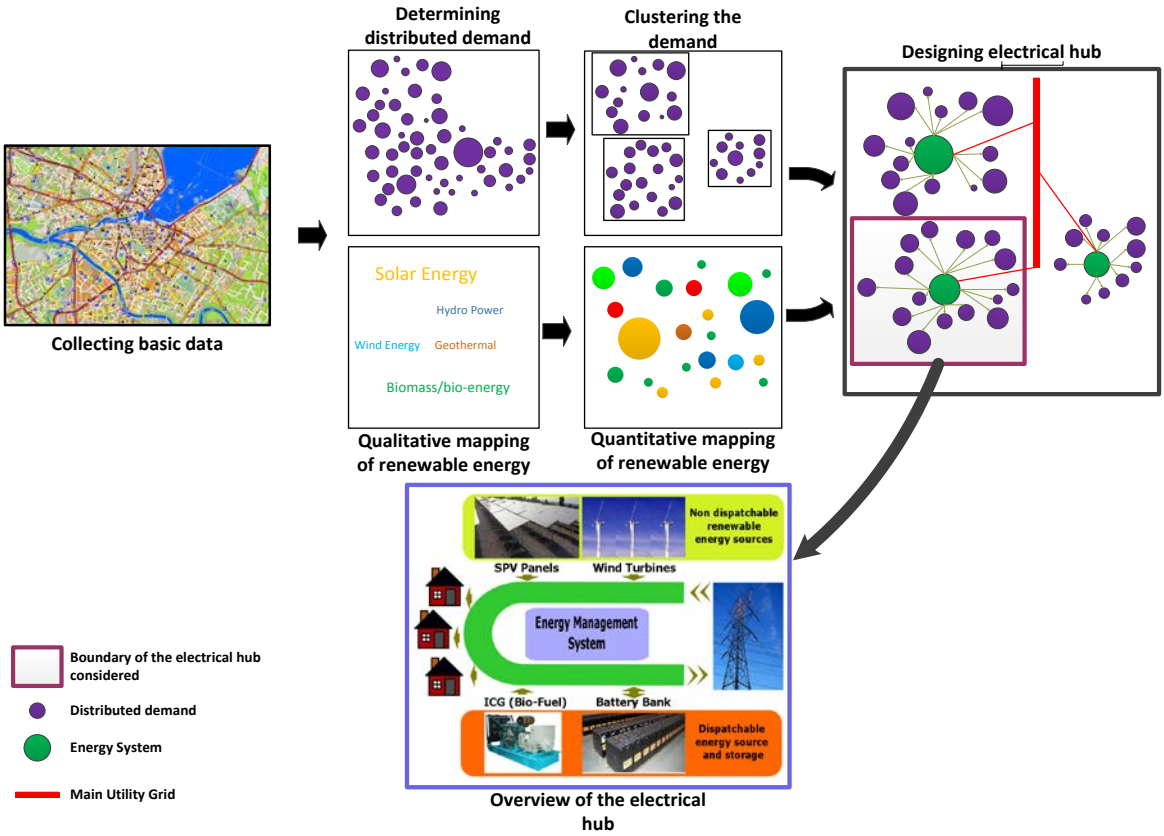

Fig. 2. 1 : Overview of the design problem

The task of the simulation block is to compute performance indicators that are used to formulate objective functions considering life cycle operation of the system. Energy flow of the system is evaluated considering the hourly time series of the renewable power generation, demand and electricity price in the grid. A bi-level dispatch strategy is used to determine the energy interactions with storage, ICG and grid, depending upon the renewable energy generation, demand and the electricity price in the grid (elaborated in Sections 2.4.1 and 2.4.2)in Chapter 2. A set of dispatch rules, obtained from the optimization algorithm, are used to optimize the power flow within the energy hub. Use of energy storage in a particular time step is linked with its operation in the previous time steps; this makes a coupling between the mathematical model and the simulation blocks. In addition, time series grid interactions (as discussed in Section 2.3.2), hourly fuel consumption, loss of load probability etc. are obtained based on the life cycle simulation which is used in mapping decision space variables into the optimization block. An extended explanation about each block is provided in sections 2.3, 2.4 and 2.5.

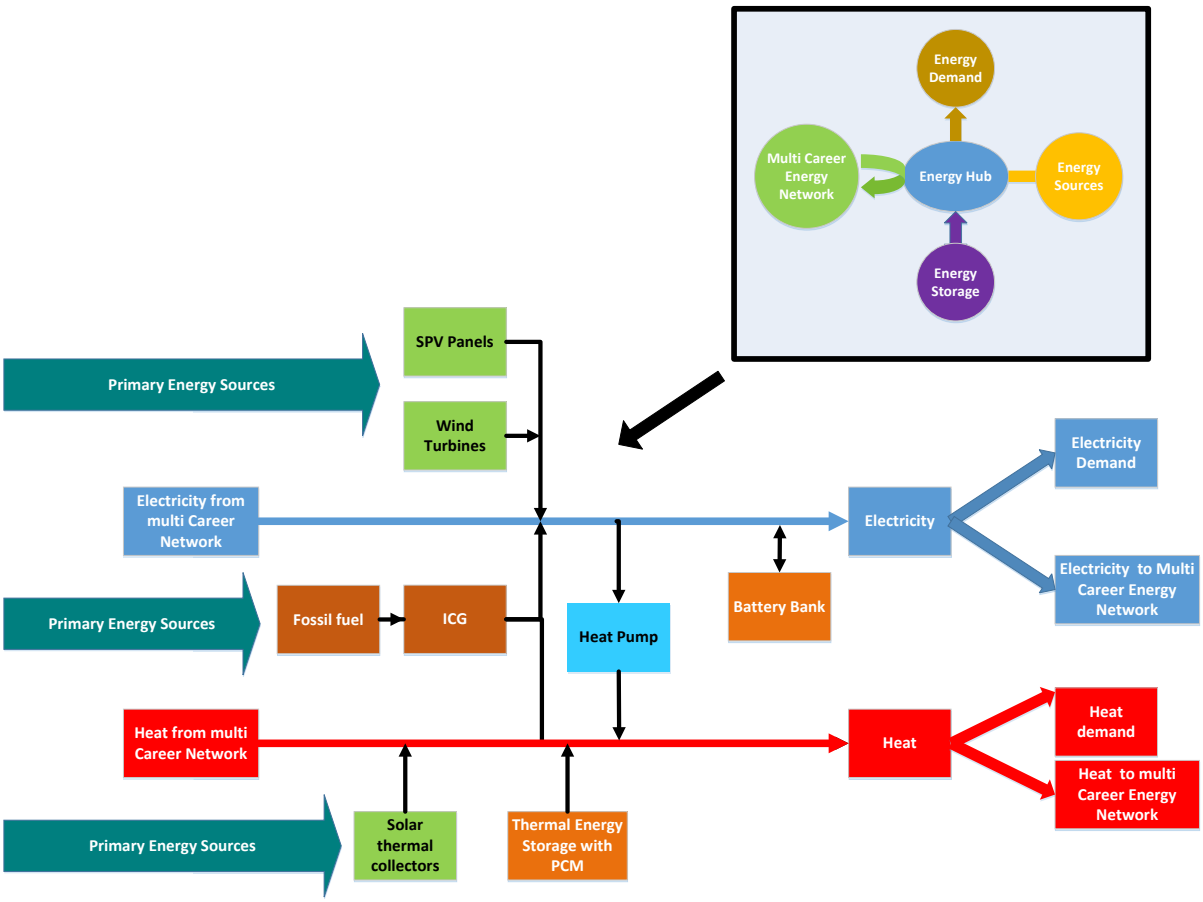

(a)

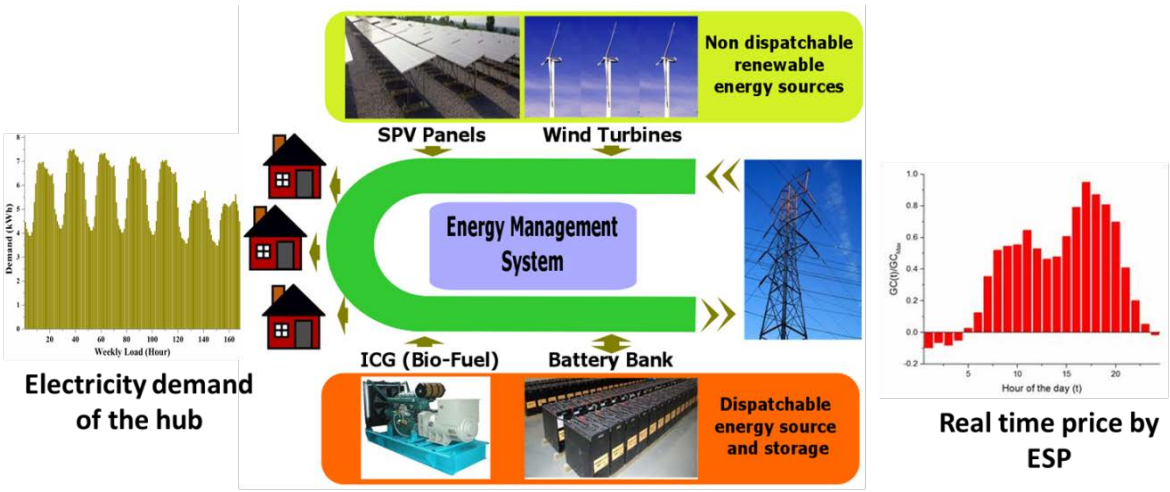

(b)

Fig. 2.2: Overview of the energy hub (a) outline of the multi-energy hub considered in the thesis and (b) the outline of the energy hub considered in Chapter 2 (present chapter) concerning the electricity part.

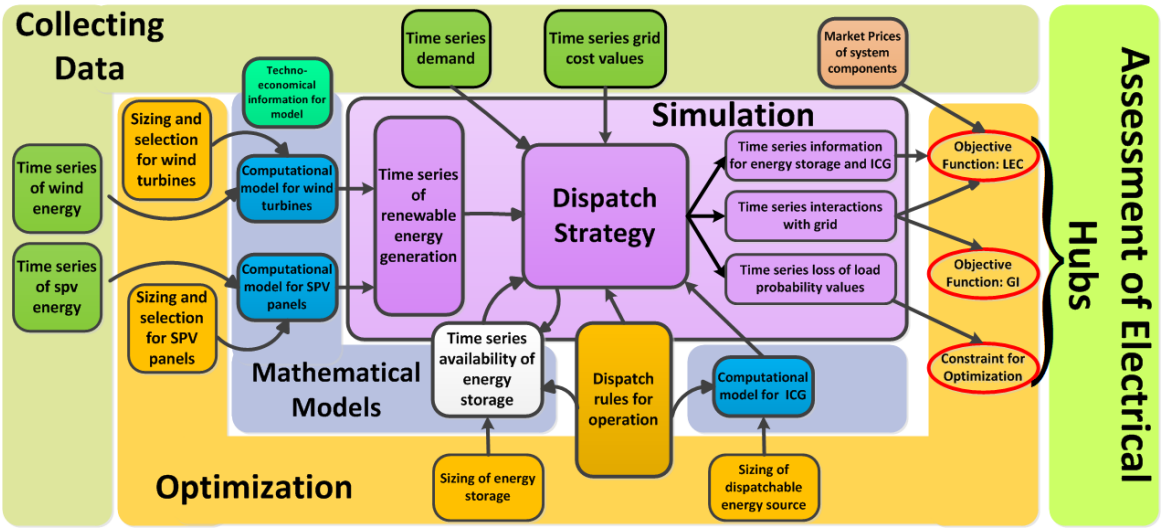

Fig. 2.3: Outlook of the computational tool

2.3. Mathematical model for the energy hub

The mathematical model developed in this study consists of several parts devoted to analyze the energy and cash flow of the system, grid interactions and power supply reliability. This is used to formulate LEC and Grid Integration (GI) level which are considered as objective functions (F∈Ƒ: set of objective functions) to be optimized. Power supply reliability is considered as a constraint as defined in Section 2.3.3. Decision space represents variables of the system design and operation (dispatch strategy); the system design variables consist of the type (technology) of SPV panels, wind turbines and the capacities of SPV panels, wind turbines, ICG and battery bank in the optimum system design (N∈Ɲ: set of decision space variables related to system design). This section formulates the time series of renewable power generation using SPV and wind based on the corresponding values of the decision space variables. Moreover, the computational model is illustrated which is used to determine State of Charge (SOC) and lifetime of the battery bank (Section 2.3.12), fuel consumption of the ICG (Section 2.3.12) and the grid interaction levels depending upon the operating conditions determined by the dispatch strategy (discussed in Section 2.4.1). Section 2.3.2 presents the model used to evaluate the autonomy level of the system considering grid integration. Finally, Section 2.3.4 determines the LEC considering all the cash flows related to system design and system operation.

2.3.1. Energy flow model

The main objective of the energy flow model is to evaluate the power generation and energy conversion processes within the system as discussed in Section 2.2.3. A comprehensive description of the computational model which is used to determine the electricity generation through the dispatchable/non-dispatchable sources and the other energy conversion processes is presented in this section.

2.3.3.1. Modeling non-dispatchable energy technologies

The heat and power generation from solar Thermal and PV panels depend on the solar irradiation on the panels. Hourly global irradiation data on a horizontal plane (G_t) was collected in order to compute diffuse fraction (f) according to Eq. 2.1. Following that, the diffuse solar irradiation (G_t^d) on horizontal plane is calculated according to Eq 2.2.

$$f = \begin{cases} (0.995 - 0.081\,MT\,, MT \leq 0.21) \\ (0.724 + 2.738\,MT - 8.32\,MT^2 + 4.967\,MT^3\,, 0.21 \leq MT \leq 0.76) \\ (0.18\,, 0.76 \leq MT\,) \end{cases} \quad (2.1)$$

$$G_t^d = \mathrm{f}.G_t$$

(2.2)

In Eq. 2.1, MT denotes clearness index. Eq. 2.3 is used to compute the clearness index.

$$MT = {}^{G_t}/_{H_0} \quad (2.3)$$

where H_0 denotes extraterrestrial solar radiation.

Klucher model [24] is used to compute the diffuse solar irradiation on tilted surface ($G_{d\beta}^t$) (Eq 2.4 and 2.5)

$$\mathrm{F} = 1 - (G_t^d/G_t)^2 \quad (2.4)$$

$$G_t^{d,\beta} = G_t^d\left[0.5\left(1 + \cos(\beta/2)\right)\right].\left[1 + \mathrm{F}\sin^3(\beta/2)\right].\left[1 + \mathrm{F}\cos^2(\theta)\sin^3(\theta_z)\right]$$

(2.5)

The beam radiation ($G_t^{b,\beta}$) and reflected solar radiation ($G_t^{r,\beta}$) are computed by using Eq. 2.6 and 2.7.

$$G_t^{b,\beta} = \left(G_t - G_t^d\right).\cos(\theta)/\cos(\theta_Z) \quad (2.6)$$

$$G_t^{r,\beta} = \rho.\mathrm{G}.\left(1 - \cos(\beta)\right)/2 \quad (2.7)$$

Finally, total solar irradiation on tilted surface G_β using Eq 2.8.

$$G_t^{\beta} = G_t^{d,\beta} + G_t^{b,\beta} + G_t^{r,\beta} \tag{2.8}$$

In these equations θ, θ_z and β denote angle of incidence for an arbitrarily inclined surface oriented toward the equator, zenith angle and tilt angle of SPV panel. Further, ρ is the albedo coefficient.

Thereafter, a semi empirical formula proposed by Durisch et al. [26] is used to determine the energy efficiency of the SPV panels η_t^{SPV} for time step $t(t \in T : set\,of\ all\,hours\,in\,the\ year)$ according to Eq 2.9.

$$\eta_t^{SPV} = p^{SPV}\left[\mathrm{q}^{SPV}\left(\frac{G_t^{\beta}}{G_0^{\beta}}\right) + \left(\frac{G_t^{\beta}}{G_0^{\beta}}\right)^{m^{SPV}}\right]\left[1 + r^{SPV}\left(\frac{\theta_t^{SPV}}{\theta_0^{SPV}}\right) + s^{SPV}\left(\frac{AM}{AM_0}\right) + \left(\frac{AM}{AM_0}\right)^{u^{SPV}}\right], \quad \forall t \in T \tag{2.9}$$

In Eq. 2.9, AM is the air mass value [27] and θ_t^{SPV} is the solar cell temperature. Standard values for G_0^{β}, θ_0^{SPV}, AM_0 are taken respectively as G_0^{β} = 1000 Wm^{-2}, θ_0^{SPV} = 25°C and AM_0 = 1.5. Parameter values of p^{SPV}, q^{SPV}, r^{SPV}, s^{SPV}, m^{SPV}, u^{SPV} for different SPV technologies, such as mono-crystalline, polycrystalline and amorphous silicon cells, are taken from Ref. [54] (Appendix A1-1). Θ_t^{SPV} was computed using Eq. 2.10.

$$\theta_t^{SPV} = \theta_a + h\, G_t^{\beta} \tag{2.10}$$

where *h* denotes the Ross coefficient (Appendix A1-1) and θ_a is the ambient temperature of the location.

The hourly power supply from the SPV panels P_t^{SPV} is calculated according to Eq. 2.11.

$$P_t^{SPV} = G_t^{\beta}\, \eta_t^{SPV}\, A^{SPV} N^{SPV}, \quad \forall t \in T \tag{2.11}$$

A^{SPV} and N^{SPV} $(N^{SPV} \in \mathrm{N})$ represent the area of a single SPV panel as well as the number of SPV panels.

Similar to the energy conversion model of the SPV panels, the energy flow model for wind turbines consist of two main components: i) a model to evaluate the wind speed at the hub level of the wind turbine and ii) a model to evaluate the electrical power generation from wind turbines. Hourly wind speed at 10 m anemometer height is used to calculate wind speed at hub level (v_t) of the wind turbine using a power law approximation. The "power curve" of the wind turbine, provided by the manufacturer, is used and modeled by applying n_s number of cubic spline interpolation functions [55], [56], taking (n_s+1) points from the power curve of the wind turbine according to Eq. 2.12

$$\tilde{P}_t^w = \begin{cases} \tilde{P}_t^w = 0, & v_{CI} > v_t \\ \tilde{P}_t^w = a_1^w v_t^3 + b_1^w v_t^2 + c_1^w v_t + d_1^w, & v_{CI} < v_t < v_1 \\ \tilde{P}_t^w = a_2^w v_t^3 + b_2^w v_t^2 + c_2^w v_t + d_2^w, & v_1 < v_t < v_2 \\ \qquad \cdots\cdots\cdots\cdots & \\ \qquad \cdots\cdots\cdots\cdots & \\ \tilde{P}_t^w = a_{n_s}^w v_t^3 + b_{n_s}^w v_t^2 + c_{n_s}^w v_t + d_{n_s}^w, & v_{n_s-1} < v_t < v_{n_s}(v_R) \\ \tilde{P}_t^w = P_R, & v_R < v_t < v_{CO} \\ \tilde{P}_t^w = 0, & v_t > v_{CO} \end{cases}, \forall t \in T \tag{2.12}$$

In Eq. 2.12, a_i^w, b_i^w, c_i^w, and d_i^w are coefficients of the polynomial function which vary depending on the "power curve". v_R, v_{CI}, v_{CO} and P_R denote rated wind speed, cut-in wind speed, cut-off wind speed and rated power of the wind turbine. Finally, net power generation (P_t^W) is calculated using Eq. 2.13.

$$P_t^W = \tilde{P}_t^W(\mathrm{v_t})\ \mathrm{N^w}\ \eta^{\text{W-losses}}, \forall t \in T \tag{2.13}$$

In Eq. 2.13, $N^W\,(N^W \in \mathrm{N})$ denotes the number of wind turbines which is optimized using the optimization algorithm, $\tilde{p}_t^W$ denotes power generated by one wind turbine calculated using the power curve and $\eta^{\text{W-losses}}$ accounts for other losses that take place in the energy conversion.

2.3.3.2. Modeling dispatchable energy technologies

Three dispatchable energy technologies are considered for the energy system in this thesis; i.e. Internal Combustion Generator (ICG), Combined Heat and Power generator (CHP) and a boiler. ICG possess the capability to cater the electricity demand, CHP caters both electricity and heat demand and boiler can be used to cater the heat demand. Chapter 2 considers the ICG in the energy hub model and the other components are considered in the Energy Hub model of Chapter 3. Energy flow model for the dispatchable sources are devoted towards computing the fuel consumption of each source based on the part load operating conditions. Eq. 2.14 is used to compute the fuel consumption of the ICG.

$$FC_t^{ICG} = a_0^{ICG} + a_1^{ICG} P_t^{ICG} + a_2^{ICG} P_t^{2_{ICG}} + a_3^{ICG} \left|\sin(a_4^{ICG}(P_t^{ICG} - P_{\min}^{ICG}))\right|, \forall t \in T,\ P_{\min}^{ICG} < P_t^{ICG} < P_{\max}^{ICG} \tag{2.14}$$

A model with two degrees of freedom is used (operating load factor and heat to power ratio) to model the operating cost of CHP (Eq. 2.14). In this equation, $P_{\max}^{ICG}$ and $P_{\min}^{ICG}$ denotes maximum and minimum power output of ICGs. a_0^{ICG} to a_3^{ICG} are constant which varies depending upon the type of

ICG. The importance of this equation is its capability to represent the valve point effect which is usually not presented in simple polynomial equations.

A model with two degrees of freedom is used (operating load factor and heat to power ratio) to model the fuel consumption of CHP according to the Eq. 2.15

$$FC_t^{CHP} = a_0^{CHP} + a_1^{CHP} P_t^{CHP} + a_2^{CHP} P_t^{CHP2} + a_3^{CHP} H_t^{CHP} + a_4^{CHP} H_t^{CHP2} + a_5^{CHP} H_t^{CHP} P_t^{CHP}, \forall t \in T \qquad (2.15)$$

In Eq. 2.15, P_t^{CHP} and H_t^{CHP} denote the power (electricity) and heat output from CHP. a_0^{CHP} - a_5^{CHP} depends on the type of co-generation plant and taken from the manufacturers.

A battery bank and a thermal storage based on Phase Change Material (PCM) are considered in this study as the energy storage model. Thermal storage is having complex characteristics when it comes to both charging and discharging cycles although it has higher second law efficiency. Multi-phase heat transfer and change of conduction to convection dominant behavior during the discharge process and charging process makes it difficult to model it. However, these complex heat transfer phenomena's are not considered in this study. The energy flow model for the battery bank is simplified in a similar manner. State of Charge (SOC) model is used to compute the charge levels of both battery bank and thermal storage. SOC of the battery is calculated according to Eq. 2.16

$$\mathrm{SOC_{t+1}} = \mathrm{SOC_t(t)}.\left(1 - \sigma^{\mathrm{bat}}{}_{\mathrm{t}}\right) + \mathrm{I_{bat_t}} \Delta \mathrm{t}.\, \eta_{\mathrm{ch_t}} / \mathrm{C_{bat}} \qquad (2.16)$$

In Eq. 2.16, σ^{bat} denotes self-discharge coefficient, which was taken as 0.02%, η_{chg} and C_{bat} denotes the round cycle efficiency of the battery bank and its capacity. A similar approach is used for the thermal storage. Similar to the dispatchable energy source, battery bank is considered in the energy hub model of Chapter 2 and both battery bank and thermal storage are considered in Chapter 3. State of Charge (SOC) of the battery bank is determined using finite state machines as describes in Section 2.4.2. Capacity of the battery bank N^{Bat} ($N^{Bat} \in \mathbb{N}$) is optimized using the optimization algorithm. The Rain-Flow Algorithm [59] is used to determine the life time of the battery bank depending on the number of charge/discharge cycles. Based on that number of replacement for the battery bank, life cycle cash flow for the energy storage is calculated.

2.3.2. Grid interaction level

The electricity grid is a critical infrastructure which is vulnerable to cascade failures [60]. Strong interactions via both importing and exporting electricity are discouraged from a perspective of grid

stability. Stability of the grid is considered in two different steps in the design process of the grid integrated energy system [43]. Firstly, curtailments for grid interactions are introduced. Due to hourly, daily and seasonal changes in both electricity demand and renewable energy supply, it is difficult to determine these parameters which should ideally be dynamic. Hence, grid curtailments are introduced as an upper bound for the energy interactions with the grid in this work. Secondly, a method is used to minimize the net interactions considering either importing or exporting energy from the grid or both. The two methods can be used as a performance indicator to evaluate the autonomy level of the system. It is important to note that these methods cannot replace the technical procedures used to access and monitor the stability and performance of the grid, which need to be carried out after the optimization of the system design.

The maximal limit for grid interaction (both to and from) is given by EG_{Lim} (i.e., the maximal power units that can be sold to the grid within a time step) and IG_{Lim} (e.g., the maximal power units that can be purchased from grid within a time step) belonging to the first category. Curtailments are introduced for thermal interactions in a similar way in Chapter 3. Three different performance indicators are used in Chapter 2 to measure the interaction with the grid which are developed based on [45], [61]. These indicators are entirely based on grid interactions with the electricity grid. The first indicator, GI_{IG} is based on the total electricity amount purchased from the grid (Eq. 2.17), this indicator depicts the support of the grid to maintain the reliability level of the energy hub. The second indicator, GI_{EG} is the total energy amount that is sold or exported to the grid (Eq. 2.18). Due to the integration of renewables, selling electricity to the grid becomes essential in order to minimize the operating cost of the system; though, excess transfer of electricity can reduce the stability of the grid. Finally, energy flows in both directions are considered as the third indicator (GI_{IEG}) as shown in Eq. 2.19.

$$GI_{\mathrm{IG}} = \sum_{\forall t \in T} P_t^{IG} / \sum_{\forall t \in T} P_t^{ELD} \tag{2.17}$$

$$GI_{\mathrm{EG}} = \sum_{\forall t \in T} P_t^{EG} / \sum_{\forall t \in T} P_t^{ELD} \tag{2.18}$$

$$GI_{\mathrm{IEG}} = \frac{\sum_{\forall t \in T} P_t^{EG} + P_t^{IG}}{\sum_{\forall t \in T} P_t^{ELD}} \tag{2.19}$$

In these equations, P_t^{ELD} denotes electricity demand of the electrical and P_t^{IG} and P_t^{EG} denotes the power imported and exported to and from the grid; the formulation for both these parameters depends on operating state. For an example, P_t^{EG} can be defined according to Eq. 2.20 for a one

simple operating state in an energy hub only considers the electricity flow i.e. State 3 (described in Section 2.4.2) which is different in other operating states.

$$P_t^{EG} = P_t^{RE} + P_t^{ICG} - P_t^{ELD}, \forall t \in T \tag{2.20}$$

In this equation, ELD_t and P_t^{RE} denote electricity load demand of the application and renewable power generation ($P_t^W + P_t^{SPV}$).

It is important to consider the interactions with the grid besides being limited to interactions maintained with the electricity grid. Interactions with the thermal grid are not considered in most of the instances when it comes to the concept of energy autonomy. Therefore, the formulation presented in Eq.2.17-19 is extended to consider grid integration level for multi energy hubs according to Eq. 2.21.

$$GI^{ME}{}_{\mathrm{IG}} = \frac{\sum_{\forall t \in T} P_t^{IG,E} + \gamma P_t^{IG,H}}{\sum_{\forall t \in T} P_t^{ELD} + \gamma \sum_{\forall t \in T} P_t^{HLD}} \tag{2.21}$$

In this equation, $P_t^{IG,H}$, P_t^{HLD} and γ denote electricity, heat imported from the grid, electricity and heat load of the energy hub and the weighting factor for heat to power conversion taken as the reciprocal of coefficient of performance of a heat pump (based on the second law of thermodynamics).

2.3.3. Power supply reliability

Loss of power supply (LPS) is considered to be occurring whenever power generation within the system is less than the demand (according to Eq. 2.22) and the mismatch cannot be supplied by both battery bank (due to the limitations in energy storage) and grid (due to the grid curtailments).

$$LPS_t = ELD_t - P_t^{RE} - P_t^{ICG} - P_t^{Bat-Max} - IG_{Lim}, \forall t \in T \tag{2.22}$$

$P_t^{Bat-Max}$ denotes maximum power flow from the battery depending upon the state of charge.

Finally, loss of load probability (LOLP) is calculated using LPS according to Eq. 2.23, which is used as the performance indicator to evaluate the power supply reliability.

$$LOLP = \frac{\sum_{\forall t \in T} LPS_t}{\sum_{\forall t \in T} P_t^{ELD}} \tag{2.23}$$

A similar approach is used to consider both heat and electricity when computing the loss of load probability in Eq. 2.24.

$$LOLP = \frac{\sum_{\forall t \in T} LPS^{E}{}_{t} + \gamma LPS^{H}{}_{t}}{\sum_{\forall t \in T} P_t^{ELD} + \gamma \sum_{\forall t \in T} P_t^{HLD}} \tag{2.24}$$

In this equation, $LPS^{E}{}_{t}$ and $LPS^{H}{}_{t}$ denote loss of electricity and heat (during break down) take place in the operation of the energy system.

2.3.4 Utilization of renewable energy

Various reasons such as stochastic nature of the demand and renewable energy potential, grid curtailments, limitations in energy storage makes it challenging to utilize renewable energy. This leads to a number of problems including poor energy efficiency, dependence on grid or dispatchable energy source which results in either poor autonomy or higher GHG emissions due to the combustion of fossil fuels. In order to rectify this issue utilization of renewable energy is considered as a major criterion to be optimized in energy system design. This study uses Waste of Renewable Energy (WRE) as the performance indicator which should be minimized in the design process. WRE represents the energy losses that take place in system due to seasonal changes in demand, renewable energy potential, and limitations in the energy storage and grid curtailments that has been amply used in resent literature [20], [39], [44]. WRE is formulated as Eq. 2.25 considering only the electrical part of the energy system.

$$WRE = \frac{\sum_{t=1}^{8760} P_t^{RE} - P_t^{SB-Max} - P_t^{ELD} - P_t^{TG-Max}}{\sum_{t=1}^{8760} P_t^{ELD}} \tag{2.25}$$

In this equation, $P_{SB\text{-}Max}$ denotes maximum energy that can be stored in time step t, depending upon the state of charge and $P_{TG\text{-}Max}$ denotes maximum units (kWhs) that can be sold to the grid depending upon the grid curtailments. Utilization of renewable energy technologies in multi-energy hubs is not taken into discussion in this thesis. Hence, the definition of WRE is only limited to the electrical part of the energy system.

2.3.5 CO2 Emissions

Minimizing CO2 emissions in different phases of the project is considered as one of the objectives of the energy system designers. Levelized CO2 (LCO2) is taken as the performance indicator to evaluate

this aspect in the thesis in Chapter 10 (only considering the electrical part of the energy hub). CO2 generation due to energy system components and their replacement is considered first. Afterwards CO2 generated due to grid interactions (when purchasing electricity) and power generation in ICG is considered secondly. Finally, total CO2 emission (TCO2) of the system is calculated combining both these aspects which is subsequently used to calculate the LCO2 according to Eq. 2.26.

$$TCO_2 = \sum_{\forall s \in S} ICO2_s + h \sum_{t=1}^{t=8760} (P_t^{IG,E} CGF_t + CICG_t(LF) P_t^{ICG}) \tag{2.26}$$

In this equation, $ICO2_s$ denote the lifecycle CO2 emission of system components including replacement for ICG and battery bank. CFG denotes the CO2 intensity for electricity unit taken from the grid and CICG denotes the CO2 intensity of each unit generated by ICG depending upon the load factor of the ICG.

2.3.6 Life Cycle Cost Model

The developed Life Cycle Cost (LCC) model evaluates the cash flows taking place during different time periods of the project. The cost model consists of three components: i) an Initial Capital Cost (ICC), ii) a fixed annual cash-flow and a iii) variable annual cash-flow. Accordingly, investment should be made at the beginning as well as annually. The ICC of system components comprises the purchase and installation costs for the systems components. The ICC of the whole system is determined considering the initial financial investment for the wind turbines, SPV panels, battery bank, power electronic devices (such as DC/AC converters and inverters) etc.

Life Cycle Cost (LCC) of the system consists of two components i.e. ICC and Operation and Maintenance cost (OM). ICC of system components comprise Acquisition Cost (AC) and installation cost. Installation cost of system components are taken as a fraction of AC (α) (Table A1-2 in the appendix) according to Eq. 2.27.

$$ICC_s = (1+\alpha)\ AC \quad \forall s \in S \tag{2.27}$$

ICC of the complete system (ICC_0) is calculated considering initial expenditure on system components (ICC^s) ($\forall s \in S$: set of system components) such as ICG (ICC_{Gen}), wind turbines (ICC_W), SPV panels (ICC_{SPV}), battery bank (ICC_B) and inverters (ICC_{Inv}) etc. according to Eq. 2.28.

$$ICC_0 = \sum_{\forall s \in S} ICC_s \tag{2.28}$$

Regular maintenance costs for wind turbines, SPV panels, fuel cost for ICG are considered under fixed annual cash flow (OM^F). Replacement costs for ICG, Battery bank (calculated based on the number of replacements) and power electronic devices are considered as variable annual cash flow (OM^V). Finally, present value of the operation and maintenance cash flows (for system components ($\forall s \in S$: set of system components) such as SPV panels, wind turbines, ICG etc.) is calculated according to Eq. 2.29.

$$OM_P = \sum_{\forall s \in S} OM_s^F \, CRF_s + \sum_{\forall h \in H} \sum_{\forall s \in S} p_s^h \, OM_S^V \tag{2.29}$$

In this equation, CRF_s denotes Capital Recovery Factor for s^{th} component for operation and maintenance. The real interest rate denoted by p is calculated using both interest rates for investment and local market annual inflation ratio. H denotes the set of all years.

In Eq. 2.29 CRF denotes the Capital Recovery Factor, which is computed using Eq. 2.30. In Eq. 2.30, p^{CRF} denotes the annual real interest rate, and h denotes the lifetime of the project in years. Annual real interest rate p^{CRF} is finally calculated using Eq. 2.31 where f^{CRF} and g^{CRF} denote return on investment and local market annual inflation rate (Table A1-2: in Appendix).

$$\mathrm{CRF}_S = \frac{\mathrm{p}\,(1-p^{CRF\mathrm{h}})}{1-\mathrm{p}^{CRF}} \tag{2.30}$$

$$\mathrm{p}^{CRF} = \frac{1+\mathrm{f}^{CRF}}{1+\mathrm{g}^{CRF}} \tag{2.31}$$

The Fixed Annual Cash-flow (FAC) consists of two items: FAC^{GI} which is the cash flow for grid integration (GI) and the fixed operation and maintenance cost. FAC^{GI} depends on the energy interaction with the grid. There is a cash inflow when selling electricity to the grid and a cash outflow when purchasing electricity from the grid. The cash flow depends on the Real Time Pricing of a unit kWh in the grid. FAC^{GI} is calculated based on hourly simulations over the year using Eq. 2.32.

$$FAC^{GI} = \sum_{\forall t \in T} P_t^{IG} \, GC_t^{IG} - P_t^{EG} \, GC_t^{EG} \tag{2.32}$$

In this equation, P_t^{IG} and P_t^{EG} denote energy (kWh) imported from the grid and exported to the grid respectively. GC_t^{IG} and GC_t^{EG} denote the cost of energy in the grid for purchasing and selling. Subsequently, Total Grid Integration cost TGI is calculated considering present value of all the cash flows of FAC^{GI}.

Variable annual cash-flow includes the replacement cost of the battery bank, ICG and power electronic devices, which depends on operating conditions, operating hours and life expectancy. The present values of all the variable annual cash-flows are subsequently calculated. The Net Present Value of the system comprises all the cash flows mentioned above. Finally, net present value is used to calculate Levelized Energy Cost (LEC) considering the demand of the energy hub throughout the lifetime of the project according to Eq. 2.33.

$$LEC = \frac{\left(ICC + OM_P + TGI\right)}{\sum_{\forall h \in H} \sum_{\forall t \in T} P_{h,t}^{ELD}} \tag{2.33}$$

2.4. Dispatch strategy and simulation

Choice of the energy management system, for a particular time step will influence the performance of the system in next dew time steps to come. Hence, it is important to understand the influence of dispatch strategy in system sizing. On the other hand dispatch strategy depends on the system configuration. Therefore, both these aspects are coupled together. Hence, it is important to de-couple these two. Simplified dispatch strategy is used in this context in system configuration optimization which will evaluate the critical aspects of energy management important for system sizing. More comprehensive dispatch strategies will be used for real time operation after designing the system.

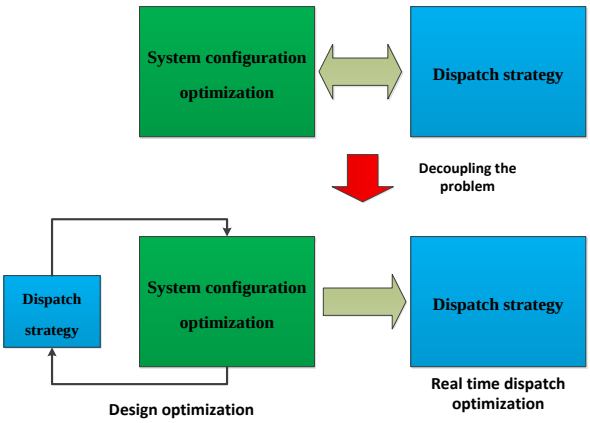

Fig. 2.4 Interrelationship of system configuration and dispatch strategy

Optimization method used to optimize these systems can be classified into two categories based on the method used to optimize dispatch strategy. For the cases where state of the system is optimized for each time step a bi-level optimization algorithm is used. In this case, system configuration and operation strategy are optimized in two different levels. In this process, primary algorithm is used to optimize the system configuration and secondary algorithm is used to optimize the operation (Fig.

2.5). The optimum operation strategy is derived for each time step for each configuration selected in the primary algorithm where 8760 time step needs to be optimized considering one year. This becomes an exhaustive task where objective function for dispatch strategy needs to be simplified and selective time steps need to be used instead of considering 8670 time steps. As per highlighted before, this dilutes basics physics of the problem first by linearizing the objective functions and secondly selecting representative time steps.

Second method relates with the control strategy based on finite state machines. In this method, transition function is optimized instead of energy flow in each time step (Fig. 2.5). This method is amply used in designing standalone hybrid energy systems and grid connected energy systems. Optimizing transition function instead of state of the system for each time step simplifies the optimization problem. System configuration and operation strategy can be optimized at the same level using this method. Hence, this method minimizes the deficiencies pertaining to the bi-level optimization algorithm and encouraged authors to use the second method.

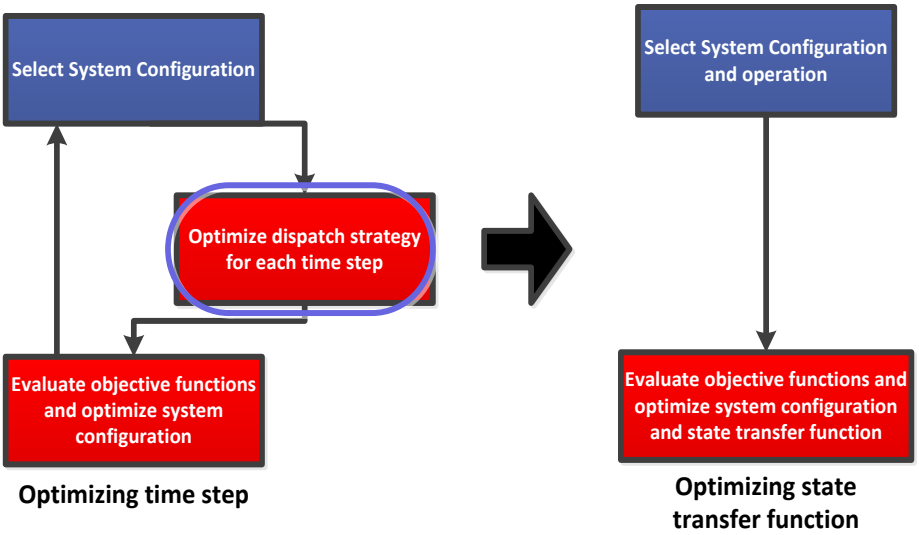

Fig.2.5 Comparison of two optimization approaches

A bi-level dispatch strategy is introduced in this section which is used in order to achieve this task along with the decision space variables used to optimize dispatch strategy (dϵD: set of decision space variables for system control). Section 2.4.1.1, introduces the primary algorithm based on fuzzy logic and Section 2.4.1.2 introduces the secondary algorithm based on finite state machines. Hourly simulation of the system based on the dispatch strategy generates the time series of hourly fuel consumption and State of Charge (SOC) which are used to calculate the costs related to ICG and the life time of battery bank, system reliability and the grid integration levels. Finally, Section 2.4.2

provides a brief overview about the meteorological and demand data used in the specific application.

2.4.1. Novel dispatch strategy for the energy hubs

Choice of the energy management system for a particular time step, will influence the performance of the system during next time steps. Hence, it is important to understand the influence of the dispatch strategy in system sizing. On the other hand, dispatch strategy depends on the system configuration. Therefore, both system design and dispatch strategy are coupled together. Hence it is important to de-couple these two in order to optimize the energy system. Simplified dispatch strategy is used in system configuration optimization since it is difficult to use the methods used to optimize the dispatch strategy alone. Simplified dispatch strategy will evaluate the critical aspects of energy management important for system sizing. Different methods have been suggested to achieve this task in the recent literature is reported in Ref. [63].

With the grid integration, the electrical power flow becomes more complex compared to typical hybrid energy systems, used for standalone applications. Conditions of the grid need to be considered when determining the system operating states in addition to the renewable energy generation and demand. Several recent studies were focused on this aspect: Augustin and Lopez [64] used evolutionary algorithm to maximize profits for grid connected wind farms with H_2 storage via optimal operations of the system considering the real time price. In their study, the optimum real time price for the grid to store wind energy, feeding to the grid and convert H_2 into electricity is determined along with other system design parameters. However, they did not consider catering a particular demand. Lopez [65], Lopez and Augustin [66] studied the impact of battery bank with real time price of grid when delivering an electricity demand to an industrial application. An enumerative method is used to optimize the rules of the dispatch strategy in this regard without considering power supply. There are a number of recent publications focused on optimal control of grid integrated renewable energy systems as reviewed in Ref. [67]. However, for the best of author's knowledge none of these research studies combine the energy management with optimal system design considering real time pricing of grid and grid curtailments for designing grid integrated hybrid energy systems. More importantly, most of the studies are entirely based on white box models. This thesis introduces both grey and black box models to optimize distributed energy systems. Chapter 2 (this chapter) introduces grey box model based on fuzzy logic which is extended in Chapter 3 to consider black box model when representing dispatch strategy.

Schematic overview of the energy management system is presented in Fig. 2.6 and 2.7. Four parameters are considered when determining the state of the system. These are state of the charge (SOC) of the battery bank, power generation in SPV panels and wind turbines, cost of electricity in grid and demand. Depending on these parameters, charging or discharging conditions of the battery bank, operating load factor of the ICG and grid interaction levels are determined. This is performed in two stages where first stage is used to determine the operating condition of the ICG using a fuzzy rule based controller. Second stage is used to manage the battery bank and grid interactions. Although schematic representation of the energy management system looks simple it is more complicated.

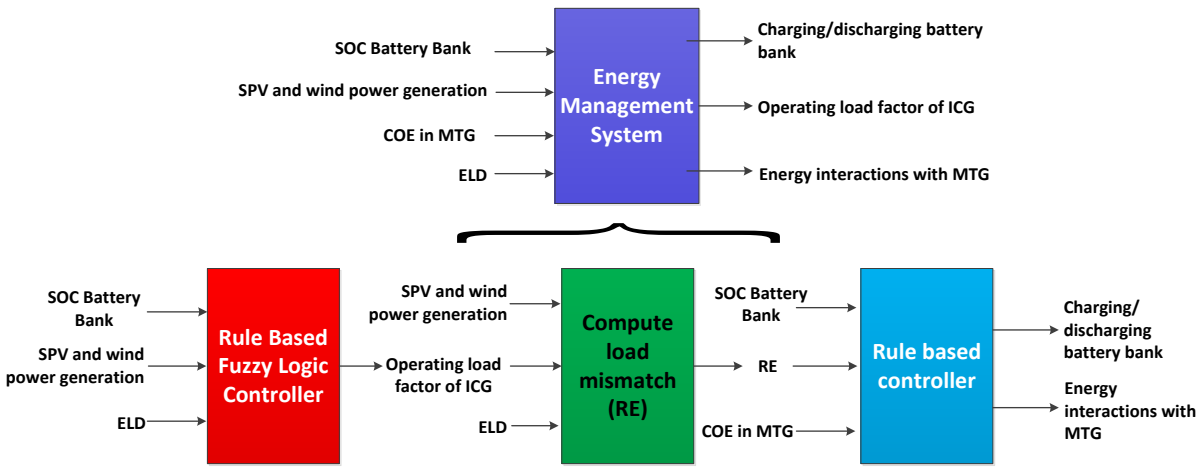

Fig.2.6 overview of the energy management system

2.4.1.1. Primary level dispatch strategy

As mentioned before, the operating state (load factor) of the ICG (y_t) is determined in the first step, based on two input variables x_t^1 and x_t^2 representing normalized depth of Discharge (DoD) of the battery bank and the normalized load mismatch between demand and the renewable energy generation (Eq. 2.34).

$$x_t^1 = \frac{P_t^{ELD} - P_t^{RE}}{\max_{\forall t \in T}(P_t^{ELD} - (P_t^{SPV} + P_t^{w}))} \tag{2.34}$$

The depth of discharge of the battery bank is calculated in a similar way using the SOC battery bank. Normalized values of DOD are designated by x_t^2 similar to Eq. 2.34.

Takagi-Sugino method [68]–[70] is used in this study to load factor of the ICG. Fuzzy implication R^l for l^{th} fuzzy subspace is defined according to Eq. 2.35

$$R^l\text{: If } g_l(x^1_t, \text{ is } A^1 \ldots\ldots x^k_t \text{ is } A^k) \text{ then } y_t = h(x^1_t, x^2_t, \ldots x^k_t,) \tag{2.35}$$

In this equation, x^1_t - x^k_t ($x \epsilon \chi$: set of all input variables of the fuzzy controller) denotes premise input variables for the fuzzy controller for the time interval t ($\forall t \in T$),y_t denotes output variable of the fuzzy logic controller whose value is inferred. A^l denotes the fuzzy sets having a linear membership function representing a fuzzy subspace where rule R^l can be applied. y_t^l is calculated for implication rule R^l using Eq. 2.36 using the function h^l in the consequence.

$$y_t^l = w_0^l + w_1^l x^1_t + w_2^l x^2_t \ldots\ldots + w_k^l x^k_t \tag{2.36}$$

where w_0^l, w_1^l (($w \epsilon W$: set of decision space variable related to fuzzy controller ($W \subset D$)) denotes coefficient determined by the system designer. y_t^l is further simplified considering the two inputs according to Eq. 2.37

$$y_t^l = (w_1^l x^1_t + w_2^l x^2_t)/ (w_1^l + w_2^l) \tag{2.37}$$

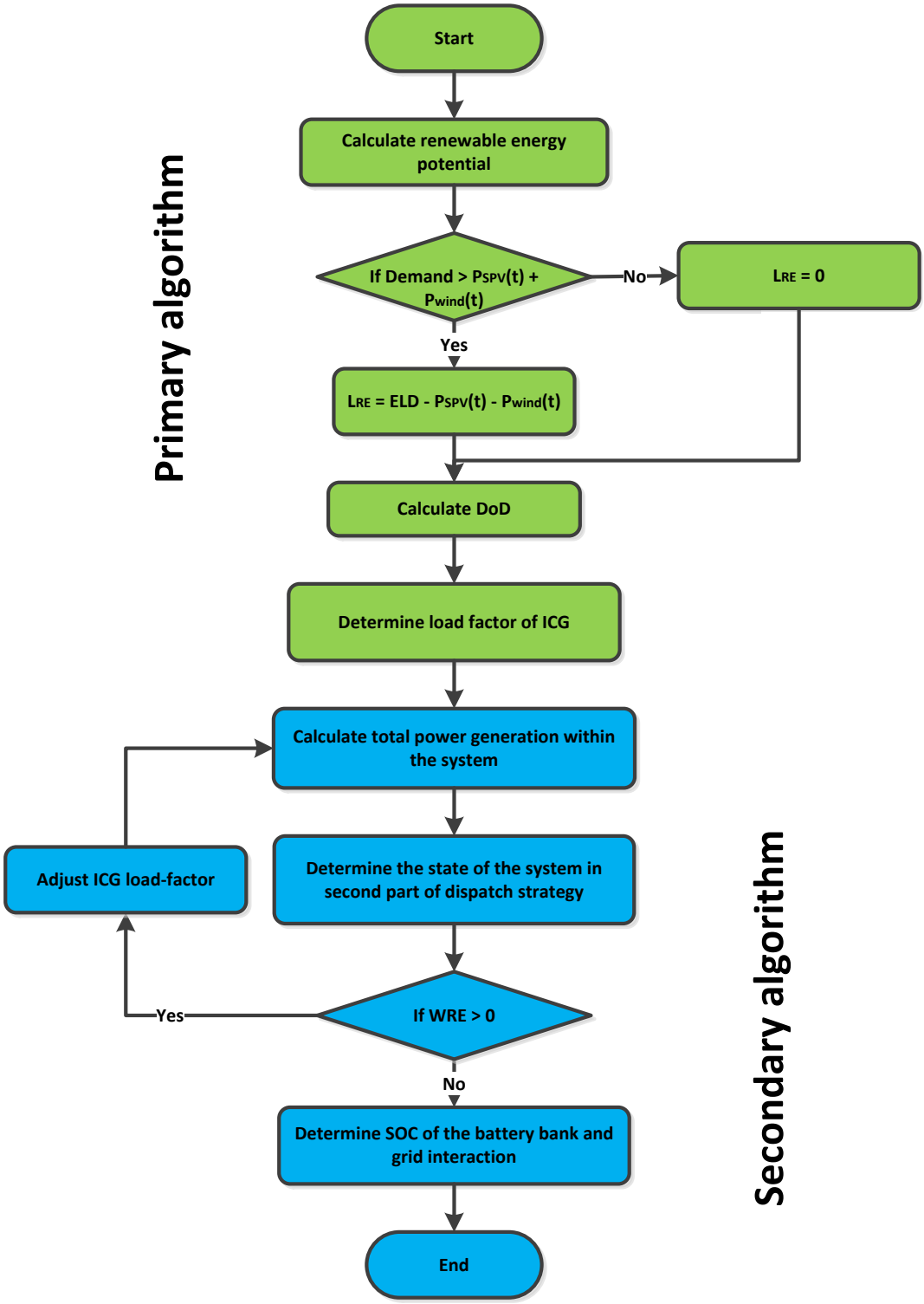

Fig. 2. 7: Flow chart of the Dispatch Strategy considering the operation of internal combustion generator, battery bank and grid interactions

Finally, y_t is calculated using center of gravity method according to Eq. 2.38 where μ_l denotes the membership function value for the corresponding rule R^l.

$$y_t = \frac{\sum \mu_l y_t^l}{\sum \mu_l} \tag{2.38}$$

An extended description of this method can be found in Ref. [71]–[74] . The weight coefficients corresponding to all the nine subspaces (w∈W) are optimized using the optimization algorithm considering these as decision space variables. After determining the ICG operating state, the net power generated in the energy hub is determined by combining both the non-dispatchable and dispatchable energy sources. The mismatch between demand and power generated is calculated afterwards. Load factor of the ICG is adjusted whenever the excess power generation is larger than the available storage capacity of the battery bank and EG_{Lim}. In the case of demand being larger than the generated power, Load Mismatch (LM) is calculated which is the difference between demand and power generated. The load mismatch is used to determine the operating state of secondary level dispatch strategy.

2.4.1.2. Secondary level dispatch strategy

Eight main operating system states are identified for the second stage of the dispatch strategy based on the conditions of the input variables for the rule based controller as well as curtailments for grid interactions (Fig. 2.8). A short description about the critical parameters (l **∈ L:**$(\mathrm{L} \subset \mathrm{D})$: set of all decision space variables related to secondary level controller) used to optimize the state transfer is presented in Table 2.1 followed by a graphical presentation in figure Fig. 2.9.

The first four operating states corresponds to instances where generation (combining wind, SPV and ICG) is less than the demand of the energy hub. In State 1, corresponds to the instances where price of electricity in grid is higher (GI_t^{IG}) > Lim_{BD} and GI_t^{EG}< Lim_{BTG}) and it is economical to take the mismatch from battery bank. Discharging the battery bank minimizes its life time, especially when reaching lower SOC levels. In order to overcome this problem, a minimal SOC level, which can be reached during the discharging process (SOC_{min}), is determined using the optimization algorithm (Fig. 2.9).

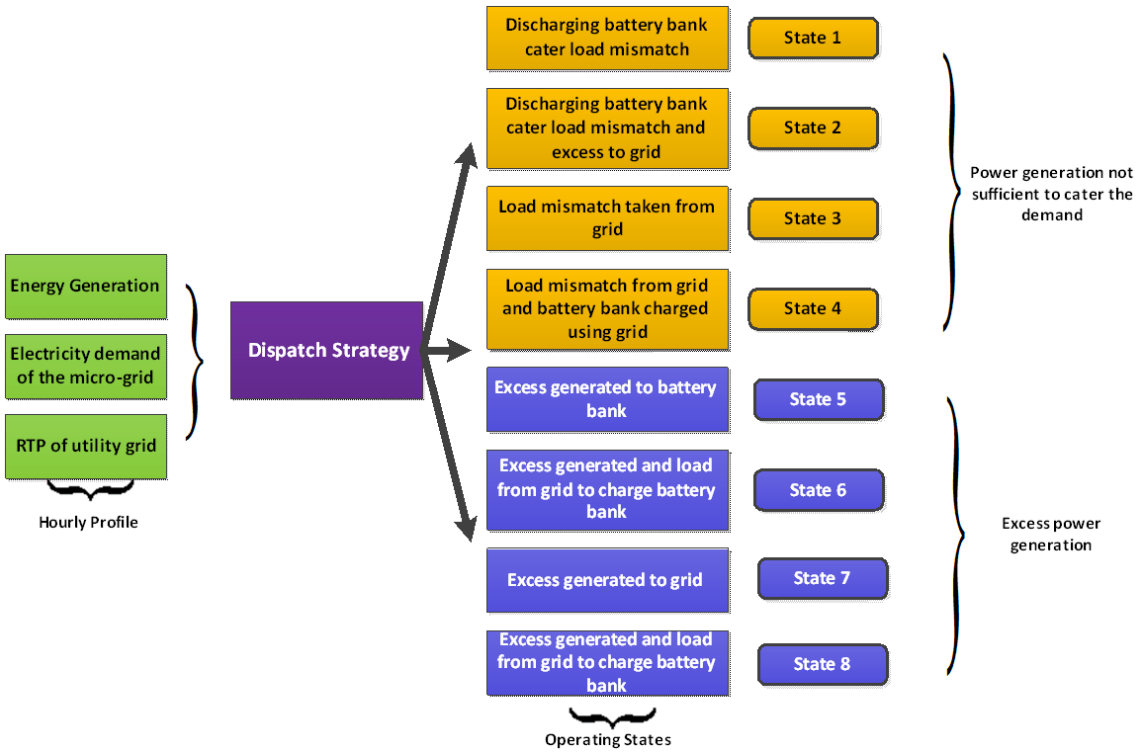

Fig. 2.8: Operating states of the system

When the cost of electricity in the grid increases further, it is economical to discharge the battery bank (GI_t^{IG} > Lim_{BD} and GI_t^{EG} > Lim_{BTG}) and sell electricity to the grid while supplying the mismatch between demand and generation. System moves to State 2 in such instances. However, discharging battery bank may lead to instances where energy hub needs to purchase electricity at a larger price from the grid at a later stage. In addition, depth of discharge of the battery bank needs to be considered since it reduces the lifetime of the battery bank. Hence, minimal SOC for the battery discharging process ($SOC_{Min,G}$) needs to be determined through the optimization algorithm.

The system operates at State 3, when the price of grid electricity is cheaper (GI_t^{IG} < Lim_{BD} and Lim_{GTB} < GI_t^{IG}). Load mismatch between demand and generation is taken from the grid in State 3. When the price of grid electricity goes down further (GI_t^{IG} < Lim_{BD} and Lim_{GTB} > GI_t^{IG}), it is economical to charge the battery bank using the grid electricity. However, as the charging of the battery bank from the grid reduces their storage capacity for renewable energy, a set point (SOC_{Set}) is introduced as the maximum limit for charging (instead of a full charging the battery bank), similar to the set point in the combined dispatch strategy for hybrid energy systems. SOC_{Set} is optimized taking upper bound as the maximum state of charge and lower bound as the $SOC_{Min,G}$ using the optimization algorithm.

Table 2. 1: Brief description about the variables in the dispatch strategy (I ϵ L (L ⊂D))

Acronym used	Description
Lim_{BC}	Critical cost for $GC_{EG}(t)$ above which selling the excess power generated to the grid is economical compared to battery charging
Lim_{BD}	Critical cost for GI_t^{IG} below which purchasing power from grid is economical compared to battery discharging
Lim_{GTB}	Critical cost for GI_t^{IG} below which purchasing power from grid to charge battery bank is economical
Lim_{BTG}	Critical cost for $GC_{EG}(t)$ above which selling stored energy to grid is economical
SOC_{min}	Critical SOC of the battery bank below which discharging is not economical to cater the load mismatch
$SOC_{Min,G}$	Critical SOC of the battery bank below which it is not economical to discharge and/or to sell the stored energy to grid
SOC_{Set}	Maximum state of charged to be reached when charging the battery bank

State 5-8 correspond to instances where generation is in excess compared to the demand. System moves into State 5 when price of grid electricity is low (GI_t^{EG} < Lim_{BC} and Lim_{GTB} < GI_t^{IG}) where excess generation is directed to battery bank. When the price of grid electricity is quite low it is economical to charge the batteries from the grid after charging the battery bank from excess power generated (GI_t^{EG} < Lim_{BC} and Lim_{GTB} > GI_t^{IG}). State 7 corresponds to instances where cost in the grid is competitive compared to charging batteries. In such instances, excess generated will be directed to the grid. When the price of electricity in the grid increases further, it is economical to discharge the battery bank in addition to directing excess electricity generated (GI_t^{EG} > Lim_{BC} and GI_t^{EG} > Lim_{BTG}). However, all these energy interactions need to take place considering the storage limitations of battery bank, EG_{Lim} and IG_{Lim} which makes the energy interactions more complicated. The logic flow diagram used in the secondary level dispatch strategy consists of 18 states which are based on the main eight states described. A more comprehensive description about these states is presented in Appendix 2.

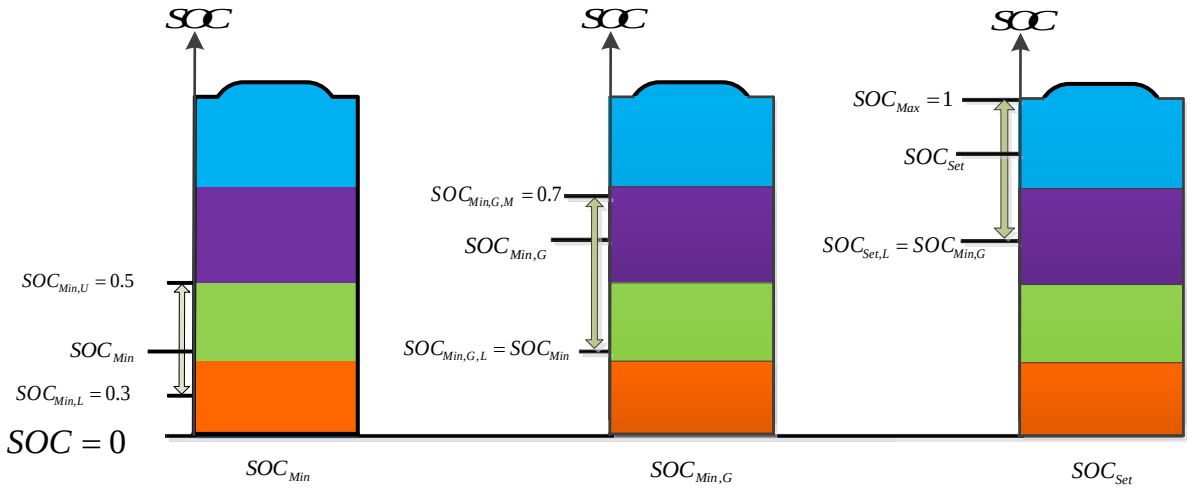

Fig. 2.9: Selection of the decision space variables for the battery bank

2.4.2. Time Series meteorological and demand data for simulation

The chapter 2 limits its scope to the electrical part of the energy hub in the assessment. The hourly average values of wind speed, global horizontal solar irradiation and ambient temperature data are required for the simulation. The site of Hambantota, a south coastal city of Sri Lanka, was considered for this study due to its strong wind and solar energy potential. All the aforementioned meteorological data are issued from the corresponding local meteorological station. The demand of a particular application is highly specific to the latter. In this study, demand is considered to vary according to the load variation suggested by the IEEE system reliability committee [75]. Load profiles are generated following a summer-weekly demand since seasonal demand variations are trivial in Sri Lanka being located near to the equator.

The cost of electricity is a function of time in a smart grid, depending from several factors. A hypothetical cost function is considered for the hourly electricity prices based on the demand in the region. Hourly electricity price is assumed to be proportional to the electricity consumption in the region, a maximal cost of electricity being reached at the peak hours of the demand. The price for selling electricity to the grid is considered to be proportional to the purchasing price of electricity from the grid. A sensitivity analysis of the impact of the cost of electricity function on the optimal solution was subsequently carried out. The effect of demand curve and the profile of grid cost on optimum system design are to be presented in future publications.

2.5. Optimization of the system design and dispatch strategy

Designing energy hubs integrated to the grid is challenging due to a number of reasons as discussed before. A heuristic algorithm has been amply used in the literature [19], [29]–[31], [36], [67], [76],

[77] and shown to be much efficient when optimizing these systems when compared to enumerative methods [78]which are used in existing software such as Homer [79]. A heuristic algorithm to optimize the system design and dispatch strategy which can handle non-linear objective functions efficiently in this Chapter considering the electrical part of the energy hub. This section illustrates optimization algorithm used in this study along with the decision space variables considered for the optimization which are introduced in Section 2.2.3 and 2.2.4, objective functions considered for the optimization defined in Section 2.2.3 and the constraints.

2.5.1. Decision space variables

Determining the optimal capacities of the system components as well as the type of components is the main objectives of the optimization algorithm. Basic system components are selected according to Table 2.2: their corresponding type and capacity are also determined using the same optimization algorithm. Six decision space variables are used to represent the whole system configurations.

Optimizing the dispatch strategy is another part of the optimization algorithm. The operation of the ICG and the battery bank need to be optimized together with the grid interaction. Both load mismatch and battery bank SOC are used to determine the state of operation of the ICG. The weight coefficients defined in Section 2.4.2 are optimized using the same algorithm. Three parameters are used to manage the energy flow to the battery bank according to its State of Charge (SOC) as illustrated in Fig. 2.9. SOC_{Min} is optimized considering a SOC range of [0.3, 0.5]. Critical parameters for battery charging and discharging are optimized considering upper and lower bounds as shown in Fig. 2.9. Similarly four variables are used to control the grid interaction as explained in Section 2.3.3. A total number of 19 decision space variables are selected to represent the state transfer function, with their span is defined according to Table A1-3 in Appendix.

2.5.2. Objective functions and constraints considered

The goal of this study is to maximize the autonomy of the system in renewable energy integration process while minimizing its cost. It is a multi-objective optimization task where two objective functions need to be minimized simultaneously. All three indicators introduced in Section 2.3.2 are used as the objective functions along with LEC introduced in Section 2.3.4. LOLP is considered as a constraint (defined in Section 2.3.3) in the optimization algorithm. List of objective functions considering different scenarios are presented in Table 2.2.

Table 2.2: List of Objective functions considered

Scenario*	Objective Function 1-Objective Function 2 (F_1-F_2)	Sensitivity	Constraints
A	LEC-Grid Interactions considering imports (GI_{IG})	Not considered	Loss of load probability (LOLP)
A	LEC-Grid Interactions considering Exports (GI_{EG})	Not considered	
A	LEC-Grid Interactions considering imports (GI_{IEG})	Not considered	
B	LEC-Grid Interactions considering imports (GI_{IG})	Grid curtailments considering 30%, 60% and 90% of the peak demand	
B	LEC-Grid Interactions considering imports (GI_{IG})	Market price of SPV panels and wind turbines considering 10%, 20% and 30% reduction	
B	LEC-Grid Interactions	Market price of grid electricity considering 10%,	

*Pareto fronts in Scenario A corresponds to Section 2.6.1 and Section B corresponds to Section 2.6.2

2.5.3. Optimization algorithm

As discussed in Section 2.2.3, the optimization algorithm is closely connected with the mathematical model and simulation of the system. The computational model and lifecycle simulation which map decision space variables into the objective space are described in detail in Sections 2.2, 2.3 and 2.4. Fig. 2.10 presents the simplified flow diagram of the optimization algorithm used in this study. The optimization algorithm starts with the random creation of decision vectors including variables related to system design and operation strategy which will create the initial population. Subsequently, set of vectors selected as the initial population is mapped to the objective space through the computational model and the life cycle simulation presented in Section 2.3 and Section 2.4 which will provide the values for the objective functions ($F \in \mathcal{F}$) and constraints. Initial archive is created from the non-dominant set of solutions in the population according to the criterion defined by Deb et-at [80]. A Steady ε-State Evolutionary Algorithm [81] is used in this study for updating of archive and reproduction of the population which is proven as a method to maintain the diversity while reaching the final set of Pareto solutions within short period of time. Polynomial mutation operator [82] and simulated binary crossover operator [83] are used along with differential evolutionary operators [77]–[79] in the reproduction of the population. Constraints for the optimization algorithm are handled at two different levels: constraint tournament method [82] is

used to handle the constraints in the optimization algorithm and loss of load probability is considered as a constraint while states of the control system were defined to handle the constraints due to grid curtailments. A computer program is written in C++ using Visual studio plat form. Computational time for the Pareto front depends on the objective functions selected and the number of generations considered; on average computational time was two hours for both Scenario A and B in this study.

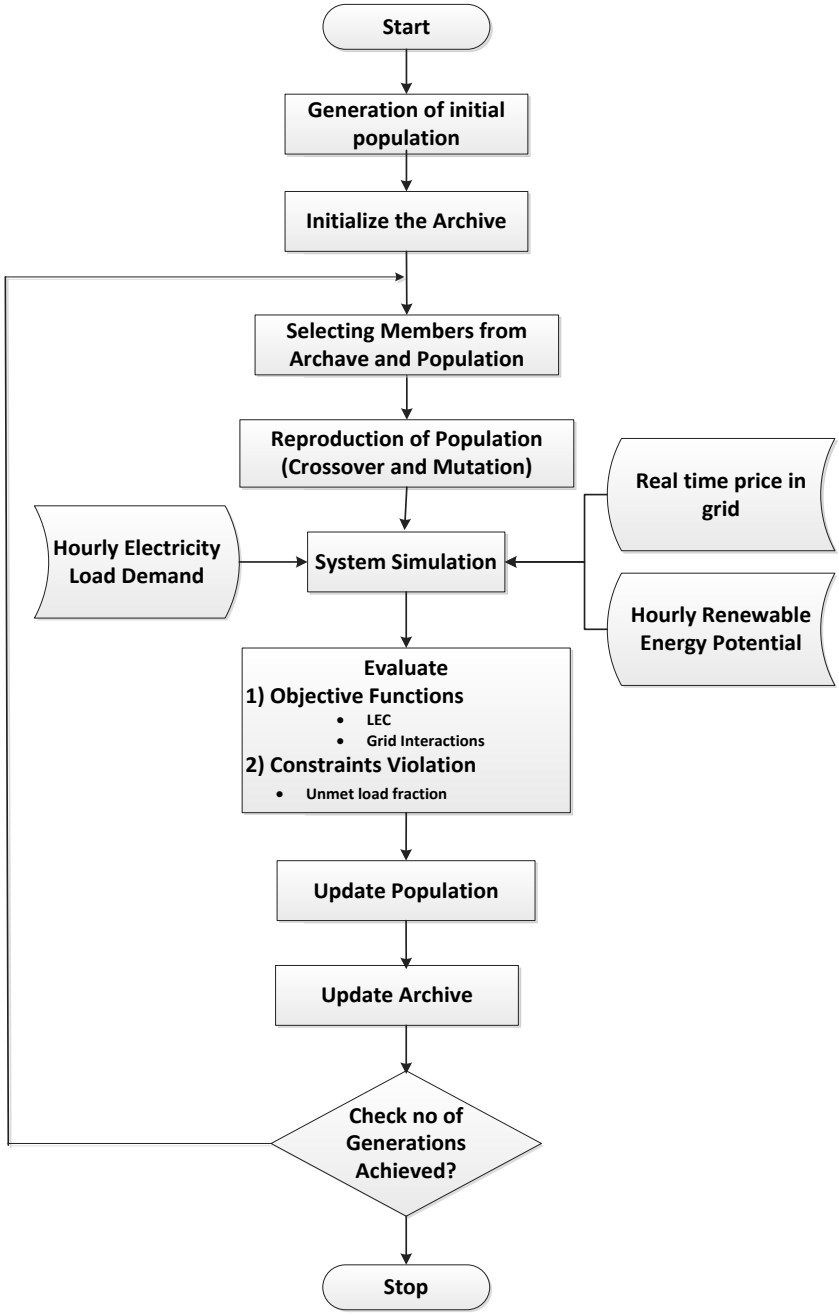

Fig. 2. 10: Optimization algorithm for energy Hubs

2.6. Results and discussion

Selecting optimal combination of energy technologies, storage becomes vital in integrating SPV and wind energy into energy hubs. Autonomy of the system needs to be maximized in integrating renewable energy technologies while minimizing the lifecycle cost of the system. Pareto fronts obtained in Section 2.5 considering LEC and grid integration level is useful in this regard. These Pareto fronts are used in this section to analyze

- Sensitivity of imports, exports and both to lifecycle cost, energy mix and renewable energy utilization of the system
- Sensitivity of grid curtailments and market conditions on renewable energy integration

Accordingly, this section is divided into two parts. The impact of grid interactions on energy hub and energy flow is discussed in Section 2.6.1. Section 2.6.2 is devoted to a sensitivity analysis of other techno-economical parameters impacting the results.

2.6. Sensitivity of grid interactions and energy mix

The support of the grid is essential to maintain the power supply reliability of the energy hub with the integration of renewable energy sources, while minimizing the lifecycle costs. Maximizing the autonomy of the energy hub is important when considering the grid. Therefore, the lifecycle cost and the autonomy of energy hub may become conflicting, meaning that it can be difficult to optimize both of them simultaneously. A Pareto front presents all the possible combination of solutions, which are optimal and non-dominant between each other. It helps the system designers to better understand the characteristics of the system accounting for the changes at the grid integration level.

Three different performance indicators were considered in this study to assess the grid integration level, as defined in Section 2.3.3. Three Pareto fronts are computed taking levelized energy cost (LEC) and grid integration (LEC-GI) as objective functions, considering the import and export limits for the grid interactions as 50% of the peak demand of the hub. The Pareto fronts which are calculated and plotted in Fig. 2.11 correspond to the three different methods for grid interactions with LEC. LEC-GI_{IG} denotes Pareto front obtained considering LEC and electricity imports from grid corresponding to Eq. 2.17 and LEC-GI_{IG} denotes Pareto front obtained considering LEC and electricity exports (Eq. 2.18). Finally, LEC-GI_{IEG} Pareto front considers interactions in both modes along with LEC as objective functions.

A significant reduction in the (LEC) is observed when moving from one Pareto front to the other. The LEC is rather low throughout LEC-GI_{EG} (exporting) Pareto front compared to the other two. LEC notably increases in LEC-GI_{IEG} Pareto front when grid interactions are less than 5% which is the same for LEC-GI_{EG}. Set of solutions in LEC-GI_{IEG} Pareto front follows the trend of LEC-GI_{IG} when grid interactions are greater than 5%. These variations are mainly due to the differences of power generation mix and modes of grid interactions which are taken into discussion in next two paragraphs.

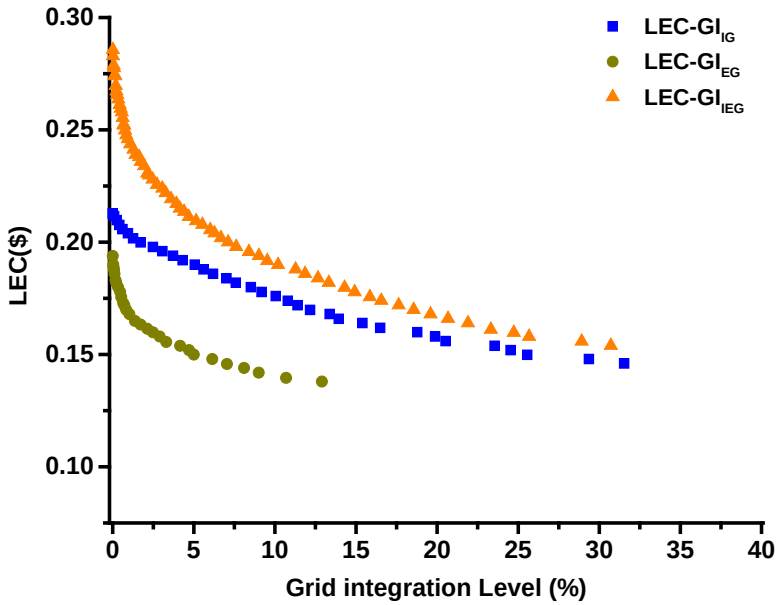

Fig. 2. 11: Pareto fronts obtained for three different performance indicators of the grid interaction with Levelized Energy Costs

In order to analyze the import, export and both interactions with the grid simultaneously, GI_{IG}, GI_{EG} and GI_{IEG} are plotted for three Pareto fronts considering all the modes of interactions with grid as a percentage of annual demand (Fig. 2.12). Among the three Pareto fronts, percentage exports to the grid (GI_{EG}) remains almost constant in LEC-GI_{IG} Pareto front. Meanwhile, GI_{IG} gradually reduces in with the increase of grid interactions in LEC-GI_{EG} Pareto front. However, GI_{IEG} is notably high (above 45%) in LEC-GI_{EG} Pareto front when compared to LEC-GI_{IG} Pareto front. This result in higher LEC in LEC-GI_{IG} Pareto front compared to LEC-GI_{EG} which is observed in Fig. 2.11. Energy flows of the LEC-GI_{IEG} Pareto front reveals that the total interactions with the grid (GI_{IEG}) are notably lower for the LEC-GI_{IEG} Pareto front compared to the two others Pareto fronts. A lower GI_{IEG} value indicates less energy interactions with the grid. This implies that the energy hub tends accordingly to operate as a standalone system in this case where variations of the renewable energy supply and the demand are absorbed by the system itself resulting higher LEC due to the less interactions with the energy market through the grid.

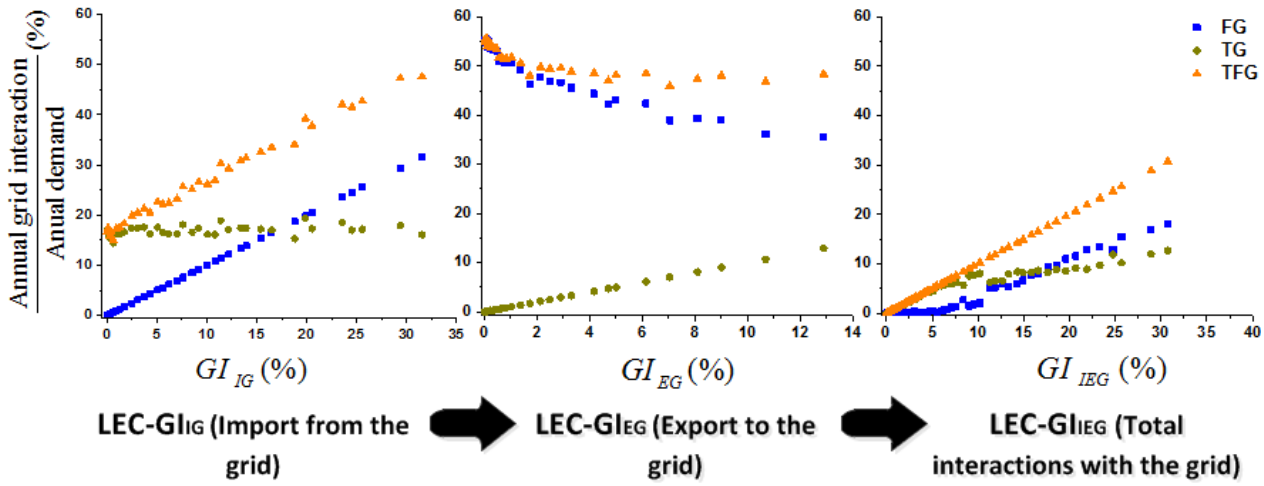

Fig. 2.12 : Comparison of the energy interactions with the grid (import, export and both) for three Pareto fronts (LEC-GI_{IG}, LEC-GI_{EG}, LEC-GI_{IEG} from left to right) obtained considering LEC and grid interactions

Analyzing the power generation within the energy hub from SPV panels and the wind turbines is one of the main goals of the study. Design solutions from LEC-GI_{IG} (System A) and LEC-GI_{IEG} (System B) Pareto fronts are selected in order to achieve this objective. The power generation from the non-dispatchable energy sources (SPV panels and wind turbines), the dispatchable energy source (ICG) as well as the total electrical power generated are plotted for both systems in Fig. 2.13 as a fraction of total annual demand of the energy hub. From the two Pareto fronts, it can be argued that the grid integration of wind and solar energy technologies through the energy hubs is achieved in a satisfactory way being more than 60% of the annual demand of the hub. System B shows annual wind and solar energy contributions larger than 100% (as a percentage of total annual demand). Minimal contributions from SPV and wind turbines reach 80% for System A in the corresponding Pareto front. More importantly, there are instances in which SPV and wind contributions are larger than the annual electricity demand, the energy hub operating as an “Energy plus” (generating more than the annual demand) system in both cases. However, it is important to analyze the Wasted Renewable Energy (WRE) due to limitations in energy storage and grid curtailments along with the generation to get a proper overview of the system.

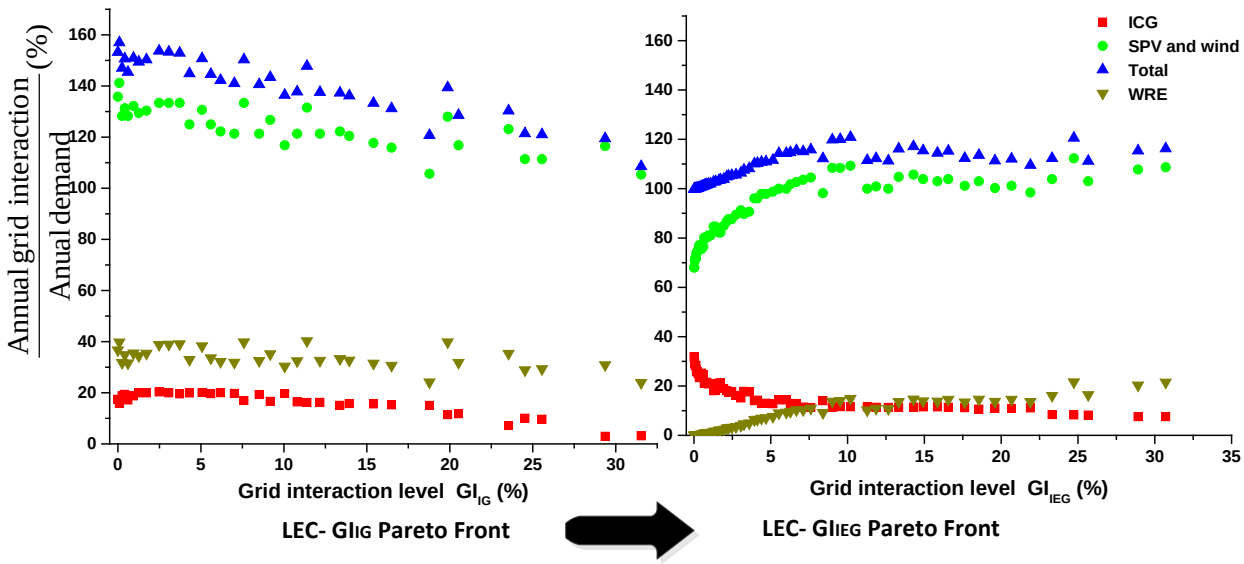

Fig. 2.13 : Power generation using ICG, SPV panels and wind turbines for optimal systems in the LEC-GIIG and LEC-GIIEG Pareto fronts (left System A and right System B)

When considering the WRE of System A, it is clear that around 30- 40% renewable energy generated will be lost due to limitations in storage and grid interactions which reach up to 20% in System B. In addition, around 15% of the generation within the system is exported in System A. Considering the generation, WRE and fraction exported to the grid; around 60-85% of the demand of the energy hub is catered using non-dispatchable energy sources. Considering the economic scenario (lowest LEC) it reaches around 60%. This is a major achievement when compared to the level of non-dispatchable renewable energy contribution in present cases which will be around 20-30% [46] in direct integration to grid. This clearly demonstrates the potential of energy hub to integrate non-dispatchable renewable energy sources. Nonetheless, it is important to highlight that utilizing renewable energy is a major challenge in energy Hubs although higher integration levels can be achieved.

Both plots show that the ICG plays a major role whenever grid interaction is weak. For System B, a dispatchable energy source is essential in order to minimize the grid interactions further and to operate in an autonomous way. An energy hub based only on non-dispatchable energy sources and energy storage is not economically sound when a perfect autonomy is targeted. Contributions from the ICG are gradually mitigated with the increase of grid interaction, reaching a condition where it is economically justified to operate the system without it.

2.7. Conclusions

This focuses on evaluating the potential of energy hubs in integrating non-dispatchable renewable energy technologies such as SPV panels and wind turbines with minimum impact to grid. A novel optimization algorithm in introduced with the support of a bi-level dispatch strategy to optimize energy hubs considering both real time price and curtailments for import and export in the grid. A gray model based on fuzzy logic is introduced to control the operation of ICG in the primary algorithm while finite automata theory is used to in the secondary algorithm to control the energy interactions with grid and battery bank. Finally, multi objective optimization is conducted considering LEC and grid integration level.

The results obtained from the Pareto analysis shows that energy hub can help to increase the share of wind and SPV generation beyond 60% of the annual demand of the energy hub. From an economic perspective, the assessment of the energy system shows that limitations for purchasing electricity from the grid are more critical than selling: this is promising when one considers the present grid architecture. Furthermore, larger grid interaction curtailments increase the LEC of the system and hinder the integration of renewable energy sources to the grid. The LEC-GI_{IG} Pareto front indicates that energy hubs can actively participate to the energy market by generating quantities of electricity far larger than the demand of the energy hub. However, an autonomous operation of energy hubs is not encouraged, as it notably increases the electrical power generation by the ICG minimizing the SPV and wind integration. In conclusion, it can be stated that energy hub is effective in increasing the non-dispatchable renewable energy share with minimum impact to the grid when considering present Sri Lankan context. Nonetheless, limitations in the initial capital investment need also to be addressed in this prospect, especially for developing countries like Sri Lanka, which is a real challenge for solar and wind energy.

3 Energy System Optimization Using Reinforcement Learning

This chapter extends the modeling framework introduced in Chapter 2. A black box model introduced to conduct energy system optimization replacing the grey box model introduced in Chapter 2. Reinforcement learning (machine learning technique) is used as the black box model. Both fully connected neural network and a convolution neural network are considered for the model. Subsequently, the results obtained from the novel approach are compared with the model introduced in Section 2.

This chapter is based on manuscript under preparation:

A.T.D. Perera, PU Wickramasinghe, V. M. Nik, and J.-L. Scartezzini, “Energy system optimization using reinforcement learning,” to be finalized in future

Author contribution for the journal paper:

In this article, ATD, designed the research with the support of PU, VMN and JLS. ATD initiated the concept of using reinforcement learning. ATD and PU designed the architecture of the neural network. PU developed the C++ code for neural network (both fully connected and convolution). ATD extended the energy system model and the optimization algorithm. VMN provided the demand profile. ATD wrote the manuscript except sections (2 and 4.5 (written by VMN and PU respectively)). PU, DM and JLS supported in revising and finalizing the Manuscript.

Readers are encouraged to read following conference proceedings for further information

1. A.T.D. Perera, V.M. Nik, Dasaraden Mauree, J-L Scartezzini. "Design optimization of Electrical Hubs using hybrid evolutionary algorithm" ASME Energy Sustainability Conference 2016 USA

3.1. Introduction

Distributed energy systems such as energy hubs play a vital role in integration of non-dispatchable renewable energy technologies such as Solar PV (SPV) and wind energy into the energy infrastructure while mitigating the adverse impacts due to fossil fuel based power generation. In addition, energy hubs have shown the potential to cater the demand of multi-energy services such as electricity, heating and cooling [1,2]. Furthermore, energy nexus of transportation, water distribution etc. is also discussed widely in recent literature. As a result, energy hubs have become an attractive energy solution for improving the sustainability of cities [3].

Distributed energy systems such as energy hubs brought significant changes into energy infrastructure. Simple dispatchable energy sources are replaced by an energy system which consists of non-dispatchable energy technologies, energy storages with different characteristics and energy conversion devices such as heat pump and vapor compression cycles. The energy flow within the distributed energy system becomes more complicated compared to a system with simple dispatchable energy source. According to Perera et-al [4] and Piacentino[5] et-al there are two different approaches to design such distributed energy systems. The first one is a policy based approach which defines a specific strategy for the energy system to operate. Markov Decision Process (MDP) is used to evaluate the performance of the system on long run. However, complex architecture of energy systems made this approach to become challenging to use. Energy systems having complex architectures results in complex energy flows within the energy systems. As a result, the number of possible states that the system can operate notably increases which makes it difficult to arrive at an optimum policy [6,7]. The second approach is a valued based method where bi-level optimization algorithm is used [8]. The value of operation for a particular time step is minimized by the dispatch strategy at the primary level which is used to optimize the configuration of the energy system at the secondary level which include the size and choice of energy system components [9]. The main advantage of the former method is that it can be used to design complex energy systems due to its capability to consider complex energy flows at the primary level at the dispatch optimization although it might need longer computational time, up to several days for certain instances [4,10].

Due to the capability exhibited by the bi-level optimization algorithm it has been widely used to design distributed energy hubs having complex architectures [11]. Weber et-al [9] used bi-level optimization algorithm for dispatchable sources with fuel cells. A set of selected days and hours of the year are considered in this study for the dispatch strategy instead of considering the entire year. Jayasekara et-al [12] designed combined cooling, heating and power (CCHP) system using the bi-

level optimization algorithm where entire year is considered in the primary level dispatch optimization. Evins [10] considered energy system optimization along with the building design which demonstrated the flexibility of the approach although it took three days to arrive at the optimum. Both Murrey et-al [13] and Paolo et-al [14] used the bi-level optimization algorithm to design energy systems with long term energy storage. According to Murrey et-al [13], future forecast for non-dispatchable renewable energy sources, grid conditions play an important role in the energy system optimization. These aspects can be included into the optimization process by introducing model predictive control (MPC) into the energy system optimization process. Paul et-al incorporated MPC into the dispatch strategy in the optimization process of the energy system. However, they limited the scope to the selected days and hours and did not consider 8760 time steps. Furthermore, uncertainty in renewable energy generation, demand and grid conditions were not considered in their work and the time horizon for the forecast was matching for short term storage.

Energy transition is demanding for energy sector by moving from centralized to decentralized systems and even to the energy internet [15,16] in order to facilitate large scale integration of renewable energy technologies. Energy internet can be simply understood as a multiplex network that links a set of distributed energy systems. However, the main difference between the typical distributed energy systems and an energy internet is related interactions maintained in cyberspace. The energy internet converts the physical energy network into a cyber physical network [17]. This allows computing and communication cores to be embedded into the energy infrastructure which enables monitoring, coordinating and controlling at a significantly higher level [18,19]. The strong inter-links between the energy systems help to cater the imbalances due to the fluctuations in renewable energy generation and demand, allowing larger scales of the renewable energy integration. However, we need to understand that the stronger connectivity among energy systems does not undermine the importance of autonomy maintained by each energy system. Both aforementioned approaches used to design distributed energy systems have been extended to arrive at the optimum design for energy internets. Two different methods have been used to design (Fig. 3.1)energy internets i.e.; 1) each energy hub is optimized separately and subsequently designing the network, 2) considering the entire energy internet as a single component and optimizing it. Unfortunately, both these techniques consider two extreme ends and do not align with the objectives of the energy internet. Considering each energy system separately and optimizing the design ends up with the designs that are less prepared for energy interactions. On the other hand, considering the entire energy internet as a single structure neglects the autonomy of each energy hub. Hence, it is important to come to an in-between solution where certain amount of information is shared between the energy hubs. However, most of the information that is shared among the

energy systems might be difficult to formulate as a part of the objective functions through a white box model due to its complexity. At the same time, electric vehicles and smart devices will operate based on price signals in near future where reasonable 'learning' might require understanding the demand responses. Same applies to the peer-to-peer trading within micro-grids. All the aforementioned changes take place in the energy sector cannot be solely white box methods. Data driven approaches based on black box methods might be immensely helpful in such contexts

In order to address the limitations in the present state of art in energy system optimization, this study introduces a black box approach to reinforcement learning, replacing the white and grey box models used so far to present the operation of the energy system during the design process. Reinforcement learning is a data driven approach that can be easily used to learn from the environment. Reinforcement learning has been recently used for the dispatch optimization although not used to design distributed energy systems. Notable changes are introduced into the optimization process of the energy system towards incorporating the reinforcement learning into the design optimization process. Subsequently, the performance of the novel method is evaluated in comparison with a grey box model.

A multi energy hub consisting of wind turbines, Solar PV (SPV panels), Solar Thermal (ST Panels) combined heating and Internal Combustion generator (ICG), heat pump, battery bank, thermal storage assisted by Phase Change Material (PCM) is considered in this study. It is assumed that the multi-energy hub is operating connected to both electrical and thermal network. A novel optimization algorithm is introduced to design distributed energy systems that use reinforcement learning to present the dispatch strategy. Fully connected neural network is used initially for the dispatch optimization. The performance of the novel optimization algorithm is compared with grey-box model developed using fuzzy logic. In order to consider the hourly forecast of wind speed, solar irradiation, electricity demand, heat demand, price of electricity and heat in grid convolution neural networks (CNN) are introduced. Subsequently a comprehensive assessment is conducted considering the influences of dispatch model on the energy system taking grey box model, fully connected neural network and the CNN.

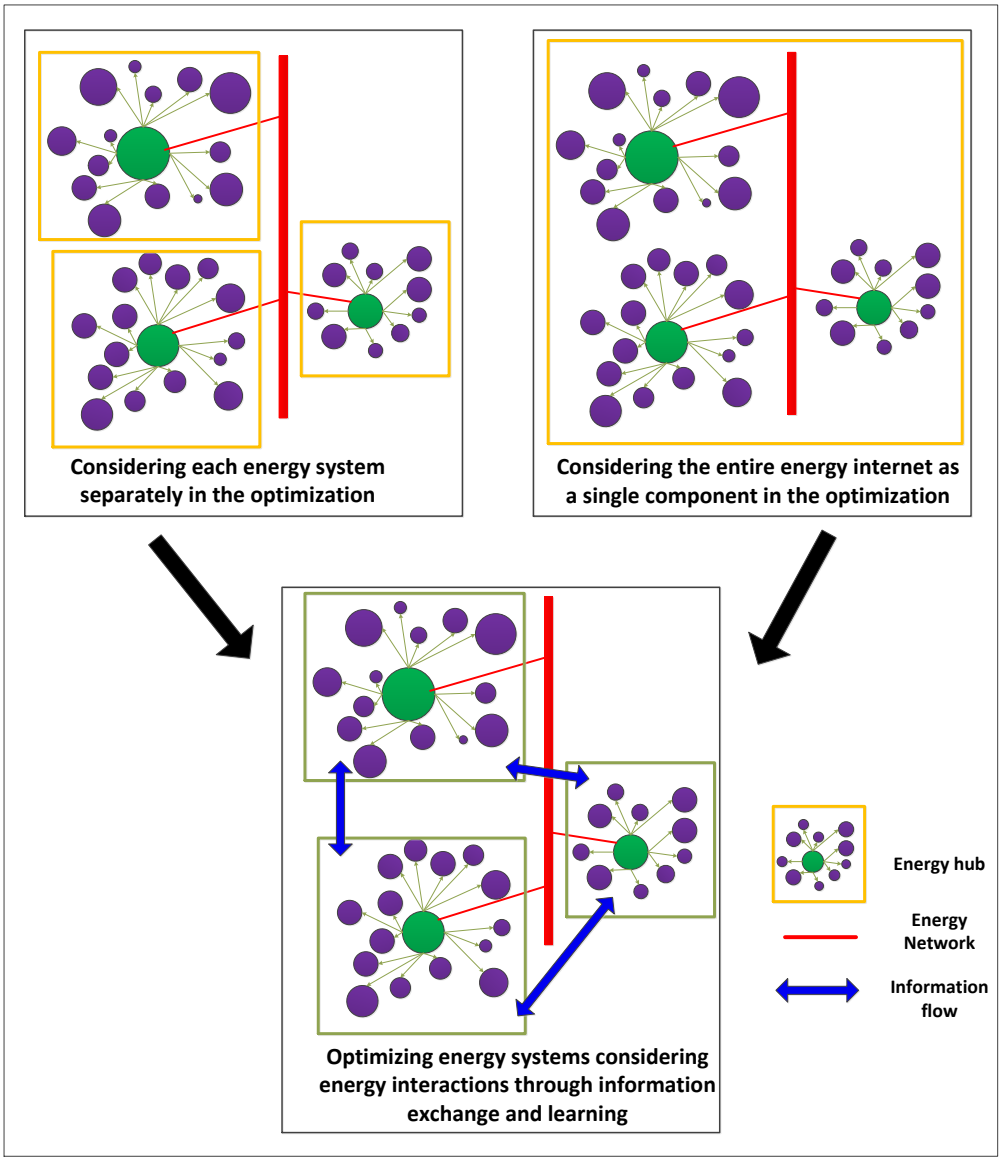

Fig. 3.1: Two boxes on top present the approaches used in the present state of art when designing distributed energy systems. The top-left box considers each energy system separately and optimize them. Subsequently, the network is optimized taking the individually optimized energy systems. The top-right box considers the entire energy internet as a single system and optimize the super structure in one single step. The one in the bottom is what we expect from the energy systems in future. It learns by interacting with the neighboring energy systems and adapt to the local conditions in both design and generation. Information flow among the energy systems facilitate this process.

3.2. Outline of the building simulation model

The energy demand was simulated for a conceptual urban area with 40 buildings in Lund, located in the southern Sweden. The buildings are selected from a set of statistically representative buildings for the city, which were investigated by the Swedish National Board of Housing, Building and Planning (Boverket) [20]. The model for simulating the energy performance of the buildings is made as a linear explicit discrete time-variant system based on the lumped system analysis approach in Simulink/Matlab [21]. Each building is represented as one zone where the law of conservation of

energy is governed at each time step (hour), considering the heat losses due to transmission and ventilation and the heat gains from the solar radiation and the internal gains from tenants and appliances. Modelling buildings as a lumped system enables running faster simulations with less required details on buildings. The energy demand of buildings is calculated while the cooling strategy is hybrid cooling (natural and mechanical), however the cooling demand (considering the latent cooling load) is very small in Sweden, compared to heating demand [21][22][23]. The model has been used to simulate the energy performance of the Swedish building stock considering past and future climate both for current [21][22] and retrofitted conditions [23][24][25].

The energy demand of the considered buildings was simulated for the typical weather conditions of Lund during 1976-2005 according to the RCA3-ERA40 climate scenario. RCA3 is the third generation the Rossby Centre – the climate modelling unit of the Swedish Meteorological and Hydrological Institute (SMHI) – regional atmospheric model [26]. ERA40 is a reanalysis-driven simulation of climatic conditions that constitutes a realistic description of the state of the atmosphere and represents the real conditions with a high accuracy (for more details check [22][27][28]). Typical weather conditions were synthesized by distinguishing the representative years based on the distribution of the outdoor temperature and creating the typical downscaled year (TDY) [29]. The synthesis and application of TDY in energy and hygrothermal simulations are discussed in earlier works [29] [30,31].

3.3. Overview of the energy system and the computational model

Multi-energy hub catering the thermal and electricity demand of a neighborhood is considered in this study. Multi-energy hub is connected to the local electricity and thermal grid (Fig. 3.2). The energy system consists of both dispatchable and non-dispatchable energy technologies that generate electricity and heating. Solar PV panels (SPV) and wind turbines are used as non-dispatchable renewable energy technologies that generate the electricity while solar thermal panels (ST) are used as the non-dispatchable thermal energy source. A fossil fuel based boiler and an internal combustion generator with the capability for generating heat and electricity (co-generation) are considered as dispatchable sources. A battery bank and a thermal storage using PCM are considered as energy storage medium. Heat pump is introduced as a link between thermal and electrical layers of the energy system which generates heat using electricity. The energy hub is connected to the thermal and electricity grid respectively which acts as a spinning reserve when there is a mismatch between demand and generation. A detailed description about the energy system model used in this chapter is presented in Chapter 2.

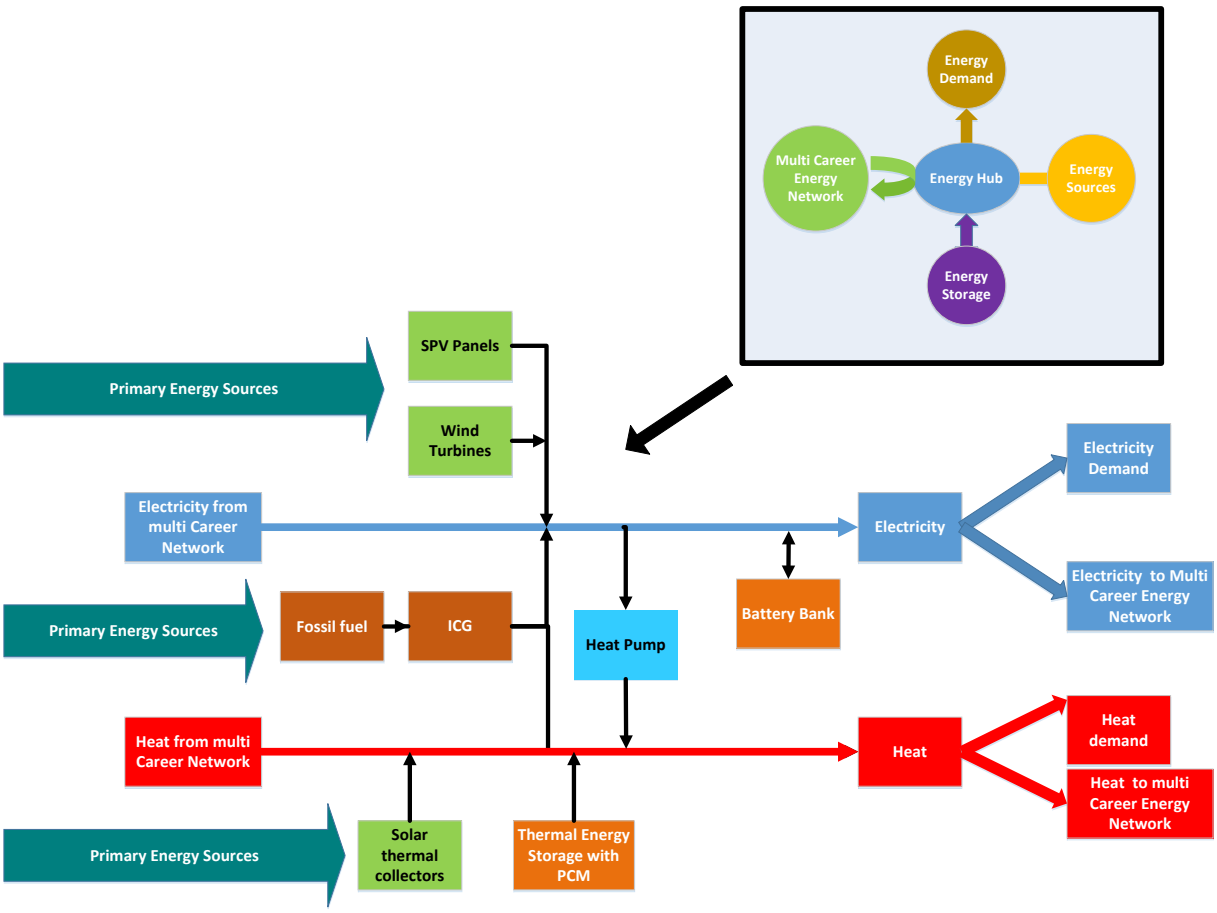

Fig. 3. 2: Outline of the multi energy hub

3.4. Dispatch strategy

Integrated energy systems consisting of renewable energy technologies, energy storage, energy conversion devices such as heat pumps which are operating in a grid integrated mode can have a complex energy flow within the system. Energy flow within the system needs to be optimized in order to guarantee the proper utilization of different components used. This formulates a dispatch optimization problem within the energy system optimization problem. The design of the energy system is strongly coupled with the dispatch optimization while the dispatch strategy is strongly influenced by the energy system design. Combining these two aspects together are important. This section presents the applicability of black box models to consider dispatch strategy in the energy system optimization process.

3.4.1. From white box models to black box models

Dispatch strategy optimization during the energy system design process formulates a sequential decision problem. The operation of the energy system needs to be optimized at each time step for the entire time series considered for the design problem. A series of decisions need to be taken one

after the other in such instances where a specific decision at a time step can reasonably influence the decision at another time step which is known as the Markov property. Markov property states that the decision made at state s_t is solely based on s_{t-1} without considering the influence of $\{s_0, s_1, s_2, s_{3....} s_{t-2}\}$. Two main approaches can be found in addressing such problems i.e. MPC and reinforcement learning [37,38]. According to Gorges [38], the main advantage of MPC is that it guarantees the stability as well as robustness. In contrast to MPC, reinforcement learning has a number of advantages since it 1) is a model free method, 2) does not require convexity guarantee and 3) has a higher adaptability. The stability is not considered at the hourly scale simulation of the energy system. Usually transient analysis is conducted for the optimized design following the energy system optimization in order to guarantee stability in the operation. In addition, ongoing increase of complexity of the energy system makes it difficult to guarantee convexity. Furthermore, the interactions between energy systems are expected to be maintained with other auxiliary services such as transportation, water services etc., which makes the learning process to be an important element where reinforcement learning is very good at. All the aforementioned reasons encourage the present study to move into black box method such as reinforcement learning to assist energy system optimization.

3.4.2. Grey box approach

Black box models are entirely based on the learning process instead of depending much on models that are based on basic problem physics. Grey box models lies in between white box and black box models and can be used as a really good benchmark to evaluate the performance of the black box models. Towards this direction, the grey box model developed by Perera et-al [4] is extended to evaluate the performance of black box models (as explained in Chapter 2). Readers are encouraged to go through the original paper which provides a comprehensive overview of the model. A direct extension to the previous model is performed by considering the electricity and flow and heat flow separately due to the limitations of grey box models to handle higher dimension action spaces. This simplification enables considering both heat and electricity flows although energy conversion pathways between electricity to heat notably simplified in the control strategy due to the reduction in the action space.

3.4.3. Reinforcement learning with neural networks

Reinforcement learning has been gradually getting popular during last two decades. It has been applied in a number of fields where state and action spaces are high dimensional. It has attracted the attention of the scientific community due to the human level (and sometime above) control capabilities it has demonstrated [39]. Reinforcement learning facilitates the system to learn by

understanding the consequences of different actions made by the system when interacting with the surroundings. Assume that there exists an agent who controls the actions of a system at different states. The intention of the agent is to maximize the reward at the end of the sequential decision making process. Depending the actions made by the agent at different states, the reward it obtains at the end of the sequential decision making process is going to be changed. This trial and error approach is the fundamental concept behind the reinforcement learning with certain inherent characteristics:

1. Optimum strategy that the agent should be taken needs to be understood solely through trial and error.
2. The actions made by the agent at a time step may subject to strong temporal correlation.
3. Agents may go through a long series of actions before they realize the impact of one specific action on the reward.

Two main approaches are used by the reinforcement community to address sequential decision problems. These methods are known as value function method and policy function method. In addition to both these main streams, there are techniques such as actor-critic method which are a combination of both these approaches. The value function method tries to improve the value of the reward at each time step. By improving the value of the reward at each step it tries to improve the reward of the entire sequential decision problem. In contrast, the policy function tries to come up with a policy for the state transition which maximizes the reward by conditions of the surroundings and the action space. High dimensional state and action space that have to be considered in complex real world problems make it challenging to come up with both policy and value function. Deep neural networks have been used as a technique to approximate these functions effectively. Hence, these two approaches are known to be value function approximation and policy function approximation. Both policy as well as value function methods have its own pros and cons. When considering applications such as energy system optimization where a long sequential decision problem is involved, policy function can perform better than value function method.

3.4.4. Significance of neuro-evolution based enforcement learning

Policy function approximation method can be further classified into two main sub groups, i.e. policy gradient method and policy search method (which is also known as direct reinforcement). The main difference between these two methods is that the policy gradient usually depends on gradient based technique while the policy search depends on black box techniques for the optimization. The policy search is gradually getting popular due to its capability for notable reduction in computation time and the capability to handle complex control problems [40]. A neural network is trained in this

context using an evolutionary algorithm which is also known as neuro-evolution. Although neuro-evolution has been popular few years ago, deep-learning based on convex methods outperformed neuro-evolution in reinforcement. However, this was proven to be wrong by Salimans et-al [41] in Open AI in 2017. They proved that policy search performs better than policy gradient method for MuJoCo humanoid task. Furthermore, they showed that policy search produces more robust results when compared to policy gradient. This created a new interest among the reinforcement learning community to use policy search again. Recently, Zhang et-al [42] showed that a notable reduction in computational time can be achieved by using policy learning. Furthermore, they showed that evolutionary algorithm can be used to optimize policy learning problems up to three million variables. Such a large number of variables have not been optimized using heuristic algorithms before. Recently, Ha and Schmidhuber showed that deep recurrent neural networks also can be effectively used along with policy evolution[43]. Therefore, this study uses policy search method based on neuro-evolution to assist energy system optimization

3.4.5. Architecture of the neural network considered in this study

Two neural network architectures are used in this study. These are fully connected neural network and convolution neural network. The feature space considered for the fully connected neural network is different from the one used for the Convolution neural network. Fully connected neural network considered a 1-D input vector of the present conditions in demand, renewable energy potential and grid prices for heat and electricity. The input features are further improved when moving to convolution neural network which considers a 2D input vector (Fig. 3.3). A comprehensive overview about the use of fully connected neural networks on the dispatch strategy is presented in Ref. [44]. This section presents an extended explanation about the use of convolution neural networks.

Traditionally Convolutional Neural Networks (CNNs) are used to process images. The architecture enables efficient processing of image data. The images being processed are viewed as 2D matrices where the two dimensions of an image correspond to its height and width. The advantage of CNNs in this setting is the possibility of reformulating energy data as 2D matrices and using already well-established CNN machinery to process the data. This is done by taking features as one dimension and the time as the other dimension (Fig. 3.3).

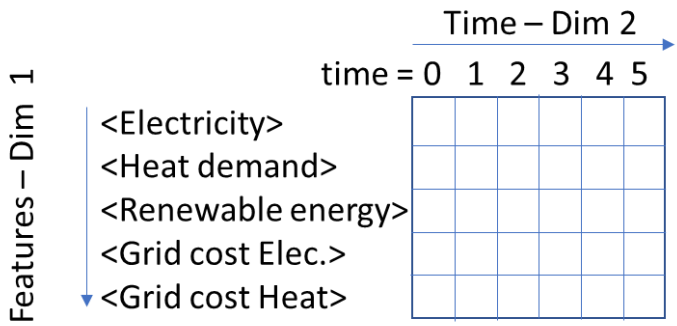

Fig. 3. 3: Reformulating energy data as a 2D matrix

Once the input is given to a CNN it processes the data according to the defined architecture (Figure 3). The architecture consists of multiple layers similar to a Fully-Connected Network (FCN). But, instead of performing matrix multiplication at each layer, CNNs perform convolutions. Similar to each layer having multiple neurons in FCNs, a CNN has multiple kernels for each layer. Unlike each neuron outputting a scalar in a FCN, a kernel at a given layer outputs a 2D feature map (F_s^{t+1} in Fig. 3.4). Since there are several kernels at a given layer, we get multiple 2D feature maps at each layer. These multiple layers are concatenated into a single 3D matrix (the new dimension corresponding to feature maps from each kernel in the layer, D^t in Figure 4) and it is passed onto the next layer. Convolution operation for location (x, y) in feature map F_s^{t+1} is defined as Eq. 3.1:

$$F_j^{i+1}(x,y) = \sum_{0\le k<D^t} \sum_{\substack{-\mathcal{H}^t/_2 \le i \le \mathcal{H}^t/_2 \\ -\mathcal{W}^t/_2 \le j \le \mathcal{W}^t/_2}} F^i\left(x-j+\mathcal{W}^t/_2, y-i+\mathcal{H}^t/_2, k\right) \times K_j^i\left(i+\mathcal{H}^t/_2, j+\mathcal{W}^t/_2, k\right) \tag{3.1}$$

Here $0 \le x < W - \mathcal{W}^t$ and $0 \le y < H - \mathcal{H}^t$ (matrix indexing starts from 0). The convolution defined by using this range for x, y is called 'valid' convolutions since the convolution is not evaluated at the boundary.

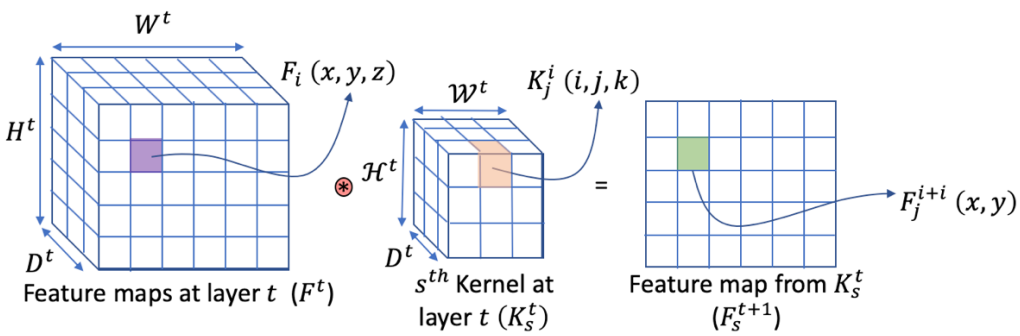

Fig. 3. 4: ***Convolution operation***

Using these convolution layers, the final architecture is defined as in Fig. 3.5. It consists of three convolutional layers. One of the basic assumptions in using CNNs is the feature invariance across

dimensions. In this scenario the assumption is only valid across time dimension and not along the feature dimension. Therefore, in the very first convolution layer, the kernel is defined such that its height equals number of features. This ensures the assumption is not violated since the kernel does not move in this direction when computing the feature map in the first layer. After the convolution layers, the output vectors are vectorized, which is simply reshaping the multi-dimensional vector into a 1D vector. Afterwards, fully connected layers compute the final output. The final output is used to determine the operating load factor of the ICG, state of charge of the battery bank and thermal storage. Depending upon energy flow through these parameters, interactions between the thermal and electric grid are computed.

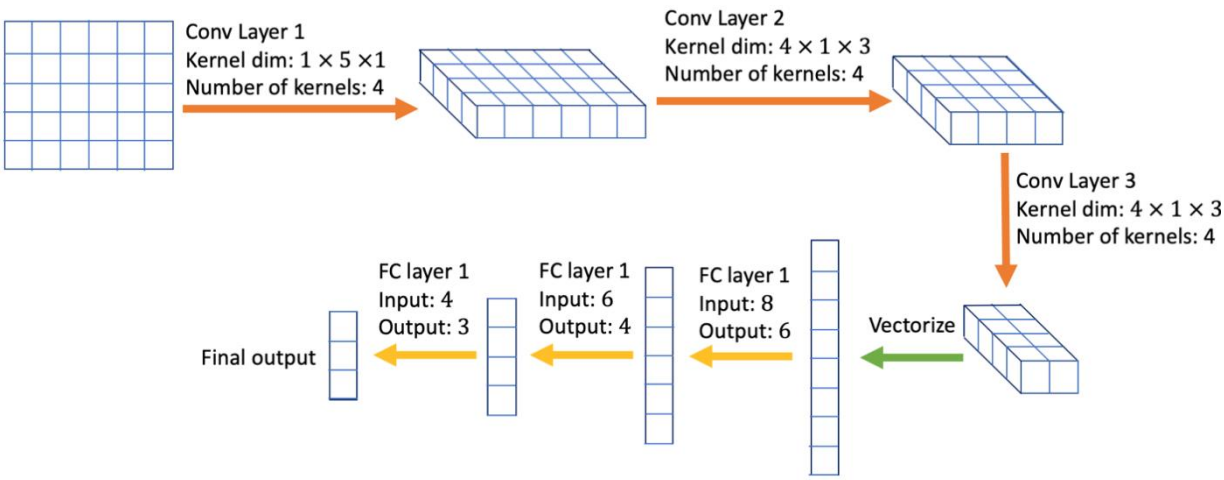

Fig. 3. 5: Network architecture: Kernel dimensions (dim) uses the notation $D^t \times \mathcal{H}^t \times \mathcal{W}^t$.

3.5. Design optimization of the system

A number of different methods have been proposed to optimize distributed energy systems including mixed integer linear programing, mixed integer non-linear programming, heuristic algorithms, enumerative methods etc. Heuristic methods have been amply used considering the system sizing problem (even in bi-level optimization algorithms secondary algorithm that relates to system sizing are often based on heuristic methods) due to two reasons. These are prices related to the system component are nonlinear and heuristic methods can be easily used to conduct Pareto optimization effectively. Furthermore, heuristic methods become the only available method when combining energy system designing and using dispatch strategies based on Markov-Decision Processes. Therefore, heuristic algorithms have been amply used for design optimization of distributed energy systems. However, the main disadvantage when using heuristic methods is the high computational time compared to other methods. Furthermore, heuristic methods do not guarantee the optimum, therefore they should be carefully selected.

3.5.1. Moving into heuristic methods

Optimization of both energy system configuration and dispatch strategy are taken into consideration in this study. Architecture of the neural network should be optimized along with system configuration which is a challenging task due to the extension of decision space. Convex optimization methods such as gradient decent, stochastic gradient decent etc. have been commonly used to optimize the architecture of neural networks. However, heuristic methods such as evolutionary algorithms and particle swarm have been amply used to optimize the architecture of neural networks especially considering evolving neural networks. Neuro-evolution has been successfully used in reinforcement learning as described in Section 4.4. Hence, heuristic methods can be effectively used to optimize both the architecture of the neural network and the state transition points for the dispatch strategy. However, this extends the decision space for the optimization problem which might result in reaching towards sub-optimal especially when using a heuristic method.

A co-operative co-evolutionary algorithm (COCE) is used in this study to assist the optimization process. COCE is an extension to the co-evolution algorithms. Co-evolutionary algorithms have become an effective method when handling larger decision spaces compared to simple evolutionary algorithms. Recently, it is getting popular for multi objective optimization problems. However, the main limitation of co-evolutionary algorithms is the difficulty of handling optimization problems which are not variable separable. COCE becomes effective in such instances [45].

3.5.2. Overview of the COCE

Implementation of COCE brings an extension to the co-evolutionary algorithms used for optimization. Decision space is partitioned into several parts which are presented by several sub-populations instead of using a single population that represent the whole decision space (Fig. 3.6). Each sub-population considers a subset of the decision space variables as the decision space for the optimization. The entire set of sub population covers the entire decision space. Each sub population is initialized randomly as the first step. In step 2, basic reproduction operators such as mutation and cross-over operators are acting on each sub-population simultaneously. Archives of the Pareto front obtained for each sub-population (known as sub archive) in Step 2 are fed into Step 3. After reaching the number of the generations defined by the user, archived Pareto solutions form each sub-population is taken and fed into Step 3. In Step 3, Pareto solutions are given the opportunity to compete with each other based on constraint tournament method in order to obtain the global archive. Global archive is fed in to step 2 again. A sub-population is recreated for the next generation

taking members from global archive and the final population of the previous step randomly. This routine is conducted for number of generations.

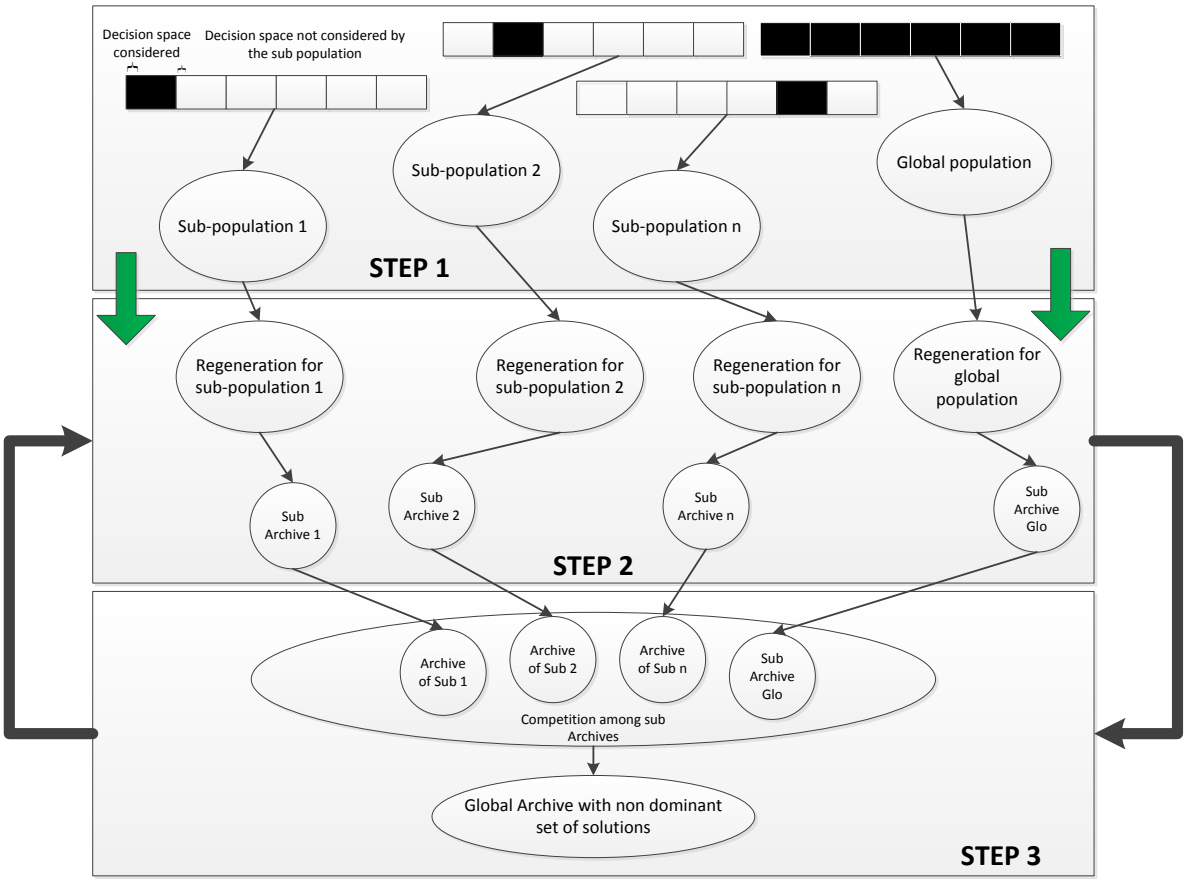

Fig. 3. 6: Outline of the optimization algorithm

3.6. Results of the case study

Introducing the changes into the optimization process of energy systems can have an influence on both design and operation of the energy system. Hence, it is interesting to analyze both these aspects separately. Pareto optimization is conducted in this study considering Net Present Value (NPV) and total grid integration level (GI) as objective functions to support the analysis. The comparison of the objective function values obtained using grey-box method and black box method is presented in Section 6.1. Subsequently, the design of the energy system is considered. Section 6.2 is devoted to analyze the influence of the optimization strategy of the system design. Few design solutions from each Pareto front are taken and subsequently analyzed based on several performance indicators. Finally, Section 6.3 is devoted to generalize the observation obtained in Section 6.2 and understand the specific aspects that control strategy is having more influence.

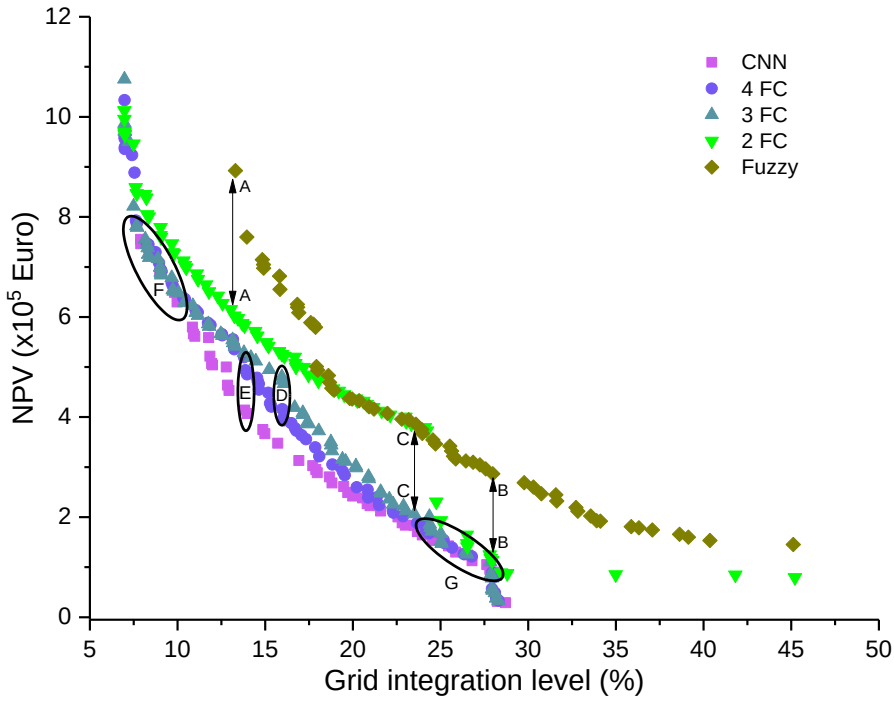

Fig. 3. 7: Pareto fronts obtained for 5 different methods considering NPV and Grid interactions as the objective functions

3.6.1. Inter-comparison of the Pareto fronts

Five different Pareto fronts are taken, considering five different models used to represent the dispatch strategy during the energy system optimization. Fuzzy logic is used for the grey box model. Three different fully connected neural network architectures are considered which are having different number of hidden layers. Pareto fronts named as 2 FC, 3 FC and 4 FC are respectively having two, three and four hidden layers. In addition to the grey box model and the fully connected neural networks, CNN is considered which is having the architecture described in Section 5.5. All these Pareto fronts can be classified into three classes i.e. grey box models, fully connected neural networks (FNN) and CNN. There is a significant change in the objective function values when moving from one to another for the Pareto fronts of the three different classes.

Previous studies on electrical hubs by Perera et-al [33] showed that grey models are an efficient method to reach the optimum design configuration for simple energy hubs which only considers the electrical aspect. However, Fig. 3.7 shows that increasing the complexity of energy system cannot be accommodated by grey models. Even simple neural network with two hidden layers can outperform the grey model based on fuzzy logic. Except for the grid interaction levels between 17 to 23 %, 2 FC outperform the grey model with a notable margin. In certain instances, 2 FC can reduce the NPV of the energy hub by 60% when compared to the grey model. For example, when comparing A-A and B-B solutions (Fig. 3.7) from the two Pareto fronts which are having similar grid interactions, the NPV reduce respectively by 33 and 57 %. Furthermore, it is observed that higher autonomy levels (grid

interactions below 14%) cannot be achieved when using the grey models. Further reduction in NPV can be observed when moving from 2 FC to 3 FC and to 4 FC. These results clearly demonstrate that black box methods can easily outperform grey box models with the increase of complexity in the energy system.

When comparing the black box methods, a significant reduction in NPV can be observed within FNN models. For example, the NPV reduces from 3.86 to 2.06 $x10^5$ when moving from 2 FC to 3 FC Pareto fronts along C-C reducing it by 47 %. However, such a significant reduction in NPV is not observed when moving from 3 FC to 4 FC. The maximum difference in NPV between 3 FC and 4 FC is observed within D-D which is around 12%. Further increase in hidden layers beyond four (4 FC) did not improve the NPV. Hence, it is prudent that four hidden layers are sufficient to handle the complexity of the energy hub considered in this work. However, FNN is used only to consider the present demand, renewable energy generation and grid conditions. Notable changes are introduced into both operation and neural network structure when moving from 4 FC to CNN. Future forecast of renewable energy potential, demand, grid prices are considered for the CNN scenario which are not considered for the FNN scenarios. Considering future forecast renewable energy technologies, demand and grid costs notably increase the input features considered by the neural network. Such a large pool of input variables is difficult to be handled by using a fully connected neural network. This made it to use CNN instead of using a fully connected neural network.

A noticeable reduction in NPV can be observed when moving from 4 FC to CNN compared to the difference observed in-between 4 FC and 3 FC. The NPV reduced by 18% when moving from 4 FC to CNN along E-E (the maximum difference reach 20%). Hence, it is clear that considering both future forecast and introducing changes to the architecture of the neural network are beneficial. However, it is observed that most of the black box models merge with each other in regions F and G. Furthermore, a significant increase in NPV is observed when moving from region G to F, irrespective of the method used to represent the dispatch strategy. This clearly demonstrates that the energy system superstructure that is used at present is difficult to be operated in the fully autonomous mode. Further integration of long term energy storage, energy nexus such as vehicle to grid, renewables to chemicals etc. would be interesting to analyze from the perspective of making the energy hub fully autonomous. Such extensions to the energy hub will make the architecture of the neural network to become more complex where significant changes in NPV would be possible.

3.6.2. Comparison of the system configuration

Section 6.1 shows that the methodology used to present the dispatch strategy is having a notable impact on the objective function values. However, it is interesting to analyze whether the model

used to present the dispatch strategy only influence the operation of the energy system or it has an impact beyond the operation towards the design of energy system. To achieve this task, three Pareto solutions are taken from each Pareto front having similar grid integration level as tabulated in Table 3.1. For example, CNN-B, 4FC-B, 3FC-B, 2FC-B and FZZ-B present Pareto solutions from different Pareto fronts having similar grid integration levels. Similarly, scenarios A and B present Pareto solutions having similar grid integration levels. However, a Pareto solution for FZZ-A is not tabulated since fuzzy model does not have Pareto solutions with grid integration level below 13%.

When analyzing the design solutions, one prominent observation is the higher generation of the dispatchable source. The power generation from the ICG reaches above total annual demand for all the models except CNN. This is due to the fact that it is economical to operate the ICG at higher load factors and inject the excess to the grid than simply following the demand. Furthermore, it is observed that the renewable energy that is not utilized (WRE) goes above 20% for many scenarios. This is not considered as a good practice when designing grid integrated distributed energy systems [33]. However, it can be justified when considering the lower grid interactions maintained with the multi energy grid. When moving from the performance indicators to the system configuration, no direct relationship is observed that justifies the difference in NPV when analyzing the system design. However, certain common characteristics can be observed within the Pareto solution of one specific model. For example, the size of the thermal storage is small for Fuzzy and 3FC models. Moreover, 3FC-A and B are having 11 storage units in the bank while FZZ-B and C are having 34 and 49 respectively. The size of thermal storage for these four designs is significantly small when compared to this size for 2FC and CNN. Furthermore, lower ICG capacities are observed for 2FC and 3FC systems. For example, 2FC-C is having an ICG with a capacity of 115 kW which is the smallest among the design solutions in Table 3.1. However, the most important observation is that the design solutions of 2FC and 3FC are having higher percentage of power generation using the ICG, compared to CNN, although the capacities are small. After considering all the aforementioned factors and the design solutions in Table 3.1 it can be concluded that:

- an increase in renewable energy capacity is observed when moving from 2FC to 3FC (while the size of storage drops) though the ICG capacity stays more or less the same
- an increase in ICG capacity and thermal storage is observed when moving from 3FC to 4 FC with a slight drop in the renewable energy capacity
- an increase in the size of battery bank is observed when moving from 4FC to CNN

Table 3. 1 Selected design solutions from the five Pareto fronts having similar grid interactions

Model	Name	NPV (x10^5 Euro)	GI (%)	ICG[1] generation	WRE[2] (%)	SPV capacity (kW^E)	Wind capacity (kW^E)	# battery banks	ICG capacity	ST capacity (kW^T)	# thermal storage banks
CNN	CNN-A	4.64	12.85	94.3	29.48	68	990	10	205	9	82
	CNN-B	3.75	14.87	69.4	23.92	68	990	9	205	9	82
	CNN-C	3.13	16.92	52.0	16.86	68	990	9	190	9	76
4FC	4FC-A	5.63	12.55	125.8	21.71	68	850	1	210	10	99
	4FC-B	4.55	14.65	94.7	42.19	25	890	12	190	8	71
	4FC-C	3.64	17.07	70.5	30.46	65	850	1	225	7	100
3FC	3FC-A	5.63	12.56	120.2	26.34	68	1000	1	175	6	11
	3FC-B	5.12	14.46	106.2	19.89	65	1000	1	155	6	11
	3FC-C	4.19	16.68	73.2	35.20	68	965	9	200	12	57
2FC	2FC-A	6.27	12.57	124.2	15.72	66	785	2	170	6	100
	2FC-B	5.62	14.55	116.2	10.70	62	690	2	150	6	99
	2FC-C	5.00	16.76	103.9	26.22	66	995	7	115	6	100
Fuzzy	FZZ-B	7.15	14.84	113.7	19.20	67	990	1	205	30	34
	FZZ-C	6.09	16.91	95.1	14.59	67	990	1	220	13	49

[1)] Power generation using ICG as a percentage of the annual demand

Although the observed variations in the system design are not straight forward when moving from one model to another, it is clear that the model used to present the dispatch strategy is having a significant impact on the energy system design. However, understanding the influence of dispatch model is important which makes it possible to improve the super structure of the energy system as well as the method used to present dispatch strategy in the energy system optimization. This requires an overall qualitative assessment of the Pareto solutions besides being limited to few selected design solutions from each Pareto front.

3.6.3. A comparison of the performance indicators

In order to understand the impacts of the model used to represent the dispatch strategy in a broader scale, three performance indicators (power generation of ICG, grid injection) are taken and plotted against the grid integration level (Fig. 3.8 and 3.9). By analyzing the ICG generation plot a clear relationship between the operation of ICG and NPV can be observed. Power generation using the ICG is the lowest in CNN which is followed by 4FC, 3FC and 2FC being analogous to the NPV. A similar observation can be made when analyzing the grid injection levels of the Pareto solutions obtained using different models. 2FC and fuzzy models are having the highest grid injection while CNN is having the lowest. The most interesting fact is that 2FC and 3 FC systems tend to have a higher power generation using the ICG as well as injection while having a lower ICG capacity. This specific observation reveals an interesting overview about the model the dispatch strategy.

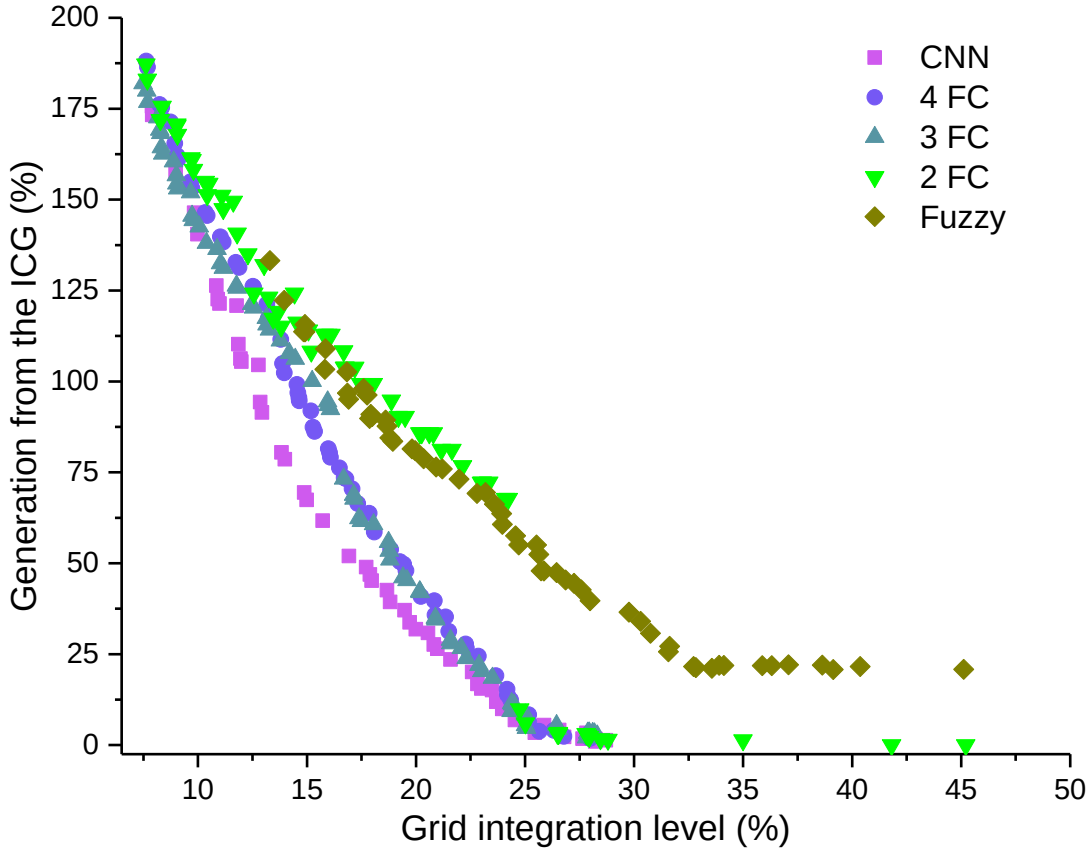

Fig. 3. 8: Generation using ICG as a percentage of the annual energy demand for the Pareto solutions

The systems with lower ICG capacity contribute by generating more power using the ICG. At the same time, these systems having smaller ICG capacity injects more power to the grid. These observations indicate that the ICG of these systems operate more frequently when compared 4FC and CNN systems. Hence, we can imagine that the ICG of 2FC and 3FC systems to follow the operation as shown in Fig. 3.10 (a). It operates as a base load more frequently while the mismatch is taken from the grid. Since the mismatch between demand and renewable generation (using wind and solar) fluctuates significantly, the lead factor may change notably when trying to follow the mismatch (load following strategy). Operating at lower load factors may results in a significant increase in the operation cost. Hence, these generators operate at a higher load factor and inject the excess to the grid. However, having a very large ICG capacity is not favorable when adapting such a strategy due to the grid curtailments for injection. This leads the 2FC and 3FC systems to have lower ICG capacities. In contrast, 4FC and CNN use ICG for the peak shaving. As explained in Section 6.2, the size of thermal storage increases when moving from 3FC to 4FC and the battery bank get further enlarged when moving from 4FC to the CNN. Larger energy storage allows the system to withstand the fluctuations in the demand without much support from the ICG. ICG is only used for the instances where mismatch is quite significant which cannot be withstand by energy storage and the

grid (due to grid curtailments). This requires careful energy management in between grid, energy storage and the ICG since a careful shift over from storage, to grid and to ICG is more challenging than simply taking the base load from the ICG. This makes it important to have more knowledge transfer such as future prediction of renewable energy, demand and prices in the grid. At the same time, it demands for more advanced approximation techniques.

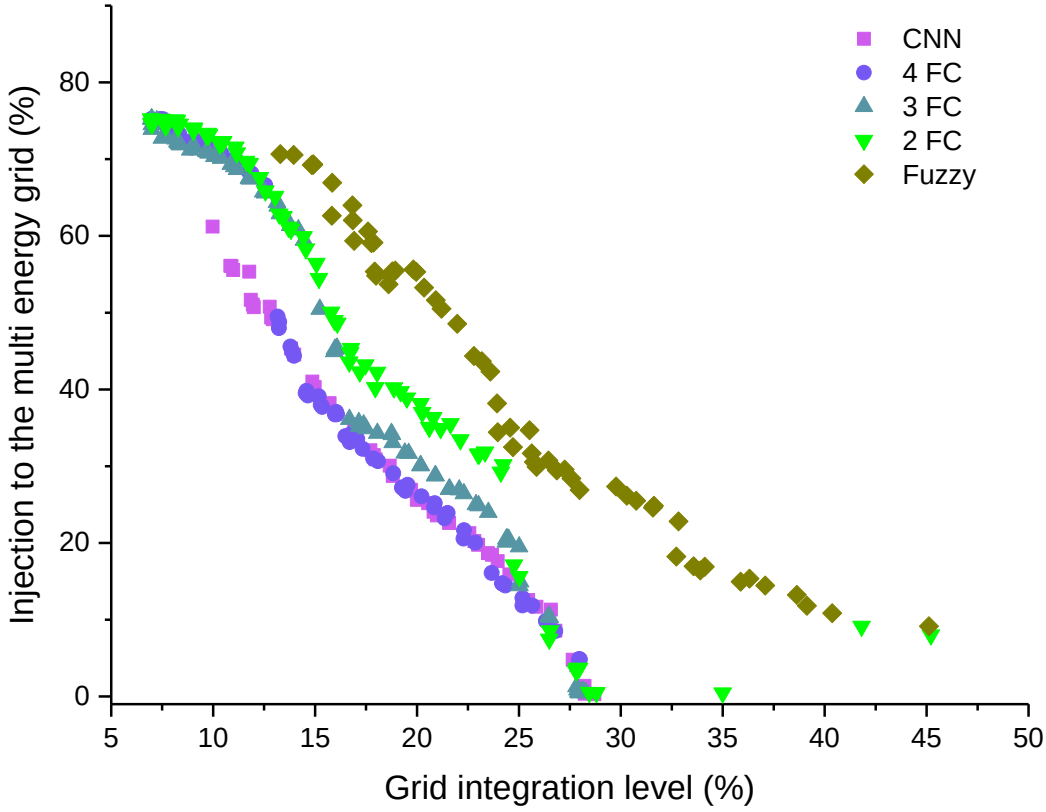

Fig. 3. 9: Grid injection as a percentage of the annual energy demand for the Pareto solutions

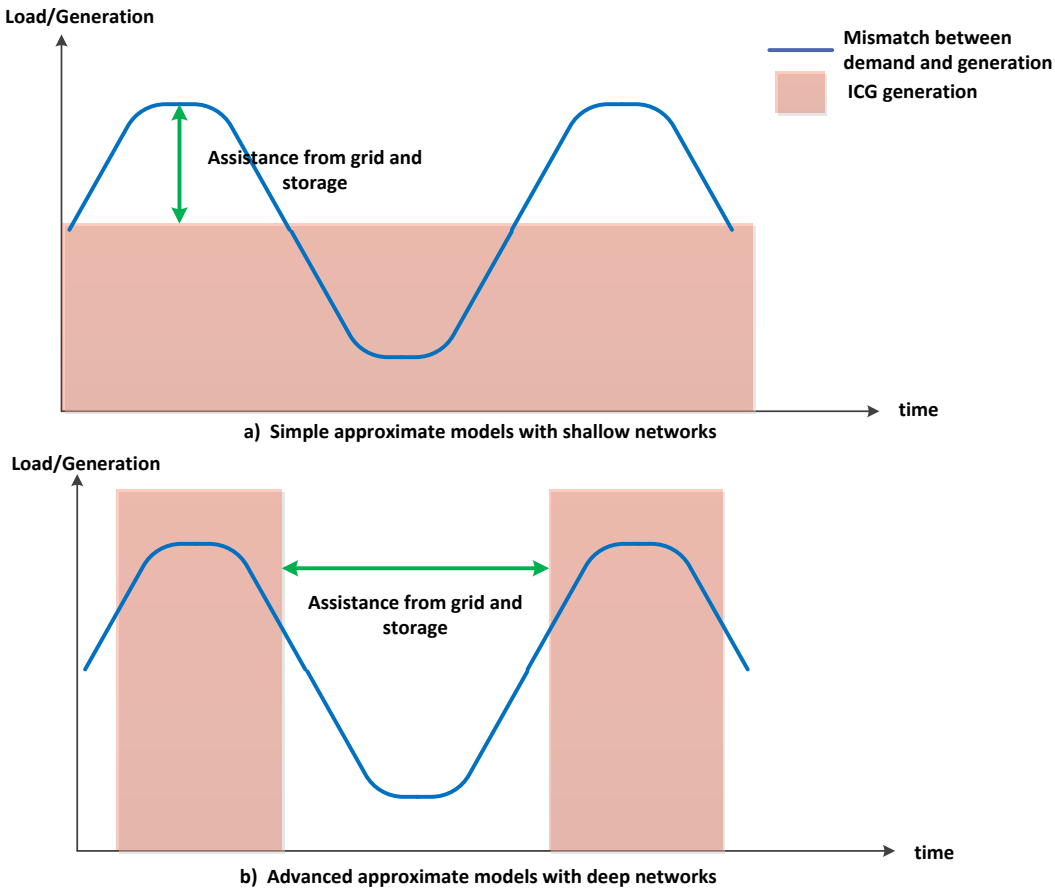

Fig. 3. 10: Possible operation of ICG for (a) shallow and (b) deep neural networks

3.7. Conclusions

Distributed energy systems are getting more and more popular due to the large scale deployment of renewable energy technologies such as solar PV and wind. However, it is a challenging task to design such distributed energy systems due to the intermittence nature of the renewable energy potential and fluctuations in the demand. Complex super structures having different energy conversion as well as storage technologies have been introduced in order to accommodate the fluctuations in energy demand and generation. Furthermore, energy systems are gradually becoming cyber physical systems with strong interactions that need to be maintained with the energy internet. Such progress of energy systems demands for a notable change in the present techniques used to design distributed energy systems.

Black box methods are an interesting alternative to be considered in such a context. This study proposes reinforcement learning to consider the dispatch strategy in the energy system optimization process. Policy search method is used to represent the dispatch strategy initially using fully connected neural networks. Subsequently, convolution neural networks are introduced to derive the dispatch strategy considering future forecast of renewable energy potential, energy demand for

electricity, heating and the grid process for electricity and heating. Finally, a grey model based on fuzzy logic is used to bench mark the novel method based on black box models.

Results of the study reveal that fully connected neural network outperform the grey box models with a notable improvement in the objective function values. The NPV, can be reduced up to 60% by simply using a feed forward neural network with two hidden layers. It clearly indicates that black box methods are more suitable when considering energy systems with enlarged state space. Increasing the number of hidden layers results in an increase in the performances up to four hidden layers. The increase in hidden layers does not improve the performance of the energy system further. Introduction of future forecast into the dispatch strategy by using CNN had a notable impact on the objective function values. NPV was improved by 20% when compared to fully connect neural network with four hidden layers. Finally, the results of the study reveal that the method used to represent dispatch strategy is having a notable impact on the design of the energy system. Advanced approximation methods with deep neural networks facilitated by information such as future predictions helps the system to shift over from one alternative to another with a minimum impact on the grid. Furthermore, it helps to have higher storage and dispatchable energy source capacities with minimum power generation from the dispatchable source.

4 Towards Realization of Energy Internet: Designing Distributed Energy Systems Using Game-Theoretic Approach

This computational model developed in Chapter 2 and 3 can be used to design a single energy system. This chapter extends the model introduced in Chapter 2 and 3 to consider an energy internet, consisting of multiple energy systems that interact with each other. A game-theoretic approach is introduced considering fully co-operative and non-cooperative scenarios. A distributed optimization algorithm is introduced to conduct the optimization. Finally, the novel approach is compared with the present practices.

This is chapter is based on:

A.T.D. Perera, V. M. Nik, Zhengchao Wang and J.-L. Scartezzini, "Towards realization of energy internet: designing distributed energy systems using game-theoretic approach," to be finalized in future

Author contribution for the journal paper:

In this article, ATD, designed the research with the support of VMN, DM and JLS. ATD conducted the analysis and prepared the first draft of the manuscript. VMN provided the demand profiles. VMN,ZW and JLS supported in revising and finalizing the Manuscript.

4.1. Introduction

Integration of renewable energy technologies into the energy infrastructure has been extensively discussed in recent past due to rapid depletion of fossil fuel resources and environmental concerns [1,2]. Large scale integration of non-dispatchable renewable energy technologies often used to be followed up by reinforcement of the grid which imposes economic constraints. Furthermore, maintaining reliability and robust operation becomes challenging following large scale integration of non-dispatchable energy technologies. Distributed energy systems such as micro-grids, energy hubs etc. have become attractive solution in this context which has shown the potential to integrate higher fractions of non-dispatchable energy technologies [3,4]. Both dispatchable energy technologies and energy storage devices help to withstand the fluctuations in demand and generation with a minimum impact on the grid [5]. However, designing distributed energy systems consist of different energy technologies is a difficult task.

Design optimization of energy system is a rich area of study [6,7]. A number of different approaches used to design distributed energy systems for both stand-alone and grid integrated applications including multi-vector energy systems. Energy systems with complex super structures have been optimized using different techniques. Deterministic, robust and stochastic optimization methods have been adapted in order to consider the uncertainty in the optimization process [8]. Energy nexus of auxiliary services connected to energy systems such as vehicle to grid, water management, waste management etc. have been discussed besides being limited to the boundary of the energy system [9]. In addition, energy system design has been optimized along with other infrastructure planning. For example, Evins [10] optimized the energy system design along with building design, while Wu et-al [11] did that along with building renovation. Increasing the design space extends the boundaries of the energy system, enabling to make more decisions at a more holistic manner. However, such holistic optimization can increase the calculation time for optimization problems; for example up to three days along with parallel compotation [10]. All in all, the energy system designing process has evolved significantly which facilitates to accommodate different aspects closely relevant to the energy system into the design process.

Towards the energy transition, it is important to improve the dissemination of distributed energy systems catering the local energy demand while harnessing the renewable energy potential. This makes it important to design energy systems considering the interactions among them (through multi-energy grids). Designing such energy infrastructure becomes very challenging due to two main reasons:

1. Expansion of the decision space that needs to be explored

2. Difficulties in considering the interactions among energy systems

Moving from a single distributed energy system to a set of energy systems interacting with each other extends the decision space. It is required to optimize both connectivity and strength of the network in this context besides being limited to the energy system which will further expand the decision space. Such expansion of the decision space makes the optimization process to be more challenging. Maroufmashat et-al [12] conducted optimization of the energy systems together with the energy network connection for a case study that consists of three distributed energy systems connected to each other. Secondly, energy markets are gradually translating into a more open environment where distributed energy systems behave as agents with much higher autonomy. A fully cooperative scenario considers that all the decisions related to the entire energy infrastructure are made by one entity. As a consequence, the fully cooperative scenario will misrepresent the transition that takes place in energy infrastructure where agents with higher autonomy are expected to be taking part [13,14]. Towards this end, Jing et-al [15] conducted energy system optimization considering the cooperative scenario and represented distributed energy systems using multiple agents during the decision making process. Bargaining process of different agents are considered during the decision making process through an agent based model. Moving ahead from the cooperative scenario to non-cooperative scenario by considering the optimization problem as a non-cooperative problem will help to study the liberalized energy markets. Furthermore, it will allow accommodating more sustainable energy technologies depending upon the preference of the agents (representing each distributed energy system) while guaranteeing reliable and robust operation of the energy system. Therefore, such representation is essential for the realization of the broader concept of energy internet where different stake holders related to energy services meet each other in a common energy market.

Considering the importance of non-cooperative agents towards realization of energy internet, this study focus on optimizing energy infrastructure with multiple non-cooperative agents and compare the solutions with cooperative scenario and other practices used in the present state of the art. The cooperative method formulates a single objective function considering all the aspects of energy infrastructure. This includes the energy grids, distributed energy systems and other auxiliary components related to the energy systems. The non-cooperative approach considers each agent (such as a distributed energy system) as a unit that tries to maximize its own profit while interacting with an open energy market having several such agents that do not cooperate with each other. Designing energy systems for a non-cooperative energy market is a challenging task since it converts the optimization problem into a set of distributed optimization problems (where each agent

represents a distributed energy system). In order to guarantee the equilibrium in the market, the optimization process should be conducted for several rounds until the Nash-equilibrium is guaranteed. This will extend the computational time making the optimization process further challenging. Towards addressing these challenges a novel computational algorithm is introduced in this study. Subsequently, the results obtained from the novel optimization algorithm is compared at two different levels. First, the results are compared with distributed energy systems optimized considering grid curtailments where boundary of the optimization problem is simply considered as the distributed energy system (individual system scale). Secondly, the results are compared with a cooperative scenario where boundary is extended to several energy systems. Promising paths for the energy transition are taken into discussion based on the comparison of non-cooperative scenario with both individual system scenario and cooperative scenario.

4.2. Coordinated design and operation of energy systems for energy internet

The concept of energy internet is developed with the intention of allowing stronger interactions among multi-energy systems connected by multi-energy networks. Energy internet allows higher integration level of renewable energy technologies while enabling self-healing and plug and play devices. Design and operation of energy infrastructure play an important role in this process towards the realization of energy internet where cyber-physical interactions to be considered. Multi energy network support the physical interactions while information exchange among the distributed energy systems enables cyber interactions with the support of communication technology. This requires making energy systems to be more intelligent. In addition, interactions among distributed energy systems are essential to provide the flexibility to integrate renewable energy technologies and cater the requirement of prosumers.

4.2.1. Different practices for controlling multi agent micro-grids

Coordination among distributed energy systems can be achieved through different architectures [16]. Different control strategies such as centralized, decentralized, distributed and hierarchical have been proposed to achieve the coordination. Among these techniques, distributed control strategies have received much attention due to its capability to include plug and play devices and improve robustness, scalability and efficiency according to Hu et al. [17]. Two major approaches have been adapted when using distributed control strategies i.e. cooperative and non-cooperative distributed control strategies. In the cooperative scenario, distributed energy systems cooperate with each other and agree together in order to improve the performance of all the energy systems together. In contrast, the non-cooperative scenario assumes that distributed energy systems make decisions independently. Nash and Stackelberg equilibria are commonly used solutions concepts for non-

cooperative scenarios. Non-cooperative scenario is gradually getting popular due to its capability to provide higher autonomy at the level of distributed energy system. However, the coordinated operation of the energy system solely depends on the design and the connectivity. In this study, both coordinated and non-coordinated approaches are practiced with the design approach practiced in present in order to understand more promising ways for the realization of energy internet.

4.2.2. Three different design and operation scenarios

An energy internet consists of several energy systems connected through a network. The design process of the energy internet can be conducted in different ways considering the interactions among the energy hubs within the energy internet.

Energy system optimization considering pre-defined grid curtailments (ESPG)

Design of energy internets is a challenging task which required simultaneous optimization of the energy systems and grid. Optimization needs to be performed at three levels in order to achieve this i.e. 1) operation of the energy systems, 2) system configurations of the energy systems, and 3) connectivity and strength of network [18]. The design process of energy internet is initiated as a process with two steps by Fazlollahi et-al [18] where energy system is optimized initially where the design optimization of the energy system is conducted using a bi-level optimization algorithm. The operation strategy of the energy system is optimized along with the system design using the bi-level optimization algorithm. Subsequently, the energy network (electricity or heat) is optimized as the second step. However, the influences of grid curtailments are not considered in detail at the first level where energy system is optimized using the bi-level optimization algorithm. Perera et-al [19–21] extended this approach by considering predetermined grid curtailments. ESPG presents this approach where energy system is optimized initially considering a set of predetermined grid curtailments and subsequently the energy network is optimized as shown in Fig 4.1.

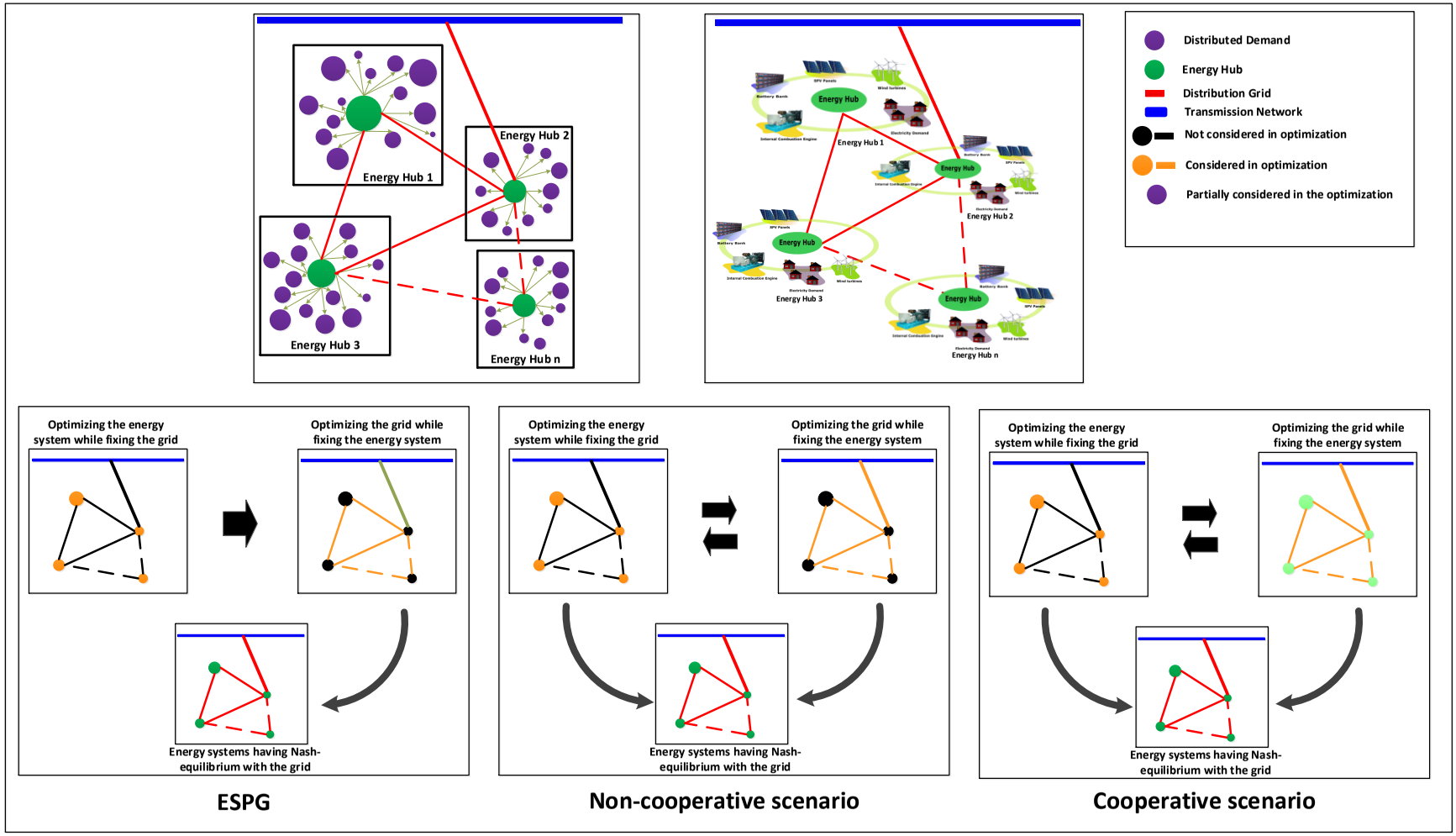

Fig. 4. 1: Three scenarios considered for the optimization of the energy internet.

Fully cooperative scenario (FCS)

The main limitation with the ESPG scenario is that it optimizes energy hubs without any knowledge about the neighboring energy hubs. This may lead to a significant congestion in the grid which leads to a sub-optimal system design. Fully cooperative scenario (FCS) facilitates the sharing of information among the agents, making the energy systems to be aware of the adjacent energy systems. Usage of multi energy grid, which presents the allowance for purchasing and injection, is shared among all the energy hubs. Subsequently, each energy hub is optimized considering its grid interactions and NPV as the objective functions based on the information shared among the energy hubs about the limitations for grid interactions. The energy internet is optimized at the secondary level where the energy hub design and grid connectivity are considered as decision space variables. Pareto solutions obtained for each energy hub at the primary level are considered as the decision space variables at the secondary scale. Following the optimization of the energy internet (secondary scale), the limitations for the grid interactions are determined. These limitations are again used to optimize the energy hubs individually using the primary algorithm. This process is iteratively conducted until it converges.

Non-cooperative scenario

Non-cooperative scenario presents the situation where interactions between the energy systems fall in between FCS and ESPG. All the energy systems are optimized separately and subsequently the grid is optimized in ESPG scenario. An iterative process is introduced in FCS scenario where grid and energy hub are optimized one after the other. Non-cooperative scenario follows a similar iterative approach to the FCS. However, the objective function and the decision space are limited to the grid connectivity and its cost without considering the energy system in both objective and decision spaces. Such a consideration leads to a situation where grid acts as a separate agent (similar to an energy system) which tries to maximize its profits.

4.3. Modeling approach

The energy infrastructure is expected to be consisting of several energy hubs connected through an electricity network. However, each energy hub has a distribution grid, as marked in Box 1 in Fig. 4.2, which is not considered in order to simplify the study. This converts the design problem as shown in Box 2, where each energy hub and its connectivity need to be optimized. However, the design optimization of the energy systems and grid, while allowing higher independency to the energy systems, is not a process that can be achieved in a single step considering a non-cooperative scenario. Hence, an iterative approach should be adopted while optimizing the energy systems design and the connectivity in two different stages; one after the other till the Nash equilibrium is

reached. A techno-economic model is developed in order to optimize the energy hub. Another techno-economic model is also developed to optimize the network. This section presents a brief overview about the techno-economic models for optimizing the energy system and network separately.

4.3.1. Outline of the case study

Three cities of Landskrona, Lund and Malmö in the southern Sweden are considered in this study to calculate the energy demand and renewable generation profiles. These cities have the oceanic climate with relatively mild winters compared to other locations at similar latitudes, because of their proximity to the sea affected by Gulf Stream.

The type of weather data can affect the energy calculations considerably [22]. For the purpose of this work, typical hourly weather data sets were synthesized considering six future climate scenarios for the 30-year span of 2070-2099 [23] [24]. Future weather data sets were simulated by RCA4 regional climate model with the spatial resolution of 12.5km, downscaling four global climate models (GCMs) – namely, CNRM-CERFACS-CNRM-CM5, ICHEC-EC-EARTH, IPSL-IPSL-CM5A-MR and MPI-M-MPI-ESM-LR – forced by two representative concentration pathways (RCPs) [25]; the first two are forced by RCP4.5 and RCP8.5 and the last two by RCP8.5. In total, six future climate scenarios have been used to create one typical downscaled year (TDY) for each city during 2070-2099 (for more details, the reader is referred to [23] [26]).

The energy demand of the residential buildings in a typical neighborhood in the cities was simulated by considering certain number of residential buildings in each city. The size of each neighborhood was set in a way to do not exceed the peak energy demand of 420 kW. Accordingly, the neighborhoods in Landskrona, Lund and Malmö respectively contain 39, 46 and 59 buildings that statistically represent the majority of residential buildings in each city. The models for building energy simulations were developed in Simulink toolbox of Matlab according to the BETSI investigation by the Swedish National Board of Housing, Building and Planning (Boverket, 2009) [27]. Simulations were done on the hourly time scale, calculating the total energy demand profiles, including the demand for heating, cooling, hot water, fans and considering if heat recovery is used in the building or not. The building simulations have been verified and used in some previous works (e.g. [28] [29] [30] [31]).

4.3.2. The design problem of Distributed Energy Hub

Energy hub consisting of wind turbines, PV panels, battery bank and an internal Combustion Generator (ICG) is considered in this study (Fig. 4.2). The energy hub caters the heating and

electricity demand of the considered neighborhoods in this study. It is assumed that heat pumps are used in all the buildings which convert the thermal demand into electricity demand. The energy hub interacts with the grid by selling and purchasing energy depending upon the fluctuations in the energy demand and renewable potential. However, the limitations for the grid interactions are imposed depending on the strength of connectivity, demand and generation of the other energy hubs. Net Present Value (NPV) and grid integration levels are considered as the objective functions when optimizing the energy hub while power supply reliability is considered as a constraint. Optimization process for all the three scenarios remains the same except for one specific factor which is grid curtailments. Grid curtailments for both injecting and purchasing electricity to the distribution network are considered as a constraint for the entire time period in ESPG scenario. However, these curtailments are updated during the iterative process for both NS and FCS.

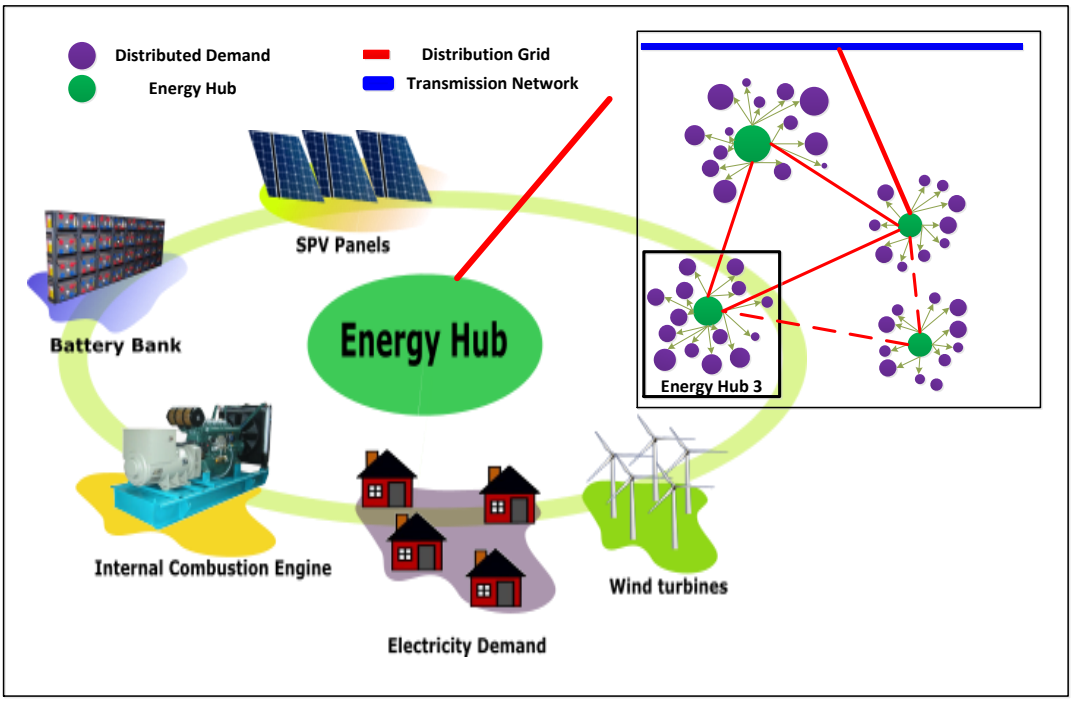

Fig. 4. 2: Configuration of a single energy hub which is connected to the energy internet. The mode of connections depends on whether the scenario is ESPG, FCS or NC.

4.3.3. Distributed network planning problem

Design of the network is conducted at the secondary level. A Pareto optimization is conducted considering two objective functions at the secondary level. However, formulation of the objective function is different from one to another when moving from one scenario to another.

Both ESPG and FC scenarios consider the entire energy internet is considered in the optimization process and the grid interactions maintained with the transmission line and the total cost for the entire energy internet is considered in this scenario. The NPV^{IE} is computed considering the net present value of all the energy hubs and the operation and maintenance cost for the distributed network (Eq. 4.1).

$$NPV_{ESPG/FCS}^{IE} = \sum_{\forall h \in H} NPV^{h} + \sum_{\forall l,m \in H} NPV^{x_{lm}} \tag{4.1}$$

In, Eq. 4.1, x_{lm} denotes the installation, operation and maintenance cost for the line connecting energy hub *l* and *m*. NPV^{h} denote the net present value of a single energy hub computed according to Chapter 2. The decision space for both ESPG and FC scenario consists of energy hub design e^{h} ($p\forall \in P^{h}, \forall h \in H$) for each energy hub and connectivity strength for x_{lm} ($x\forall \in X$). The formulation changes when moving from ESPG to NS scenario. As explained in 2.2, it only considers the cost for the connectivity according to Eq.4.2.

$$NPV_{NS}^{IE} = \sum_{\forall l,m \in H} NPV^{x_{lm}} \tag{4.2}$$

Grid interactions maintained with the transmission network (IT) is computed in a similar manner for the three scenarios. Both selling and purchasing are minimized when reaching lower IT levels. Eq. 4.3 is used to compute the IT.

$$IT = \frac{\sum_{\forall t \in T} P_t^{IE,EG} + P_t^{IE,IG}}{\sum_{\forall h \in H} \sum_{\forall t \in T} P_{t,h}^{ELD}} \tag{4.3}$$

In this equation, $P_t^{IE,EG}$, $P_t^{IE,IG}$ and $P_{t,h}^{ELD}$ respectively denote energy exported and imported from the transmission network and the energy demand for each energy hub respectively.

4.4. Optimization frame work

Optimizing both hub and the network is a challenging task. The complexity becomes more when considering different operation scenarios as discussed in Section 2.2. A brief overview about the optimization frame work is presented in this part without going deep into the mathematical formulation. When considering the ESPG scenario, method proposed by Samira et-al [18] and Perera et-al [19,20] are used directly (described in Chapter 2). Energy system is optimized considering two objective functions formulated in Eq. 4.3 and 4.4. A Pareto optimization results in a set of solutions

for each energy system as shown in Box A in Fig. 4.3. Subsequently, the network is optimized along with the energy system in the second step as shown in Box B. The optimization process terminates after finishing the optimization of the network for ESPG scenario. However, the optimization process it further extended in FCS and NC scenarios. Both these scenarios go through an iterative process as shown in Fig. 4.4. Similar to ESPG scenario, Energy system and grid are optimized at two different stages (Box A and B). Subsequently, grid curtailments are redefined in Box C based on the results of the Box B. Afterwards, the energy hub is optimized again in Box A for the new grid curtailments. The iterative process take place until the equilibrium is reached. The main difference between FCS and NC is related with the formulation of objective functions formulated in Section 3.3.

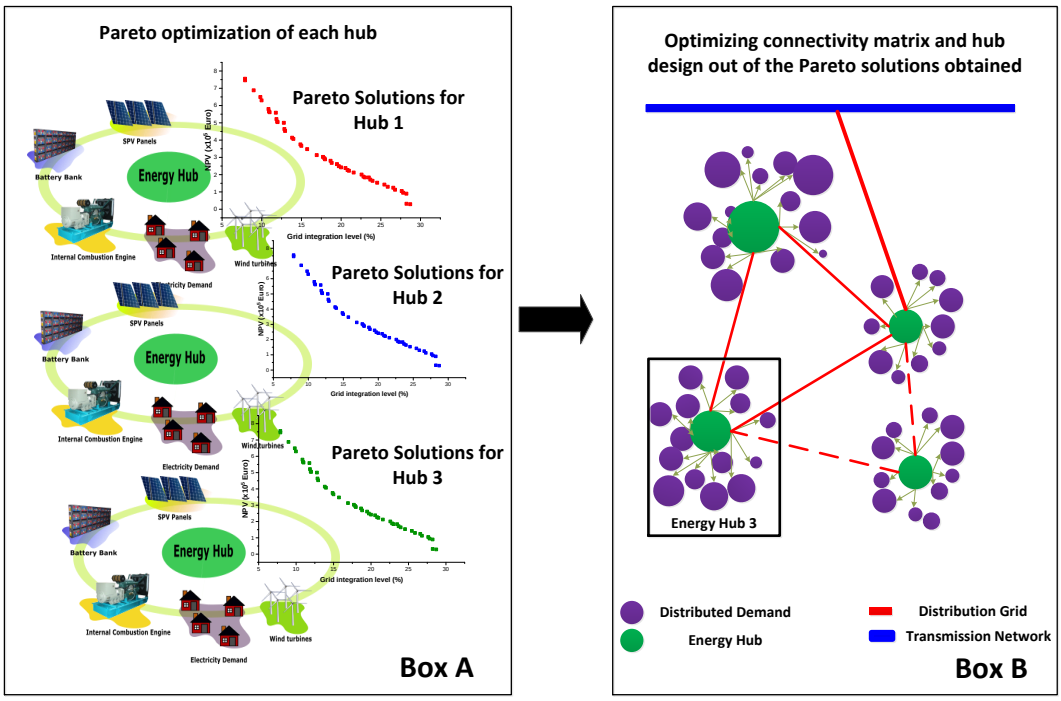

Fig. 4. 3: Graphical Presentation of the optimization algorithm for ESPG scenario

4.5. Results and discussion

Optimizing the design of a group of energy systems is a difficult task especially when considering the interactions within the group. The energy systems demand for higher autonomy while expecting support from the grid whenever there is a shortage or excess in generation. Maintaining the optimum balance between these two ends is difficult. It is interesting to analyze how these different scenarios introduced in this study helps to balance the autonomy and while guaranteeing better connectivity to assist energy systems to with stand the fluctuations in demand and generation.

4.5.1. Analysis of ESPG

ESPG presents the design for the set of energy systems and the grid considering minimum prior knowledge between each other. As a result, the energy system is designed solely considering the upper and lower limits which are imposed artificially to design each energy system while the grid is subsequently designed based on the requirements of the energy system. As a result, the energy system is unaware of the demand and generation of its neighbors and fails to adapt its generation mix to maximize its profit while optimizing the interactions with the neighbors through the grid. In order to analyze these aspects further, Pareto fronts obtained for the four energy hubs are presented in Fig. 4.5.

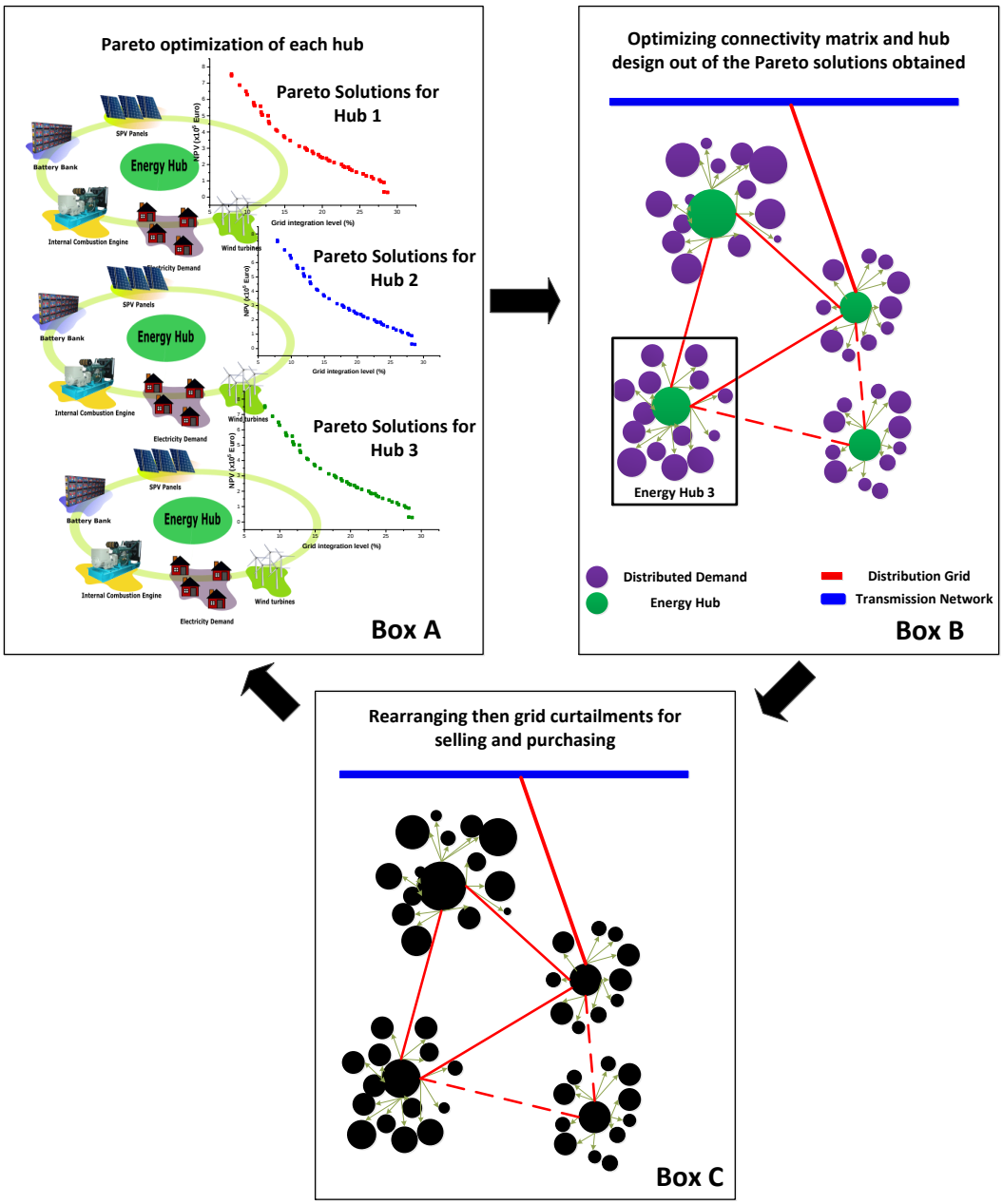

Fig. 4. 4: Formulation of the optimization problem for FCS and NC

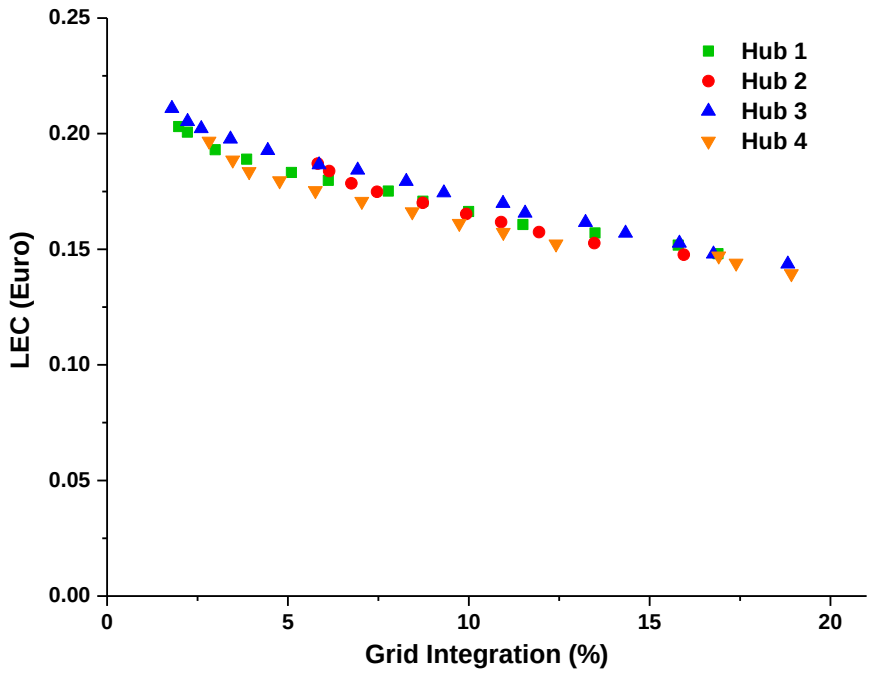

Fig. 4. 5: Pareto fronts obtained considering LEC and Grid Integration levels as the objective functions for the four different energy hubs. Each Pareto front is obtained by conducting the optimization separately considering set of upper bounds for grid interactions based on ESPG.

When analyzing the Pareto fronts, it is prudent that a gradual reduction in the LEC is observed for the Pareto solutions while increasing the grid interactions. Furthermore, a slight shift in NPV is observed when moving from the Pareto fronts obtained for different hubs which can be justified due to the changes observed in energy demand and renewable energy potentials. Towards analyzing the changes observed in NPV for different hubs, two Pareto solutions with similar grid integration levels from different hubs are taken and tabulated in Table 4.1. The two scenarios are taken considering Pareto solutions having grid interaction levels close to 5% and 10% respectively. When analyzing the Pareto solutions it is prudent that the LEC, within a scenario does not show a significant fluctuation as observed in Fig. 4.5. In addition, the number of wind turbines reaches the upper limit set of the optimization for many design solutions except with S1H3 and S1H1. The main deviation is observed when analyzing the SPV capacity. A notable drop in SPV capacity is observed in S1H1 and S2H3 when compared to the other Pareto solutions, having 31 and 42 SPV panels respectively. As a result, the grid injection notably reduces. Hence, it is clear that significant changes in both design and operation can be observed when moving from one energy hub to the other. The most important fact is that these optimum solutions have been obtained solely considering the energy demand and generation of the specific hub without considering the demand and the generation of the others which can lead to many deficiencies during the operation.

Table 4. 1: Pareto solutions having similar grid interactions for the four hubs.

Scenario	Hub	Pareto Solution	GI (%)	LEC(Euro)	Grid Injection (%)	Grid Purchase (%)	SPV panels	wind turbines	ICG Capacity (kWh)
1	1	S1H1	5.10	0.18	3.6	1.5	50	28	100
	2	S1H2	5.83	0.19	0.5	5.3	31	30	100
	3	S1H3	5.86	0.19	4.5	1.4	47	10	100
	4	S1H4	5.76	0.18	3.4	2.3	51	30	100
2	1	S2H1	10.00	0.17	8.8	1.2	99	30	100
	2	S2H2	10.90	0.16	6.3	4.6	74	30	100
	3	S2H3	9.31	0.17	3.3	6.0	42	30	80
	4	S2H4	10.96	0.16	8.7	2.3	106	30	100

4.5.2. Analyzing the fully cooperative scenario

The fully cooperative scenario (FCS) presents the entire opposite of ESPG. FCS considers the generation and demand of the other energy systems as well as the grid congestion during the optimization process of the specific energy hub. As a result, it provides the opportunity to minimize the design and operation of the specific energy system as well as the entire system consisting of several energy hubs along with the grid. The distributed optimization algorithm introduced in Section 4 is used to arrive at the Pareto solutions considering the FCS scenario. The LEC-GI Pareto front obtained following the Epsilon-Nash equilibrium is presented in Fig. 4.6.

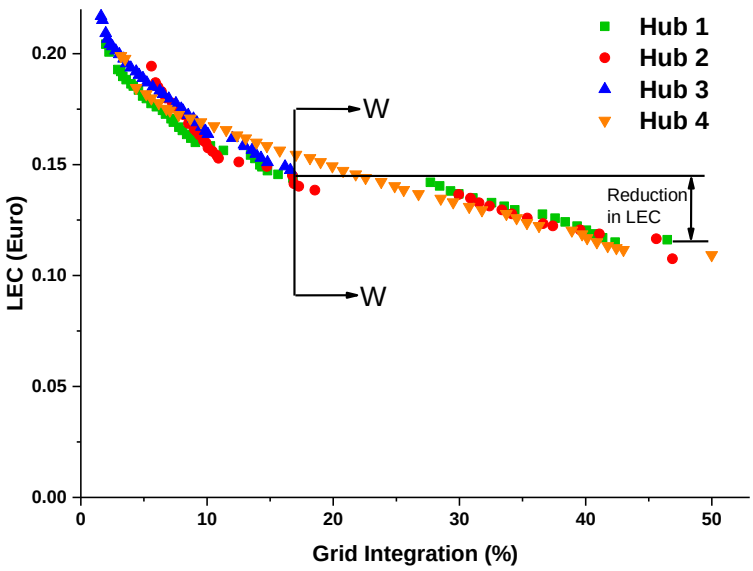

Fig. 4. 6: LEC-GI Pareto fronts obtained for the four hubs after Epsilon-Nash equilibrium condition. The LEC-GI Pareto front extends significantly when compared to ESPG introducing Design solutions having higher grid integration levels and lower LEC. Pareto solutions towards the left side of W-W line are the ones introduced in FCS which will result in a reduction around0.05 Euros in LEC.

Pareto front obtained shows a steep reduction in LEC with the increase of grid interactions for design solutions which are having grid interaction levels less than 10%. The reduction in LEC is notably high for these design solutions when compared to ESPG. For example, the LEC reduces from 0.2042 to 0.1455 Euros when increasing the grid integration level from 2 to 15.6% by reducing the LEC by 28% for Hub 1. In addition, the Pareto front obtained for FCS is having design solution with higher grid integration levels when compared ESPG. The Pareto solutions towards the right hand side of W-W line are the newly added designs when moving from ESPG to FCS. For example, the grid integration level has increased from 16.9 to 46 % with an increase almost three times when moving from the design solution having highest grid interactions in Hub 1 under ESPG scenario to the same design solution in FCS. The higher grid interactions results in a significant drop in LEC. For example, the LEC reduces from 0.148 to 0.1161 Euros reducing it by when moving from the design solution having highest grid interactions in Hub 1 under ESPG scenario to the same design solution in FCS 31%. Further, reduction in LEC can be observed when comparing Hub 4. These results clearly show that it is possible to reduce the lifecycle cost notably by improving the interactions with the neighboring energy hubs. The energy network plays a vital role in this context which will enable higher interactions among different energy hubs.

The Pareto fronts obtained for the energy system presents the alternative design solutions from the energy system perspective. However, the main advantage of FCS is that these solutions obtained for each energy hub can be used to optimize the entire energy superstructure consisting of both the energy hubs and grid. The Epsilon-Nash equilibrium for the fully cooperative scenario presents Pareto solutions for each hub as well as the energy superstructure including all the energy hubs and grid. Hence, it’s interesting to move from the Pareto solutions obtained for each energy hub to the optimum solutions obtained for the energy superstructure which will provide a more holistic view. Towards this end, the two Pareto solutions having lowest LEC and grid interactions respectively for the entire energy superstructure are taken and both grid and energy system configuration of these solutions are tabulated in Table 4.2.

Table 4. 2: Pareto solutions having lowest NPV from ESPG and FCS

Scenario	Hub	Pareto Solution	GI (%)	LEC(Euro)	Grid Injection (%)	Grid Purchase (%)	SPV panels	wind turbines	ICG Capacity (kWh)
Lowest cost-FCS	1	FLCH1	29.95	0.14	13.4	16.6	84	4	60
	2	FLCH2	18.54	0.14	7.1	11.4	119	30	80
	3	FLCH3	3.95	0.19	2.4	1.6	37	0	100
	4	FLCH4	41.74	0.11	17.1	24.7	120	29	40
Optimum ESPG	1	ESH1	5.10	0.18	3.6	1.5	50	28	100
	2	ESH2	5.83	0.19	0.5	5.3	31	30	100
	3	ESH3	5.86	0.19	4.5	1.4	47	10	100
	4	ESH4	5.76	0.18	3.4	2.3	51	30	100

When comparing the design solutions obtained for the fully ESPG and FCS, a notable drop in LEC can be observed for each hub as a result of the significant improvement in the grid interactions. For example, the total grid interactions increase from 5.1 to 29.95% when moving from ESH1 to FLCH1 while reducing the LEC from 0.18 to 0.14 with a percentage reduction in 24%. Similarly, the LEC reduce by 40% when moving from ESH4 to FLCH4. This clearly shows that the interaction among the energy systems can lead to a significant drop in the lifecycle cost. When analyzing the grid interactions carefully, it is observed that both grid injection and purchasing have improved in FLC scenario except for FLCH3. As the result of the improvements in grid interactions, the requirements of the dispatchable energy sources get reduce. This can be observed when comparing the ICG capacities of FLCH4 and FLCH1 (40 and 60 kWh respectively) which are significantly low when compared to the ICG capacities obtained for ESPG scenario. Similarly the number of SPV panels has increased in all the design solutions for the FSC scenario except FLCH3. Therefore, it is clear that the interactions among the energy systems can lead to notable changes in the energy system design which result in a significant drop of the lifecycle cost.

4.5.3. Analyzing the non-cooperative scenario (NS)

The design solutions obtained for non-cooperative scenario falls in between the ESPG and FCS. There are interactions among the energy systems and the grid although not strong as the FCS. The changes introduced to the optimization process when moving from FCS to NCS influence the design of each energy hub and the entire superstructure. Hence, it is important to analyze the changes in both energy hubs as well as the superstructure.

In order to analyze the design solutions of the energy hubs, Pareto solutions for Hub 1 are plotted for both FCS and NS (Fig. 4.7). When analyzing the Pareto solutions it is clear that the LEC obtained for NS are slightly higher than the solutions obtained for FCS in many instances (marked in Region L).

Furthermore, there are few design solutions where FCS shows slightly higher LEC as marked in Region M. Finally, both Pareto fronts overlap each other when the grid interactions are very low and very high. In order to understand the possible causes for the deviation, three Pareto solutions having similar LEC are taken from each Pareto front (FCS and NS which belong to Region L) and tabulated in Table 4.3. When analyzing the design solutions, a significant increase in grid interactions can be observed when moving from FCS to NS for the same LEC. For example, GI increase from 5.2 to 9.31 when moving from F1 to N1, increasing the total grid interactions by 80%. However, when comparing the grid purchasing levels, Pareto solutions which belong to the same case (having similar LEC from the two different Pareto fronts) are having similar grid purchasing levels. Therefore, the deviation is entirely due to the grid injection. This can be understood when comparing the grid injection levels of the Pareto solutions. When analyzing the scenarios further it was found that the increase in grid injection is due to the changes in the energy system design. The design solutions obtained for NS are having larger number of wind turbines when compared to the FCS. For example FC3 is having 7 wind turbines while N3 is having 28. The number of wind turbines has increase by four times while increasing the grid injection notably. However, LEC and the grid purchase remain almost the same when moving from NS3 to FC3. It shows that more energy sources need to be added to the energy system when considering NS due to the mutual understanding between different energy hubs. As a result both grid integration level and LEC increase when moving from FCS to NS.

It is interesting to analyze the influences of cooperative and non-cooperative scenarios on the other energy hubs (presented in Fig 4.8(a), (b) and (c)). Hence, the Pareto solutions obtained for each energy hub at the epsilon-Nash equilibrium are plotted in a similar manner. When analyzing Hub 2 (Fig. 4.8 (a)), the Pareto fronts obtained considering FCS and NS deviate from each other following a similar pattern to the Hub 1. However, the difference between the two Pareto fronts has reduced in Hub 2. When moving from Hub 2 to 3, the differences between the Pareto fronts reduce further (Fig. 4.8(a) and (b)). Finally, the two Pareto fronts overlap with each other in Hub 4. The connectivity of different hubs explains the gap between the Pareto fronts obtained using FCS and NS. Hub 1 is connected towards both Hub 4 and 2 and the transmission network. Hub 2 is connected to both Hub 1 and 3. FCS can take the benefit of higher connectivity of energy hub and lead to a notable reduction in LEC when compared to the NS. Both Hub 3 and 4 are less connected when compared to the other two. Especially, Hub 4 is far away from Hub 1 which results in significant investment on the grid. Therefore, these two hubs get less opportunity to interact when compared to the others. As a result, a significant deviation cannot be observed when moving from FCS to NS.

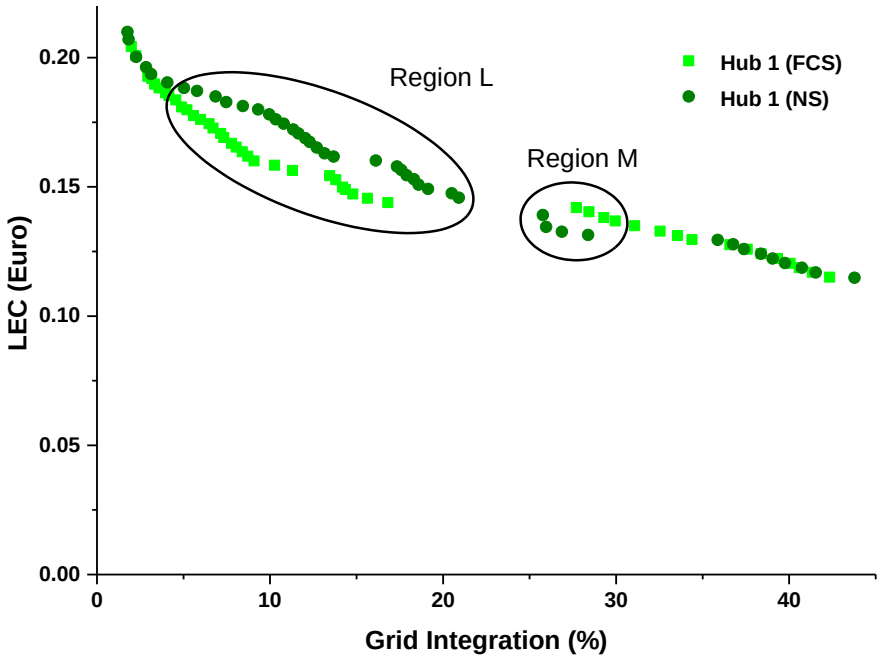

Fig. 4. 7: A comparison of Pareto solutions for Hub 1 for FCS and NS scenarios

Table 4. 3: Three Pareto solutions having similar LEC are taken from each Pareto front (FCS and NS which belong to Region L)

Scenario	Case	Pareto Solution	GI (%)	LEC(Euro)	Grid Injection (%)	Grid Purchase (%)	SPV panels	wind turbines	ICG Capacity (kWh)
FCS	1	F1	5.20	0.180	3.628	1.571	54	13	100
NS	1	N1	9.31	0.180	8.069	1.246	57	29	100
FCS	2	F2	8.71	0.162	7.223	1.492	110	6	100
NS	2	N2	13.68	0.162	12.100	1.583	120	30	100
FCS	3	F3	16.81	0.144	7.340	9.473	120	7	80
NS	3	N3	20.91	0.146	11.863	9.048	120	28	80

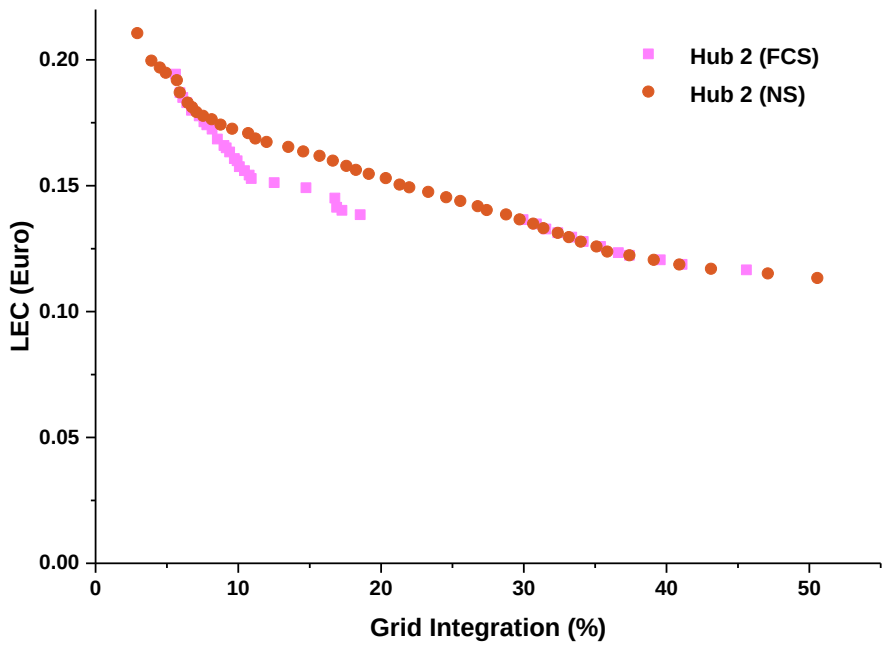
Hub 2 (FCS)
Hub 2 (NS)
LEC (Euro)
0.00
0.05
0.10
0.15
0.20
0
10
20
30
40
50
Grid Integration (%)

(a)

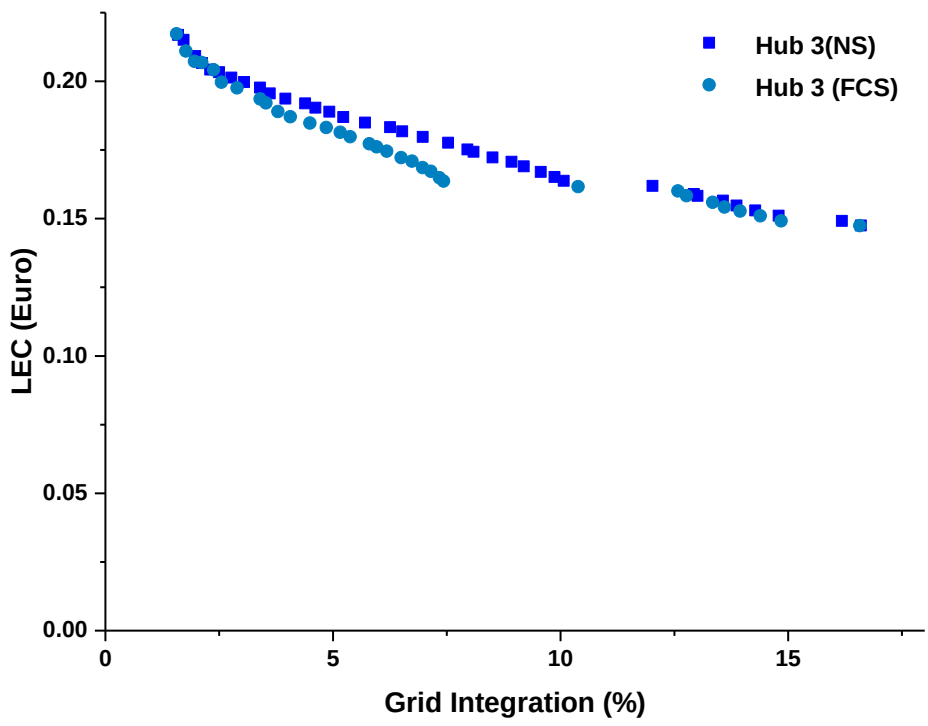
Hub 3(NS)
Hub 3 (FCS)
LEC (Euro)
0.00
0.05
0.10
0.15
0.20
0
5
10
15
Grid Integration (%)

(b)

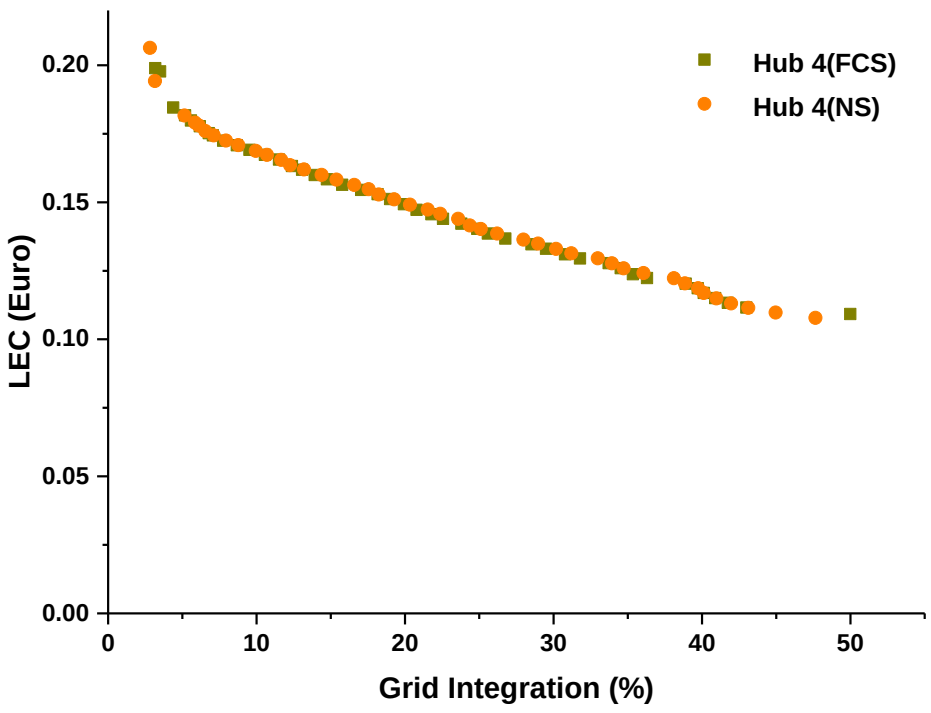

(c)

Fig. 4. 8: Presents the comparison of FCS and NS using Pareto fronts obtained for (a) Hub 2, (b)Hub 3 and (c) Hub 4

4.5.4. Analyzing the Energy Internet for NS and FCS

Pareto analysis of each hub presents the overview from a specific energy system perspective. However, it is important to consider the entire energy internet in order to get a more holistic understanding about the influences of cooperative and non-cooperative scenarios. Such a holistic assessment provides the opportunity to understand the impact of energy interactions among different energy hubs on the performance of the energy internet. Towards this end NPV and interactions with the transmission network are plotted for the Pareto solutions of the energy internet at the epsilon-Nash equilibrium (Fig. 4.9) which is followed by a detailed analysis taking several design solutions from the Pareto front.

The Pareto front of NPV-IT presents the design solutions obtained considering Net Present Value of the energy internet (including the lifecycle cost of all different energy hubs and the grid) and the interactions energy internet maintains with the transmission line for the FCS. When moving into the NS, Pareto optimization is conducted considering the NPV of the grid and the interactions energy internet maintains with the transmission line for the FCS. Hence, for NS, Fig. 4.9 presents the NPV of the energy internet for the Pareto solutions obtained considering NPV of the grid and IT at the

epsilon Nash equilibrium. However, when analyzing the Fig. 4.9, it is clear that the design solutions obtained for NS are non-dominant and presents a Pareto front in the objective space of NPV-energy internet and IT. Therefore, both are referred as Pareto fronts hereafter. Both Pareto fronts overlap each other at the beginning where grid interactions are at minimum. Subsequently, they divert from each other with the increase of grid interactions resulting a significant difference in NPV up to 13%. A notable reduction in NPV is observed for FCS with the increase in IT in Region P. However, the difference between NPVs gradually get reduces when reaching the end of Pareto front where grid interactions are at the maximum.

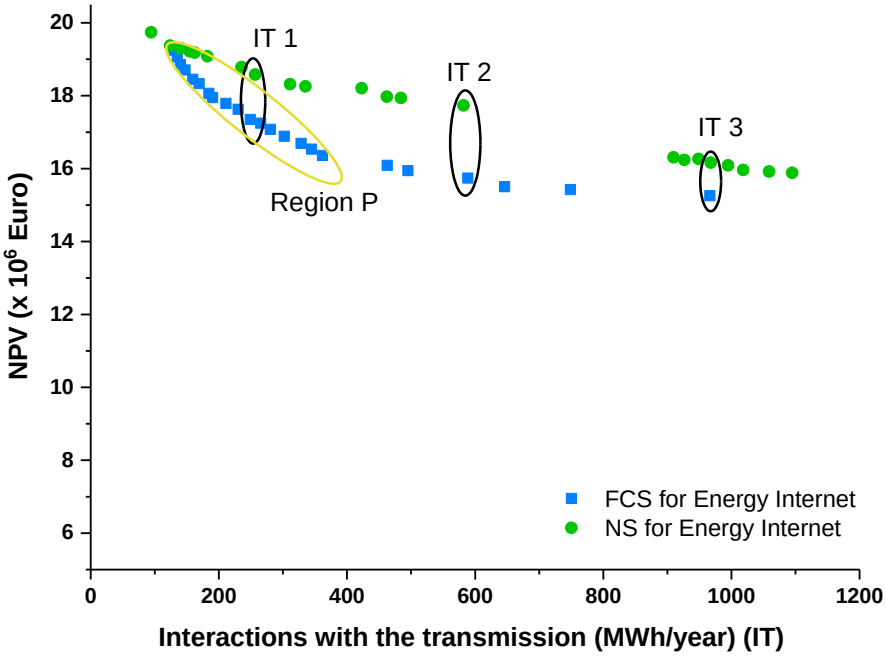

Fig. 4. 9: A comparison of the two Pareto fronts obtained for the energy internet considering FCS and NS scenarios

In order to analyze the Pareto fronts quantitatively, three Pareto solutions are taken from each Pareto front. Subsequently, the strength of the grid connectivity of each Pareto solution and energy hub design are tabulated in Table 4.4, 4.5, and 4.6. When analyzing the Pareto solutions it is clear that Hub 1 is having higher grid interactions for both FCS and NS which is maintained above 240 kW for all the design solutions tabulated in Table 4.5. Hub 1 is connected to the transmission line and having very short connection distance which justify the strong connectivity irrespective of the scenario. The connection distance between Hub 2 and 3 is trivial when compared to the distance between Hub 2-1 and Hub 4-3. This justifies the strong connection for Hub 3. The main difference between the two scenarios lies with connectivity strength of Hub 2. FCS scenario is having a higher connectivity for Hub 2 which notably reduces when moving into Hub 4. As shown in Table 4.4.6, Hub 2, 3 and 4 are having low grid interaction level for NS scenario (except for NIT 3 where Hub 2 is

having a higher GI level). Hence, by connecting each other, these three can form an island without depending much upon transmission network. Such island operation will minimize the cost of grid although it will significantly increase the overall cost of the energy internet. As a result, a significant improvement in grid connectivity is observed when moving into FCS scenario which results in notable change in the energy system design. However, Hub 4 is at the end of the network, being only connected to Hub 3. Hence, it is important to have a higher grid interaction with Hub 3 which makes it to have a stronger grid connection than Hub 2 for the NS scenario except for NIT3.

Table 4. 4: Connectivity strength of each energy hub for the selected designs, NPV and grid interactions maintained with the transmission line for the energy internet

Scenario	Name	NPV ($x10^6$)	IT (MWh /year)	Hub 1 (kW)	Hub 2 (kW)	Hub 3 (kW)	Hub 4 (kW)
FCS	FIT 1	17.35	249	290	100	270	60
	FIT 2	15.74	589	290	190	280	90
	FIT 3	15.26	966	290	160	280	190
NS	NIT1	18.58	257	280	20	210	60
	NIT2	17.73	582	280	20	210	60
	NIT3	16.16	968	240	80	280	60

It is interesting to further assess the impacts of the two different operation scenarios on the design of two energy hubs. A notable difference in grid interactions, cost and system configurations can be observed for the energy hubs when comparing NS and FCS scenarios. When comparing the two scenarios, it is observed four hubs will have unique system design under FCS while Hub 3 and 4 will have the same design for NIT 1, 2 and 3 design solutions. The design solutions obtained for Hub 3 and 4 (NIT 1-3-3 and NIT 1-3-4) are the Pareto solutions having the lowest grid integration level with the highest LEC. Moving from NS to FCS, Pareto solutions obtained for the energy hubs are neither the cheapest nor the most autonomous. A significant change in LEC is observed when moving from one solution to the other within the energy hub including energy hubs 3 and 4. For example, LEC reduce from 0.185 to 0.113 Euros when moving from FIT 1-4 to FIT 3-4. More importantly, the cheapest LEC is observed for Hub 2 (Solution FIT1-2 for Grid Scenario FIT 1) and Hub 4 (Solution FIT2-4 and FIT3-4 for Grid Scenario FIT 2 and 3) in FCS. Hence, it's clear that it utilizing the local renewable energy potential reduce the LEC being the opposite of NS scenario. Furthermore, the grid interactions of Hub 2, 3 and 4 improve significantly compared to NS scenario. GI reaches 41.74 (FIT 3-4) and 12.93 % (FIT 2-3) respectively for Hub 3 and 4 for FCS, which was below 3% for NIT1-3-3 and NIT1-3-4. As a result, significant improvement in renewable energy capacity can be observed for Hub 3 and 4. The design solutions obtained for FCS complement each other in order to operate the energy internet as a single energy hub. This can be observed when the three Pareto solutions for

Hub 3 and 4. FIT 1-3 and FIT 3-3 do not have any wind turbines while FIT 1-4 and FIT 3-4 are having 29 wind turbines each. In contrast, FIT 2-3 has 30 wind turbines while FIT 2-4 does not have any. This clearly presents that proper organization between the energy hubs can be seen for FCS from the system design perspective which enables them to coordinate properly as an energy internet.

Table 4. 5: Design of four energy hubs for the selected three design solutions of FCS

	Grid Scenario	Name	LEC(Euro)	GI (%)	Grid Injection (%)	Grid Purchase (%)	SPV panels	wind turbines	ICG Capacity (kWh)
Hub 1	FIT 1	FIT 1-1	0.181	4.90	3.37	1.53	52	13	100
	FIT 2	FIT 2-1	0.162	8.71	7.22	1.49	110	6	100
	FIT 3	FIT 3-1	0.137	29.95	13.39	16.56	84	4	60
Hub 2	FIT 1	FIT 1-2	0.153	10.91	6.51	4.40	120	30	100
	FIT 2	FIT 2-2	0.151	12.52	7.31	5.21	120	30	100
	FIT 3	FIT 3-2	0.138	18.54	7.13	11.41	119	30	80
Hub 3	FIT 1	FIT 1-3	0.190	4.61	3.12	1.49	41	0	100
	FIT 2	FIT 2-3	0.159	12.93	7.59	5.34	86	30	80
	FIT 3	FIT 3-3	0.194	3.95	2.36	1.60	37	0	100
Hub 4	FIT 1	FIT 1-4	0.185	4.39	1.46	2.93	38	29	100
	FIT 2	FIT 2-4	0.142	23.80	16.42	7.38	111	0	100
	FIT 3	FIT 3-4	0.113	41.74	17.05	24.69	120	29	40

Table 4. 6: Design of four energy hubs for the selected three design solutions of NS

	Grid Scenario	Name	LEC(Euro)	GI (%)	Grid Injection (%)	Grid Purchase (%)	SPV panels	wind turbines	ICG Capacity (kWh)
Hub 1	NIT 1	NIT 1-1	0.147	20.51	11.93	8.58	120	26	80
	NIT 2	NIT 2-1	0.119	40.73	17.84	22.89	118	29	40
	NIT 3	NIT 3-1	0.105	53.35	20.75	32.60	120	30	20
Hub 2	NIT 1-2	NIT 1-2-2	0.211	2.93	0.29	2.64	28	30	120
	NIT 3	NIT 3-2-2	0.113	50.56	17.04	33.52	114	30	40
Hub 3	NIT 1-3	NIT 1-3-3	0.217	1.56	0.07	1.49	22	23	100
Hub4	NIT 1-3	NIT 1-3-4	0.206	2.82	0.01	2.81	24	30	100

4.6. Conclusions and future perspectives

Energy internet is an emerging area of research which allows large scale penetration of non-dispatchable renewable energy technologies such as wind and SPV. Although several studies have focused on operation of such energy internets consisting of several distributed energy systems, a comprehensive study has not been conducted on promising techniques that can be used to design such energy internets. Towards addressing this research gap, this study introduces a distributed

optimization algorithm that can be used to optimize energy internet. Following that, three design strategies to design energy internet are considered assuming different behaviors for the distributed energy systems (agents) namely 1) energy system design with predefined grid curtailments (ESPG) scenario, 2) fully cooperative scenario (FCS) and 3) non-cooperative scenario (NS). The results obtained from this study reveals that energy internets design by using ESPG tends to have higher LEC up to 30% when compared to FCS as a consequence of the lack of proper coordination between the grid and distributed energy hubs. Hence, it is essential to move towards more promising ways that can reduce the cost by improving the interaction among the energy hubs. FCS presents the complete opposite of the ESPG, where energy hubs interact with the grid and neighboring energy hubs efficiently.

Distributed optimization is introduced in this study to conduct optimization considering FCS. As a result, it is possible to extend energy system optimization considering larger number of energy hubs while considering non-linear objective functions. The study reveals that FCS scenario notably increases the grid interactions. Improving the interactions results in a reduction internal combustion generator usage and an improvement in installed PV capacity. This justifies the reduction in LEC when for FCS compared to ESPG scenario. The NS lays in-between FCS and ESPG enabling the energy hubs to maintain reasonable energy interactions with the grid and neighboring energy hubs. From the analysis, it was revealed that the Pareto fronts NS, located far from the transmission network, show similar behaviors as FCS. However, in terms of higher renewable energy integration and lower cost of the energy system the final design of the energy internet favors the energy hubs that are closely located to the transmission network. As a result, the energy internet loses the opportunity to harness the renewable energy potential from the energy hubs far away from the transmission line. This leads to a gap in LEC up to 15% when compared to FCS while creating a significant inequity within the energy internet in terms of grid integration, renewable energy installation and lifecycle cost.

The assessment conducted in the study reveals that the concept of energy internet enables the co-existence of distributed energy systems while integrating higher renewable energy integrations levels. A significant improvement in renewable energy integration and a reduction in LEC can be achieved through NS and FCS where distributed optimization algorithms help to reach the optimum designs. FCS provides better opportunity for all the energy hubs irrespective of how far they are located from the transmission line. Furthermore, FCS enables stronger interactions in-between energy hubs. However, we need to understand that stronger interactions may often lead to stronger dependencies. As a result, there is a tendency for cascade failures whenever one or few energy hubs

fail to operate according to the expectations of the energy internet. Hence, promising methods to improve the resilience while maintaining the interactions should looked upon. Hierarchical operation of distributed energy systems along with leader follower strategy might be promising in this context.

5 Energy System Optimization Using Supervised and Transfer Learning Techniques

Optimization of distributed energy systems may take extensive computational time in certain instances. The optimization process should start from the beginning when the input parameters such as demand, renewable energy potential etc. are varying. This makes it challenging to compute the potential for renewable energy technologies at regional and national scale where a large number of distributed energy systems need to be optimized along with grid. This chapter evaluates the potential of supervised and transfer learning techniques to address the limitations in the present state of the art. A surrogate model is developed with the assistance of a supervised learning technique in order to by-pass computationally intensive Actual Engineering Model (AEM) used to map the decision space variables into the objective space. Eight different neural network architectures are considered in the process of developing the surrogate model. Transfer learning is used to adapt the surrogate model (trained using supervised learning technique) for different scenarios where solar energy potential, wind speed and energy demands are notably different from the scenario the surrogate model is initially trained on. Subsequently, a hybrid optimization algorithm (HOA) is developed combining Surrogate and AEM in order to speed up the optimization process while maintaining the same accuracy.

This chapter is based on (preprint version):

A.T.D. Perera, P.U Wickramasinghe, Vahid Nik, Jean-Louis Scartezzini, "Supervised and transfer learning methods to assist energy system optimization" (Accepted)

Author contribution for the journal paper:

In this article, ATD and PU designed the research with the support of VMN and JLS. PU developed the surrogate model. ATD developed the AEM, hybrid optimization algorithm (HOA). PU analyzed the results of the surrogate model (5.4). ATD conducted energy system analysis (Section 5.6). ATD (all the parts except Section 5.4) and PU (Section 5.4) prepared the first draft. VMN and JLS supported in revising and finalizing the Manuscript.

Readers are encouraged to read following conference proceedings for further information

1. A.T.D. Perera, Udaranga Wickramasinghe, Vahid Nik, Jean-Louis Scartezzini, Optimum design of distributed energy hubs using hybrid surrogate models (HSM), CISBAT 2017, Switzerland

5.1. Introduction

Distributed energy systems can play a vital role when integrating SPV and wind energy technologies. A number of different concepts such as virtual plants, smart micro grids, energy hubs, integrated energy systems etc. are emerging within the umbrella of distributed energy systems due to its capabilities to integrate non-dispatchable energy technologies with a minimum impact to the grid [1,2]. Distributed energy systems integrate system component which possess different characteristics, enabling to cater the demand reliably during the periods with lower wind and solar energy potential. Devices with different characteristics may result in a complex energy flow within the energy system [3]. As a result, dispatch optimization needs to be considered during the design optimization of the energy system. Considering both system design and operation strategy during the optimization process makes energy system optimization a challenging task [4]. Uncertainties in energy demand, renewable energy potential, market prices of the system components etc. further add to the difficulty [5].

A number of recent studies have focused on optimum design of distributed energy systems for multiple energy services considering both grid connected and standalone operation using bi-level optimization algorithms [4,6,7]. In these algorithms, the operation strategy (dispatch) is optimized at the secondary level, which is used to compute the operation cost of the system considering hourly changes in demand and renewable energy potential and grid conditions [8–10]. Primary level computation is used to optimize the selection of energy system components based on the dispatch strategy optimized at the primary level. Bi-level optimization algorithms require higher computational time especially in the context of considering non-dispatchable renewable energy technologies. For example, the bi-level optimization algorithm developed by Evins [10] took approximately three days to optimize to design distributed multi-energy hubs using parallel computation (operation of the energy system is optimized considering 8760 time steps using Mixed Integer Linear Programing (MILP) and system design using heuristic algorithms). Higher computational time required to formulate objective functions by using Actual Engineering Models (AEM) is considered as one major limitation. To evaluate the impact of uncertainties during the energy system optimization process it is therefore important to look into promising methods to reduce the computation time in the energy system design process [11].

Recently, surrogate models or meta-models have been used in a number of different fields to reduce the computational time of optimization problems. A surrogate model is used to by-pass the AEM, which takes more computational time when mapping decision space variables into objective space. Black-box methods such as neural networks, support vector machines (SVM), random forests etc.

have been used to develop surrogate models. According to recent literature, surrogate models have shown the potential to speed up computation more than 100 times while maintaining an up to 90% higher accuracy [12]. This has made surrogate models popular in a wide area of engineering fields such as civil, automobile, aerospace and manufacturing engineering. Surrogate models have been used frequently for building simulation in order to reduce the simulation time in building energy optimization problems [13,14]. Furthermore, components of energy systems have been optimized using surrogate models. For example, Miao et-al [15] and Cheng et-al [16] designed the PEM fuel cell using a surrogate model while Thomsen et-al [17] and Halder et-al [18,19] used surrogate models to optimize the design of wave energy converters. Kadhim and Rona [20,21] optimized the design of an axial turbine used in liquefied natural gas plants. Most of these studies used surrogate models to replace time consuming computational fluid dynamic (CFD) models. However, moving from a single component to an energy system entails a number of complexities.

Surrogate models have been seldom used to support energy system optimization. Bornatico et-al [22] use surrogate model to optimize collector area and storage size of a solar thermal energy system. Simply two variables related to the design are considered in this chapter while surrogate model is directly coupled with the heuristic optimization algorithm to obtain Pareto fronts considering multiple objectives. Sanchez and Martin used a surrogate models to presents the complex formulation of chemical plant operation when optimizing the design of an Ammonia production using renewable energy technologies [23]. Similarly to Bornatico et-al [22], the operation strategy of the energy system is not considered when developing the surrogate model. When moving into distributed energy systems variables related to the dispatch strategy also need to be considered. This will extend the number of decision variables significantly and make the surrogate model to be complicated. Furthermore, using surrogate model alone may lead to sub-optimal design solutions due to the limitations in approximating. Hence, it is important to look into promising methods that can be used to combine surrogate models with AEMs during the optimization process which has not been considered in the present state of art from the energy system design perspective. In addition to these limitations, bi-level often requires to restart from the beginning whenever there is a reasonable change in the renewable energy potential, demand and techno-economic data increasing the computational time notably. This limits the applicability of such optimization models in regional and national scale where large number of distributed energy systems need to be optimized. None of these limitations have been addressed in present state of the art.

Towards addressing the limitations the design process of an electrical hub operating in connection to the grid is considered in this chapter. Electrical hub consists of wind turbines SPV panels, wind

turbines, battery bank and an internal combustion generator (ICG). A computation platform is developed by combining a surrogate model with an optimization algorithm to assist energy system optimization. To overcome the above stated limitations this following objectives are expected to be met in this study:

- Both system design and dispatch strategy are considered (besides being limited to system design only) in the surrogate-model and the optimization process. A comprehensive study is conducted to obtain the best fitting surrogate model after considering eight configurations.
- A novel computational algorithm is developed to assist the optimization process which combines both surrogate and actual engineering model.
- Since the supervised learning model cannot be used directly when moving into other cases (where renewable energy potential, energy demand, techno-economic data might be different from the specific case the supervised learning model is trained for) a transfer learning technique is proposed to adapt the surrogate model. Such methods can significantly reduce the computational time when analyzing energy systems at regional or national scale significantly reducing the computational time.

The research paper is arranged as follow. Section 5.2 of this article presents an outline of the computational model proposed in this Chapter. Section 5.3 presents the actual engineering model (AEM) used to develop the surrogate model as well as to optimize the energy system. Section 5.4 describes the supervised and transfer learning techniques used when developing the surrogate model. Section 5.5, presents the novel optimization algorithm developed. Applicability of the model considering different cases and future applications of the model are taken into discussion in Section 5.6.

5. 2. Overview of the computational model

Energy system designing processes are often conducted as a simulation based optimization problem. The response of the energy system to the varying renewable energy potential, demand and grid conditions should be assessed when mapping decision space variables into the objective space. Usually, a time series simulation of 8760 time steps (24x360) or a set of representative time steps are considered during the simulation which can be considered as a Markov Decision Process (MDP). The objective function values depend on both system configuration and operation strategy. Hence, optimizing both system configuration and dispatch strategy while going through the time series simulation usually takes more computational time (in certain instances up to several days). This section presents an outline of the computational algorithms used and the proposed novel frame work based on supervised and transfer learning methods. Section 5.2.1 explains the present

approaches while Sections 5.2.2 and 5.2.3 present newly introduced computational models that can be used to reduce computational time when designing distributed energy systems. Section 5.2.4 presents an approach that can be used to generalize the computational model for other locations with the support of a transfer learning technique.

5.2.1. Actual engineering model (AEMs)

Energy system operation (selection of dispatchable source, storage and grid) has a direct influence on optimum system sizing. Therefore, operation of the energy system should be considered on an hourly basis to take into account the changes in renewable energy potential, demand and grid conditions. According to [24,25], two approaches are used in this context, aligned with dynamic programing [24,25]. The first method is closely related to the value function method where operation strategy of the energy system is optimized on an hourly basis. This is usually practiced when designing a complex poly-generation system, which will result in extensive computational time. The second method is based on a policy function method where it is assumed that there is an optimum policy that governs the operating state of the energy system, which has to be optimized along with the system configuration. The operation of the energy system needs to be considered on an hourly scale throughout the years in both the scenarios, which will result in higher computational time (Fig. 5.1). Hence, irrespective of the method used, the energy system optimization process takes a more computational time. This study uses the second approach for AEM. AEM is used to obtain a training data set to train the surrogate model. Furthermore, it is used to map decision space variables to the objective space in the proposed novel computational algorithm with the support of the developed surrogate model.

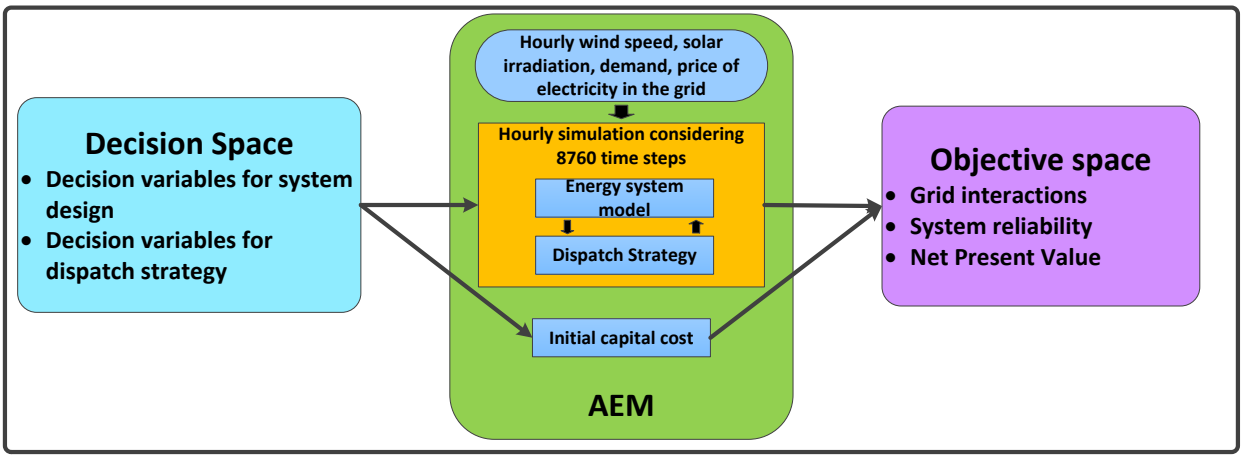

Fig. 5. 1: Flow chart for the Actual Engineering Model (AEM). Decision space variables are mapped into the objective space through the AEM.

5.2.2. Supervised learning to develop surrogate model

Surrogate models are black box models such as neural network, Support Vector Machines (SVM) etc. They simply present the relationship between input and output bypassing a computationally extensive model, which takes longer computational time (Fig. 5.2). Although surrogate models are fast in computation, black box models cannot completely replace actual engineering models (AEM), which are computationally extensive. Such data driven approaches can be used to minimize the extensive computational processes and detailed information related to both analytical and numerical models. Specific to the energy system optimization process, surrogate models are used to reduce the computational time required for time series simulation when mapping decision space variables to the objective space. Three steps are required when using the surrogate models to design energy systems:

1) Create a data set for training and validating the surrogate model
2) Use a supervised learning method to develop the surrogate model
3) Optimize the energy system using the surrogate model

The AEM described in Section 5.2.1 is used to create the data set that is used to create the surrogate model. Subsequently, several supervised learning techniques have been used to train the surrogate model and evaluate its performance. A comprehensive overview of these techniques can be found in Section 5.4. The surrogate model only maps the decision space variables into the objective space. In order to optimize the design, an optimization algorithm needs to be used to obtain optimum design by using the surrogate model.

5.2.3. Hybrid Optimization Algorithm combining surrogate and AEM models

AEMs are more accurate in comparison to surrogate models when computing the objective function values. However, it takes much longer to compute the objective function values using AEM. Furthermore, developing a surrogate model with a very high level of accuracy will demand extensive training of the surrogate model and this in turn will demand a larger set of training data resulting in more computational time. An optimum combination of a surrogate model and an AEM will help to sort out this issue while significantly minimizing the computational time required for the energy system design process. The Hybrid Optimization Algorithm (HOA) combines both AEM and surrogate models in order to speed up the computation (Fig. 5.3). A surrogate model is initially used with the optimization algorithm to generate the initial Pareto front. Thereafter, the initial Pareto front is used as the starting point for the secondary stage optimization which is using AEM. The higher computational speed of the surrogate model helps the optimization algorithm to reach the Pareto front faster. However, AEM is used in the second stage which maps decision space variables into the

objective space with a better accuracy. In HOA, the surrogate model helps reach the actual Pareto front within a short period of time, which is later refined using the AEM.

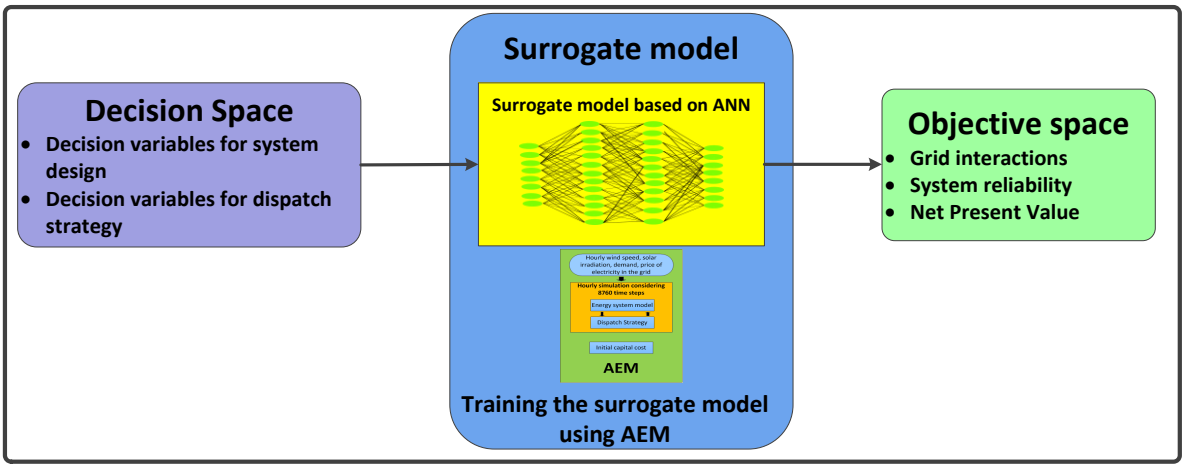

Fig. 5. 2: Flow chart for the surrogate model. Decision space variables are mapped into the objective space through the surrogate model. AEM is used to generate a data set in order to train the surrogate model.

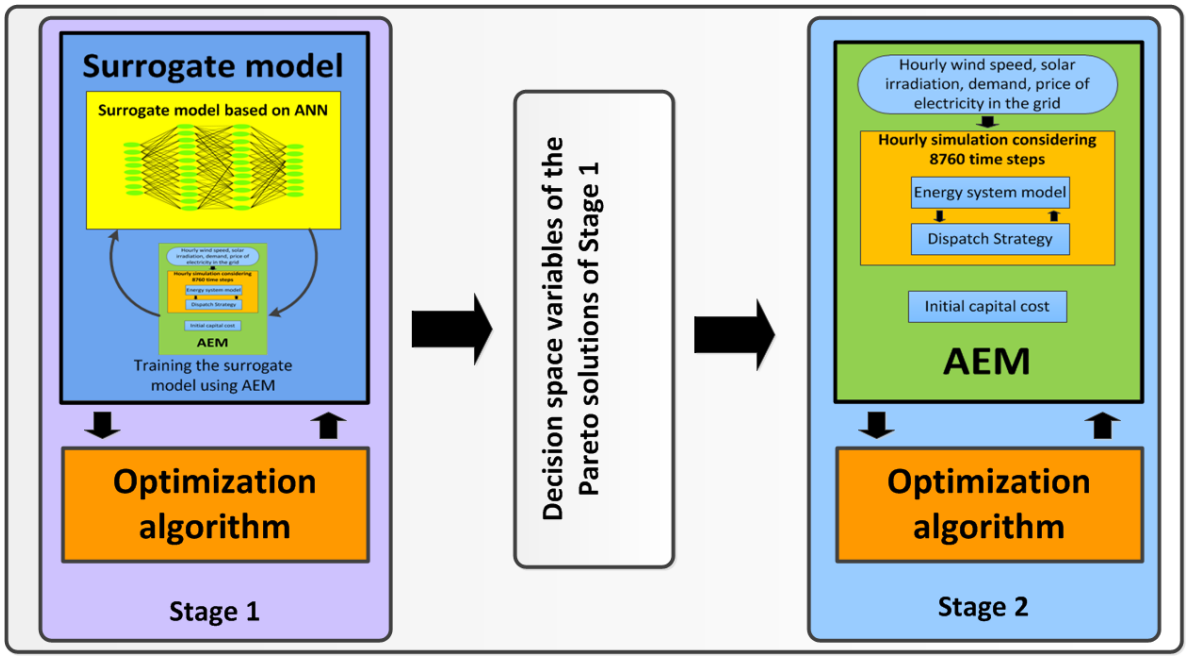

Fig. 5. 3: Flow chart for HOA combining the surrogate model and AEM. The surrogate model helps to come up with a better starting point to the AEM, thus speeding up the computation process.

5.2.4. Transfer supervised learning algorithm

The development presented in Sections 5.2.2 and 5.2.3 are focused on optimizing distributed energy systems for a specific location. Often, it is required to start the optimization process from the beginning when moving to another location. This is one major limitation which hinders the use of AEM at national or regional scale planning where a large number of distributed energy systems need

to be optimized considering their interactions. One major advantage of a data driven approach is that the model obtained using supervised learning can be adapted to other locations with certain changes. The adapting process is not as intensive as the initial training process (Fig. 5.4). As a result, the computational time required to develop the surrogate model is significantly reduced. The process used to adapt the surrogate model is known as transfer learning. The main advantage of transfer learning is that it minimizes the amount of labeled data required for the training process while minimizing the time required to generate the labeled data and the training process. Fig. 5.4 presents the approach used in the present study for the model adaptation. The surrogate model initially developed for a specific location is adapted for another location using transfer learning. A set of labeled data is generated for the new location using the AEM for the transfer learning process. Accelerated GPU (Graphics Processing Unit) computing is used to speed up the process of generating data. By using the labelled data generated for the new location, the surrogate model is transfer learned. Finally, the Surrogate Model trained using Transfer Learning (SMTL) replaces the surrogate model trained using supervised learning in the HOE as shown in Fig. 5.4.

5.3. Mapping of decision space variables to the objective space using AEM

An energy hub consisting of renewable energy sources, energy storage and ICG operating connected to the grid is considered in this chapter when developing the AEM. Techno-economic aspects related to the energy system are considered in the computational model using lifecycle simulation. The computational model evaluates the lifecycle cost, system autonomy, reliability, utilization of renewable energy, etc. through a life cycle simulation. The AEM presents the simulation based computational model used to map decision space variables representing both system design and operation strategy into the objective space. Grid integration level and NPV are considered as the objective functions. The formulation of objective functions is explained in Chapter 2 in detail.

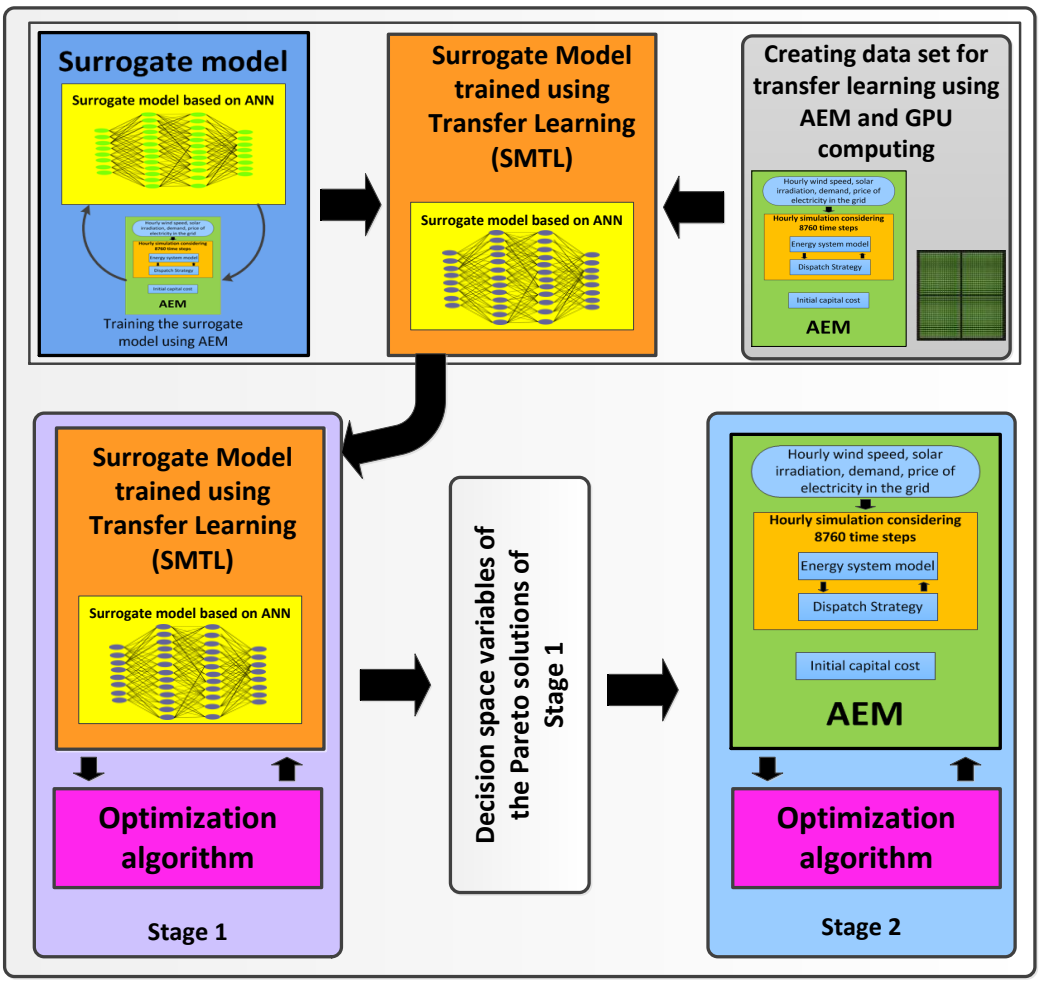

Fig. 5. 4: Outline of the architecture used to develop SMTL and combine the SMTL with the HOA.

5.4. Hybrid surrogate model to present energy system

There are number of different methods such as Support vector Machines (SVM), Artificial Neural Networks (ANN), Linear Regression (LR) etc. can be used to develop surrogate models. In recent past, ANN has shown to be promising in number of areas with the arrival of deep learning. Therefore, ANN are selected to be used for the surrogate model in this study. In simple, ANN consist of set of neurons where each neuron facilitates a non-linear mapping between input and output. However, arriving at the optimum architecture for the neural network is a difficult task due to the larger number of combinations that are possible to consider. Hence, a pool of combinations are considered for the architecture which consist of neural networks having different number of layers and neurons per each layer as shown in Table 5.1. The architectures considered in this study consist of neural networks consisting of two layers up to thirteen while increasing the complexity of the architecture.

Optimization is done using Levenberg-Marquardt backpropagation (Damped least square) method. Mean Square Error (MSE) is used as the loss function and no regularization term is used. Training, validating and testing datasets used in the training of initial model consist of 448000, 192000 and 640000 respectively. Afterwards, transfer learning is used to adapt the initial neural network to other scenarios. Transfer learning is a strategy in machine learning used to adopt a model trained on one dataset to another which is not exactly same, but is related. In this case, it is done by continuing the training of the initial model on a dataset corresponding to the scenario that needs to be adopted. This dataset is smaller in-size compared to the dataset used in the initial training. It consists of 7000 samples for training, 3000 samples for model validation and 10000 for testing. During the transfer learning stage, same parameters are used as in the initial training stage apart from the difference in dataset.

The performances of these neural networks are evaluated based on Mean Absolute Error (MAE).Based on this metric, it is observed that increasing number of layers as well as increasing the number of neurons per layer decrease the MAE. However, for the architectures that are tested, best performance is obtained with a shallow network with 2 layers and each of them consisting of 50 neurons. Results for y1 (output Variable 1 (O1)) one is summarized in Table 5.1. When analyzing the results it is prudent that accuracy of the prediction accuracy increases when increases while increasing the number of layers. This can be observed when moving from AR1 to AR6 where the mean AEP reduces from 4.35 to 2.85. However, extending the ANN by adding layers will demand for higher computational time for training while demanding more computational time during the prediction. Hence, the possibility to improve the prediction error by widening the neural network is subsequently considered. AR7, 8 and 9 are introduced by widening the neural network. When moving from AR6 to AR7 a significant drop in the Mean AEP is observed. However, an improvement in Mean AEP is observed when moving from AR6 to AR8 with the significant widening of the neural network architecture even with two hidden layers. To analyze the influence of both widening and deepening, two more hidden layers are added to AR8 and created AR 9. A significant improvement in Mean AEP is observed as a result of the modification. However, the modification introduced in AR9 increase the number of parameters as well as the prediction time notably. As a result, AR9 cannot be used besides its higher accuracy. AR8 is used in this study as the architecture for the surrogate model.

Table 5. 1: Architecture of the neural networks considered in this study

Neural Network	Number of hidden layers	Number of neurons in each layer	Mean AEP
AR1	2	16,8	4.35
AR2	3	18,14,8	3.39
AR3	5	18,18,14,10,6	2.79
AR4	5	20,18,18,16,16	2.80
AR5	9	20,18,18,18,18,16,16,16,16	2.93
AR6	13	20,18,18,18,18,18,18,16,16,16,16,16,16	2.85
AR7	2	25,25	3.09
AR8	2	50,50	2.33
AR9	4	50,50,50,50	1.48

5.5. Optimization algorithm

Optimization algorithms have been used in two different parts of this study. An optimization algorithm is used initially to train the surrogate model. Afterwards, it is used to optimize the energy system. A concise overview of the stochastic gradient decent (SGD) algorithm used to train the surrogate model is presented in Section 5.4. This section is focused on the second application where optimization of the energy system is considered.

Both AEM and the surrogate model map decision space variables into the objective space. AEM uses a time series simulation where both system configuration and policy function related to the dispatch strategy are considered as the decision space variables (Table 5.2). The surrogate model uses a fully connected feed forward neural network to map the decision space variables into the objective space. An optimization algorithm is required to arrive at the optimum solution irrespective of the method used to map the decision space variables. When it comes to energy system optimization, there are a number of instances where the objective functions have been formulated considering the restrictions in optimization algorithm. As a result linear programing and mixed integer linear programing have been amply used when designing distributed energy systems. At the same time, a number of recent studies have used heuristic methods to design distributed energy systems. However, the objective functions obtained using surrogate models based on neural networks are neither linear nor convex. The optimization algorithm introduced in this study should possess the

capability to interact with both AEM and the surrogate model. Hence, it is inevitable to consider an optimization technique other than a heuristic method.

5.5.1. Implementation of the optimization algorithm along with AEM and surrogate model

The optimization algorithm is connected with the surrogate model and AEM according to Fig 5. 5. Two orange blocks represent the elements of the optimization algorithm. The light blue and green blocks represent the elements of the surrogate model and AEM respectively. The steady ε-State Evolutionary Algorithm [34] is used for the optimization algorithm which is proven as a method to maintain the diversity while reaching the final set of Pareto solutions. The polynomial mutation operator [35] and simulated binary crossover operator [36] are used along with differential evolutionary operators [77]–[79] in the reproduction of the population. The Constraint Tournament Method [35] is used to consider the constraints that are not handled at the level of dispatch strategy. Computational time for the Pareto front depends on the objective functions selected and the number of generations considered.

The optimization algorithm follows Path 1(orange block-blue block and orange block) when optimizing the energy system using the surrogate model. The decision vector required to evaluate is transferred to the blue box. The surrogate model directly maps the decision vector to the objective space which helps to obtain the objective function values and constraint violation. These values are transferred to the orange-block, which evaluates the objective function values and subsequently updates the population and archive. Similar to the surrogate model, Path 2 is followed when using the AEM (orange block-green block and orange block). The decision vector required to evaluate is transferred to the green block. As opposed to Path 1, a detailed time-series simulation is conducted to map the decision vector into objective space. Hourly wind speed, solar irradiation and energy demand data are used for the time series simulation as explained in Chapter 2. Subsequently, objective function values and constraint violation are transferred to the orange-block to update the population and achieve.

5.5.2. Hybrid optimization algorithm (HOA) combining AEM and surrogate model

Section 5.5.1 describes the outline of the optimization algorithm when using either the surrogate model or AEM. However, the same structure cannot be adapted when combining these two algorithms. The surrogate model is faster when computing the objective function values. However, the accuracy of objective functions and constraints might not be very high in certain instances. In contrast, AEM takes longer for the computation but shows higher accuracy when computing the objective functions and constraints. Hence, the surrogate model is used to arrive at a better starting

point to the optimization algorithm based on AEM. As shown in Fig 5.6, an optimization algorithm based on the surrogate model is used as the first step. Subsequently, the population and archive (Pareto solutions) are moved to the next step. However, it is important to check the values for objective functions and constraints before direct use in the AEM (since there are certain limitations in the surrogate model when computing both objective functions and constraints). Therefore, in Step 2, AEM is used to simulate both archive and population (obtained using the optimization algorithm based on the surrogate model). Afterwards, dominance of the Pareto solutions is rechecked and, population and archive (set of Pareto solutions) are updated. The updated archive and population are transferred to Step 3. Updated archive and population obtained from the surrogate model are an efficient starting point for the optimization algorithm. Thereafter, the optimization algorithm will use the AEM in order to further improve the Pareto solutions using AEM.

Table 5.2: Decision space variables considered for the optimization problem including both system configuration and operation strategy

Variable	Lower bound	Upper bound	Interval	Description
SPV Type ($^{NTY\text{-}SPV}$)	0	3	1	Mono-crystaline, Polycrystaline and Amorphous[1]
# SPV Panels N_{SPV}	0	120	1	
Type of Turbines ($N^{TY\text{-}W}$)	0	2	1	1, 5 kW
# Wind Turbines	0	30	1	
# Battery banks	0	20	1	0-240[3] kWh
ICG Capacity (kVA)	0	15	0.5	
$W_{i,j}$ (weight matrix)	0%	100%	Continuous	
Seven rules ($r\,(r \in \mathrm{N})$)corresponding to the finite states			Continuous	

[1] 0.5 kW maximum capacity

[3]Each battery bank having 12 kWh capacity

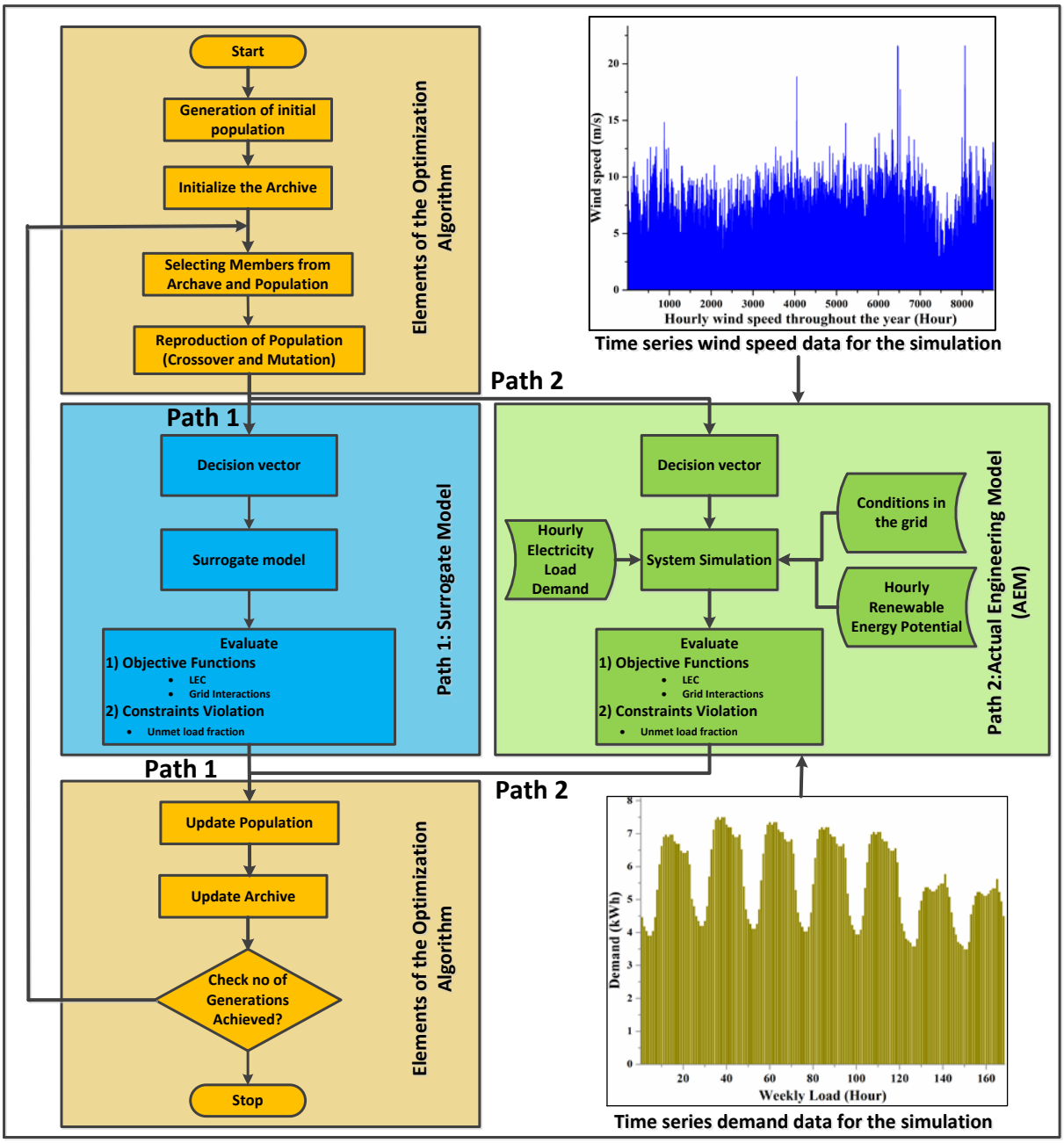

Fig. 5. 5: Presents the implementation of the optimization for the surrogate model and AEM. The two orange boxes represent the elements of the optimization algorithm common for both the surrogate model and AEM. Path 1 is taken when using the surrogate model (blue box) while Path 2 is taken when using the AEM (green box).

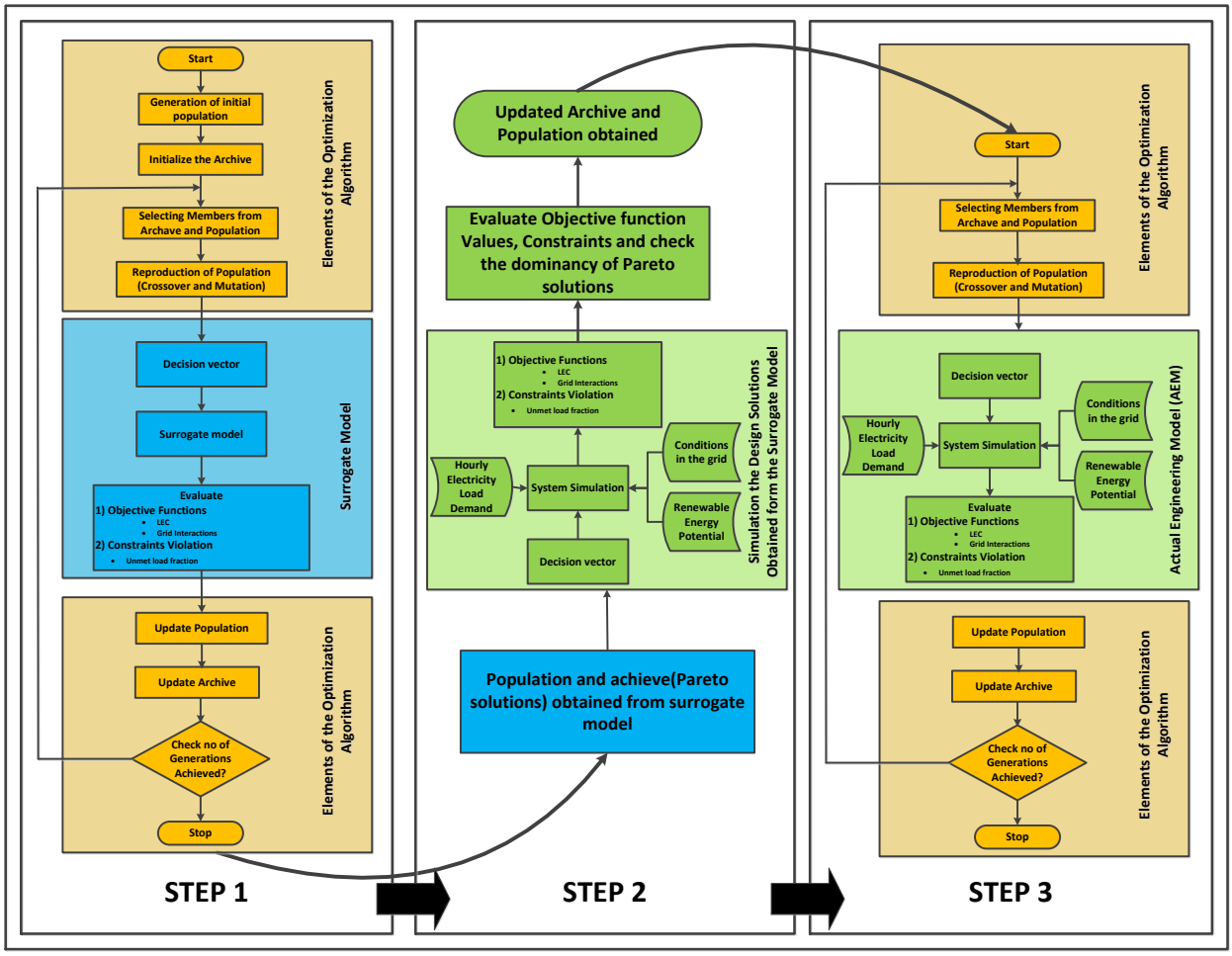

Fig. 5. 6: Presents the implementation of the Hybrid Optimization Algorithm (HOA), which consists of three steps. A surrogate model is used initially to reach a better starting point with regard to the AEM in a short period of time (Step 1). In Step 2, Pareto solutions obtained using the surrogate model are simulated again using the AEM and the Pareto solutions are updated based on the objective function and constraint values obtained using the AEM. Subsequently, these Pareto solutions are transferred into the optimization algorithm which uses AEM in Step 3 in order to obtain the final Pareto solutions.

5.6. Results and discussion

The results and discussion section is mainly divided into two main parts. The first part demonstrates the development of supervised and transfer learning models used for the replication of the AEM. The second part is devoted to analyzing the performance of different techniques that are used to combine AEM with surrogate models that are developed using supervised and transfer learning techniques.

5.6.1. Comparison of the Pareto fronts obtained using AEM and surrogate models

Pareto fronts obtained considering both AEM and surrogate models are presented in Fig 5. 7. The Pareto fronts overlap when the grid integration levels are higher (Region Q in Fig 5. 7). However,

they start to divert from each other when grid integration levels are below 10% (Region P Fig 5. 7). NPV begins to increase at a much higher rate for the Pareto front obtained using the surrogate model when grid integration levels are below 10%. As a result, a significant difference in NPV can be seen when the grid integration levels are within the range of 1-5%. The difference in NPV between AEM and the surrogate model slightly decreases when reaching the fully autonomous state (due to the sudden increase in NPV observed in AEM Pareto front when reaching the fully autonomous state). The Pareto front only indicates the reflection of the decision space variables on the objective space. The most important factor to be analyzed is the similarity between the decision space variables corresponding to Pareto solutions which are obtained using two models that are close to each other.

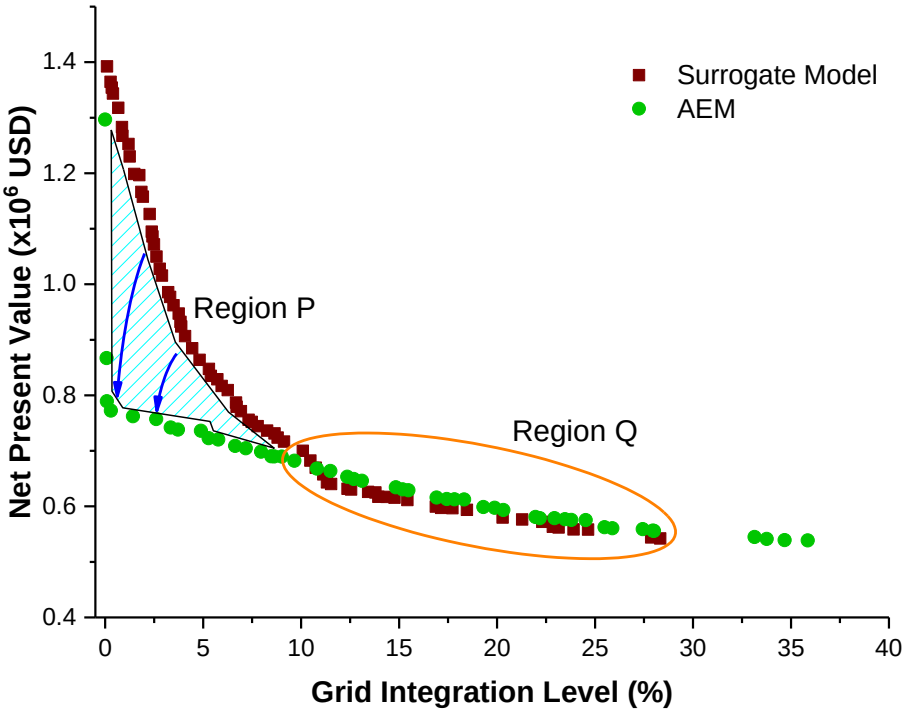

Fig. 5. 7:: Presents the two Pareto fronts obtained using Surrogate and AEM. Region Q represents the region where both Pareto fronts overlap with each other. Region P represents the sector which a significant deviation among the two Pareto fronts can be observed. Semi supervised techniques such as Active learning can be used to further improve the accuracy of the surrogate model by taking samples from Region P and further training the AEM.

In order to understand the applicability of the surrogate model, Pareto solutions with similar grid integration values are taken from both Pareto fronts and tabulated in Tables 5.3 and 5.4. Table 5.3 contains the design solutions which maintain grid interaction levels above 10% while Table 5. 3 presents the design solutions with grid interaction levels less than 10%. Comparing the design solutions is challenging due to the higher dimensionality of the decision space. Besides taking all the

decision space variables, system configuration variables are tabulated in both Table 5. 3 and 4. The ratio between solar PV to wind turbine installed capacity and dispatchable to non-dispatchable installed capacity is taken to support the analysis. Designs A, B, C and D respectively present design solutions with similar grid interaction levels. Respectively, A-AEM and A-S are obtained using actual engineering and surrogate models.

Table 5. 3: Comparison of Pareto solutions of the AEM and surrogate model obtained for grid interactions higher than 10%

		NPV ($x10^6$USD)	GI (%)	SPV capacity	Wind capacity	wind : SPV	Battery banks	ICG capacity	ICG :non-dispatchable
A	A-AEM	0.6461	13.10	67.6	75	1.11	9	10	7.01
	A-S	0.6261	13.43	59.8	85	1.42	11	10	6.91
B	B-AEM	0.6132	17.44	67.6	70	1.04	8	10	7.27
	B-S	0.5966	17.73	63.7	90	1.41	10	7.5	4.88
C	C-AEM	0.5935	20.32	62.4	75	1.20	8	10	7.28
	C-S	0.5798	20.29	55.9	90	1.61	9	7.5	5.14
D	D-AEM	0.5605	25.89	58.5	65	1.11	8	10	8.10
	D-S	0.5582	24.64	58.5	85	1.45	10	10	6.97

Table 5. 3 presents the Pareto solutions from the section where both AEM and surrogate models overlap (with grid integration equal or above 10%). When comparing the Pareto solutions, it is clear that the design solutions look close to each other when comparing the wind turbine, solar PV, battery bank and ICG capacities. When comparing the two sets, it can be seen that the solar PV capacity is slightly higher in the Pareto solutions obtained using AEM. For example, installed solar PV capacity decreases by respectively 7.8, 3.9 and 6.5 kVA when moving from AEM to surrogate models (respectively in A, B, C), resulting in a change of 11.5, 5.7 and 10.4 % respectively. In contrast, wind turbine capacities are higher in Pareto solutions obtained using the surrogate model. For example, wind turbine capacity increase by 10, 20 and 15 kVA when moving from AEM to surrogate models (respectively in A, B, C), resulting in a change of 13, 29 and 15 % respectively. When compared to solar PV capacity, wind turbine capacity shows a significant deviation. As a result, the ration of wind turbine capacities to solar PV capacities increases when moving from the AEM to the surrogate model. Similarly, a deviation in ICG and battery bank capacities can be observed. Finally, it can be concluded that the system configuration shows notable deviations although the objective function values looks quite closer each other when the grid integration level is above 10%.

Table 5. 4: Comparison of Pareto solutions of the AEM and surrogate model obtained for grid interactions less than 10%

		NPV ($x10^6$USD)	GI (%)	SPV capacity	Wind capacity	wind : SPV	Battery banks	ICG capacity	ICG :non-dispatchable
E	E-AEM	0.6680	10.81	67.6	80	1.18	9	10	6.78
	E-S	0.7000	10.09	70.2	65	0.93	14	10	7.40
F	F-AEM	0.7204	5.77	68.9	85	1.23	10	10	6.50
	F-S	0.8167	5.95	71.5	45	0.63	20	10	8.58
G	G-AEM	0.7420	3.35	75.4	80	1.06	11	10	6.44
	G-S	0.9772	3.32	58.5	40	0.68	20	12.5	12.69
H	H-AEM	0.7573	2.60	75.4	85	1.13	11	10	6.23
	H-S	1.1578	1.93	55.9	25	0.45	20	15	18.54
I	I-AEM	0.7623	1.42	68.9	85	1.23	10	10	6.50
	I-S	1.1986	1.49	81.9	0	0.00	20	25	30.53

When moving from Table 5. 3 to Table 5. 4, a clear deviation in objective function values can be noticed. A significant increase in NPV is observed when moving design solutions obtained using AEM to the surrogate model (as observed in Fig 5. 7). This makes it interesting to analyze the design solutions further in order to reason out the deviations observed. When comparing the design solutions of the two sets, a slight deviation in solar PV panel capacity is observed. Major deviations can be observed in the two sets when considering wind turbine, ICG and battery bank capacities. Wind turbine capacity drops when reducing the grid interaction levels for the Pareto solutions of the surrogate model. For example, wind turbine capacity drops from 65 kVA to zero when moving from E-S to I-S. As a consequence of the reduction in wind turbine capacity the ratio of wind turbine to solar PV capacity gradually drops in Pareto solutions obtained using the Surrogate model when reducing the grid interactions. In contrast, the capacities of both battery bank and ICG increase with the reduction in grid interactions. For example, the ICG capacity increases from 10 to 25 kVA. As a consequence of the reduction in wind turbine capacity and increase in the ICG capacity, the ration between dispatchable to non-dispatchable capacities increases significantly when minimizing grid interaction levels for the Pareto solutions obtained using the surrogate model. Such clear patterns in system configuration are not visible for the Pareto front solutions obtained using the AEM although complex patterns can be observed for the decision space variables corresponding to the dispatch strategy.

The patterns observed in the Pareto solutions obtained using the surrogate model such as increase in energy storage, dispatchable energy source and reduction in non-dispatchable energy capacity (wind turbines since seasonal fluctuations in wind speed are significant compared to solar energy potential) are typical conditions expected in standalone operation [26,40]. However, introducing grid

integration and advanced energy management enables the system to maintain a higher autonomy without a significant change in the energy system for the specific example. As a result, a noticeable pattern in system configuration is not observed for the Pareto solutions obtained using the AEM. When comparing the design space variables, it is evident that the complexity introduced by the decision space variables corresponding to the dispatch strategy has not been properly learnt by the surrogate model using the supervised learning method when grid integration levels are low. As a consequence, the Pareto front obtained using the surrogate model diverts from the one obtained using AEM following the general trend. However, the surrogate model presents better results when it comes to higher grid integration scenarios. This makes it important to further train the surrogate model considering scenarios where grid integration levels are low. Active learning techniques can be used in this context that can help to improve the accuracy of the surrogate model (Fig 5. 7).

5.6.2. Assessment of computational time for AEM, surrogate and hybrid models

The analysis conducted in Section 5. 6.2 demonstrates that the surrogate model can approximate the objective function values close to the Pareto solutions obtained using AEM in certain parts of the Pareto front. Furthermore, the surrogate model can provide a reasonable approximation for the decision space variables for a certain part of the Pareto front. However, it is clear that the surrogate model cannot be used alone to derive the Pareto solutions although it is efficient when computing the objective functions. The HOA introduced in this study becomes attractive in this context since it combines both surrogate and AEM. However, it is important to evaluate the boundary conditions valid for approximating the Pareto solutions using the surrogate model followed by AEM. When analyzing these Pareto fronts, the ratio of generation (REG) between AEM and surrogate model plays a vital role (Fig 5. 8). A higher REG (greater than 1) implies that the optimization algorithm uses the AEM for a larger number of generations than the surrogate model. Increasing the REG will extend the computational time since AEM takes longer for the computation. In contrast, AEM provides an accurate mapping of the decision space variables into the objective space. Hence, determining the optimum REG is important considering both convergence and computation time. Towards achieving this goal, a multi objective optimization is conducted considering different REG values. Among these scenarios, HOA 1 presents the case where the surrogate model is used for a larger number of generations when compared to HOA 2 and 3. Similarly, HOA 3 presents the case where AEM is used for a larger number of generations when compared to HOA 2 and 1. When comparing the HOA, no significant difference can be seen when moving from one to another (Fig 5. 8). More importantly, the objective function values of HOA 1 (which uses the surrogate model for a larger number of generations compared to HOA2 and 3) tend to follow the Pareto front obtained using AEM even

when the grid integration levels are below 10%. Hence, it can be stated that the surrogate model can be effectively merged with AEM using the HOA. Furthermore, the computational time decreases by 83% for the optimization process when using HOA 1, which is a significant achievement. However, it is interesting to assess the adaptability of the model for other cases where renewable energy potential and demand are different.

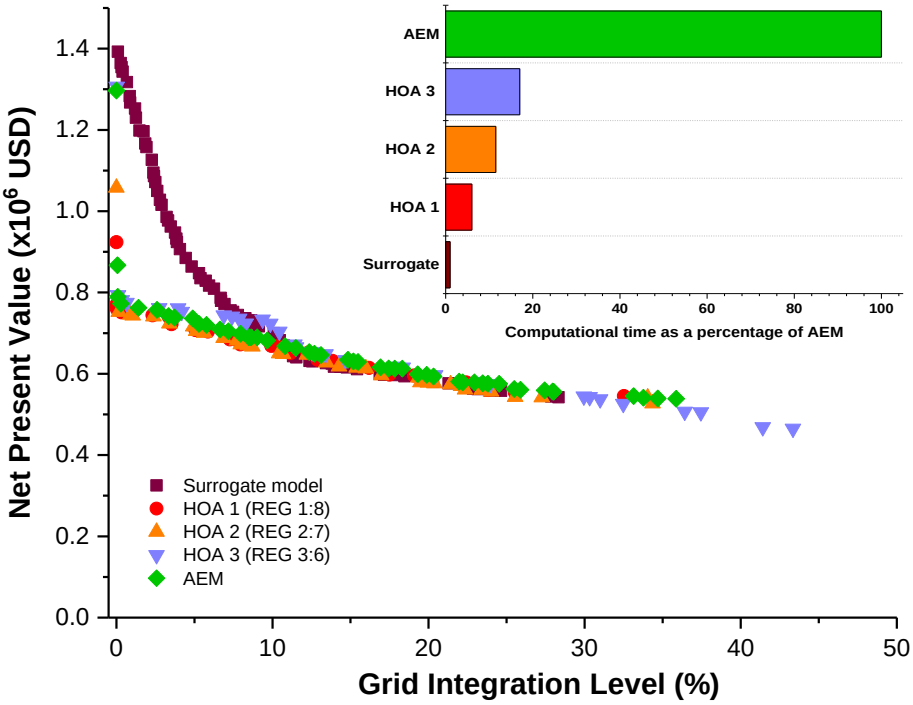

Fig. 5. 8: Presents Pareto fronts obtained using different ratios of surrogate model to AEM. The three optimization algorithms with different combination ratios can reach the Pareto solutions in a fraction of the time taken by the AEM

5.6.3. Comparison of the Pareto fronts for transfer-supervised learning

Sections 5.6.2 and 5.6.3 show the potential surrogate model to approximate the mapping of decision space variables into the objective space which can be used to minimize the computational time required for the energy system optimization. The main advantage of developing a surrogate model is its diverse applicability through modal adaptation. As discussed before, transfer learning facilitates adapting the surrogate model developed using supervised learning. In order to assess the model adaptation capability, six different scenarios are taken where the renewable energy potential for solar PV (SPV 1 and SPV 2), wind (Wind 1 and Wind 2) and demand (Demand 1 and Demand 2) profiles are different from one another. AEM is used to generate the Pareto solutions for different scenarios as the first step of the analysis (Fig 5. 9).

The changes observed in the Pareto fronts in Fig 5. 9 are consequences of the changes introduced in demand, solar and wind energy potential. It is interesting to assess the capability of transfer learning

to adapt the surrogate model trained for the initial conditions. When comparing the Pareto fronts obtained using AEM, it is prudent that SPV 1 and 2 closely follow the Initial Scenario. However, notable changes in the Pareto fronts are observed for Scenarios Demand 1, 2 and Wind 1, 2. For example the shape of the Pareto front notably changes when moving from initial scenario to Wind 2 as a consequence of the changes introduced in the scenario. It is interesting to evaluate the adaptability of the surrogate model through transfer learning (SMTL). Towards this end, Pareto fronts obtained entirely using SMTL are compared with AEM for different scenarios (Fig 5. 10). When comparing the Pareto fronts obtained using AEM and SMTL, it is clear that SMTL provides a good approximation when considering the objective function values for all scenarios. For example, Pareto fronts obtained using SMTL and AEM for Scenarios SPV 1 and 2 closely follow each other when minimizing the grid interactions until a grid interaction level of 10% is reached (similar to the Pareto front obtained using AEM and the surrogate model for Initial Scenario) (Fig 5. 10). Demand 1 Scenario introduces a significant change to the Pareto front obtained using AEM (Fig 5. 9). Nonetheless, SMTL provide a better approximation to the AEM for the scenario Demand 1. When considering the scenario Wind 2, Pareto front solutions obtained using AEM show a complex variation in the objective space when compared to the Initial Scenario. However, it is observed that the SMTL has the potential to closely follow the AEM when decreasing grid interactions to 6%. In conclusion, it can be stated that the objective function values obtained using STML alone provide a better approximation, similar to the surrogate model trained using supervised learning. Hence, STML becomes a better substitute for the surrogate model and can be effectively used whenever boundary conditions are changed.

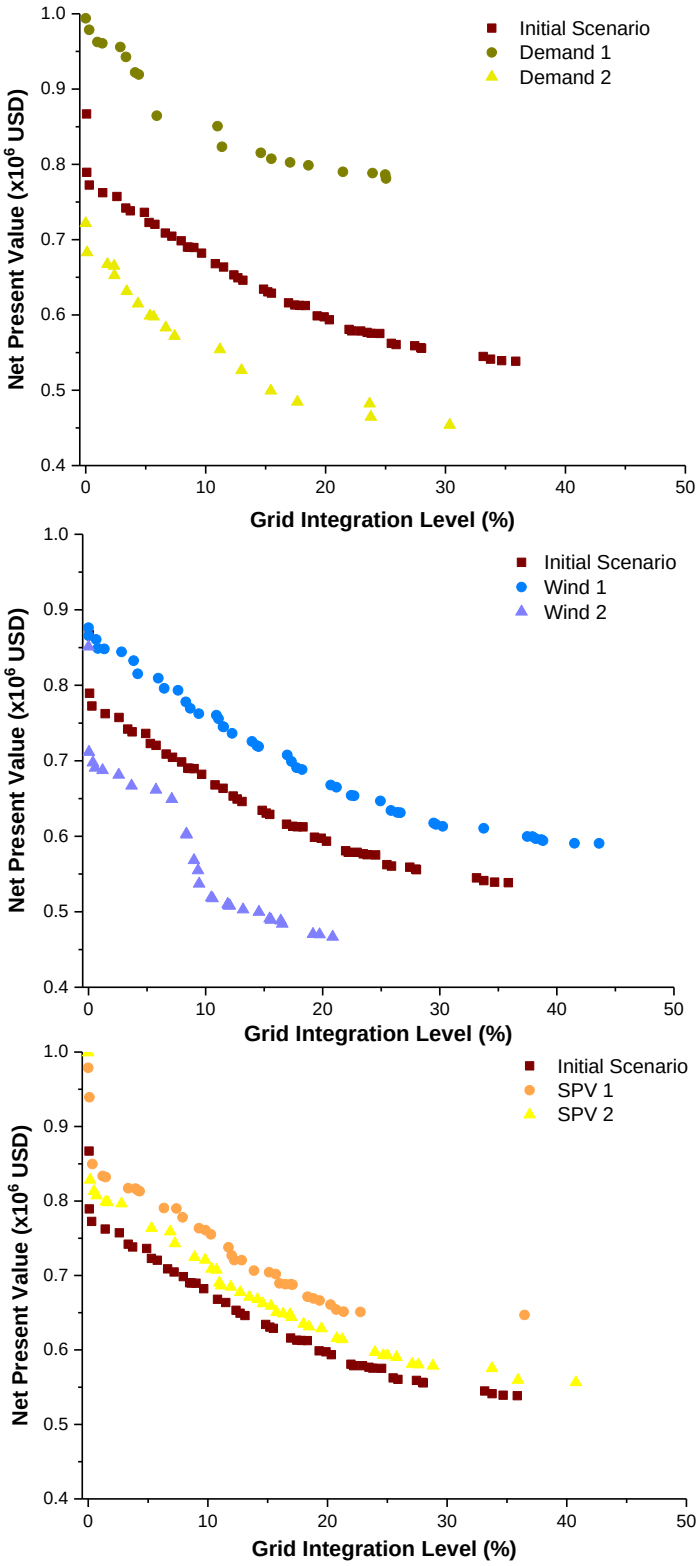

Fig. 5. 9: From top to bottom presents the Pareto fronts obtained using the AEM for six different scenarios.

Similar to the surrogate model, SMTL is combined with AEM by using HOA (SMTL replaces the surrogate model) and found that REG of 1:8 is sufficient for the Pareto front to be similar to the

initial scenario where the surrogate model is trained using supervised learning. This makes it interesting to analyze the entire computational time required to train the computational model and conduct the optimization. The computational time includes the time required to generate the data set for transfer learning, computational time for transfer learning and optimization (Fig 5. 11). When compared with the optimization algorithm based on AEM, a significant drop in computational time can be observed when using SMTL along with the HOA (REG of 1:8). The computational time required all together for generating the data points using the AEM for transfer learning, transfer learning for the model and subsequently optimizing the energy system takes 15.3 % of the computational time required for the AEM. Such a significant drop in the computational time required for energy system optimization will enable optimizing energy systems at regional and national scale consisting of a large number of distributed energy systems.

5.7. Conclusions

Distributed energy systems play a vital role in the renewable energy integration process. Optimum design of distributed energy systems is a computationally intensive process which may take several days in certain instances. Furthermore, the optimization process is not flexible enough to adapt to changes in renewable energy potential, demand and other input data. As a result, an optimization algorithm needs to be implemented from the beginning, when there are changes in the aforementioned factors. Therefore, it is challenging to evaluate the potential for distributed energy systems in regional and national scale using bottom up models.

Supervised and transfer learning techniques have been used in this study to improve the computational speed and model adaptation. The surrogate model developed shows the potential to approximate the objective function values of the Pareto solutions with a higher efficiency. However, there is a significant deviation in system design for the Pareto solutions obtained using the surrogate model. When analyzing the Pareto solutions further, it is revealed that the surrogate model possesses the potential to predict the general trend of renewable energy components, battery bank and ICG. However, it fails to predict the changes in system operation variables. This specific weakness can be improved using active learning which will be an extension to the present study. The surrogate model can be effectively combined with the AEM using the novel optimization algorithm introduced in this study (HOA). The novel computational algorithm can reduce the computational time of the optimization process significantly (by up to 94 %).

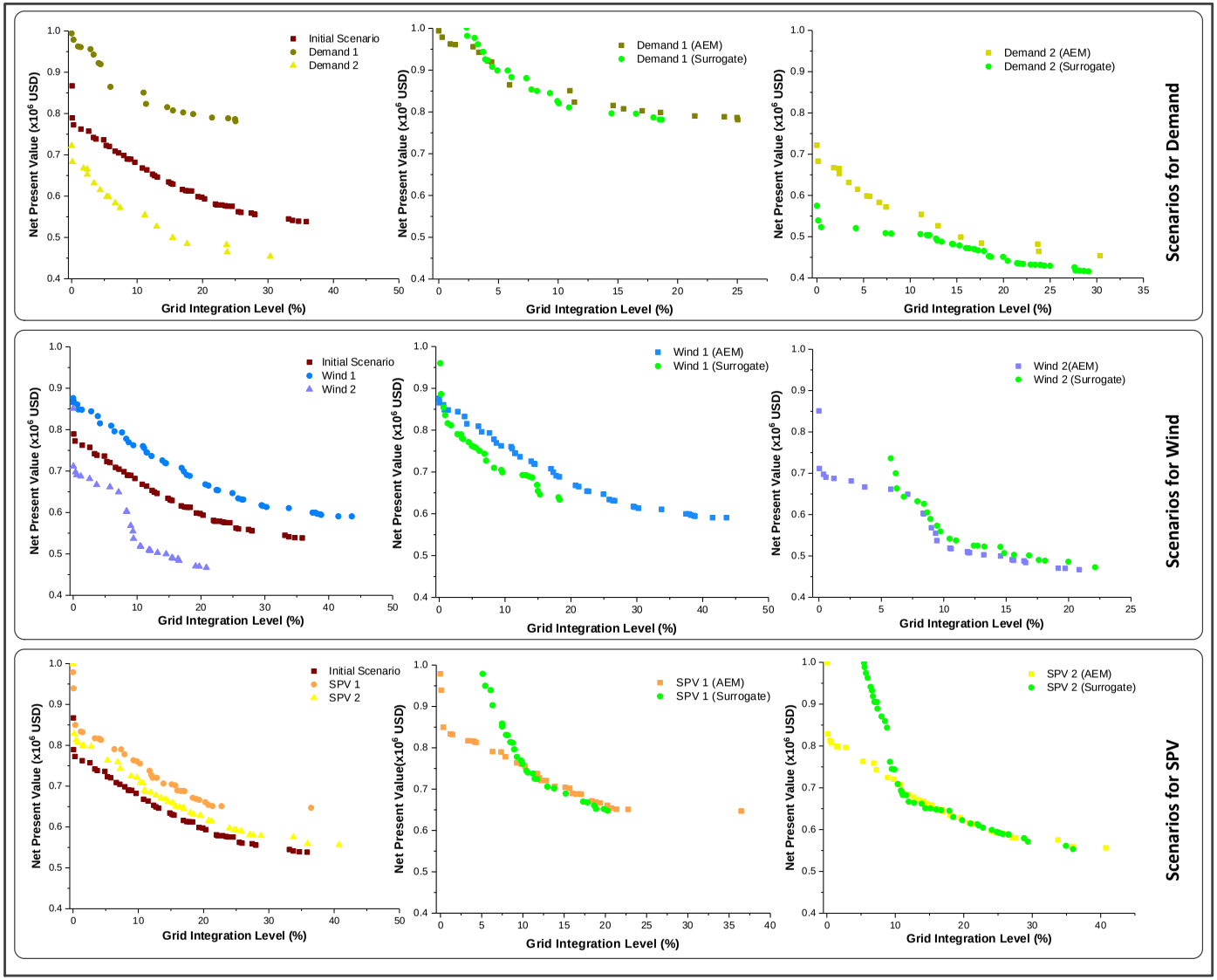

Fig. 5. 10: Presents the Pareto fronts obtained using the surrogate model that is trained using transfer learning (SMTL) technique for a data set consisting of 10000 data points.

The surrogate model initially trained for one specific scenario is later adapted using transfer learning for six different scenarios where solar, wind and demand profiles are notably different. A data set (10000 data points) is generated using the AEM to train the surrogate model. SMTL is developed with the assistance of the initial surrogate model through transfer learning. SMTL has the potential to approximate the Pareto solutions with the support of an optimization algorithm with a similar accuracy achieved by the surrogate model trained using supervised learning. HOA that combines the surrogate model and STML can reach the Pareto solutions within a fraction of time taken by the AEM reducing the computational time by 84%. Such a significant reduction in computational time facilitates use of the proposed method for evaluating the potential of a large number of distributed energy systems at regional and national scale.

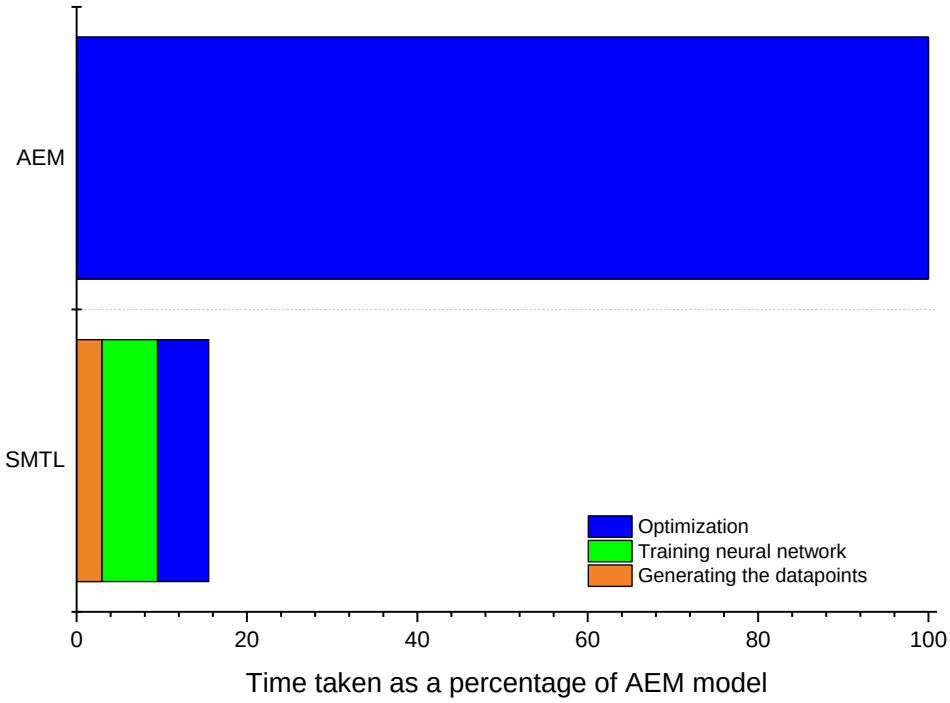

Fig. 5. 11: Presents a comparison of the computational time required for the classical approach based on AEM and the novel approach based on SMTL

6 Designing Climate Resilient Distributed Energy Systems

Climate change and extreme climatic events influence both energy demand and power generation. The challenge is therefore to design climate resilient energy systems that withstand extreme climate and respond appropriately to uncertainties of the climate. Improving the climate resilience of the energy systems involves i) converting climate relevant data into energy system relevant data and ii) designing energy systems that withstand extreme climate events and cope with climate uncertainties. Both these aspects are closely interrelated and have not been discussed in the literature despite their timely importance. To achieve this objective, a regional climate model (RCM) is used to generate hourly weather data for six future climate scenarios. Weather data sets are generated considering a 30-year time span and used in energy demand and power generation (solar and wind) calculations, for 180 single years (30x6). The 180 single-year time series climate data set is subsequently used to develop three representative years (two extremes and typical) and five expected scenarios (developed as pseudo-sequential time series) for energy system optimization. A novel computational algorithm based on the hybrid stochastic-robust optimization (SRO) method is used to consider climate uncertainty and extreme climate conditions. GPU-computing is used to accelerate the computation in the optimization process. Subsequently, Pareto optimization is conducted considering Net Present Value (NPV) and Grid Integration (GI) level as objective functions. Finally, the novel computational algorithm is benchmarked against three algorithms based on deterministic and stochastic models.

This chapter is based on (preprint version):

ATD Perera, Vahid M. Nik, Jean-Louis Scartezzini, Tianzhen Hong, “Designing distributed energy systems resilient to climate uncertainty and extreme climate events” (Manuscript under review)

Author contribution for the journal paper:

ATD, VMN, JLS and TH designed the research. VMN run the climate model and building simulation. VMN analyzed the climate uncertainty of demand and renewable energy generation. ATDP developed the energy system optimization algorithm and conducted the energy system analysis. ATD, VMN, JLS and TH wrote the manuscript.

Readers are encouraged to read following conference proceeding for further information

1. A.T.D. Perera, Vahid Nik and Jean-Louis Scartezzini, Impacts of extreme climate conditions due to climate change on the energy system design and operation, Applied Energy Conference 2018, Rhodes-Greece.

6.1. Introduction

As the 5th assessment report of the state of the global climate describes, climate change will accelerate, causing increasingly frequent and stronger extreme climate events, which makes human, built and natural systems more vulnerable. Failure in climate change mitigation and adaptation can lead to disaster and serious short- and long-term issues [1]. Energy supply may be disrupted by disaster events resulting in partial or total blackouts [2]. The consequences can be very costly in cities and urban areas that accommodate large populations. According to the United Nations, 3.5 billion people live in urban areas around the world and by 2050 more than half of the World population will live in cities [3]. Around two-thirds of global primary energy consumption are attributed to urban areas, leading to 71% of the directly energy-related global greenhouse-gas (GHG) emissions. The urban sector hence plays an important role in both climate change adaptation and mitigation [4,5]. The conjunction of projected population and economic growth with climate change will place greater stress on energy resources, systems and infrastructures [6]. Conserving energy and using alternative renewable forms of energy and generation will improve disaster management and resilience against extreme climate events.

Buildings are the most important users of urban energy systems. Studying the impacts of climate change on the energy performance of the residential building stock in major cities of Sweden showed that the 20-year average heating demand might decrease by around 30% in the years 2081-2100 compared to 1991-2010 [7]. Considering the hourly profiles of heating and cooling demand, deviations can reach values above 50% and 400% for the 20-year average values, respectively. This illustrates the critical conditions for energy systems covering hourly peak demands in the future. The existence of large uncertainties in estimating future climatic conditions makes the assessment more difficult; for the case of Sweden, uncertainties can induce differences of around 30% in the 20-year average values of heating demand, while for cooling demand they can amount to more than 500% [7,8]. Naturally, these differences will increase when narrowed down to the hourly time scale, making the design and adaptation of energy systems more difficult. Auffhammer et-al. [9] show that the impact of climate change on the peak demands becomes even more critical due to its influence on power generation. All in all, due to extreme weather conditions, impacts of climate change on the peak demand are well beyond the net annual change in energy demand and it is important to consider the impact of the change in demand on the power generation.

Effects of climate change are not limited to the demand side but rather extendable to energy systems and infrastructures, which has been investigated for some cases in the USA [10], Greece [11], Norway [12] and Australia [13]. Energy conversion efficiencies of thermal power generation

plants can be affected by climate change [14]. Similarly, a notable change in renewable energy potential can be observed due to climate change(and its uncertainties), which can affect renewable energy generation (and its estimation), especially wind [15,16], hydropower [17] and solar energy [18], however the size of the impact depends on the renewable source and geographical location. For example, according to Seljom et al. [12], effects of climate change on the wind power potential are very limited. A comprehensive assessment of the impact of climate change on solar and wind energy potential is reported in Ref. [19,20]. Fluctuations in the performance indicators of energy systems (obtained using a deterministic model) due to climate and price uncertainty are presented by Mavromatidis et-al. [21]. Dowling [22] assessed the impact of climate change on the energy system at regional scale considering the whole Europe based on several scenarios (design optimization is not considered in this work). However, none of the recent studies have focused on developing climate resilient energy systems.

Integration of non-dispatchable renewable energy technologies, such as solar PV and wind energy, into urban energy infrastructure plays a vital role in the process of climate change mitigation and adaptation. Distributed energy systems, such as energy hubs, have become an attractive option that supports the energy transition in an urban context [23,24]. However, large scale integration of non-dispatchable renewable energy technologies can lead to increasing vulnerability of the grid, which in turn may lead to cascade failures, especially during extreme climate events. Hence, it is essential to guarantee the resilience of renewable based energy systems.

The resilience of energy systems has mostly been a matter of discussion with regard to energy economy and security, usually adopting a global or holistic view [9]. Studying and assessing the resilience of urban energy infrastructures is a new topic, for which few studies exist (e.g. [24–29]). The coverage is even smaller when it comes to considerations related to the uncertainties of climate change and integration of renewables. Sharifi and Yamagata [25] have divided the probable threats and challenges associated with the functionality of urban energy systems into two groups of climate and non-climate induced. Some of the climate induced problems are due to having more frequent and stronger extreme events (e.g. temporal events [31] and heat-induced sagging, hurricanes [32]) and long term effects of climate change (e.g. drought and water shortage [33]).

6.1.1. Objectives of the study

According to Panteli and Mancarella [34], quantifying the risks introduced by weather poses a challenge due to its high stochasticity and multi-dimensional impact. In this context the challenge is to guarantee the resilience of energy infrastructure. According to the International Energy Agency (IEA) report on climate resilience of energy systems, resilience of the energy infrastructure is defined

as the "*capacity of the energy system or its components to cope with a hazardous event or trend, responding in ways that maintain their essential function, identity and structure*" [35,36]. Energy systems are expected to be robust, resourceful and recoverable under extreme climate events. Within this context two major research gaps exists in the current state of the art:

I. Translating climate data into energy system relevant data [22], such as developing weather and demand profiles (to be used in energy system sizing process) considering both climate uncertainty and extreme climate.
II. Methods to optimize the energy systems considering both climate uncertainty and extreme climate.

To address these research gaps, this chapter aims to develop climate scenarios that represent both climate uncertainty and extreme climate using a regional climate model in combination with a novel computational model to design climate resilient distributed energy systems (Fig. 6. 1). Within this context the current study attempts to reach the following objectives:

I. Integrate climate scenarios based on a regional climate model to support energy system optimization.
II. Introduce a novel optimization algorithm to consider climate uncertainty, extreme conditions and resilience.
III. Speed up the computation using graphical processor unit (GPU) programing
IV. Benchmark the performance of the novel computational algorithm to design climate resilient energy systems.

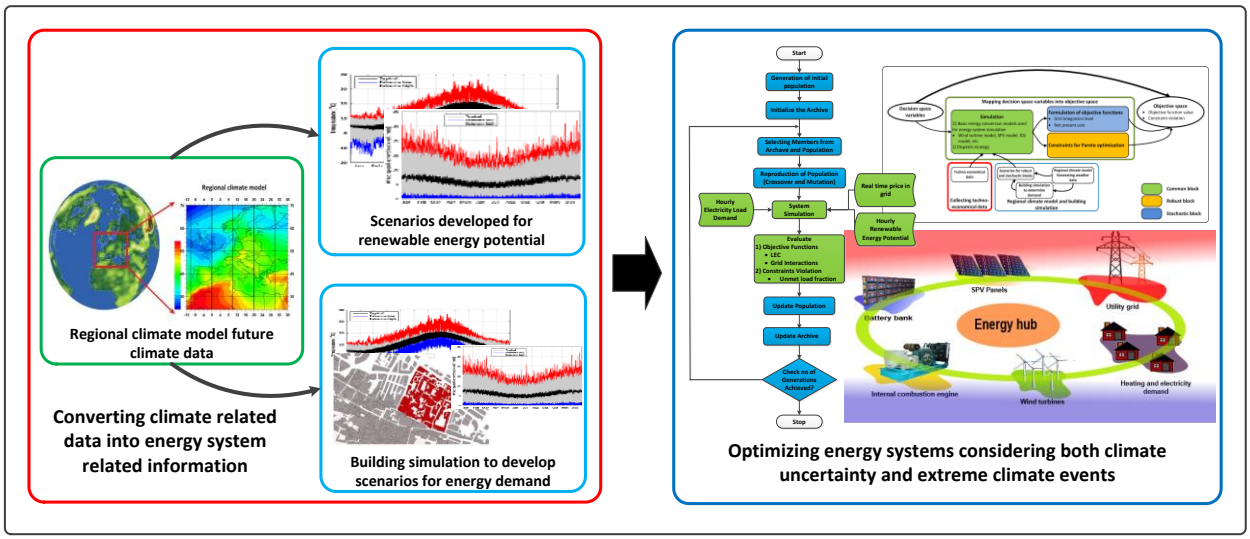

Fig. 6. 1: Addressing the research gaps in the present state of the art

6.1.2. Structure of the chapter

This chapter is organized as follows: Section 6. 2 presents the state of the art of energy system optimization considering uncertainty and promising directions to incorporate climate resilience into the energy system optimization. In Section 6. 3, we present the use of regional climate models to develop typical and extreme climate scenarios considering monthly and hourly distributions of weather data sets. A novel computational algorithm hybridizing the stochastic and robust approaches is introduced in Section 6. 4 to design climate resilient energy systems. A detailed description of the mathematical model and implementation using accelerated GPU computing is presented in Section 6. 4. Finally, in Section 6. 5, the performance of the novel computational algorithm is compared with three simpler computational algorithms. Promising pathways to integrate renewable energy technologies while guaranteeing climate resilience are discussed in Section 6. 5. Furthermore, the capability of climate resilient energy systems to handle normal operating conditions is also taken into discussion in Section 6. 5. Finally, summary and future research directions are presented in the Conclusion section.

6.2. Promising directions to extend existing computational methods

Robustness, resourcefulness and recoverability are the three main pillars that guarantee the resilience of urban energy systems [5]. Robustness is defined as seamless operation of the energy system and its capability to withstand extreme weather as well as gradual changes. Capability to manage operations effectively during an extreme weather event is known as resourcefulness. Finally, the ability to restore the operations following an extreme event is known as recoverability [35,36]. Under the broad definition of resilience, an energy system is expected to be robust during extreme climate conditions while accommodating climate variations and uncertainties without a significant drop in efficiency. Handling uncertainties in the energy system optimization process is vital to guarantee the robust operation and resourcefulness of the energy system facing climate change and extreme conditions.

A number of studies have focused on design optimization of energy systems under uncertainty. Soroudi and Amraee [37] reviewed different methods that can be used to represent uncertainty in the energy system design process. They highlighted the importance of hybrid models to present the uncertainty in a more accurate manner and the benefits of heuristic methods to soften the computation procedure. Mavromatidis et-al. [38] characterize the uncertainties that need to be considered when designing distributed energy systems; they highlight the importance of improving the reliability of data. Zheng et-al [39] reviewed algorithms for optimizing the operation of energy systems considering uncertainty; they highlighted the importance of improving computational

methods to incorporate a larger number of scenarios. Sharifi and Yamagata [25] critically discussed the importance of considering climate resilience during the energy system design process, explaining the need for extending the available approaches to take into account uncertainties.

6.2.1. Existing methods to consider uncertainty in energy system design optimization

Recent literature on energy system optimization that considers the uncertainty of demand, renewable energy generation, grid condition, etc. can be classified into two main groups based on the number of days considered for time series simulation. Certain research groups conducted entire annual time series simulations (ETS) considering 8760 time steps for each scenario, when conducting stochastic optimization (e.g. [40–44]). Other groups limited the simulation to a set of selected days and hours (SSD) (e.g. [21,45–48]). In the latter case (SSD), limiting the number of time steps makes it feasible to increase the number of scenarios considered for stochastic optimization. Both stochastic and robust optimization methods have been implemented using this technique. A bi-level stochastic programming approach based on mixed integer linear programing (MILP) (at both levels) is adapted in most of the instances in these studies [21,45–48]. A bi-level optimization approach facilitates considering the unit commitment problem in detail, which makes it feasible to design complex energy systems. In contrast, reducing the length of the time series can notably influence the final design obtained, especially when considering non-dispatchable energy technologies; for example, Ref. [46,47] if you use three to five days to represent 365 days this may end up in a notable deviation from the actual condition. More importantly, such an approach cannot be used directly to represent extreme climate events that may take place for periods longer than one week. Such extreme events can occur in different seasons and the probability will be higher for future climatic conditions.

Several research studies have considered the ETS (8760 time steps) in stochastic optimization [40–44]. Such a detailed representation enables the model more accurate and closer to reality, especially in the context of representing energy systems with a larger capacity of non-dispatchable energy technologies. However, a relatively simple dispatch strategy needs to be used in the design optimization process (one of the main limitations using this method) when incorporating ETS. In addition, non-linear optimization methods should be accommodated, which will significantly increase the computation time. As a result, the number of scenarios considered in the stochastic optimization process is notably reduced. For example, Narayan and Ponnambalam [40] limited the scenarios in stochastic optimization down to 200. Limiting the number of scenarios considered for stochastic optimization (especially when using scenario reduction methods following Monte Carlo simulation) often eliminates extreme climate conditions. Therefore, a notable improvement is

essential when extending the ETS based on the entire time series simulation to accommodate both climate uncertainty and extreme climate events.

6.2.2. A promising way to consider climate resilience

A novel computational algorithm is developed in this chapter to accommodate climate resilience into the energy system design process by extending the ETS approach. Robust programing is used to compute the performance related to the reliability of the system (through introducing constraints to guarantee a minimum performance level) while stochastic programing is used to evaluate objective function values considering the climate uncertainty.

Simulation-based optimization may take much longer to evaluate objective functions [40]. Hence, incorporating a large number of scenarios becomes time consuming [40,41]; as a result, scenarios with very low expected values have to be omitted in the stochastic optimization process. Extreme climate occurs during shorter time spans (days to weeks) in comparison to the time span of the time series simulation (one year). Furthermore, extreme climates have a relatively low frequency of occurrence. Scenarios corresponding to extreme climatic conditions will therefore have a lower expected value (which cannot be considered in the stochastic optimization process due to the computational limitations). In contrast, robust optimization considers healthy operation of the system under extreme conditions [49–51] and constitutes therefore an appropriate way to consider the resilience of a system under extreme conditions. However, it does not evaluate the performance of a system in non-extreme scenarios.

Besides inducing more frequent and stronger extreme conditions, climate change leads to computational challenges due to uncertainties in estimating climatic conditions (see Section 6. 3 for more details about climate uncertainties as well as [7,8]). Energy systems should possess the potential to manage climate uncertainty without a significant drop in performance. Stochastic programing is a better way to consider the uncertainty when formulating the objective functions compared to robust programing [52]. With their unique pros and cons, hence it is important to use both robust and stochastic programing, which will guarantee resilient operation of the energy system in climate extremes.

The novel algorithm introduced here integrates the stochastic and robust programing in a hybrid way to handle both climate uncertainty and extreme climate. The stochastic optimization approach will address the uncertainties in energy demand and the renewable energy potential due to climate change. Furthermore, uncertainties due to the grid conditions are accommodated through stochastic optimization. Smooth operation of the system under extreme conditions (due to extreme climate

events) is guaranteed through robust optimization. Hybridizing the two approaches has been practiced for unit commitment problems related to power systems [53–58] although yet to be applied for energy system design. The dispatch strategy proposed by Perera et-al [57] is used to consider complex interactions for the unit commitment problem, addressing the limitations of recent literature with ETS. GPU computing is used to increase the number of scenarios through large scale parallelization while reducing the computational time. A comprehensive overview of synthesizing scenarios for stochastic-robust optimization is presented in Section 6. 3 while a detailed overview of the computational model is presented in Section 6. 4.

6.3. Synthesizing representative weather data sets from regional climate models

Developing climate scenarios as input for stochastic and robust programing plays a vital role in the energy system optimization process. In this chapter, six future climate scenarios are taken into account through synthesizing of outputs of a regional climate model (RCM) and creating two groups of typical and extreme weather data sets (based on hourly and monthly distributions); in addition five expected scenarios (all concepts are described in detail hereafter) are developed. RCMs are climate models to downscale global climate models (GCMs) dynamically to regional scale. GCMs, forced by representative concentration pathways (RCPs), are used to simulate future climate conditions on a global scale and develop future climate scenarios. Since the spatial and temporal resolution of GCMs' outputs are coarse, they need to be downscaled to finer resolutions by means of statistical or dynamical downscaling technique. Although the common practice for technical applications is statistical downscaling, it has the disadvantage of only considering the long-term trends of climate change and neglecting extreme weather conditions (there is another downscaling technique, namely stochastic downscaling, with the similar disadvantage). The weather data used in this work has been downscaled using RCA4 [59]; the 4th generation of the Rossby Centre RCM. Compared to the statistical downscaling, RCMs have a better representation of topography and mesoscale processes with the advantage of generating physically consistent data sets across different variables with fine spatial and temporal resolutions [60–62].

6.3.1. Major challenges in dealing with future climate

Two major challenges in the impact assessment of climate change are climate uncertainties and large data sets. There exist several models and scenarios for simulating future climate conditions while no single simulation can be considered as the most probable [63,64]. Meanwhile it is recommended to perform the impact assessment for periods of 20 to 30 years and avoid short time spans [65]. Therefore, a valid impact assessment should consider several long-term future climate scenarios. This increases the size of data sets (e.g. six 100-year scenarios with the hourly time

resolution), the number of simulations (e.g. simulating the building stock of a city for each climate scenario) and the complexity of further analyses (e.g. designing and optimizing urban energy systems). Designing resilient energy systems for future conditions requires to deal with these challenges since it is critical to consider extreme conditions (on an hourly basis) and climate uncertainties. To do so, some previously developed methods are applied in this chapter and developed further for the purpose of energy system optimization.

6.3.2. Deriving climate scenarios for stochastic and robust optimization

In this work, the hourly weather data were synthesized [65] considering six future climate scenarios for the 30-year span of 2070-2099. Future weather data sets are the outputs of RCA4 regional climate model with the spatial resolution of 12.5km, downscaling these driving models: CNRM-CERFACS-CNRM-CM5, ICHEC-EC-EARTH, IPSL-IPSL-CM5A-MR and MPI-M-MPI-ESM-LR (which are called CNRM, ICHEC, IPSL and MPI hereafter, respectively). These driving models are forced by two RCPs [66]; the first two are forced by RCP4.5 and RCP8.5 and the other two by RCP8.5, resulting in six future climate scenarios in total (these weather data sets are called 'RCM data' in this work). This requires creating three different sets of climate data i.e. extreme weather data for robust programing, climate scenarios for stochastic optimization and typical weather data for reference algorithms (in order to compare the performance of the novel algorithm).

6.3.2.1. Extreme weather data for robust programing

RCM data were used to synthesize two groups of representative weather data sets for a 30-year period, each group including three one-year weather data sets: one typical downscaled year (TDY), one extreme cold year (ECY) and one extreme warm year (EWY) [67]. The difference between the two groups is in the time scale for picking the representative data, which varies between picking the representative month and the representative hour. The method for generating TDY, ECY and EWY on the monthly basis is explained in detail in [67]. In short, the method is based on Finkelstein–Schafer (FS) statistics [68]: picking the months with a cumulative distribution temperature that is most similar to that of the whole data sets (6×30=180 years in this case) as the typical months and constructing TDY based on them. For ECY and EWY, the months with the largest differences are picked as the extremes of cold and warm. The method and its usefulness have been verified in different applications [60,67]. The method was developed further so as to track all possible extremes at each time step for any climate variable (outdoor air temperature in this work). To do so, the typical and extreme values of a climate variable were picked according to the hourly distribution at each time step (hour) considering all the years and climate scenarios (6×30=180 data points at each time step). This results in three time series (with the length of 8760 hours), each containing the most

typical, the lowest and the highest values at each time step. It is important to remember that these data sets (arranged based on hourly distributions) are generated only for calculation purposes and they cannot be considered as weather data since they do not reflect the natural variations of the climate system (unlike TDY, ECY and EWY which are arranged based on monthly distributions and reflect natural variations). This is visible in Fig. 6.2 and Fig. 6.3, showing the hourly profiles of the outdoor air temperature and wind speed at the wind turbine level, respectively. The figures on the left compare the typical and extreme data sets with all the 180 probable future conditions (light grey lines) while the three representative data sets were synthesized based on the monthly distributions. The figures on the right do a similar comparison when the representatives are arranged based on the hourly distributions. Naturally, the ones on the right include the extremes at each hour, although their annual profile does represent natural variations of climate. However, it is important to remember that each hourly value is a possible future condition (according to climate models) that can challenge the energy and urban infrastructures in future.

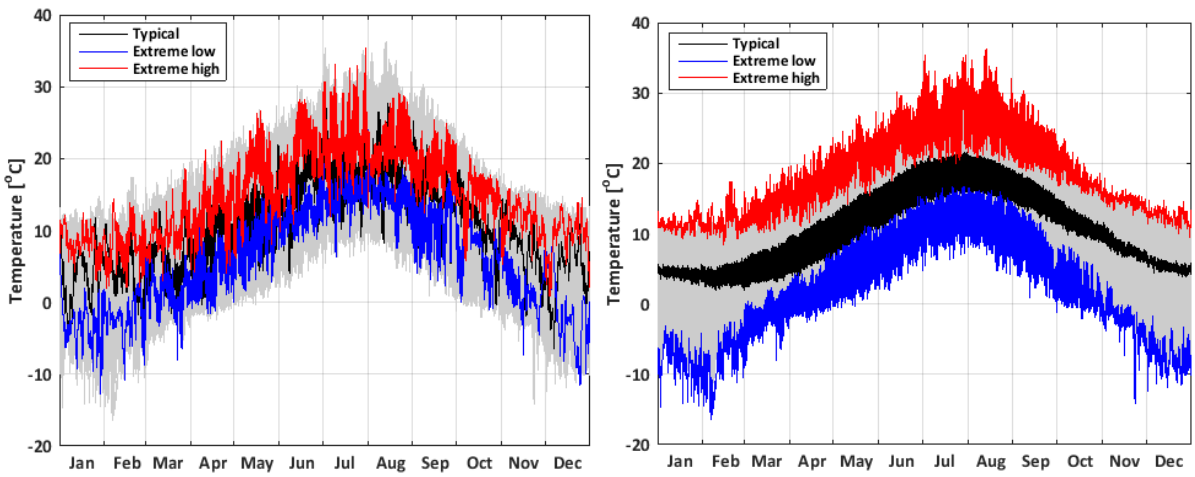

Fig. 6. 2: Hourly distribution of the outdoor temperature for six climate scenarios during 2070-2099 (180 profiles –light grey lines) and the typical and extreme conditions when they are picked based on the (left side) monthly distributions according to [67] and (right side) the hourly distributions of temperature.

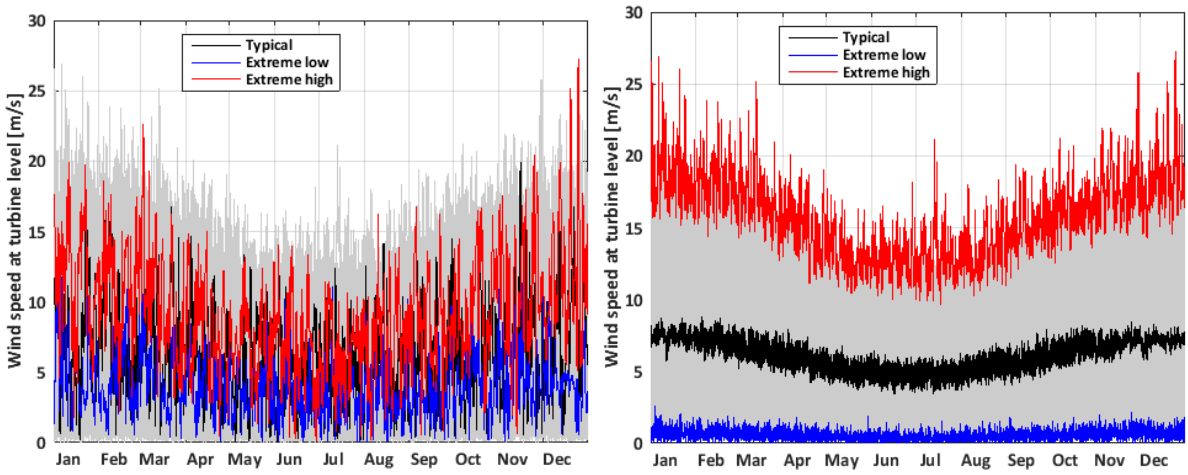

Fig. 6. 3: Hourly distribution of the wind speed at the wind turbine level (60 m) for six climate scenarios during 2070-2099 (180 profiles – light grey lines) and the typical and extreme conditions when they are picked based on the (left side) monthly distributions and (right side) hourly distribution of wind speed.

6.3.2.2. Expected scenarios for stochastic optimization

Another approach, developed for the purpose of this work, is synthesizing sets of scenarios for the future weather conditions, arranged on the basis of the expected values of the desired climate variables. To do so, all the 180 years of weather data (6 scenarios, each for a 30-year period) are accommodated in one year, meaning that at each time step (hour) of a year, there are 180 possible values. Considering the cumulative distribution of the values at each hour and calculating their percentiles, the values (e.g. wind speed) for different probabilities can be calculated. For example, looking at the wind speed, which varies between 0 to 20 m/s during one year in **Error! Reference source not found.** 6.4, and by dividing the range of values into 9 sequences as in the figure legend, the first 5% ('5% - lower' in Fig. 6.4) represent the lowest wind speed values during the whole year, while the last 5% ('5% - higher 2' in Fig. 6.4) represent the highest wind speed. In other words, the first one is a pseudo-sequential time series with one value at each time step that represents the percentiles between 0 and 5, while the last one is for the percentiles between 95 to 100. Four scenarios have been generated in this work by synthesizing pseudo-sequential time series for three (20-60-20 %), five (10-20-40-20-10 %), seven (10-15-15-20-15-15-10 %) and nine (5-5-15-15-20-15-15-5-5 %) sequences (the probability of the scenario is given within the brackets). These scenarios are called 'expected scenarios' in this work. It is noteworthy to remember that the time series of the expected scenarios do not represent the natural variations of the climate system.

It is possible to adapt the method to any variable with many possible values at each time step, as was adopted in this work for creating the expected scenarios for renewable generation potentials and energy demand, which is discussed in the result section. Such detailed information is not

available for grid curtailments and grid prices, therefore only three sequences (20-60-20 %) were considered, based on Ref. [57] and Ref. [69] respectively.

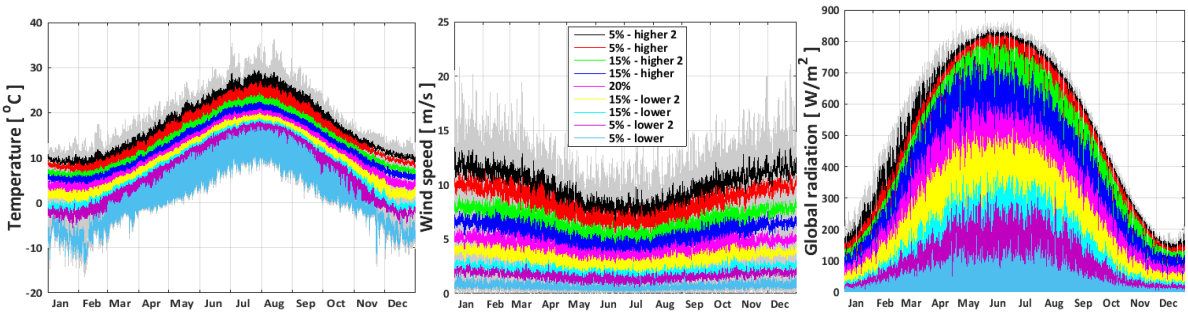

Fig. 6. 4: Hourly distribution of the (left) outdoor air temperature, (middle) wind speed, and (right) global radiation for six climate scenarios during 2070-2099 (180 profiles – light grey lines) and the hourly time series of expected values considering nine probability values.

6.4. Computational model for energy system optimization

The energy system design process combines three steps, i.e. i) deriving a meteorological data set using a regional climate model, ii) building simulation to consider different scenarios for energy demand, and iii) energy system optimization. The first two have already been discussed in Section 6. 3. Building simulations were performed for the building stock in Lund in Sweden, using a verified model, which is thoroughly discussed in some previous works (e.g. [9]). The energy demand of a combination of 40 buildings, representing a typical urban area in Lund, was used for the purpose of this work. This section describes the energy system optimization process. A brief overview of the energy system is presented in Section 6. 4.1. Decision space variables considered for the optimization are presented in Section 6. 4.2. The formulation for the energy flow within the energy hub, objective functions and constraints considered when optimizing the energy hub are presented in Section 6. 4.3. An outline of the optimization algorithm is presented in Section 6. 4.4. A brief overview of the reference algorithms developed to compare the performances of the novel computational algorithm is presented in Section 6. 4.5

6.4.1. Outline of the energy system

The energy hub concept was introduced by Geidl et-al. [70,71] to incorporate energy technologies with different characteristics in order to cater the demand for multi-energy services (Fig. 6. 5). This concept has already received the attention of a wider group of researchers working on distributed generation. Furthermore, it has shown potential to incorporate more renewable energy technologies [23,72–74]. The energy hub considered in this chapter is operated in connection with the local electricity grid. It injects electricity to the grid when there is excess generation (and also when the cost of selling is competitive) and purchases electricity from the grid to cater the mismatch between demand and generation. Grid curtailments have been introduced both for selling and

purchasing electricity to and from the grid to guarantee the stability of the grid. The energy hub considered in this chapter consists of wind turbines and Solar PV (SPV) panels which are non-dispatchable energy technologies. An Internal Combustion Generator (ICG) is used as the dispatchable source. A battery bank is used as the energy storage assisting ICG and grid to absorb fluctuations in both demand and generation. It is assumed that the heating demand is catered using heat pumps.

6.4.2. Decision space variables

Variables related to both system design (ϵN) and operation strategy (ϵL) are considered as the decision space variables. Time series simulation is used to map decision space variables into the objective space as explained in Section 6. 4.3. The decision space includes (ϵX (NUL)) both discrete and continuous variables. Variables related to system design are represented using discrete variables while continuous variables are used to present the dispatch strategy. Number of wind turbines, SPV panels and battery bank as well as size of internal combustion generator are considered as decision space variables. The technology used for SPV panels and the performance curve of wind turbines notably influence the power generation and cost. Hence, the type of wind turbine and SPV panel are also considered as decision space variables along with their capacity.

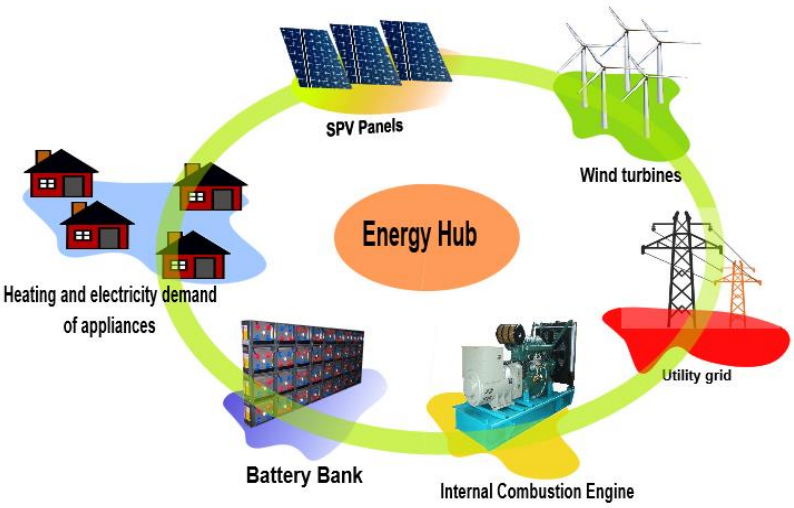

Fig. 6. 5: Outline of the energy system

6.4.3. Formulation of objective functions and constraints

The computational model which formulates the objective functions and constraints maps decision space variables into the objective space. Energy system optimization is performed using a simulation-based optimization algorithm. As shown in Fig. 6.6, the decision space variables are mapped into the objective space through a life cycle simulation which computes the objective function values and constraint violation (in case there is constraint violation). Collecting techno-

economic data helps to formulate the model used for the simulation. RCM and building simulation helps to develop the scenarios that need to be considered for stochastic and robust conditions as described in Section 6. 3. Scenarios related to stochastic and robust programing use a similar computational model for time series simulation. Hence, the computational model corresponding to this part is common for both, which is introduced as the Simulation block in Fig. 6. 6. Objective function values are computed using the Stochastic block, which corresponds to stochastic programing. Constraint violation is evaluated using the Robust block.

6.4.3.1. Simulation block

The Simulation block the computational model which is common to both robust and stochastic programing.. Evaluation of the energy flow based on hourly simulation is the part common to both sections. Hourly wind speed, solar irradiation, energy demand etc. are taken as the input to the Simulation block which determines the renewable power generation within the system. Based on the power generation, interactions with the grid, energy storage and the internal combustion generator are determined using the dispatch strategy.

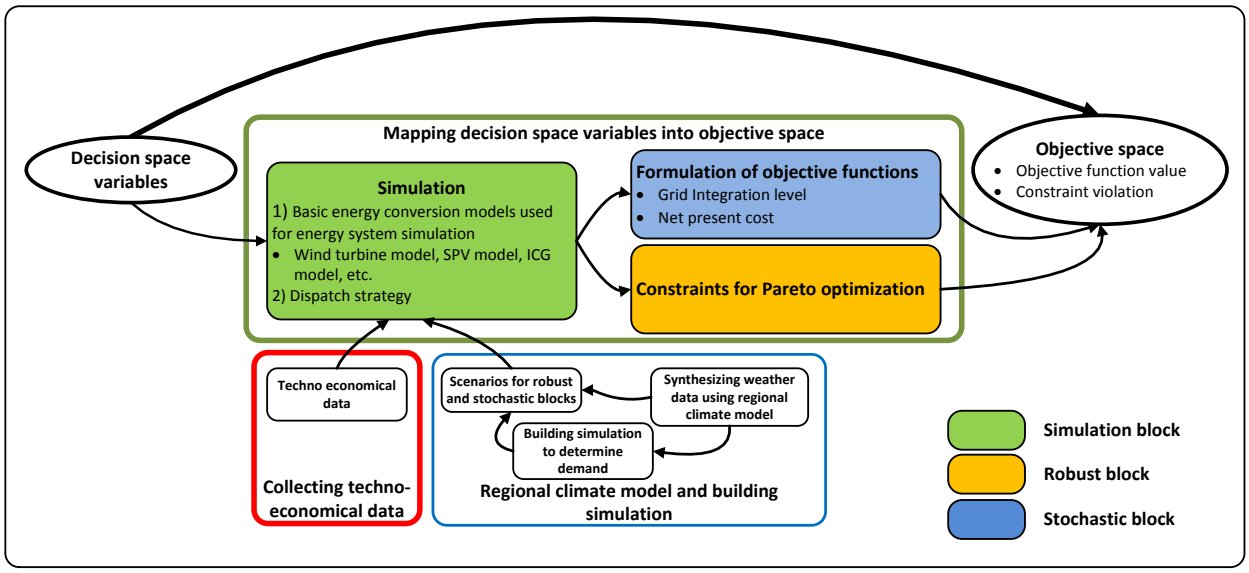

Fig. 6. 6: Mapping decision space variables into the objective space

Energy flow model

Energy flow through system components such as solar PV (SPV) panels, wind turbines etc. is considered under the energy flow model. Based on the hourly solar irradiation, solar power generation ($P_{t,s}^{SPV}$) is computed using Eq. 6.1

$$P_{t,s}^{SPV} = G_{t,s}^{\beta} \eta_{t,s}^{SPV} A^{SPV} N^{SPV} \eta_{Sys}^{SPV}, \quad \forall t \in T, \forall s \in \Omega \tag{6.1}$$

In this equation, t denotes the time step ($\forall t \in T$) and *s* denotes the scenario that belongs to the set of *Ω,* which presents all the scenarios (union of *Ψ* and *π* sets of scenarios representing stochastic and robust scenarios respectively). In Eq. 6.1, $G_{t,s}^{\beta}$, A^{SPV}, N^{SPV} $(N^{SPV} \in \mathrm{N})$ denote the global solar irradiation on a tilted SPV panel, surface area of the SPV panel and number of SPV panels in the system respectively. η_{Sys}^{SPV} takes into account the minor losses in the SPV system due to dust accumulation and the power losses in the inverters. $\eta_{t,s}^{SPV}$ denotes the efficiency of the SPV panel which is computed using Eq. 6.2.

$$\eta_{t,s}^{SPV} = p^{SPV}\left[\mathrm{q}^{\mathrm{SPV}}\left(\frac{G_{t,s}^{\beta}}{G_0^{\beta}}\right)+\left(\frac{G_{t,s}^{\beta}}{G_0^{\beta}}\right)^{m^{SPV}}\right]\left[1+r^{SPV}\left(\frac{\theta_{t,s}^{SPV}}{\theta_0^{SPV}}\right)+s^{SPV}\left(\frac{AM}{AM_0}\right)+\left(\frac{AM}{AM_0}\right)^{u^{SPV}}\right], \quad \forall t \in T, \forall s \in \Omega \tag{6.2}$$

In Eq. 6.2, Standard values for G_0^{β}, θ_0^{SPV}, AM_0 are taken respectively as G_0^{β} = 1000 Wm^{-2}, θ_0^{SPV} = 25°C and AM_0 = 1.5. Parameter values of p^{SPV}, $\mathrm{q}^{\mathrm{SPV}}$, r^{SPV}, s^{SPV}, m^{SPV}, u^{SPV} for different SPV technologies, such as mono-crystalline, polycrystalline and amorphous silicon cells, are taken from Ref. [75]. AM denotes the air mass value and $\theta_{t,s}^{SPV}$ is the cell temperature. Similarly, power generation from the wind turbines is computed using Eq. 6.3.

$$P_{t,s}^{W} = \tilde{P}_{t,s}^{W}(\mathrm{v}_{\mathrm{t,s}}^{Hub})\ \mathrm{N}^{\mathrm{w}}\ \eta^{\text{W-losses}}, \forall t \in T, \forall s \in \Omega \tag{6.3}$$

In Eq. 6.3, $\tilde{p}_{t,s}^{W}$ denotes the power generated by a single wind turbine. According to Thapar et-al [76], wind turbine models using presumed shapes (based actual shape of the performance curve of the wind turbines) are more accurate. Hence, the cubic-spline interpolation method is used in this chapter to present the power curve of wind turbine (based on actual wind turbine found in market). In Eq. 6.3, N^{W} $(N^{W} \in \mathrm{N})$, $\mathrm{v}_{\mathrm{t,s}}^{Hub}$ denote the number of wind turbines and wind speed at the wind turbine hub height. Similar to Eq. 6.1, $\eta^{\text{W-losses}}$ presents the minor losses that take place in the energy conversion. Power generation in the internal combustion generator and the energy flow through the battery bank are computed in a similar manner. Detailed energy flow models used for the simulation can be found in Ref. [77–80] (in deterministic format).

Dispatch strategy

The dispatch strategy helps to accommodate the fluctuations in demand and generation while determining the interactions with the grid, energy storage and internal combustion generator. A bi-level dispatch strategy introduced in Ref. [57] is used in this chapter. The primary level of the

dispatch strategy determines the operating load factor of the internal combustion generator based on renewable energy potential, energy demand, cost of energy in the grid and state of charge level of the battery bank. The fuzzy-automata theory is used at the primary level. The secondary level determines the interactions with the storage and the grid. The finite automata theory is used to assist the secondary level of the dispatch strategy. Both fuzzy rules and state transfer points of the dispatch strategy are considered as decision space variables. Based on the energy flow simulation, interactions with the grid, fuel consumption and wearing of internal combustion generator, charge/discharge cycles of the battery bank etc. are computed. These are used in both robust and stochastic blocks to formulate objective function values and constraints. A detailed description of the dispatch strategy is presented in Ref. [57].

6.4.3.2. Robust block formulating constraints

Performance indicators that guarantee robust operation under extreme scenarios are computed through the Robust block. Reliability of the system is assumed as the main priority. Maintaining reliability is expected to maintain a reliable power supply during extreme climate events. Hence, loss of load probability (LOLP) is considered as a constraint in the optimization problem. LOLP has been amply used in literature as a measure to evaluate the reliability of power systems [81–84]. Energy systems are simulated considering the extreme scenarios and energy flow is computed using the Simulation block in order to compute LOLP. Loss of power supply (LPS) will occur whenever there exists a mismatch between renewable power generation and demand that cannot be catered using the battery bank, internal combustion generator and grid. LPS is computed using Eq. 6.4.

$$LPS_{t,s} = ELD_{t,s} - P_{t,s}^{RE} - P_{Max}^{ICG} - P_{t,s}^{Bat-Max} - IG_{Lim}, \forall t \in T, \forall s \in \pi \tag{6.4}$$

In Eq. 6.4, $P_{t,s}^{Bat-Max}$, IG_{Lim}, P_{Max}^{ICG}, $ELD_{t,s}$ denote maximum possible power flow from the battery bank (depends on the state of charge), maximum power purchased from the grid, nominal power of the internal combustion generator and electricity load demand. $P_{t,s}^{RE}$ denotes renewable energy generation using both SPV panels and wind turbines. LOLP is computed using Eq. 6.5

$$LOLP = Max_{s\in\pi}\left(\frac{\sum_{\forall t\in T} LPS_{t,s}}{\sum_{\forall t\in T} ELD_{t,s}}, 0\right) \tag{6.5}$$

The main weakness of Eq. 6.5 is that it considers the entire time series (period on one year) when computing the loss of load probability. This might lead to erroneous results (since it averages the condition over one year) when considering extreme events which prevail for a shorter period,

leading to higher loss of load probability during extreme climate events. To avoid this issue LOLP-Ex is introduced as an improved replacement according to Eq. 6.6.

$$LOLP-Ex = Max_{s\in\pi}\left(Max_{t\in T}\frac{\sum_{t=t_0}^{t=t+d} LPS_{t,s}}{\sum_{t=t}^{t=t+d} ELD_{t,s}}, 0\right) \tag{6.6}$$

In Eq. 6.6, 'd' denotes the time period that the extreme climate condition is expected to prevail.

6.4.3.3. Stochastic block formulating objective functions

Stochastic-robust optimization has recently become popular for dispatch optimization problems [53–58]**.** Different methods have been used in these studies to consider both stochastic and robust aspects of energy system operation. In most of the instances, stochastic and robust parts of the objective function are combined by weighting the impact of each other [53,58]. In certain instances, penalty cost is introduced through robust programing [54]**,** which is quite similar to introducing it as a constraint. When moving from dispatch optimization to energy system design, the context of the problem changes notably. Due to shorter time spans (mainly) during extreme climate conditions and the relatively low frequency of occurrence, the weight that should be assigned for the robust part in the objective function will be quite low. Hence, it is only considered as a constraint in the formulation of the optimization problem. Net present value (NPV) of the system and grid integration level are considered as the objective functions. The computational model introduced in the common block is used to simulate energy flow within the system. Based on the energy flow, the cash flow of the system is computed for different scenarios within the stochastic block. Similarly, the autonomy level of the system is computed based on the hourly simulation.

Net Present Value (NPV)

Expected net present value ($\mathbb{E}(NPV)$) is computed considering all the cash flows that have taken place within the lifetime of the system. The NPV includes two main parts i.e. initial capital cost (ICC) and operation and maintenance cost (OM). The price uncertainty related to the ICC, which includes the acquisition and installation costs, is not considered in this chapter. Hence, ICC is computed only considering the deterministic part. ICC is considered at the beginning of the project. Scenarios introduced considering climate and grid uncertainty will result in a notable change in the OM. Expected value of the OM is included ($\mathbb{E}(OM)$) along with the deterministic value of ICC which formulates the $\mathbb{E}(NPV)$ according to Eq. 6.7.

$$\mathbb{E}(NPV) = \mathbb{E}(OM) + ICC \tag{6.7}$$

OM consists of two main components fixed (OM_{Fixed}) and variable costs ($OM_{Variable}$). Eq. 6.7 can be extended considering these two components separately according to Eq. 6.8. OM_{Fixed} considers recurrent annual cash flows (such as maintenance cost of wind turbines, SPV panels, fuel and operation cost for ICG). $OM_{Variable}$ considers the replacement cost for ICG and battery bank. Replacement time for the ICG is determined considering the operating hours and Rain-flow algorithm using the common block. Both fixed and variable operation and maintenance costs are evaluated on annual basis when computing the expected NPV.

$$\mathbb{E}(NPV) = ICC + \sum_{\forall s \in \Omega} \delta_s \left(\sum_{\forall c \in C} (OM_{c,s}^{Fixed} CRF_c) + \sum_{\forall h \in H} \sum_{\forall c \in C} PRI^l OM_{c,h,s}^{variable} \right), \ \forall t \in T, \forall s \in \Psi, \forall c \in C, \forall h \in H \tag{6.8}$$

In Eq. 6.8, CRF_c denotes the Capital Recovery Factor for the cth component. PRI denotes the real interest rate calculated using both interest rates for investment and the local market annual inflation ratio. 'δ' and h denote the expected value of the scenario and the year considered.

Grid integration (GI) level

The autonomy level of a distributed energy system depends on the level of the interactions it maintains with the grid. Maintaining minimum grid interactions is always recommended from the perspective of grid stability. Therefore, grid curtailments are considered for both selling and purchasing electricity to and from the grid. According to Perera et-al [57], the autonomy level of a distributed energy system can be measured in different ways. In this chapter, GI is evaluated based on the units purchased form the grid (Eq. 6.9) in order to maintain a stable operation of the distributed energy system.

$$\mathbb{E}(GI)_{\forall s \in \Psi} = \sum_{\forall s \in \Omega} \delta_s \frac{\sum_{\forall t \in T} P_{t,s}^{FG}}{\sum_{\forall t \in T} ELD_{t,s}}, \ \forall t \in T, \forall s \in \Psi \tag{6.9}$$

In Eq.6.9, $P_{t,s}^{FG}$ denotes the energy purchased from the grid.

6.4.4. Optimization algorithm

Different methods based on convex optimization, non-convex optimization, linear programing, mixed integer linear programing and heuristic methods have been used to design distributed energy systems [85,86]. Heuristic methods have been shown to be an effective way to design distributed energy systems in recent years [87]. Soroudi and Amraee [37] highlight the importance of developing methods based on heuristic methods in order to design energy systems under uncertainty. Heuristic algorithms have been amply used for both stochastic [88] and robust [89] optimization problems. This chapter uses the steady state ε-dominance method to conduct Pareto

optimization. The constraint tournament method [90] is used to handle the constraints in the optimization process. A polynomial mutation operator [90] and a simulated binary crossover operator [91] are used along with differential evolutionary operators in the reproduction of the population. Net Present value (NPV) (Eq. 6.8) ($F_1 \in \mathcal{F}$) and Grid integration level (GI) $F_2(F_2 \in \mathcal{F})$ (Eq. 6.9) introduced in Section 6. 4.3.3 are used as the objective functions.

6.4.5. Implementation of the computational algorithm

Simulation based optimization is a time consuming activity, which becomes more challenging when accommodating large number of scenarios that consider lengthy simulations. Hence, efficient implementation of the computational program plays a vital role. In order to accomplish this objective, Graphical Processor Unit (GPU) computing is introduced in this study to conduct time series simulation. GPU computing facilitates large scale parallelization of computational program. As a result, GPU computing has already been used in different fields such as image processing, machine learning, bio-informatics etc. However, GPU computing is not well known among the energy system design community despite its potential to speed up computational processes. When considering stochastic optimization, GPU computing makes it feasible to handle a large number of scenarios within a reasonable computational time. For example the number of scenarios considered in this work (5835 scenarios) is way higher than the number of scenarios considered by Narayan and Ponnambalam (200 scenarios) [40].

The formulation of the objective functions is described using three blocks in Section 6. 4.3 for the ease of understanding. The computational algorithm begins in a similar manner following the mathematical model as shown in Fig. 6. 7. The techno-economic and weather data are collected and provided to the computational algorithm. The Simulation block (considered as one part), which includes the set of computational models, is divided into a stochastic and a robust part and implemented in both CPU and GPU. Scenarios related to the stochastic programing part are implemented in the GPU, which supports large scale parallelization. Scenarios related to the robust part and deterministic part are implemented in Central Processing Unit (CPU). Subsequently, the objective function values and constraints are computed in the CPU aggregating the computation performed in both CPU and GPU. Based on the objective function values, the population and archive are updated following the dominance check using the CPU.

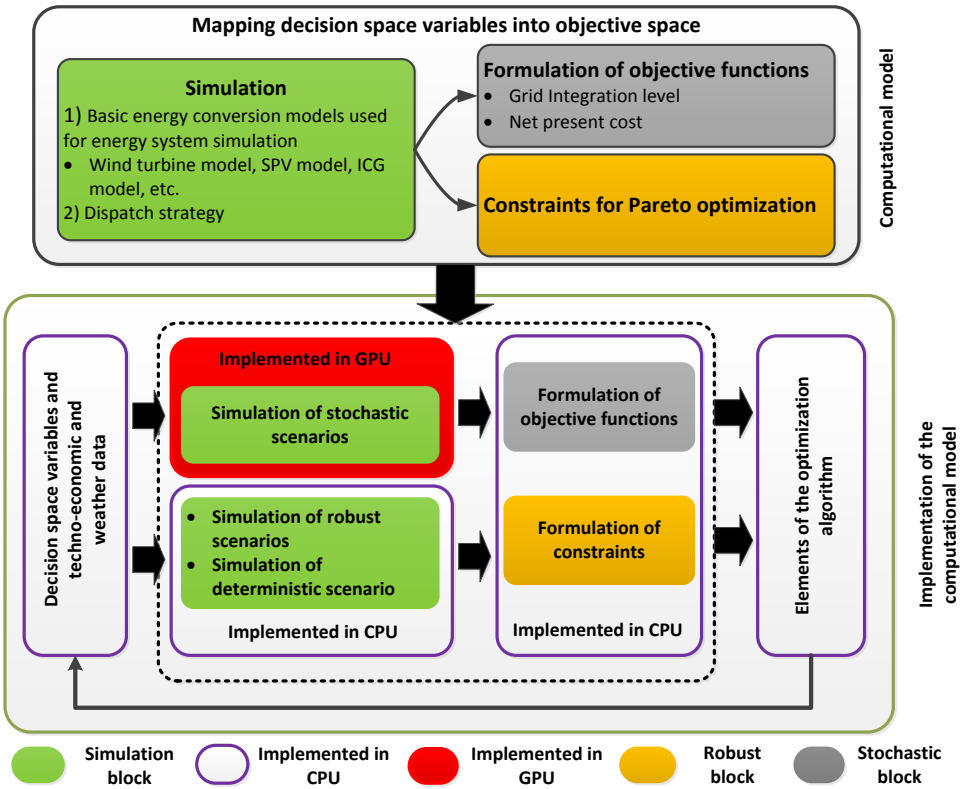

Fig. 6. 7: Implementation of the computational algorithm

6.4.6. Reference algorithm

Several reference algorithms are used to compare the performance of the novel algorithm introduced in this chapter (Fig.6.8).

- **Deterministic model with typical weather data (DT)**

The deterministic model is generally used to design distributed energy systems based on typical weather data as is the case in this work. Several typical weather data sets are available, of which TMY is one of the well-known formats, widely used for energy simulations. In this work, instead of using TMY or similar available data sets, typical weather data have been synthesized using outputs of the RCA4 regional climate model, which is called Typical Downscaled Year (TDY). TDY is used to simulate the energy demand of the buildings and the energy system (check Section 6. 3 for more details). Both objective functions and constraints are derived based on the deterministic model.

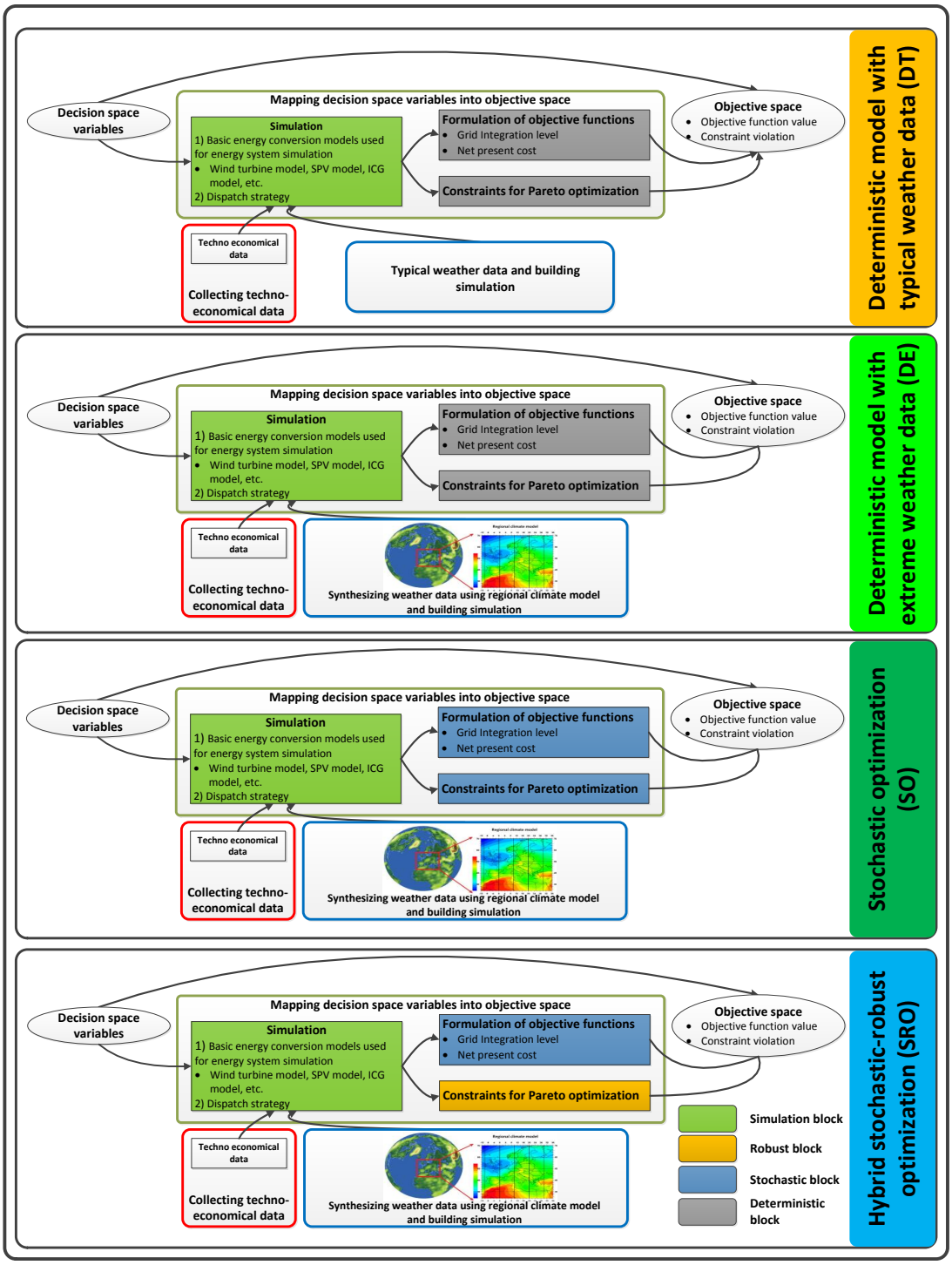

Fig. 6. 8: Comparison of different algorithms used as reference algorithms to compare the performance of the proposed SRO. Respectively from top to bottom, outline of DT, DE, SO and SRO are presented. Climate scenarios obtained from regional climate model are introduced DE onwards (when moving from top to bottom). Deterministic formulation is replaced entirely by using the stochastic models in SO. The robust programing method is used in SRO to evaluate the constraints.

- **Deterministic model with extreme weather data (DE)**

The main weakness in the deterministic model is not considering the extreme climate conditions. Therefore, it is difficult to guarantee the robustness of the energy system under extreme events. The DE algorithm is used to design the energy system replacing the typical weather data by extreme climate conditions (extreme high and low – check Section 6. 3).

- **Stochastic optimization (SO)**

As discussed before, stochastic programing is a more realistic way to represent uncertainties, especially when compared to deterministic models. Stochastic programing is used to compute both objective functions and constraints for the optimization algorithm in this algorithm (Fig. 6. 8).

- **Hybrid stochastic-robust optimization (SRO)**

SRO is the novel method introduced in this study and detailed in Section 6.4.1-3.3. Compared to SO, robust programing is used in SRO to consider the extreme events.

6.5. Results and Discussion

Climate uncertainty and extreme climate events can have an adverse impact on both energy demand and generation. Hence, it is important to quantify the impact of such events accurately using probable scenarios. The first part of the results and discussion section of this paper is devoted to understanding the influence of different methods used to synthesize the climate data on the representation of extreme climate events and climate uncertainty. Furthermore, the computational challenges that need to be faced when representing climate uncertainty and extreme climate events are discussed. The second part of the section is devoted to understanding the impact of extreme climate on energy system performance and renewable energy integration. Finally, the novel algorithm introduced in this chapter is benchmarked using the reference algorithm.

6.5.1. Energy demand and weather data

Estimating peak demand and preparing for extreme climatic conditions is vital for the design of resilient energy systems. Results in this section illustrate the role of weather data and the importance of the selected approach in estimating peak demand and extreme conditions.

6.5.1.1. Effects of time scale in synthesizing typical and extreme weather conditions

The monthly average of cooling, heating and total energy demand are plotted in Fig. 6.9 for two types of typical weather data, synthesized on the basis of the monthly and hourly distribution of outdoor air temperature. Calculated values are very similar for both typical conditions; the only considerable difference is that the typical conditions based on the hourly distribution underestimate the average need for cooling during summer. In Fig. 6.10, differences of the extreme cold (ECY) and

warm (EWY) years from typical year (TDY) in calculating the total energy demand of buildings are plotted for the monthly and hourly based representative weather data sets (TDY, ECY and EWY based on the monthly and hourly distribution of air temperature). According to the graphs, the larger peak demands during cold and warm seasons belong to ECY and EWY synthesized on the basis of the hourly distribution. This is clearly visible in **Error! Reference source not found.**. 6.11, which compares the differences from typical conditions in heating demand for ECY and in cooling demand for EWY. Boxplots of the differences during cold (Jan-Feb & Oct-Dec) and warm (May-Sep) seasons are illustrated in Fig. 6.12, confirming the fact that not considering extreme climatic conditions will result in underestimating peak demand. Moreover, by performing calculations only for monthly-representative extreme conditions, the scale of peak demand at the hourly basis is diminished, which may cause failure in supplying the required energy during extreme climatic conditions. This is obvious for the case of cooling demand during warm seasons in Fig. 6.11.

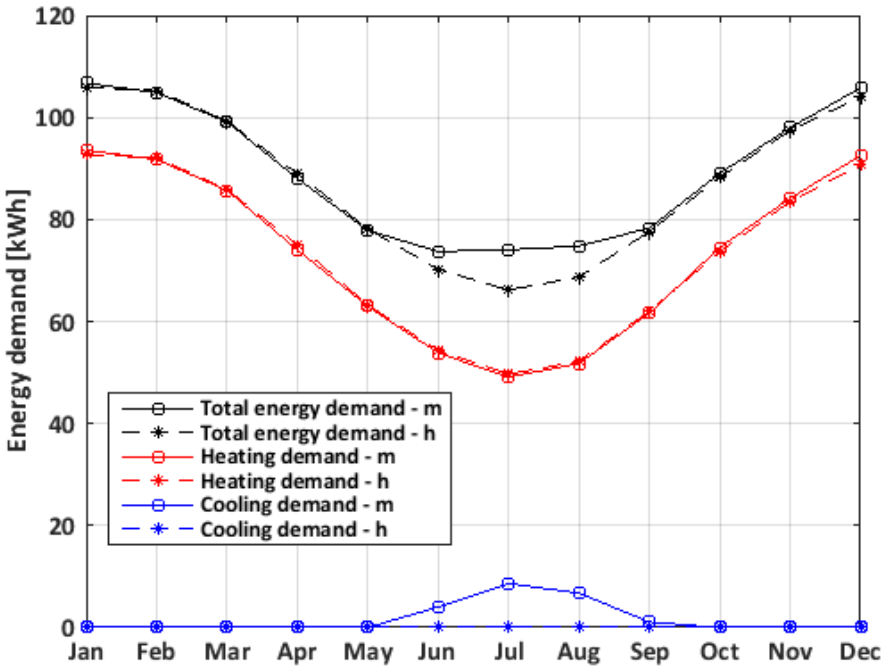

Fig. 6. 9: Monthly average of cooling, heating and total energy demand for buildings in Lund during 2070-2099 for two sets of typical (TDY) weather conditions, synthesized based on the monthly (m) and hourly (h) distribution of outdoor air temperature.

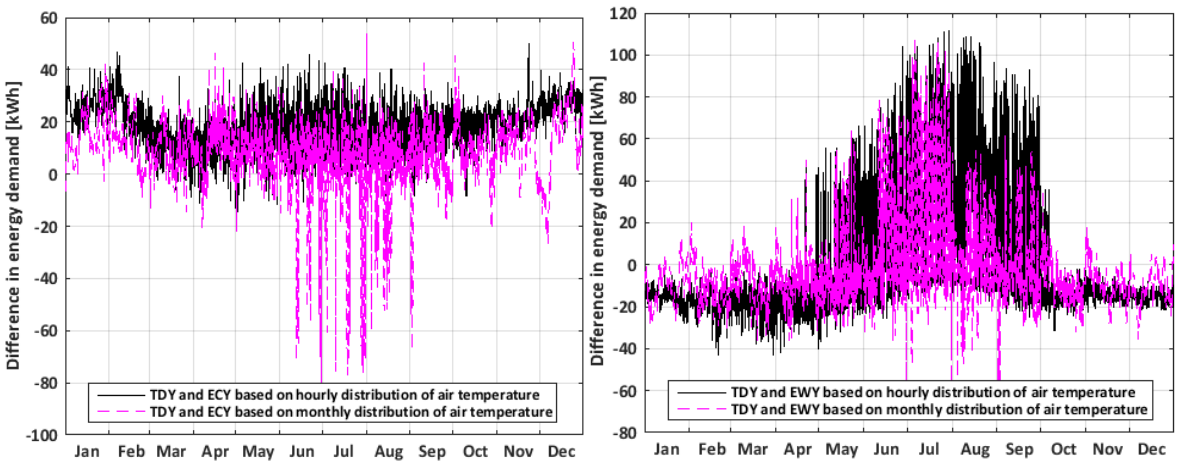

Fig. 6. 10: Hourly differences in the total energy demand when the representative weather data sets are synthesized based on the monthly or hourly distribution of the outdoor air temperature ($Demand_{Extreme}$-$Demand_{Typical}$): (left) difference between typical and extreme cold conditions; (right) difference between typical and extreme warm condition.

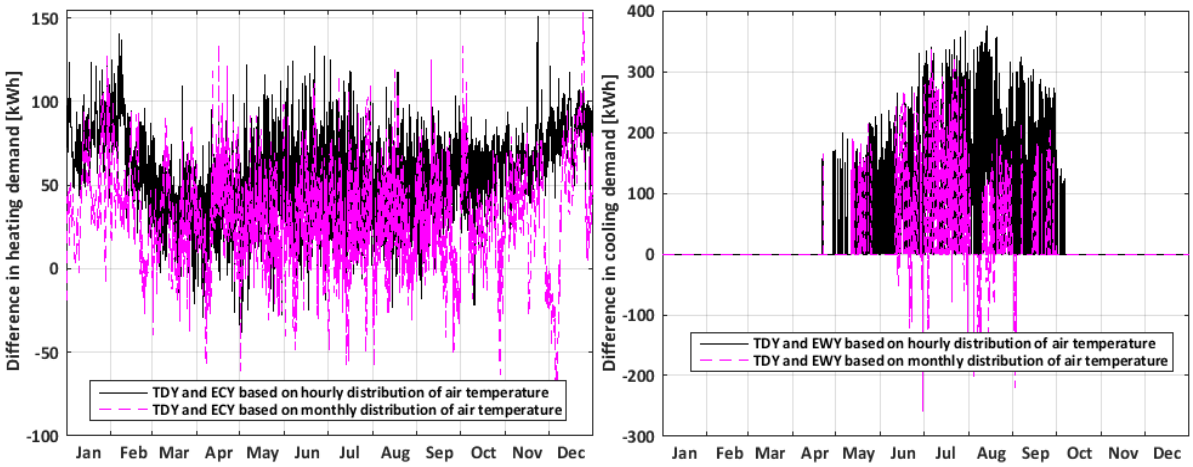

Fig. 6. 11: Hourly differences in (left) heating demand and (right) cooling demand. Comparing differences when the representative weather data sets are synthesized based on the monthly or hourly distribution of the outdoor air temperature ($Demand_{Extreme}$-$Demand_{Typical}$).

Based on the abovementioned outcomes, more than the long-term outputs of RCMs, the representative weather data sets synthesized based on the hourly distribution of the outdoor air temperature have been used for all the calculations hereinafter.

6.5.1.2. Presenting climate uncertainty and extreme climate

Hourly profiles of the total energy demand for typical and extreme weather data sets (based on the hourly distribution of air temperature) are compared with all the 180 profiles (calculated using the RCM weather data) in Fig. 6.13. Energy demand for extreme climate conditions is derived using ECY and EWY, which is subsequently used for the robust optimization. Similarly, 180 generated energy demand scenarios using the RCM weather data are used to present climate uncertainty during the

stochastic optimization. A group which consists of sets of scenarios that present climate uncertainty is created in order to evaluate the influence of the number of scenarios on the accuracy of climate uncertainty representation. The group consists of four sets of scenarios each having respectively three, five, seven and nine scenarios used to represent climate uncertainty. The demand profiles for each set of scenarios are plotted in Fig. 6.14 (considering three, five, seven and nine probability values). The expected value of each scenario is also included in the plot.

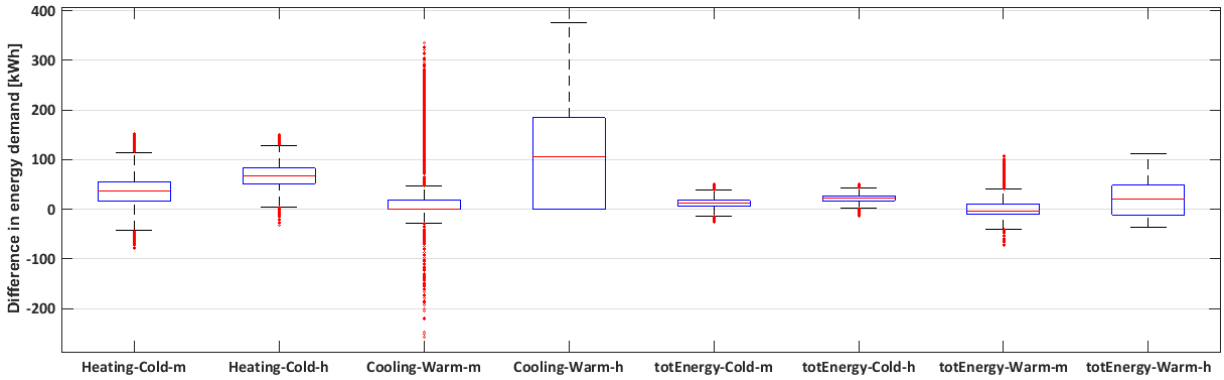

Fig. 6. 12: Distribution of the hourly differences in heating, cooling and total energy demand ($Demand_{Extreme}$ - $Demand_{Typical}$) when the representative weather files are synthesized based on the monthly (m) or hourly (h) distributions of the air temperature. "Cold" and "Warm" refer to the cold and warm seasons. The average values of the differences are 35.8, 66.7, 34.7, 106.4, 11.8, 21.9, 4.8 and 21.9 kWh (respectively, from left to right in the figure) while the average demand for typical cases is 238.4, 237.3, 11.6, 0, 98.8, 98.4, 75.7 and 72.2 kWh.

The seasonal variations are visible in profiles based on ECY and EWY in Fig. 6.13; energy demand increases due to extreme heating demand during cold seasons (ECY – check the high values of the blue line in Fig. 6.13 during cold season) and due to extreme cooling demand during warm seasons (EWY – check the high values of the red line in Fig. 6.13 during warm season). These seasonal changes are not distinguishable for the lower expected values of the expected scenarios in Fig. 6.14 , however the higher values can represent the extreme values during both warm and cold seasons (for example check the black solid lines in Fig. 6.14 which reflect the changes in energy profile due to seasonal changes while this is not the case for the cyan line). By increasing the number of sequences of expected values in the expected scenarios (and naturally narrowing down to smaller probabilities), the chances for covering the extreme values with lower probabilities increase. For example, by comparing the expected scenarios with three and nine sequences in **Error! Reference source not found.**. 6.14, it is obvious that '5% - higher 2' for nine sequences covers larger extremes with lower probability compared to '20% - higher'. This is elaborated further in Fig. 6.15, which presents the boxplots of the differences in the energy demand for extreme conditions from the typical conditions during the warm and cold seasons on the hourly time scale. The energy demand for typical conditions is calculated using TDY and for extremes using ECY, EWY. P9, P7, P5 and P3 in

Error! Reference source not found.. 6.15 reflect the differences between the last expected values (the highest values in each expected scenario or black solid lines in Fig. 6.14) and typical conditions. According to Fig. 6.15, using ECY and EWY results in considering a larger span of extreme conditions, however the expected values are also useful in estimating the span of extreme conditions, especially when they are divided into larger number of sequences (for example, compare the boxplot of P9 in the cold and warm season respectively with the ECY and EWY boxplots in Fig. 6.15).

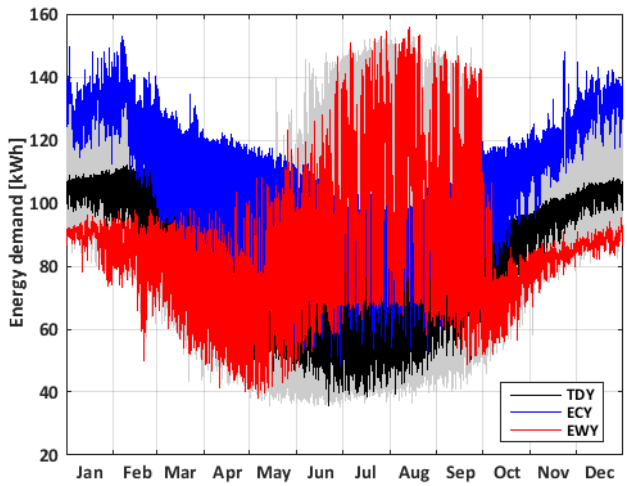

Fig. 6. 13: Hourly distribution of the total energy demand for six climate scenarios during 2070-2099 (180 profiles – light grey lines) and the typical and extreme scenarios based on the hourly distribution of outdoor air temperature.

6.5.2. Impacts of extreme weather conditions on the performance of energy systems

Energy systems are optimized considering GI and NPV as objective functions. Pareto fronts obtained using different methods: DT, DE, SO and SRO are presented in Fig. 6. 16. In addition, Pareto fronts are obtained considering Ext-LOLP as a constraint (SRO-Ex) optimization to assess the impact of refining the loss of load probability (LOLP) indicator to match with extreme climate events further. The five Pareto fronts can be grouped into two groups;

- Group 1: set of Pareto fronts obtained using stochastic programing (SRO, SO, SRO-Ex)
- Group 2: set of Pareto fronts that are based on deterministic models (DT and DE)

To analyze the Pareto fronts further, four different sets are created taking one Pareto solution from each Pareto front that have a similar grid integration level. Performance indicators of these Pareto solutions and the system configuration details are tabulated in Table 6. 1.

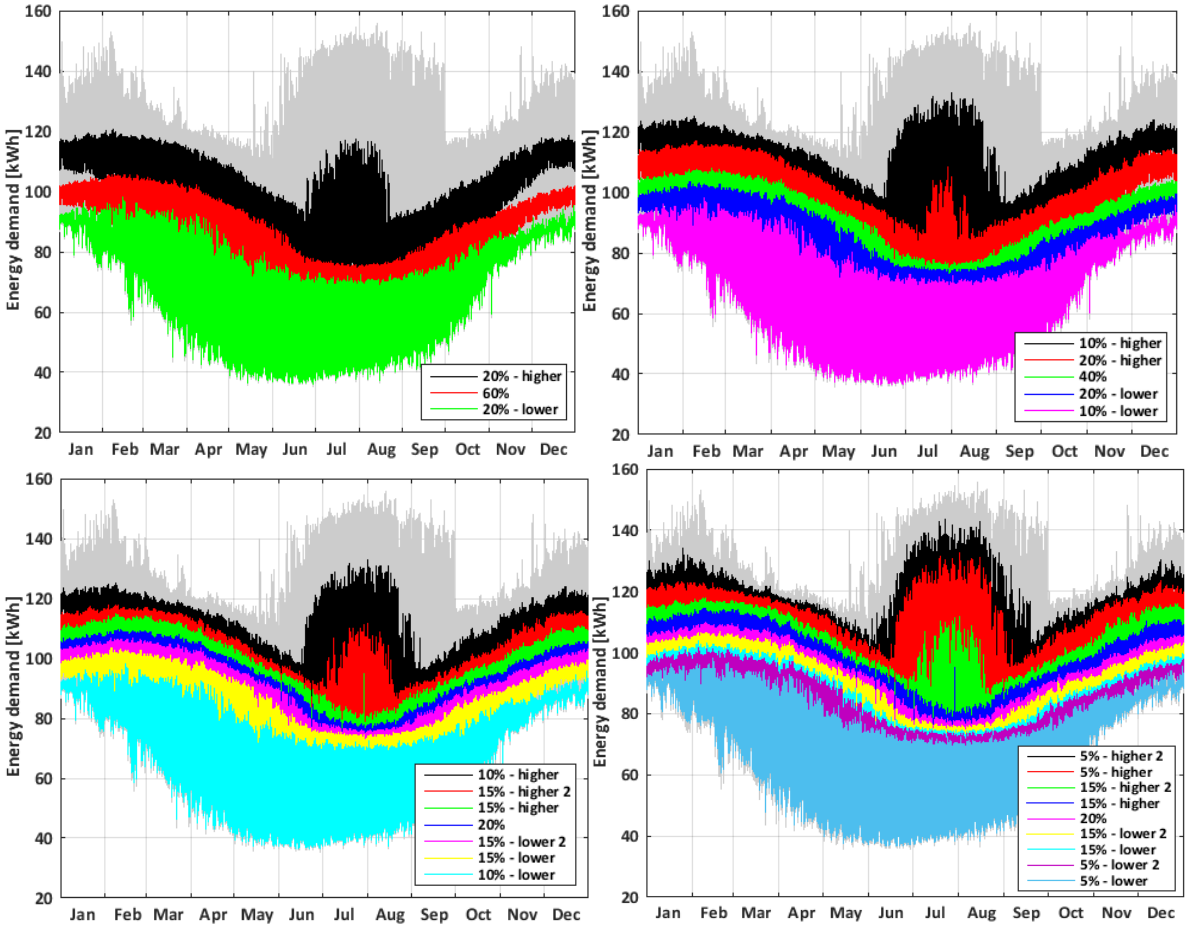

Fig. 6. 14: Hourly distribution of the total energy demand for six climate scenarios during 2070-2099 (180 profiles – light grey lines) and the hourly time series of expected values considering (top-left) three, (top-right) five, (bottom-left) seven and (bottom-right) nine probability values.

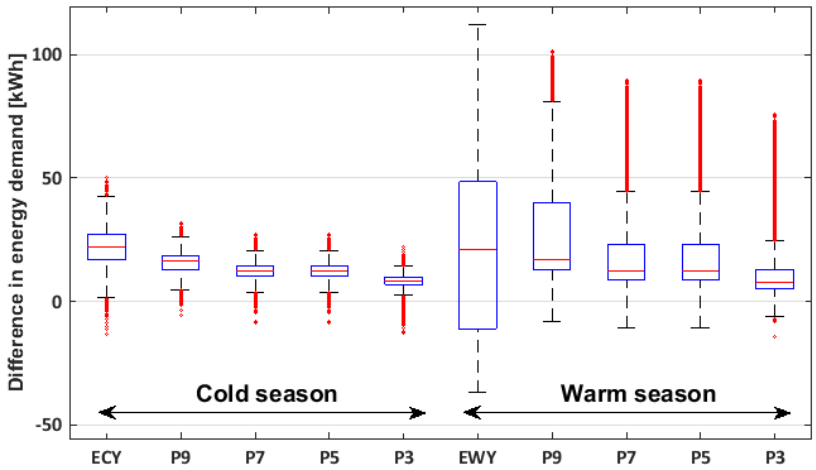

Fig. 6. 15: Distribution of the hourly differences in total energy demand ($Demand_X$ -$Demand_{Typical}$) during cold and warm seasons considering extremely cold (ECY) and warm (EWY) years - based on hourly distribution – and extremely high expected values (black solid lines in Error! Reference source not found.**) for nine (P9), seven (P7), five (P5) and three (P3) probability values.**

6.5.2.1. Pareto fronts considering NPV and GI

When analyzing the Pareto fronts that belong to Group 1, a noticeable increase in the objective function values is observed when moving from DT to DE. As shown in Table 6. 1, NPV increases by 61.1% (when moving from DT to DE) in Set A and by 71.2 % in Set D. Furthermore, a totally contrasting picture is seen when comparing the installed renewable energy capacity of DT and DE. For example, the renewable energy capacity drops from 735 kVA to 25 kVA when moving from DT to DE in Set A. A similar behavior is observed when comparing the installed renewable energy capacity of DE with the Pareto fronts belong Group 2. In addition, it is observed that DT is having the highest ICG capacity. Hence, it can be concluded that considering the extreme climate conditions through deterministic models results in poor renewable energy capacity. In addition, considering extreme conditions through deterministic models portray a negative picture about distributed energy systems from the economic perspective. It can be concluded that it is not a good practice to use deterministic approaches to consider extreme climate events when designing distributed energy systems.

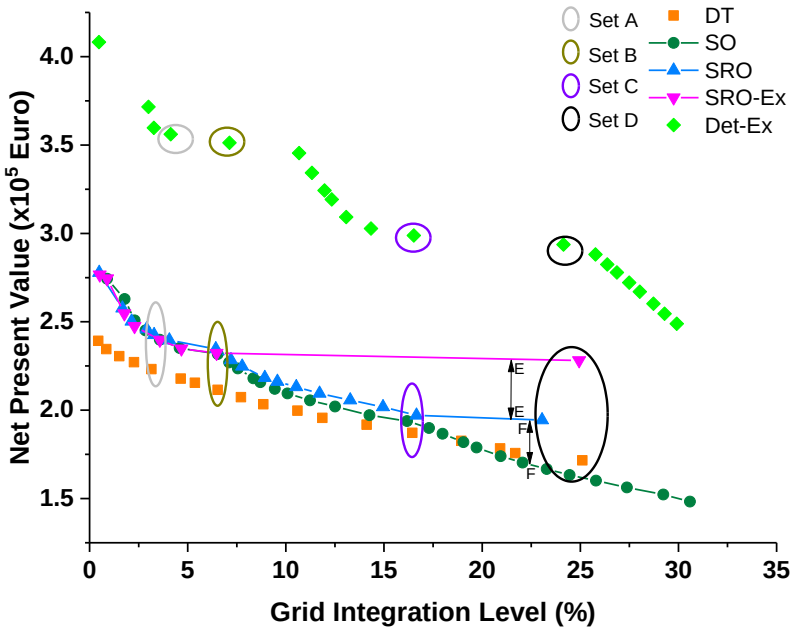

Fig. 6. 16: Pareto fronts obtained considering NPV GI. Four colored circles represent four sets of Pareto solutions created selecting one Pareto solution from each Pareto front having grid interaction levels close to each other. E-E and F-F respectively show the difference in NPV for SRO-SRO-Ex and SRO-SO Pareto fronts.

When moving from Group 1 to Group 2 (methods based on stochastic programing), the three Pareto fronts move very closely to each other until these reach the Pareto solutions that belong to Set B. Thereafter, SRO-EX Pareto front deviates from the other two Pareto fronts (belongs to Group 2). Similarly, SRO and SO deviate from each other after reaching the Pareto solutions marked as Set C.

Hence, system designs of the Pareto fronts which belong to Group 2 are quite close to each other when the grid integration level is low. Renewable energy capacity, wind turbine capacity as a percentage of total renewable energy capacity, ICG capacity and energy storage size of Set A (Tabulated in Table 6. 1) (for SO, SRO, SRO-EX) demonstrate this specific point. Following the deviation in Pareto fronts, a significant difference in ICG capacity can be observed in Set B where the deviation in NPV is at the highest. The ICG capacity increases from 40 kVA to 60 kVA and finally to 80 kVA when moving from SO to SRO and SRO-EX. Such a variation clearly shows that the ICG plays a major role in distributed energy systems when guaranteeing the robust operation under extreme conditions. Furthermore, renewable energy capacity is maintained above 400 kVA for all the Pareto solutions of Group 2 (except for Pareto solution SRO in Set D) having a minimum renewable energy contribution of 49%. Reaching such a high level of renewable energy generation is a significant achievement (especially for the case of SRO and SRO-EX which impose stringent restrictions to guarantee the robust operation of the system under extreme conditions).

Table 6. 1: Performance and system configuration of the Pareto solutions from different Sets

Set	Pareto front	NPV ($x10^5$ Euro)	GI(%)	RE capacity (kVA)	Wind energy (%)	Number of battery banks	ICG capacity (kVA)	NPV Increase[1] (%)
A	DT	2.23	3.15	735	12.2	20	60	
	SO	2.40	3.58	495	92.9	13	80	7.43
	SRO	2.43	3.29	490	89.8	14	80	8.70
	SRO-EX	2.40	3.58	495	92.9	13	80	7.43
	DE	3.60	3.27	25	80.0	16	120	61.16
B	DT	2.11	6.52	555	7.2	20	60	
	SO	2.32	6.54	985	60.9	17	60	9.58
	SRO	2.35	6.43	980	59.2	17	60	10.94
	SRO-EX	2.32	6.47	425	98.8	7	80	9.81
	DE	3.51	7.13	25	80.0	3	120	66.11
C	DT	1.87	16.44	360	1.4	6	60	
	SO	1.94	16.18	405	93.8	11	60	3.57
	SRO	1.97	16.66	440	90.9	18	60	5.29
	DE	2.99	16.52	25	80.0	3	100	59.67
D	DT	1.72	25.11	285	1.8	1	60	
	SO	1.63	24.45	535	48.6	10	40	-4.84
	SRO	1.94	23.05	375	96.0	17	60	13.29
	SRO-EX	2.28	24.94	430	93.0	1	80	32.96
	DE	2.94	24.14	25	80.0	2	100	71.15

[1]Compared to DT Pareto front

6.5.2.2. Performance gap due to neglecting the climate uncertainty

The Pareto fronts that belong to Group 2 follow each other closely up to a point (when increasing the grid integration level) and subsequently deviate, resulting in a notable difference in NPV (as

marked by E-E and FF). It is important to investigate the causes that create such a significant difference in NPV. Furthermore, it is important to figure out its relationship with climate uncertainty and extreme climate. To achieve this objective, Pareto solutions obtained using both deterministic and stochastic methods are further assessed using the four sets created earlier (Set A-D). Pareto solutions obtained using a deterministic model are simulated again considering both stochastic and extreme scenarios to assess the influence of climate uncertainty and extreme climate conditions (Table 6. 2 presents the results obtained for solutions in Set B, C and D in Table 6. 1). In addition, the influence of extreme climate on the Pareto solutions obtained using stochastic programing (Group 2) is also assessed further (see Table 6. 3).

A significant performance drop can be observed when simulating the Pareto solutions of Group 1 considering stochastic scenarios (shown in Table 6. 2 and Fig 6.17). For example, the NPV increases by 44% in DT-Sim-D while GI increases by 43% in DT-Sim-B when considering the climate uncertainty. When moving into NPV, it increases by 92% in DE-Sim-B. Therefore, it is clear that climate uncertainty has a significant influence on the performance of the energy system. Performance degradation due to climate variation is evident throughout the Pareto front, which is shown by the grey line connecting B-DT-Sim and D-DT-SIM. As a result of the performance degradation, the design solutions for DT show inferior performance (higher NPV and grid integration level) when compared to all the other Pareto fronts obtained using stochastic methods (Group 2). This means that neglecting climate uncertainty will induce energy system design that is not flexible enough in facing the external environment and its variations. Hence, the design solutions obtained using the deterministic model will end up with a notable performance gap due to the climate uncertainty being dominated by the design solutions obtained using stochastic methods (Fig. 6. 17).

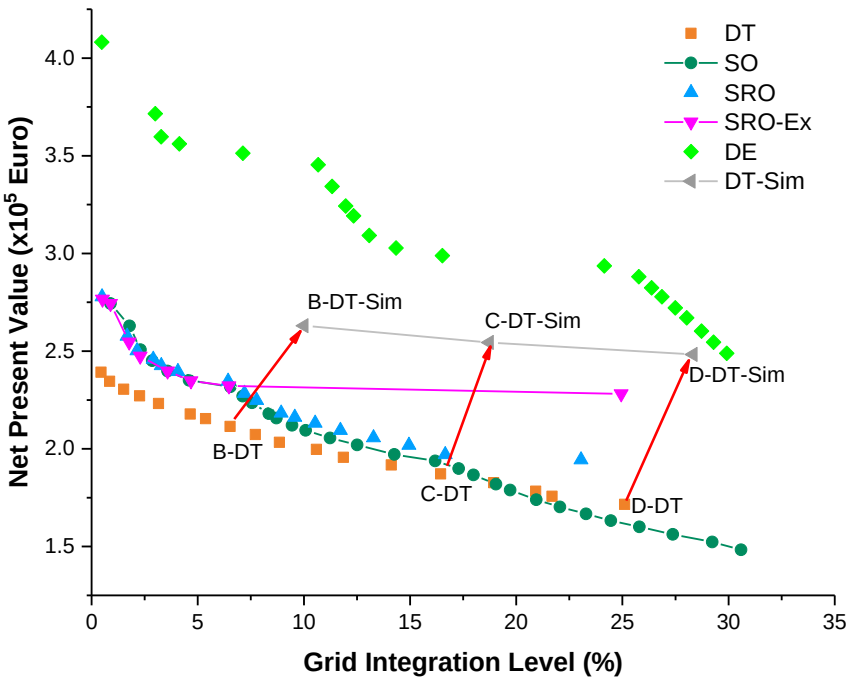

Fig. 6. 17: Performance gap due to the climate uncertainty. The gray line connecting B-DT-Sim, C-DT-Sim and D-DT-Sim shows the expected values of the objective functions after considering the uncertainty. The gray line is dominated by SO, SRO and SRO-EX Pareto fronts.

6.5.2.3. Impact of extreme climate conditions

Extreme climate conditions notably influence the reliability of energy systems. Both LOLP-SRO and LOLP-EXT present a better overview of the reliability of the system when moving from climate uncertainty to extreme climate events. LOLP-SRO averages the loss of load considering a horizon of one year (when evaluating the influence of extreme events) while LOLP-EXT averages the loss of load considering a time interval of two weeks, which moves through the entire year when computing LOLP and guarantees that maximum LOLP within the two-week time window is less than the constraint set. As a result, LOLP-EXT guarantees the smooth operation of the system in extreme conditions in a better way than LOLP-SRO. Furthermore, LOLP-EXT is more relevant in the context of extreme climate events since such events prevail for shorter periods of time. Both LOLP-SRO and LOLP-EXT are computed for Group 1 (Table 6. 2) and 2 (Table 6. 3). When analyzing Group 1, it is clear that a significant increase in LOLP can be observed. However, LOLP-Ext is kept below 1% when considering DT-Sim B to D. However, LOLP-EXT reaches 12% for SO-D, which is well below the expectations concerning power supply reliability. This clearly demonstrates that considering climate uncertainty using stochastic programing is not sufficient enough. In addition, it justifies the gap in NPV E-E in Fig. 6. 16. LOLP-EXT values for Pareto solutions obtained using SRO (SRO-B-D) are below 1% (although this violates the constraint set for LOLP as 0.1%). The results clearly show the

importance of combining robust and stochastic optimization methods in order to guarantee the robust operation under extreme climate conditions. Hence, neglecting extreme climate events will result in a **major** drop in power supply reliability. To maintain robust operation under extreme climate events, the proposed computational algorithm is therefore clearly significant. Finally, it can be stated that both, extreme climate events and the method used to assess the impact of extreme climate events (on the reliability), influence the objective function values and subsequently energy system design.

Table 6. 2: Performance of the Pareto solutions obtained using deterministic models under climate uncertainty and extreme climate events

	Sim[2]-NPV	Sim-GI	Increase in NPV (%)	Increase in GI (%)	LOLP[3]-SRO (%)	LOLP-EXT (%)	GI[4]-Ext (%)
DT-Sim-B	2.63	10.00	24.65	53.42	0.033	0.58	39.25
DT-Sim-C	2.54	18.73	36.08	13.93	0.033	0.59	41.07
DT-Sim-D	2.48	28.33	44.38	12.81	0.034	0.59	45.31
DE-Sim-B	4.00	13.66	13.99	91.60	0	0.00	7.13
DE-Sim-C	3.46	18.82	15.84	13.90	0	0.00	16.52
DE-Sim-D	3.48	13.18	18.40	-45.40	0	0.00	24.14

[2]Expected value considering the scenarios used for stochastic optimization [3]LOLP considering extreme events, [4]GI considering the conditions of extreme scenarios will prevail entire year

Table 6. 3: Reliability and grid integration level of Set B-D (Group 2) at extreme climate events

	LOLP[3]-SRO (%)	LOLP-EXT (%)	GI[4]-Ext (%)
SO-B	0.03	0.58	39.48
SO-C	0.07	0.63	47.08
SO-D	2.75	11.91	57.28
SRO-B	0.03	0.58	39.17
SRO-C	0.05	0.59	46.78
SRO-D	0.07	0.79	47.27
SRO-EX-B	0.00	0.00	30.23
SRO-EX-D	0.00	0.00	41.13

[3]LOLP considering extreme events, [4]GI considering the conditions of extreme scenarios will prevail entire year

Extreme climate notably influences the design and operation of energy systems, which can clearly be observed when comparing the grid interaction levels during extreme (Table 6. 2 and 3) and normal climatic conditions (Table 6. 1). When considering Group 1 (deterministic models), a notable increase in GI is observed in DT since DE considers the extreme conditions as the usual operation conditions. Similar to DT, a notable increase is observed in Group 2 (stochastic models) when moving from the expected value of grid integration level to the grid integration levels during extreme climate events. The grid integration level increases (when catering extreme climate conditions) when moving from SRO-EX to SRO and subsequently into SO. For example, GI-EXT increases from 41% to

47% and subsequently to 57% when moving from SO to SRO and subsequently SRO-EX when considering Set D. This is due to the fact that SO does not consider extreme events during the optimization process. Hence, the design solutions rely on the grid when catering the demand during extreme climate events since the ICG capacity is small. However, reliance on the grid gradually decreases when moving from SO to SRO and subsequently into SRO-EX. For example, the capacity of ICG increases respectively from 40 kVA to 60 kVA and subsequently to 80 kVA when moving from SO to SRO and finally to SRO-EX in Set D (Table 6. 1). A larger ICG capacity facilitates withstanding the fluctuations in demand and generation during extreme conditions. However, maintaining such flexibility adds an additional margin to the NPV when considering higher grid integration levels. Finally, it can be stated that both design and operation of the energy system play a vital role towards making energy systems robust in extreme climate conditions. A hybrid approach combining stochastic and robust programing methods (as proposed in this study) can facilitate the design of optimum energy systems considering both climate uncertainty and extreme climate events.

6.6. Conclusions and future perspectives

Climate change and the risk of more frequent and stronger extreme climate events demands for climate change adaptation and improving the climate resilience of energy infrastructure, which consists of two main steps:

I. Quantifying the impacts of climate change, extreme conditions and uncertainties on energy demand and renewable energy generation.

II. Designing the energy system considering changes in demand and renewable energy generation due to climate change.

This chapter tries to combine both these aspects in an effective manner in order to support the energy system design process. A novel hybrid stochastic robust optimization algorithm is proposed in this chapter to consider both climate uncertainty and extreme climate conditions. Climate uncertainty is considered through the stochastic programing while extreme climate conditions are considered through robust analysis. Accordingly, scenarios are created to represent climate uncertainty and extreme climate conditions in energy system optimization using climate data from a regional climate model.

From the comprehensive analysis on the demand profiles, it is found that synthesizing typical and extreme weather data sets based on the hourly distribution of the climate variables can better present the extreme climate conditions for the purpose of optimizing energy systems. Having larger

number of scenarios makes it possible to reflect extreme climate events through the scenarios used for stochastic optimization. However, the number of scenarios considered for stochastic optimization has to be limited considering the computational time. Hence, it becomes appropriate to consider climate uncertainty and extreme climate events in two different steps. Accordingly, the stochastic part of the optimization algorithm represents the climate uncertainty and the robust part represents the extreme climate events.

The energy system analysis reveals that climate uncertainty can cause a significant performance gap when using deterministic models to optimize energy systems. This will lead to a number of problems for the energy infrastructure that has already been developed using deterministic models. Hence, it is important to improve the climate resilience of existing energy infrastructure to withstand the climate uncertainties where the proposed novel computational algorithm can be used. Stochastic programing presents climate uncertainty in a much better way when compared to deterministic methods. However, stochastic programing alone cannot guarantee the robust operation of the energy system under extreme climate conditions. Hence, it is essential to come up with a hybrid approach combining stochastic and robust programing methods as proposed in this study.

The results of the study reveal that a higher renewable energy fraction (above 40% of the annual demand) can be maintained while keeping stringent conditions for power supply reliability. Hence, making energy systems resilient to extreme climate events adds an additional margin to the NPV but it does not undermine the opportunities to integrate renewable energy technologies into distributed energy systems. This chapter does not consider the influence of urban climate when deriving the energy demand. It would be interesting to extend the computational platform introduced in this chapter to consider urban climate in the future since it can intensify the influence of extreme climate conditions.

7 From Stochastic Optimization to Flexibility of Energy Systems

The flexibility of energy system has been widely taken into discussion recently focusing on the operation of the energy system. However, in order to improve the performance of energy systems under the uncertainties of renewable energy potential, demand and grid conditions it is important to consider their flexibility already at the early design stage. This requires an extension to the present methodologies used to evaluate energy system flexibility (often focused on operation of the energy system) and optimization methods used (often based on deterministic methods). A novel method is introduced in this chapter to evaluate flexibility which considers multiple criteria under different operating scenarios using fuzzy logic. GPU (Graphics Processing Unit)-accelerated computing is introduced to speed up the computation process when computing the expected values of the objective functions considering a pool up to 5832 scenarios. Subsequently, a Pareto optimization is conducted considering Net Present Value (NPV), Grid Integration (GI) level and system flexibility.

This chapter is based on (preprint version):

A.T.D. Perera, Vahid Nik, P.U. Wickramasinghe, Jean-Louis Scartezzini, "Redefining energy system flexibility for designing distributed energy system" (Manuscript under review in Applied Energy)

Author contribution for the journal paper:

In this article, ATD, VMN and PU designed the research with the support of JLS. ATD developed the computational model and implemented in GPU with the support of VMN. VMN developed the weather, demand profiles with the input of ATD. ATD conducted the analysis. ATD (entire manuscript except the Section 7.2.2) and VMN (Section 7.2.2)) prepared the first draft of the manuscript. PU and JLS supported in revising and finalizing the Manuscript

Readers are encouraged to read following conference proceedings for further information

1. A.T.D. Perera, Vahid Nik, P.U. Wickramasinghe, Jean-Louis Scartezzini, Integrating renewable energy technologies into distributed energy systems maintaining system flexibility, IEEE-EFEA 2018, Rome-Italy.

7.1. Introduction

Integrating non-dispatchable energy technologies such as wind and solar PV (SPV) energy is essential to decarbonize the grid; these technologies are variable due to the fluctuating nature of the energy potential. Hence, it is difficult to improve the contribution of solar and wind energy beyond a certain limit while maintaining power quality and reliability of the grid. According to Sansavini et al. [1], direct replacement of dispatchable energy sources by Variable Renewable Energy (VRE) may lead to cascade failures in the grid, resulting in blackouts. Detail assessment of power grids conducted by Ueckerdt et al. [2] suggests that it is challenging to cover more than 30-35% of the annual demand using VRE without a notable improvement in the present status of the grid. Recently, the National Renewable Energy Laboratory (NREL) - USA showed that VRE can be increased by up to 30% in the Eastern Grid of United States — one of the largest power systems in the world — through improvement of the grid flexibility [3]. Although integrating renewable energy into the existing energy infrastructure is vital, direct integration of VRE technologies will lead to several problems. Hence, the flexibility of existing energy infrastructures should be improved in order to facilitate the large scale integration of renewable energy while keeping existing energy infrastructures reliable.

The flexibility of engineering systems has been discussed for more than three decades, in a wide spectrum of areas such as manufacturing [4]–[6], transportation [7]–[9], energy, etc. Flexibility is defined as the adaptability of a system to a range of possible environments that it may encounter [5]; this includes both internal and external factors [10]. When moving into energy infrastructure, flexibility has been defined in different ways, focusing on different aspects. The definition of system flexibility has been very specific in certain instances, focused on certain aspects [11]. Furthermore, it has been defined considering different temporal resolutions starting from the level of micro seconds to months [12]. Referring to the recent literature, e.g. Alizadeh et al. [13], it can be concluded that flexibility does not have a general definition: the definition highly depends on the characteristics of the systems. In general, the recent literature on energy system flexibility can be classified into three groups: flexibility of i) generation, ii) distribution and iii) demand [14,15]. Lund et al. [16] highlight that generation flexibility from the perspective of energy systems, such as smart grids [17,18], micro-grids and energy hubs [19,20], plays a vital role when improving the contribution of distributed renewable energy technologies.

Flexibility of energy systems has been discussed in several recent studies focusing on renewable energy integration. Sensitivity of thermal storage [17]–[20] , vehicle to grid (V2G) [25–27], dispatchable sources [12,28] and demand flexibility [29–31] with regard to renewable energy integration are some of the considered areas. A number of different methods have been introduced in these studies to quantify the flexibility and to assess the energy system in order to evaluate the

potential of integrating renewable energy sources [32]. For example, Ulbig and Anderson [33] considered power provision capacity, power ramp-rate capacity, energy provision capacity and ramp duration as performance indicators in flexibility evaluations. By contrast, Nuytten et-al [22] defines flexibility as the capability of the installation to change the use of energy demand over time. Most of these definitions are based on very specific technical indicators; however, there are a few definitions focusing on a broader set of performance indicators, to present energy flexibility combined with multi-criterion decision making [13]. Among them, Oree and Hassen [34] use a multi-criterion decision-making method to quantify flexibility. Hence, it is clear that flexibility of the energy system has been defined in different ways to cater the requirements of given applications.

7.1.1. Research gaps in the present state of art

When moving into energy hubs, virtual power plants and smart micro grids, the uncertainty of a number of different aspects, such as renewable energy potential, demand and grid condition (price, curtailments for selling and purchasing etc.) needs to be considered. A complex optimization problem [12] is formulated when trying to optimize the design of the energy system [35] considering these uncertainties. As a result, substantial computational resources are required to achieve this task. Keeping aside the stochastic components, design optimization of the energy hub for a deterministic problem formulation may even take several days [36]. Hence, the majority of recent publications on energy system flexibility focus on their operation without addressing design aspects [13,32]. According to Kondziella and Bruckner [32], considering both system design and operation is vital when evaluating flexibility. Hence, computational algorithms that can optimize an energy system considering its flexibility within a reasonable computational time, while accommodating a number of different scenarios to represent the uncertainties in demand, generation and grid would clearly show promising directions to integrate more VRE sources while guaranteeing robust operation although not considered so far in present state of art.

Uncertainties in the external environment may lead to performance degradation in energy systems. Higher flexibility implies that the system can withstand changes in external environment with a minimum degradation on its performance indicators in long term. However, the terms ‘performance’ and ‘degradation’ are quite open ended and might extensively depend on the application, which makes it is difficult to quantify the impact of performance change. Furthermore, multiple performance indicators should be considered in this context. These aspects have not been considered in the literature with respect to energy system design [16]. Hence, the flexibility concept needs to be re-introduced to match with the requirements of the energy system designing problem. This will enable us to design energy systems which are resilient to external changes, especially during the renewable energy integration process.

7.1.2. Objectives of the chapter

The following three objectives have been defined in order to address the research gaps in preset state of art (see Section 7. 1.1.):

- Combine the energy system flexibility concept with scenarios considered for stochastic optimization;
- Redefine energy system flexibility to accommodate multiple criteria and preferences of the energy system designer.
- Improve computational algorithms to support energy system design considering uncertainties due to several external factors.

These three objectives are closely connected to each other. In addition, the chapter focuses on deriving optimum ways to integrate renewable energy technologies while maintaining the flexibility of the system Fuzzy logic is used to quantify the impact of performance degradation due to the uncertainties in the external environment (renewable energy potential, demand and grid conditions). Introducing fuzzy logic helps to understand the subjective inputs of the stake holders when quantify flexibility considering multiple criterions. Based on that, the flexibility of an energy system is defined considering multiple attributes as described in detail in Section 7.3. A novel accelerated computing algorithm based on a Graphics Processing Unit (GPU) is introduced for the first time in energy related design optimization. GPU computing allows large scale parallelization enabling it to compute the objective function values for a pool of scenarios considered in the stochastic optimization. As a result, computation time of the objective function evaluation reduces significantly while making it possible to evaluate a large pool of scenarios and used along with heuristic algorithms. A detailed description of the novel computational algorithm is presented in Section 7. 4. Subsequently, the flexibility of distributed energy systems at different grid integration levels is assessed in Section 7. 5, using a Pareto set obtained considering Net Present Value (NPV) and grid integration level (GI) as objective functions. Finally, promising directions for the integration of renewable energy technologies while maintaining system flexibility are discussed under Conclusions and future perspectives.

7.2. Overview of the energy hub and the scenarios for energy system simulation

A brief overview of the energy system and the scenarios considered for the stochastic optimization is presented in this section.

7.2.1. Outline of the energy hub

This chapter investigates design options for a multi energy hub [37,38] that caters the heating and electricity demand of residential urban areas in Lund, Sweden, simulated by modelling a certain

number of statistically representative buildings. The multi-energy hub consists of wind turbines, SPV panels, a battery bank and an Internal Combustion Generator (ICG); it is operating in grid connected mode. We assume that the heating demand of the neighborhood is catered using heat pumps; therefore, heating demand is converted to electricity and considered as part of the total electricity demand as presented in Fig. 7.1. Grid curtailments are introduced when selling and purchasing electricity from the grid. A time-of-use (TOU) pricing scheme is introduced when pricing electricity. Hourly time series of wind speed, solar irradiation and energy demand are used considering several scenarios as described under Section 7. 3. Similarly, scenarios are considered for grid curtailments for both purchasing and selling electricity to and from the grid.

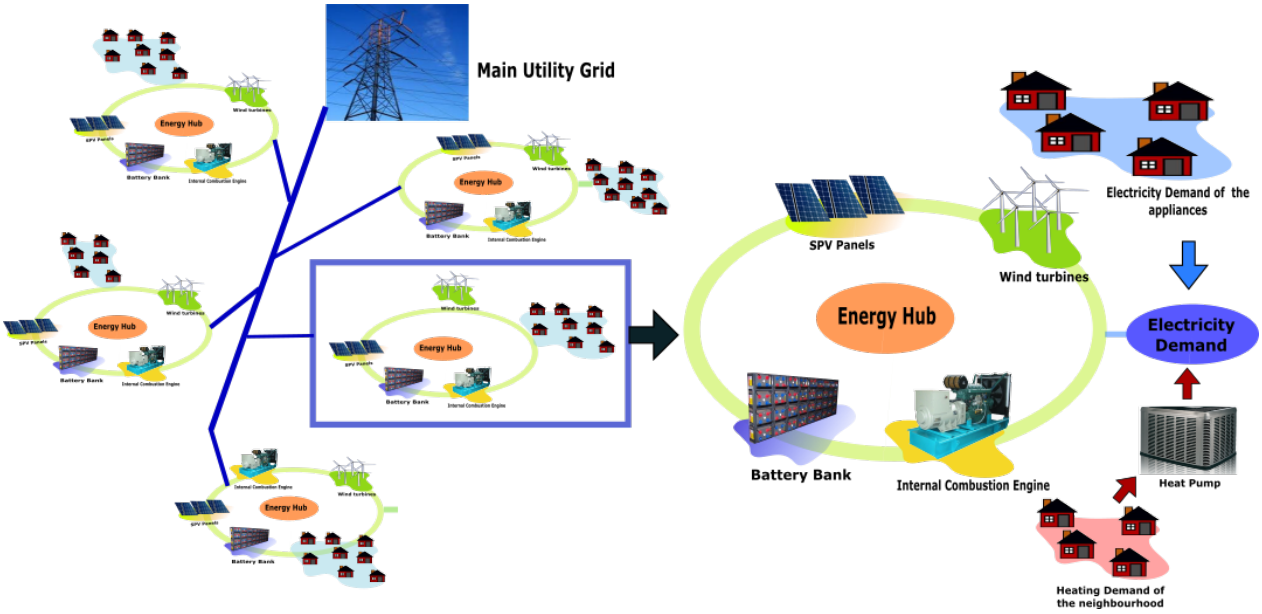

Fig. 7. 1: Overview of the grid integrated energy hub

7.2.2. Scenarios for energy demand and generation for stochastic optimization

Several probabilistic scenarios representing the conditions in the grid (price of electricity and grid curtailments), energy demand and renewable energy generation are created in this work, considering a typical urban area in Lund (a major city in southern Sweden with oceanic climate). The energy demand of 40 statistically representative residential buildings was simulated in the Simulink toolbox of Matlab [39] [40] for the 30-year time span of 1976-2005 and the RCA3-ERA40 climate scenario. ERA40 is a reanalysis-driven simulation of climatic conditions, constituting a realistic description of the state of the atmosphere and representing the real conditions with a high accuracy (for more details on the considered energy and climate models, the reader is referred to [39] [40]). The 30-year energy demand and renewable generation potentials were mapped as one-year probability distributions. Based on these probability distributions, scenarios for wind energy and

solar energy potential are taken for stochastic optimization and subsequently to evaluate flexibility (Fig. 2).

Forty (40) buildings were selected out of 52 buildings which represent the residential building stock in Lund, according to the BETSI investigation by the Swedish National Board of Housing, Building and Planning (Boverket) in year 2009 [41], which is the major source of information for the energy performance of residential buildings in Sweden. The Simulink model is used for simulating the energy performance of buildings separately, on an hourly time scale. The model takes into account the energy needed for heating, cooling, hot water, and fans and considers if the building has a heat recovery system. The model and its results have been verified and used in previous works of the authors (e.g. [39] [40]). Such detailed information is not available for grid curtailments and grid prices, therefore three different scenarios were considered, each based on [19] and [42] respectively.

Since retrofitting buildings affects their energy performance, a retrofitting approach including four retrofitting measures was applied to the considered buildings to investigate how the changes on the demand-side effects, and hopefully helps the performance of the urban energy system. The applied retrofitting measures include increasing the insulation of cellar/basement, facades and attics/roofs and replacing windows with more thermally efficient windows. According to a previous study, applying these four retrofitting measures together and considering the hourly energy demand of buildings. Considering the fact that Lund is a heating dominated city, heating demand will decrease on average while cooling demand will increase during warm summer days due higher insulation. The retrofitting strategies and their performance for current and future climate have been thoroughly investigated in the previous works of the authors [43] [44].

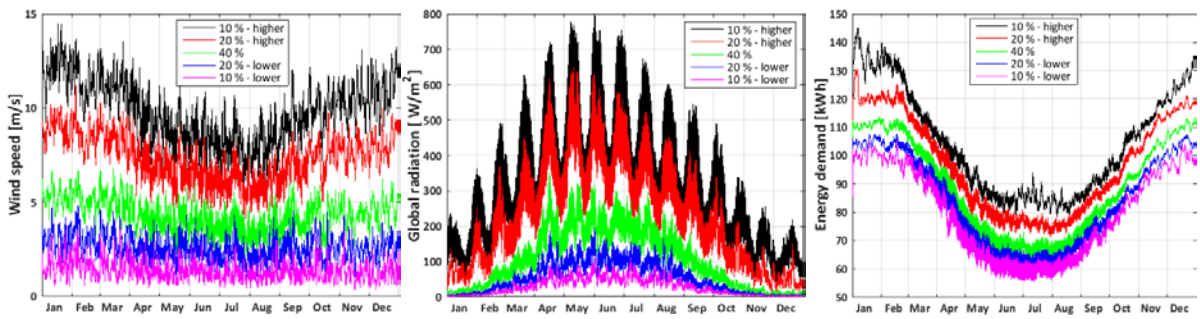

Fig. 7. 2: Moving average of the hourly time series of expected values for wind speed, global radiation and energy demand, considering five probability values.

7.3. Overview of the computational model

The computational model used to present the energy flow of the energy system and dispatch strategy is briefly presented in Sections 7.3.1 and 7.3.2. The energy flow model evaluates the power

generation within the system components and the interactions with the grid. This includes the power generation using renewable energy technologies, ICG and energy interactions that are taking place with grid and energy storage when catering the energy demand. The formulation of objective functions and constraints for the Pareto optimization are presented in Section 7. 3.3.

7.3.1. Outline of the dispatch strategy

The dispatch strategy used in this study consists of two levels as shown in Fig. 7. 3. The first level consists of a fuzzy logic based controller which determines the operating load factor of the ICG. Fuzzy logic has been amply used in dispatch optimization of hybrid energy systems [49–52] being one of the most promising methods for implementing energy management strategies in hybrid energy systems [53]. The operating load factor of the ICG is determined based on the State of Charge (SOC) of the battery bank, the difference in Electric Load Demand (ELD) (following the conversion of thermal demand into electricity) and power generation using renewable energy sources. After computing the power generation using the ICG, the net power generation within the system is computed. This is inserted in the second stage of the dispatch strategy which evaluates the interactions with the battery bank and grid. The finite automata theory is used in the second stage of the dispatch strategy. The nomenclature used for the dispatch strategy is presented in Table 7.1. The reduced state space for the second stage of the dispatch strategy is presented in Table 7.2. Fuzzy rules for the fuzzy controller (w_{ij}) and state transition points for the secondary level controller are optimized using the optimization algorithm. An extended explanation of the dispatch strategy can be found in Ref. [19].

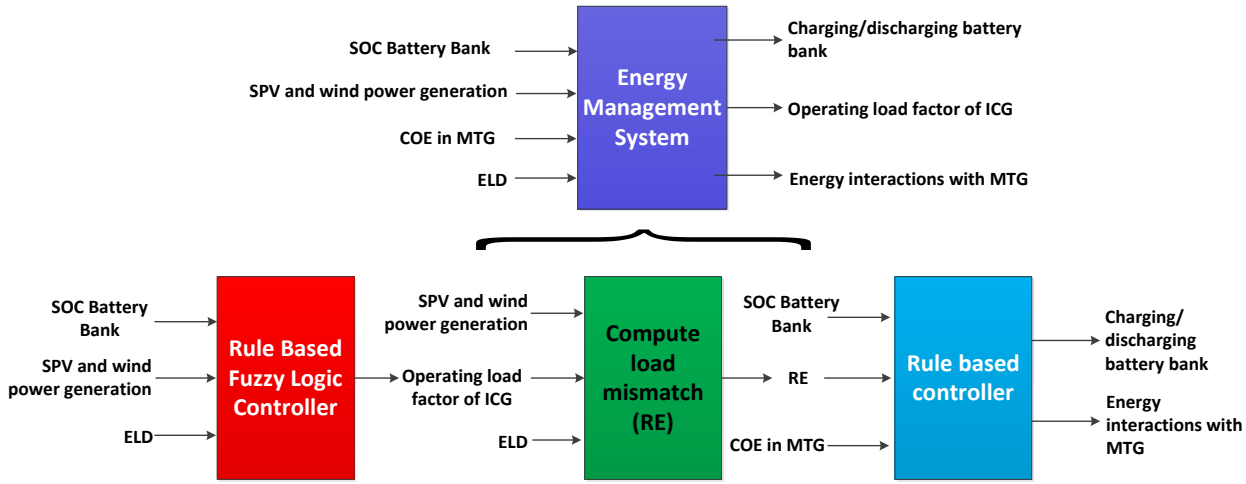

Fig. 7. 3: Outline of the dispatch strategy

Table 7. 1: Decision space variables used for formulating the state transfer function

		Description
Decision space variable	Lim_{BC}	Critical cost for $GCT_{t,s}$ above which selling the excess power generated to the grid is economical compared to battery charging
	Lim_{BD}	Critical cost for $GCF_{t,s}$ below which purchasing power from grid is economical compared to battery discharging
	Lim_{GTB}	Critical cost for $GCF_{t,s}$ below which purchasing power from grid to charge battery bank is economical
	Lim_{BTG}	Critical cost for $GCT_{t,s}$ above which selling stored energy to grid is economical
	SOC_{min}	Critical SOC of the battery bank below which discharging is not economical to cater the load mismatch
	$SOC_{Min,G}$	Critical SOC of the battery bank below which it is not economical to discharge and/or to sell the stored energy to grid
	SOC_{Set}	Maximum state of charged to be reached when charging the battery bank using the grid
Other parameters	GCT	Price of electricity when selling to grid
	GCF	Price of electricity when purchasing from grid
	COE	Cost of Energy
	MTG	Main distribution grid

Table 7. 2: Operating states for the secondary level of the dispatch strategy

State	Description of the state	Condition of the battery bank	Grid interaction	COE in Grid
State 1	Excess power is generated and COE in MTG is higher enough to sell excess power generated instead of battery charging	Self-discharge	Excess power generated is transferred to grid	$GCT_{t,s} > Lim_{BC}$ and $GCT_{t,s} < Lim_{BTG}$
State 2	Excess power generated is directed to the grid and battery bank discharge	Battery bank can be discharge up to $SOC_{Min,G}$	Power can be directed to the grid up to $P^{TG\text{-}Lim}$ depending on excess generation	$GCT_{t,s} > Lim_{BC}$ and $GCT_{t,s} > Lim_{BTG}$
State 3	Excess power generated is directed to the battery bank	Battery bank can be charged up to maximum SOC	No interactions	$GCT_{t,s} < Lim_{BC}$ and $GCF_{t,s} > Lim_{GTB}$
State 4	Excess power generated is directed to the battery bank and further charged using	Battery bank is charged using excess renewable energy and grid	Power from grid to charge battery bank	$GCT_{t,s} < Lim_{BC}$ and $GCF_{t,s} < Lim_{GTB}$
State 5	Excess power generated is larger than the maximal transferable, it needs to be dumped, which will produce waste of renewable energy (WRE).	Battery bank reaches maximum state of charge	Power is directed to the grid up to $P^{TG\text{-}Lim}$	At any condition
State 6	Mismatch in demand and generation taken from the grid	Self-discharge	Mismatch is catered	$GCF_{t,s} < Lim_{BD}$ and $GCF_{t,s} > Lim_{GTB}$
State 7	Mismatch is taken from the grid while charging the battery bank	Battery bank is charged up to SOC_{Set} using the grid	Power taken from the grid to charge the battery bank	$GCF_{t,s} < Lim_{BD}$ and $GCF_{t,s} < Lim_{GTB}$
State 8	Mismatch is taken from the battery bank	Battery bank can be discharged up to SOC_{min}	No interactions	$GCF_{t,s} > Lim_{BD}$ and $GCT_{t,s} < Lim_{BTG}$
State 9	Mismatch is taken from the battery bank and excess in the battery bank is injected to the grid	Battery bank can be discharged up to $SOC_{Min,G}$	Power to the grid from battery bank	$GCF_{t,s} > Lim_{BD}$ and $GCT_{t,s} > Lim_{BTG}$
State 10	Mismatch is greater than the maximum that can be taken combining battery bank and grid. Loss of power supply will take place in this case	Battery bank reaches the minimum state of charge	Maximum limit that can be taken from the grid	At any condition

7.3.2 Flexibility

There are a number of instances where the system flexibility is defined in different ways within the same field [5,10,61]. For instance, according to Cheng et-al [62], manufacturing flexibility is defined in different ways, such as the ability to respond effectively to changing circumstances, the capacity for taking new action to meet new circumstances, the capacity to continue functioning effectively despite changes in the environment etc. Similarly, a number of definitions can be found for system flexibility in the energy sector [13]. System flexibility has often been discussed related to renewable energy integration from the perspective of power system operation [16]. However, most of the studies focus on resilience of the system rather than flexibility (since flexibility is defined as the capability of the system to meet the changes during the operation with a minimum impact on its performance indicators in the broad sense).

Aligned with the general definition used for flexibility, this chapter introduces flexibility of the energy system as the capacity of the system to resist performance degradation due to changes in the external environment. However, the terms 'performance' and 'degradation' are quite open ended and might extensively depend on the application. In general, multiple criteria are used to evaluate the performance of energy systems (although rarely considered under the aspect of flexibility). In this chapter, six performance indicators are considered when evaluating flexibility. These are

- NPV
- Waste of Renewable Energy (WRE)
- loss of load probability GI
- NI
- fuel consumption of the generator

According to Perera et-al [54], these performance indicators provide a better overview of the performance of the energy system. The process of computing the system flexibility consists of six steps as presented in Fig. 7. 4:

***Step 1*:** The process begins with defining the scenarios for the stochastic optimization. These scenarios will represent the uncertainties. The scenarios considered for stochastic optimization are considered to evaluate the flexibility. A detailed description of the formulation of the scenarios is presented in Section 7. 2.2.

Step 2: The values for the performance indicators such as NPV, GI etc are computed for each scenario based on the time series simulation.

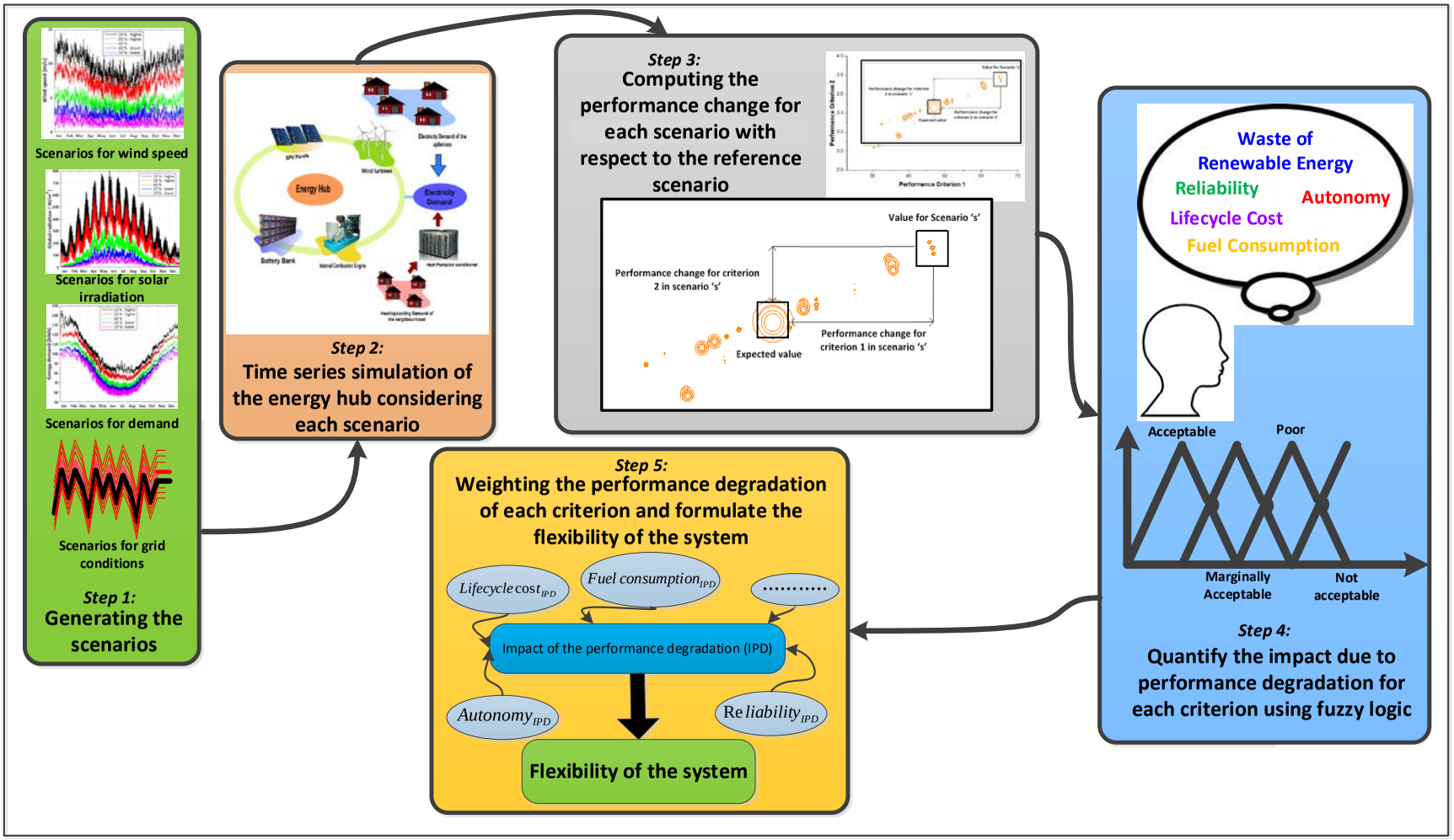

Fig. 7. 4: Steps followed to evaluate system flexibility

Step 3: The next challenge is to evaluate the performance change for each indicator. Degradation should be measured with respect to a reference value. When using stochastic programming, the expected value of the performance indicator can be used as the reference value (R_P). Performance change (PC) for a specific indicator for a given scenario ($PC_{P,S}$) can be calculated according to Eq. 7. 1, where CI is the value of the pth criterion for scenario s:

$$PC_{p,s} = (R_p - CI_{p,s}) / R_p \;\; \forall p \in P and \left|P\right| = n, \forall s \in \Omega \, and \left|\Omega\right| = m \tag{7.1}$$

For minimization objectives (a specific criterion that the system designer tries to minimize, such as cost, loss of load probability etc.), Performance Degradation (PD) is greater than zero whenever PC is less than zero, and vice versa for maximization objectives.

For example, performance change for NPV is computed for scenario's' ($\forall s \in \Omega$) according to Eq. 7. 2.

$$PC_{NPV,s} = (NPV_S - \mathbb{E}(NPV)) / \mathbb{E}(NPV) \;\; \forall s \in \Omega \tag{7.2}$$

Step 4: Performance changes are unavoidable due to the changes in the external environment. The main difficulty in this process is to evaluate the Impact of Performance Degradation (IPD) from the perspective of the stakeholder. IPD is highly dependent on the specific performance indicator and the application. For instance, a 15% reduction with respect to the reference value might be acceptable for renewable energy utilization but not for the system reliability or NPV. Furthermore, it is difficult to directly quantify the IPD depending on the performance change due to ambiguity. This is related to the fact that in most of the instances stakeholders use subjective measures such as acceptable, marginally acceptable, inadequate and poor instead of precisely quantified values. For example, a stakeholder might say that performance degradation is acceptable for the NPV if it is within 5%. But the quantitative IPD value for a performance change of 4% (for the same performance indicator) cannot be obtained using such a qualitative description. Fuzzy-logic can be used in such instances to quantify the IPD combining subjective inputs from system designers and the quantitative (objective) changes obtained for different scenarios [63].

Four classes are defined (i.e. acceptable, marginally acceptable, poor, not acceptable) for each performance indicator, based on the PD value (Table 7.3). Subsequently, triangular fuzzy numbers are used to represent each class. Based on that, the IPD is calculated for each criterion using a scale of 0 to 2. However, it is important to map the impact of performance degradation of different criteria into a single performance indicator. The procedure followed in Fuzzy TOPSIS to form a single performance indicator based on several criteria with fuzzy values is used in this chapter. Classification of four classes and the weights for different performance indicators are obtained based on Ref. [54].

The fuzzy performance degradation matrix (X_{PD}) is developed considering all the criteria under each scenario as the next step (using a linguistic rating for the other criteria similar to NPV as presented in Table 7.3) according to Eq. 7. 3.

$$X_{PD} = \begin{pmatrix} x_{11} & \cdots & x_{1n} \\ \vdots & \ddots & \vdots \\ x_{m1} & \cdots & x_{mn} \end{pmatrix}_{m\times n} \quad \frac{\rightarrow Criteria}{\downarrow Scenario} \; \forall p \in P and \left|P\right| = n, \forall s \in \Omega \, and \left|\Omega\right| = m \tag{7.3}$$

Step 5: A weighted performance degradation matrix X_{WPD} is computed according to Eq. 7.4 in order to map all the different ideas into a single indicator. A weighting matrix (Wp = (w_1, w_2…w_n)) is used to define the relative importance of each criterion.

$$X_{WPD} = \begin{pmatrix} \tilde{x}_{11} & \cdots & \tilde{x}_{1n} \\ \vdots & \ddots & \vdots \\ \tilde{x}_{m1} & \cdots & \tilde{x}_{mn} \end{pmatrix}_{m\times n} \quad \frac{\rightarrow Criteria}{\downarrow Scenario} \; \forall p \in P and \left|P\right| = n, \forall s \in \Omega \, and \left|\Omega\right| = m \tag{7.4}$$

In this equation, $\tilde{x}_{ij=} w_j \times x_{ij}$.

Expected value of IPD ($\mathbb{E}(IPD)$) is computed using Eq. 7. 5.

$$\mathbb{E}(IPD)_{\forall s\in\Omega} = \sum_{\forall s\in\Omega} \psi_s \sum_{\forall p\in P} \widetilde{x_p} \tag{7.5}$$

The sensitivity of the weight matrix is discussed in detail under Section 7. 5.3. Finally, flexibility of the system is defined using EIPD according to Eq. 7.6, extending the concept used in Fuzzy TOPSIS to arrive at the coefficient of closure.

$$Flexibility = \frac{1}{1+\mathbb{E}(IPD)} \tag{7.6}$$

Table 7. 3: Performance degradation, linguistic rating and triangular fuzzy numbers to present IPD considering for NPV [54,64]

Performance degradation	Linguistic rating	Triangular fuzzy number to present IPD
(0, 0, 5%)	Acceptable	(0,0,0.5)
(5%, 10%, 15%)	Marginally acceptable	(0.5,1,1.2)
(10%, 15%, 20%)	Poor	(1,1.2,1.5)
(15%, 20%,[max])	Not acceptable	(1.2,1.5,2)

7.4. Computational algorithm for optimization and performance analysis

Design optimization of distributed energy systems has been amply discussed in recent literature and reviewed in Ref. [65,66]. Heuristic algorithms such as particle swarm, simulated annealing and evolutionary algorithms are used to optimize distributed energy hubs due to the complexity of the objective functions [67]. The computational time to reach an optimum solution is however quite high when using heuristic algorithms since they require repetitive evaluation of the objective function(s). This is one major drawback in the use of heuristic methods for simulation-based optimization problems. Stochastic optimization can prolong the optimization process even further since several simulations are required to present different scenarios when computing the expected values of the objective functions. For this reason heuristic methods have become less popular for stochastic optimization problems. In order to address the problem, Graphical Processing Unit (GPU) accelerated computing is used in this chapter.

Given a sequence of data to process, The Central Processing Unit (CPU) will take one item from the sequence, process it and move to the next item in the list to process. For example, consider the execution of a 'for loop'. The CPU processes the data corresponding to the iteration index at each iteration. In certain instances, the data items in a sequence that is being processed are independent from each other. This means processing the ith item in a sequence does not require waiting for inputs from the data at the $(i-1)^{th}$ position in the sequence. However, given the sequential nature of the CPU processing, the ith item has to wait till (i-1) finishes processing. A GPU (Graphical Processing Unit) becomes useful in such instances. GPU is a collection of hundreds (or sometimes thousands) of CPUs. As a result, when there is a sequence of data, the steps are independent from each other, and the GPU can execute the processes in parallel, which significantly reduces the computational time. In GPU programming, each GPU is used along with a Central Processing Unit (CPU), which enables large scale parallelization of the computational program [68]. Therefore, a number of different threads can be run simultaneously. This method is amply used in such diverse applications as image recognition, computer gaming, molecular dynamics etc. [68]. It is introduced as a promising method to increase the computational speed of evolutionary algorithms in the literature [69,70].

7.4.1. Outline of the computational algorithm

The computational algorithm consists of two main parts: the first part evaluates the objective function values and the second part derives the Pareto front based on the objective function values. Both parts are computed using CPU (as shown in Fig. 7. 5) in the case of deterministic optimization problems (which is discussed in detail in Section 7. 4.2). Large-scale parallelization of the computer algorithm is feasible when using the GPU. Hence, it can be productively used to evaluate the performance indicators for different scenarios. The scenarios are subsequently used to compute the

expected values of the objective functions when conducting stochastic optimization. After computing the objective function values, CPU can be used to complete the steps in the optimization algorithm as shown in Fig. 7. 5.

Decision space variables are those corresponding to the energy system design and dispatch strategy:

- Type and capacity of the wind turbines and SPV panels, which represent renewable energy components.
- ICG and battery bank capacities, which represent dispatchable source and energy storage.
- Weight matrix, which represents fuzzy logic rules.
- State transition points as presented in Table 7.2.

Net present value of the system, grid integration level and system flexibility are considered as objective functions (as explained in Section 7. 3.3). Loss of load probability is considered as a constraint and maintained below 2%. A Steady ε-State Evolutionary Algorithm [71], based on the ε-dominance technique, was accordingly used in this study to conduct the optimization process. A detailed description of the decision space variables and operators used for optimization can be found in Ref. [19,72].

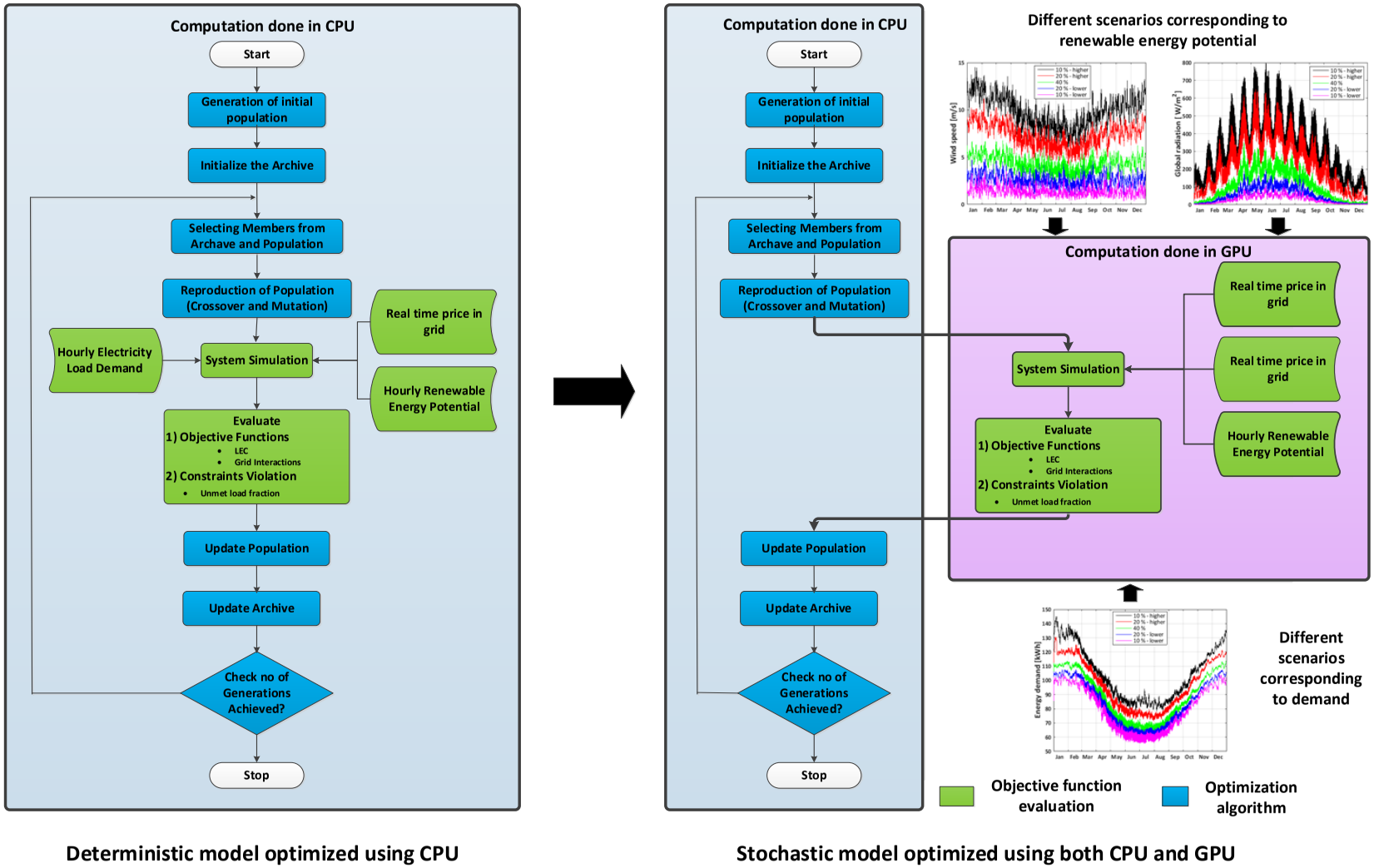

Deterministic model optimized using CPU

Stochastic model optimized using both CPU and GPU

Fig. 7. 5: Comparison of the two algorithms used to optimize distributed energy systems considering a deterministic model (present practice) and a stochastic model (introduced in this chapter). The flowchart on the left presents the commonly used approach (only) using the CPU while the one on the right presents the proposed novel approach.

7.4.2. Performance assessment and sensitivity to the number of scenarios

A brief overview of the sensitivity of the number of considered scenarios to computational time and accuracy is discussed using a NPV-GI Pareto front in this section (since it is used to evaluate the flexibility of energy systems in Section 7. 5). Increasing the number of scenarios used for the stochastic optimization will improve the accuracy while increasing the computational time [73]. At the same time, the number of objective functions and their nature (whether it formulate course objective space with many local optima's) will influence the number of generations required to converge towards the true Pareto front [74].

Pareto optimization is conducted considering NPV and GI as objective functions taking 729, 1728, 3375 and 5835 scenarios named as L, M, N and O respectively. The stochastic nature of wind speed, solar irradiation, energy demand, price of grid electricity and grid curtailments is considered when developing the scenarios. However, the number of scenarios used to present price of grid electricity and grid curtailments was kept constant when moving from L to O (only the number of scenarios for solar irradiation, wind speed and energy demand was increased). Pareto fronts obtained for the four cases are presented in Fig. 7. 6.

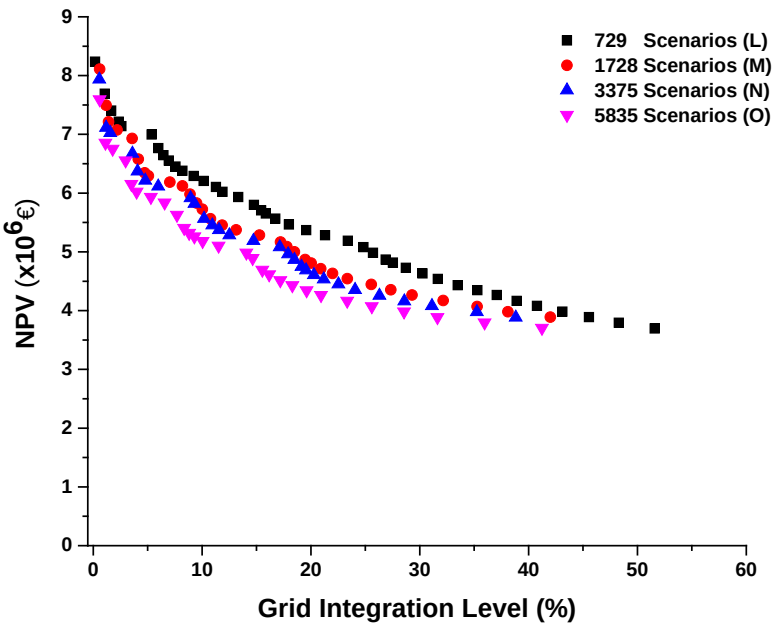

Fig. 7. 6: NPV-GI Pareto front obtained considering 729, 1728, 3375 and 5835 scenarios

It is a known fact that a higher number of scenarios results in better accuracy. In this specific case, a lower NPV is observed when increasing the number of scenarios (this specific aspect is discussed in Section 7. 5.1). When moving from Case L to M (729 to 1728 scenarios), a significant difference in

Pareto solutions can be observed. The difference between the Pareto fronts gradually decreases when moving from Case M to N and subsequently to Case O. The results of the Pareto optimization tend to converge when increasing the number of scenarios, which is trivial in stochastic optimization problems. Although increasing the number of scenarios will help to come up with a more accurate Pareto front, it results in increasing computational time (as shown in Fig. 7. 7). It is interesting to assess the improvement in computational time due to the introduction of GPU compared to using the CPU. Such a comparison is challenging since the stochastic optimization algorithm introduced in this study is using both CPU and GPU while the deterministic model is using only the CPU.

Total computational time (T_{Tot}) is the sum of the time taken for simulation (T_{Sim}) and optimization (T_{Opt}) as indicated in Eq. 7. 7 (all in seconds):

$$T_{Tot} = T_{Opt} + T_{Sim} \tag{7.7}$$

T_{Opt} is quite low when compared to T_{Sim}, considering the stochastic model used in the GPU computation. For the same reason, computational time increases linearly with the number of scenarios (Fig. 7. 7). This makes it possible to approximate T_{Tot} as T_{Sim}. Based on this assumption, increasing the number of scenarios in CPU will result in a linear increase in computational time assuming sequential processing. Therefore, the ratio of CPU time to GPU time ($R_{CPU/GPU}$) can be approximated according to Eq. 7.8

$$R_{CPU/GPU} = \frac{T_{Tot}^{CPU} N_{Scenarios}}{T_{Tot}^{CPU+GPU}} \tag{7.8}$$

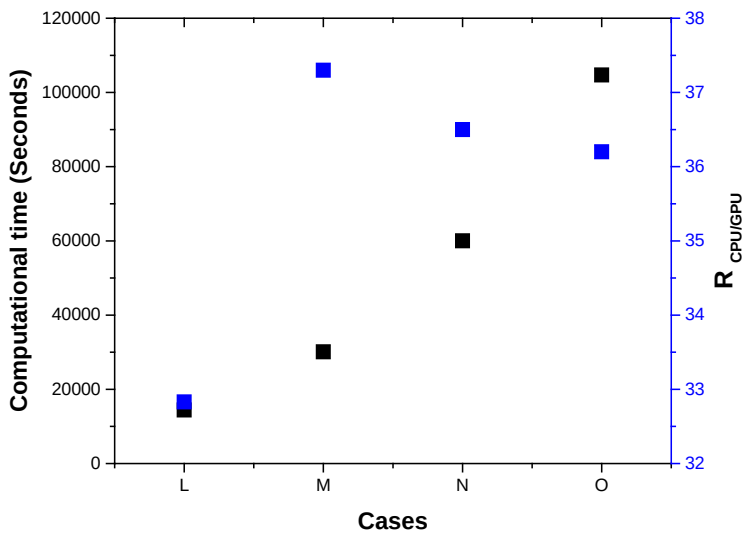

Fig. 7. 7: Impact of increasing the number of scenarios on computational time (obtain NPV-GI Pareto after 20000 generations) and performance improvement when using the GPU. The algorithm is implemented using Visual C++ (Visual

Studio 2015) and CUDA 7.5. The computational time is for a system with GeForce GTX 960 graphics card and an Intel(R) Core(TM) i7-6700-3.40GHz CPU.

The $R_{CPU/GPU}$ values for different numbers of scenarios, as presented in Fig. 7. 7, vary within the range of 30 to 40. This indicates that a 30 to 40-fold increase in processing speed can be obtained when introducing GPU. However, we need to understand that $R_{CPU/GPU}$ values present the maximum improvement that we can achieve. In practical problems this can be lower due to a higher ratio between T_{Opt} and T_{Sim} when using the CPU compared to the GPU.

7.5. Results and discussion

The challenge addressed in this study is to assess distributed energy systems considering techno-economic and environmental aspects. In the first part of this section, we use autonomy level and lifecycle costs of the system as the two main indicators for the assessment. Pareto optimization is conducted initially considering NPV and GI level to evaluate the system. However, it is more appropriate to conduct the assessment considering system flexibility under external uncertainties, such as changes in renewable energy potential, demand, grid condition etc. Therefore, the performance of the obtained Pareto design solutions is assessed under the uncertainty of demand, renewable energy potential and grid conditions to quantify the flexibility of the system. Promising paths to improve energy system flexibility are evaluated in the second part of this section. Pareto optimization is conducted considering NPV, GI and flexibility as objective functions and the obtained solutions are assessed using techno-economic factors to get a broad overview of the system flexibility.

7.5.1. 2D Pareto front considering NPV-GI

Improving the autonomy level of distributed energy systems and minimizing the lifecycle cost are two conflicting objectives, which are difficult to optimize simultaneously. The autonomy level of the system is directly related with the onsite generation. There are many instances where power generation using non-dispatchable energy sources (such as solar PV and wind) becomes economically viable compared to power generation using dispatchable source and grids at the scale of energy hubs. However, combining energy storage and dispatchable sources with non-dispatchable renewable energy technologies in order to maintain higher autonomy levels adds additional cost to the system. On the other hand, allowing more interactions with the grid while using it as a virtual storage is an economical option from the energy hub perspective. However, this is not beneficial when considering grid stability. These conflicting observations make the design process of energy hubs difficult, especially considering the possible changes that could occur in renewable energy potential, demand, grid price etc., which cannot be comprehensively evaluated based on a deterministic model.

Pareto solutions of LEC and GI present all the non-dominant solutions when considering the two objectives. Pareto front results obtained considering these objective functions are presented in Fig. 7. 8 along with the flexibility. When analyzing the Pareto front, it is prudent that NPV increases when the autonomy level of the system is improved. The increase of NPV is significant when attaining grid interaction levels below 10% since the system is approaching the condition of a stand-alone energy system where all the fluctuations in demand and generation will be handled by the energy system. Fig. 7. 8 (a) presents the expected values of the objective functions. However, the objective function values can notably change in different scenarios due to the uncertainties discussed before.

It is interesting to assess the impact of building retrofitting where demand profile shifted providing a higher flexibility from the demand side. Towards achieving this objective, Pareto optimization is conducted considering the same objectives Fig. 7. 8 (b) presents the comparison of Pareto fronts obtained considering present building stock and the retrofitting scenario. However, conducting such a comparison is challenging due to the changes in demand profile and flexibility introduced as a consequence of building renovation. Hence, flexibility of the energy system is considered as a constraint when conducting the optimization of the energy system. Furthermore, both objective functions are normalized according to [75], in order to support further comparison (8 (b). When comparing the two Pareto fronts obtained for present and retrofitting scenarios, a clear shift in normalized NPV is observed. Furthermore, Pareto front obtained for retrofitting conditions extends for higher grid integration levels while minimizing the NPV. These points clearly indicate that flexibility in the demand side notably helps to minimize the design and operation cost of the energy system when considering the same flexibility level of the energy system. On the other hand, it reflects the wide applicability of the flexibility model introduced in this study being sensitive to the flexibility of the demand side during the energy system optimization process.

It is interesting to analyze the objective function values of the Pareto solutions for different scenarios. Seven Pareto solutions from different parts of the Pareto front are selected and the objective function values for the corresponding system designs under different scenarios are plotted in Fig. 7. 9. Each color represents a different Pareto solution while each circle represents a scenario. The radius of each point is proportional to the probability of the scenario. The expected value of each solution is presented by a square. 729 different scenarios are considered in the stochastic optimization. Out of the seven Pareto solutions selected, two Pareto solutions are analyzed further, as presented in Fig. 7. 10. When analyzing Fig. 7. 10, it is prudent to look at a number of scenarios that have objective function values close to each other. In this way, several clusters of objective function values can be observed such as the one in Region W. Although there are 729 different scenarios, there are only 30 different clusters that have a significant difference in objective function

values. This reveals that the system can withstand the changes introduced in certain scenarios without any significant change to the NPV and GI, which results in a notable reduction of scenarios that show a distinguishable change in the objective function values. It suggests the capability of using a scenario reduction method [73] in the stochastic optimization process for energy system sizing problems without a significant drop in the accuracy. However, the factors that do not have a significant impact on the grid integration level or NPV might have an influence on other performance criteria such as renewable energy utilization, fuel consumption etc., which are considered when assessing the flexibility.

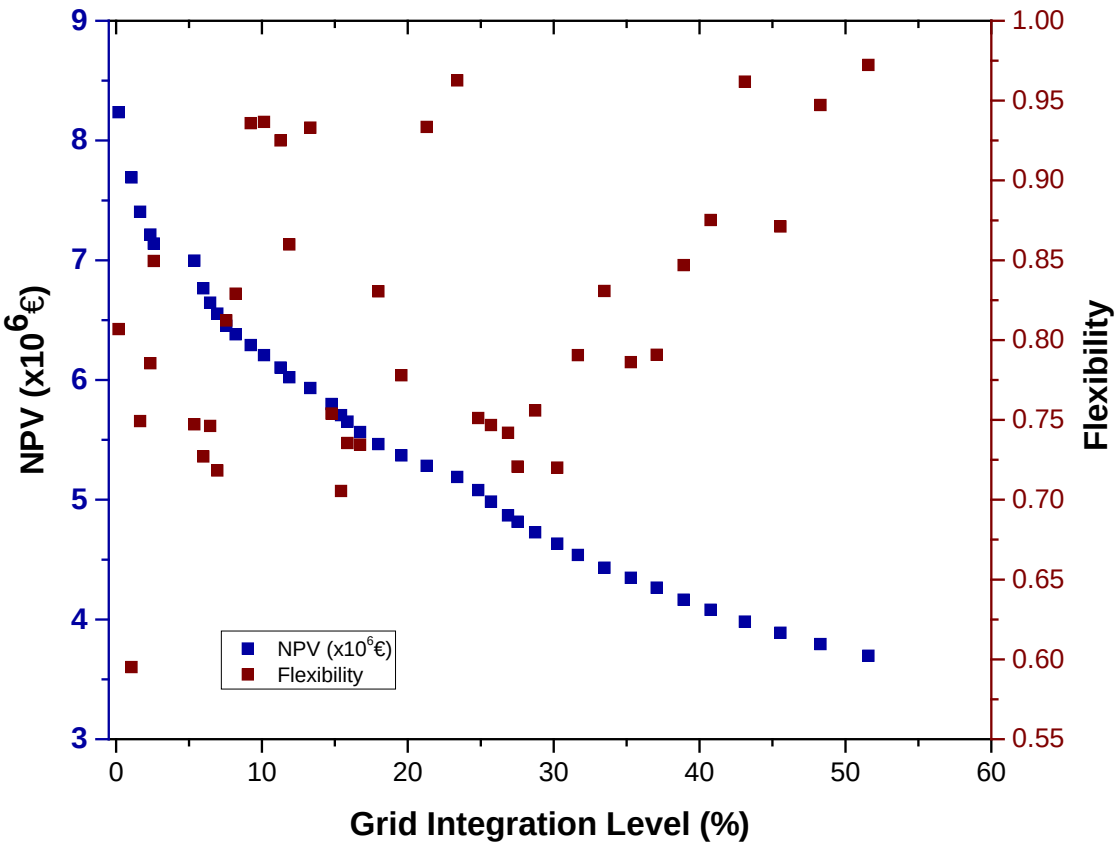

(a)

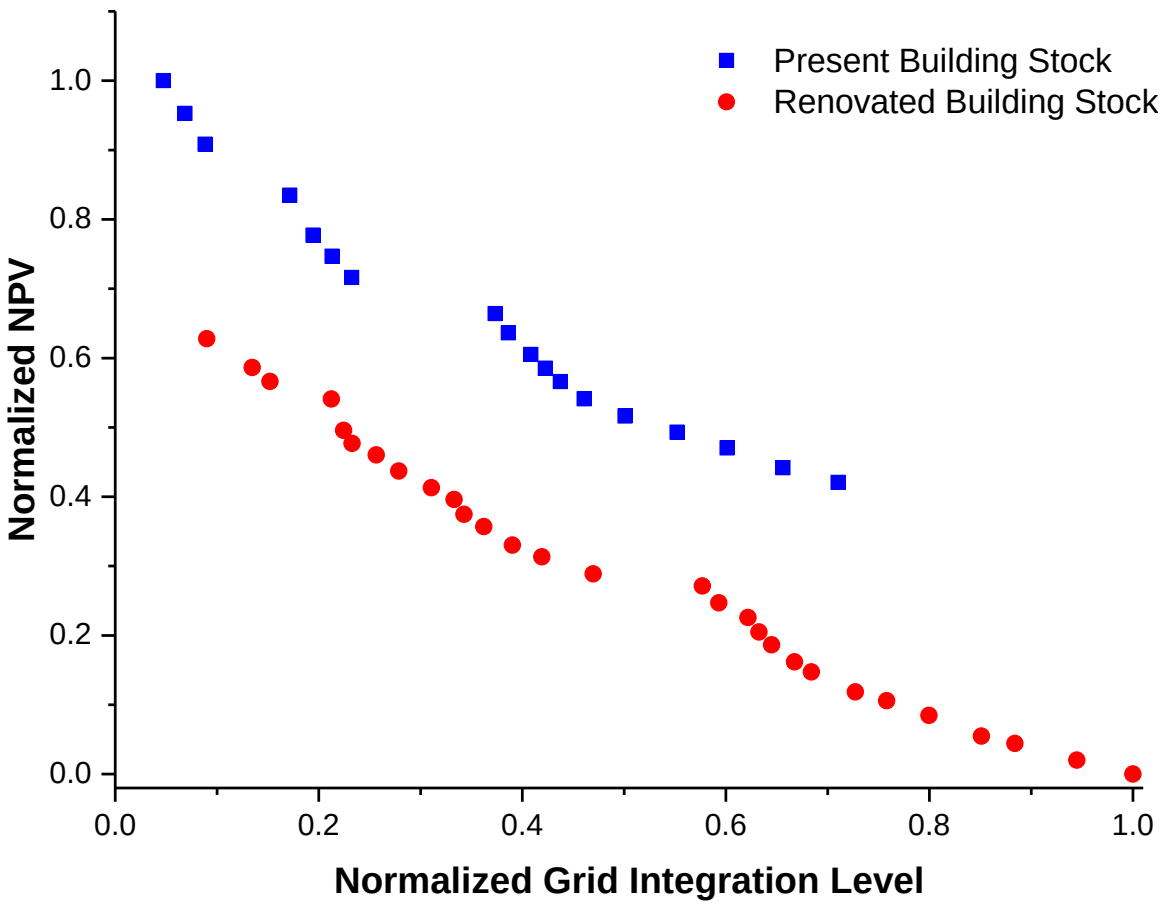

(b)

Fig. 7. 8: (a) presents design solutions of the Pareto front considering NPV and grid integration level and corresponding flexibility values of the design solutions and (b) presents the same Pareto front obtained considering present and refurbished building stocks. The flexibility is considered as a constraint in the Pareto optimization in addition to the power supply reliability. Normalized objective functions (normalization performed according to [75]) for the two scenarios are presented in Fig. 7. 8 (b)

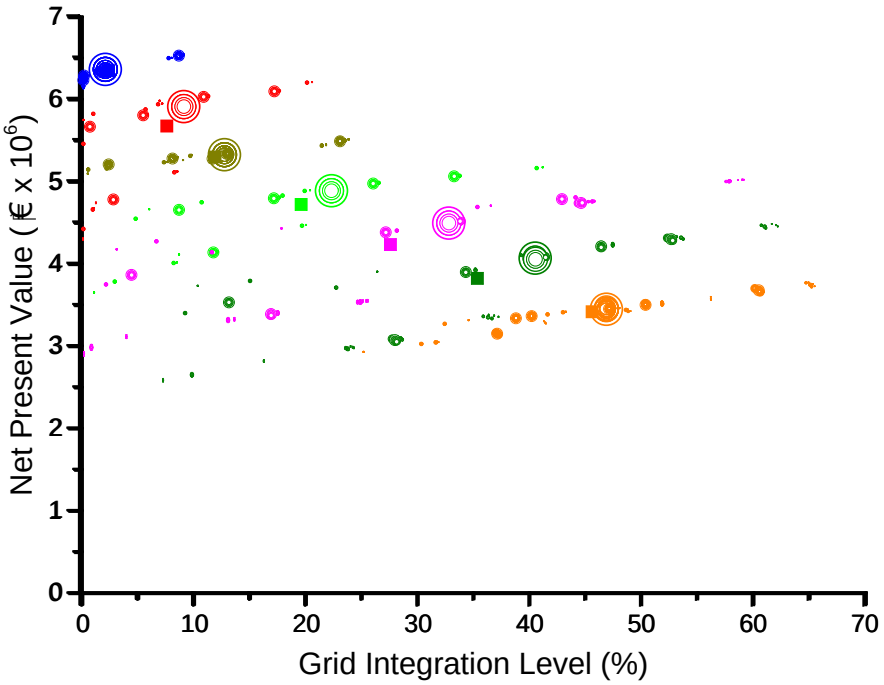

Fig. 7. 9: Objective function values for different scenarios for the seven selected Pareto solutions taken from the NPV-GI Pareto front. Each color represents a different Pareto solution while each circle represents a scenario. The radius of each point is proportional to the probability of the scenario. The expected value of each solution is presented by a square.

When assessing the objective function values for different scenarios, it is clear that the objective function values are distributed within a larger range. For example, in the Pareto solution with the lowest expected GI in Fig. 7. 9 and 10 (plotted in orange, the grid interaction level varies between 25% and 67%. Similarly, a significant difference in NPV is observed: between 2.94 and 3.78 x 10^6 €. More importantly, the expected values of the Pareto solutions show lower GI and NPV values (better performances) compared to the scenarios with the highest probability of occurrence (which might be equal to the objective function value if we use a deterministic model based on TDY or TMY) in most of the instances. For example, if we consider the vertex V-X in Fig. 7. 10, point V presents the objective function value for the scenarios with highest probability of occurrence (which might be the objective function value if a deterministic model is used to optimize instead of stochastic optimization). Point x represents the expected value after considering all scenarios. This difference (the difference between the objective function values for the cluster of scenarios having highest probability of occurrence and the expected value) is quite significant in certain Pareto solutions in Fig. 7. 9 (purple and dark green). This is due to the fact that the system tends to perform way better in certain scenarios when compared to the scenario with the higher probability of occurrence. As a result, a notable reduction in expected values is observed when compared to the scenario that has

the highest probability of occurrence. Having a better expected value for the objective function than the cluster of scenarios with the highest probability of occurrence is a positive sign, which will encourage further investments. This clearly suggests the advantage of stochastic methods in comparison to deterministic models when designing distributed energy systems.

When considering the Pareto optimal solutions, the number of scenarios where the system performs better than expected is lower than the number of scenarios where the system performs poorly. However, most of the scenarios where the system performs better than expected are extreme cases with very high improvement in objective functions and very low probability of occurrence. These extreme scenarios notably increase when the number of scenarios grows. This is the reason why objective function values improve when the number of scenarios is higher (Fig. 7. 6). There is always a high risk directly incorporated is extreme scenarios in real world operation due to low probability of occurrence and very high improvement in system performance. Improving the flexibility of the system can prevent the occurrence of such significant changes in system operation, which will minimize risks related to the uncertainty of the external environment.

A higher flexibility level guarantees that the performance indicators considered for flexibility do not change significantly with the changes in the external environment. For example, considering the two Pareto optimum design solutions presented in Fig. 7. 10, the flexibility of the system increases from 0.78 to 0.87 when moving from the solution with scenarios marked in green to that with scenarios marked in orange. Subsequently the impact is noticeable; objective function values for different scenarios are scattered all over the objective space (Fig. 7. 10) for the design solution with lower flexibility. This clearly shows that the objective function values change notably between different scenarios of the same Pareto solution when the flexibility of the system decreases.

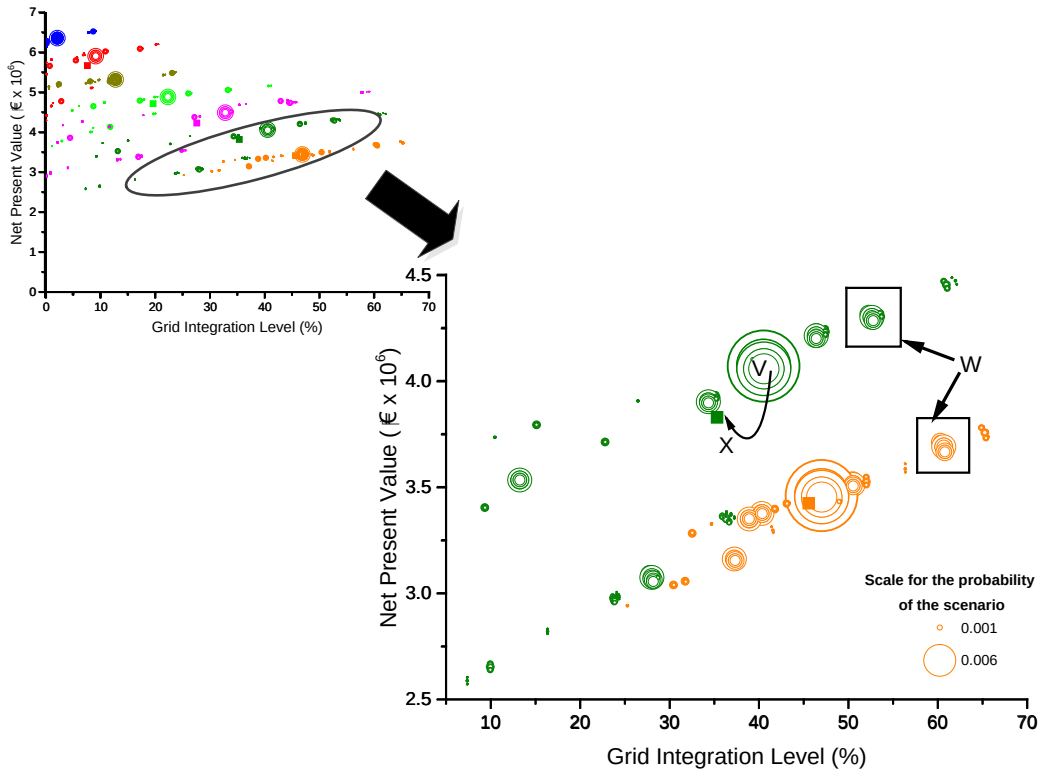

Fig. 7. 10: Further analysis of the objective function values for different scenarios of two Pareto solutions. Design solutions marked in green and orange have a flexibility level of 0.78 and 0.87 respectively. Region W presents clusters that have objective function values close to each other. Vertex V-X shows the reduction in objective function values when moving from scenarios that have the highest probability of occurrence (which might be the objective function values in case of deterministic optimization) to the expected values of the objective functions.

Naturally, lower flexibility levels are expected when reaching lower grid integration levels. However, flexibility of the system does not follow such a trend according to Fig. 7. 8 because of the intervention of the ICG (further discussed in Section 7. 5.2). In certain parts of the Pareto front, gradual improvement in system flexibility can be observed locally with the increase of grid interactions. Nonetheless, the pattern suddenly diminishes, reducing the flexibility significantly. Such behavior emphasizes the importance of looking into promising methods to improve the flexibility of the system, especially considering renewable energy integration processes. This requires an extension to the Pareto optimization where flexibility should be considered as a separate objective function.

7.5.2. 3D optimization considering LEC-GI and flexibility

In order to assess ways to improve system flexibility, Pareto optimization is conducted considering NPV, GI and flexibility. GI and NPV are considered as objective functions to be minimized and

flexibility to be maximized. The Pareto front obtained considering these three objectives is presented in Fig. 7. 11. The well distributed Pareto solutions clearly show that these three objectives are conflicting and cannot be optimized simultaneously. More importantly, energy system flexibility can be maintained at a high level irrespective of the grid integration level. However, the main question that arises in this context is: how far can renewable energy integration be achieved while maintaining the flexibility?

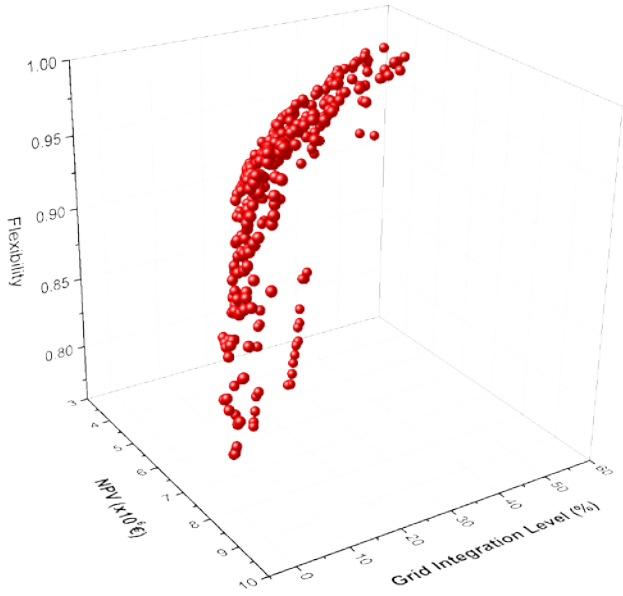

Fig. 7. 11: 3D Pareto front considering NPV, grid Integration Level and Flexibility as objective functions

It is important to identify the promising pathways to integrate non-dispatchable renewable energy technologies while maintaining system flexibility. In this context, constraints in grid integration level and lifecycle cost should be carefully considered. For this purpose, two plots that present the system flexibility along with the renewable energy fraction are plotted considering grid integration level (Fig. 7. 12) and NPV (Fig. 7. 13). The first few design solutions with the lowest NPV in Fig. 7. 12 have very low renewable energy penetration levels. However, a significant increase in renewable energy generation is observed with the increase of NPV. This can induce a notable increase in the renewable energy fraction, which reaches above 45% of the total annual demand of the energy hub. However, the flexibility of the system decreases significantly for most of the designs when the renewable energy fraction reaches values beyond 30%. This means that the performance of the system can notably change when operating under real world conditions due to the changes in external environment as discussed in Section 7. 5.1.

System flexibility tends to improve with improved grid connectivity (Fig. 7. 13). The electricity grid operates as a buffer which absorbs the fluctuations. Hence, the system possesses higher flexibilities

except for the scenarios with a renewable penetration level above 30%, which results in lower flexibility at certain instances. When considering lower grid integration levels, the flexibility is varying significantly. This is due to the fact that the system approaches a level of stand-alone where the fluctuations in demand and generation should be absorbed by the system. However, design solutions that depend on dispatchable sources and storage show higher flexibility even at lower grid integration levels, which is discussed later in this section.

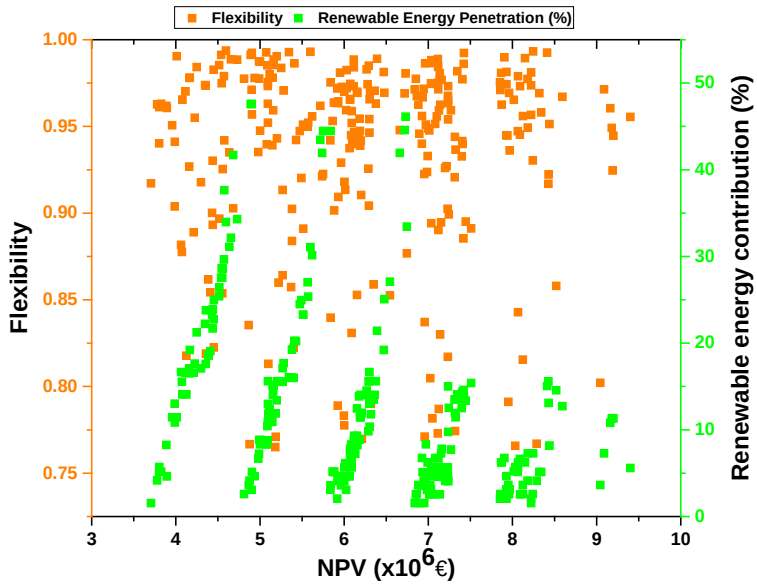

Fig. 7. 12: Flexibility, renewable energy level and NPV for the Pareto solutions of NPV-GI and flexibility Pareto front.

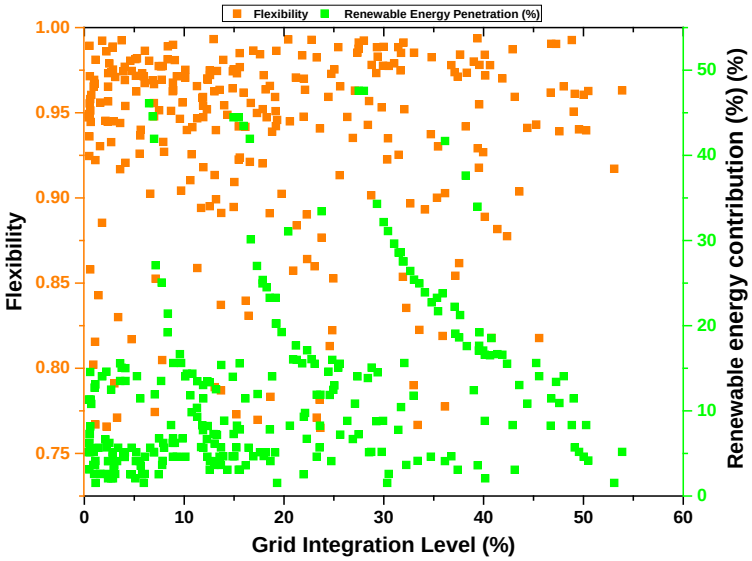

Fig. 7. 13: Flexibility, renewable energy level and GI for the Pareto solutions of NPV-GI and flexibility Pareto front.

In order to further assess the renewable energy integration process, Pareto solutions are plotted in Fig. 7. 14 considering renewable energy fraction and flexibility. It is interesting to assess the design

solutions that have the potential of generating a similar percentage of renewable energy with different flexibility levels. To do so, design solutions from four regions of the flexibility-renewable energy fraction plot, named as A, B, C and D, are selected. Region A includes design solutions that have the highest renewable energy penetration levels. However, the flexibility of the system is trivial when compared to all the other regions. When moving from Region A to B, renewable energy penetration slightly drops. However, a significant improvement in system flexibility is observed. It is interesting to find the driving force that improves the system flexibility. When moving from Region B to C both the system flexibility and renewable energy penetration level decrease. Similarly, both the renewable energy fraction and flexibility further decrease when moving from Region C to D. Three to four design solutions were taken from each region and tabulated in Table 7.4 in order to continue the discussion further.

Region A includes design solutions with the highest renewable energy penetration levels. The SPV capacity of the system is notably high in these systems when compared to the others with a higher ratio of SPV panel capacity to wind turbine capacity (See A1 to A3). Higher renewable energy penetration levels have been maintained while minimizing the grid interaction levels (A1 and A2) or contributions from ICG (A3). As a result, the flexibility of the system has notably dropped below 0.78 in all these design solutions. At the same time, the wasted renewable energy fraction exceeds 5%. Therefore, it is clear that although higher penetration levels of renewable energy are observed, these design solutions have major drawbacks.

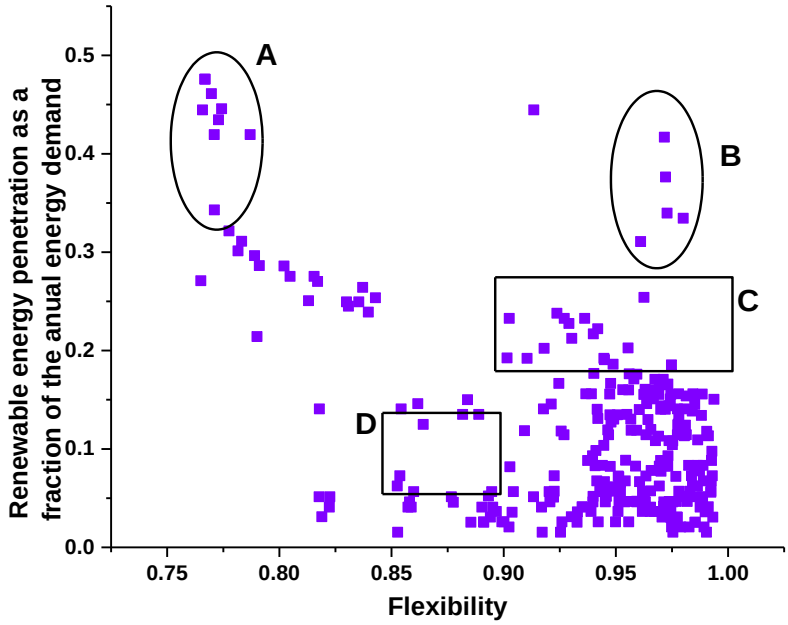

Fig. 7. 14: Renewable energy penetration level and system flexibility for the Pareto solutions of NPV-GI and flexibility Pareto front.

When moving from the design solutions in Region A to Region B, a notable improvement in system flexibility is observed. However, the renewable energy integration level drops by 5 to 10 % (except B4) while increasing the grid integration level to beyond 20%. The grid injection level is notably high in B4 (the only design solution reaching a renewable energy integration level of above 40%) when compared to all the other design solutions. Hence, a significant fraction of the renewable energy generation is injected to the grid instead of being used within the system. In general, grid interactions maintained by the design solutions in Region B are notably high when compared to the other regions. Furthermore, a notable drop in SPV capacity and simultaneous increase in wind turbine capacity is observed when moving from design solutions of Region A to those of Region B. As a result of higher grid integration level, design solutions in Region B are more flexible than in Region A. Furthermore, a good balance between wind and solar PV technologies is maintained in Region B, which results in a notable reduction of wasted renewable energy.

Renewable energy fraction, grid interactions, grid injection and waste of renewable energy notably decrease in Region C in comparison to Region B. Size of the battery bank, SPV panels and wind turbines decrease notably when moving into design solutions of Region C. However, the ratio between installed wind turbine and SPV panel capacity remains the same as in Region B. When moving from Region C to Region D, the renewable energy integration level further decreases. Furthermore, the system flexibility level decreases compared to the design solutions in Regions B and C. In general, the highest lifecycle cost and lowest grid interaction levels are observed in Region D. Higher ICG capacity depicts that the system tends to depend more on the dispatchable source for catering the demand while maintaining less interactions with the grid. Due to the dependence on the ICG, design solutions in Region D tend to be more flexible for the changes in external environment. This can justify a higher flexibility even at lower grid interaction level which was observed previously when analyzing the NPV-GI Pareto front in Section 7. 5.1

Table 7. 4: Performance comparison of few selected cases from Fig. 7. 14

	NPV ($x10^6$ €)	Flexibility	Grid Integration (%)	Grid injection (%)	Renewable fraction (%)	Wasted renewable (%)	SPV Capacity (kW)	Wind capacity (kW)	Battery banks	ICG capacity (kW)
A1	5.862	0.7710	6.99	10.12	41.95	5.521	342	40	19	80
A2	5.913	0.7743	6.86	10.79	44.57	6.604	364.5	40	19	80
A3	4.302	0.7667	27.50	8.14	47.58	6.072	355.5	120	15	40
B1	3.974	0.9625	33.03	1.48	25.41	0.073	139.5	180	19	40
B2	4.928	0.9611	20.43	3.55	31.07	0.362	162	240	20	60
B3	5.936	0.9801	23.78	6.97	33.44	0.371	121.5	380	19	80
B4	4.120	0.9717	36.14	18.85	41.69	2.412	279	180	18	40
C1	7.416	0.9885	3.59	0.43	15.57	0.001	90	100	9	120
C2	5.539	0.9391	9.69	0.48	15.61	0.003	99	80	12	80
C3	4.752	0.9653	24.84	0.16	15.99	0.003	67.5	160	20	60
C4	5.545	0.9246	9.58	0.69	16.66	0.002	108	80	12	80
D1	6.192	0.8177	2.84	9.33	5.14	0.183	18	60	19	100
D2	7.095	0.8225	0.43	12.46	5.14	0.903	18	60	20	120
D3	6.284	0.8599	3.39	7.04	5.67	0.001	22.5	60	19	100
D4	7.171	0.8526	0.52	14.33	6.23	0.001	36	40	18	120

7.5.3. Sensitivity of the weight matrix

The flexibility level of the system is an integrated measure of several performance indicators. Depending upon the relative importance given to each performance indicator, values obtained for flexibility might change. The relative importance of each criterion is brought together using the weight matrix. The weight matrix and triangular fuzzy numbers can be obtained in different ways. In this study, we follow experts' opinion to obtain both. This is followed up by a method proposed by the authors in Ref. [54] which provides a detailed overview.

Two additional scenarios with different weight matrices are considered in order to evaluate the sensitivity of the considered weight matrix (see Fig. 7. 15 and Table 7.5). Scenario P presents the weight matrix used so far for the assessment. Scenario Q, considers a situation where NPV is given more priority compared to Scenario P. Furthermore, grid interactions are considered at two different levels, i.e. electricity purchased from the grid and net interactions. When moving from Scenario Q to Scenario R, the priority level of the NPV is further increased. In addition, total net interaction with the grid is considered instead of considering the energy purchased from the grid.

Table 7. 5: Weight matrix for three cases

Case	NPV	WRE	Loss of load probability	Load from grid	Net grid interactions	Generator Fuel consumption
P	0.3	0.15	0.2	0.25	0	0.1
Q	0.4	0.1	0.2	0.1	0.1	0.1
R	0.6	0.05	0.1	0	0.2	0.05

A distinguishable difference in flexibility values can be observed for the three different weight matrices. This clearly indicates that the preference of the system designer can have a distinguishable influence on the flexibility values, which can result in changes of up to a maximum of 10%. However, it is difficult to observe a common trend for the three weight matrices except for the design solutions in Region F where the flexibility value of weight matrix P is in-between the two other matrices. Pareto solutions between Region F and line E-E show flexibility values very close to each other. Fluctuations in flexibility are quite significant for all three scenarios when moving into the design solutions on the left side of line E-E. At certain instances, flexibility values obtained for the three scenarios are close to each other. A distinguishable difference can be observed when moving from P to Q and R. However, the Pareto solutions do not show a significant difference in flexibility above 10% when moving from one scenario to the other. In other words, the flexibility represents the vulnerability of the system performance due to the changes in external environment, which does not change significantly for the three weight matrices considered.

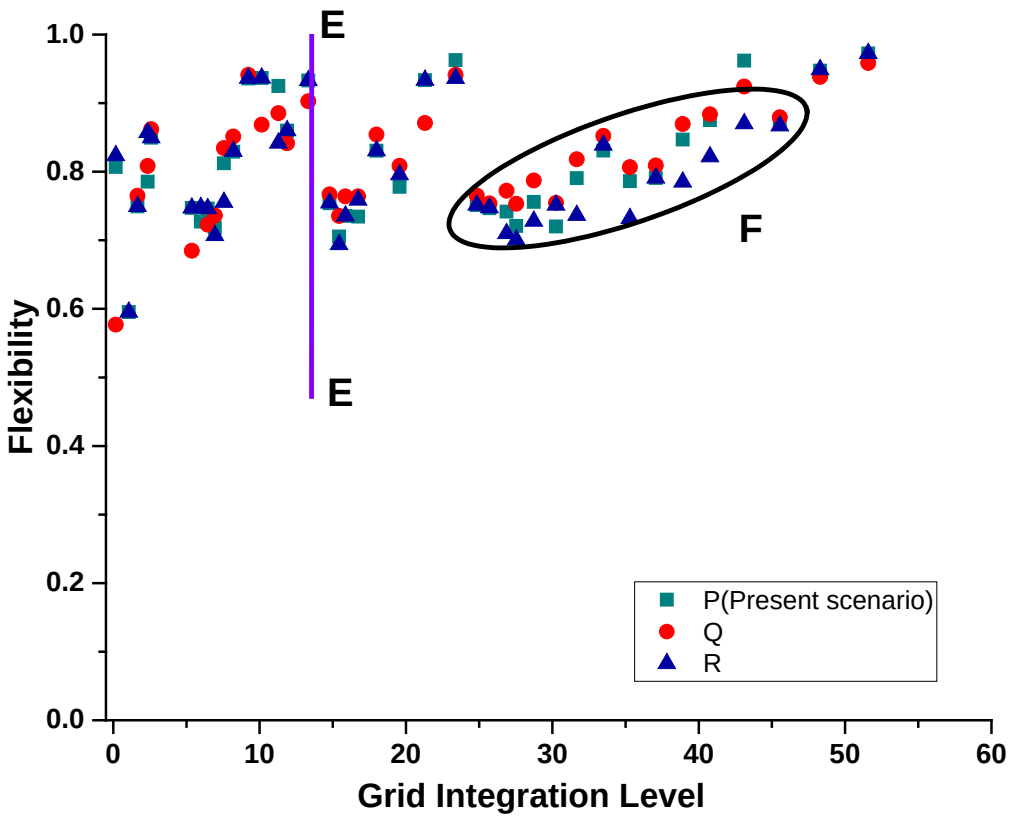

Fig. 7. 15: Comparison of three weight matrices

7.6. Conclusions and future perspectives

Changes in the external environment can strongly influence the performance of the energy system, which is usually not considered in the design process of energy systems. Energy systems should be designed to resist the performance degradation due to changes in the external environment caused by the stochastic nature of renewable energy potential, demand and grid conditions. This study shows that extending the flexibility concept to the energy system design process while combining it with stochastic optimization can be helpful to address the aforementioned problems.

The flexibility concept is redefined in this study in order to address three main limitations in the existing pool of knowledge:

I. how to aggregate stochastic optimization and the flexibility concept
II. how to evaluate the flexibility of an energy system considering different performance indicators with different priority levels in the energy system design process
III. how to integrate subjective input from the system designers/investors with regard to the impact of performance degradation with the flexibility concept.

In order to address these research problems, a pool of scenarios is developed using pseudo–sequential time series of demand, renewable energy potential, and grid conditions, extending the

deterministic model used to optimize the energy system. Changes in performance indicators under different scenarios are used to compute the flexibility level. Six different criteria are considered (with different priority levels) when defining energy system flexibility. Fuzzy logic is used to integrate the subjective input from the system designers/investors in the process of quantifying the impact of performance degradation. Subsequently, the sensitivity of the weight matrix used to prioritize different performance indicators is evaluated.

Stochastic Pareto optimization is conducted considering NPV, GI and system flexibility as the objective functions. Both CPU and GPU are used for the computational algorithm and the scenarios are simulated simultaneously using the GPU. A significant improvement in computational time is observed when using the GPU compared to CPU with sequential processing. A noticeable reduction in objective function values is observed when using a stochastic method compared to a deterministic model. Extreme scenarios with a lower probability of occurrence improve the objective function values notably, which results in an improvement of the expected value of the objective function. However, such scenarios - with a notable improvement in objective function values - will impose a risk on energy system investment unless flexibility of the energy system is guaranteed.

Significant changes in performance indicators can be observed due to the changes in external environment, which can account for variations of up to 40% of the expected value of NPV and of more than 100% for GI. This clearly indicates the vulnerability of the system under the uncertainty of external factors which needs to be minimized. Pareto optimization considering flexibility as an objective function is used to assess this aspect. Results of the 3D Pareto front reveal that changes in external environment can have a significant impact on the performance indicators for design solutions with a renewable energy contribution beyond 30% due to lower flexibility. Even with higher grid integration levels, it is challenging to integrate renewable energy technologies to cater more than 30% of the annual demand. When minimizing the grid interactions by up to 10%, renewable energy generation within the system level will decrease by up to 15% of the annual demand.

The assessment of the energy system considering system flexibility highlights that reaching higher renewable energy penetration levels is still a challenge although this is not recognizable when using a deterministic model. For this reason we find a number of recent publications showing penetration levels of non-dispatchable energy sources of beyond 80% of annual demand. The interesting question that lies ahead is: how far can we get assistance from future improvements in energy storage (within the system) and grid (outside) to integrate non dispatchable renewable energy technologies while maintaining the flexibility of the energy system? Furthermore, we should carefully consider whether the speed of technological improvements within these two sectors is sufficient to

cater the speed of renewable energy integration. The additional cost required for future scenarios when improving energy system flexibility will help to address these problems. This requires an extension to the flexibility concept introduced in this study beyond the boundaries of the energy system while taking into account grid stability, which will help system designers to come up with an optimum balance between energy system improvements and grid improvements.

8 The Impact of Urban Climate on Energy Systems

Rapid growth of cities, concerns on global warming and depletion of fossil fuel resources call for sustainable energy solutions for cities. Distributed energy systems such as energy hubs offer promising solutions in this context. Evaluating the energy demand at urban scale is vital to support the design of energy hubs. However, most of the recent studies are based on bottom-up models and do not consider the energy demand in detail. More specifically, the influence of the urban climate on urban energy demand has not been considered so far in the energy system design process. In order to address this research gap, a novel computational platform is developed in the first part of this chapter, combining an urban climate model with a building simulation tool and an energy system optimization model. The second part of the Chapter is devoted to quantifying the impact of urban climate on energy system design and assessing the consequences of neglecting this specific aspect on energy system performance. Three case studies are conducted considering three building densities for the city of Nablus (building density at the periphery, center and future center of the city) in Palestine. Three scenarios representing 1) standalone buildings (present practice) 2) shadowing and longwave reflection (radiation heat transfer from the walls and the roofs of the buildings to the urban climate and to the sky) of neighboring buildings and 3) urban climate are considered for each case study when computing the energy demand. Subsequently, the energy system is optimized considering Net Present Value (NPV) and system autonomy level as the objective functions (Pareto optimization).

This chapter is based on (preprint version):

A.T.D. Perera, Silvia Coccolo, Jean-Louis Scartezzini, Dasaraden Mauree, , "Quantifying the impact of urban climate by extending the boundaries of urban energy system modeling" Applied Energy 2018 (222), PP. 847–860

Author contribution for the journal paper:

In this article, ATD, SC and DM designed and conducted the research with the support of JLS. ATD (Sections 8.1, 8.2.1, 8.2.1.1, 8.2.1.2, 8.4 (entire section), 5.3, 5.4 and 6), SC and DM prepared the first draft of the manuscript. JLS supported in revising and finalizing the Manuscript.

Readers are encouraged to read following journal paper and the conference proceedings for further information

1. Dasaraden Mauree, Silvia Coccolo, A.T.D. Perera , Vahid Nik, Jean-Louis Scartezzini, Emanuele Naboni, "A new framework to evaluate urban design using urban microclimatic modelling in future climatic conditions", Sustainability, 2018, 10(4), 1134
2. Dasaraden Mauree, A.T.D. Perera, Jean-Louis Scartezzini, Influence of Buildings Configuration on the Energy Demand and Sizing of Energy Systems in an Urban Context, Applied Energy Conference (ICAE), 2017 UK

8.1. Introduction

Energy requirements in urban areas are rising at a rapid rate with the increase in urban population [1], [2]. In the context of actions against climate change, rapid depletion of fossil fuel resources and health concerns due to the emission of noxious gasses, a shift toward sustainable energy solutions in cities is therefore essential. The transition from fossil fuel based urban energy systems to 100% renewable energy systems [3], [4] is expected to be achieved within a few decades. To reach this goal, it is important to upscale planning from net-zero buildings to energy sustainable neighborhoods, districts and cities, since energy optimization of a district or a community is more cost effective than optimizing each building separately [5]. The objective is to lead urban planners to consider energy efficiency of the urban form and renewable energy integration simultaneously during the planning process [6]. Developing a holistic computational platform that bridges urban climate, building simulation and energy systems will be immensely helpful in this context.

Renewable energy integration and energy system design at urban and neighborhood scale have been widely discussed in recent studies at individual building, community, district and urban scale [7]–[11]. A comprehensive review on this is presented by Kastead et-al [12]. Perera et-al [13] have shown that integrated energy systems such as energy hubs can be used to integrate non-dispatchable renewable energy technologies beyond 60% of the annual demand. Morgan et-al [14] showed that more than 80% of the demand of a community can be supplied using onsite renewable energy technologies. Movraj et-al [15] have evaluated the influence of grid constraints when integrating renewable technologies into energy hubs. All these studies portray an optimistic picture of renewable energy integration at urban and neighborhood scale. However, simple integration of renewable energy technologies at any scale (building, community, urban or even direct grid integration) will result in poor utilization of the generated renewable energy [16]. Therefore, optimization tools are needed to reach the optimum energy mix.

Recently, a number of groups have developed optimization algorithms to implement efficient energy systems at urban and community scale while minimizing lifecycle cost, environmental impact, grid dependency etc. Samira et-al [8], [17], [18] introduced a bi-level optimization algorithm to design distributed energy systems considering the dispatch strategy, which was later extended to include thermal networks. Optimum design of distributed energy hubs and the electrical and thermal distribution networks is addressed by Moraj et-al [19]. Simultaneous optimization of multiple energy hubs considering the interactions and the energy network is performed by Maroufmashat et-al [20]. A detailed cross comparison of different optimization algorithms used to design distributed energy systems can be found in Ref. [21]–[23]. These studies are solely focused on the generation and

distribution aspects of the energy infrastructure where demand is considered as direct input to the optimization model. Therefore, the sensitivity of factors such as urban climate, building density and urban form on the demand is not properly considered.

Improving energy efficiency and sustainability in the urban context depends on four leverages, i.e. urban morphology, building form and technology, occupant behavior and energy system [24]. The contribution of all these leverages is subject to the urban climate. On the other hand, the building stock itself has a notable impact on the urban micro climate. Quantifying the influence of urban climate on the building energy demand considering all the aforementioned factors is a challenging task. However, it is essential since the thermal behavior of the collective building stock is different from that of a stand-alone building; especially in an urban context [25]. According to Moonen et-al [26], a building in an urban area (compared to a stand-alone building) will more likely experience 1) higher air temperature due to urban heat islanding (UHI) effect, 2) lower wind speeds due to the wind shelter effect 3) reduced energy losses during the night due to the low sky view factor 4) changes in solar heat gain due to shadowing 5) changes in radiation balance due to the interactions in neighboring buildings. Neglecting the aforementioned factors may lead to significant miscalculation of the demand, beyond 30% according to Bozonnet et-al [27], which will have a notable impact on energy system design. However, capturing the influence of solar radiation, long wave radiation and urban climate is a challenging task for hourly building simulation to be used for energy system sizing [25].

A number of groups have investigated effective methods to combine building simulation and energy system optimization. Evins [28] optimized the system configuration and building design by coupling energy system optimization with building simulation. A bi-level optimization algorithm is used in this context to optimize the energy system along with the building envelope, which takes considerably higher computational time (nine days without parallel processing). However, a standalone building is considered in this context without considering thermal interactions caused by the surrounding buildings. Wu et-al [29] optimized the building renovation level and energy system design simultaneously in order to identify the optimum energy system design and the buildings requiring renovation in the Swiss village Zernez. A representative set of buildings in which the energy interactions among the buildings are not considered, was selected in this study to represent the whole village.

Fonseca et-al [30] introduced a city energy analysis tool to optimize urban energy systems using a bi-level optimization algorithm. A detailed hybrid model combining a physical model with a set of statistically representative archetypes is used in this study to obtain the energy demand in the

context of energy system sizing [31]. The hybrid mode used in this work provides a better representation of the energy demand in an urban context. However, the energy interactions among the buildings are not considered in this study. Morgan et-al [14] developed a computational platform combining building simulation and an energy system optimization tool. The platform has the capability to assess the impact of shadowing and the long wave radiation at urban scale. However, the impact of the micro-climate is not considered in this work. A Swiss village with low building density is considered in this study; the sensitivity to shading and long wave radiation is therefore trivial. Furthermore, the impact of the building stock on energy system sizing is not considered. In conclusion, it can be stated that none of these studies comprehensively assess the impact of adjacent buildings on the thermal and electricity demand (due to lighting) in energy system sizing. Effects of shadowing and boundary layer are not considered in most of the instances. An adequate representation of buildings and their effects such as drag force, generation of turbulence etc. is crucial in the evaluation of local meteorological variables[32], [33] and therefore in the calculation of the building energy demand [34], [35] as it can impact the convective heat transfer coefficient [36]. Hence, it is important, with a view of energy system sizing, to represent the micro-climate accurately in the building simulation process.

Following these considerations, the present study focuses on extending the computational platform used to design urban energy systems by introducing an urban meteorological model. The computational platform consists of a building simulation model and an energy system sizing tool with an urban meteorological model as shown in Fig. 8. 1. The introduction of the urban meteorological model facilitates presenting the influence of urban climate on building simulation and subsequently on the energy system design process. The influence of the urban climate on the energy demand is quantified considering different urban densities to introduce the present and future scenarios of Nablus, a city in Palestine. The demand profile notably influences the energy system design. Misrepresentation of the urban micro climate can lead to a performance gap in the energy system. This performance gap can be avoided through adequate representation (by using the computational platform introduced in this study) of the urban micro climate as shown in the final part of the Chapter 8. A concise overview of the computational platform combining different models is presented in Section 8. 2. An extended explanation of the building simulation model and the urban climate model is presented in Section 8. 3 followed by a description about the energy system optimization tool in Section 8. 4. The influence of long wave radiation, urban climate and occupancy at urban context on the energy system sizing problem is taken into discussion in Section 8. 5.

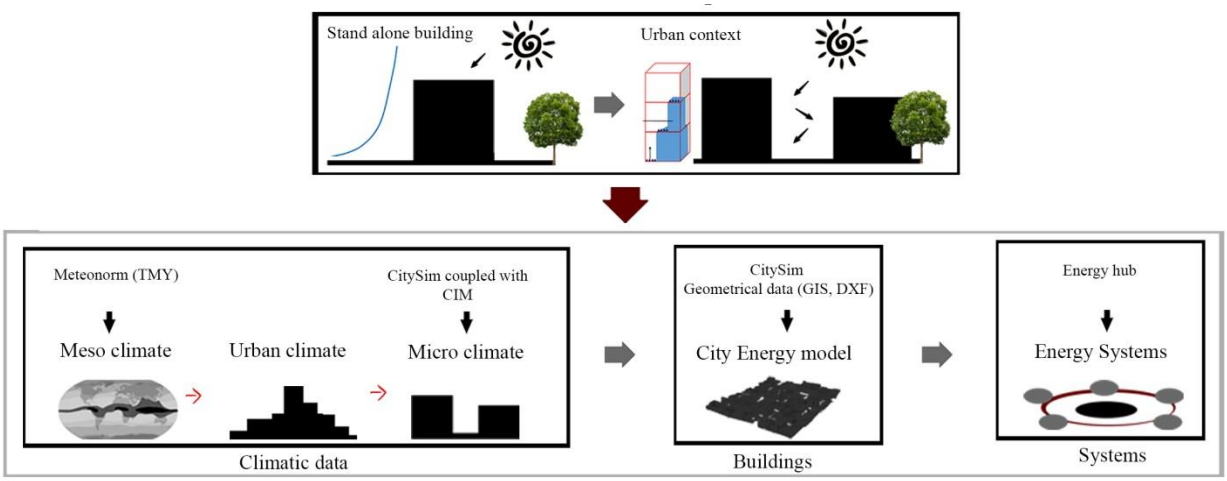

Fig. 8. 1: Schematic overview of the computational platform.

8.2. Overview of the computational platform and the case studies

This section presents an overview of the computational platform developed in this study and the case study used to apply the novel computational platform. The platform combines urban microclimatic conditions, urban design, energy demand of building and optimization of energy system modelling. It is an attempt in the direction of creating a comprehensive design tool that offers a compromise between energy planning needs and the complexity of the urban metabolism. The platform is used to assess a real case study in order to quantify the influence of urban climate on the energy system. A brief over-view of the city considered for the case study and the methodology used to develop building archetypes that represent the compactness of the city at different levels is presented in Section 8. 2.2.

8.2.1. The computational platform

Urban energy planning is a lengthy process that involves a considerable number of steps [37]. Energy system optimization plays an important role in this context as does evaluating the energy demand of the building stock. The coupling of buildings and urban climate is the main challenge to be faced when determining the energy demand of buildings using a bottom-up method. Taking into account the influence of urban climate on buildings and vice-versa may result in a significant change in the projected heating and cooling demand of the building stock and may lead to notable changes in energy system design. Hence, it is important to consider the impact of urban climate at the early design stage of the energy system. The main objective of the proposed computational platform is to combine an urban climate model with a building simulation model and an energy system optimization model in order to design urban energy systems.

8.2.1.1. Challenges in modeling the urban climate and promising paths

The interaction between building stock and urban climate should be carefully decoupled when combining the urban climate model with building simulation. Developing an urban climate model alone is a challenging task due to the geometric complexity and the wide range of spatial and temporal scales required to characterize atmospheric phenomena [25]. A computational fluid dynamic (CFD) model is usually required to achieve a very high level of accuracy. A CFD model requires excessive computational resources and time when computing a time series data for wind distribution and temperature in an urban canyon layer. Therefore, simpler models which reduce the computational time and intensity are necessary. According to [25], urban canopy models can be effectively used to address the challenge with an acceptable level of accuracy. The multi-layer Canopy Interface Model (CIM) [32], [38] is hence used in order to provide the microclimate data for building simulation.

8.2.1.2. Work-flow of the computational platform

The urban energy planning process begins with the acquisition of required spatial and temporal data as inputs to the computational model. GIS based tools (e.g. QGIS) are used to collect the building information for the simulation. The 3D geometries of the buildings in the urban area are modelled using Rhinoceros, based on the information from QGIS. This is done to prepare the DXF data files as input for CitySim Pro[39] and CIM.

CitySim is an extension to SUNTool [40], which can consider the shading effect of adjacent buildings and longwave radiation due to the interaction among buildings. CitySimPro [39], [41] a software developed at the EPFL Solar Energy and Building Physics Laboratory (LESO-PB) is used in this study to simulate the building stock. CitySimPro uses a bottom-up approach when evaluating the hourly energy demand taking into account the fine details of the building stock. The radiation model inside CitySim, the Simplified *Radiosity* Algorithm (SRA) [42] can consider the shading effect of adjacent buildings and longwave radiation due to the interaction of buildings. Building simulation generally considers properties of the thermal shell, visible surface properties, occupancy profile, openings of the building through doors and windows etc. However, it is time consuming to collect all details precisely for each building forsimulations at building scale. Therefore, basic envelope details are obtained considering the construction year of the building. In addition, each building is represented by a single zone instead of multiple zones when evaluating the energy flow. Citysim computes the surface temperature of each building, which is subsequently imported to CIM. Based on the resulting wind speed, the air temperature is recalculated and fed back to Citysim to re-calculate the energy demand.

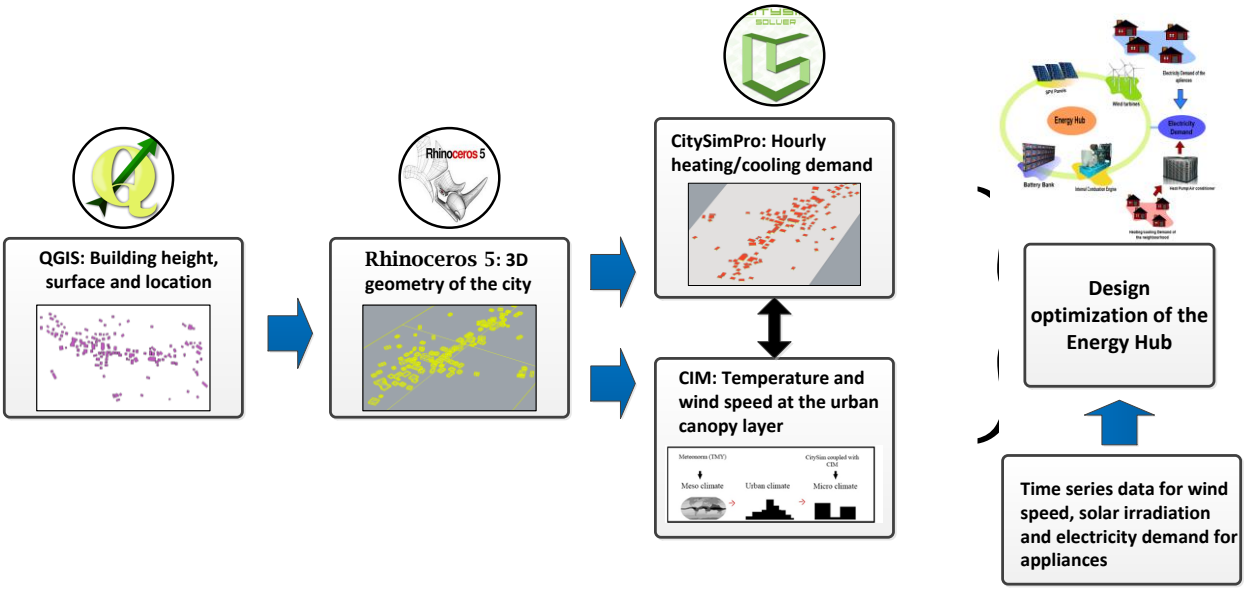

Fig. 8. 2: Work flow of the computational platform

The hourly energy demand obtained from CitySim is subsequently used to optimize the energy system. A multi energy hub consisting of non-dispatchable renewable energy sources, storage and dispatchable energy sources is considered in this study. The energy hub optimization model presented in Ref. [13], [43] is used to optimize the system design of the energy system. An hourly time series of renewable energy potential and prices of system components are taken as the input to the computational model. A detailed description of the computational model used to design the energy system is presented in Section 8. 4.

8.2.2. Outline of the Case Studies

The computational platform developed in this study is used to quantify the influence of urban climate on energy system design. A detailed description of the selected case study and the considered building stock is presented in this section.

8.2.2.1. City of Nablus

The city of Nablus (32°13’ N, 35°16’ E), located in the northern part of the West Bank, is considered for the case study. The city presents a Csa climate (C: temperate; s: dry summer; a: hot summer), characterized by warm temperatures, low precipitations and high temperatures during the summer time. Nablus is located at 550 m above sea level and presents a particular topography, as it is positioned in a narrow valley, between Mount Ebal (940 meters) in the North, and Mount Gerizim (870 meters) in the South. In order to perform this study, the Al-Habaleh district (circa 130 buildings) is analyzed, within the old city; the district is characterized by dense constructions and narrow streets. The average annual temperature corresponds to 17.9°C, with maximum temperatures during the summer time equaling to 36.8°C, and the lowest temperature (during the month of

December) equaling 1°C (extracted from Meteonorm database [44]). The total annual precipitation corresponds to 315 mm, and precipitation is completely absent during the summer season (from June to September). The wind blows mostly during the summer time, with an average speed of 3.5 m s^{-1} during the month of July.

8.2.2.2. Use of archetypes

Urban morphology is usually complex. Furthermore, buildings within a city are distributed with different densities and usually have diverse thermal characteristics. This makes it difficult to quantify the influence of urban climate on energy system design. In order to simplify, we worked with archetypes representing the urban fabric. Urban archetypes are amply used to simplify the complexity of the urban morphology in an effective way [24], [45]. The urban archetype influences the thermal performance, solar access and the ventilation as shown by Sanaieian et-al [46]. In this chapter, we limit the scope to a single urban archetype focusing more on the urban density. The height and the distance between buildings in urban archetypes present an average value of the building stock considered. By analyzing the old city center of the city of Nablus as well as the peripheral areas, the density of the two city areas was defined. The city center has a volume to site area ratio equal to 2.6. The periphery has a volume to site area ratio equal to 1.5. In order to represent these two configurations, we used archetype modelling, using both density characteristics, as presented in Figure 3.

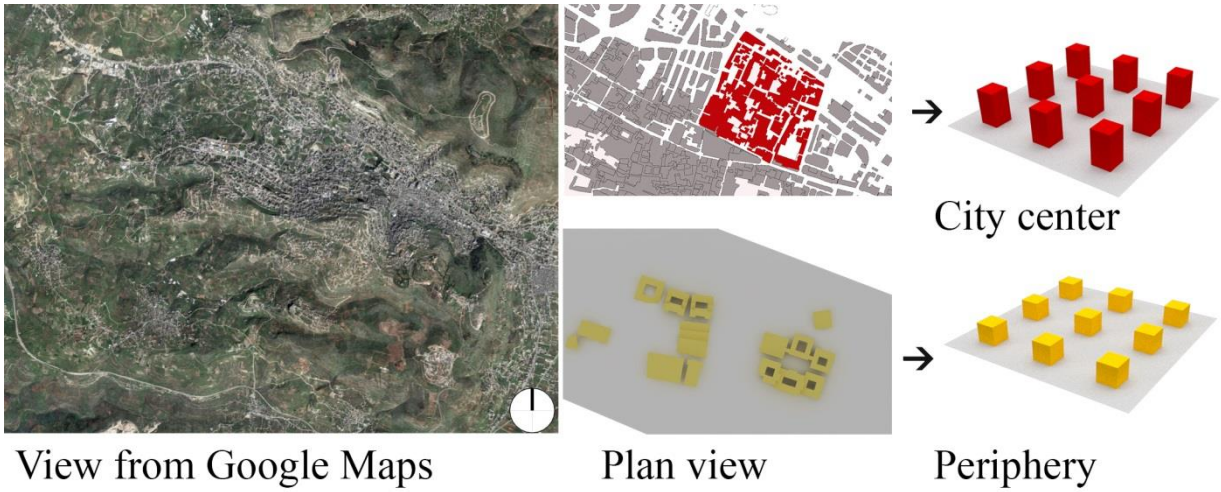

Fig. 8. 3: Archetype modelling as a function of the density of the site

8.3. Computational model for urban micro climate and building simulation

The coupling of a building simulation model (such as CitySim) with meteorological models is essential to represent the impact of buildings on climatic variables and to provide enhanced building energy simulation. Phenomena such as the Urban Heat Island [47] are not represented in TMY or a

Meteonorm dataset, since they are usually collected outside of the city. This data then needs to be transformed to take into account the particularities of the urban climate and to provide useful data to building energy models. This is why it is proposed here to use the CIM-CitySim coupled model and to extend it further.

CIM is a 1D meteorological model [48] that can work offline as a stand-alone module while using as input data a climatic dataset (such as Meteonorm [44]). Alternatively, it can be coupled with a 3D meteorological model (such as WRF [49]). For the purpose of this study, since we are addressing the issue of energy systems, a typical meteorological year supplied by Meteonorm is used as boundary condition for CIM. The values are averaged over a period of 20 years for the irradiation and over 10 years for the wind speed and air temperature. CIM computes high resolution vertical profiles of the variables (such as the wind speed, direction and air temperature) considering the urban environment (for example considering the presence of buildings and their density). CIM resolves a diffusion equation derived from the Navier-Stokes equations but reduced to one direction only.

The differential equations for the momentum and the potential temperature can be written as Eq. 8. 1 and 8. 1'

$$\frac{\partial u}{\partial t} = \frac{\partial}{\partial z}\left(\mu_t \frac{\partial u}{\partial z}\right) + f_m^s \tag{8.1}$$

$$\frac{\partial \theta}{\partial t} = \frac{\partial}{\partial z}\left(\kappa_t \frac{\partial \theta}{\partial z}\right) + f_\theta^s, \tag{8.1'}$$

where u is the mean horizontal wind component in the *x*- or *y*-direction, f_m^s and f_θ^s are the terms representing the momentum and heat fluxes exchanged between the flow and "solid" surfaces (ground or buildings here). The diffusion coefficients are computed according to a 1.5-order turbulent closure (Eq. 8. 7 and 8.8) as proposed by Monin and Yaglom [50] according to Eq. 8. 2:

$$\mu_t = C_e\sqrt{e}l \quad \text{and} \quad \kappa_t = \Pr \mu_t, \tag{8.2}$$

where C_e is a constant, e is the turbulent kinetic energy (TKE), $\Pr$ is the Prandtl number that represents the ratio between the momentum and heat diffusion coefficients, and hence depends on the stability of the atmosphere [51]. Subsequently, differential equations for momentum, potential temperature and TKE are solved using the finite volume method. Equations are taken from [48] take into account the obstacles density and height in the canopy.

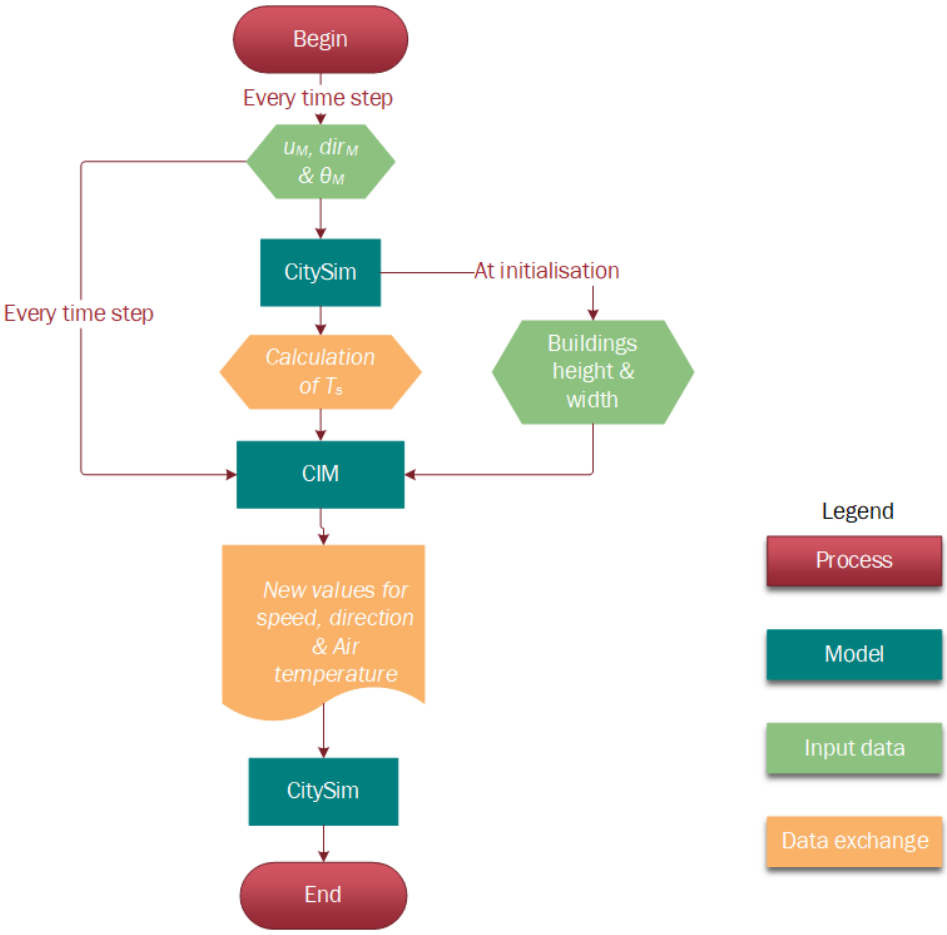

Fig. 8. 4: CIM-CitySim flowchart adapted from Ref. [34]

The model has been coupled with the CitySim building simulation software (see Fig. 8. 4) in order to determine the energy demand of a district [34]. The CIM-CitySim coupling has been tested in multiple cities [35], [52]–[54] and the method presented in this chapter could thus also be applied to other regions. Furthermore, the use of such a methodology has also been previously used to evaluate the building energy consumption at the city scale [55], [56]. Although the building geometries are simplified in CIM, the simulation of the wind speed is coherent with past findings [32], [57], [58]. The coupling of CitySim and CIM provides enhanced boundary conditions for both models. As described in Fig. 8. 4 the simulation takes place in three steps. First a simulation with CitySim is performed with the Meteonorm data to obtain the surface temperatures. Secondly, CIM is forced with the surface temperature from CitySim to simulate the flow in the column module and to recalculate a high resolution vertical profile of meteorological variables, such as the air temperature and the wind speed. Finally, CitySim is provided with localized meteorological data to simulate the energy demand. The modification of the variables influences two main processes that are computed by CitySim.

First, the convective heat transfer coefficient for each surface *i* at time step *t* ($h_t^{c,i}$ $(Wm^{-2}K^{-1})$) is given by Eq. 8. 3:

$$h_t^{c,i} = 2.8 + 3U_t, \quad \forall t \in T, \forall i \in I \tag{8.3}$$

where U_t is the wind speed. $h_t^{c,i}$ is then used in the calculation of the flux $Q_t^{ch,i}$ (Eq. 8. 4):

$$Q_t^{ch,i} = h_t^{c,i}(\theta_t^{s,i} - \theta_t^{air}) \forall t \in T, \forall i \in I \tag{8.4}$$

where $\theta_t^{s,i}$ is the surface temperature in K and θ_t^{air} is the air temperature in K. The longwave heat transfer is calculated as a function of the difference between the environmental temperature (θ_t^{air}) and the surface temperature. Secondly, the longwave flux $Q_t^{lw,i}$ is computed in a similar manner considering the radiation heat transfer. The entire coupling process between CIM and CitySim is presented in Fig. 8. 4. A full description of the CIM model as well as the equations used to take into account the obstacles density and height in the canopy can be found in Mauree et al. [32].

8.4. Energy System design tool

The main objective of the energy hub model is to optimize the energy system design. A multi energy hub (MEH) catering the energy demand for cooling, heating and power (CCHP) is considered in this chapter. The energy hub model introduced by Geidl et-al [59], which has been amply used to design and assess poly-generation systems [60], is used.. This model integrates energy technologies with different characteristics. Solar PV panels (SPV) and wind turbines are used as the non-dispatchable energy technologies in the energy hub (Fig. 8. 5). An internal combustion generator or a gas turbine is used as the dispatchable source. A battery bank is used as the energy storage device. A ground source heat pump and a vapor compression air conditioner are used to cater the heating and cooling demands respectively. The MEH is expected to operate in connection to the Medium Voltage Grid (MVG). A time series of grid electricity prices is considered to represent the real time price in the MVG. Grid curtailments are introduced when selling and purchasing electricity to and from the MVG. Both system design and the operation strategy of the energy hub are optimized using the optimization algorithm. A concise description of the energy flow and cash flow models is presented in this section along with the formulation of objective functions. A bi-level dispatch strategy used for the energy flow management and the optimization algorithm used for the Pareto optimization are presented in the last part of this section.

8.4.1. Energy and cash flow model

The inputs to the computational model that computes the power generation using SPV panels and wind turbines are the hourly global solar irradiation on the tilted solar PV panel surface and wind speed at the wind turbine hub level. It is challenging to consider the impact of the urban context when sizing the energy systems. This requires prior selection of appropriate roofs and facades to install SPV panels, which constitutes another optimization problem within the energy system optimization problem already addressed. In order to simplify the procedure, a shading factor is introduced in this work. Wind turbines are expected to be installed in close proximity to the city in which the wind speed is adjusted to match the urban context according to Ref. [61]. An extended explanation about the computational model is presented in Chapter 2. The objective functions considered for the Pareto optimization are presented in Table 8.1.

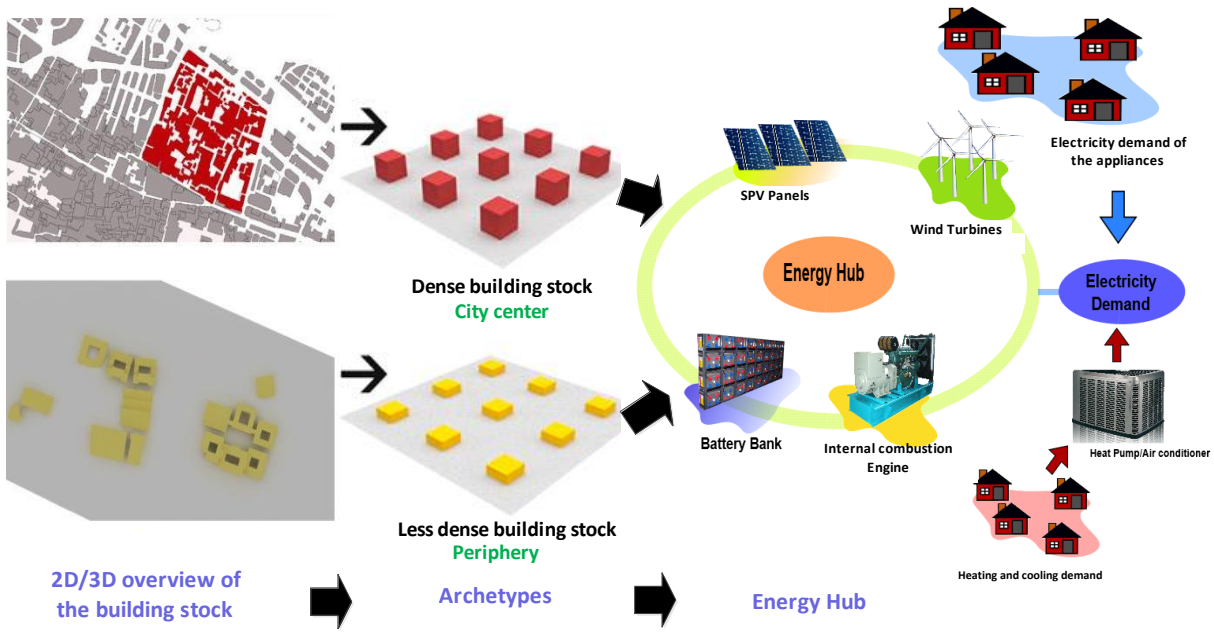

Fig. 8. 5: Overview of the energy system

Table 8. 1: Objective functions and the constraints considered for Pareto optimization.

Location	Objective Function 1-Objective Function 2 (F_1-F_2) formulated in Chapter 2	Scenario	Constraints
Nablus city center	NPV-Grid Interactions	Standalone, Meteonorm, CIM	Power supply reliability
Nablus Periphery	NPV -Grid Interactions	Standalone, Meteonorm, CIM	
Nablus future city center	NPV -Grid Interactions	Standalone, Meteonorm, CIM	

8.5. Results and discussion

The influence of the urban climate is an important factor to be considered when designing urban energy systems. However, the impact of urban climate on the energy system is not direct. It expresses itself in the heating and cooling demand of the building stock, which makes it more complex. A comprehensive assessment of the impact of urban climate on the energy demand and its importance on the energy system design is discussed in this section.

8.5.1. Influence of urban climate on the energy demand

The heating and cooling demand, as quantified by means of archetype modelling, presents an interesting information on the influence of urban climate on the energy demand. In order to reach a better understanding of the impact of meteorological data and urban compactness, a comprehensive assessment is performed for the archetype building stock in the city of Nablus, focusing on the variation of the heating and cooling demand. In order to support the analysis, three scenarios are considered i.e. standalone, Meteonorm and CIM. The standalone scenario neglects the thermal interactions with the neighboring buildings when computing the energy demand for the archetype. This is the method often practiced when computing energy demand for a stock of buildings. Meteonorm considers the shading effect and long wave radiation due to the adjacent buildings. Finally, CIM considers the microclimate in addition to the Meteonorm model. The influence of building density on energy demand in different urban densities is subsequently analyzed for each scenario. This is then used to understand the changes required in energy system design in Section 8. 5.3.

8.5.1.1. Influence of the urban density on energy demand

Urban compactness notably influences building energy demand, which needs to be taken into account in energy system sizing. Three cases (represented by three different archetypes of building stock) are considered in this work in order to assess its impact. Case 1 corresponds to the building

density it the center of the city of Nablus. Case 2 considers the building density at the periphery, which is less compact compared to the center. Case 3 considers a future expansion scenario for Case 1, in which the building density of Case 1 is expected to grow further. Case 3 has the highest building density, followed by Cases 1 and 2. The peak and annual demand for each case are presented in Table 8.2. Furthermore, the percentage increase in annual demand and peak demand is presented in Table 8.2.

Peak and annual demand for the standalone scenario of Cases 1 and 3 are the same; they are different from Case 2. The height of the building archetypes is considered to be same even after expansion, which makes the set of buildings look the same in the standalone scenario. The heights of the buildings are reduced when moving into the periphery, which results in a reduction of the energy demand (when considering the standalone scenario for Case 2). The percentage increase in annual and peak demand is trivial for Cases 1 and 2 when moving from the standalone to the Meteonorm scenario. This shows that the influence of shadowing and longwave radiation is negligible when considering Cases 1 and 2. However, a noticeable increase in both peak and annual demand is observed when moving from the standalone scenario to the Meteonorm scenario in Case 3. This reveals that the influence of shadowing and longwave radiation is observed at very high urban densities. A noticeable increase in annual and peak demand is observed when moving from the standalone to the CIM scenario. This suggests that the wind speed and air temperature at the urban canyon layer have a noticeable impact. When moving to Case 3, this increases the annual and peak demand by 13% and 10% respectively. These results make it interesting to further analyze the influence of the wind speed and ambient temperature on energy demand. To achieve this, wind speed and ambient temperature values at higher temporal resolution are taken.

Table 8. 2: Influence of the urban compactness on the energy demand

Case		Standalone	Meteonorm	CIM
3	Annual Demand (GWh/year)	1.16	1.21	1.41
	Peak heating/cooling demand (kWh)	536.6	557.1	619.3
	Increase in annual demand compared to Standalone (%)		4.13	17.73
	Increase in Peak Demand compared to Standalone (%)		3.69	13.36
2	Annual Demand (GWh/year)	0.73	0.73	0.82
	Peak heating/cooling demand (kWh)	334.4	334.8	363.8
	Increase in annual demand compared to Standalone (%)		0.27	10.95
	Increase in Peak Demand compared to Standalone (%)		0.11	8.07
1	Annual Demand (GWh/year)	1.16	1.15	1.33
	Peak heating/cooling demand (kWh)	536.6	537.5	582.3
	Increase in annual demand compared to Standalone (%)		-0.26	13.22
	Increase in Peak Demand compared to Standalone (%)		0.17	7.85

8.5.1.2. Influence of wind speed and ambient temperature

In order to assess the influence of the urban climate, the heating and cooling demand of buildings in the city center are taken into consideration. For these buildings, the annual heating demand obtained from Meteonorm is close to the value obtained from CIM, although the cooling demand shows a significant difference. The average cooling demand in the city center increases from 9.68 to 17.83 $kWhm^{-2}$ when changing the climatic data from Meteonorm to CIM. In order to assess this further, hourly demand profiles for three summer days (21st-23rd June) obtained using both CIM and Meteonorm are plotted in Fig. 8. 6. The two demand profiles reveal that the increase in the demand for CIM is not uniform throughout the time line. Hence, moving from one to another creates a shift in the entire demand profile. A notable increase in the cooling demand is observed towards the peak, while it gradually decreases when moving away from the peak. For example, the peak demand is approximately doubled with the CIM meteorological data during a sunny day (average octas equals to 0), passing from 43 GWh to 20 GWh at 13:00 hours. A detailed explanation of this observation is presented in Section 8. 5.2. Such extreme increases in hourly demand profile can have a notable impact on the energy system which is not reflected in the annual average demand discussed in detail in Section 8. 5.2.

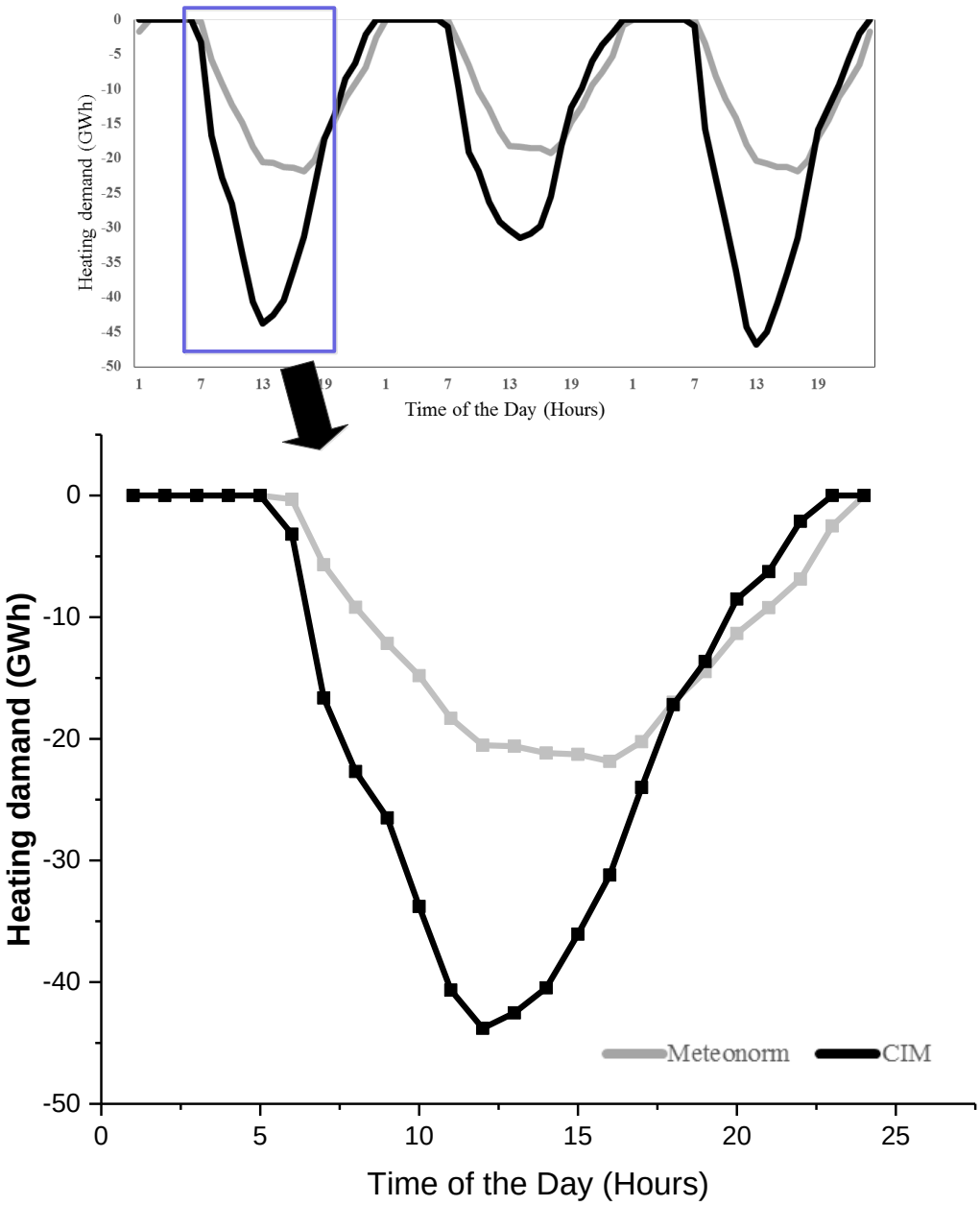

Fig. 8. 6: Hourly demand for heating demand for Nablus center from 21st- 23rd June.

8.5.2. Role of CIM in presenting higher resolution meteorological variables

The main objective of coupling a building simulation tool with an urban climate model is to capture the influence of the presence of buildings in the urban context. In this context, CIM is used to calculate the high resolution vertical profiles of meteorological variables. These variables are then used as boundary conditions for CitySim, the building simulation tool. Hence, a detailed comparison of the temperature and wind profiles obtained from CIM with Meteonorm (simple meteorological data which do not consider the presence of buildings) can provide a better justification of the changes observed in heating and cooling demands in Section 8. 5.1.

When analyzing the annual average wind speed and temperature, a difference in 1.5 ms^{-1} and 0.5°C is observed between CIM and Meteonorm respectively. However, this difference is trivial when compared to the changes observed for the building energy demand of the building stock at the center of Nablus (which can no longer explain the changes in energy demand). Hence, it is important to move into a higher temporal resolution. When moving into a monthly resolution, a difference of up to 1.5°C in temperature and of 2.2 ms^{-1} in wind speed is observed. However, when moving further up to an hourly scale, the temperature difference can reach up to 14°C as observed in Fig. 8. 7. By contrast, the wind speed difference is quite constant throughout the year (at the hourly temporal scale when compared to temperature) as shown in Fig. 8. 8. The reason for this is that the drag force calculation does not change throughout the year since the density of obstacles remains the same and the reduction in the wind speed will consequently be more or less the same as well. CIM is using 1-D Navier-Stokes equations in this process, which can be improved by increasing the dimensions considered. This will result in introducing more fluctuations into the wind speed. However, it is noteworthy that there is a significant increase in the temperature during the summer time as opposed to the winter time for the Nablus case. In general, it can be concluded that CIM provides a better representation of the urban climate, which will help to get a better understanding of the meteorological variables. More importantly, the impact of urban climate is not linear, which will induce a direct shift in the energy demand.

It is interesting to assess the direct influence of urban microclimate on the cooling and heating demand at an hourly time resolution. To achieve this objective, air temperature values obtained from both CIM and Meteonorm are plotted along with the energy demand for a single day (in Fig. 8. 9) in February. The peak demand is higher with the CIM weather profile during the daytime, and lower during the nighttime. This behavior is directly related to the air temperature, which is lower during the night time (by 2°C) and higher during the daytime (by 5°C). The temperatures of the surfaces within the urban environment are heated by the sunlight during the daytime, consequently increasing the temperature. Naturally, this behavior is evident during sunny days and limited for cloudy days. Additionally, the studied day is characterized by a moderate breeze during the daytime, according to the Meteonorm climatic data (5.5 ms^{-1}), which is reduced to a gentle breeze according to the CIM meteorological data (3.7 ms^{-1}). This can be explained using the concepts of urban heat islanding and cold air pools, which are however not the main focus of this chapter (interested readers are referred to Ref. [34] for a detailed description). As a result, the demand profile obtained using CIM has a peak demand higher than the one obtained using Meteonorm. At the same time, the lowest demand is also obtained for CIM, which will result in a higher fluctuation in the demand profile. Higher peak demand will result in requiring a larger system capacity while higher fluctuation

in the demand profile will make the design and operation of the energy system more challenging. Hence, taking into account the urban climate will introduce more fluctuations and higher peak demands on a seasonal basis which will influence the energy system design. These issues are discussed in detail in the following section.

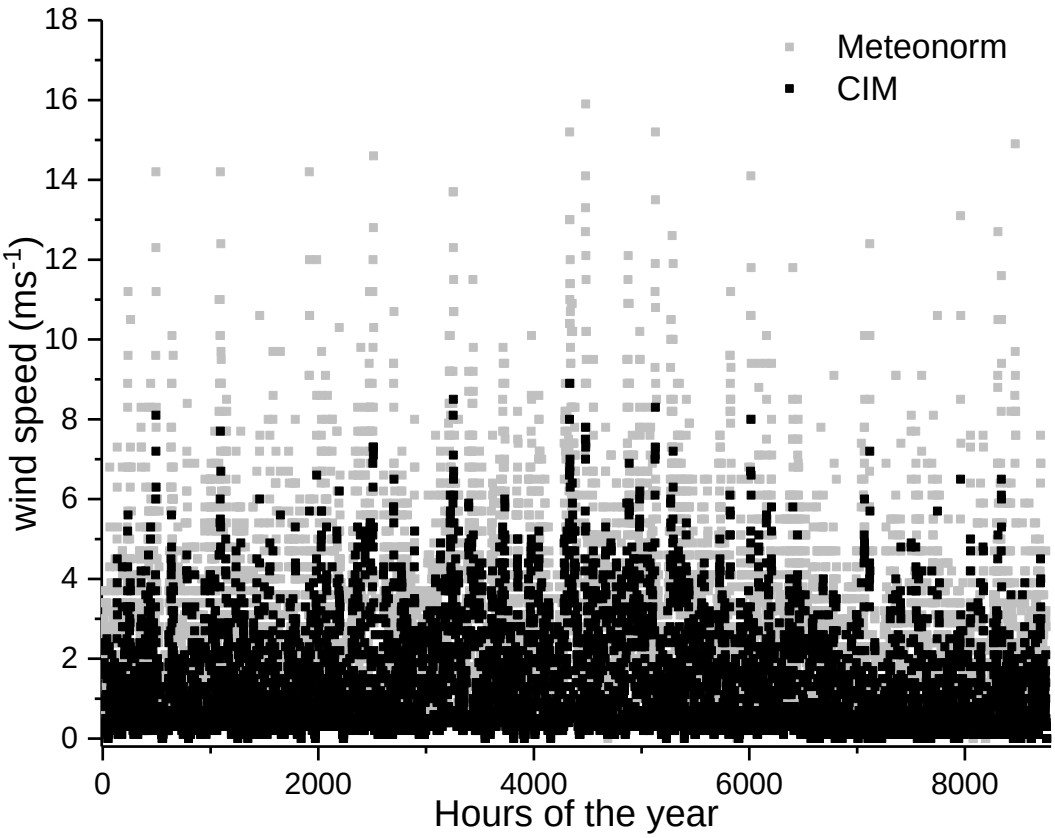

Fig. 8. 7: Wind speed (ms^1) obtained from Meteonorm (grey) and computed with CIM (black) for the dense scenario in Nablus

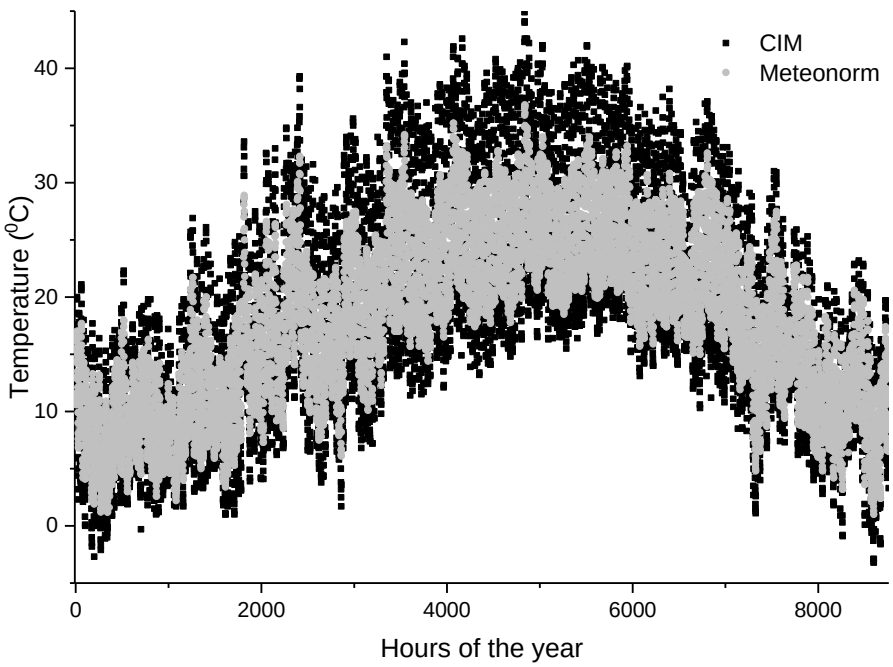

Fig. 8. 8: Air temperature (°C) obtained from Meteonorm (grey) and computed with CIM (black) for the dense scenario in Nablus

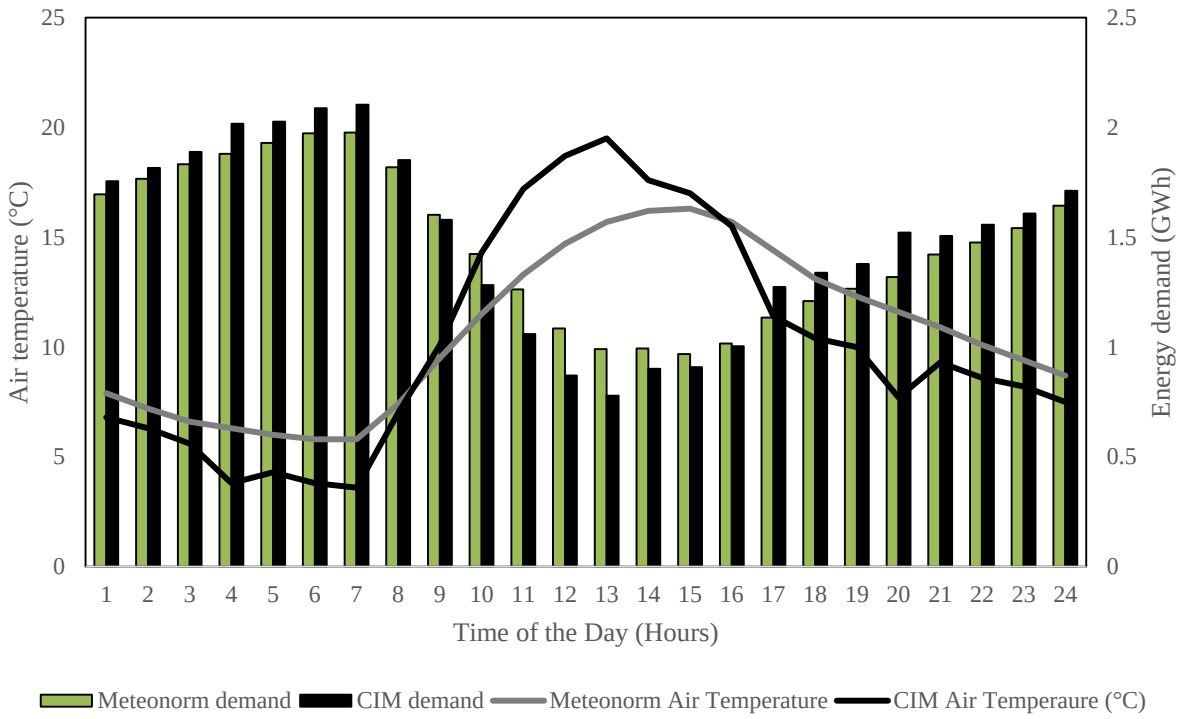

Fig. 8. 9: Air temperature and energy demand for the city of Nablus on 2nd of February.

8.5.3. Influence of the urban climate on the energy system

The notable influence of the urban climate on building energy demand is clearly reflected in Section 8. 5.2 especially considering the dense areas. The effect of urban climate on the energy demand can

have a notable impact on the performance of the energy system. Hence, it is interesting to conduct a comprehensive analysis on the impact of the microclimate on the energy system based on a set of performance indicators commonly used to assess the energy system. This is conducted in two steps in line with Section 8. 5.1; the impact of shadowing and long-wave radiation at the building scale will be evaluated initially, followed by an assessment of the impact of the micro-climate. Building archetypes are used in this context to provide a normalized overview.

Energy systems are optimized considering NPV and GI as the objective functions taking the urban archetype of the center of Nablus. A detailed analysis of the impact of system autonomy on lifecycle cost and system configuration is given in Ref. [13]. Pareto fronts are obtained considering three scenarios i.e. neglecting the shadowing effect (both shadowing and long wave radiation) and adjusted wind speed (both wind speed and surface temperature) (Scenario "stand-alone"), considering the shadowing effect but neglecting the adjusted wind speed (Scenario Meteonorm) and considering both shadowing and adjusted wind speed (Scenario CIM) (Fig. 8. 10). A clear Pareto front is observed for all three scenarios, which suggests that the NPV and GI level are conflicting objectives, for which it is difficult to reach to a single optimum solution considering both objectives. Pareto fronts obtained for Standalone and Meteonorm scenarios have objective function values quite close to each other except in a part of Region B (Fig. 8. 10), where, Meteonorm presents marginally higher NPV compared to the Standalone scenario. However, a significant increase in objective function values is observed when moving to Scenario CIM which is due to the increase in energy demand as discussed in Section 5.2. The NPV increases by 20% in Region B, which decreases by 7-10 % when moving into Region C while increasing the grid interactions. When moving into autonomous operation of the system, the Pareto fronts appear to be close to each other since the magnitude of the gradient is higher in this region. A closer look at the Pareto fronts shows that the difference in objective function values observed in Region B is maintained in Region A (in certain instances the difference increases as well). In conclusion, it can be stated that the increase in demand observed in building simulation is reflected and often magnified in the energy system design.

It is interesting to assess the impact of urban density on energy system design. To achieve this objective, energy system optimization is performed for the urban archetype representing the building density of the periphery of Nablus as the second case study. A third case study is introduced considering the future expansion of the city, in which the building density is expected to increase further. Both these case studies align with the case studies introduced in Section 8. 5.1 (to quantify the effect of urban climate on the energy demand). A Pareto optimization is conducted considering

NPV and GI and the objective functions for three scenarios illustrated before (i.e. Standalone, Meteonorm and CIM). Subsequently, the objective function values for each case study are normalized considering the three Pareto fronts obtained for each case study in order to make it easy for the readers to understand the deviation due to the building density (Fig. 8. 11).

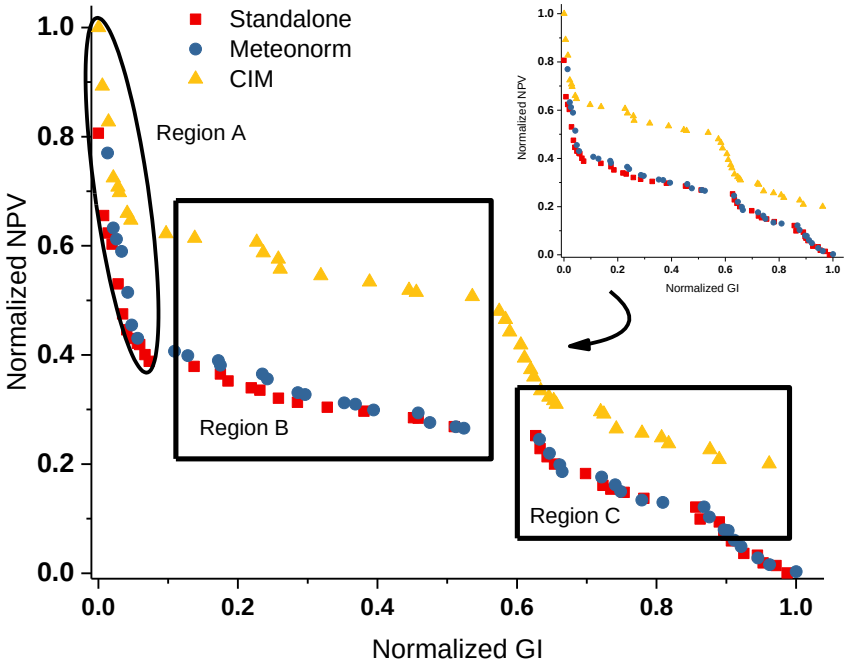

Fig. 8. 10: Pareto front obtained considering NPV and GI as the objective functions. Values of the objective functions are normalized considering minimum and maximum objective function values obtained for the three Pareto fronts in order to simplify the analysis.

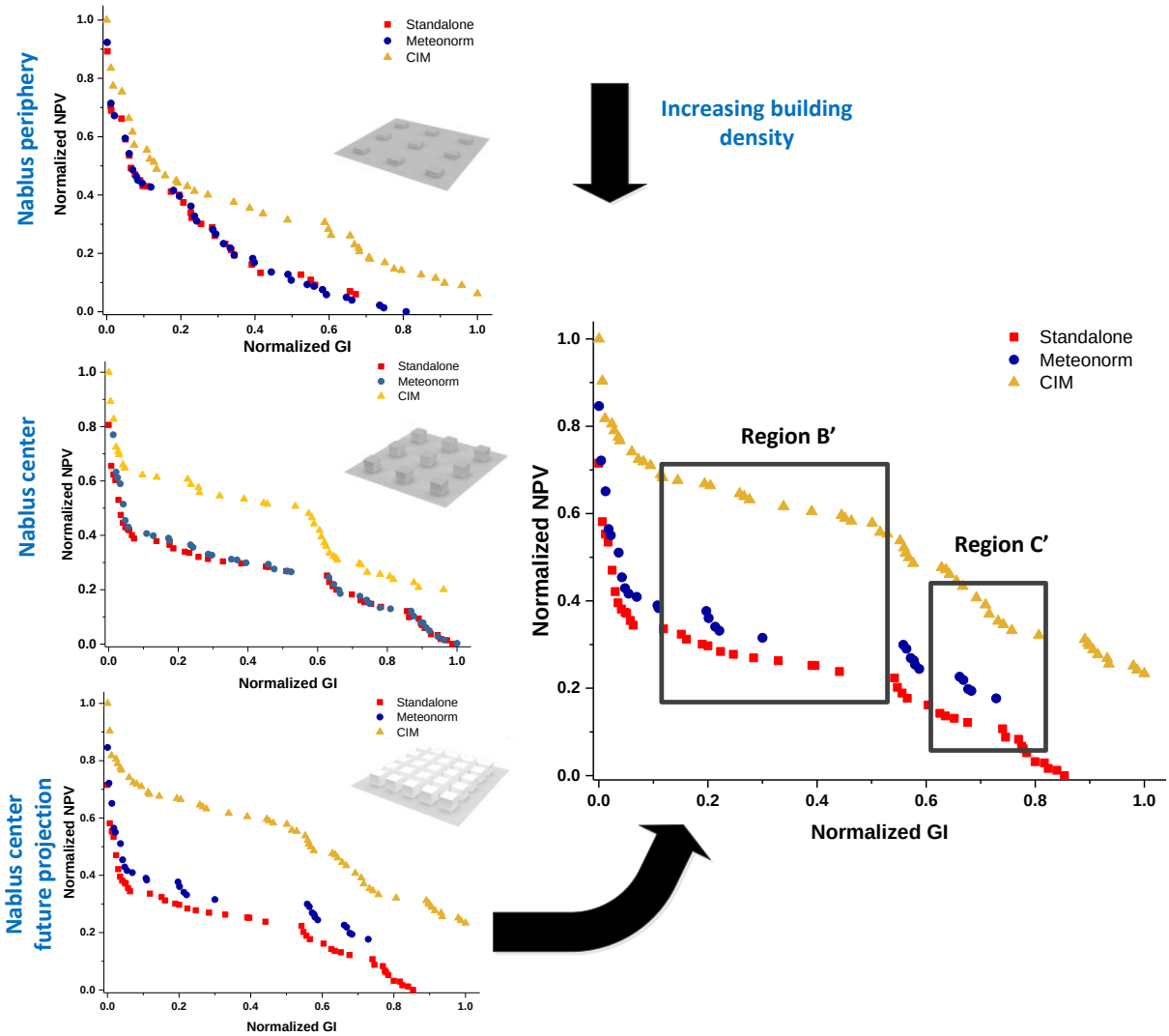

Fig. 8. 11: Top to bottom plots in the left side of the figure presents the three Pareto fronts obtained for each case study i.e. Periphery of Nablus (PN), Center of Nablus (CN) and Future Center of Nablus. The three Pareto fronts obtained for Future Center of Nablus (FCN) are enlarged on the right hand side image in order to elaborate the regions introduced in the figure

Pareto fronts obtained for the three case studies (Fig 11.) are used to get a qualitative understanding of the influence of urban climate in the context of energy system sizing (which is assessed quantitatively in Section 8. 5.4). When comparing the three case studies, it is observed that the Pareto fronts for Meteonorm and Standalone follow close to each other for both the periphery and the center of Nablus (discussed previously in this section). However, a clear separation of these two Pareto fronts is observed when moving into the future center of Nablus, which takes into account an increase in the objective function values of up to 10% (future center of Nablus-CIM). These results show that neglecting the influence of shadowing and long wave radiation may lead to a deviation in NPV of up to 10%. The deviation observed can be further increased in cities that have skyscrapers and much higher building densities. The influence of building density on energy system sizing can be

clearly understood when comparing standalone and CIM scenarios for future center of Nablus. The differences in the objective function values (stand alone and CIM) increase by up to 40% when considering the future center of Nablus which is on average a 20% increase when compared to buildings in the periphery of Nablus. These results show that the urban climate can have a notable influence on the energy system design process, especially in highly dense cities.

8.5.4. Consequences of neglecting urban climate in energy system sizing

A quantitative analysis is conducted in this section to understand the influence of urban climate (extending the qualitative analysis conducted in Section 8. 5.3) and the consequences of neglecting it during the energy system design process. Pareto solutions are taken for further assessment from the three Pareto fronts of the future center of Nablus which presented the highest deviation in objective function values.

Four sets of design solutions (with similar grid purchase values) are taken from the three Pareto fronts and tabulated in Table 8.3. When considering each set, it is clear that the NPV has increased by 3-6% when moving from the Standalone to the Meteonorm scenario while it increases by more than 20% when moving from the standalone scenario to CIM. For example, NPV has increased by 4.8% when moving from 1-SA to 1-MET while it has increased by 20.3% when moving from 1-SA to 1-CIM. These quantitative values align with the qualitative explanation provided in Section 8. 5.3. The increase in NPV is well beyond the increase in the demand. It can be concluded that increase in demand as well as the fluctuations introduced to the demand profile due to the urban climate result in a notable increase in NPV.

When analyzing Table 8.3 further, it is clear that both the ICG contribution and capacity follows the pattern of NPV when moving from the standalone to the CIM scenario. The percentage contribution of the ICG increases by 3-10% when moving from the standalone to the CIM scenario. For example, ICG generation increases by 3.2% when moving from 4-CIM to 4-SA while it increases by 10% when moving from 1-SA to 1-CIM. A clear pattern is not observed for system configuration except for the ICG capacity when moving from the standalone to the CIM scenario. As discussed in Section 8. 5.1, the increase in demand is not uniform throughout the year when moving from the standalone to the CIM scenario. As a result, a uniform increase in renewable energy components, energy storage and dispatchable source is not observed. A notable increase in daily peaks is observed in the demand curve which results in introducing more fluctuations into the demand profile calling for support from the dispatchable source whenever the grid is not catering the mismatch. This results in higher ICG capacity and contribution when moving from the standalone scenario to CIM. In general, the

changes brought to the demand pattern due to the urban climate result in changes in the energy system configuration.

The effect of urban climate is considered in CIM and neglected in the standalone scenario. Where urban climate is not considered, the system will be designed based on the demand profile obtained for the standalone scenario. The system designed for the standalone scenario will have to cater the demand profile of CIM due to the effect of urban climate which is not considered at the design point. This will result in a performance gap. The performance gap clearly presents the consequences of not considering the urban climate at an early point of energy system design. To assess the impact further, performances of the four energy systems obtained for the standalone scenario (already presented in Table 8.3) are evaluated considering the demand profile of the CIM scenario (for the future center of Nablus). When analyzing the results, a notable performance gap can be observed for all the performance indicators (Table 8.4). NPV increase by 5-8% while grid dependency increases by up to 57%. More importantly, all the design solutions violate the constraint on power supply reliability set at the formulation of the optimization problem. A significant increase in ICG contribution is observed due to the increase in the peak demand as discussed before. In general, it can be concluded that neglecting the urban climate may lead to a notable performance gap. More importantly, energy systems fail to maintain the reliability of the power supply which is considered as an important constraint in design optimization.

8.5.5. Overall computational time required

Computational time required for the overall process and the additional computational burden due to the consideration of urban climate is an important aspect which needs to be evaluated. Simulations are run on a single processor (1.2GHz) for each scenario and for each city for one full year (8760 time step) for both CIM and CitySim. The energy hub model is implemented in Intel(R) Core(TM) i7-6700-3.40 GHz CPU. CIM simulations are more computationally extensive compared to the CitySim ones (Table 8.5). Since CIM is dependent on the number of vertical levels, it takes significantly more time to run for a domain with higher buildings. Higher buildings imply that there are additional cells so that a surface layer can be developed above the displacement height. It is clear that CIM adds an additional computational load to energy system sizing, extending the computational time by approximately four times. However, the extension of the computational time can be easily justified when considering the improvements obtained in the energy system design.

Table 8. 3: Computational time in seconds for each simulation for CIM, CitySim and energy hub model

	CIM (s)	CitySim(s)	Energy hub model (s)
Center of city	39752	252	7160
Periphery of city	39759	237	7320

8.6. Conclusions and future perspectives

Providing sustainable energy solutions to rapidly growing cities is a challenging task. Urban energy systems play a major role in this context. Computational platforms combining different fields of expertise will help the energy engineers to face this challenge. This chapter highlights the importance of filling the research gap by combining energy system optimization with building simulation and urban climate modeling. The complexity of modeling the urban climate and subsequent coupling with a bottom up building simulation tool and an energy system designing tool make it difficult to develop a computational platform that can bridge all these elements. This chapter presents an effective way to address the problem by combining CIM, CitySim and an energy hub model as a computational platform to address the aforementioned research gap.

Results of the chapter reveal that the response of a cluster of buildings is different from that of a single building. Therefore, it is difficult to make predictions based on the performance of a single standalone building due to the interaction among the buildings and the micro-climate. The study shows that more fluctuations in demand profile (heating and cooling) are observed when moving from standalone buildings to dense urban areas. This makes it more challenging to design urban energy systems. Furthermore, both peak and annual energy demand can increase respectively by 13% to 18% when considering urban climate. All these results emphasize that the urban climate plays a major role in energy demand. Therefore, it is important to look at the energy efficiency of an entire building stock at neighborhood or urban scale considering the interactions among buildings and the micro-climate and not to limit the efforts to energy efficiency at building scale.

The influence of urban climate on energy demand has a significant impact on the energy system. The increase observed in peak and annual demand results in an increase in NPV of the energy system. NPV of the energy system increases up to 40% when considering the effect of urban climate in highly dense urban scenarios. Therefore, neglecting the influence of urban climate can result in a significant performance gap for all the performance indicators of the energy system, which can reach up to 50% in certain scenarios. This highlights the importance of developing a computational platform combining urban climate, building simulation and energy system optimization. Furthermore, both active and passive strategies should be introduced to minimize the adverse

impacts due to urban climate. Introducing green areas and water bodies into the cities, building renovation and green roofs and facades would be promising remedies [67]. The computational platform introduced in this chapter should be extended further to accommodate the influence of the aforementioned factors. In addition, it is important to evaluate the effectiveness of different urban configurations in order to minimize the adverse impact of increasing urban densities. In conclusion, the impact of the urban morphology on the energy systems should be carefully considered during the urban planning process. A computational platform introduced in this chapter can be immensely helpful in this context. However, it is important to extend the boundaries of the computational platform to consider other aspects such as transportation, outdoor comfort etc. which will help the urban planners to produce better designs.

Table 8. 4: Comparison of the three scenarios by taking Pareto solutions that are having grid purchase values close to each other

Scenario[1]	Name	NPV ($x10^6$ Euro)	Grid Purchase (MWh)	Export to the grid (%)	ICG generation (%)	PV panel capacity (kVA)	Wind turbine capacity (kVA)	Total renewable capacity (kVA)	PV capacity (%)	Battery bank capacity (kWh)	ICG capacity (kVA)
SA	1-SA	4.80	5.74	53.05	26.33	210	680	890	23.60	20	100
MET	1-MET	5.03	5.27	45.32	32.77	155	560	715	21.68	19	120
CIM	1-CIM	5.77	5.68	42.18	36.42	150	600	750	20.00	19	140
SA	2-SA	4.41	23.84	43.77	28.79	140	560	700	20.00	15	100
MET	2-MET	4.54	22.11	48.16	30.02	170	560	730	23.29	19	100
CIM	2-CIM	5.44	22.89	47.03	37.03	175	580	755	23.18	4	140
SA	3-SA	4.21	55.59	46.97	25.17	140	580	720	19.44	15	100
MET	3-MET	4.35	58.74	42.83	27.16	130	560	690	18.84	19	100
CIM	3-CIM	5.22	66.12	47.26	31.41	170	580	750	22.67	4	140
SA	4-SA	3.90	117.09	47.18	17.08	155	540	695	22.30	19	80
MET	4-MET	4.14	113.93	51.06	18.08	210	540	750	28.00	20	80
CIM	4-CIM	4.84	111.82	52.60	21.33	255	540	795	32.08	20	100

1) SA, MET and CIM denote Standalone, Meteonorm and CIM scenarios

Table 8. 5: Performance gap due to neglecting the urban climate in energy system optimization

Name	Demand	NPV ($x10^6$ Euro)	Increase in NPV(%)	Grid Purchase (MWh)	Increase in Grid purchase	Export to the grid (%)	ICG generation (%)	Increase in ICG Generation (%)	Constraint violation
1-SA	SA	4.80	5.34	5.74	57.67	-11.50	26.33	15.19	no
1-SA-R	FCN-CIM	5.07		13.57			31.04		yes
2-SA	SA	4.41	6.87	23.84	35.65	-17.46	28.79	14.74	no
2-SA-R	FCN-CIM	4.73		37.05			33.77		yes
3-SA	SA	4.21	7.61	55.59	20.37	-19.34	25.17	16.15	no
3-SA-R	FCN-CIM	4.56		69.81			30.01		yes
4-SA	SA	3.90	7.48	117.09	15.95	-17.25	17.08	17.8	no
4-SA-R	FCN-CIM	4.22		22.89			37.03		yes

9 Towards Energy System Friendly Urban Form

Standard and newly designed archetypes are used in this chapter to quantify the influence of urban morphology on energy demand, renewable energy integration and the energy system design process. An energy hub is designed for a set of archetypes selected to quantify the impact of urban morphology on energy system requirements.

This chapter is based on (preprint version):

A.T.D. Perera, Silvia Coccolo, Jean-Louis Scartezzini, "Impact of urban form on energy efficiency and renewable energy integration" (Manuscript in review, Scientific Reports)

Author contribution for the journal paper:

ATD, SC, JLS designed the research. SC conducted the building and urban energy simulation. SC and ATDP analysed the energy demand. ATDP conducted the energy system analysis. ATDP, SC and JLS wrote the manuscript

9.1. Introduction

The energy sustainability of cities has been widely discussed in recent years and even included into the United Nations Sustainable Goals [1]. However, no satisfactory method to quantify the impact of the complex chain of effects and reactions that impact urban energy infrastructure has been presented to date.

The interactions among buildings in the urban environment play a vital role when considering the energy demand in cities. According to Baker and Steemer [2], five factors leverage building energy performance in the urban context, i.e. urban climate, urban morphology, building physics, HVAC systems and occupant behavior. Energy efficiency and the sustainability of cities have been addressed from different perspectives [3] within this context by Baker and Steemer [2]. Among these, two approaches complementary to each other can be clearly observed when referring to recent literature. These are to improve the energy efficiency of cities by:

i) increasing the efficiency of building stock and introducing sustainable energy technologies into the urban energy infrastructure;

ii) enhancing the urban form and morphology through efficient urban planning.

The first of these approaches relates with mapping the potential of renewable energy technologies at the urban scale, optimal integration of renewable energy technologies, optimal operation of urban energy systems, improving energy efficiency building stock through methods, such as building renovation, etc. Arranging urban configuration by introducing different zones depending upon function, locating green areas, etc. in order to change the urban climate are considered under the second. Both play a vital role in improving the energy efficiency and sustainability as demonstrated in detail in recent literature [4,5]. When it comes to the first approach, Perera et-al. [6] have shown the potential of distributed energy systems such as energy hubs to integrate renewable energy technologies into urban energy infrastructure. Fazlollahi et-al [7,8] introduced a novel method to optimize urban energy systems combining several distributed energy systems with the energy network. Having a better understanding of the energy demand is essential when designing distributed energy systems. Fonseca et-al [9,10] introduced City Energy Analysis to design urban energy systems carefully considering the energy demand at building scale using statistically representative building archetypes. Le Guen et-al [11] developed a computational platform that considers the energy demand in detail including interactions among buildings when designing distributed energy systems. This platform is used to obtain the best levels for building renovation and energy system improvements. Perera et-al assessed the impact of urban climate on energy system design [13]. All these studies are focused on improvements considering both buildings and energy

systems. However, none of these studies considered the influence of urban morphology; Hence, it is difficult to directly extend such methods to urban planning. In addition, the interactions among buildings have not been considered in most studies, although these significantly influence energy efficiency and renewable energy integration. Hence, it is important to move beyond building level to consider urban form, which can notably reduce the energy consumption and support renewable energy integration according to Salat [14].

From the perspective of urban form and morphology, several studies have been conducted investigating the "best" urban form in terms of sustainability of the urban environment. The discussion on the "compact city" versus the "dispersed city" [15,16] can be brought as one example. Urban planning plays a leading role in urban energy consumption. Ratti et-al [18] present the relationship between energy consumption in cities and urban texture and relate the influence of urban texture on energy efficiency. Different attempts have been made to quantify the influence of urban form on the energy demand. Liu et-al. [19] evaluate the impact of urban density on heat transfer of building stocks simply considering the distances between buildings. However, such a method cannot be extended to complex urban morphologies. Ratti et-al. [18] introduce the concept of urban archetypes in order to handle the complexity in urban morphology. Okeil [20] evaluates the effectiveness of harnessing solar energy in different urban forms introduced by Ratti et al. [18]. Sanaieian et al [21] evaluate the impact of urban form on thermal performance, solar access and ventilation using archetypes while Taleghani et-al [22] evaluate the impact of urban archetypes on outdoor thermal comfort. These studies clearly reflect that the urban form has a notable impact on the energy demand and that urban archetypes can be used to get a better understanding of the impact of urban morphology. However, none of these studies focuses on the impact of building archetypes on renewable energy integration and energy system configuration.

The two approaches mentioned above (improving the energy efficiency of urban form and improving the energy efficiency at the building scale and integrating renewable energy technologies) are adopted in this study to improve the energy efficiency and sustainability at the urban scale. Merging the two can speed up the energy transition in the urban sector. Towards this end, the study focuses on quantifying the impact of urban morphology on energy demand and its consequences for energy system design, which can lead to improved energy sustainability in future cities through optimum urban planning.

The impact of the urban form on the peak and annual energy demand and building integrated solar PV generation

is evaluated in a first step using modular urban archetypes defined by Ratti et-al [18] at different scales (Fig 9. 1). The urban morphology can be very complex in certain instances and might be difficult to represent using simple archetypes. To handle this issue, integrated urban archetypes are introduced by extending the modular urban archetype defined by Ratti et-al [18]. Towards addressing the main research problem, the design of distributed energy systems is optimized considering the energy demand of a selected set of urban archetypes. Pareto optimization considering cost and system autonomy is conducted to optimally design the energy system. Subsequently, the impact of urban form on cost, autonomy and renewable energy integration level are evaluated for both simple and integrated urban archetypes to understand the influence of urban form on the energy infrastructure.

9.2. Urban Archetypes

An urban archetype (Fig 9. 1) can be defined as a set of several environmental and architectural parameters commonly used to describe the urban environment. Urban archetypes can be used to represent a typical neighborhood in terms of geometric and volumetric properties when working at the urban scale [23]. Several studies used urban archetypes to investigate the relationship between the urban form and environmental variables such as shadow density and daylight distribution [18,23,24]. Five modular urban configurations adapted from [26] are selected in this study (Table 9. 1). These five modular archetypes can be considered as the building blocks for complex urban morphologies that can be observed in a city. The characteristics of the urban archetypes are i) ground floor area (m^2), ii) number of floors (-), iii) treated floor area (m^2), iv) Floor Area Ratio (FAR), v) Site Coverage (%) and vi) Form Factor (FF) (-). Sky View Factor (0-1) defined as the ratio between the radiation received by a planar surface and the one from the entire hemispheric radiating environment. Floor Area Ratio (-), corresponds to the ratio of the gross floor area to the site area. Site Coverage (%), defined as the ratio of buildings footprint to the site area. Form Factor (-), defined as the ratio between the ratio between the external envelope and the gross area of the building.

9.3. Modular archetypes to complex urban forms

Modular archetypes represent buildings in a simple neighborhood. It is important to get an understanding of the impact of the scaling-up process when moving from a simple neighborhood to urban scale. Both horizontal and vertical growth need to be considered in this context. Vertical growth corresponds to adding more floors to an existing modular archetype, which will increase the floor area while maintaining the same ground floor area and site coverage. In contrast, horizontal expansion extends ground floor area while maintaining the number of floors. The dimensions of the plan view of the modular archetype remains the same in the vertical expansion. Similarly, horizontal expansion can be achieved while proportionately increasing the dimensions of the modular

archetype by a constant factor. However, it is difficult to observe such a proportionate expansion of modular archetypes when considering horizontal growth. Often, it can be observed that different modular archetypes are mixed to form complex urban forms when considering horizontal growth.

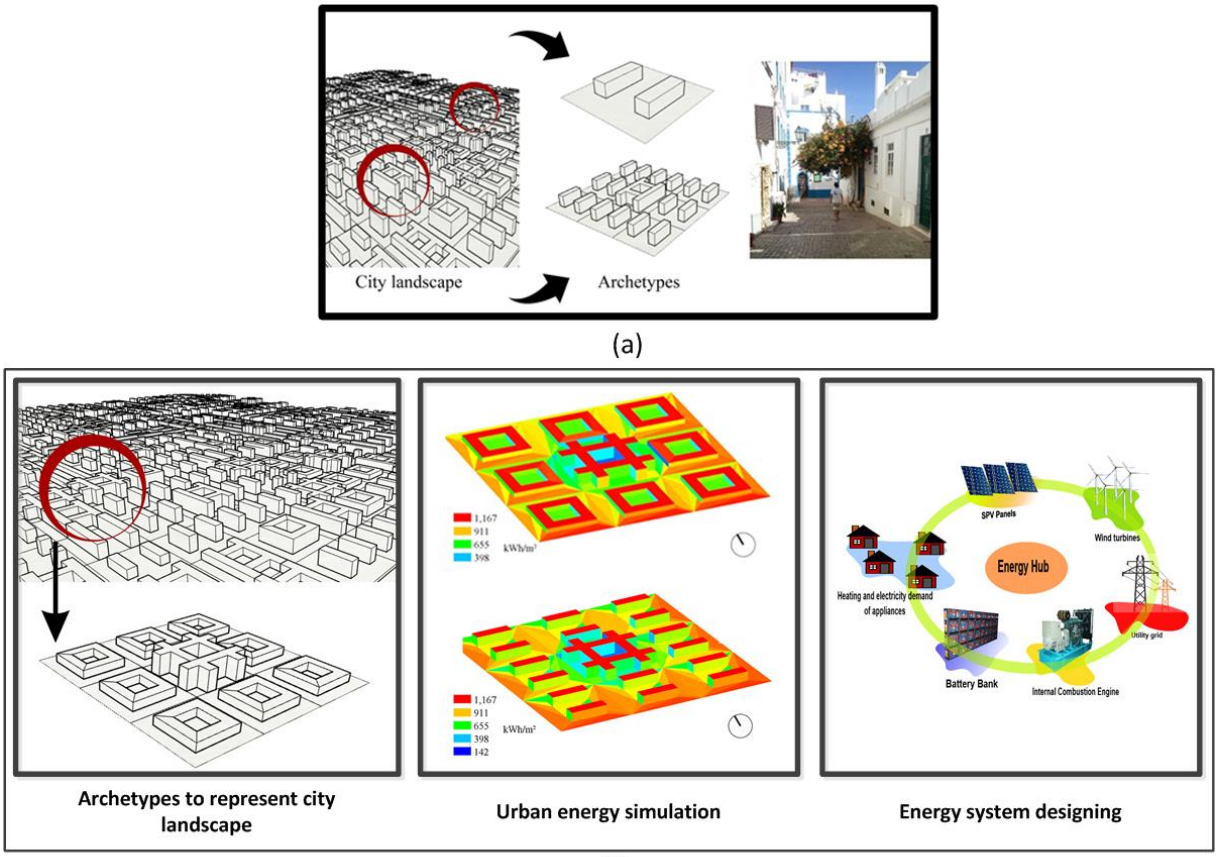

Fig. 9. 1: Conceptual design of the urban archetypes.

Table 9. 1: Urban characteristic of the modular archetypes.

Case studies	Ground floor area (m^2)	Site Coverage (%)	Urban configurations, plan and 3D view. Adapted from [26]
A	900	0.009	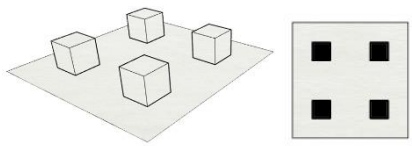
B	3,000	0.03	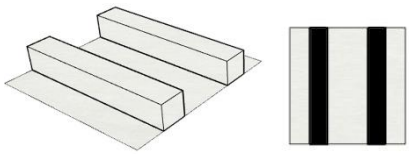

C	1,500	0.015	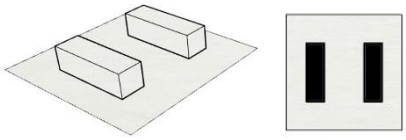
D	4,050	0.04	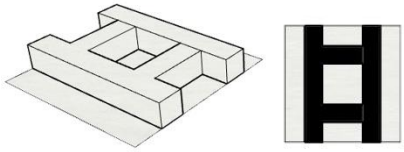
E	3,000	0.03	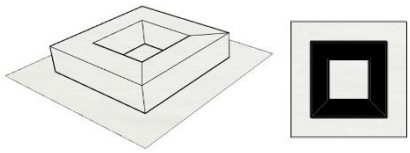
F	5,100	0.05	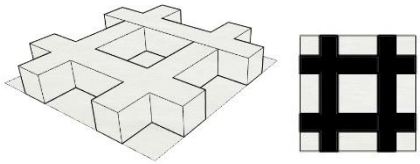

This chapter considers the evolution of modular archetypes from simple neighborhoods to complex urban forms through both vertical and horizontal expansion. Ten different cases were considered for each modular archetype as a function of the number of floors in order to assess the impact of vertical growth. In order to consider the impact of horizontal growth, this chapter considers a grid that formulates integrated urban archetypes based on modular archetypes. The grid consists of nine cells. The central grid cell consists of the modular archetype. In order to create a new district starting from the composition of the archetypes, we decided to aggregate the archetypes upon a 9-cell grid (Table 9.2), where the central one corresponds to the highest case study (with 10 floors), and the cells around are defined by selecting the other case studies, with the objective of reaching a total area of 145,000 m^{-2}, with a maximum tolerance of 5,000 m^{-2} and a relative difference lower than 5%. The total area is defined as the average area of all case studies, multiplied by the 9-cell grid.

Following a deep analysis of the results, three configurations were selected; their geometrical characteristics are summarized in Table 9. 2. Their total area corresponds to 147,000 (m^2).

Table 9. 2: Aggregation typologies.

Aggregation Case Study	Central Cell	Border cells and Area (m^2)	Total Area District (m^2)	Images
Ag1	F10	B4/ 12,000	147,000	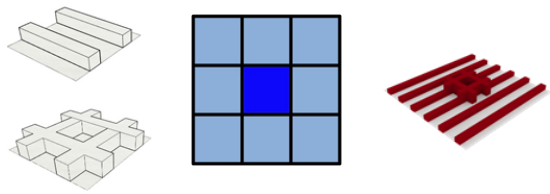
Ag2	F10	C8/ 12,000	147,000	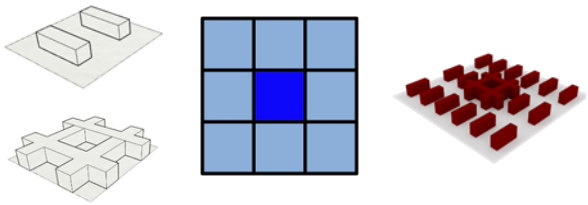
Ag3	F10	E4/ 12,000	147,000	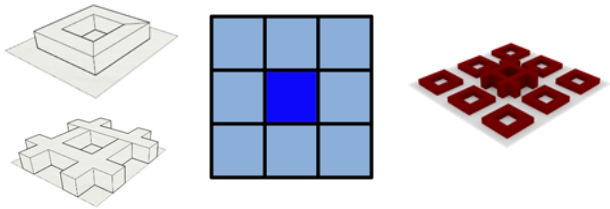

9.4. Computational platform and case study

A computational platform developed to design urban energy systems, which consists of several computational tools. A comprehensive overview of the computational platform is presented in Ref. [11,13]. The computational platform includes a GIS database (QGIS) of building location, building height, year of construction etc., a parametric modelling tool (Rhinoceros 5), an urban simulation model (CitySim) and an energy simulation model. CitySim is amply used in literature [11,27,28], and well validated with on-site monitoring and procedure tests [29–31]. Hourly electricity, heating and cooling demands, as well as SPV generation using rooftop PV are computed using CitySim. The building envelope presents an averaged glazing ration of 20%, without differentiation of facade orientation. The glazing U-value corresponds to 1.2 $W \cdot m^{-2}K^{-1}$ and the g-value to 0.5. The U-value of the envelope is defined according to the CitySim and Lesosai database [32]. All buildings are equipped with heating and cooling systems, which start to work if the indoor air temperature is lower than 20°C or higher than 26°C. The buildings are considered to have a residential function; consequently the occupancy, lighting and appliance profiles are applied according to national and international normative [33] [34]. The electricity required for lighting and appliances is defined hourly

according to the profile we defined, adapted from [33] [34]. The lighting power density corresponds to 5 $W \cdot m^{-2}$ [34], and the power density of appliances to 2 $W \cdot m^{-2}$ [33].

9.4.1. Case study

The energy and electrical models are applied to two climatic conditions: the warm climate of Dubai (United Arab Emirates) and the temperate climate of Hemberg (Switzerland). The weather data used for the analyses were created with the software Meteonorm [35], for a Typical Meteorological Year (TMY), based on the average irradiance data of the period 1991-2010 and the average temperature of the period 2000-2009. The village of Hemberg (47°18'N, 9°10' E, 935m asl, annual solar irradiance: 1,165 $kWh \cdot m^{-2}$, Heating Degree Days: 4,044) presents a Cfb climate (C: warm temperate; f: fully humid; b: warm summer). During the winter time, the lowest temperature recorded during the month of January corresponds to -12.1°C. The summer is quite warm, with a maximum temperature of 29.1°C during the month of July, and an average temperature of 16.3°C. The wind speed is constant throughout the year, with an average wind speed of 3 $m \cdot s^{-1}$. The precipitations are quite high, with a total of 1,018 mm per year.

The city of Dubai (25°16'N, 55°20'E, 0 m asl, Cumulative Solar Irradiance: 1,997 $kWh \cdot m^{-2}$, Cooling Degree Days: 6,196) is characterized by a BWh climate (B: arid; W:desert; h:hot) corresponding to a hot desert climate [36]. The maximum air temperature reaches 45°C during the month of July, while the average temperature during the summer time corresponds to 35°C, and during the winter time to 20°C. Precipitations are mostly absent during the year, and just a few events are registered during the winter time, with less than 40 mm of rain per year. The relative humidity is high, and the wind speed is limited to circa 3.7 $m \cdot s^{-1}$.

9.4.2. Energy system design tool

A multi energy hub that caters the heating, cooling and electricity demand of the location is considered in this chapter. The energy hub is operated in a grid connected mode both selling and purchasing electricity to and from the grid while accommodating fluctuations in demand and generation. Grid curtailments are introduced when interacting with the grid for purchasing and selling electricity to stabilize the grid. The energy hub consists of renewable energy technologies, a dispatchable energy source and energy storage. Solar PV and wind turbines are considered as renewable energy technologies, which are non-dispatchable. An Internal Combustion Generator (ICG) is used as the dispatchable energy source, which helps to absorb the fluctuations in demand along with the battery bank. Heating and cooling demands are catered using heat pump and air-conditioners respectively.

9.5. Results

The annual energy demand for cooling and heating per unit area, respectively assessed for Dubai and Hemberg, is presented in Fig 9. 2(a) and (b). Both Q-Q and S-S lines in the figures show that there is a significant drop in the energy demand when increasing the number of floors. For example, the annual cooling demand decreases from 240 to 99 kWh/m^2 when moving from A1 to A6 in the Dubai case study. A similar decrease in energy demand can be observed for Hemberg. However, there is a significant variation in the cooling demand between modular archetypes with the same number of floors as shown in circle P in Fig 9. 2 (a). Cooling demand decreases from 104.35 to 67.58 kWh/m^2 by 35% when moving from A5 to D5, which have the same number of floors as highlighted in circle P. This clearly highlights the impact of the modular archetype on the energy demand. However, the impact of the modular archetype on the energy demand is lower in the case of Hemberg (which can be understood by comparing P and R circles). This makes it interesting to use indexes such as FF and FAR in order to generalize the observations.

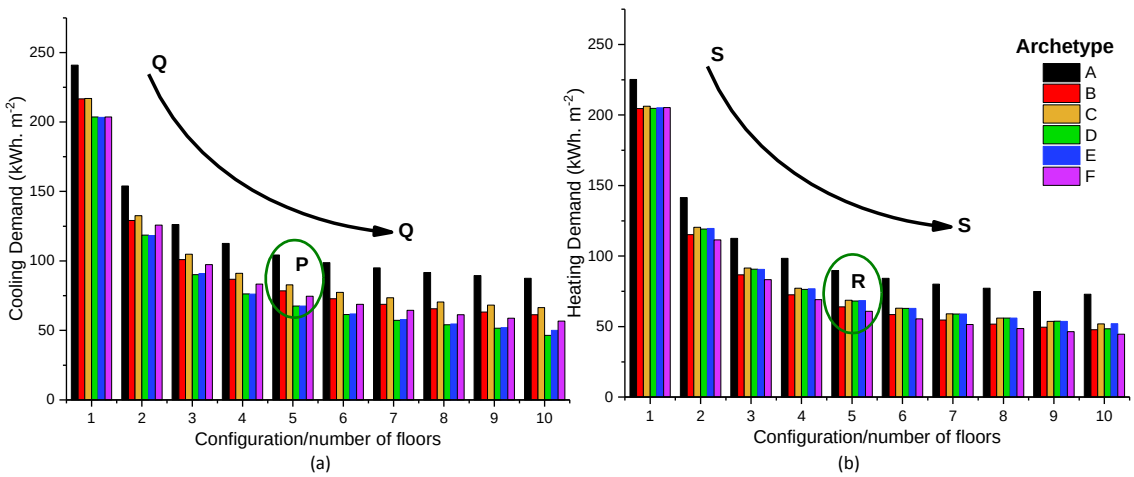

Fig. 9. 2: Annual cooling and heating demand respectively for Dubai and Hemberg. Lines Q-Q and S-S show that annual energy demand for cooling and heating generally decreases with an increase in the number of floors. Circle P shows that there is a significant difference in energy demand per unit area (even for the same number of floors) for the case of Dubai, which is lower in Hemberg as shown in circle R.

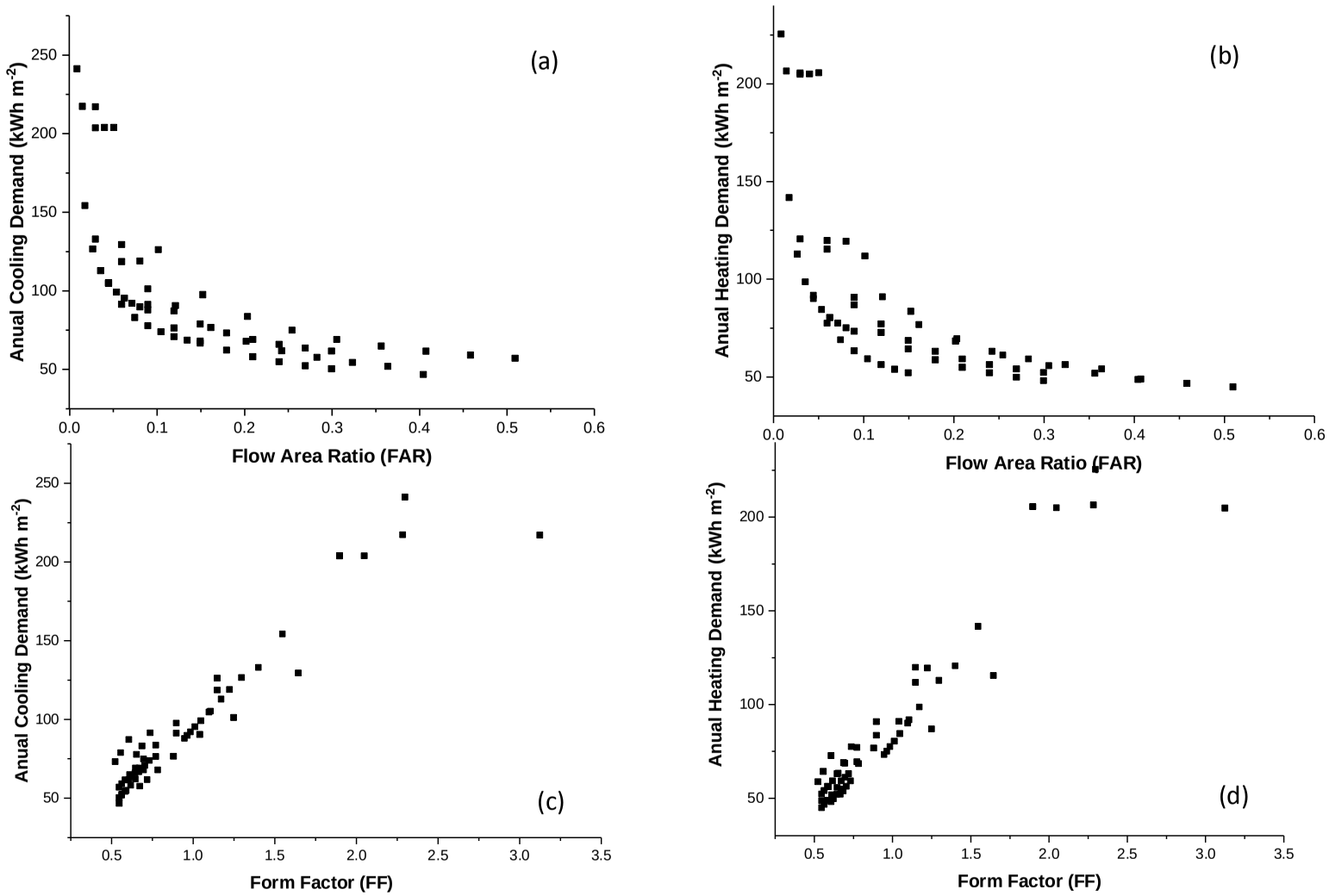

Fig. 9. 3: Variations of (a) cooling and (b) heating demand for Dubai and Hemberg with Floor Area Ratio (FAR) are presented in Fig 9. 3(a) and (b). Variations of cooling and heating demand for Dubai and Hemberg with Form Factor (FF) are presented in Fig 9. 3(c) and (d).

The variation of FAR and FF with energy demand is similar in the Dubai and Hemberg case studies (Fig. 9.3 (a-d)). The energy demand decreases in a polynomial manner with increasing FAR while the energy demand linearly increases with the FF for both locations. For example, by increasing the Form Factor from 0.55 (Case Study F10) to 1.18 (Case Study A4), the heating demand increases by 100%, from 44.6 to 98.3 $kWh \cdot m^{-2}$ for the case of Hemberg. Consequently, the lower the FF, the lower is the heating demand. In general, the building has a low internal volume compared to a high external envelope, increasing the thermal losses, which results in a higher energy demand. This specific aspect is reflected in both FF and FAR. However, when analyzing Fig 9. 3 (b) it can be noticed that the urban archetypes with a similar heating demand (around 205 $kWh \cdot m^{-2}$) can have a different FF, passing from 1.9 (case study E1) to 3.1 (case study B1). This reflects that both FF and FAR only provide a general trend. Hence, it is important to analyze the influence of demand profile in an hourly resolution to get a broader idea of the influence of urban morphology on the energy system with regard to the design process. This is done in the next section.

9.5.1. Influence on the hourly energy demand

The next task is to consider the entire set of modular archetypes used so far to analyze the demand profile on an hourly scale (Fig 9. 4). For this purpose, five archetypes are selected (A10, B3, C6, D2 and E3) from the entire set of 60 archetypes, representing different modular types with different numbers of floors. However, the selected archetypes have a total floor area close to 9,000 m^2, which makes it reasonable to compare the energy system in order to highlight the impact of morphology.

Hourly cooling and heating profiles for Dubai and Hemberg are presented in Fig 9. 4 (a) and (b). The demand profiles for both locations present complex variations on the hourly scale, which complicates performance analysis. Hence, the hourly cooling demand profile for Dubai is taken and divided into three sections marked by colored rectangles in Fig 9. 4(c). The rectangles colored in blue and marked as S provide a similar variation in demand, which is different from the purple rectangle marked as U. Subsequently, two frames are taken and enlarged, each presenting a time span of 48 hours. Frame 1 presents a typical distribution of the cooling demand during summer while Frame 2 presents the demand profile during autumn and spring.

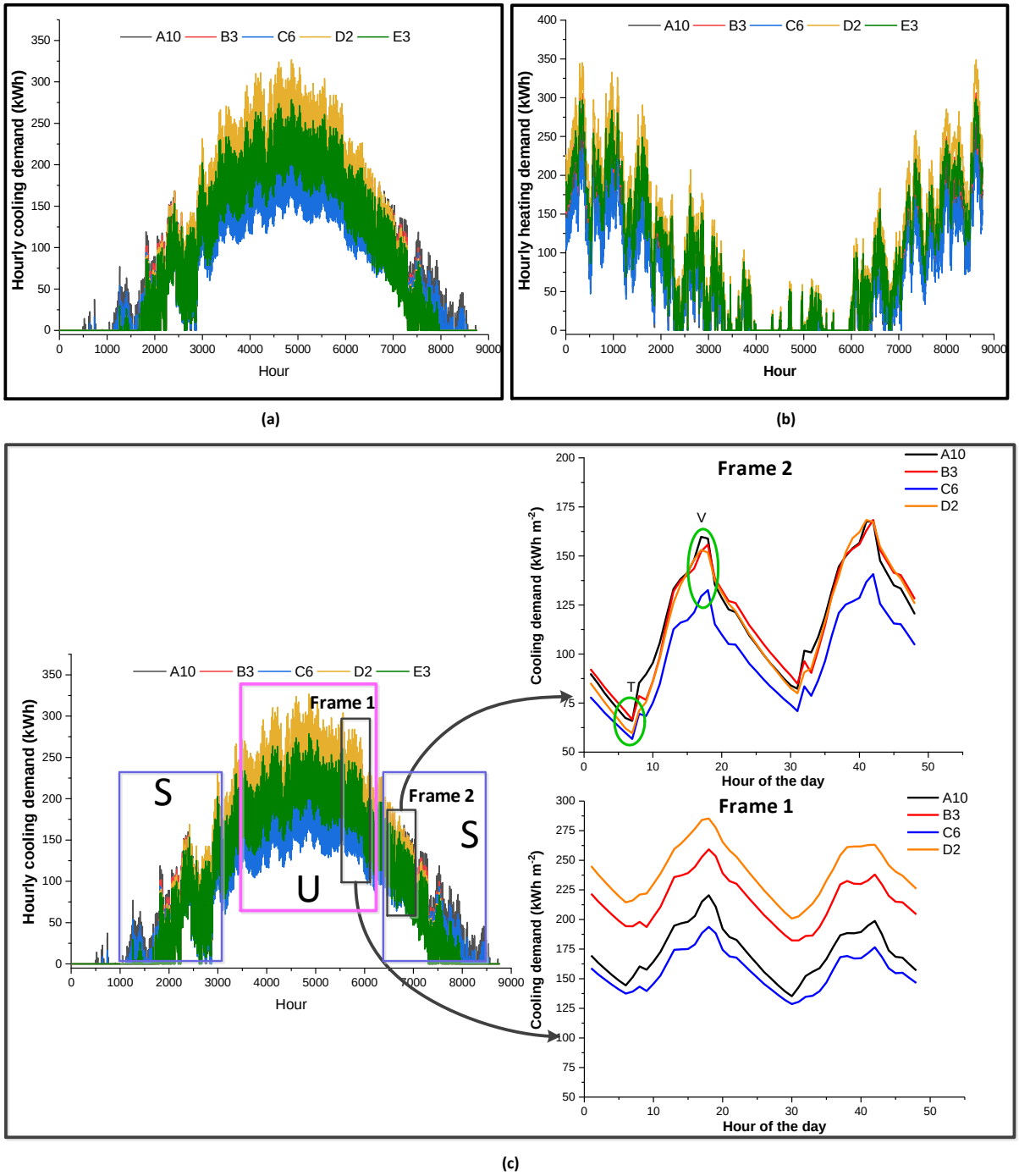

Fig. 9. 4: Hourly variation of cooling (a) and heating demand (b) respectively for Dubai and Hemberg case studies. (c): A detailed analysis of the hourly cooling demand profile of Dubai. Rectangles U and S present the demand during summer and autumn and spring respectively. Frames 1 and 2 are used to further analyze the demand profile.

Following the changes observed in annual energy demand (as shown in Fig 9. 2), it is expected that the hourly demand profile will shift following the annual demand. Such a clear shift in the demand profile can be observed when analyzing Frame 2 in Fig 9. 4(c). A clear separation of the demand profiles can be observed in this context with relatively less fluctuations in the demand profile.

However, when moving from Frame 2 to Frame 1, a few significant changes can be observed. First, it is no longer possible to differentiate the demand profiles in Frame 1 when compared to Frame 2. In certain instances, a significant difference in cooling demand can be observed when considering C6 and the rest (as marked by Circle V in Frame 2) while they are very close to each other in other instances (as marked by circle T in Frame 2). When considering Frames 1 and 2, it can be concluded that the difference in the energy demand is quite negligible in valleys as marked in circle T when compared to the energy demand during the peak period as shown in Frame 1. As a result, energy systems designed for archetypes such as D2 need to operate at very low part-loads when compared to the energy systems installed in C6, which can have a significant impact on their design, especially when considering life cycle cost, environmental impact and autonomy level. The impact of the archetype on the energy system is discussed in next section.

9.5.2. Impact of the modular archetype on the energy system

The stochastic nature of renewable energy potential and demand makes the renewable energy integration process more challenging, especially when designing distributed energy systems while maintaining system autonomy. Therefore, maintaining energy autonomy at building and neighborhood scale is considered as a main priority when integrating renewable energy technologies. A Pareto front considering Net Present Value (NPV) and Grid Integration (GI) level, which presents all the non-dominant solutions considering these two objectives, is helpful to understand the marginal cost of improving the system autonomy. Therefore, a Pareto front considering NPV and GI is used to obtain the design of the energy system, which is subsequently assessed considering NPV, system autonomy, renewable energy integration level and energy efficiency.

The Pareto fronts obtained considering NPV and autonomy level for the selected urban archetypes and the meteorological conditions of Hemberg are presented in Fig 9. 5(a). When analyzing the Pareto fronts, it is prudent to increase NPV when minimizing the grid integration level (for system autonomy improvement). The Pareto fronts of B3 and E3 evolve quite close to each other. Beside these two Pareto fronts a clear shift in Pareto fronts can be observed when moving from one urban form to another. For example, the Pareto solutions have an NPV below $2x10^6$ CHF for urban form C6 but above $3x10^6$ CHF for urban form D2 when reaching the stand-alone condition, which represents a significant increase in cost. More importantly, the shape of the Pareto fronts shows a significant difference when moving from one urban form to another. A sudden drop in NPV is observed when increasing the GI levels for the standalone condition (fully autonomous) for both A10 and D2. A gradual drop in NPV is observed for other urban forms. The Pareto fronts reveal that urban form has a notable impact on the energy system design and grid integration process.

Besides performing a qualitative analysis, it is important to quantify the influence of the urban form from a cost and system autonomy perspective. When looking at C6 and A10 Pareto fronts, it is prudent that both reach the same NPV level when increasing the grid interactions. However, there is a significant difference in the grid interaction levels that `have the same NPV. C6 maintains a grid integration level of 14% at a cost of 1.1 $x10^6$ whereas A10 presents an integration level of 29% for the same cost level. This clearly demonstrates that a higher autonomy level can be maintained for a much reduced price when selecting an appropriate urban configuration. Furthermore, a grid integration level of 10% can be reached for 1.2 $x10^6$ CHF when using C6 whereas the cost increases to 2.6 $x10^6$ CHF using D2, which is a significant increase in the NPV. In brief, urban form has a price from an energy system perspective.

It is interesting to assess the impact of climate on the energy efficiency of the urban form. When moving from Hemberg to Dubai, the Pareto fronts follow the same pattern when arranged in the order of increasing cost (Fig 9. 5(b)). However, the shape of the Pareto fronts looks more homogenous for Dubai. A sudden drop in NPV is observed when increasing the grid integration level from stand-alone, followed by a gradual reduction in NPV when further increasing the grid integration level. However, a significant increase in NPV is observed when moving from C6 to A10, which is not observed for Hemberg. Furthermore, a clear separation of two Pareto fronts is observed for B3 and E3 when considering Dubai due to a distinguishable difference in cooling demand. In general, noticeable changes are observed in the Pareto fronts when moving from Hemberg to Dubai, although the order of increasing NPV remains the same. It can be stated that the influences of urban climate on the energy consumption of buildings depend on the urban form, which may lead to a notable change in the energy demand pattern when moving from one location to another. This results in notable changes for the energy system under different autonomy levels.

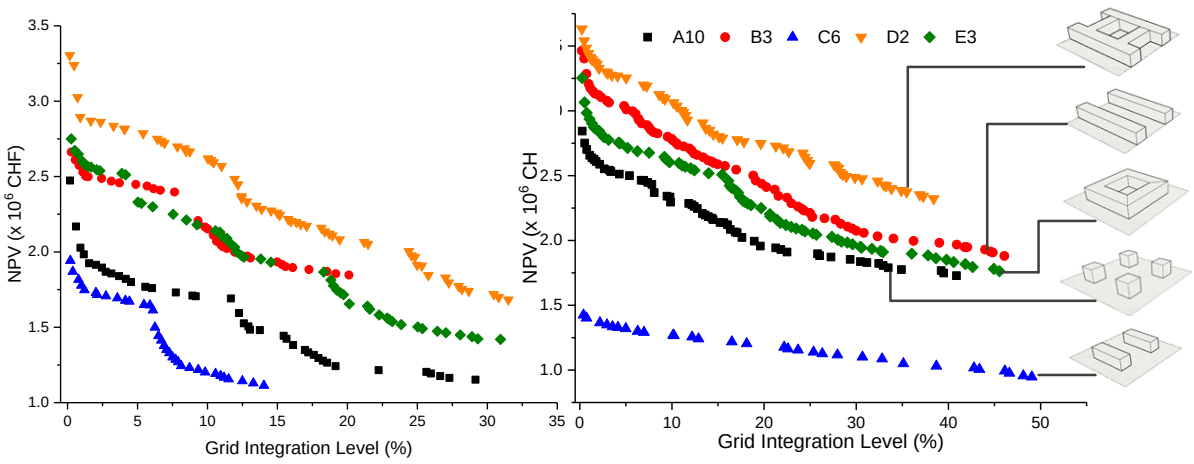

(a) (b)

Fig. 9. 5: Pareto fronts for five urban forms considering NPV and Grid Integration level for the climate of (a) Hemberg and (b) Dubai (R).

9.5.2.1. Impact of the energy demand on energy system design and operation

Urban form can influence both peak demand and demand pattern, which may lead to a notable change in annual energy demand and varying demands on the energy system as well as a notable change in the NPV for the same autonomy level. It is important to assess whether increases in peak demand or annual demand influence the cost of an energy system in a similar manner. To this effect, four Pareto solutions are taken each for urban forms that have similar grid interaction levels. The NPV of these Pareto solutions are taken as a ratio of the NPV of C6 (N/N_{C6}) (urban form with the lowest peak and annual demand). Similarly, the ratios of the peak demand of the urban form to the peak demand of C6 (P/P_{C6}) and the annual energy demand (A/A_{C6}) are computed (as shown in Fig 9. 6). The ratios of N/N_{C6} to P/P_{C6} and N/N_{C6} to A/A_{C6} are computed in order to compare the impact on the energy system due to the changes in peak and annual demand (as a result of a change in the urban form).

Fig 9. 6(a) and (b) show that both N/N_{C6}: A/A_{C6} and N/N_{C6}: P/P_{C6} ratios have values greater than one except for one grid integration scenario of A10 and E3. This indicates that the cost of the system increases at a larger ratio beyond the increase in peak demand and annual demand when moving from C6 to other scenarios. More importantly, both ratios (i.e. N/N_{C6}:A/A_{C6} and N/N_{C6}:P/P_{C6}) reach 1.8 for D2 in Scenario 3, which indicates that there is a significant increase in cost well beyond the increase in annual or peak demand. This clearly highlights the importance of evaluating the sensitivity of energy systems to urban form. When analyzing the demand profile of A10, B3, E3 D2 and C6, D2 presents the highest peak demand. Nonetheless, the demand requirements when there is no cooling

or heating (which corresponds to the minimum demand) remain the same for all scenarios (since the demand for appliances is taken to be similar). Hence, demand fluctuation in D2 is significant compared to the other scenarios, which results in a cost increase that are linear neither with the peak demand nor with the annual demand. The same argument can be advanced to reason out the fluctuations in other three urban forms. Hence, it is clear that the influence on of urban form cannot be simply inferred using building or urban simulation which makes it essential to integrate energy system designing into urban planning process.

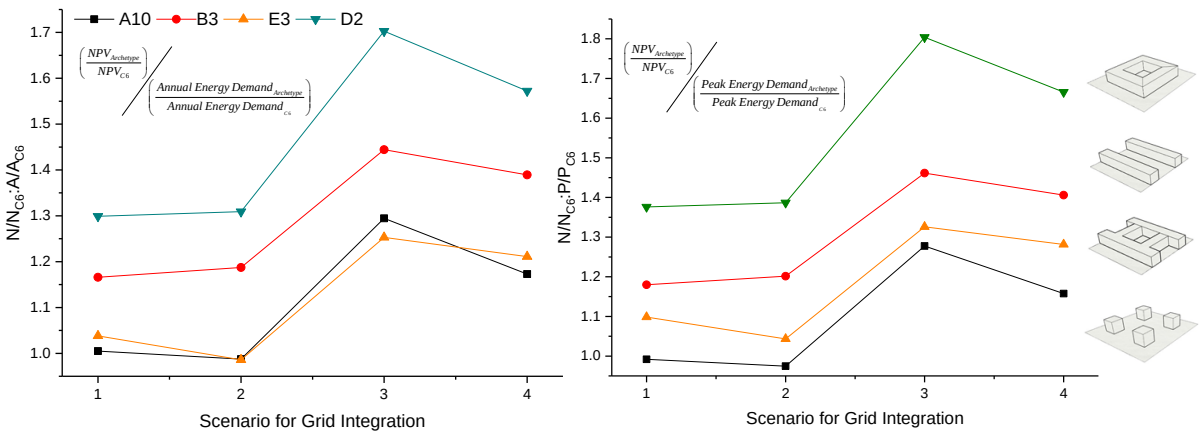

(a) (b)

Fig. 9. 6: Variation of (a) N/N_{C6}:A/A_{C6} and (b) N/N_{C6}:P/P_{C6} for different scenarios of grid integration

9.5.3. Renewable energy integration at building and system level

Roofs receive more solar irradiation than facades and are therefore often preferred for BIPV for financial reasons. Nonetheless, integration of PV panels into facades is rapidly getting popular due to the price reduction PV panels. Therefore, solar irradiation on both facades and roofs is considered in this study. The annual solar energy received per unit floor area is plotted for 60 different forms for Dubai and Hemberg in Fig 9. 7. As you may observe, the peak energy received reaches 23.6 and 35.9 respectively in the C1 configuration for Hemberg and Dubai. For the E10 configuration, the minimum solar energy received reaches 0.23 and 0.32 kWh. The roof area remains the same while the number of floors increases. This simply explains the reason for the decrease of solar energy received per unit area with the increase of floors for the same urban form. However, the most important fact is the sensitivity to urban form of received solar energy. Significant changes can be observed when moving from one urban form to another. For example, the difference is of an order of magnitude when moving from C to E. It can be concluded that the urban form has a notable impact on solar energy technology efficiency at building level.

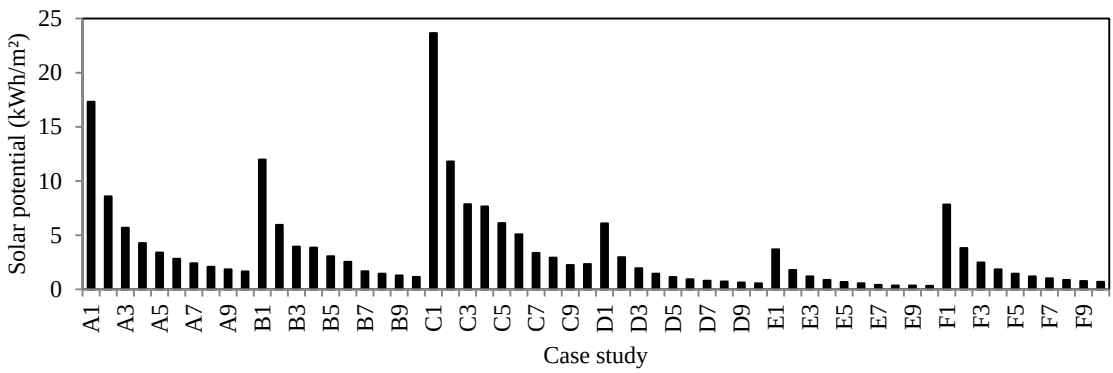

(a)

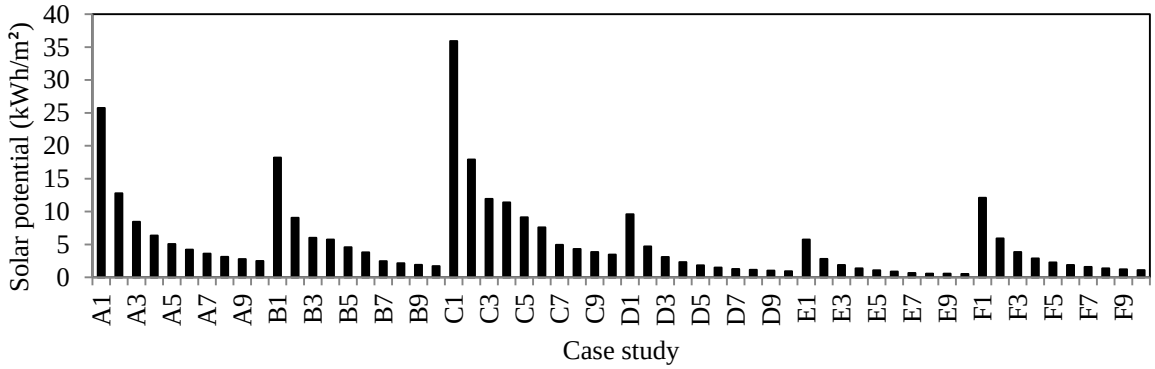

(b)

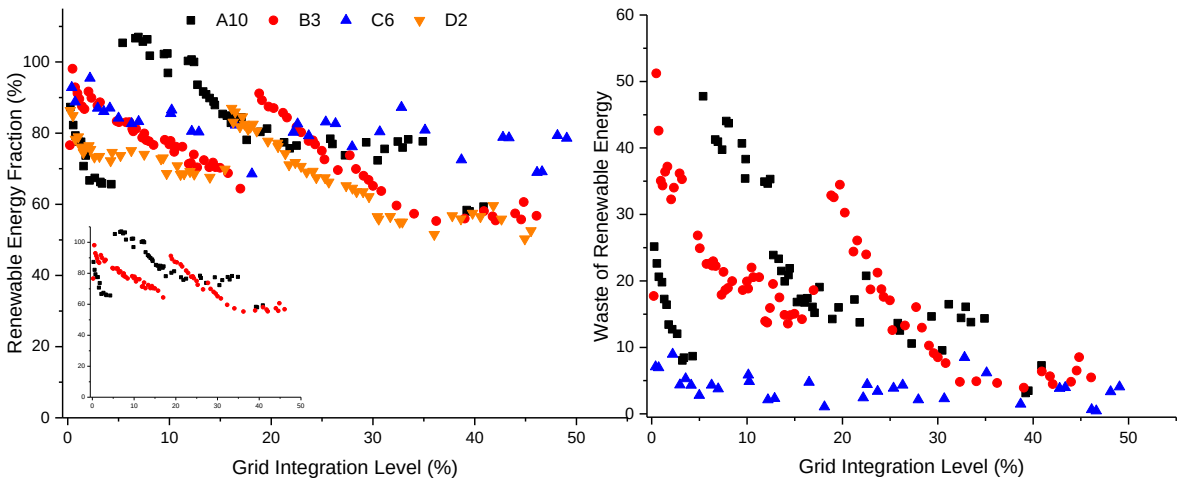

Fig. 9. 7: Renewable energy integration into Archetypes. Annual solar irradiation per unit floor area for different urban forms for (a) Dubai and (b) Hemberg. (c) Fluctuations in the renewable energy fraction (left) and Waste of Renewable Energy (WRE) for the Pareto solutions considering NPV and grid Integration level as objective functions (right) for Dubai case.

Besides performing a qualitative assessment of the potential for building integrated renewable energy technologies, it is important to evaluate the provisions for renewable energy integration at the system level. Characteristics of the demand profile are of notable influence in this context and these depend on the urban form as discussed previously. When analyzing the renewable energy percentage of A10, B3 and E3, we can see that the renewable energy contribution decreases up to a certain point as the grid integration level increases and then suddenly jumps up again (Fig 9. 7(c)). Afterwards it starts to decrease again, but apparently without a common pattern except for B3 and E3. A gradual decrease in renewable energy generation is observed when considering Pareto solutions of urban form C, which is totally different from the other three. In general, the fluctuation of renewable energy contribution with respect to grid integration level is significantly influenced by the urban form. When considering the renewable energy penetration level for the four urban forms considered, an optimistic picture can be observed. Renewable energy generation passes beyond the demand in certain instances (A10), in which the excess is sold to the grid. The renewable energy generation reaches around 50-60% of the annual demand when reaching the minimum NPV for Forms A10, B3 and C6. It oscillates between 70% and 80% in urban form C, which corresponds to a 20% increase in renewable energy penetration level when compared to the others. In general, irrespective of urban form, energy hubs can incorporate non-dispatchable renewable technologies for more than 50% of the annual energy demand.

The renewable power generated within the system cannot be utilized completely in certain instances due to grid curtailments and storage limitations. Therefore, it is important to assess the utilization of renewable energy as well as the generation. The part of renewable energy which cannot be used (waste of renewable energy or WRE) within the system is presented in Fig 9. 7 (c) for the Pareto solutions of the urban forms of A10, B3 and C6. In general, maintaining WRE below 10% is known to be a good practice when designing grid integrated energy systems. When analyzing the WRE for the three urban forms, it is clear that a significant amount of the renewable energy generated within the system has to be dumped due to grid curtailments and storage limitations. WRE reaches 50% for certain design solutions of A10 and B3, which is considered well above the usual practice for grid integrated energy systems. In contrast, WRE is kept below 10% in C6. However, WRE falls below 10% when increasing the grid integration level to above 40% for all the design solutions of all three urban forms. It can be concluded that urban form has a notable impact on renewable energy utilization especially for instances when the grid integration level is low. Hence, effective renewable energy generation can significantly influenced by urban form.

9.5.4. From the modular archetypes to cities

Three Pareto fronts are created for the three aggregated urban forms as presented in Fig 9. 8. Pareto fronts of the aggregated urban forms show a significant drop in NPV when comparing D2 and E3. This is due to the fact that the basic urban forms were more densified when generating the aggregated urban forms, which reduced the demand per unit area. The most important fact is that a significant change in NPV is not observed when moving from one integrated archetype to the other. The three Pareto fronts for the integrated archetypes are sandwiched in between C6 and A10. This depicts the fact that when moving into aggregated urban forms combining different simple urban forms, the aggregated urban forms tend to behave uniquely being different from the parent urban forms. More importantly, no significant difference in the energy system is observed between the aggregated urban forms. However, this specific aspect needs to be studied further, deriving more integrated urban forms using the basic urban forms used in this study and subsequently applying them in real world situations.

9.6. Conclusions and perspectives

The results of the chapter reveal that the urban form has a notable impact on the energy demand. The annual demand can increase by 35% due to the urban form (for Hemberg) when considering the six urban forms considered in this chapter. These values are strongly influenced by the climatic conditions. Although performance indicators such as form factor and floor area ratio can be used to get an overview about the influence of urban form on the energy demand these do not provide detail information. Analyzing the energy demand of the archetypes at hourly resolution helps to get an overview about the influence of urban form on the demand profile which can be split into two. A direct shift (clear separation) in demand profile can be seen among the archetypes for a period of time in the year, while for the rest, these moves very close to each other. As a consequence, a significant fluctuation in demand profile can be seen for some archetypes notably influencing the energy system design. As a result, the autonomy level of the system can be improved by 10-15 % by selecting a more efficient urban form and more importantly, the cost of the energy system can be reduced by 30-50% by appropriate urban planning.

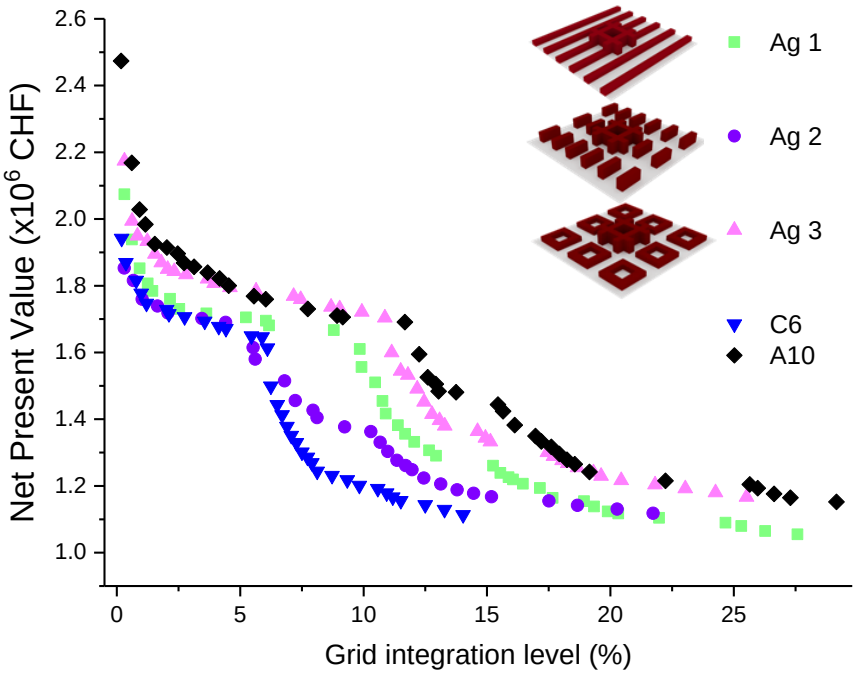

Fig. 9. 8: Comparison of the Pareto fronts obtained for integrated urban archetypes.

The influence of urban form is further assessed focusing on the renewable energy integration perspective. As a consequence of the change in demand profile due to urban form, waste of renewable energy levels notably changes. Except one (C6), all the archetypes have higher WRE when reaching fully autonomous operation which increase up to 50% of the annual demand in certain instances. The chapter also shows that urban form can have an impact on building integrated renewable energy technologies such as BIPV. Optimum selection of the urban form can maximize the onsite renewable energy generation significantly. In general, urban form has a significant impact on the renewable energy integration. When comparing the two cities it is observed that a notable change in the NPV is observed when moving from Dubai to Hemberg (when comparing) from the perspective of objective function values of the Pareto fronts. Nonetheless, the impact of urban configuration on the energy system is visible irrespective of the location. Archetype C6 performed well for both the locations when compared to the other archetypes which resulted in a significant improvement in the NPV values.

Extrapolating the conditions of simple urban forms to complex urban forms that can be observed in actual cities will not produce accurate results. However, aggregated urban forms developed on the basis of simple urban forms can provide an indication regarding the behavior of complex urban forms. An aggregated urban form shows a behavior that is different from the parent forms that are used to develop them. More importantly, no significant difference is observed when moving from

one to another considering demand, renewable energy integration and energy system. This indicates that the influence of the urban form is trivial whenever we introduce a neighborhood into a highly dense large city, in which the complexity of the urban form is not altered by the introduction. However, the configuration of a neighborhood should be carefully considered when introducing a stock of buildings at the periphery of the city or in suburbs, in which the configuration of the buildings can notably influence the energy performance of the neighborhood. More importantly, the study reveals that the impact of urban form on the energy system (in terms of cost) is well beyond the impact on annual energy demand or peak demand. Therefore, it is difficult to deduct the influence of urban morphology simply by using building or urban energy simulation. The urban form influences the energy system with regard to cost, system autonomy and renewable energy integration. This makes it essential to optimize the configuration of the neighborhood along with the energy system and to combine urban planning and energy system optimization in order develop energy efficient future cities.

10 Integrated Assessment and Decision Making in the Energy System Designing Process

An integrated approach is presented in this chapter to design electrical hubs combining optimization, multi-criterion assessment and decision making. Levelized Energy Cost (LEC), Initial Capital Cost (ICC), Grid Integration Level (GI), Levelized CO2 emission (LCO2), utilization of renewable energy, flexibility of the system, loss of load probability (LOLP) are considered as criteria used to assess the design. The novel approach consists of several steps. Pareto analysis is conducted initially using 2D Pareto fronts to reduce the dimensions of the optimization problem. Subsequently, Pareto multi objective optimization is conducted considering LEC, GI and ICC which were identified as the best set of objective functions to represent the design requirements. Next, fuzzy TOPSIS and level diagrams are used for multi-criterion decision making (MCDM) considering the set of criteria and the boundary matrix that represents the design requirements of the application.

This chapter is based on (preprint version):

A.T.D. Perera, V.M. Nik, D. Mauree, and J.-L. Scartezzini, "An integrated approach to design site specific distributed electrical hubs combining optimization, multi-criterion assessment and decision making", Energy 2017 (134), PP. 103-120

Author contribution for the journal paper:

In this article, ATD, designed the research with the support of VMN, DM and JLS. ATD conducted the analysis and prepared the first draft of the manuscript. VMN, DM and JLS supported in revising and finalizing the Manuscript.

Readers are encouraged to read following journal papers and conference proceedings for further information

1. Morgane Le Guen, Lucas Mosca, A.T.D. Perera, Silvia Coccolo, Nahid Mohajeri, Jean-Louis Scartezzini, "Improving the energy sustainability of a Swiss village through building renovation and renewable energy integration", Energy and Buildings, 2018
2. Nahid Mohajeri, A.T.D. Perera, Silvia Coccolo, Morgane Le Guen, Lucas Mosca, Jean-Louis Scartezzini "Assessments of sustainable development scenarios for a Swiss village to 2050 through renewable energy integration." (Manuscript in review: Renewable Energy)
3. Karni Siraganyan, A.T.D. Perera, Dasaraden Mauree, Jean-Louis Scartezzini, Role of solar energy and storage technologies to make neighborhood more autonomous. (Manuscript in Review: Energies)
4. Morgane Le Guen, Lucas Mosca, A.T.D. Perera, Silvia Coccolo, Nahid Mohajeri, Jean-Louis Scartezzini, Achieving energy sustainability in future neighborhoods through building refurbishment and energy hub concept: a case study in Hemberg, Switzerland, CISBAT 2017, Switzerland
5. A.T.D. Perera, Dasaraden Mauree, Jean-Louis Scartezzini, The energy hub concept applied to a case study of mixed residential and administrative buildings in Switzerland, CISBAT 2017, Switzerland
6. Karni Siraganyan, Dasaraden Mauree, A.T.D. Perera, Jean-Louis Scartezzini, Evaluating the need for energy storage to enhance autonomy of neighbourhoods, CISBAT 2017, Switzerland
7. Antoine Kuehner, Nour Mdeihli, Silvia Coccolo, A.T.D. Perera, Nahid Mohajeri, Jean-Louis Scartezzini, Extending building integrated photovoltaics (BiPV) using distributed energy hubs: a case study in Cartigny, Switzerland, CISBAT 2017, Switzerland
8. Henri Bittel, A.T.D. Perera, Dasaraden Mauree, Jean-Louis Scartezzini, Locating multi energy systems for a neighborhood in Geneva using k-means clustering, CISBAT 2017, Switzerland

10.1. Introduction

Integrating renewable energy technologies is important to make energy systems sustainable and face the challenges due to escalating prices of fossil fuel resources, GHG emissions and security problems due to nuclear energy. Wind and solar energy are becoming more promising choices in this regard. However, stochastic nature of these energy sources limits the direct integration of these energy technologies up to 40% of the demand in order to maintain the stability of grid [1], [2]. Smart micro grids [3]–[5], virtual power plants [6]–[8], grid integrated and stand-alone hybrid energy systems [9]–[11] are getting popular on this regard as methods to integrate higher fractions of Solar PV (SPV) and wind energy. These systems consist of dispatchable energy sources and storage which can absorb the fluctuations of SPV and wind energy while maintaining the reliability of the power supply. However, a number of aspects (technical, environmental, economical, social) need to be considered in the designing process especially considering site specific requirements [12].

Optimum design and operation of distributed energy system is a challenging task with higher penetration levels of non-dispatchable renewable energy technologies such as SPV and wind. A number of studies have focused on addressing this research problem for both grid integrated and stand-alone operating modes [13]. At the same time, different approaches have been used to optimize these systems depending upon the system configuration as reviewed in Ref. [9], [14]–[16]. Multiple conflicting objectives are considered in the optimization process considering a number of diversified factors such as cost, environmental impact [17]–[19], utilization of renewable energy [20], system reliability [10], [21], [21], [22], social impact [23], exergy efficiency [24]etc., depending upon the requirements of the design. A detailed list of different objective functions considered in multi objective optimization of energy systems is presented by Tan et-al [25]. According to Fadaee and Radzi [12], research studies on multi objective optimization energy systems should be more focused on catering site specific requirements. This makes it essential to consider a number of sites and design specific requirements which are beyond objective functions used for multi-objective optimization. In addition, this makes it essential to select proper objective functions for Pareto optimization out of the set of criterions used to assess the project. In addition it is important to continue energy system design beyond multi-objective optimization as suggested by Bhattacharyya [26] where multi criterion assessment and decision making needs to be combined with the designing process.

Multi criterion assessment and decision making plays a major role when designing energy systems where a set of criterions need to be considered when arriving at the final. A number of different techniques have been used in this context which are reviewed in detailed in Ref. [27], [28]. Multi-

criterion decision making has been amply used in various applications related to locating energy systems [29]–[31], performance evaluation of energy systems [32]–[34], configuration selection etc [35]–[38]. However, most of these applications are different from energy system designing. When it comes to energy system designing, non-dominant set of solutions used for multi criterion decision making needs to be obtained using Pareto optimization which is a lengthy process compared to most of the previous examples. Sayyaadi et-al [24], Perera et-al [39] and Mazza et-al [40] have used multi criterion decision making following multi objective optimization to design a poly-generation system, stand-alone hybrid energy system and a distribution network. Objective functions used for Pareto optimization are used directly used as the criterions for multi-criterion decision making process in these studies. Hence, this approach cannot be used whenever set of criterions used to assess the energy system increases notably; especially for practical applications of distributed energy systems where much diversified criterions are expected to be evaluated. In such instances, it is important to have an integrated approach consisting of several steps in order to identifying criterions that need to be considered for the assessment, select most the appropriate criterions as objective functions for Pareto optimization and support multi-criterion decision making considering all the criterions used to assess the system.

This chapter presents an integrated approach that can be used to design grid integrated electrical bubs (simplified version of a multi energy hub only considering the electrical parts) consisting of SPV panels, wind turbines, battery bank and an Internal Combustion Generator (ICG). Eight criterions are considered to assess a grid integrated electrical hub. A novel integrated approach consisting of several steps is introduced to design the electrical hub depending upon the importance of each criterion. A Pareto analysis is conducted with different combinations of objective functions to reduce the dimensions of the optimization problem and select the most suitable objective functions. Decision making process is extended beyond the Pareto optimization (values of the objective function) considering all the aspects of the design using a boundary matrix to present the boundaries of the customer expectation. Section 10.2 provides a brief overview about the system considered in this chapter. Section 10.3 provides a detail description about the criterions used to assess the system and optimize. Section 10. 4 presents a concise description about the dispatch strategy. Section 10. 5 optimization algorithm and different combinations of objective functions considered. A detailed description about the novel integrated approach is presented in Section 10. 6. Finally, application of the novel method is taken into discussion in section 10. 6.

10.2. Computational model for the electrical hub and assessment criterions

A computational model is developed in this chapter to formulate criterions that are used to assess the electrical hub. Some of these criterions are directly used as objective functions in the optimization process and some other are considered in the decision making process. This section presents a brief overview about the energy system and the dispatch strategy adapted in brief.

10.2.1. Overview of the Electrical Hub

An Electrical Hub operating as a distributed energy system connected to the grid is considered in this chapter (Fig. 10.1). The Electrical Hub discussed in this paper is related to a rural electrification project for a small model village (peak demand of 29 kWh) in Hambanthota district. Hambantota is situated in the southern coastal belt in Sri Lanka which is having significant solar and wind energy potential according to the surveys carried out in Sri Lanka. Hence, an energy system configuration consisting of SPV panels, wind turbines, ICG and a battery bank is considered for the Electrical Hub.

A steady state hourly simulation is used to assess the energy flow in the system. Hourly wind speed and global horizontal solar irradiation are taken from meteorological databases. An isotropic model is used calculate the tilted solar irradiation on the SPV panel. Finally, power output from the solar panels is calculated using Durisch model [41]. The main advantage of this model is its capability to consider cell temperature, air mass, tilted solar irradiation when evaluating the efficiency of Solar PV panels which provides a better accuracy in modeling SPV panels [42]. Similarly, the power low approximation is used to convert the wind speed from anemometer to hub level height. Cubic Spline interpolation technique [43] is used to represent the power curve provided by the manufacturer of the wind turbines. Finally, renewable power generated (P_{RE}) using SPV panels and wind turbines are computed on hourly basis. A detailed description about the model used to compute the energy flow through the renewable energy components can be found in Ref. [11].

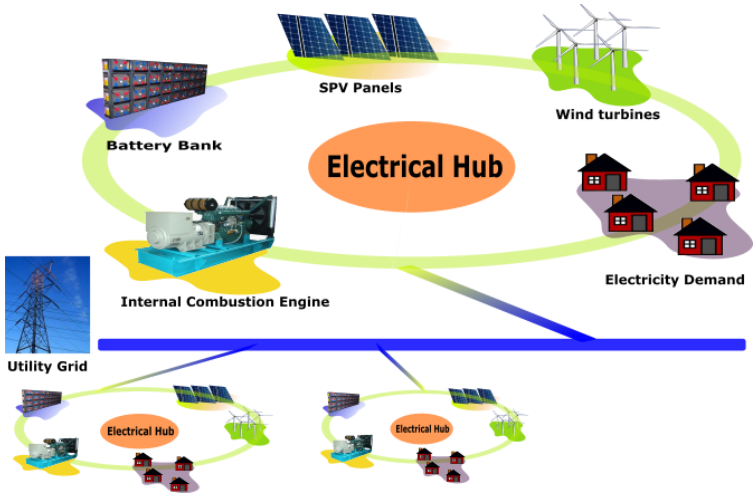

Fig. 10. 1*:* Overview of the electrical Hub

10.3. The assessment criterions and their formulation

Eight criterions are used to assess the energy system. These criterions are covering wider spectrum interests by users of the energy system including economic, environmental, energy efficiency and reliability. A concise description about the each criterion is presented in this section.

10.3.1. Power supply reliability

Power supply reliability becomes a vital factor to be considered in the designing process. Stochastic nature of the renewable energy potential, maintenance downtime of system devices and limitations in grid interactions and energy storage can result in breakdown in the power supply. Loss of power supply (LPS) due to downtime of system devices is not considered in this study. Loss of load probability (LOLP) as defined in Chapter 2 in used to measure the power supply reliability.

10.3.2. Grid integration Level

Autonomy of the system plays a major role in the renewable energy integration process. Strong interactions with grid will make the grid to be vulnerable to cascade failures. Hence, autonomy of the system is considered as a vital factor to be evaluated in renewable energy integration process especially in distributed generation. Instead of taking system autonomy (i.e. determines the percentage of demand generated within the system), grid integration level which is the complimentary to system autonomy is considered in this work. This will convert the maximization problem into a minimization problem that will make the decision making problem trouble free. The definition of GI level introduced in Chapter 2 is used in this part.

10.3.3. Utilization of renewable energy

Various reasons such as stochastic nature of the demand and renewable energy potential, grid curtailments, limitations in energy storage makes it challenging to utilize renewable energy. This leads to a number of problems including poor energy efficiency, dependence on grid or dispatchable energy source which results in either poor autonomy or higher GHG emissions due to the combustion of fossil fuels. In order to rectify this issue utilization of renewable energy is considered as a major criterion to be optimized in energy system design. This study uses Waste of Renewable Energy (WRE) as the performance indicator which should be minimized in the design process. WRE represents the energy losses that take place in system due to seasonal changes in demand, renewable energy potential, and limitations in the energy storage and grid curtailments that has been amply used in resent literature [20], [39], [44]. The formulation for WRE introduced in Chapter 2 is used in this chapter.

10.3.4. Fuel Consumption of ICG

Dispatchable energy sources play a major role when integrating renewable energy technologies into integrated energy systems. However, reliance upon dispatchable energy sources based on fossil fuel resources makes the system to be vulnerable to dynamic pricing due to higher depletion of fossil fuel resources. In addition, Fuel transportation becomes challenging for places away from cities and frequent use of ICG will lead to frequent maintenance. Minimizing fuel consumption will lead to minimize all the aforementioned limitations and make the system to become more sustainable. Fuel consumption of the ICG (FC) is calculated considering the operating load factor (LF) as presented in Chapter 2.

10.3.5. Initial Capital investment

Two economical parameters are considered in this assessment: initial investment required and Levelized Energy Cost (LEC) considering lifecycle cash flow of the system. Initial Capital Cost (ICC) required consist of acquisition cost (I_{AC}), installation cost of the components (wind turbines, SPV panels, battery bank, ICG, power electronic devices etc) and other services charges that required to be paid to Energy Service Provider (I_{ESP}) to operate as grid integrated energy system. I_{AC} comprise of cash flows related to purchasing of system components considering present Sri Lankan market. Cash flows related to land clearance and installation costs are considered under I_{Ins}. Investment for the land is not considered in this work. Finally, ICC is calculated as explained in Chapter 2.

10.3.6. Levelized Energy Cost

Levelized Energy Cost (LEC) is calculated considering the total cash flows of the system. LEC mainly consist of three components i.e. ICC and operation and maintenance cost (OM), and cash flow due

to grid interactions. OM consists of two main components, these are fixed (OM_{Fixed}) and variable $OM_{Variable}$ costs. OM_{Fixed} considered recurrent annual cash flows for maintenance of wind turbines, SPV panels, fuel and operation cost for ICG etc. $OM_{Variable}$ considers the replacement cost for ICG and battery bank. Replacement time for the ICG is determined considering the operating hours and Rain-flow algorithm is used to determine the replacement time for the battery bank. Net cash flow due to GIs (GICF) is computed considering cash inflow due to selling excess generated and buying the mismatch based on the real time price of the grid. Finally, NPV of all the three main cash flows are combined and Net Present Value (NPV) of the project is calculated. A detailed description about the methodology used to compute NPV is presented in Chapter 2.

10.3.7. Levelized CO2 Emissions

Minimizing CO2 emissions in different phases of the project is considered as one of the objectives of the energy system designers. Levelized CO2 (LCO2) is taken as the performance indicator to evaluate this aspect in this work. CO2 generation due to energy system components and their replacement is considered first. Afterwards CO2 generated due to grid interactions (when purchasing electricity) and power generation in ICG is considered secondly. Finally, total CO2 emission (TCO2) of the system is calculated a in Chapter 2.

10.3.8. Flexibility of the system

Flexibility of the system is defined as the ability of the system to adjust for the changes that take place in internal or external environment changes. Flexibility will make the system impervious to changes in the inputs and the outputs which are essential when it comes to distributed generation. Hourly time series for renewable energy potentials, demand, price of grid electricity etc., are considered as inputs to the computational model that are stochastic in nature. Hence it is important to consider the flexibility of the system to get adapted to the changes of these factors. In addition to these factors, flexibility of the system needs to be measured considering volatility of market prices in fuel, electricity, and energy storage needs to be considered in economic terms. All the aforementioned factors can be considered as the external factors which system needs to flexible. In addition, internal factors due to malfunctioning or maintenance of system components such as wind turbines, SPV Panels, ICG etc., need to be considered within the broad scope of flexibility. However, most of the recent studies in energy systems design did not consider all these aspects simultaneously due to the complexity and most of the studies limit their scope to power supply reliability. This chapter also limits the scope to internal factors considering the changes in renewable energy potential, demand and grid curtailments. A detailed description about the methodology used to compute flexibility is presented in Chapter 7.

.

10.4. Dispatch Strategy of the E-hub

A bi-level dispatch strategy combining fuzzy and finite state automata theory is used in this chapter to determine the operating load factor of the ICGs and, energy interactions with battery bank and grid. Finite state automata have been amply used in representing dispatch strategy when designing hybrid energy systems [48], [49]. Fuzzy rules are defined considering the state of charge level of the battery bank and the difference in Electric Load Demand (ELD) and generation. The fuzzy rules are optimized using the algorithm presented in Section 10.6. Interactions with the grid and energy storage are determined in the secondary level after determining the net power generation of the system, mismatch between demand and generation, real time electricity price in grid and state of charge of the battery bank. State transfer function is derived considering seven decision variables (Table 10.1) which are optimized using the optimization algorithm. Subsequently, the ten possible states that the system operates considering the SOC of battery bank, renewable energy generation, COE in grid, upper bounds to purchase ($P_{FG\text{-}Max}$ (t)) or sell electricity to grid ($P_{TG\text{-}Max}$ (t)) (grid curtailments) is presented in Table 10. 2.

Table 10. 1: Decision space variables used for formulating the state transfer function

Decision space variable	Description
Lim_{BC}	Critical cost for GCT(t) above which selling the excess power generated to the grid is economical compared to battery charging
Lim_{BD}	Critical cost for GCF(t) below which purchasing power from grid is economical compared to battery discharging
Lim_{GTB}	Critical cost for GCF(t) below which purchasing power from grid to charge battery bank is economical
Lim_{BTG}	Critical cost for GCT(t) above which selling stored energy to grid is economical
SOC_{min}	Critical SOC of the battery bank below which discharging is not economical to cater the load mismatch
$SOC_{Min,G}$	Critical SOC of the battery bank below which it is not economical to discharge and/or to sell the stored energy to grid
SOC_{Set}	Maximum state of charged to be reached when charging the battery bank using the grid

10.5. Design optimization of the system

Optimum design and control of integrated energy systems combining renewable energy technologies for both stand-alone and grid integrated applications is a rich area of study. A number of publications have presented different techniques for optimization including heuristic, direct search, numerical methods where different objective functions are considered [12], [16], [50]. The

response of the energy system to the changes in demand, renewable energy potential etc. needs to be considered where hourly simulation is required. Simulation of the system considering time series of demand, renewable energy potential and grid conditions result in objective functions neither linear nor analytical. Simultaneous optimization of design and control strategy makes mapping of decision space variable into objective space complicated. Lopez et-al [51] has shown that evolutionary algorithms are efficient in optimizing such integrated energy systems for stand-alone applications. Different architectures of algorithms have been adapted to optimize integrated energy systems which have shown to be promising for both grid connected and stand-alone operation [12], [16], [50].

Table 10. 2: Operating states of the system secondary level dispatch strategy

State	Description of the state	Condition of the battery bank	Grid interaction	COE in Grid
State 1	Excess power is generated and COE in MTG is higher enough to sell excess power generated instead of battery charging	Self-discharge	Excess power generated is transferred to grid	$GCT(t) > Lim_{BC}$ and $GCT(t) < im_{BTG}$
State 2	Excess power generated is directed to the grid and battery bank discharge	Battery bank can be discharge up to $SOC_{Min,G}$	Power can directed to the grid up to TG_{Lim} depending on excess generation	$GCT(t) > Lim_{BC}$ and $GCT(t) > Lim_{BTG}$
State 3	Excess power generated is directed to the battery bank	Battery bank can be charged up to maximum SOC	No interactions	$GCT(t) < Lim_{BC}$ and $GCF(t) > Lim_{GTB}$
State 4	Excess power generated is directed to the battery bank and further charged using	Battery bank is charged using excess renewable energy and grid	Power from grid to charge battery bank	$GCT(t) < Lim_{BC}$ and $GCF(t) < Lim_{GTB}$
State 5	Excess power generated is larger than the maximal transferable, it needs to be dumped which will produce waste of renewable energy (WRE).	Battery bank reaches maximum state of charge	Power is directed to the grid up to TG_{Lim}	At any condition
State 6	Mismatch in demand and generation taken from the grid	Self-discharge	Mismatch is catered	$GCF(t) < Lim_{BD}$ and $GCF(t) > Lim_{GTB}$
State 7	Mismatch is taken from the grid while charging the battery bank	Battery bank is charged up to SOC_{Set} using the grid	Power taken from the grid to charge the battery bank	$GCF(t) < Lim_{BD}$ and $GCF(t) < Lim_{GTB}$
State 8	Mismatch is taken from the battery bank	Battery bank can be discharge up to SOC_{min}	No interactions	$GCF(t) > Lim_{BD}$ and $GCT(t) < Lim_{BTG}$
State 9	Mismatch is taken from the battery bank and excess in the battery bank is injected to the grid	Battery bank can be discharge up to $SOC_{Min,G}$	Power to the grid from battery bank	$GCF(t) > Lim_{BD}$ and $GCT(t) > Lim_{BTG}$
State 10	Mismatch is greater than the maximum that can be taken combining battery bank and grid. Loss of power supply will take place in this case	Battery bank reaches the minimum state of charge	Maximum limit that can be taken from the grid	At any condition

Evolutionary Algorithm based on Ɛ-dominance technique is used in this study for multi-objective optimization. This method is a proven technique to maintain diversity of the Pareto front while reaching the best set of solutions. Optimization algorithm is combined with the computational model that formulates the objective functions. Hence, a simulation based optimization of the system is performed. Several combinations of the objective functions are considered as shown in Table 10. 3 based on the formulations described in Section 10. 3. Power supply reliability is considered as the constraint in all the optimizations.

Table 10. 3: Different combinations of objective functions considered for optimization and decision space variables

Scenario[1]	Objective functions considered	Constraint function	Decision space variables
A	Case 1: LEC-ICC Case 2: LEC-LCO2 Case 3: LEC-GI Case 4: LEC-WRE	Loss of Load probability	• Number and type of SPV panels • Number and type of wind turbines • Size of Battery bank • Size of ICG • Variables for finite state machines • Variables of fuzzy controller
B	LEC-GI-ICC		

(1)Scenario A relates to Cases for Pareto analysis and B relates for multi-criterion decision making

10.6. Frame work for the multi criterion assessment and decision making

Optimum design and operation of Electrical Hubs is a multi-step process which consists of several phases as shown in Fig. 10.2. Multi-criterion assessment starts with understanding the main requirements that need to be met in the energy system designing project. This will help understand and define criterions that need to be considered in the optimization, assessment and multi criterion decision making. As the second step, classifying these performance indicators based on the relative importance to the specific project is performed. In this study, performance indicators are classified into three groups i.e. Preference Indicators (PI), Basic Indicators (BI) and Critical Indicators (CI) depending upon its importance and relevance to the application. Power supply reliability and LEC are taken as the most influential factors to the design which cannot be waived to increase the performance of other indicators. Power supply reliability is considered as a constraint in the optimization process which is not considered further in the decision making process. LEC is carefully considered along with all the other criterions in the decision making process to make sure that expectation of the system design is met.

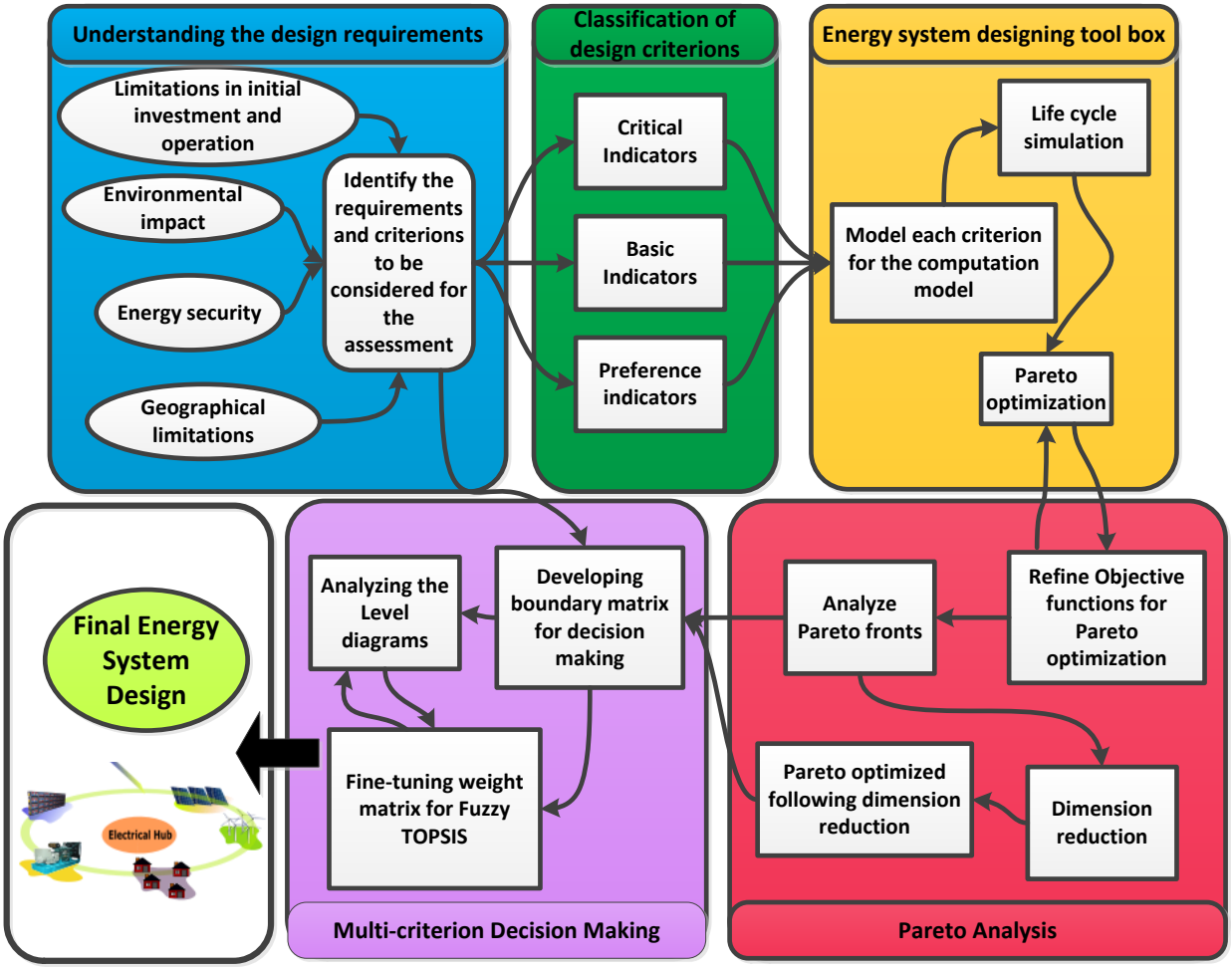

Fig. 10. 2*: Different parts of the decision making Process*

BIs are selected from the pool of criterions considering the site specific information and the requirement of the applications. These criterions are having a less priority lower compared to CIs. In this work, ICC, LCO2, WRE, GI and system flexibility level are considered as BIs. These are considered as objective functions in the Pareto optimization and subsequently in the Pareto analysis (except system flexibility which is computed following the Pareto optimization considering the performance of the Pareto solutions). Finally, PIs are considered as other criterions need to be considered in the design. After the classification of criterions, these criterions need to be mathematically modeled which can subsequently be used for optimization. This is usually performed by an energy system designing tool box as explained in Section 10. 3, 10.4 and 10.5.

A number of techno-economical criterions can be suggested to consider in Pareto optimization. However, extending the dimensions of the objective space makes the optimization process more difficult. Extending the dimensions will increase the set of Pareto solutions. Each and every solution in the Pareto front presents a unique system design, operation strategy or both. Hence, increasing

the set of non-dominant solutions will make the ranking process more challenging. Hence, a 2D Pareto analysis is used to identify the performance indicators which can be promoted as objective functions to determine final set of solutions while reducing the dimensions of the optimization problem.

Selecting final system design by using the Pareto front obtained will limit the opportunity to fully consider the design requirements and the influence of the other criterions which are not considered for the Pareto optimization. Hence, decision making needs to be performed moving beyond the graphical analysis of the Pareto front obtained using CI and few selected BI where multi-criterion decision making technique is required. This will help to consider the pool of criterions including CI, BI and PIs with its relative importance. However, it is important to define the boundary matrix which gives the maximum value (for a minimization problem) that you can reach considering a specific criterion based on the design requirements. This is obtained considering the design requirements of the energy system, boundary values obtained in the 2D Pareto analysis and the boundary values of the 3D Pareto front. Finally, Fuzzy TOPSIS method is used with the support of Level diagrams for the multi criterion decision making process. Fuzzy TOPSIS have been amply used as a multi-criterion decision making technique for energy related applications and combining with multi objective optimization.

The fuzzy TOPSIS method consists of several steps:

Step 1: Performance criterions for all the design solutions are normalized using Eq. 10.1.

$$CN_{m,n} = \frac{c_{m,n} - c_{\min,n}}{c_{\max,n} - c_{\min,n}}$$

(10.1)

In this equation, $C_{m,n}$, denotes normalized value for m^{th} criterion value for nth Pareto solution. $C_{m,n}, C_{max,n}$, and $C_{min,n}$ denotes respectively the value for m^{th} criterion value for nth Pareto solution, maximum and minimum values obtained by the Pareto solutions for the same criterion.

Step 2: A positive ideal solution (I^+) and a negative ideal solution (I^-) is introduced which represents two ideal solutions considering best and worst performance for all the criterions.

Step 3: Weight matrix is developed which as a 1 x p matrix which present the relative weight for each criterion (for p criterions).

Step 4: Arrive at Ideal Positive Solution (I+) and Ideal Negative solution (I-) taking the best and worst criterion value under each criterion. Design solutions are expected to be close to the positive ideal solution and far from the negative ideal solution.

Step 5: Positive distance matrix (d+) is computed taking Euclidian distance between I+ and $CN_{m,n}$ for each Pareto solution as shown in Eq. 10.2.

$$d_m^+ = \sqrt{\sum_{i=1}^{n} w_i (I_i^+ - CN_{i,m})^2}$$

(10.2)

Similarly, negative distance matrix is calculated.

Step 6: Coefficient of closure (CC) is defined as a minimization objective (most preferred solution is having the minimum value) which is calculated according to Eq. 10.3.

$$CC = \frac{d_m^+}{d_m^+ + d_m^-}$$

(10.3)

10.7. Results and discussion

The path that needs to follow to arrive at the final system design is quite lengthy. This chapter elaborates the final part of the design process which combines multi-objective optimization with multi-criterion decision making. As the first step, the role of each performance indicator in the assessment process is investigated considering the local conditions and specific design requirements. As discussed previously, energy system optimization process has turned from classical cost optimization to Pareto optimization where set of non-dominant solutions can be obtained considering conflicting objectives. The main advantage in this process is the system designer is having the choice to select the best solution considering the limitations of each criterion and its relative importance. This is an extensive task starting from selecting the best criterions to consider in the optimization process and subsequently the decision making process. This section elaborates how to address these issues using the novel method introduced in this paper through a case study. First part of this section is devoted on how to filter the best suited criterions for Pareto optimization. Second part of this section is dedicated to the selection of the design based on Pareto front obtained considering the objective functions identified in the first part.

10.7.1. Analyzing 2D Pareto fronts

Main challenge in the design process is to select most relevant criterions to assess the system design. This becomes more difficult when selecting several criterions for Pareto optimization from the pool of criterions selected to assess the system. In order to identify the criterions to be used in the optimization, 2D Pareto front is created considering the main objective as one objective function and the others respectively as the first step. In this work, LEC is considered as the main objective function and, LEC-CO2 emission, LEC-ICC, LEC-GI and LEC-WRE are taken for the design. Cross comparison of the values for objective functions are carried out to understand the limitations in improving each objective.

In order to analyze the Pareto fronts further, design solutions of four Pareto fronts are plotted for similar objectives in Fig. 10.3. When analyzing the objective space, it is clear that design solutions of LEC-ICC Pareto front presents a non-dominant set of solutions since LEC and ICC are considered as the objectives. In addition, a notable increase in ICC is observed when moving from Pareto solutions of LEC-ICC Pareto front to LEC-WRE, LEC-GI and LEC-LCO2 accordingly. More importantly, design solutions of the four Pareto fronts can be clustered into two main clusters i.e. Cluster A and Cluster B as shown in Fig. 10.3. When considering the design solutions of two Pareto fronts in Cluster B, both are quite close to each other. Although it is not as close as Cluster B, design solutions of two Pareto fronts in Cluster A are quite close. Therefore LEC-ICC Pareto can be used to represent LEC-WRE Pareto front when considering LEC-ICC objective space.

In a similar manner, design solutions of the Pareto fronts are plotted in LEC-LCO2 objective space (Fig. 10.4). Similar to the previous case, LEC-LCO2 Pareto front presents the non-dominant frontier. When considering LEC-LCO2 and LEC-GI Pareto fronts both are located close to each other as these were clustered in Fig. 10.3. If we consider the scatter plot of design solutions of Pareto front considering all the five objectives; LEC-ICC and LEC-LCO2 Pareto fronts can be considered as the boundaries when considering its projections in LEC-LCO2 objective space.

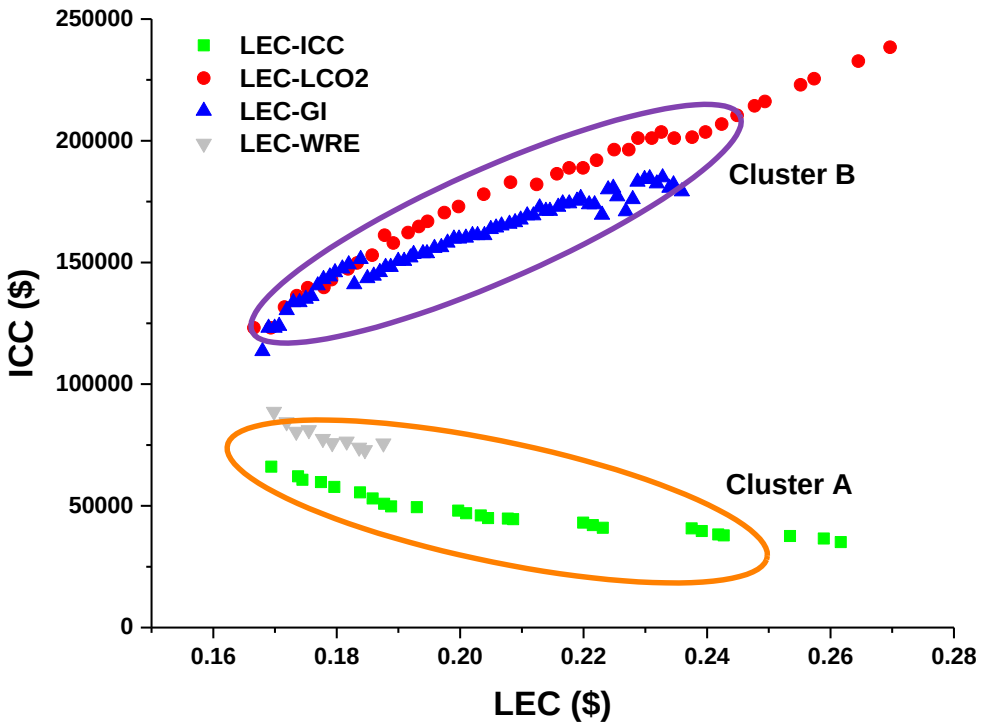

Fig. 10. 3*:* Variation of ICC with LEC for four Pareto solutions

Let us consider the possibility of replacing LCO2 by GI in the Pareto optimization process which will reduce the dimensions of the optimization problem. In this case, design solutions clustered in Cluster C will be lost which will result in loosing (dropping out) Pareto solutions marked in Region B. In addition, Pareto solutions marked in Region A will be lost. When considering most of the applications, the possibility that final design solution reaching Region B is quite less due to the higher LEC which is at least more than 50% larger when compared to the minimum. Comparing the region covered by LEC-ICC and LEC-GI Pareto fronts (area enclosed by light green and blue scatterplots, and light blue dash line) Region A is negligible. Hence, it can be concluded that GI level is a good indicator in representing LCO2 based on the projection in LEC-LCO2 objective space which will minimize the dimensions in the optimization process.

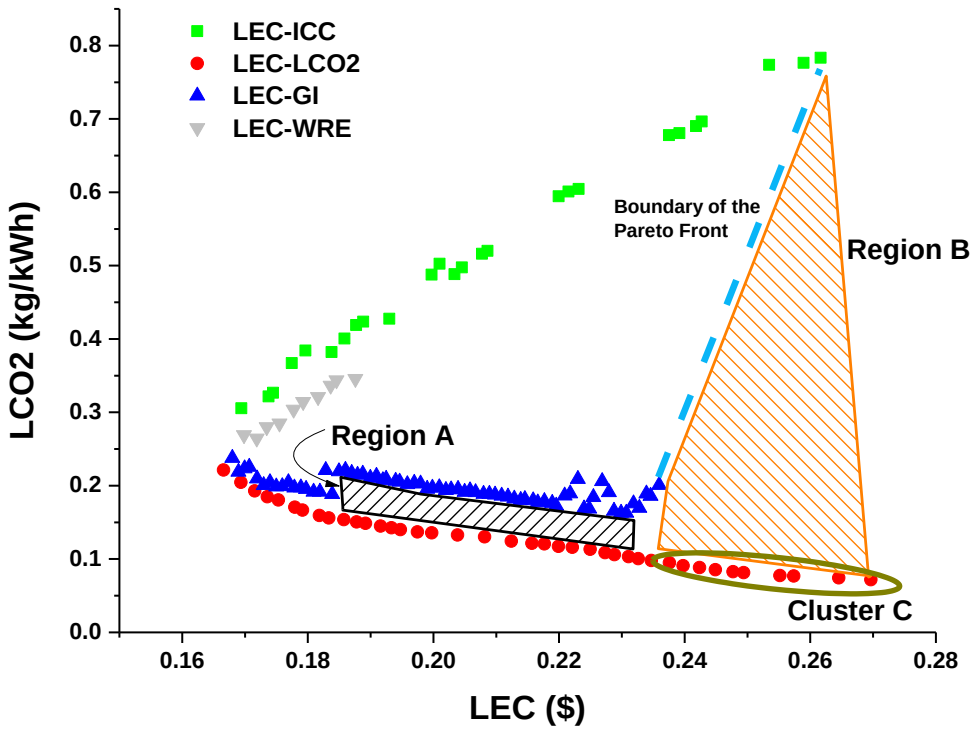

Fig. 10. 4*:* Variation of LCO2 with LEC for four Pareto solutions

Scatter plots of four Pareto fronts are presented in LEC-GI objective space to analyze the system further (Fig. 10.4). The two main clusters observed since the beginning can be seen even in this case. LEC-WRE and LEC-ICC Pareto fronts meet each other; although the latter extends further. LEC-GI Pareto front presents set of solutions which are dominant as expected. LEC-GI and LEC-LCO2 are closely located to each other. However, when compared to Fig. 10.3 the difference in the solutions of two Pareto fronts are not uniform (Region C) in this case. In certain instances, it extends up to a 10% difference in grid integration level. Therefore, representing GI using LCO2 will lead to take away some important design solutions which are interesting to be considered in the multi criterion decision making process.

Utilization of renewable energy is considered as the fourth criterion to conduct Pareto optimization with LEC. The Pareto front obtained and the objective function values for the design solutions of the other Pareto fronts are plotted in Fig. 10.6. Clear separation of the LEC-CO2 and LEC-GI Pareto fronts are observed in this plot although LEC-WRE and LEC-ICC can be clustered together. When considering the renewable energy utilization of the design solutions of LEC-GI Pareto solutions, WRE is less than 15 % and majority of the solutions are clustered within 10% up to 15%. In contrast, majority of the design solutions are having WRE more than 20% when it comes to LEC-LCO2 Pareto front which is not preferred in usual system designing. Hence, LEC-GI can be considered as realistic upper bound.

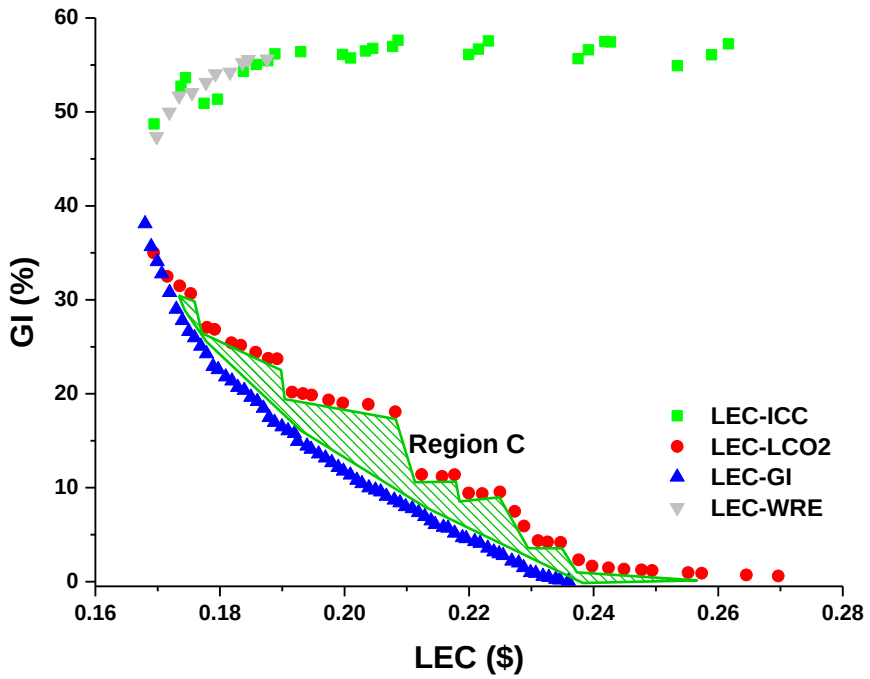

Fig. 10. 5:Variation of GI with LEC for four Pareto solutions

After conducting the graphical analysis it is prudent to say that the four objectives considered to optimize the system design along with LEC can be classified into two groups in which one objective function can present the group. This will reduce the five dimensional optimization problem (including LEC) into a three dimensional optimization problem along with LEC. Further, this will improve both accuracy and efficiency while reaching the optimum set of results and scarifying few design alternatives. When considering the first group (Cluster A in Fig 3) ICC can be considered as better alternative than WRE. ICC provides a better upper bound when considering LCO2 and GI along with an extended boundary considering LEC. Furthermore, LEC-ICC Pareto front overlaps with LEC-WRE Pareto front except for a small part in LEC and WRE objective space. Hence, it can be concluded that ICC is a better performance indicator to present both ICC and WRE. Similarly, GI can be used to represent the other group. Finally, LEC, GI and ICC gives a better representation of the five objective functions discussed while reducing the complexity of the optimization process.

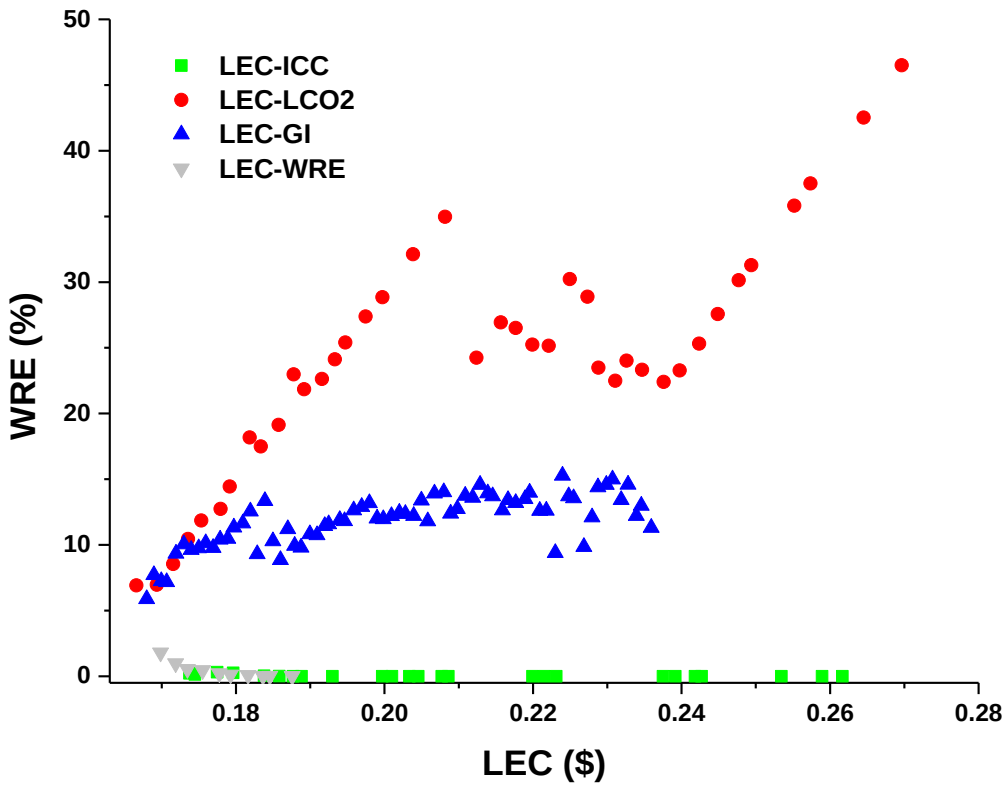

Fig. 10. 6: Variation of WRE with LEC for four Pareto solutions

10.7.2. 3D Pareto front considering LEC-ICC-GI

The 2D Pareto analysis helped to reduce the number of dimensions in the optimization problem. However, the four 2D Pareto fronts obtained in previous section only provided the boundaries of the objective space in which final design solution is located. In order to obtain non-dominant set of solutions, multi-objective optimization is carried out considering the objective functions identified in Section 10.7.1.

The Pareto front obtained from the optimization considering LEC, ICC and GI are presented in Fig. 10.7. Scatter plot clearly demonstrate that there exists a well distributed Pareto surface. Contour plot generated is using the scatter plot in order to help the system designer to visualize the distribution of Pareto solutions. Scatter plot and the contour diagram clearly delineates that the three objectives considered for the optimization are conflicting to each other in which it is difficult to optimize these three objectives simultaneously. It is simple to select one Pareto solution using both scatter and contour plot. Nonetheless, decision making is not straight forward since it is required to consider other factors such as LCO2, flexibility of the system, WRE etc., in the decision making process.

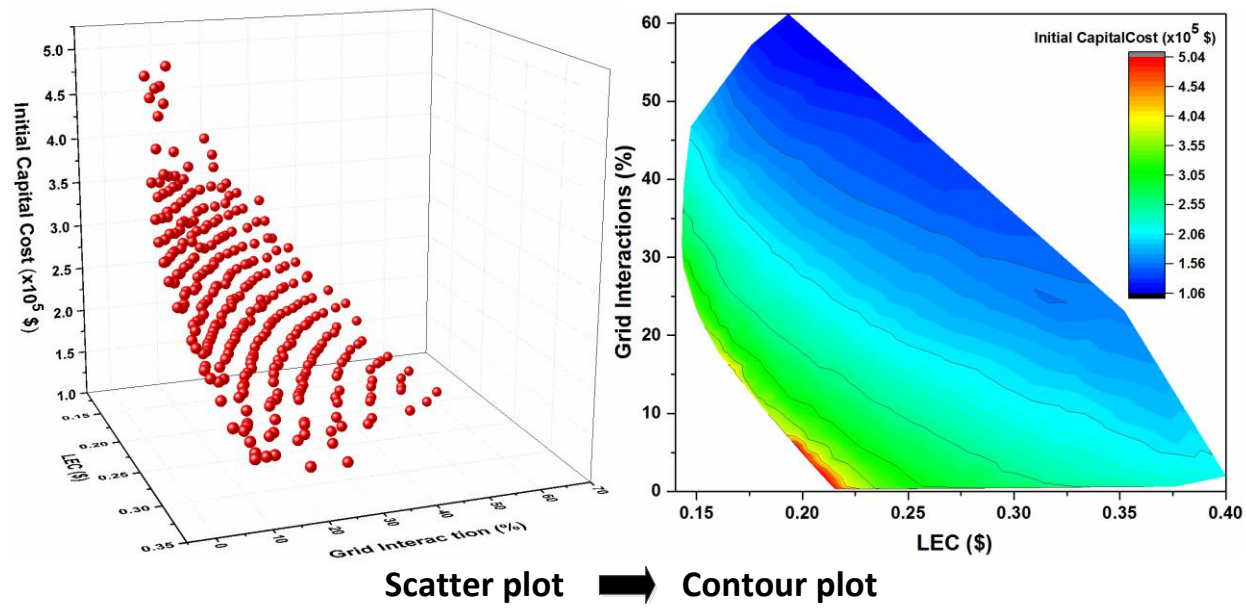

Fig. 10. 7: Scatter and contour plot of the Pareto front considering LEC, grid integration level and Initial Capital cost.

10.7.3. Multi Criterion Decision Making (MCDM) Process

In this work, seven criterions are used to assess the performance of the system .Whenever, the number of criterions used to assess the system increase beyond three, direct graphical representation methods cannot be used to assess the solution space. Hence coming up with the final system design is not straight forward. Multi criterion decision making process helps the designer to arrive at the final design solution considering conflicting criterions as discussed in Section 10.5. The main challenge in using the multi-criterion decision making technique is deriving the weight matrix for Fuzzy TOPSIS considering relative importance of each criterion. This section presents path followed in order to achieve the final design solution.

MCDM process is sensitive to the specific application of the energy system. Prioritizing the criterions and identifying the expectations for the design plays a major role in this context. Identifying the upper bounds (since the design problem is formulated as a minimization problem) for the design requirements play a major role in this context. Whenever one or several criterions are improved performance of some other criterions will degrade. Hence, close comparison of each criterion is important in the multi-criterion decision making process. Normalized criterion values will be useful in such an ambiance to identify the upper limits for design requirements and the required changes. Finally, multi criterion decision making needs to be carried out considering the importance of each criterion specifically to the application being within the boundary matrix.

The application of the suggested method is tried on the case of electrification a small, model rural village in Hambanthota, a district in southern coastal belt of Sri Lanka. Reliability of the system is considered vital which made it to be considered as a constraint in the optimization which does not considered to be compromised for an improvement in other criterion. The village is already connected to the grid which requires having a competitive electricity price after designing the new system (compared to the grid) which is considered as a special design requirement. Initial capital investment is also a main constraint to be considered since it is challenging to go for bank loans for community based energy systems which is considered as a design priority. Flexibility of the system had to be considered seriously since coastal weather changes rapidly which results in notable changes in wind and SPV energy potentials. In addition, minimizing grid integration level is considered as a main objective which is expected to achieve through the design. Finally the acceptance matrix which presents the boundary for each criterion where the customer is ready to accept the design is created which is presented in Table 10. 4.

10.7.3.1. Analyzing the Level Diagrams

MCDM process starts after understanding the boundary for the final design with an initial guess for the weight matrix. Results obtained for each weight matrix is evaluated while improving the weight matrix in order to cater the objectives. Level diagrams are used in this context to identify the possible directions that can be taken in improving the weight matrix. An intermediate (Case A) and the final weight matrix arrived (Case B) in the decision making process are presented in Table 10. 5. Best six design solutions corresponding both Case A and Case B are presented in Table 10. 6 and 10.7. 2D and set of 3D contour plots obtained for both Case A and B are presented in Fig. 10.8, 10.9 (a) and (b)

Table 10. 4: Boundary matrix for the criterions based on the requirements of the customer. Green denotes acceptance and red denotes rejection for different regions of normalized value for criterions. Green color denotes acceptable and red denotes not acceptable

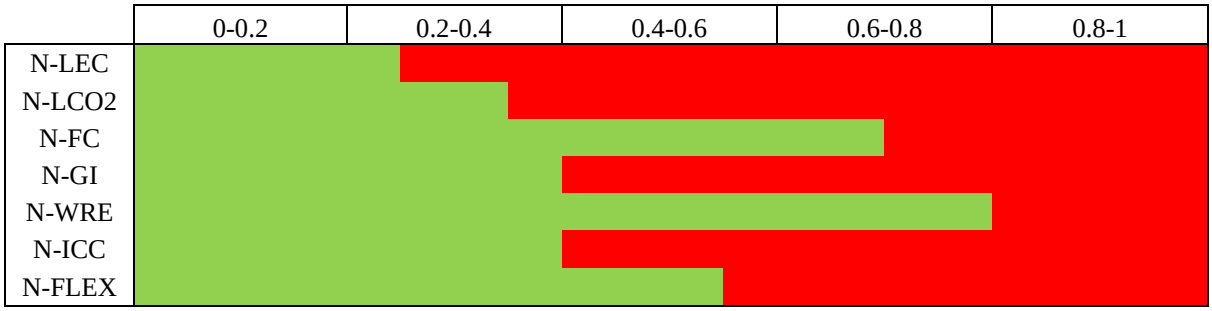

Table 10. 5: Weight matrix considered for Case A and Case B

Case	LEC	LCO2	FC	GI	WRE	ICC	Flex.
A	0.255	0.136	0.043	0.128	0.064	0.187	0.187
B	0.245	0.131	0.041	0.163	0.061	0.180	0.180

Analyzing the 2D scatter plot is considered first step in the decision making process which provides a better representation of all the criterions simultaneously as in Fig. 10.8. In addition, 2D scatter plots supports the decision makers at the early stage of decision making process to bring all the global optimums close to the boundary matrix (or into the boundary matrix). When considering the two scatter plots in Fig. 10.8 it is prudent that surface of the scatter plots for Case A is rough except ICC. As a consequence, global maximum moves significantly (interchange with local maximum) with a marginal change in weight matrix. This makes it difficult to analyze the possibility to improve the specific criterions. When moving to Case B in the same diagram (left to right) much smoother surface is observed for most of the criterion except flexibility. This makes it easy to analyze the systems further. However, 2D scatter plots can be used only at the beginning where major changes in weight matrix is performed in order to bring the criterions considered closed to the boundary matrix. Sensitivity of changing the weight for one criterion over the other cannot be evaluated directly using 2D contour plots which make it difficult to use as a method to fine tune the weight matrix. This can be visualized further using 3D contour plots considering two criterions along with CC.

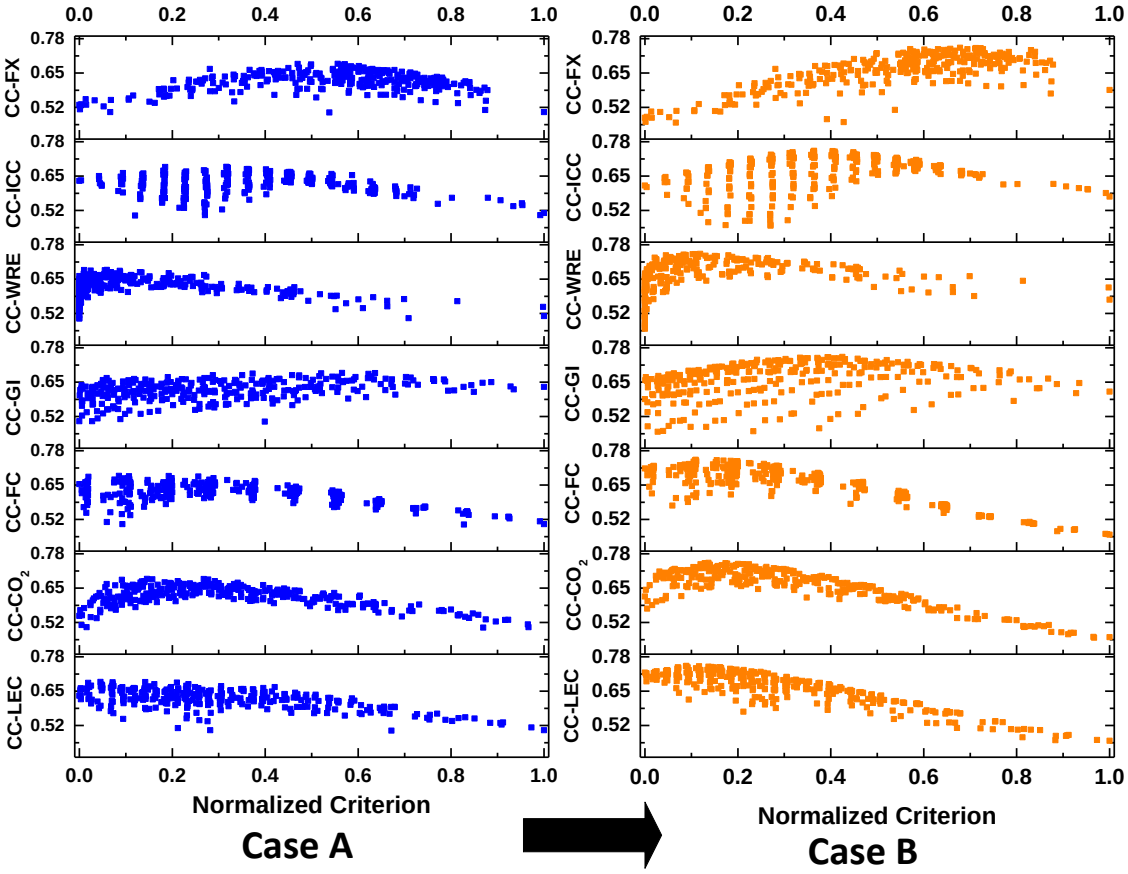

Fig. 10. 8*:* 2D scatter plots for Case A and Case B

3D contour plots are helpful in understanding the impact of changing the weight of one criterion over the others. Contour plots are presented in Fig. 10.9 (a) and (b) considering different criterions used for MCDM. When analyzing the contour plots for two cases, several local optimums are observed in Case A (plots in left hand for both Fig. 10.9 (a) and (b)). However, when moving to Case B one global optimum is observed in most of the instances except in normalized flexibility and LEC which shows complicated variation with several local maximums. This agrees with the previous observation in 2D scatter plot. In order to analyze the 3D contour plots further, two contour plots from Fig. 10.9 (a) (NLEC-GI and NLEC-Fx) are taken for Case A and illustrated in detailed in Fig. 10.10.

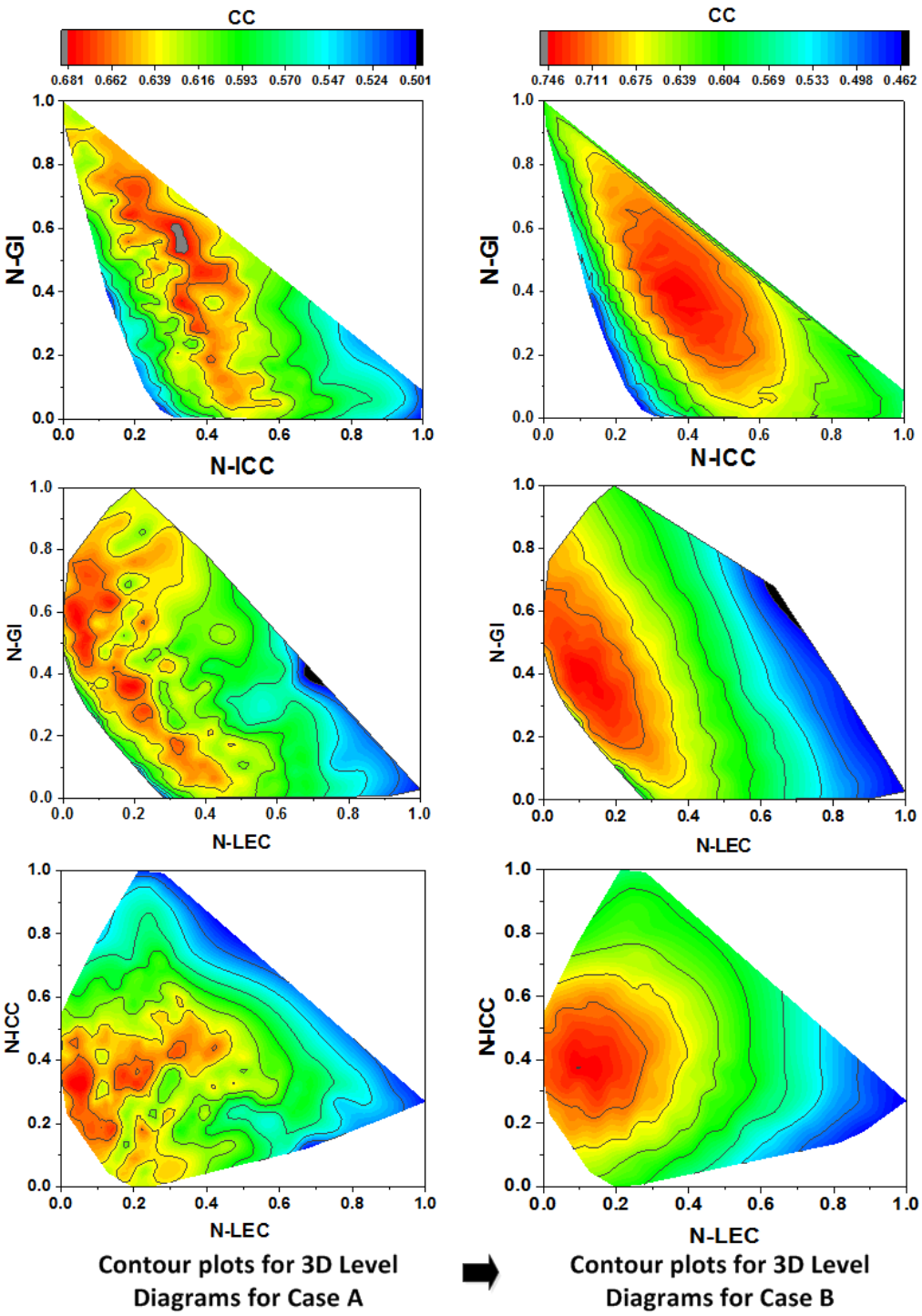
CC
0.681 0.662 0.639 0.616 0.593 0.570 0.547 0.524 0.501
CC
0.746 0.711 0.675 0.639 0.604 0.569 0.533 0.498 0.462
N-GI
N-ICC
N-GI
N-ICC
N-GI
N-LEC
N-GI
N-LEC
N-ICC
N-LEC
N-ICC
N-LEC
Contour plots for 3D Level Diagrams for Case A
Contour plots for 3D Level Diagrams for Case B

(a)

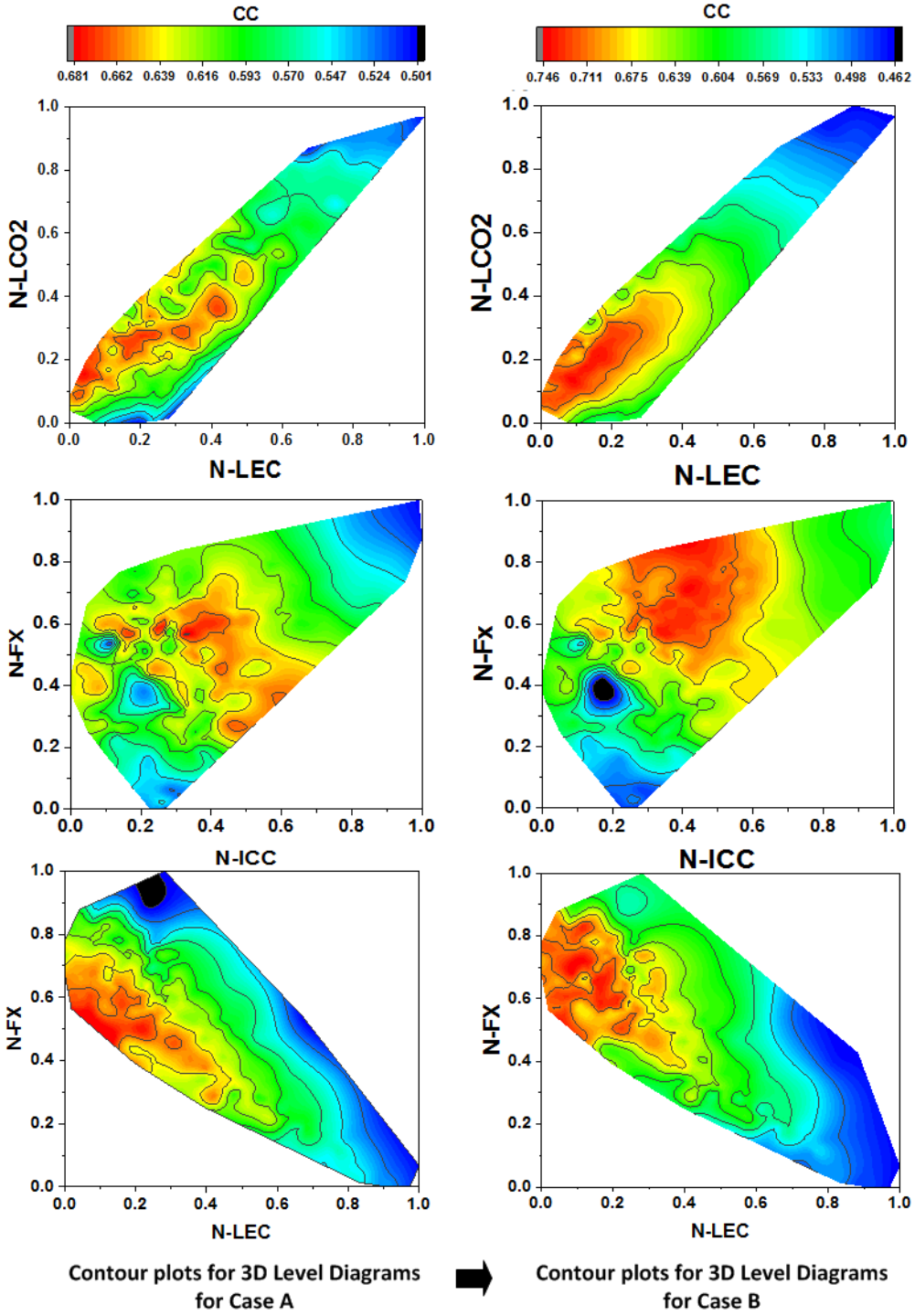

(b)

Fig. 10. 9 (a): A comparison of 3D contour plots considering CC with different criterions (b): A comparison of 3D contour plots considering CC with different criterions for Case A and B

When analyzing the NFG-NICC contour plot for Case A in Fig. 10.10, best ranked solutions (red colored region) are distributed in P and Q regions. The distribution of these two regions forms a frontier with a negative gradient. This demonstrates that these objectives are conflicting to each other and a significant reduction in N-FG can be obtained with a marginal increase in N-ICC. A similar pattern is observed when analyzing NFX and NLEC Pareto front (Fig. 10.10 (right hand)). Best ranked solutions are distributed in region R and S. These two objectives also produce a Pareto front in which it is difficult to improve both simultaneously. However, this indirectly implies both GI and flexibility improves with a marginal scarify in LEC in which improvements in GI is more significant compared to flexibility as observed in P and Q regions in left plot in Fig. 10.10 and R and S regions in right plot (numerical values are later presented in Table 10. 6 and 10.7). In a similar manner, it can be shown that a significant improvement in GI with a marginal scarify of ICC when analyzing the NGI-NICC contour plot for Case A in Fig. 10.9 (a). Therefore, it is clear that a notable improvement in GI can be achieved while scarifying the criterion values for ICC and LEC.

The analysis can be extended further to evaluate the possibility of improving the other criterions and the consequences of improving them. In order to analyze the consequences of improving LCO2, NLEC-NLCO2 plot for Case A (Fig 10.9 (b): first left one from the top) is taken. The set of high ranked solutions is distributed within (marked in red) linearly with a positive gradient. This reveals that LEC and LCO2 are parallel objectives in which one will increase with the increase of the other. When analyzing the contour plots for Case A, it is observed that GI can be improved which will convert existing distributed maximas into a global maximum (or merge both together) resulting an increase in LEC as shown in regions P and Q in Fig. 10.10. However, a major improvement in flexibility will interchange global maximum and local maximum which will increase the LEC beyond the expectations (from R to S) since this will increase N-LEC beyond 0.25 which is the boundary. Improvement in flexibility and grid integration levels is required to meet the expectations of the customer according to the boundary matrix. When analyzing the contour plot it is clear that increasing the weight of grid integration and marginally increasing the weight of the system flexibility will drive towards the expectations. The observations of the contour plot analysis is used to improve the weight matrix and finally arrived to at weight matrix for Case B which is given in Table 10. 5.

Contour plots obtained after revising the weight matrix are plotted in the same diagram (Fig. 10.9 (a) and (b)) in order to make the comparison simple. When analyzing the contour plots for Case B it is prudent that most of the contour plots are quite smooth with one global maximum for most of the instances. This makes the analysis and decision making easier. Local minimums located at different

locations of the contour map makes it challenging to analyze the consequence changing the weight of one criterion in which decision makes should go back and forth again and again from one plot to another as discussed before in order to find the promising directions to change the weight matrix. Contour plot for Case B clearly shows that all the criterions are within the boundary and a notable improvement in criterions is not possible.

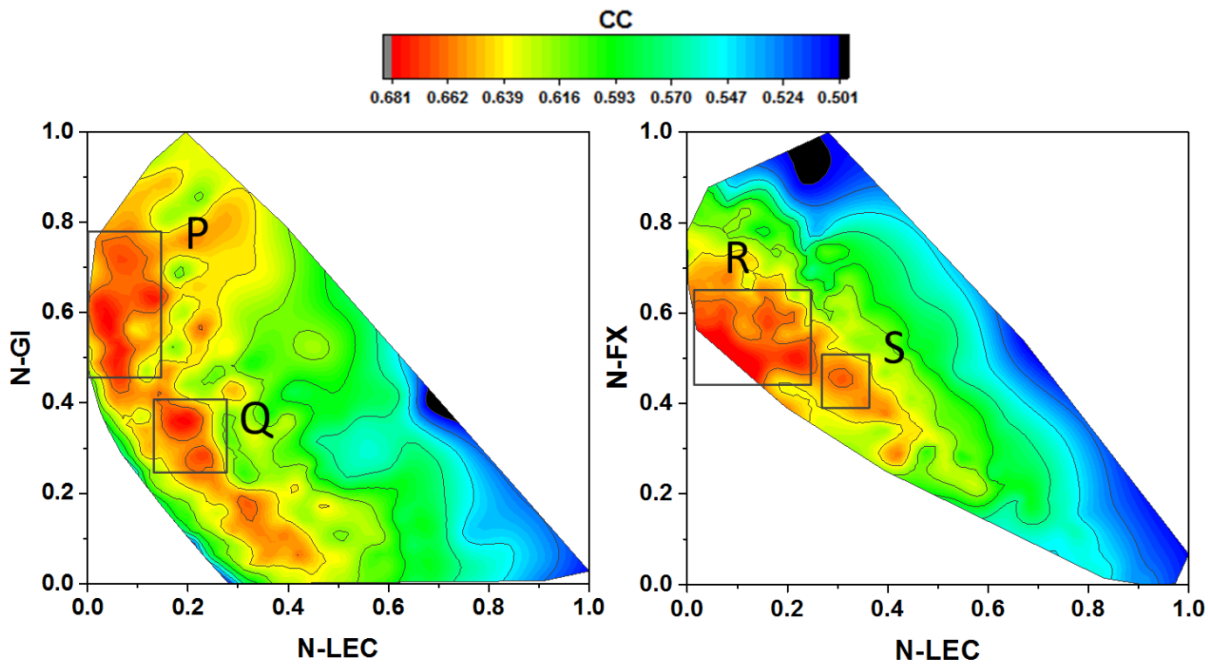

Fig. 10. 10: Possible changes in contour plot with the changes in weight matrix. Global maximum move from P to Q in NGI-NLEC plot while global maximum might move R to S in NFX-NLEC plot

10.7.3.2. Analyzing the best candidates for each weight matrix

2D and 3D Level diagrams help the decision makers to reach towards the best fitting weight matrix. However, final system design should be arrived after closely examining the best ranked design solutions. On the other hand, analyzing the best set of solutions obtained after revising the weigh matrix, helps the decision maker to get a quantitative understand about the promising changes that should be made in weight matrix especially for very small changes in the weight matrix. Hence, analyzing the contour plots and best set of solutions are complimentary tasks which help the system designer to come up with final system design.

Assessing the best ranked solutions, started with selecting the best six design solutions for Case A (are tabulated in Table 10. 6). When analyzing the design solutions, it is prudent that most of the design solutions perform well when considering several criterions. A1 adheres to most of the design criterions except with GI. A1 maintains a normalized grid integration level of 0.57 which is greater than the accepted limit of 0.4 which is the same for A2 and A5. These two design solutions are

having normalized grid integration level of 0.64 and 0.62 respectively which is higher than 0.4. A4 and A6 design solutions performs close to each other for most of the criterions being within the boundary matrix including grid integration level. However, A6 is marginally outside the boundary matrix when considering the expectations of the design. Therefore, A4 becomes the only design solution within the design requirements.

Contour plots provide the possible directions to improve the weigh matrix further. After several iterations we arrived at the weight matrix for Case B which is Table 10. 5 to see the possibility of improving the design further. A significant change in the weight matrix is not performed when moving to Case B. Hence, four design solutions that appeared in the best six alternatives are appearing in Table 10. 7 (B1, B3, B4 and B5). B6 does not fulfill the design requirements since LEC is beyond the critical LEC defined in the boundary matrix. Both B1 and B2 both meet the design requirements. B2 outperform B1 when it comes to grid interactions and B1 outperforms B2 when it comes to LEC, LCO2, fuel consumption and waste of renewable energy. System configuration will change when considering the capacities of SPV panels and wind turbines. When moving from B2 to B1. The final decision solution arrived is highly subjective to the decision maker whether the designer appreciates the notable improvement in grid integration level in B2 or the overall improvement B1. In this case B1 is considered as the system design solution.

10.7.3.3. Sensitivity of different criterions

Multiple-criterions need to be considered in the designing process of energy systems. However, all of them cannot be considered in the Pareto optimization. Most of the instances, decision making is performed based on the criterions considered for Pareto optimization. This will omit several important criterions from the decision making process. It Important to assess the consequences of limiting the decision making process into few criterions that are considered in the Pareto optimization process. In order to achieve this, four cases are considered (i.e., Case C, D, E and F) removing one or two criterions from the weight matrix from the decision making process. The ratio among the weights for the other criterions was the other criterions as in for Case B in the weight matrix. Case C does not consider System flexibility, Case D does not consider grid integration level, Case E does not consider LCO2 and fuel consumption and finally Case F does not consider initial capital cost. Weight matrix for each case is tabulated in Table 10. 8. The best design solution obtained under each weight matrix is presented in Table 10. 9.

When analyzing the design solutions for Cases C, D, E and, F it is clear that removing a criterion from the weight matrix will results in a notable increase of the performance indicator (considering a minimization problem) of the specific criterion removed from the weight matrix. For example, for

cases C and D, which respectively remove flexibility and grid integration level from the weigh matrix, the N-Flex increases from 0.499 to 0.678 for and N-GI level increases from 0.373 to 0.887 for Case D. Same can be observed in Case F. This will result poor performance under these criterions which are outside the decision matrix in this case which will not be preferred by the end users. However, due to the weaknesses (over simplification of the design space) in the existing methods used for multi-criterion decision making system designers will end-up in such designs.

The sensitivity of each criterion considered for the multi-criterion decision making is different depending upon the weight matrix, the considered criterion, its relationship with the other criterions and the boundary matrix. For example, when considering Case E, increase in N-LCO2 after taking away from the weight matrix is insignificant when compared to Case C, D and F. This can be justified by assessing the level diagrams, LCO2 and LEC are parallel objectives (as discussed in 6.3.1) within the close proximity of the weight matrix selected (as shown in Fig. 10.9.(a) NLEC-NLCO2 diagram). Hence, both these objectives can be simultaneously minimized within the proximity of the weight matrix selected with strong coupling. Higher, weight matrix on both LCO2 and LEC results in lower emissions as well as LEC. Removing LCO2 from weight matrix does not influence due to the weight imposed by LEC though a notable reduction in LEC is observed due to the removing of weight in LCO2. This coupling makes it difficult to fine tune the weight matrix where Contour Level diagrams are extremely useful to find the proper directions to improve the weight matrix. However, the coupling between LEC-LCO2 is limited to a one part of the decision space as observed when analyzing Fig. 10.3, 10.4 and 10.5. Hence, a notable change in LCO2 can be observed for a different setting of the weigh matrix.

Table 10. 6: Best six solutions ranked based on weight matrix for Case A

System	Criterion Values							Normalized criterion values							CC	System configuration			
	LEC[1]	LCO2[2]	FC[3]	GI[3]	WRE[4]	ICC[5]	Flex.	NLEC	NLCO2	NFC	NGI	NWRE	NICC	NFlex		SPV[6]	Wind[7]	Battery[8]	ICG[9]
A 1	0.155	0.261	0.038	27.9	1.02	2.32	0.362	0.05	0.15	0.09	0.57	0.06	0.32	0.56	0.685	12.9	50	2880	27.5
A 2	0.179	0.356	0.063	31.4	0.18	1.80	0.309	0.14	0.27	0.19	0.64	0.01	0.18	0.47	0.684	10.9	35	960	30
A 3	0.161	0.270	0.043	25.7	0.95	2.33	0.372	0.07	0.16	0.11	0.52	0.05	0.32	0.57	0.683	12.9	50	2880	30
A 4	0.197	0.363	0.079	18.5	0.42	2.33	0.327	0.21	0.28	0.26	0.37	0.02	0.32	0.49	0.683	13.6	40	1920	30
A 5	0.148	0.219	0.022	30.7	1.50	2.34	0.367	0.02	0.09	0.02	0.62	0.09	0.32	0.56	0.681	15.6	50	2880	30
A 6	0.185	0.312	0.065	17.4	1.52	2.51	0.372	0.16	0.21	0.20	0.35	0.09	0.36	0.57	0.677	13.6	55	1920	30

Table 10. 7: Best six solutions ranked based on weight matrix for Case B

System	Criterion Values														CC	System configuration			
	LEC[1]	LCO2[2]	FC[3]	GI[3]	WRE[4]	ICC[5]	Flex.	NLEC	NLCO2	NFC	NGI	NWRE	NICC	NFlex		SPV[6]	Wind[7]	Battery[8]	ICG[9]
B1	0.197	0.363	0.079	18.5	0.42	2.33	0.327	0.21	0.28	0.26	0.37	0.02	0.32	0.49	0.680	13.6	40	1920	30
B 2	0.203	0.374	0.087	14.3	1.17	2.50	0.326	0.23	0.29	0.29	0.29	0.07	0.36	0.50	0.678	10.9	55	1920	30
B 3	0.185	0.312	0.065	17.4	1.52	2.51	0.372	0.16	0.21	0.20	0.35	0.09	0.36	0.57	0.676	13.6	55	1920	30
B 4	0.161	0.270	0.043	25.7	0.95	2.33	0.372	0.07	0.16	0.11	0.52	0.05	0.32	0.57	0.675	12.9	50	2880	30
B 5	0.155	0.261	0.038	27.9	1.02	2.32	0.362	0.05	0.15	0.09	0.57	0.06	0.32	0.56	0.675	12.9	50	2880	27.5
B 6	0.222	0.381	0.094	9.6	1.33	2.70	0.296	0.31	0.30	0.32	0.19	0.08	0.41	0.45	0.674	12.2	55	1920	27.5

Table 10. 8: Best six solutions ranked based on weight matrix for Case B, C, D, E and F

System	Criterion Values														CC	System configuration			
	LEC[1]	LCO2[2]	FC[3]	GI[3]	WRE[4]	ICC[5]	Flex.	NLEC	NLCO2	NFC	NGI	NWRE	NICC	NFlex		SPV[6]	Wind[7]	Battery[8]	ICG[9]
B1	0.197	0.363	0.079	18.5	0.42	2.33	0.327	0.210	0.277	0.256	0.373	0.024	0.318	0.499	0.680	13.6	40	1920	30
C	0.166	0.254	0.043	21.1	2.06	2.51	0.439	0.089	0.137	0.109	0.425	0.119	0.364	0.678	0.746	16.32	55	1920	30
D	0.186	0.397	0.062	43.7	0.00	1.23	0.301	0.167	0.321	0.186	0.887	0.000	0.042	0.458	0.750	4.76	25	960	30
E	0.251	0.406	0.108	3.1	1.94	2.87	0.191	0.420	0.333	0.377	0.059	0.112	0.454	0.281	0.677	12.92	60	1920	30
F	0.227	0.303	0.078	2.7	3.14	3.40	0.277	0.326	0.200	0.252	0.051	0.181	0.587	0.419	0.724	19.04	65	3840	27.5

[1]LEC in $, [2]LCO2 in kg/kWh, [3]fuel consumption in l/kWh, [3]grid integration level (%), [4]WRE (%), [5]ICC (x10[5]$), [6]SPV capacity in kW, [7]wind turbine capacity in kW Battery [8]bank size in kWh and [9]ICG capacity in kW

Table 10. 9: Weight matrix for Case B, C, D, E and F

Case	LEC	LCO2	FC	GI	WRE	ICC	Flex.
B	0.245	0.131	0.041	0.163	0.061	0.180	0.180
C	0.299	0.159	0.050	0.199	0.075	0.219	0
D	0.293	0.156	0.049	0	0.073	0.215	0.215
E	0.296	0	0	0.197	0.074	0.217	0.217
F	0.299	0.159	0.050	0.199	0.075	0	0.219

10.8. Conclusions

A comprehensive frame work to design distributed electrical hubs consists of wind turbines, SPV panels, battery bank and an ICG operating connected to the grid is taken into discussion in this chapter. Selecting the objective functions for Pareto optimizing and subsequently multi-criterion decision making, considering set of criterions in order to meet the design requirements is focused in the chapter. Seven criterions are defined covering wider spectrum of interests including cost, environmental impact, energy efficiency etc in the designing process. A novel method is introduced to evaluate the flexibility of the energy system based on several criterions. A bi-level multi criterion decision making process is introduced to reach to the final design solution. 2D Pareto optimization is used to select the best representative objective functions to consider in Pareto optimization. Subsequently, LEC, grid integration level and initial capital cost found out to be the best representative objective functions reducing the dimension of the problem up to a 3D optimization problem without losing large number of possible solutions. Pareto front obtained considering three objective functions are ranked using seven criterions. Fuzzy TOPSIS is used to rank the non-dominant solutions using 2D and 3D level diagrams. The results obtained from the Pareto analysis emphasize the weakness in present practice limiting decision making process to the objective functions considered for the Pareto optimization. This will lead to poor performances in other criterions not considered in the decision making which can be addressed by the novel method introduced in this chapter through appropriate selection of objective functions and extending the criterions considered in the decision making process.

Following the sensitivity of weight matrix it is prudent that considering all the criterions related to the design is important during the decision making process. However, considering all these criterions both at the multi objective optimization and multi criterion decision making level is a challenging task. This chapter is using direct method to achieve this task analyzing each Pareto front and contour plots with in a region selected. However, this work can be further extended using dimension reduction techniques such as Principle Component Analysis (PCA). More research work needs to be

focused in this context where proper mechanisms need to be developed combining these methods with multi-objective optimization and multi-criterion decision making.

11 Conclusions and Future Perspectives

The thesis presents a novel approach towards energy system optimization, which addresses several research gaps in the present state of the art. A conclusion section is included in each chapter, summarizing the contribution while highlighting the limitations of the methodology developed. This chapter looks at the highlights of the thesis at a more holistic level, considering the interrelationship between the chapters. It consists of two parts. Section 11.1 presents the major contributions of this thesis while Section 11.2 highlights the limitations and future prospects.

11.1. Major contributions to the present state of the art

Rapid depletion of fossil fuel resources and climate change demand a major transition in the energy sector. Distributed energy systems play a vital role in this transition by integrating non-dispatchable renewable energy technologies such as solar PV and wind. Chapters 2 and 3 present a novel way to model and optimize distributed urban energy systems. Chapter 2 introduces a grey box model based on fuzzy logic to be used in energy system design while Chapter 3 introduces black box models. Introducing grey box models is a major achievement since it demonstrated that an alternative path can be taken when designing distributed energy systems. Grey box models perform well for electrical energy hubs and show the potential to reach penetration levels of about 80% for renewable energy technologies with grid assistance. However, it was found that grey box models cannot be used to consider energy systems that have complex energy interactions. Black box methods based on reinforcement learning are introduced in order to handle the complexity of energy systems, outperforming grey box models. Reinforcement learning with the support of convolution neural networks performed well when designing energy systems considering the forecast of demand, renewable energy potential and grid conditions in the dispatch strategy. Reinforcement learning tends to be the only alternative that can consider the complex cyber

physical interactions that energy systems are expected to maintain with urban systems during the energy system optimization.

Chapter 4 of the thesis introduces a distributed optimization technique to design energy internets, a fleet of energy systems connected with each other through a multi energy network. The introduced distributed optimization algorithm can be used to design energy systems that are operating in fully co-operative and non-co-operative scenarios. The main advantage of using a distributed optimization algorithm for the co-operative scenario is that it can limit the information that needs to be shared among the agents. This helps to improve privacy. The novel optimization algorithm shows a good capability to reach the Epsilon-Nash equilibrium. Although the present study limits its scope to cooperative and non-cooperative scenarios, the developed computational model can be easily extended to consider the leader-follower games leading to a Stackelberg equilibrium, which can be used to design energy internets with hierarchies.

Top down approaches based on statistical models or shallow learning techniques are often used for energy planning at regional and national scale. As a result, there is a risk that the decisions made at regional and national scale are erroneous. Bottom up models - widely used for energy system optimization - are limited to localized applications. For more accurate planning, they need to be extended to regional and national scale. One of the main advantages of the grey and black box models introduced in Chapters 2 and 3 is their higher adaptation capacity. Chapter 5 of the thesis shows that transfer learning can be effectively used to adapt the developed black box models so that energy system optimization at different locations can be performed faster reducing the computational demand by 5/6. Such a reduction in computational time allows energy systems optimization to be conducted at regional and national scale and hence to improve decision making.

Climate uncertainty and extreme climate events due to climate change have a severe impact on energy systems. However, the impact of climate change is expected to be even higher in the future as the concentration of CO2 in the atmosphere increases. Improving the resilience of urban energy systems is important in order to face these challenges, especially in the energy sector. However, converting climate relevant data into energy system relevant data is a difficult task, especially considering the dynamics of regional climate. One of the main contributions of this study is to introduce a novel method to present uncertainty in demand and generation due to climate change by using a pool of scenarios derived from a regional climate model. The approach has been extended to consider extreme climate events as well. To be able to consider a large pool of scenarios of over 5000 the novel approach introduced in Chapters 2 and 3 has been extended further to conduct stochastic-robust optimization to design energy systems. Graphical Processor Unit (GPU) computing

is introduced in the energy system optimization process for assistance. One of the major findings of this study is that thus optimized energy systems can maintain renewable energy integration levels above 50% while guaranteeing robust operation during extreme events. This allows making progress in the energy transition while being resilient to climate change.

Facing the challenges brought by climate change is more challenging in highly dense cities due to phenomena such as the urban heat island (UHI) effect. UHI intensifies adverse impacts due to climate change. Energy infrastructure plays a vital role in facing UHI effects in highly dense cities with high rise buildings. The energy demand for cooling is strongly influenced in such instances. Therefore, considering the influence of urban climate is essential during the urban energy system design process. This requires a further extension of the urban energy system model used in the present. One achievement of this thesis is the extension proposed to the urban energy system model to consider the impact of urban climate on the energy system. Towards achieving this objective, the canopy interface model (CIM) is coupled with an urban simulation model and an energy system optimization model, and a computational platform is developed.

It was revealed that the urban climate can have a notable impact on the performance of the energy system due to the fluctuations of the demand caused by the UHI and cooling pool effect. This can lead to a performance gap of up to 40% in indicators such as cost and grid integration level. Furthermore, failing to consider the adverse impacts of urban climate will lead to poor power supply reliability, especially during extreme climate events. The model developed in Chapter 8 is extended further in Chapter 9 to understand efficient urban forms that can minimize the adverse effects due to urban climate.

It is important to bring the energy system design process closer to a wider community of stake holders. High end modeling, simulation and optimization techniques introduced in Chapters 2 - 9 are supporting the progress of the present state of art from the technical perspective. However, it is difficult to communicate this message to a wider community of stake holders. Hence, it is important to translate the message into a simpler one. Combining energy system optimization with decision making techniques provides more opportunity to the stake holders to be implicated in the design process. This enables considering multiple criterions that are sensitive to a wider community during the design process. However, considering such a wider pool of criterions makes the optimization process complicated. To address this difficulty, the performance indicators must be prioritized based on the input of the stake holders. Chapter 10 presents a novel method that can be used for such objective space reduction. Besides prioritizing objective functions, Chapter 10 introduces a promising method to consider a wider pool of criterions in the decision making process through

multi-criterion decision making. Fuzzy logic is used to consider ambiguity in the decision making process related to inputs from a wide community of people with different backgrounds. This enables the urban energy system model introduced in Chapters 2 and 3 to easily integrate with business models. Furthermore, introducing a decision making technique in the energy system optimization process makes the model easier to use by energy planners and the wider community of stake holders in urban energy systems.

A novel approach to design urban energy systems is introduced in this study. Grey and black box models are introduced to conduct the energy system design process. Subsequently, the model is extended into number of directions. It has been shown that the proposed approach enables designing energy internets consisting of multiple energy systems interacting with each other and can be effectively used with transfer learning to design energy systems at regional and national scale due to its adaptability. Furthermore, stochastic and robust programing techniques can be easily connected with the presented approach, which enables considering climate uncertainty and extreme climate events. It has also been shown that the complexity of urban climate can be considered in the energy system design process through the novel approach presented. All these advances achieved through the novel approach introduced in this study demonstrate its flexibility. However, it is important to validate the applicability of the model in different climatic conditions.

The different extensions introduced to the model are validated at different geographical locations, which clearly demonstrate the wider applicability of the model. The case studies for Chapter 2 and Chapter 10 are conducted in Hambanthota, a coastal city in Sri Lanka with tropical climate conditions. Methods presented in chapters 3, 4, 6 and 7 are applied for Sweden considering Nordic climate conditions. Ten cities from different climate zones in Sweden are considered in Chapter 6. The city of Nablus in Palestine is considered for Chapter 8. Nablus is located in the northern part of the West Bank and has Mediterranean climate conditions. Chapter 9 is based on two case studies conducted in Dubai, United Arab Emirates and Hemberg, Switzerland. These two cities present totally contrasting climate conditions. Dubai has a tropical desert climate while Hemberg has a moderate climate strongly influenced by the Alps. Although not included as separate chapters, a number of case studies are conducted for Junction-Geneva, Cartigny-Geneva and Ecublens-Lausanne in Switzerland. These studies are published in conference and journal proceeding papers included in the beginning of Chapter 10. The computational model is now in the process of being tested for 16 European capitals considering different climate conditions. All these case studies conducted at different geographic locations demonstrate the wider applicability of the developed approach.

11.2. Limitations of the methodology developed and improvements

According to George Box, the famous British statistician, 'all the models are wrong but some are useful'. The approach presented in this this study has a number of limitations. One main limitation is the time resolution. Steady state hourly simulation is conducted, which is the usual practice for energy system optimization problems. However, the one-hour time resolution is too big when considering the stability of the grid. Similarly, a one-hour time resolution is too bulky to consider the changes in urban boundary layers which may lead to a number of limitations in computing the energy demand. Hence, from a control perspective, the design solutions obtained through a typical energy system optimization method may be subject to issues in real time operation,; it is therefore important to evaluate the stability of the design solutions in a much finer time resolution.

Another major limitation of the study is the simple representation of power flow. In Chapter 4, power flow computation is conducted simply using DC approximations. Furthermore, it is assumed that the network is designed in a radial manner in order to avoid an optimum power flow problem (OPF). Although such an assumption is reasonable if the aim is to simplify the problem and make it solvable, the n-1 reliability cannot be guaranteed. Hence, the connectivity matrix obtained for the energy internet in Chapter 4 should be further optimized to guarantee n-1 reliability (this extension is currently under implementation). However, it is inevitable to use DC approximation in this context to make the problem into a mixed integer linear program, which weakens the physics of the problem to a certain level. Therefore, it is important to look into better methods to represent the power flow in a more accurate manner when designing distributed energy systems.

Linking building stock with urban energy infrastructure is considered in detail in this study. However, buildings themselves are only a part of urban energy systems. There are numerous other energy flows that need to be considered, such as transportation, water distribution, waste management etc. Nexus, maintained by energy systems with these sectors, plays a vital role in the process of improving the urban sustainability. Furthermore, it provides more diversity to energy systems configuration. For example, biomass and biogas generation from waste management can be a part of the energy system. In general, the diversity of energy system components considered could have been improved by considering seasonal storage such as pumped hydro, compressed air, H2/fuel cell etc. Such extensions to the energy system model are expected to be added in the future.

Energy demands required for this study are entirely taken from computational models developed for building/urban simulation. The demand profile has a significant impact on energy system sizing. It would be interesting to compare the results with actual monitored demand data since many simplifications are performed when conducting building and urban simulations. For example,

CitySim, the model used for building/urban simulation, uses a single zone model for the energy simulation in order to simplify the complexity of a building stock. However, such a simplification may lead to changes in the simulated demand. Since such assumptions are difficult to avoid, it is important to quantify their influences on energy system design. The same limitation applies to occupation profiles. Urban architypes are used in Chapter 8 to simplify the complex urban form when computing the energy demands. Moving from building scale to urban scale brings a number of challenges into the simulation process. Although addressing these limitations is not the major focus of this study it is important to understand the impacts of these limitations on energy system design.

Urban micro climate plays a vital role when designing energy systems as it influences both energy demand and generation. An urban canopy model is used in this study to consider the impacts of urban climate on energy systems. The urban canopy model used in this study uses the 1-D Navier-stroke model. This limits the representation of urban complexity up to a certain limit. Combining the Computational Fluid Dynamics (CFD) model with an energy system optimization and a building simulation model can be an attractive solution that can help to overcome this limitation. Moving from the urban canopy model to CFD will increase the complexity of the Navier-Stroke equation from 1D to 3D. However, CFD models demand much higher computational time. This specific aspect is currently under investigation in our research group. Furthermore, it would be interesting to combine the climate scenarios introduced in Chapter 6 with the urban climate model. This could lead to the design of climate resilient urban energy infrastructures.

Uncertainty can be presented in many ways. Often multiple methods are used to quantify the impact of uncertainties. This study limits its scope to a set of factors in the process of evaluating uncertainty. The set of factors considered can be further extended based on different applications. Furthermore, stochastic, robust and stochastic-robust optimization methods are used to consider the uncertainties in the optimization process. Possibility based approaches to quantify uncertainty are not considered in this study. Methods such as fuzzy logic might be helpful in this context since they can be effectively used to consider uncertainty without a significant increase in the pool of scenarios. Hence, possibilistic based approaches would be an interesting area for further consideration that can address the limitations of dimensionality.

The evolution of an energy system over its life span is not considered in this study. The evolution of renewable energy price, market price for fuel etc. plays a major role. Methods such as stochastic dynamic programing can be used in order to consider the evolution of energy systems over the time horizon. Such an extension will be helpful to understand the energy transition pathways. A case study is conducted to identify promising energy transition pathways for a village in Switzerland

(Hemberg) as a part of this thesis. However, the scenarios considered for the transition pathways are artificially synthesized besides using dynamic programing. Hence, the transition pathways might be sub-optimal and highly vulnerable to uncertainties in energy market. This leads to a major limitation of the present study. The analysis used in the thesis attempts to provide a single energy solution instead of a transition pathway. Presenting an energy transition pathway instead of a design solution might be a better approach to attract more investments instead of presenting high-end, expensive final solutions.

Introducing distributed optimization into the energy system optimization process is another achievement of the present study. It enables considering fully cooperative, non-cooperative and leader follower scenarios when designing energy systems. However, it is important to conduct this process at the scale of urban systems where the energy system becomes an agent. However, determining the criterions for the equilibrium will be challenging in such a context. Furthermore, it will require a co-simulation platform that can combine different systems that have responses with different time resolutions. Furthermore, it will require arbitration methods beyond the Nash or Stackelberg equilibrium when the agents have multiple interests. The computational models introduced in Chapters 3 and 4 can be directly extended to solve such multi-agent reinforcement learning problems. Artificial intelligence could be used to understand the adaptation of energy infrastructure at urban scale, which would be an interesting extension to the thesis.

Integrating decision making into optimization is an important step that brings the design tool closer to the users. Chapter 10 presents a promising method to facilitate such an integration. However, there are certain limitations in the proposed method. First, the uncertainties of the performance indicators used for the multi-criterion decision making are not considered in the decision making process. Considering the uncertainties of performance indicators is usually considered as an important part in the decision making process. Hence, the model should be extended to consider this specific aspect. In addition, it is important to combine business models with the decision making process. Such an extension allows to move beyond energy systems and consider other auxiliary services. Transportation, agriculture chemical production etc. can also be linked with the energy system design process and can be included into the business model. Finally, a multi criterion decision making technique is discussed just for a single system. It would be an interesting task to conduct the design process of a multi energy internet considering different bargaining powers and different priorities of agents by combining the work of Chapters 4 and 10.

Usually, a set of performance indicators are used to guide the design process of the energy systems. Energy system designers try to maximize/minimize performance indicators such as cost, reliability,

efficiency etc. to improve the performance of the energy system. However, an important aspect is overseen in this process: the co-existence of energy systems with the other parts of complex urban systems. Most of the performance indicators that are used to optimize the design of an energy system do not guarantee optimum functioning as a part of a complex urban system. Hence, having higher performances at the design stage of the energy system will not guarantee smooth and efficient functioning as a part of a complex urban system. This is where the concept of co-existence and niche diversity from the ecology and evolution theory comes in. Present engineering approaches tend to optimize a selected set of performance indicators of the energy system treating it as a niche, neglecting co-existence of the energy system as a part of the complex urban system in the optimization process. As a consequence, the energy system may fail to operate efficiently as a part of the complex urban system. Hence, improving co-existence and niche are important where niche separation plays a vital role. The main contribution of this thesis is that it opens up a promising new pathway to address this important issue.

List of References Chapter by Chapter

Chapter 1

[1] Ćosić B, Krajačić G, Duić N. A 100% renewable energy system in the year 2050: The case of Macedonia. Energy 2012;48:80–7. doi:10.1016/j.energy.2012.06.078.

[2] Connolly D, Lund H, Mathiesen BV, Leahy M. The first step towards a 100% renewable energy-system for Ireland. Appl Energy 2011;88:502–7. doi:10.1016/j.apenergy.2010.03.006.

[3] Mathiesen BV, Lund H, Karlsson K. 100% Renewable energy systems, climate mitigation and economic growth. Appl Energy 2011;88:488–501. doi:10.1016/j.apenergy.2010.03.001.

[4] Lund H, Mathiesen BV. Energy system analysis of 100% renewable energy systems—The case of Denmark in years 2030 and 2050. Energy 2009;34:524–31. doi:10.1016/j.energy.2008.04.003.

[5] Xydis G. Comparison study between a Renewable Energy Supply System and a supergrid for achieving 100% from renewable energy sources in Islands. Int J Electr Power Energy Syst 2013;46:198–210. doi:10.1016/j.ijepes.2012.10.046.

[6] Sansavini G, Piccinelli R, Golea LR, Zio E. A stochastic framework for uncertainty analysis in electric power transmission systems with wind generation. Renew Energy 2014;64:71–81. doi:10.1016/j.renene.2013.11.002.

[7] Brouwer AS, van den Broek M, Seebregts A, Faaij A. Impacts of large-scale Intermittent Renewable Energy Sources on electricity systems, and how these can be modeled. Renew Sustain Energy Rev 2014;33:443–66. doi:10.1016/j.rser.2014.01.076.

[8] Rajeev T, Ashok S. Dynamic load-shifting program based on a cloud computing framework to support the integration of renewable energy sources. Appl Energy 2015;146:141–9. doi:10.1016/j.apenergy.2015.02.014.

[9] Cerovac T, Ćosić B, Pukšec T, Duić N. Wind energy integration into future energy systems based on conventional plants – The case study of Croatia. Appl Energy 2014;135:643–55. doi:10.1016/j.apenergy.2014.06.055.

[10] Osório GJ, Lujano-Rojas JM, Matias JCO, Catalão JPS. A probabilistic approach to solve the economic dispatch problem with intermittent renewable energy sources. Energy 2015;82:949–59. doi:10.1016/j.energy.2015.01.104.

[11] Raza SS, Janajreh I, Ghenai C. Sustainability index approach as a selection criteria for energy storage system of an intermittent renewable energy source. Appl Energy 2014;136:909–20. doi:10.1016/j.apenergy.2014.04.080.

[12] Mohammadi M, Noorollahi Y, Mohammadi-ivatloo B, Yousefi H. Energy hub: From a model to a concept – A review. Renew Sustain Energy Rev 2017;80:1512–27. doi:10.1016/j.rser.2017.07.030.

[13] Zhang X, He M, Zhang Y. A review of research on the Kalina cycle. Renew Sustain Energy Rev 2012;16:5309–18. doi:10.1016/j.rser.2012.05.040.

[14] Imran M, Haglind F, Asim M, Zeb Alvi J. Recent research trends in organic Rankine cycle technology: A bibliometric approach. Renew Sustain Energy Rev 2018;81:552–62. doi:10.1016/j.rser.2017.08.028.

[15] Barley CD, Winn CB. Optimal dispatch strategy in remote hybrid power systems. Sol Energy 1996;58:165–79.

[16] Dufolopez R, Bernalagustin J. Design and control strategies of PV-Diesel systems using genetic algorithms. Sol Energy 2005;79:33–46. doi:10.1016/j.solener.2004.10.004.

[17] Deshmukh MK, Deshmukh SS. Modeling of hybrid renewable energy systems. Renew Sustain Energy Rev 2008;12:235–49. doi:10.1016/j.rser.2006.07.011.

[18] Tian M, Su Y, Zheng H, Pei G, Li G, Riffat S. A review on the recent research progress in the compound parabolic concentrator (CPC) for solar energy applications. Renew Sustain Energy Rev 2018;82:1272–96. doi:10.1016/j.rser.2017.09.050.

[19] Athukorala AUCD, Jayasuriya WJA, Ragulageethan S, Sirimanna MPG, Attalage RA, Perera ATD. A techno-economic analysis for an integrated solar PV/T system with thermal and electrical storage #x2014; Case study. 2015 Moratuwa Eng. Res. Conf. MERCon, 2015, p. 182–7. doi:10.1109/MERCon.2015.7112342.

[20] Elbahjaoui R, El Qarnia H, Naimi A. Thermal performance analysis of combined solar collector with triple concentric-tube latent heat storage systems. Energy Build 2018;168:438–56. doi:10.1016/j.enbuild.2018.02.055.

[21] Srinivas T, Reddy BV. Hybrid solar–biomass power plant without energy storage. Case Stud Therm Eng 2014;2:75–81. doi:10.1016/j.csite.2013.12.004.

[22] Fathima AH, Palanisamy K. Optimization in microgrids with hybrid energy systems – A review. Renew Sustain Energy Rev 2015;45:431–46. doi:10.1016/j.rser.2015.01.059.

[23] Perera ATD, Wijesiri A. Designing smart hybrid renewable energy systems with V2G. 2014 7th Int. Conf. Inf. Autom. Sustain. ICIAfS, 2014, p. 1–5. doi:10.1109/ICIAFS.2014.7069612.

[24] Timothée C, Perera ATD, Scartezzini J-L, Mauree D. Optimum dispatch of a multi-storage and multi-energy hub with demand response and restricted grid interactions. Energy Procedia 2017;142:2864–9. doi:10.1016/j.egypro.2017.12.434.

[25] Geidl M, Koeppel G, Favre-Perrod P, Klockl B, Andersson G, Frohlich K. Energy hubs for the future. IEEE Power Energy Mag 2007;5:24–30. doi:10.1109/MPAE.2007.264850.

[26] Geidl M, Andersson G. Optimal Power Flow of Multiple Energy Carriers. IEEE Trans Power Syst 2007;22:145–55. doi:10.1109/TPWRS.2006.888988.

[27] Piacentino A, Cardona F. EABOT – Energetic analysis as a basis for robust optimization of trigeneration systems by linear programming. Energy Convers Manag 2008;49:3006–16. doi:10.1016/j.enconman.2008.06.015.

[28] Perera ATD, Nik VM, Mauree D, Scartezzini J-L. Electrical hubs: An effective way to integrate non-dispatchable renewable energy sources with minimum impact to the grid. Appl Energy 2017;190:232–48. doi:10.1016/j.apenergy.2016.12.127.

[29] Evins R. Multi-level optimization of building design, energy system sizing and operation. Energy 2015;90, Part 2:1775–89. doi:10.1016/j.energy.2015.07.007.

[30] Fazlollahi S, Bungener SL, Becker G, Maréchal F. Multi-Objective, Multi-Period Optimization of Renewable Technologies and storage system Using Evolutionary Algorithms and Mixed Integer Linear Programming (MILP). In: Iftekhar A. Karimi and Rajagopalan Srinivasan, editor. Comput. Aided Chem. Eng., vol. Volume 31, Elsevier; 2012, p. 890–4.

[31] Jayasekara S, Halgamuge SK, Attalage RA, Rajarathne R. Optimum sizing and tracking of combined cooling heating and power systems for bulk energy consumers. Appl Energy 2014;118:124–34. doi:10.1016/j.apenergy.2013.12.040.

[32] Murray P, Orehounig K, Grosspietsch D, Carmeliet J. A comparison of storage systems in neighbourhood decentralized energy system applications from 2015 to 2050. Appl Energy 2018;231:1285–306. doi:10.1016/j.apenergy.2018.08.106.

[33] Gabrielli P, Gazzani M, Martelli E, Mazzotti M. Optimal design of multi-energy systems with seasonal storage. Appl Energy 2018;219:408–24. doi:10.1016/j.apenergy.2017.07.142.

[34] Stadler P, Girardin L, Ashouri A, Maréchal F. Contribution of Model Predictive Control in the Integration of Renewable Energy Sources within the Built Environment. Front Energy Res 2018;6. doi:10.3389/fenrg.2018.00022.

[35] Sridhar S, Hahn A, Govindarasu M. Cyber–Physical System Security for the Electric Power Grid. Proc IEEE 2012;100:210–24. doi:10.1109/JPROC.2011.2165269.

[36] Huang AQ, Crow ML, Heydt GT, Zheng JP, Dale SJ. The Future Renewable Electric Energy Delivery and Management (FREEDM) System: The Energy Internet. Proc IEEE 2011;99:133–48. doi:10.1109/JPROC.2010.2081330.

[37] Zhou K, Yang S, Shao Z. Energy Internet: The business perspective. Appl Energy 2016;178:212–22. doi:10.1016/j.apenergy.2016.06.052.

[38] Rajkumar R, Lee I, Sha L, Stankovic J. Cyber-physical systems: The next computing revolution. Des. Autom. Conf., 2010, p. 731–6. doi:10.1145/1837274.1837461.

[39] Mavromatidis G, Orehounig K, Carmeliet J. A review of uncertainty characterisation approaches for the optimal design of distributed energy systems. Renew Sustain Energy Rev 2018;88:258–77. doi:10.1016/j.rser.2018.02.021.

[40] Panteli M, Mancarella P. Influence of extreme weather and climate change on the resilience of power systems: Impacts and possible mitigation strategies. Electr Power Syst Res 2015;127:259–70. doi:10.1016/j.epsr.2015.06.012.

[41] Manfren M, Caputo P, Costa G. Paradigm shift in urban energy systems through distributed generation: Methods and models. Appl Energy 2011;88:1032–48. doi:10.1016/j.apenergy.2010.10.018.

Chapter 2

[1] J. Blazejczak, F. G. Braun, D. Edler, and W.-P. Schill, “Economic effects of renewable energy expansion: A model-based analysis for Germany,” Renew. Sustain. Energy Rev., vol. 40, pp. 1070–1080, Dec. 2014.

[2] B. Zakeri, S. Syri, and S. Rinne, “Higher renewable energy integration into the existing energy system of Finland – Is there any maximum limit?,” Energy.

[3] E. Voumvoulakis, G. Asimakopoulou, S. Danchev, G. Maniatis, and A. Tsakanikas, “Large scale integration of intermittent renewable energy sources in the Greek power sector,” Energy Policy, vol. 50, pp. 161–173, Nov. 2012.

[4] E. E. Sfikas, Y. A. Katsigiannis, and P. S. Georgilakis, “Simultaneous capacity optimization of distributed generation and storage in medium voltage microgrids,” Int. J. Electr. Power Energy Syst., vol. 67, pp. 101–113, May 2015.

[5] B. Ćosić, G. Krajačić, and N. Duić, “A 100% renewable energy system in the year 2050: The case of Macedonia,” Energy, vol. 48, no. 1, pp. 80–87, Dec. 2012.

[6] D. Connolly, H. Lund, B. V. Mathiesen, and M. Leahy, “The first step towards a 100% renewable energy-system for Ireland,” Appl. Energy, vol. 88, no. 2, pp. 502–507, Feb. 2011.

[7] B. V. Mathiesen, H. Lund, and K. Karlsson, “100% Renewable energy systems, climate mitigation and economic growth,” Appl. Energy, vol. 88, no. 2, pp. 488–501, Feb. 2011.

[8] H. Lund and B. V. Mathiesen, “Energy system analysis of 100% renewable energy systems—The case of Denmark in years 2030 and 2050,” Energy, vol. 34, no. 5, pp. 524–531, May 2009.

[9] G. Xydis, “Comparison study between a Renewable Energy Supply System and a supergrid for achieving 100% from renewable energy sources in Islands,” Int. J. Electr. Power Energy Syst., vol. 46, pp. 198–210, Mar. 2013.

[10] G. Sansavini, R. Piccinelli, L. R. Golea, and E. Zio, “A stochastic framework for uncertainty analysis in electric power transmission systems with wind generation,” Renew. Energy, vol. 64, pp. 71–81, Apr. 2014.

[11] A. S. Brouwer, M. van den Broek, A. Seebregts, and A. Faaij, “Impacts of large-scale Intermittent Renewable Energy Sources on electricity systems, and how these can be modeled,” Renew. Sustain. Energy Rev., vol. 33, pp. 443–466, May 2014.

[12] O. Hafez and K. Bhattacharya, “Optimal planning and design of a renewable energy based supply system for microgrids,” Renew. Energy, vol. 45, pp. 7–15, Sep. 2012.

[13] F. F. Yanine and E. E. Sauma, “Review of grid-tie micro-generation systems without energy storage: Towards a new approach to sustainable hybrid energy systems linked to energy efficiency,” Renew. Sustain. Energy Rev., vol. 26, pp. 60–95, Oct. 2013.

[14] A. T. D. Perera, R. A. Attalage, K. K. C. K. Perera, and V. P. C. Dassanayake, “Converting existing Internal Combustion Generator (ICG) systems into HESs in standalone applications,” Energy Convers. Manag., vol. 74, pp. 237–248, Oct. 2013.

[15] A. H. Fathima and K. Palanisamy, “Optimization in microgrids with hybrid energy systems – A review,” Renew. Sustain. Energy Rev., vol. 45, pp. 431–446, May 2015.

[16] R. Dufo-López, J. L. Bernal-Agustín, J. M. Yusta-Loyo, J. A. Domínguez-Navarro, I. J. Ramírez-Rosado, J. Lujano, and I. Aso, “Multi-objective optimization minimizing cost and life cycle emissions of stand-alone PV–wind–diesel systems with batteries storage,” Appl. Energy, vol. 88, no. 11, pp. 4033–4041, Nov. 2011.

[17] A. T. D. Perera, R. A. Attalage, K. K. C. K. Perera, and V. P. C. Dassanayake, “Designing standalone hybrid energy systems minimizing initial investment, life cycle cost and pollutant emission,” Energy, vol. 54, pp. 220–230, Jun. 2013.

[18] I. R. Cristóbal-Monreal and R. Dufo-López, “Optimisation of photovoltaic–diesel–battery stand-alone systems minimising system weight,” Energy Convers. Manag., vol. 119, pp. 279–288, Jul. 2016.

[19] M. Bortolini, M. Gamberi, A. Graziani, and F. Pilati, “Economic and environmental bi-objective design of an off-grid photovoltaic–battery–diesel generator hybrid energy system,” Energy Convers. Manag., vol. 106, pp. 1024–1038, Dec. 2015.

[20] C. Weber, F. Maréchal, D. Favrat, and S. Kraines, “Optimization of an SOFC-based decentralized polygeneration system for providing energy services in an office-building in Tōkyō,” Appl. Therm. Eng., vol. 26, no. 13, pp. 1409–1419, Sep. 2006.

[21] S. Fazlollahi, G. Becker, A. Ashouri, and F. Maréchal, “Multi-objective, multi-period optimization of district energy systems: IV – A case study,” Energy, vol. 84, pp. 365–381, May 2015.

[22] R. Evins, “Multi-level optimization of building design, energy system sizing and operation,” Energy.

[23] A. Maroufmashat, A. Elkamel, M. Fowler, S. Sattari, R. Roshandel, A. Hajimiragha, S. Walker, and E. Entchev, “Modeling and optimization of a network of energy hubs to improve economic and emission considerations,” Energy, vol. 93, Part 2, pp. 2546–2558, Dec. 2015.

[24] K. A. Pruitt, S. Leyffer, A. M. Newman, and R. J. Braun, “A mixed-integer nonlinear program for the optimal design and dispatch of distributed generation systems,” Optim. Eng., vol. 15, no. 1, pp. 167–197, Aug. 2013.

[25] A. Piacentino and F. Cardona, “EABOT – Energetic analysis as a basis for robust optimization of trigeneration systems by linear programming,” Energy Convers. Manag., vol. 49, no. 11, pp. 3006–3016, Nov. 2008.

[26] K. A. Pruitt, R. J. Braun, and A. M. Newman, “Evaluating shortfalls in mixed-integer programming approaches for the optimal design and dispatch of distributed generation systems,” Appl. Energy, vol. 102, pp. 386–398, Feb. 2013.

[27] R. Evins, K. Orehounig, V. Dorer, and J. Carmeliet, “New formulations of the ‘energy hub’ model to address operational constraints,” Energy, vol. 73, pp. 387–398, Aug. 2014.

[28] K. Orehounig, R. Evins, and V. Dorer, “Integration of decentralized energy systems in neighbourhoods using the energy hub approach,” Appl. Energy, vol. 154, pp. 277–289, Sep. 2015.

[29] A. Maleki, F. Pourfayaz, and M. A. Rosen, “A novel framework for optimal design of hybrid renewable energy-based autonomous energy systems: A case study for Namin, Iran,” Energy, vol. 98, pp. 168–180, Mar. 2016.

[30] A. S. O. Ogunjuyigbe, T. R. Ayodele, and O. A. Akinola, “Optimal allocation and sizing of PV/Wind/Split-diesel/Battery hybrid energy system for minimizing life cycle cost, carbon emission and dump energy of remote residential building,” Appl. Energy, vol. 171, pp. 153–171, Jun. 2016.

[31] S. R. Tito, T. T. Lie, and T. N. Anderson, “Optimal sizing of a wind-photovoltaic-battery hybrid renewable energy system considering socio-demographic factors,” Sol. Energy, vol. 136, pp. 525–532, Oct. 2016.

[32] Z. Shi, R. Wang, and T. Zhang, “Multi-objective optimal design of hybrid renewable energy systems using preference-inspired coevolutionary approach,” Sol. Energy, vol. 118, pp. 96–106, Aug. 2015.

[33] A. T. D. Perera, R. A. Attalage, K. K. C. K. Perera, and V. P. C. Dassanayake, “A hybrid tool to combine multi-objective optimization and multi-criterion decision making in designing standalone hybrid energy systems,” Appl. Energy, vol. 107, pp. 412–425, Jul. 2013.

[34] O. Erdinc and M. Uzunoglu, “Optimum design of hybrid renewable energy systems: Overview of different approaches,” Renew. Sustain. Energy Rev., vol. 16, no. 3, pp. 1412–1425, Apr. 2012.

[35] A. T. D. Perera, R. A. Attalage, and K. K. C. K. Perera, “Optimal design of a grid connected hybrid electrical energy system using evolutionary computation,” in 2013 8th IEEE International Conference on Industrial and Information Systems (ICIIS), 2013, pp. 12–17.

[36] A. M. Eltamaly, M. A. Mohamed, and A. I. Alolah, “A novel smart grid theory for optimal sizing of hybrid renewable energy systems,” Sol. Energy, vol. 124, pp. 26–38, Feb. 2016.

[37] J. L. Bernal-Agustín and R. Dufo-López, “Hourly energy management for grid-connected wind–hydrogen systems,” Int. J. Hydrog. Energy, vol. 33, no. 22, pp. 6401–6413, Nov. 2008.

[38] R. Dufo-López, “Optimisation of size and control of grid-connected storage under real time electricity pricing conditions,” Appl. Energy, vol. 140, pp. 395–408, Feb. 2015.

[39] A. Rezvani, A. Khalili, A. Mazareie, and M. Gandomkar, “Modeling, control, and simulation of grid connected intelligent hybrid battery/photovoltaic system using new hybrid fuzzy-neural method,” ISA Trans.

[40] S. Safari, M. M. Ardehali, and M. J. Sirizi, “Particle swarm optimization based fuzzy logic controller for autonomous green power energy system with hydrogen storage,” Energy Convers. Manag., vol. 65, pp. 41–49, Jan. 2013.

[41] S. Berrazouane and K. Mohammedi, “Parameter optimization via cuckoo optimization algorithm of fuzzy controller for energy management of a hybrid power system,” Energy Convers. Manag., vol. 78, pp. 652–660, Feb. 2014.

[42] M. H. Athari and M. M. Ardehali, “Operational performance of energy storage as function of electricity prices for on-grid hybrid renewable energy system by optimized fuzzy logic controller,” Renew. Energy, vol. 85, pp. 890–902, Jan. 2016.

[43] L. Olatomiwa, S. Mekhilef, M. S. Ismail, and M. Moghavvemi, “Energy management strategies in hybrid renewable energy systems: A review,” Renew. Sustain. Energy Rev., vol. 62, pp. 821–835, Sep. 2016.

[44] G. Krajačić, N. Duić, Z. Zmijarević, B. V. Mathiesen, A. A. Vučinić, and M. da Graça Carvalho, “Planning for a 100% independent energy system based on smart energy storage for integration of renewables and CO2 emissions reduction,” Appl. Therm. Eng., vol. 31, no. 13, pp. 2073–2083, Sep. 2011.

[45] J. Salom, A. J. Marszal, J. Widén, J. Candanedo, and K. B. Lindberg, “Analysis of load match and grid interaction indicators in net zero energy buildings with simulated and monitored data,” Appl. Energy, vol. 136, pp. 119–131, Dec. 2014.

[46] F. Ueckerdt, R. Brecha, G. Luderer, P. Sullivan, E. Schmid, N. Bauer, D. Böttger, and R. Pietzcker, “Representing power sector variability and the integration of variable renewables in long-term energy-economy models using residual load duration curves,” Energy, vol. 90, Part 2, pp. 1799–1814, Oct. 2015.

[47] “EnergyPlus | EnergyPlus.” [Online]. Available: https://energyplus.net/. [Accessed: 25-Nov-2015].

[48] “CitySim Software | LESO-PB.” [Online]. Available: http://citysim.epfl.ch/. [Accessed: 25-Nov-2015].

[49] S. Fazlollahi, G. Becker, and F. Maréchal, “Multi-objectives, multi-period optimization of district energy systems: III. Distribution networks,” Comput. Chem. Eng., vol. 66, pp. 82–97, Jul. 2014.

[50] J. Soares, M. A. Fotouhi Ghazvini, Z. Vale, and P. B. de Moura Oliveira, “A multi-objective model for the day-ahead energy resource scheduling of a smart grid with high penetration of sensitive loads,” Appl. Energy, vol. 162, pp. 1074–1088, Jan. 2016.

[51] W. Tushar, B. Chai, C. Yuen, D. B. Smith, K. L. Wood, Z. Yang, and H. V. Poor, “Three-Party Energy Management With Distributed Energy Resources in Smart Grid,” IEEE Trans. Ind. Electron., vol. 62, no. 4, pp. 2487–2498, Apr. 2015.

[52] A. Safdarian, M. Fotuhi-Firuzabad, M. Lehtonen, and F. Aminifar, “Optimal Electricity Procurement in Smart Grids With Autonomous Distributed Energy Resources,” IEEE Trans. Smart Grid, vol. 6, no. 6, pp. 2975–2984, Nov. 2015.

[53] A. T. D. Perera, D. M. I. J. Wickremasinghe, D. V. S. Mahindarathna, R. A. Attalage, K. K. C. K. Perera, and E. M. Bartholameuz, “Sensitivity of internal combustion generator capacity in standalone hybrid energy systems,” Energy, vol. 39, no. 1, pp. 403–411, Mar. 2012.

[54] G. Notton, V. Lazarov, and L. Stoyanov, “Optimal sizing of a grid-connected PV system for various PV module technologies and inclinations, inverter efficiency characteristics and locations,” Renew. Energy, vol. 35, no. 2, pp. 541–554, Feb. 2010.

[55] F. O. Hocaoğlu, Ö. N. Gerek, and M. Kurban, “A novel hybrid (wind–photovoltaic) system sizing procedure,” Sol. Energy, vol. 83, no. 11, pp. 2019–2028, Nov. 2009.

[56] S. Diaf, D. Diaf, M. Belhamel, M. Haddadi, and A. Louche, “A methodology for optimal sizing of autonomous hybrid PV/wind system,” Energy Policy, vol. 35, no. 11, pp. 5708–5718, Nov. 2007.

[57] M. K. Deshmukh and S. S. Deshmukh, “Modeling of hybrid renewable energy systems,” Renew. Sustain. Energy Rev., vol. 12, no. 1, pp. 235–249, Jan. 2008.

[58] R. Dufo-López and J. L. Bernal-Agustín, “Design and control strategies of PV-Diesel systems using genetic algorithms,” Sol. Energy, vol. 79, no. 1, pp. 33–46, Jul. 2005.

[59] S. D. Downing and D. F. Socie, “Simple rainflow counting algorithms,” Int. J. Fatigue, vol. 4, no. 1, pp. 31–40, Jan. 1982.

[60] E. Zio and T. Aven, “Uncertainties in smart grids behavior and modeling: What are the risks and vulnerabilities? How to analyze them?,” Energy Policy, vol. 39, no. 10, pp. 6308–6320, Oct. 2011.

[61] B. Verbruggen and J. Driesen, “Grid Impact Indicators for Active Building Simulations,” IEEE Trans. Sustain. Energy, vol. 6, no. 1, pp. 43–50, Jan. 2015.

[62] A. T. D. Perera, A. N. Madusanka, R. A. Attalage, and K. K. C. K. Perera, “A multi criterion analysis for renewable energy integration process of a standalone hybrid energy system with internal combustion generator,” J. Renew. Sustain. Energy, vol. 7, no. 4, p. 43128, Jul. 2015.

[63] A. Mohammed, J. Pasupuleti, T. Khatib, and W. Elmenreich, “A review of process and operational system control of hybrid photovoltaic/diesel generator systems,” Renew. Sustain. Energy Rev., vol. 44, pp. 436–446, Apr. 2015.

[64] J. L. Bernal-Agustín and R. Dufo-López, “Hourly energy management for grid-connected wind–hydrogen systems,” Int. J. Hydrog. Energy, vol. 33, no. 22, pp. 6401–6413, Nov. 2008.

[65] R. Dufo-López, “Optimisation of size and control of grid-connected storage under real time electricity pricing conditions,” Appl. Energy, vol. 140, pp. 395–408, Feb. 2015.

[66] R. Dufo-López and J. L. Bernal-Agustín, “Techno-economic analysis of grid-connected battery storage,” Energy Convers. Manag., vol. 91, pp. 394–404, Feb. 2015.

[67] S. Upadhyay and M. P. Sharma, “A review on configurations, control and sizing methodologies of hybrid energy systems,” Renew. Sustain. Energy Rev., vol. 38, pp. 47–63, Oct. 2014.

[68] T. Takagi and M. Sugeno, “Fuzzy identification of systems and its applications to modeling and control,” IEEE Trans. Syst. Man Cybern., vol. SMC-15, no. 1, pp. 116–132, Jan. 1985.

[69] M. Sugeno, “An introductory survey of fuzzy control,” Inf. Sci., vol. 36, no. 1, pp. 59–83, Jul. 1985.

[70] M. Sugeno and G. T. Kang, “Structure identification of fuzzy model,” Fuzzy Sets Syst., vol. 28, no. 1, pp. 15–33, Oct. 1988.

[71] C.-Y. Li and G.-P. Liu, “Optimal fuzzy power control and management of fuel cell/battery hybrid vehicles,” J. Power Sources, vol. 192, no. 2, pp. 525–533, Jul. 2009.

[72] X. Li, L. Xu, J. Hua, X. Lin, J. Li, and M. Ouyang, “Power management strategy for vehicular-applied hybrid fuel cell/battery power system,” J. Power Sources, vol. 191, no. 2, pp. 542–549, Jun. 2009.

[73] S. Caux, W. Hankache, M. Fadel, and D. Hissel, “On-line fuzzy energy management for hybrid fuel cell systems,” Int. J. Hydrog. Energy, vol. 35, no. 5, pp. 2134–2143, Mar. 2010.

[74] J. Solano Martínez, R. I. John, D. Hissel, and M.-C. Péra, “A survey-based type-2 fuzzy logic system for energy management in hybrid electrical vehicles,” Inf. Sci., vol. 190, pp. 192–207, May 2012.

[75] P. Wong, P. Albrecht, R. Allan, R. Billinton, Q. Chen, C. Fong, S. Haddad, W. Li, R. Mukerji, D. Patton, A. Schneider, M. Shahidehpour, and C. Singh, “The IEEE Reliability Test System-1996. A report prepared by the Reliability Test System Task Force of the Application of Probability Methods Subcommittee,” IEEE Trans. Power Syst., vol. 14, no. 3, pp. 1010–1020, Aug. 1999.

[76] Z. Iverson, A. Achuthan, P. Marzocca, and D. Aidun, “Optimal design of hybrid renewable energy systems (HRES) using hydrogen storage technology for data center applications,” Renew. Energy, vol. 52, pp. 79–87, Apr. 2013.

[77] S. Sanajaoba and E. Fernandez, “Maiden application of Cuckoo Search algorithm for optimal sizing of a remote hybrid renewable energy System,” Renew. Energy, vol. 96, Part A, pp. 1–10, Oct. 2016.

[78] J. L. Bernal-Agustín and R. Dufo-López, “Efficient design of hybrid renewable energy systems using evolutionary algorithms,” Energy Convers. Manag., vol. 50, no. 3, pp. 479–489, Mar. 2009.

[79] S. Bahramara, M. P. Moghaddam, and M. R. Haghifam, “Optimal planning of hybrid renewable energy systems using HOMER: A review,” Renew. Sustain. Energy Rev., vol. 62, pp. 609–620, Sep. 2016.

[80] K. Deb, M. Mohan, and S. Mishra, “Evaluating the ε-Domination Based Multi-Objective Evolutionary Algorithm for a Quick Computation of Pareto-Optimal Solutions,” Evol Comput, vol. 13, no. 4, pp. 501–525, Dec. 2005.

[81] M. Laumanns, L. Thiele, K. Deb, and E. Zitzler, “Combining Convergence and Diversity in Evolutionary Multiobjective Optimization,” Evol. Comput., vol. 10, no. 3, pp. 263–282, Sep. 2002.

[82] K. Deb, “An efficient constraint handling method for genetic algorithms,” Comput. Methods Appl. Mech. Eng., vol. 186, no. 2–4, pp. 311–338, Jun. 2000.

[83] K. Deb and H.-G. Beyer, “Self-Adaptive Genetic Algorithms with Simulated Binary Crossover,” Evol. Comput., vol. 9, no. 2, pp. 197–221, Jun. 2001.

[84] A. K. Qin, V. L. Huang, and P. N. Suganthan, “Differential Evolution Algorithm With Strategy Adaptation for Global Numerical Optimization,” IEEE Trans. Evol. Comput., vol. 13, no. 2, pp. 398–417, Apr. 2009.

[85] R. Storn and K. Price, “Differential Evolution – A Simple and Efficient Heuristic for global Optimization over Continuous Spaces,” J. Glob. Optim., vol. 11, no. 4, pp. 341–359.

[86] J. Brest, S. Greiner, B. Boskovic, M. Mernik, and V. Zumer, “Self-Adapting Control Parameters in Differential Evolution: A Comparative Study on Numerical Benchmark Problems,” IEEE Trans. Evol. Comput., vol. 10, no. 6, pp. 646–657, Dec. 2006.

Chapter 3

[1] Orehounig K, Evins R, Dorer V. Integration of decentralized energy systems in neighbourhoods using the energy hub approach. Appl Energy 2015;154:277–89. doi:10.1016/j.apenergy.2015.04.114.

[2] Orehounig K, Mavromatidis G, Evins R, Dorer V, Carmeliet J. Towards an energy sustainable community: An energy system analysis for a village in Switzerland. Energy Build 2014;84:277–86. doi:10.1016/j.enbuild.2014.08.012.

[3] Mauree D, Coccolo S, Perera A, Nik V, Scartezzini J-L, Naboni E, et al. A New Framework to Evaluate Urban Design Using Urban Microclimatic Modeling in Future Climatic Conditions. Sustainability 2018;10:1134. doi:10.3390/su10041134.

[4] Perera ATD, Nik VM, Mauree D, Scartezzini J-L. Electrical hubs: An effective way to integrate non-dispatchable renewable energy sources with minimum impact to the grid. Appl Energy 2017;190:232–48. doi:10.1016/j.apenergy.2016.12.127.

[5] Piacentino A, Cardona F. EABOT – Energetic analysis as a basis for robust optimization of trigeneration systems by linear programming. Energy Convers Manag 2008;49:3006–16. doi:10.1016/j.enconman.2008.06.015.

[6] Powell WB. Approximate Dynamic Programming: Solving the Curses of Dimensionality (Wiley Series in Probability and Statistics). New York, NY, USA: Wiley-Interscience; 2007.

[7] Powell WB, Meisel S. Tutorial on Stochastic Optimization in Energy #x2014;Part I: Modeling and Policies. IEEE Trans Power Syst 2016;31:1459–67. doi:10.1109/TPWRS.2015.2424974.

[8] Dufolopez R, Bernalagustin J. Design and control strategies of PV-Diesel systems using genetic algorithms. Sol Energy 2005;79:33–46. doi:10.1016/j.solener.2004.10.004.

[9] Weber C, Maréchal F, Favrat D, Kraines S. Optimization of an SOFC-based decentralized polygeneration system for providing energy services in an office-building in Tōkyō. Appl Therm Eng 2006;26:1409–19. doi:10.1016/j.applthermaleng.2005.05.031.

[10] Evins R. Multi-level optimization of building design, energy system sizing and operation. Energy n.d. doi:10.1016/j.energy.2015.07.007.

[11] Mohammadi M, Noorollahi Y, Mohammadi-ivatloo B, Yousefi H. Energy hub: From a model to a concept – A review. Renew Sustain Energy Rev 2017;80:1512–27. doi:10.1016/j.rser.2017.07.030.

[12] Jayasekara S, Halgamuge SK, Attalage RA, Rajarathne R. Optimum sizing and tracking of combined cooling heating and power systems for bulk energy consumers. Appl Energy 2014;118:124–34. doi:10.1016/j.apenergy.2013.12.040.

[13] Murray P, Orehounig K, Grosspietsch D, Carmeliet J. A comparison of storage systems in neighbourhood decentralized energy system applications from 2015 to 2050. Appl Energy 2018;231:1285–306. doi:10.1016/j.apenergy.2018.08.106.

[14] Gabrielli P, Gazzani M, Martelli E, Mazzotti M. Optimal design of multi-energy systems with seasonal storage. Appl Energy 2018;219:408–24. doi:10.1016/j.apenergy.2017.07.142.

[15] Huang AQ, Crow ML, Heydt GT, Zheng JP, Dale SJ. The Future Renewable Electric Energy Delivery and Management (FREEDM) System: The Energy Internet. Proc IEEE 2011;99:133–48. doi:10.1109/JPROC.2010.2081330.

[16] Zhou K, Yang S, Shao Z. Energy Internet: The business perspective. Appl Energy 2016;178:212–22. doi:10.1016/j.apenergy.2016.06.052.

[17] Sridhar S, Hahn A, Govindarasu M. Cyber–Physical System Security for the Electric Power Grid. Proc IEEE 2012;100:210–24. doi:10.1109/JPROC.2011.2165269.

[18] Rajkumar R, Lee I, Sha L, Stankovic J. Cyber-physical systems: The next computing revolution. Des. Autom. Conf., 2010, p. 731–6. doi:10.1145/1837274.1837461.

[19] Derler P, Lee EA, Vincentelli AS. Modeling Cyber–Physical Systems. Proc IEEE 2012;100:13–28. doi:10.1109/JPROC.2011.2160929.

[20] BETSI. Description of the existing buildings: technical characteristics, indoor environment and energy consumption. (Bebyggelsens energianvändning, tekniska status och innemiljö). Karlskrona, Sweden: Boverket – the National Board of Housing, Building and Planning; 2009.

[21] Nik VM, Sasic Kalagasidis A. Impact study of the climate change on the energy performance of the building stock in Stockholm considering four climate uncertainties. Build Environ 2013;60:291–304. doi:10.1016/j.buildenv.2012.11.005.

[22] Nik VM. Hygrothermal Simulations of Buildings Concerning Uncertainties of the Future Climate. PhD thesis. Chalmers University of Technology, 2012.

[23] Nik VM, Mata É, Sasic Kalagasidis A. A statistical method for assessing retrofitting measures of buildings and ranking their robustness against climate change. Energy Build 2015;88:262–75. doi:10.1016/j.enbuild.2014.11.015.

[24] Nik VM, Mata E, Sasic Kalagasidis A, Scartezzini J-L. Effective and robust energy retrofitting measures for future climatic conditions—Reduced heating demand of Swedish households. Energy Build 2016;121:176–87. doi:10.1016/j.enbuild.2016.03.044.

[25] Nik VM, Mata E, Kalagasidis AS. Assessing the Efficiency and Robustness of the Retrofitted Building Envelope Against Climate change. Energy Procedia 2015;78:955–60. doi:10.1016/j.egypro.2015.11.031.

[26] Samuelsson P, Jones CG, Willen U, Ullerstig A, Gollvik S, Hansson U, et al. The Rossby Centre Regional Climate model RCA3: model description and performance. Tellus A 2011;63:4–23.

[27] Nik VM, Sasic Kalagasidis A, Kjellström E. Statistical methods for assessing and analysing the building performance in respect to the future climate. Build Environ 2012;53:107–18. doi:10.1016/j.buildenv.2012.01.015.

[28] Nik VM. Climate Simulation of an Attic Using Future Weather Data Sets - Statistical Methods for Data Processing and Analysis. Licentiate thesis. Chalmers University of Technology, 2010.

[29] Nik VM. Making energy simulation easier for future climate – Synthesizing typical and extreme weather data sets out of regional climate models (RCMs). Appl Energy 2016;177:204–26. doi:10.1016/j.apenergy.2016.05.107.

[30] Nik VM. Application of typical and extreme weather data sets in the hygrothermal simulation of building components for future climate – A case study for a wooden frame wall. Energy Build 2017;154:30–45. doi:10.1016/j.enbuild.2017.08.042.

[31] Moazami A, Nik VM, Carlucci S, Geving S. Impacts of future weather data typology on building energy performance – Investigating long-term patterns of climate change and extreme weather conditions. Appl Energy 2019;238:696–720. doi:10.1016/j.apenergy.2019.01.085.

[32] Perera ATD, Wickremasinghe DMIJ, Mahindarathna DVS, Attalage RA, Perera KKCK, Bartholameuz EM. Sensitivity of internal combustion generator capacity in standalone hybrid energy systems. Energy 2012;39:403–11. doi:10.1016/j.energy.2011.12.039.

[33] Perera ATD, Nik VM, Mauree D, Scartezzini J-L. An integrated approach to design site specific distributed electrical hubs combining optimization, multi-criterion assessment and decision making. Energy 2017;134:103–20. doi:10.1016/j.energy.2017.06.002.

[34] Downing SD, Socie DF. Simple rainflow counting algorithms. Int J Fatigue 1982;4:31–40. doi:10.1016/0142-1123(82)90018-4.

[35] Salom J, Marszal AJ, Widén J, Candanedo J, Lindberg KB. Analysis of load match and grid interaction indicators in net zero energy buildings with simulated and monitored data. Appl Energy 2014;136:119–31. doi:10.1016/j.apenergy.2014.09.018.

[36] Verbruggen B, Driesen J. Grid Impact Indicators for Active Building Simulations. IEEE Trans Sustain Energy 2015;6:43–50. doi:10.1109/TSTE.2014.2357475.

[37] Ernst D, Glavic M, Capitanescu F, Wehenkel L. Reinforcement Learning Versus Model Predictive Control: A Comparison on a Power System Problem. IEEE Trans Syst Man Cybern Part B Cybern 2009;39:517–29. doi:10.1109/TSMCB.2008.2007630.

[38] Görges D. Relations between Model Predictive Control and Reinforcement Learning. IFAC-Pap 2017;50:4920–8. doi:10.1016/j.ifacol.2017.08.747.

[39] Mnih V, Kavukcuoglu K, Silver D, Rusu AA, Veness J, Bellemare MG, et al. Human-level control through deep reinforcement learning. Nature 2015;518:529–33. doi:10.1038/nature14236.

[40] Stanley KO, Clune J, Lehman J, Miikkulainen R. Designing neural networks through neuroevolution. Nat Mach Intell 2019;1:24. doi:10.1038/s42256-018-0006-z.

[41] Salimans T, Ho J, Chen X, Sidor S, Sutskever I. Evolution Strategies as a Scalable Alternative to Reinforcement Learning. ArXiv170303864 Cs Stat 2017.

[42] Zhang X, Clune J, Stanley KO. On the Relationship Between the OpenAI Evolution Strategy and Stochastic Gradient Descent. ArXiv171206564 Cs 2017.

[43] Ha D, Schmidhuber J. Recurrent World Models Facilitate Policy Evolution. ArXiv180901999 Cs Stat 2018.

[44] Perera ATD, Nik VM, Mauree D, Scartezzini J-L. Design Optimization of Electrical Hubs Using Hybrid Evolutionary Algorithm 2016:V001T03A007. doi:10.1115/ES2016-59517.

[45] Liu Y, Yao X, Zhao Q, Higuchi T. Scaling up fast evolutionary programming with cooperative coevolution. Proc. 2001 Congr. Evol. Comput. IEEE Cat No01TH8546, vol. 2, 2001, p. 1101–8 vol. 2. doi:10.1109/CEC.2001.934314.

Chapter 4

[1] Ćosić B, Krajačić G, Duić N. A 100% renewable energy system in the year 2050: The case of Macedonia. Energy 2012;48:80–7. doi:10.1016/j.energy.2012.06.078.

[2] Lund H, Mathiesen BV. Energy system analysis of 100% renewable energy systems—The case of Denmark in years 2030 and 2050. Energy 2009;34:524–31. doi:10.1016/j.energy.2008.04.003.

[3] Sansavini G, Piccinelli R, Golea LR, Zio E. A stochastic framework for uncertainty analysis in electric power transmission systems with wind generation. Renew Energy 2014;64:71–81. doi:10.1016/j.renene.2013.11.002.

[4] Zio E, Sansavini G. Vulnerability of Smart Grids With Variable Generation and Consumption: A System of Systems Perspective. IEEE Trans Syst Man Cybern Syst 2013;43:477–87. doi:10.1109/TSMCA.2012.2207106.

[5] Guen ML, Mosca L, Perera ATD, Coccolo S, Mohajeri N, Scartezzini J-L. Improving the energy sustainability of a Swiss village through building renovation and renewable energy integration. Energy Build 2018;158:906–23. doi:10.1016/j.enbuild.2017.10.057.

[6] Bahramara S, Moghaddam MP, Haghifam MR. Optimal planning of hybrid renewable energy systems using HOMER: A review. Renew Sustain Energy Rev 2016;62:609–20. doi:10.1016/j.rser.2016.05.039.

[7] Connolly D, Lund H, Mathiesen BV, Leahy M. A review of computer tools for analysing the integration of renewable energy into various energy systems. Appl Energy 2010;87:1059–82. doi:10.1016/j.apenergy.2009.09.026.

[8] Mavromatidis G, Orehounig K, Carmeliet J. A review of uncertainty characterisation approaches for the optimal design of distributed energy systems. Renew Sustain Energy Rev 2018;88:258–77. doi:10.1016/j.rser.2018.02.021.

[9] Hussey K, Pittock J. The Energy–Water Nexus: Managing the Links between Energy and Water for a Sustainable Future. Ecol Soc 2012;17. doi:10.5751/ES-04641-170131.

[10] Evins R. Multi-level optimization of building design, energy system sizing and operation. Energy n.d. doi:10.1016/j.energy.2015.07.007.

[11] Wu R, Mavromatidis G, Orehounig K, Carmeliet J. Multiobjective optimisation of energy systems and building envelope retrofit in a residential community. Appl Energy 2017;190:634–49. doi:10.1016/j.apenergy.2016.12.161.

[12] Maroufmashat A, Elkamel A, Fowler M, Sattari S, Roshandel R, Hajimiragha A, et al. Modeling and optimization of a network of energy hubs to improve economic and emission considerations. Energy 2015;93, Part 2:2546–58. doi:10.1016/j.energy.2015.10.079.

[13] Zhou K, Yang S, Shao Z. Energy Internet: The business perspective. Appl Energy 2016;178:212–22. doi:10.1016/j.apenergy.2016.06.052.

[14] Huang AQ, Crow ML, Heydt GT, Zheng JP, Dale SJ. The Future Renewable Electric Energy Delivery and Management (FREEDM) System: The Energy Internet. Proc IEEE 2011;99:133–48. doi:10.1109/JPROC.2010.2081330.

[15] Jing R, Wang M, Liang H, Wang X, Li N, Shah N, et al. Multi-objective optimization of a neighborhood-level urban energy network: Considering Game-theory inspired multi-benefit allocation constraints. Appl Energy 2018;231:534–48. doi:10.1016/j.apenergy.2018.09.151.

[16] Sen S, Kumar V. Microgrid control: A comprehensive survey. Annu Rev Control 2018;45:118–51. doi:10.1016/j.arcontrol.2018.04.012.

[17] Hu J, Chen MZQ, Cao J, Guerrero JM. Coordinated Active Power Dispatch for a Microgrid via Distributed Lambda Iteration. IEEE J Emerg Sel Top Circuits Syst 2017;7:250–61. doi:10.1109/JETCAS.2017.2676019.

[18] Fazlollahi S, Becker G, Maréchal F. Multi-objectives, multi-period optimization of district energy systems: III. Distribution networks. Comput Chem Eng 2014;66:82–97. doi:10.1016/j.compchemeng.2014.02.018.

[19] Perera ATD, Nik VM, Mauree D, Scartezzini J-L. Electrical hubs: An effective way to integrate non-dispatchable renewable energy sources with minimum impact to the grid. Appl Energy 2017;190:232–48. doi:10.1016/j.apenergy.2016.12.127.

[20] Perera ATD, Nik VM, Mauree D, Scartezzini J-L. An integrated approach to design site specific distributed electrical hubs combining optimization, multi-criterion assessment and decision making. Energy 2017;134:103–20. doi:10.1016/j.energy.2017.06.002.

[21] Perera ATD, Coccolo S, Scartezzini J-L, Mauree D. Quantifying the impact of urban climate by extending the boundaries of urban energy system modeling. Appl Energy 2018;222:847–60. doi:10.1016/j.apenergy.2018.04.004.

[22] Moazami A, Nik VM, Carlucci S, Geving S. Impacts of future weather data typology on building energy performance – Investigating long-term patterns of climate change and extreme weather conditions. Appl Energy 2019;238:696–720. doi:10.1016/j.apenergy.2019.01.085.

[23] Nik VM. Making energy simulation easier for future climate – Synthesizing typical and extreme weather data sets out of regional climate models (RCMs). Appl Energy 2016;177:204–26. doi:10.1016/j.apenergy.2016.05.107.

[24] Nik VM. Climate Simulation of an Attic Using Future Weather Data Sets - Statistical Methods for Data Processing and Analysis. Licentiate thesis. Chalmers University of Technology, 2010.

[25] Giorgetta MA, Jungclaus J, Reick CH, Legutke S, Bader J, Böttinger M, et al. Climate and carbon cycle changes from 1850 to 2100 in MPI-ESM simulations for the Coupled Model Intercomparison Project phase 5. J Adv Model Earth Syst 2013;5:572–97. doi:10.1002/jame.20038.

[26] Nik VM. Application of typical and extreme weather data sets in the hygrothermal simulation of building components for future climate – A case study for a wooden frame wall. Energy Build 2017;154:30–45. doi:10.1016/j.enbuild.2017.08.042.

[27] BETSI. Description of the existing buildings: technical characteristics, indoor environment and energy consumption. (Bebyggelsens energianvändning, tekniska status och innemiljö). Karlskrona, Sweden: Boverket – the National Board of Housing, Building and Planning; 2009.

[28] Nik VM. Hygrothermal Simulations of Buildings Concerning Uncertainties of the Future Climate. PhD thesis. Chalmers University of Technology, 2012.

[29] Nik VM, Sasic Kalagasidis A. Impact study of the climate change on the energy performance of the building stock in Stockholm considering four climate uncertainties. Build Environ 2013;60:291–304. doi:10.1016/j.buildenv.2012.11.005.

[30] Nik VM, Mata E, Sasic Kalagasidis A, Scartezzini J-L. Effective and robust energy retrofitting measures for future climatic conditions—Reduced heating demand of Swedish households. Energy Build 2016;121:176–87. doi:10.1016/j.enbuild.2016.03.044.

[31] Nik VM, Mata É, Sasic Kalagasidis A. A statistical method for assessing retrofitting measures of buildings and ranking their robustness against climate change. Energy Build 2015;88:262–75. doi:10.1016/j.enbuild.2014.11.015.

[32] Historical Market Data n.d. http://www.nordpoolspot.com/historical-market-data/ (accessed August 15, 2017).

[33] Perera ATD, Attalage RA, Perera KKCK, Dassanayake VPC. Designing standalone hybrid energy systems minimizing initial investment, life cycle cost and pollutant emission. Energy 2013;54:220–30. doi:10.1016/j.energy.2013.03.028.

[34] Perera ATD, Attalage RA, Perera KKCK. Multi objective optimization of lifecycle cost, unmet load, and renewable energy capacity for an expansion of existing standalone internal combustion generator (ICG) systems. ASME 2011 Energy Sustain. Fuel Cell Conf., Washington, USA: n.d.

Chapter 5

[1] Asmus P. Microgrids, Virtual Power Plants and Our Distributed Energy Future. Electr J 2010;23:72–82. doi:10.1016/j.tej.2010.11.001.

[2] Chicco G, Mancarella P. Distributed multi-generation: A comprehensive view. Renew Sustain Energy Rev 2009;13:535–51. doi:10.1016/j.rser.2007.11.014.

[3] Ackermann T, Andersson G, Söder L. Distributed generation: a definition1In addition to this paper, a working paper entitled 'Distributed power generation in a deregulated market environment' is available. The aim of this working paper is to start a discussion regarding different aspects of distributed generation. This working paper can be obtained from one of the authors, Thomas Ackermann.1. Electr Power Syst Res 2001;57:195–204. doi:10.1016/S0378-7796(01)00101-8.

[4] Fathima AH, Palanisamy K. Optimization in microgrids with hybrid energy systems – A review. Renew Sustain Energy Rev 2015;45:431–46. doi:10.1016/j.rser.2015.01.059.

[5] Mavromatidis G, Orehounig K, Carmeliet J. A review of uncertainty characterisation approaches for the optimal design of distributed energy systems. Renew Sustain Energy Rev 2018;88:258–77. doi:10.1016/j.rser.2018.02.021.

[6] Agustín JLB, Lo´ pez RD. Simulation and optimization of stand-alone hybrid renewable energy systems. Renew Sustain Energy Rev 2009;13:2111–8.

[7] Baños R, Manzano-Agugliaro F, Montoya FG, Gil C, Alcayde A, Gómez J. Optimization methods applied to renewable and sustainable energy: A review. Renew Sustain Energy Rev 2011;15:1753–66. doi:10.1016/j.rser.2010.12.008.

[8] Fazlollahi S, Mandel P, Becker G, Maréchal F. Methods for multi-objective investment and operating optimization of complex energy systems. Energy 2012;45:12–22. doi:10.1016/j.energy.2012.02.046.

[9] Fazlollahi S, Becker G, Ashouri A, Maréchal F. Multi-objective, multi-period optimization of district energy systems: IV – A case study. Energy 2015;84:365–81. doi:10.1016/j.energy.2015.03.003.

[10] Evins R. Multi-level optimization of building design, energy system sizing and operation. Energy n.d. doi:10.1016/j.energy.2015.07.007.

[11] Narayan A, Ponnambalam K. Risk-averse stochastic programming approach for microgrid planning under uncertainty. Renew Energy 2017;101:399–408. doi:10.1016/j.renene.2016.08.064.

[12] Evins R. A review of computational optimisation methods applied to sustainable building design. Renew Sustain Energy Rev 2013;22:230–45. doi:10.1016/j.rser.2013.02.004.

[13] Chen X, Yang H. Integrated energy performance optimization of a passively designed high-rise residential building in different climatic zones of China. Appl Energy 2018;215:145–58. doi:10.1016/j.apenergy.2018.01.099.

[14] Kim W, Jeon Y, Kim Y. Simulation-based optimization of an integrated daylighting and HVAC system using the design of experiments method. Appl Energy 2016;162:666–74. doi:10.1016/j.apenergy.2015.10.153.

[15] Miao J-M, Cheng S-J, Wu S-J. Metamodel based design optimization approach in promoting the performance of proton exchange membrane fuel cells. Int J Hydrog Energy 2011;36:15283–94. doi:10.1016/j.ijhydene.2011.08.070.

[16] Cheng S-J, Miao J-M, Wu S-J. Use of metamodeling optimal approach promotes the performance of proton exchange membrane fuel cell (PEMFC). Appl Energy 2013;105:161–9. doi:10.1016/j.apenergy.2013.01.001.

[17] Thomsen JB, Ferri F, Kofoed JP, Black K. Cost Optimization of Mooring Solutions for Large Floating Wave Energy Converters. Energies 2018;11:159. doi:10.3390/en11010159.

[18] Halder P, Samad A. Torque and efficiency maximization for a wave energy harvesting turbine: an approach to modify multiple design variables. Int J Energy Res 2017;41:1014–28. doi:10.1002/er.3694.

[19] Halder P, Samad A, Thévenin D. Improved design of a Wells turbine for higher operating range. Renew Energy 2017;106:122–34. doi:10.1016/j.renene.2017.01.012.

[20] Kadhim HT, Rona A. Off-design performance of a liquefied natural gas plant with an axial turbine of novel endwall design. Appl Energy 2018;222:830–9. doi:10.1016/j.apenergy.2018.03.077.

[21] Kadhim HT, Rona A. Design optimization workflow and performance analysis for contoured endwalls of axial turbines. Energy 2018;149:875–89. doi:10.1016/j.energy.2018.02.001.

[22] Bornatico R, Hüssy J, Witzig A, Guzzella L. Surrogate modeling for the fast optimization of energy systems. Energy 2013;57:653–62. doi:10.1016/j.energy.2013.05.044.

[23] Sánchez A, Martín M. Optimal renewable production of ammonia from water and air. J Clean Prod 2018;178:325–42. doi:10.1016/j.jclepro.2017.12.279.

[24] Piacentino A, Cardona F. EABOT – Energetic analysis as a basis for robust optimization of trigeneration systems by linear programming. Energy Convers Manag 2008;49:3006–16. doi:10.1016/j.enconman.2008.06.015.

[25] Perera ATD, Nik VM, Mauree D, Scartezzini J-L. Electrical hubs: An effective way to integrate non-dispatchable renewable energy sources with minimum impact to the grid. Appl Energy 2017;190:232–48. doi:10.1016/j.apenergy.2016.12.127.

[26] Perera ATD, Wickremasinghe DMIJ, Mahindarathna DVS, Attalage RA, Perera KKCK, Bartholameuz EM. Sensitivity of internal combustion generator capacity in standalone hybrid energy systems. Energy 2012;39:403–11. doi:10.1016/j.energy.2011.12.039.

[27] Durisch W, Bitnar B, Mayor J-C, Kiess H, Lam K, Close J. Efficiency model for photovoltaic modules and demonstration of its application to energy yield estimation. Sol Energy Mater Sol Cells 2007;91:79–84. doi:10.1016/j.solmat.2006.05.011.

[28] Notton G, Lazarov V, Stoyanov L. Optimal sizing of a grid-connected PV system for various PV module technologies and inclinations, inverter efficiency characteristics and locations. Renew Energy 2010;35:541–54. doi:10.1016/j.renene.2009.07.013.

[29] Hocaoğlu FO, Gerek ÖN, Kurban M. A novel hybrid (wind–photovoltaic) system sizing procedure. Sol Energy 2009;83:2019–28. doi:10.1016/j.solener.2009.07.010.

[30] Diaf S, Diaf D, Belhamel M, Haddadi M, Louche A. A methodology for optimal sizing of autonomous hybrid PV/wind system. Energy Policy 2007;35:5708–18. doi:10.1016/j.enpol.2007.06.020.

[31] Perera ATD, Nik VM, Mauree D, Scartezzini J-L. An integrated approach to design site specific distributed electrical hubs combining optimization, multi-criterion assessment and decision making. Energy 2017;134:103–20. doi:10.1016/j.energy.2017.06.002.

[32] Salom J, Marszal AJ, Widén J, Candanedo J, Lindberg KB. Analysis of load match and grid interaction indicators in net zero energy buildings with simulated and monitored data. Appl Energy 2014;136:119–31. doi:10.1016/j.apenergy.2014.09.018.

[33] Verbruggen B, Driesen J. Grid Impact Indicators for Active Building Simulations. IEEE Trans Sustain Energy 2015;6:43–50. doi:10.1109/TSTE.2014.2357475.

[34] Laumanns M, Thiele L, Deb K, Zitzler E. Combining Convergence and Diversity in Evolutionary Multiobjective Optimization. Evol Comput 2002;10:263–82. doi:10.1162/106365602760234108.

[35] Deb K. An efficient constraint handling method for genetic algorithms. Comput Methods Appl Mech Eng 2000;186:311–38. doi:10.1016/S0045-7825(99)00389-8.

[36] Deb K, Beyer H-G. Self-Adaptive Genetic Algorithms with Simulated Binary Crossover. Evol Comput 2001;9:197–221. doi:10.1162/106365601750190406.

[37] Qin AK, Huang VL, Suganthan PN. Differential Evolution Algorithm With Strategy Adaptation for Global Numerical Optimization. IEEE Trans Evol Comput 2009;13:398–417. doi:10.1109/TEVC.2008.927706.

[38] Storn R, Price K. Differential Evolution – A Simple and Efficient Heuristic for global Optimization over Continuous Spaces. J Glob Optim n.d.;11:341–59. doi:10.1023/A:1008202821328.

[39] Brest J, Greiner S, Boskovic B, Mernik M, Zumer V. Self-Adapting Control Parameters in Differential Evolution: A Comparative Study on Numerical Benchmark Problems. IEEE Trans Evol Comput 2006;10:646–57. doi:10.1109/TEVC.2006.872133.

[40] Perera ATD, Madusanka AN, Attalage RA, Perera KKCK. A multi criterion analysis for renewable energy integration process of a standalone hybrid energy system with internal combustion generator. J Renew Sustain Energy 2015;7:043128. doi:10.1063/1.4928684.

Chapter 6

[1] The Global Risks Report 2016. World Econ Forum n.d. https://www.weforum.org/reports/the-global-risks-report-2016/ (accessed June 11, 2018).

[2] Field CB, Barros V, Stocker TF, Dahe Q, editors. Managing the Risks of Extreme Events and Disasters to Advance Climate Change Adaptation: Special Report of the Intergovernmental Panel on Climate Change. Cambridge: Cambridge University Press; 2012. doi:10.1017/CBO9781139177245.

[3] Brockerhoff M, Nations U. World Urbanization Prospects: The 1996 Revision. Popul Dev Rev 1998;24:883. doi:10.2307/2808041.

[4] Keirstead J, Jennings M, Sivakumar A. A review of urban energy system models: Approaches, challenges and opportunities. Renew Sustain Energy Rev 2012;16:3847–66. doi:10.1016/j.rser.2012.02.047.

[5] IEA. Energy Technology Perspectives 2016. Paris: Organisation for Economic Co-operation and Development; 2016.

[6] Perrone D, Hornberger GM. Water, food, and energy security: scrambling for resources or solutions? Wiley Interdiscip Rev Water n.d.;1:49–68. doi:10.1002/wat2.1004.

[7] Nik V. Hygrothermal Simulations of Buildings Concerning Uncertainties of the Future Climate. Chalmers University of Technology, 2012.

[8] Nik VM, Sasic Kalagasidis A. Impact study of the climate change on the energy performance of the building stock in Stockholm considering four climate uncertainties. Build Environ 2013;60:291–304. doi:10.1016/j.buildenv.2012.11.005.

[9] Auffhammer M, Baylis P, Hausman CH. Climate change is projected to have severe impacts on the frequency and intensity of peak electricity demand across the United States. Proc Natl Acad Sci 2017;114:1886–91. doi:10.1073/pnas.1613193114.

[10] Zhou Y, Clarke L, Eom J, Kyle P, Patel P, Kim SH, et al. Modeling the effect of climate change on U.S. state-level buildings energy demands in an integrated assessment framework. Appl Energy 2014;113:1077–88. doi:10.1016/j.apenergy.2013.08.034.

[11] Mirasgedis S, Sarafidis Y, Georgopoulou E, Kotroni V, Lagouvardos K, Lalas DP. Modeling framework for estimating impacts of climate change on electricity demand at regional level: Case of Greece. Energy Convers Manag 2007;48:1737–50. doi:10.1016/j.enconman.2006.10.022.

[12] Seljom P, Rosenberg E, Fidje A, Haugen JE, Meir M, Rekstad J, et al. Modelling the effects of climate change on the energy system—A case study of Norway. Energy Policy 2011;39:7310–21. doi:10.1016/j.enpol.2011.08.054.

[13] Ahmed T, Muttaqi KM, Agalgaonkar AP. Climate change impacts on electricity demand in the State of New South Wales, Australia. Appl Energy 2012;98:376–83. doi:10.1016/j.apenergy.2012.03.059.

[14] Chandramowli SN, Felder FA. Impact of climate change on electricity systems and markets – A review of models and forecasts. Sustain Energy Technol Assess 2014;5:62–74. doi:10.1016/j.seta.2013.11.003.

[15] Pryor SC, Schoof JT, Barthelmie RJ. Winds of change?: Projections of near-surface winds under climate change scenarios. Geophys Res Lett n.d.;33. doi:10.1029/2006GL026000.

[16] Sailor DJ, Smith M, Hart M. Climate change implications for wind power resources in the Northwest United States. Renew Energy 2008;33:2393–406. doi:10.1016/j.renene.2008.01.007.

[17] Kao S-C, Sale MJ, Ashfaq M, Uria Martinez R, Kaiser DP, Wei Y, et al. Projecting changes in annual hydropower generation using regional runoff data: An assessment of the United States federal hydropower plants. Energy 2015;80:239–50. doi:10.1016/j.energy.2014.11.066.

[18] Fant C, Adam Schlosser C, Strzepek K. The impact of climate change on wind and solar resources in southern Africa. Appl Energy 2016;161:556–64. doi:10.1016/j.apenergy.2015.03.042.

[19] Pryor SC, Barthelmie RJ. Climate change impacts on wind energy: A review. Renew Sustain Energy Rev 2010;14:430–7. doi:10.1016/j.rser.2009.07.028.

[20] Wang B, Ke R-Y, Yuan X-C, Wei Y-M. China's regional assessment of renewable energy vulnerability to climate change. Renew Sustain Energy Rev 2014;40:185–95. doi:10.1016/j.rser.2014.07.154.

[21] Mavromatidis G, Orehounig K, Carmeliet J. Uncertainty and global sensitivity analysis for the optimal design of distributed energy systems. Appl Energy 2018;214:219–38. doi:10.1016/j.apenergy.2018.01.062.

[22] Dowling P. The impact of climate change on the European energy system. Energy Policy 2013;60:406–17. doi:10.1016/j.enpol.2013.05.093.

[23] Perera ATD, Nik VM, Mauree D, Scartezzini J-L. Electrical hubs: An effective way to integrate non-dispatchable renewable energy sources with minimum impact to the grid. Appl Energy 2017;190:232–48. doi:10.1016/j.apenergy.2016.12.127.

[24] Perera ATD, Coccolo S, Scartezzini J-L, Mauree D. Quantifying the impact of urban climate by extending the boundaries of urban energy system modeling. Appl Energy 2018;222:847–60. doi:10.1016/j.apenergy.2018.04.004.

[25] Sharifi A, Yamagata Y. Principles and criteria for assessing urban energy resilience: A literature review. Renew Sustain Energy Rev 2016;60:1654–77. doi:10.1016/j.rser.2016.03.028.

[26] Rutherford J, Coutard O. Urban Energy Transitions: Places, Processes and Politics of Socio-technical Change. Urban Stud 2014;51:1353–77. doi:10.1177/0042098013500090.

[27] Grubler A, Bai X, Büttner T, Dhakal S, Fisk DJ, Ichinose T, et al. Chapter 18: Urban energy systems. In: Team GW, editor. Glob. Energy Assess. Sustain. Future, Pp.1307-1400 (October 2012): Cambridge University Press and IIASA; 2012.

[28] Molyneaux L, Wagner L, Froome C, Foster J. Resilience and electricity systems: A comparative analysis. Energy Policy 2012;47:188–201. doi:10.1016/j.enpol.2012.04.057.

[29] Maliszewski PJ, Perrings C. Factors in the resilience of electrical power distribution infrastructures. Appl Geogr 2012;32:668–79. doi:10.1016/j.apgeog.2011.08.001.

[30] Roege PE, Collier ZA, Mancillas J, McDonagh JA, Linkov I. Metrics for energy resilience. Energy Policy 2014;72:249–56. doi:10.1016/j.enpol.2014.04.012.

[31] Hughes L. The effects of event occurrence and duration on resilience and adaptation in energy systems. Energy 2015;84:443–54. doi:10.1016/j.energy.2015.03.010.

[32] Van Nostrand JM. Keeping the lights on during Superstorm Sandy: climate change adaptation and the resiliency benefits of distributed generation. N Y Univ Environ Law J 2015;23:92–156.

[33] Hussey K, Pittock J. The Energy–Water Nexus: Managing the Links between Energy and Water for a Sustainable Future. Ecol Soc 2012;17. doi:10.5751/ES-04641-170131.

[34] Panteli M, Mancarella P. Influence of extreme weather and climate change on the resilience of power systems: Impacts and possible mitigation strategies. Electr Power Syst Res 2015;127:259–70. doi:10.1016/j.epsr.2015.06.012.

[35] Making the energy sector more resilient to climate change. IEA Webstore n.d. https://webstore.iea.org/making-the-energy-sector-more-resilient-to-climate-change (accessed May 25, 2018).

[36] IPCC Fifth Assessment Synthesis Report. IPCC 5th Assess Synth Rep n.d. http://ar5-syr.ipcc.ch/ (accessed May 25, 2018).

[37] Soroudi A, Amraee T. Decision making under uncertainty in energy systems: State of the art. Renew Sustain Energy Rev 2013;28:376–84. doi:10.1016/j.rser.2013.08.039.

[38] Mavromatidis G, Orehounig K, Carmeliet J. A review of uncertainty characterisation approaches for the optimal design of distributed energy systems. Renew Sustain Energy Rev 2018;88:258–77. doi:10.1016/j.rser.2018.02.021.

[39] Zheng QP, Wang J, Liu AL. Stochastic Optimization for Unit Commitment #x2014;A Review. IEEE Trans Power Syst 2015;30:1913–24. doi:10.1109/TPWRS.2014.2355204.

[40] Narayan A, Ponnambalam K. Risk-averse stochastic programming approach for microgrid planning under uncertainty. Renew Energy 2017;101:399–408. doi:10.1016/j.renene.2016.08.064.

[41] Rezvan AT, Gharneh NS, Gharehpetian GB. Optimization of distributed generation capacities in buildings under uncertainty in load demand. Energy Build 2013;57:58–64. doi:10.1016/j.enbuild.2012.10.031.

[42] Sharafi M, ElMekkawy TY. Stochastic optimization of hybrid renewable energy systems using sampling average method. Renew Sustain Energy Rev 2015;52:1668–79. doi:10.1016/j.rser.2015.08.010.

[43] Urbanucci L, Testi D. Optimal integrated sizing and operation of a CHP system with Monte Carlo risk analysis for long-term uncertainty in energy demands. Energy Convers Manag 2018;157:307–16. doi:10.1016/j.enconman.2017.12.008.

[44] Gu W, Tang Y, Peng S, Wang D, Sheng W, Liu K. Optimal configuration and analysis of combined cooling, heating, and power microgrid with thermal storage tank under uncertainty. J Renew Sustain Energy 2015;7:013104. doi:10.1063/1.4904434.

[45] Duan Z, Yan Y, Yan X, Liao Q, Zhang W, Liang Y, et al. An MILP Method for Design of Distributed Energy Resource System Considering Stochastic Energy Supply and Demand. Energies 2017;11:22. doi:10.3390/en11010022.

[46] Yang Y, Zhang S, Xiao Y. Optimal design of distributed energy resource systems based on two-stage stochastic programming. Appl Therm Eng 2017;110:1358–70. doi:10.1016/j.applthermaleng.2016.09.049.

[47] Pazouki S, Haghifam M-R. Optimal planning and scheduling of energy hub in presence of wind, storage and demand response under uncertainty. Int J Electr Power Energy Syst 2016;80:219–39. doi:10.1016/j.ijepes.2016.01.044.

[48] Fuentes-Cortés LF, Santibañez-Aguilar JE, Ponce-Ortega JM. Optimal design of residential cogeneration systems under uncertainty. Comput Chem Eng 2016;88:86–102. doi:10.1016/j.compchemeng.2016.02.008.

[49] Akbari K, Nasiri MM, Jolai F, Ghaderi SF. Optimal investment and unit sizing of distributed energy systems under uncertainty: A robust optimization approach. Energy Build 2014;85:275–86. doi:10.1016/j.enbuild.2014.09.009.

[50] Akbari K, Jolai F, Ghaderi SF. Optimal design of distributed energy system in a neighborhood under uncertainty. Energy 2016;116:567–82. doi:10.1016/j.energy.2016.09.083.

[51] Billionnet A, Costa M-C, Poirion P-L. Robust optimal sizing of a hybrid energy stand-alone system. Eur J Oper Res 2016;254:565–75. doi:10.1016/j.ejor.2016.03.013.

[52] Mavromatidis G, Orehounig K, Carmeliet J. Comparison of alternative decision-making criteria in a two-stage stochastic program for the design of distributed energy systems under uncertainty. Energy 2018;156:709–24. doi:10.1016/j.energy.2018.05.081.

[53] Zhao C, Guan Y. Unified Stochastic and Robust Unit Commitment. IEEE Trans Power Syst 2013;28:3353–61. doi:10.1109/TPWRS.2013.2251916.

[54] Bagheri A, Zhao C, Guo Y. Data-driven chance-constrained stochastic unit commitment under wind power uncertainty. 2017 IEEE Power Energy Soc. Gen. Meet., 2017, p. 1–5. doi:10.1109/PESGM.2017.8273948.

[55] Liu G, Xu Y, Tomsovic K. Bidding Strategy for Microgrid in Day-Ahead Market Based on Hybrid Stochastic/Robust Optimization. IEEE Trans Smart Grid 2016;7:227–37. doi:10.1109/TSG.2015.2476669.

[56] Baringo A, Baringo L. A Stochastic Adaptive Robust Optimization Approach for the Offering Strategy of a Virtual Power Plant. IEEE Trans Power Syst 2017;32:3492–504. doi:10.1109/TPWRS.2016.2633546.

[57] Fanzeres B, Street A, Barroso LA. Contracting Strategies for Renewable Generators: A Hybrid Stochastic and Robust Optimization Approach. IEEE Trans Power Syst 2015;30:1825–37. doi:10.1109/TPWRS.2014.2346988.

[58] Ji L, Niu DX, Huang GH. An inexact two-stage stochastic robust programming for residential micro-grid management-based on random demand. Energy 2014;67:186–99. doi:10.1016/j.energy.2014.01.099.

[59] The surface processes of the Rossby Centreregional atmospheric climate model (RCA4) | SMHI n.d. https://www.smhi.se/en/publications/the-surface-processes-of-the-rossby-centreregional-atmospheric-climate-model-rca4-1.89801 (accessed June 11, 2018).

[60] Nik VM. Application of typical and extreme weather data sets in the hygrothermal simulation of building components for future climate – A case study for a wooden frame wall. Energy Build 2017;154:30–45. doi:10.1016/j.enbuild.2017.08.042.

[61] Kjellström E, Nikulin G, Hansson U, Strandberg G, Ullerstig A. 21st century changes in the European climate: uncertainties derived from an ensemble of regional climate model simulations. Tellus A n.d.;63:24–40. doi:10.1111/j.1600-0870.2010.00475.x.

[62] Belcher S, Hacker J, Powell D. Constructing design weather data for future climates. Build Serv Eng Res Technol 2005;26:49–61. doi:10.1191/0143624405bt112oa.

[63] Solomon S, Intergovernmental Panel on Climate Change, Intergovernmental Panel on Climate Change, editors. Climate change 2007: the physical science basis: contribution of Working Group I to the Fourth Assessment Report of the Intergovernmental Panel on Climate Change. Cambridge ; New York: Cambridge University Press; 2007.

[64] Christensen JH, Kjellström E, Giorgi F, Lenderink G, Rummukainen M. Weight assignment in regional climate models. Clim Res 2010;44:179–94. doi:10.3354/cr00916.

[65] NIK VM. Climate Simulation of an Attic Using Future Weather Data Sets n.d.:128.

[66] Giorgetta MA, Jungclaus J, Reick CH, Legutke S, Bader J, Böttinger M, et al. Climate and carbon cycle changes from 1850 to 2100 in MPI-ESM simulations for the Coupled Model Intercomparison Project phase 5. J Adv Model Earth Syst n.d.;5:572–97. doi:10.1002/jame.20038.

[67] Nik VM. Making energy simulation easier for future climate – Synthesizing typical and extreme weather data sets out of regional climate models (RCMs). Appl Energy 2016;177:204–26. doi:10.1016/j.apenergy.2016.05.107.

[68] Generation of a Typical Meteorological Year. | National Technical Reports Library - NTIS n.d. https://ntrl.ntis.gov/NTRL/dashboard/searchResults/titleDetail/SAND781096C.xhtml (accessed June 11, 2018).

[69] Historical Market Data n.d. http://www.nordpoolspot.com/historical-market-data/ (accessed August 15, 2017).

[70] Geidl M, Koeppel G, Favre-Perrod P, Klockl B, Andersson G, Frohlich K. Energy hubs for the future. IEEE Power Energy Mag 2007;5:24–30. doi:10.1109/MPAE.2007.264850.

[71] Geidl M, Andersson G. Optimal Power Flow of Multiple Energy Carriers. IEEE Trans Power Syst 2007;22:145–55. doi:10.1109/TPWRS.2006.888988.

[72] Perera ATD, Mauree D, Scartezzini JL, Nik VM. Optimum design and control of grid integrated electrical hubs considering lifecycle cost and emission. 2016 IEEE Int. Energy Conf. ENERGYCON, 2016, p. 1–6. doi:10.1109/ENERGYCON.2016.7513968.

[73] Perera ATD, Nik VM, Mauree D, Scartezzini J-L. An integrated approach to design site specific distributed electrical hubs combining optimization, multi-criterion assessment and decision making. Energy 2017;134:103–20. doi:10.1016/j.energy.2017.06.002.

[74] Guen ML, Mosca L, Perera ATD, Coccolo S, Mohajeri N, Scartezzini J-L. Improving the energy sustainability of a Swiss village through building renovation and renewable energy integration. Energy Build 2018;158:906–23. doi:10.1016/j.enbuild.2017.10.057.

[75] Notton G, Lazarov V, Stoyanov L. Optimal sizing of a grid-connected PV system for various PV module technologies and inclinations, inverter efficiency characteristics and locations. Renew Energy 2010;35:541–54. doi:10.1016/j.renene.2009.07.013.

[76] Thapar V, Agnihotri G, Sethi VK. Critical analysis of methods for mathematical modelling of wind turbines. Renew Energy 2011;36:3166–77. doi:10.1016/j.renene.2011.03.016.

[77] Perera ATD, Wickremasinghe DMIJ, Mahindarathna DVS, Attalage RA, Perera KKCK, Bartholameuz EM. Determining wind turbine capacity for expansion of off grid Internal Combustion Generators (ICG) system; why it bec o mes challenging? 2010 IEEE Int. Conf. Sustain. Energy Technol. ICSET, 2010, p. 1–5. doi:10.1109/ICSET.2010.5684944.

[78] Perera ATD, Attalage RA, Perera KKCK, Dassanayake VPC. Designing standalone hybrid energy systems minimizing initial investment, life cycle cost and pollutant emission. Energy 2013;54:220–30. doi:10.1016/j.energy.2013.03.028.

[79] Perera ATD, Attalage RA, Perera KKCK, Dassanayake VPC. A hybrid tool to combine multi-objective optimization and multi-criterion decision making in designing standalone hybrid energy systems. Appl Energy 2013;107:412–25. doi:10.1016/j.apenergy.2013.02.049.

[80] Perera ATD, Madusanka AN, Attalage RA, Perera KKCK. A multi criterion analysis for renewable energy integration process of a standalone hybrid energy system with internal combustion generator. J Renew Sustain Energy 2015;7:043128. doi:10.1063/1.4928684.

[81] Celik AN. Effect of different load profiles on the loss-of-load probability of stand-alone photovoltaic systems. Renew Energy 2007;32:2096–115. doi:10.1016/j.renene.2006.11.002.

[82] Abbes D, Martinez A, Champenois G. Life cycle cost, embodied energy and loss of power supply probability for the optimal design of hybrid power systems. Math Comput Simul 2014;98:46–62. doi:10.1016/j.matcom.2013.05.004.

[83] Hadj Arab A, Chenlo F, Benghanem M. Loss-of-load probability of photovoltaic water pumping systems. Sol Energy 2004;76:713–23. doi:10.1016/j.solener.2004.01.006.

[84] Heydari A, Askarzadeh A. Optimization of a biomass-based photovoltaic power plant for an off-grid application subject to loss of power supply probability concept. Appl Energy 2016;165:601–11. doi:10.1016/j.apenergy.2015.12.095.

[85] Agustín JLB, Lo´ pez RD. Simulation and optimization of stand-alone hybrid renewable energy systems. Renew Sustain Energy Rev 2009;13:2111–8.

[86] Baños R, Manzano-Agugliaro F, Montoya FG, Gil C, Alcayde A, Gómez J. Optimization methods applied to renewable and sustainable energy: A review. Renew Sustain Energy Rev 2011;15:1753–66. doi:10.1016/j.rser.2010.12.008.

[87] Bernalagustin J, Dufolopez R. Efficient design of hybrid renewable energy systems using evolutionary algorithms. Energy Convers Manag 2009;50:479–89. doi:10.1016/j.enconman.2008.11.007.

[88] Fouskakis D, Draper D. Stochastic Optimization: a Review. Int Stat Rev n.d.;70:315–49. doi:10.1111/j.1751-5823.2002.tb00174.x.

[89] Beyer H-G, Sendhoff B. Robust optimization – A comprehensive survey. Comput Methods Appl Mech Eng 2007;196:3190–218. doi:10.1016/j.cma.2007.03.003.

[90] Deb K. An efficient constraint handling method for genetic algorithms. Comput Methods Appl Mech Eng 2000;186:311–38. doi:10.1016/S0045-7825(99)00389-8.

[91] Deb K, Beyer H-G. Self-Adaptive Genetic Algorithms with Simulated Binary Crossover. Evol Comput 2001;9:197–221. doi:10.1162/106365601750190406.

Chapter 7

[1] G. Sansavini, R. Piccinelli, L.R. Golea, E. Zio, A stochastic framework for uncertainty analysis in electric power transmission systems with wind generation, Renew. Energy. 64 (2014) 71–81. doi:10.1016/j.renene.2013.11.002.

[2] F. Ueckerdt, R. Brecha, G. Luderer, P. Sullivan, E. Schmid, N. Bauer, D. Böttger, R. Pietzcker, Representing power sector variability and the integration of variable renewables in long-term energy-economy models using residual load duration curves, Energy. 90, Part 2 (2015) 1799–1814. doi:10.1016/j.energy.2015.07.006.

[3] Eastern Renewable Generation Integration Study | Grid Modernization | NREL, (n.d.). https://www.nrel.gov/grid/ergis.html (accessed September 5, 2017).

[4] Nigel Slack, The Flexibility of Manufacturing Systems, Int. J. Oper. Prod. Manag. 7 (1987) 35–45. doi:10.1108/eb054798.

[5] A.K. Sethi, S.P. Sethi, Flexibility in manufacturing: A survey, Int. J. Flex. Manuf. Syst. 2 (1990) 289–328. doi:10.1007/BF00186471.

[6] S.K. Das, The measurement of flexibility in manufacturing systems, Int. J. Flex. Manuf. Syst. 8 (n.d.) 67–93. doi:10.1007/BF00167801.

[7] A. Chen, P. Kasikitwiwat, Modeling capacity flexibility of transportation networks, Transp. Res. Part Policy Pract. 45 (2011) 105–117. doi:10.1016/j.tra.2010.11.003.

[8] E.K. Morlok, D.J. Chang, Measuring capacity flexibility of a transportation system, Transp. Res. Part Policy Pract. 38 (2004) 405–420. doi:10.1016/j.tra.2004.03.001.

[9] J.L. Gifford, Adaptability and flexibility in urban transportation policy and planning, Technol. Forecast. Soc. Change. 45 (1994) 111–117. doi:10.1016/0040-1625(94)90088-4.

[10] G. Chryssolouris, Flexibility and Its Measurement, CIRP Ann. - Manuf. Technol. 45 (1996) 581–587. doi:10.1016/S0007-8506(07)60512-5.

[11] R. De Coninck, L. Helsen, Quantification of flexibility in buildings by cost curves – Methodology and application, Appl. Energy. 162 (2016) 653–665. doi:10.1016/j.apenergy.2015.10.114.

[12] M. Welsch, P. Deane, M. Howells, B. Ó Gallachóir, F. Rogan, M. Bazilian, H.-H. Rogner, Incorporating flexibility requirements into long-term energy system models – A case study on high levels of renewable electricity penetration in Ireland, Appl. Energy. 135 (2014) 600–615. doi:10.1016/j.apenergy.2014.08.072.

[13] M.I. Alizadeh, M. Parsa Moghaddam, N. Amjady, P. Siano, M.K. Sheikh-El-Eslami, Flexibility in future power systems with high renewable penetration: A review, Renew. Sustain. Energy Rev. 57 (2016) 1186–1193. doi:10.1016/j.rser.2015.12.200.

[14] P.-H. Li, S. Pye, Assessing the benefits of demand-side flexibility in residential and transport sectors from an integrated energy systems perspective, Appl. Energy. 228 (2018) 965–979. doi:10.1016/j.apenergy.2018.06.153.

[15] G. Oluleye, J. Allison, G. Hawker, N. Kelly, A.D. Hawkes, A two-step optimization model for quantifying the flexibility potential of power-to-heat systems in dwellings, Appl. Energy. 228 (2018) 215–228. doi:10.1016/j.apenergy.2018.06.072.

[16] P.D. Lund, J. Lindgren, J. Mikkola, J. Salpakari, Review of energy system flexibility measures to enable high levels of variable renewable electricity, Renew. Sustain. Energy Rev. 45 (2015) 785–807. doi:10.1016/j.rser.2015.01.057.

[17] I. Alaperä, S. Honkapuro, J. Paananen, Data centers as a source of dynamic flexibility in smart girds, Appl. Energy. 229 (2018) 69–79. doi:10.1016/j.apenergy.2018.07.056.

[18] A. Lüth, J.M. Zepter, P. Crespo del Granado, R. Egging, Local electricity market designs for peer-to-peer trading: The role of battery flexibility, Appl. Energy. 229 (2018) 1233–1243. doi:10.1016/j.apenergy.2018.08.004.

[19] A.T.D. Perera, V.M. Nik, D. Mauree, J.-L. Scartezzini, Electrical hubs: An effective way to integrate non-dispatchable renewable energy sources with minimum impact to the grid, Appl. Energy. 190 (2017) 232–248. doi:10.1016/j.apenergy.2016.12.127.

[20] A.T.D. Perera, D. Mauree, J.L. Scartezzini, V.M. Nik, Optimum design and control of grid integrated electrical hubs considering lifecycle cost and emission, in: 2016 IEEE Int. Energy Conf. ENERGYCON, 2016: pp. 1–6. doi:10.1109/ENERGYCON.2016.7513968.

[21] S. Stinner, K. Huchtemann, D. Müller, Quantifying the operational flexibility of building energy systems with thermal energy storages, Appl. Energy. 181 (2016) 140–154. doi:10.1016/j.apenergy.2016.08.055.

[22] T. Nuytten, B. Claessens, K. Paredis, J. Van Bael, D. Six, Flexibility of a combined heat and power system with thermal energy storage for district heating, Appl. Energy. 104 (2013) 583–591. doi:10.1016/j.apenergy.2012.11.029.

[23] O. Garbrecht, M. Bieber, R. Kneer, Increasing fossil power plant flexibility by integrating molten-salt thermal storage, Energy. 118 (2017) 876–883. doi:10.1016/j.energy.2016.10.108.

[24] J. Le Dréau, P. Heiselberg, Energy flexibility of residential buildings using short term heat storage in the thermal mass, Energy. 111 (2016) 991–1002. doi:10.1016/j.energy.2016.05.076.

[25] J. Salpakari, T. Rasku, J. Lindgren, P.D. Lund, Flexibility of electric vehicles and space heating in net zero energy houses: an optimal control model with thermal dynamics and battery degradation, Appl. Energy. 190 (2017) 800–812. doi:10.1016/j.apenergy.2017.01.005.

[26] A. Schuller, C.M. Flath, S. Gottwalt, Quantifying load flexibility of electric vehicles for renewable energy integration, Appl. Energy. 151 (2015) 335–344. doi:10.1016/j.apenergy.2015.04.004.

[27] J. Després, S. Mima, A. Kitous, P. Criqui, N. Hadjsaid, I. Noirot, Storage as a flexibility option in power systems with high shares of variable renewable energy sources: a POLES-based analysis, Energy Econ. 64 (2017) 638–650. doi:10.1016/j.eneco.2016.03.006.

[28] D.P. Schlachtberger, S. Becker, S. Schramm, M. Greiner, Backup flexibility classes in emerging large-scale renewable electricity systems, Energy Convers. Manag. 125 (2016) 336–346. doi:10.1016/j.enconman.2016.04.020.

[29] A. Soroudi, A. Rabiee, A. Keane, Distribution networks' energy losses versus hosting capacity of wind power in the presence of demand flexibility, Renew. Energy. 102 (2017) 316–325. doi:10.1016/j.renene.2016.10.051.

[30] S.O. Ottesen, A. Tomasgard, A stochastic model for scheduling energy flexibility in buildings, Energy. 88 (2015) 364–376. doi:10.1016/j.energy.2015.05.049.

[31] K. Spiliotis, A.I. Ramos Gutierrez, R. Belmans, Demand flexibility versus physical network expansions in distribution grids, Appl. Energy. 182 (2016) 613–624. doi:10.1016/j.apenergy.2016.08.145.

[32] H. Kondziella, T. Bruckner, Flexibility requirements of renewable energy based electricity systems – a review of research results and methodologies, Renew. Sustain. Energy Rev. 53 (2016) 10–22. doi:10.1016/j.rser.2015.07.199.

[33] A. Ulbig, G. Andersson, Analyzing operational flexibility of electric power systems, Int. J. Electr. Power Energy Syst. 72 (2015) 155–164. doi:10.1016/j.ijepes.2015.02.028.

[34] V. Oree, S.Z. Sayed Hassen, A composite metric for assessing flexibility available in conventional generators of power systems, Appl. Energy. 177 (2016) 683–691. doi:10.1016/j.apenergy.2016.05.138.

[35] W.B. Powell, S. Meisel, Tutorial on Stochastic Optimization in Energy #x2014;Part I: Modeling and Policies, IEEE Trans. Power Syst. 31 (2016) 1459–1467. doi:10.1109/TPWRS.2015.2424974.

[36] R. Evins, Multi-level optimization of building design, energy system sizing and operation, Energy. (n.d.). doi:10.1016/j.energy.2015.07.007.

[37] M. Geidl, G. Andersson, Optimal Power Flow of Multiple Energy Carriers, IEEE Trans. Power Syst. 22 (2007) 145–155. doi:10.1109/TPWRS.2006.888988.

[38] K. Hemmes, J.L. Zachariah-Wolf, M. Geidl, G. Andersson, Towards multi-source multi-product energy systems, Int. J. Hydrog. Energy. 32 (2007) 1332–1338. doi:10.1016/j.ijhydene.2006.10.013.

[39] V.M. Nik, Hygrothermal Simulations of Buildings Concerning Uncertainties of the Future Climate, PhD thesis, Chalmers University of Technology, 2012. http://publications.lib.chalmers.se/records/fulltext/159222.pdf.

[40] V.M. Nik, A. Sasic Kalagasidis, Impact study of the climate change on the energy performance of the building stock in Stockholm considering four climate uncertainties, Build. Environ. 60 (2013) 291–304. doi:10.1016/j.buildenv.2012.11.005.

[41] BETSI. Description of the existing buildings: technical characteristics, indoor environment and energy consumption. (Bebyggelsens energianvändning, tekniska status och innemiljö), Boverket – the National Board of Housing, Building and Planning, Karlskrona, Sweden, 2009.

[42] Historical Market Data, (n.d.). http://www.nordpoolspot.com/historical-market-data/ (accessed August 15, 2017).

[43] V.M. Nik, E. Mata, A. Sasic Kalagasidis, J.-L. Scartezzini, Effective and robust energy retrofitting measures for future climatic conditions—Reduced heating demand of Swedish households, Energy Build. 121 (2016) 176–187. doi:10.1016/j.enbuild.2016.03.044.

[44] V.M. Nik, É. Mata, A. Sasic Kalagasidis, A statistical method for assessing retrofitting measures of buildings and ranking their robustness against climate change, Energy Build. 88 (2015) 262–275. doi:10.1016/j.enbuild.2014.11.015.

[45] A.T.D. Perera, D.M.I.J. Wickremasinghe, D.V.S. Mahindarathna, R.A. Attalage, K.K.C.K. Perera, E.M. Bartholameuz, Sensitivity of internal combustion generator capacity in standalone hybrid energy systems, Energy. 39 (2012) 403–411. doi:10.1016/j.energy.2011.12.039.

[46] W. Durisch, B. Bitnar, J.-C. Mayor, H. Kiess, K. Lam, J. Close, Efficiency model for photovoltaic modules and demonstration of its application to energy yield estimation, Sol. Energy Mater. Sol. Cells. 91 (2007) 79–84. doi:10.1016/j.solmat.2006.05.011.

[47] A.T.D. Perera, R.A. Attalage, K.K.C.K. Perera, V.P.C. Dassanayake, Designing standalone hybrid energy systems minimizing initial investment, life cycle cost and pollutant emission, Energy. 54 (2013) 220–230. doi:10.1016/j.energy.2013.03.028.

[48] A.T.D. Perera, A.N. Madusanka, R.A. Attalage, K.K.C.K. Perera, A multi criterion analysis for renewable energy integration process of a standalone hybrid energy system with internal combustion generator, J. Renew. Sustain. Energy. 7 (2015) 043128. doi:10.1063/1.4928684.

[49] A. Rezvani, A. Khalili, A. Mazareie, M. Gandomkar, Modeling, control, and simulation of grid connected intelligent hybrid battery/photovoltaic system using new hybrid fuzzy-neural method, ISA Trans. (n.d.). doi:10.1016/j.isatra.2016.02.013.

[50] S. Safari, M.M. Ardehali, M.J. Sirizi, Particle swarm optimization based fuzzy logic controller for autonomous green power energy system with hydrogen storage, Energy Convers. Manag. 65 (2013) 41–49. doi:10.1016/j.enconman.2012.08.012.

[51] S. Berrazouane, K. Mohammedi, Parameter optimization via cuckoo optimization algorithm of fuzzy controller for energy management of a hybrid power system, Energy Convers. Manag. 78 (2014) 652–660. doi:10.1016/j.enconman.2013.11.018.

[52] M.H. Athari, M.M. Ardehali, Operational performance of energy storage as function of electricity prices for on-grid hybrid renewable energy system by optimized fuzzy logic controller, Renew. Energy. 85 (2016) 890–902. doi:10.1016/j.renene.2015.07.055.

[53] L. Olatomiwa, S. Mekhilef, M.S. Ismail, M. Moghavvemi, Energy management strategies in hybrid renewable energy systems: A review, Renew. Sustain. Energy Rev. 62 (2016) 821–835. doi:10.1016/j.rser.2016.05.040.

[54] A.T.D. Perera, V.M. Nik, D. Mauree, J.-L. Scartezzini, An integrated approach to design site specific distributed electrical hubs combining optimization, multi-criterion assessment and decision making, Energy. 134 (2017) 103–120. doi:10.1016/j.energy.2017.06.002.

[55] J. Salom, A.J. Marszal, J. Widén, J. Candanedo, K.B. Lindberg, Analysis of load match and grid interaction indicators in net zero energy buildings with simulated and monitored data, Appl. Energy. 136 (2014) 119–131. doi:10.1016/j.apenergy.2014.09.018.

[56] A. Narayan, K. Ponnambalam, Risk-averse stochastic programming approach for microgrid planning under uncertainty, Renew. Energy. 101 (2017) 399–408. doi:10.1016/j.renene.2016.08.064.

[57] A.T. Rezvan, N.S. Gharneh, G.B. Gharehpetian, Optimization of distributed generation capacities in buildings under uncertainty in load demand, Energy Build. 57 (2013) 58–64. doi:10.1016/j.enbuild.2012.10.031.

[58] M. Sharafi, T.Y. ElMekkawy, Stochastic optimization of hybrid renewable energy systems using sampling average method, Renew. Sustain. Energy Rev. 52 (2015) 1668–1679. doi:10.1016/j.rser.2015.08.010.

[59] L. Urbanucci, D. Testi, Optimal integrated sizing and operation of a CHP system with Monte Carlo risk analysis for long-term uncertainty in energy demands, Energy Convers. Manag. 157 (2018) 307–316. doi:10.1016/j.enconman.2017.12.008.

[60] W. Gu, Y. Tang, S. Peng, D. Wang, W. Sheng, K. Liu, Optimal configuration and analysis of combined cooling, heating, and power microgrid with thermal storage tank under uncertainty, J. Renew. Sustain. Energy. 7 (2015) 013104. doi:10.1063/1.4904434.

[61] * M.I.M.W., Measuring machine and product mix flexibilities of a manufacturing system, Int. J. Prod. Res. 43 (2005) 3773–3786. doi:10.1080/00207540500147091.

[62] James M.J. Cheng, John E.L. Simmons, ames M. Ritchie, Manufacturing system flexibility: the “capability and capacity” approach, Integr. Manuf. Syst. 8 (1997) 147–158. doi:10.1108/09576069710181965.

[63] L.A. Zadeh, Fuzzy logic = computing with words, IEEE Trans. Fuzzy Syst. 4 (1996) 103–111. doi:10.1109/91.493904.

[64] A.T.D. Perera, R.A. Attalage, K.K.C.K. Perera, V.P.C. Dassanayake, A hybrid tool to combine multi-objective optimization and multi-criterion decision making in designing standalone hybrid energy systems, Appl. Energy. 107 (2013) 412–425. doi:10.1016/j.apenergy.2013.02.049.

[65] P. Bajpai, V. Dash, Hybrid renewable energy systems for power generation in stand-alone applications: A review, Renew. Sustain. Energy Rev. 16 (2012) 2926–2939. doi:10.1016/j.rser.2012.02.009.

[66] O. Erdinc, M. Uzunoglu, Optimum design of hybrid renewable energy systems: Overview of different approaches, Renew. Sustain. Energy Rev. 16 (2012) 1412–1425. doi:10.1016/j.rser.2011.11.011.

[67] J.L. Bernal-Agustín, R. Dufo-López, Efficient design of hybrid renewable energy systems using evolutionary algorithms, Energy Convers. Manag. 50 (2009) 479–489. doi:10.1016/j.enconman.2008.11.007.

[68] J.D. Owens, M. Houston, D. Luebke, S. Green, J.E. Stone, J.C. Phillips, GPU Computing, Proc. IEEE. 96 (2008) 879–899. doi:10.1109/JPROC.2008.917757.

[69] E. Alba, M. Tomassini, Parallelism and evolutionary algorithms, IEEE Trans. Evol. Comput. 6 (2002) 443–462. doi:10.1109/TEVC.2002.800880.

[70] Y. Zhang, S. Wang, G. Ji, A Comprehensive Survey on Particle Swarm Optimization Algorithm and Its Applications, Math. Probl. Eng. (2015). doi:10.1155/2015/931256.

[71] M. Laumanns, L. Thiele, K. Deb, E. Zitzler, Combining Convergence and Diversity in Evolutionary Multiobjective Optimization, Evol. Comput. 10 (2002) 263–282. doi:10.1162/106365602760234108.

[72] A.T.D. Perera, R.A. Attalage, K.K.C.K. Perera, V.P.C. Dassanayake, Converting existing Internal Combustion Generator (ICG) systems into HESs in standalone applications, Energy Convers. Manag. 74 (2013) 237–248. doi:10.1016/j.enconman.2013.05.022.

[73] J. Dupačová, N. Gröwe-Kuska, W. Römisch, Scenario reduction in stochastic programming, Math. Program. 95 (2003) 493–511. doi:10.1007/s10107-002-0331-0.

[74] A. Konak, D.W. Coit, A.E. Smith, Multi-objective optimization using genetic algorithms: A tutorial, Reliab. Eng. Syst. Saf. 91 (2006) 992–1007. doi:10.1016/j.ress.2005.11.018.

[75] A.T.D. Perera, S. Coccolo, J.-L. Scartezzini, D. Mauree, Quantifying the impact of urban climate by extending the boundaries of urban energy system modeling, Appl. Energy. 222 (2018) 847–860. doi:10.1016/j.apenergy.2018.04.004.

[76] J.-H. Shi, X.-J. Zhu, G.-Y. Cao, Design and techno-economical optimization for stand-alone hybrid power systems with multi-objective evolutionary algorithms, Int. J. Energy Res. 31 (2007) 315–328. doi:10.1002/er.1247.

[77] M.S. Ismail, M. Moghavvemi, T.M.I. Mahlia, K.M. Muttaqi, S. Moghavvemi, Effective utilization of excess energy in standalone hybrid renewable energy systems for improving comfort ability and reducing cost of energy: A review and analysis, Renew. Sustain. Energy Rev. 42 (2015) 726–734. doi:10.1016/j.rser.2014.10.051.

Chapter 8

[1] David Satterthwaite, “The implications of population growth and urbanization for climate change,” Environ. Urban., vol. 21, no. 2, pp. 545–567, Oct. 2009.

[2] R. Madlener and Y. Sunak, “Impacts of urbanization on urban structures and energy demand: What can we learn for urban energy planning and urbanization management?,” Sustain. Cities Soc., vol. 1, no. 1, pp. 45–53, Feb. 2011.

[3] H. Lund and B. V. Mathiesen, “Energy system analysis of 100% renewable energy systems—The case of Denmark in years 2030 and 2050,” Energy, vol. 34, no. 5, pp. 524–531, May 2009.

[4] B. Ćosić, G. Krajačić, and N. Duić, “A 100% renewable energy system in the year 2050: The case of Macedonia,” Energy, vol. 48, no. 1, pp. 80–87, Dec. 2012.

[5] M. Amado, F. Poggi, and A. R. Amado, “Energy efficient city: A model for urban planning,” Sustain. Cities Soc., vol. 26, no. Supplement C, pp. 476–485, Oct. 2016.

[6] Z. Shi, J. A. Fonseca, and A. Schlueter, “A review of simulation-based urban form generation and optimization for energy-driven urban design,” Build. Environ., vol. 121, no. Supplement C, pp. 119–129, Aug. 2017.

[7] N. Mohajeri, G. Upadhyay, A. Gudmundsson, D. Assouline, J. Kämpf, and J.-L. Scartezzini, “Effects of urban compactness on solar energy potential,” Renew. Energy, vol. 93, pp. 469–482, Aug. 2016.

[8] S. Fazlollahi, G. Becker, A. Ashouri, and F. Maréchal, “Multi-objective, multi-period optimization of district energy systems: IV – A case study,” Energy, vol. 84, pp. 365–381, May 2015.

[9] G. Mavromatidis, K. Orehounig, and J. Carmeliet, “Evaluation of photovoltaic integration potential in a village,” Sol. Energy, vol. 121, pp. 152–168, Nov. 2015.

[10] K. Orehounig, G. Mavromatidis, R. Evins, V. Dorer, and J. Carmeliet, “Towards an energy sustainable community: An energy system analysis for a village in Switzerland,” Energy Build., vol. 84, pp. 277–286, Dec. 2014.

[11] H. Karunathilake, P. Perera, R. Ruparathna, K. Hewage, and R. Sadiq, “Renewable energy integration into community energy systems: A case study of new urban residential development,” J. Clean. Prod., Oct. 2016.

[12] J. Keirstead, M. Jennings, and A. Sivakumar, “A review of urban energy system models: Approaches, challenges and opportunities,” Renew. Sustain. Energy Rev., vol. 16, no. 6, pp. 3847–3866, Aug. 2012.

[13] A. T. D. Perera, V. M. Nik, D. Mauree, and J.-L. Scartezzini, “Electrical hubs: An effective way to integrate non-dispatchable renewable energy sources with minimum impact to the grid,” Appl. Energy, vol. 190, pp. 232–248, Mar. 2017.

[14] M. L. Guen, L. Mosca, A. T. D. Perera, S. Coccolo, N. Mohajeri, and J.-L. Scartezzini, “Improving the energy sustainability of a Swiss village through building renovation and renewable energy integration,” Energy Build., vol. 158, no. Supplement C, pp. 906–923, Jan. 2018.

[15] B. Morvaj, R. Evins, and J. Carmeliet, “Decarbonizing the electricity grid: The impact on urban energy systems, distribution grids and district heating potential,” Appl. Energy, vol. 191, pp. 125–140, Apr. 2017.

[16] A. T. D. Perera, A. N. Madusanka, R. A. Attalage, and K. K. C. K. Perera, “A multi criterion analysis for renewable energy integration process of a standalone hybrid energy system with internal combustion generator,” J. Renew. Sustain. Energy, vol. 7, no. 4, p. 043128, Jul. 2015.

[17] S. Fazlollahi, G. Becker, and F. Maréchal, “Multi-objectives, multi-period optimization of district energy systems: III. Distribution networks,” Comput. Chem. Eng., vol. 66, pp. 82–97, Jul. 2014.

[18] S. Fazlollahi, P. Mandel, G. Becker, and F. Maréchal, “Methods for multi-objective investment and operating optimization of complex energy systems,” Energy, vol. 45, no. 1, pp. 12–22, Sep. 2012.

[19] B. Morvaj, R. Evins, and J. Carmeliet, “Optimization framework for distributed energy systems with integrated electrical grid constraints,” Appl. Energy, vol. 171, no. Supplement C, pp. 296–313, Jun. 2016.

[20] A. Maroufmashat et al., “Modeling and optimization of a network of energy hubs to improve economic and emission considerations,” Energy, vol. 93, no. Part 2, pp. 2546–2558, Dec. 2015.

[21] R. Baños, F. Manzano-Agugliaro, F. G. Montoya, C. Gil, A. Alcayde, and J. Gómez, “Optimization methods applied to renewable and sustainable energy: A review,” Renew. Sustain. Energy Rev., vol. 15, no. 4, pp. 1753–1766, May 2011.

[22] D. Connolly, H. Lund, B. V. Mathiesen, and M. Leahy, “A review of computer tools for analysing the integration of renewable energy into various energy systems,” Appl. Energy, vol. 87, no. 4, pp. 1059–1082, Apr. 2010.

[23] A. H. Fathima and K. Palanisamy, “Optimization in microgrids with hybrid energy systems – A review,” Renew. Sustain. Energy Rev., vol. 45, pp. 431–446, May 2015.

[24] C. Ratti, N. Baker, and K. Steemers, “Energy consumption and urban texture,” Energy Build., vol. 37, no. 7, pp. 762–776, Jul. 2005.

[25] L. Frayssinet, L. Merlier, F. Kuznik, J.-L. Hubert, M. Milliez, and J.-J. Roux, “Modeling the heating and cooling energy demand of urban buildings at city scale,” Renew. Sustain. Energy Rev., vol. 81, no. Part 2, pp. 2318–2327, Jan. 2018.

[26] P. Moonen, T. Defraeye, V. Dorer, B. Blocken, and J. Carmeliet, “Urban Physics: Effect of the micro-climate on comfort, health and energy demand,” Front. Archit. Res., vol. 1, no. 3, pp. 197–228, Sep. 2012.

[27] E. Bozonnet, R. Belarbi, and F. Allard, “Thermal Behaviour of buildings: modelling the impact of urban heat island,” J. Harbin Inst. Technol., vol. 14, no. Sup., pp. 19–22, 2007.

[28] R. Evins, “Multi-level optimization of building design, energy system sizing and operation,” Energy.

[29] R. Wu, G. Mavromatidis, K. Orehounig, and J. Carmeliet, “Multiobjective optimisation of energy systems and building envelope retrofit in a residential community,” Appl. Energy, vol. 190, pp. 634–649, Mar. 2017.

[30] J. A. Fonseca, T.-A. Nguyen, A. Schlueter, and F. Marechal, “City Energy Analyst (CEA): Integrated framework for analysis and optimization of building energy systems in neighborhoods and city districts,” Energy Build., vol. 113, no. Supplement C, pp. 202–226, Feb. 2016.

[31] J. A. Fonseca and A. Schlueter, “Integrated model for characterization of spatiotemporal building energy consumption patterns in neighborhoods and city districts,” Appl. Energy, vol. 142, no. Supplement C, pp. 247–265, Mar. 2015.

[32] D. Mauree, N. Blond, M. Kohler, and A. Clappier, “On the Coherence in the Boundary Layer: Development of a Canopy Interface Model,” Front. Earth Sci., vol. 4, 2017.

[33] D. Mauree, D. Sang-Hoon Lee, E. Naboni, S. Coccolo, and J.-L. Scartezzini, “Localized meteorological variables influence at the early design stage,” Energy Procedia, vol. 122, no. Supplement C, pp. 325–330, Sep. 2017.

[34] D. Mauree, S. Coccolo, J. Kaempf, and J.-L. Scartezzini, “Multi-scale modelling to evaluate building energy consumption at the neighbourhood scale,” PLOS ONE, 2017.

[35] D. Mauree, A. T. D. Perera, and J.-L. Scartezzini, “Influence of Buildings Configuration on the Energy Demand and Sizing of Energy Systems in an Urban Context,” Energy Procedia, vol. 142, pp. 2648–2654, Dec. 2017.

[36] D. Mauree, J. H. Kämpf, and J.-L. Scartezzini, “Multi-scale modelling to improve climate data for building energy models,” in Proceedings of the 14th International Conference of the International Building Performance Simulation Association, Hyderabad, 2015.

[37] M. Manfren, P. Caputo, and G. Costa, “Paradigm shift in urban energy systems through distributed generation: Methods and models,” Appl. Energy, vol. 88, no. 4, pp. 1032–1048, Apr. 2011.

[38] D. Mauree, “Development of a multi-scale meteorological system to improve urban climate modeling,” Université de Strasbourg, 2014.

[39] “CitySim Software | LESO-PB.” [Online]. Available: http://citysim.epfl.ch/. [Accessed: 25-Nov-2015].

[40] D. Robinson et al., “SUNtool – A new modelling paradigm for simulating and optimising urban sustainability,” Sol. Energy, vol. 81, no. 9, pp. 1196–1211, Sep. 2007.

[41] E. Walter and J. H. Kämpf, “A verification of CitySim results using the BESTEST and monitored consumption values,” Proc. 2nd Build. Simul. Appl. Conf., pp. 215–222, 2015.

[42] D Robinson and A Stone, “A simplified radiosity algorithm for general urban radiation exchange,” Build. Serv. Eng. Res. Technol., vol. 26, no. 4, pp. 271–284, Nov. 2005.

[43] A. T. D. Perera, V. M. Nik, D. Mauree, and J.-L. Scartezzini, “An integrated approach to design site specific distributed electrical hubs combining optimization, multi-criterion assessment and decision making,” Energy, vol. 134, pp. 103–120, Sep. 2017.

[44] J. Remund, Quality of Meteonorm Version 6.0. 2008.

[45] C. Ratti, D. Raydan, and K. Steemers, “Building form and environmental performance: archetypes, analysis and an arid climate,” Energy Build., vol. 35, no. 1, pp. 49–59, Jan. 2003.

[46] H. Sanaieian, M. Tenpierik, K. van den Linden, F. Mehdizadeh Seraj, and S. M. Mofidi Shemrani, “Review of the impact of urban block form on thermal performance, solar access and ventilation,” Renew. Sustain. Energy Rev., vol. 38, pp. 551–560, Oct. 2014.

[47] T. R. Oke, “The energetic basis of the urban heat island,” Q. J. R. Meteorol. Soc., vol. 108, no. 455, pp. 1–24, Jan. 1982.

[48] D. Mauree, N. Blond, M. Kohler, and A. Clappier, “On the Coherence in the Boundary Layer: Development of a Canopy Interface Model,” Front. Earth Sci., vol. 4, 2017.

[49] C. Skamarock et al., “A Description of the Advanced Research WRF Version 3,” 2008.

[50] A. Monin and A. Yaglom, “Statistical fluid dynamics,” Vol II MIT Press Camb., 1971.

[51] C. H. B. Priestley and W. C. Swinbank, “Vertical Transport of Heat by Turbulence in the Atmosphere,” Proc. R. Soc. Lond. Ser. Math. Phys. Sci., vol. 189, no. 1019, pp. 543–561, 1947.

[52] D. Mauree, S. Coccolo, S. Monna, J. Kämpf, and J.-L. Scartezzini, “On the impact of local climatic conditions on urban energy use: A case study,” Proc. PLEA 2016, 2016.

[53] S. Coccolo, D. Mauree, J. Kämpf, and J.-L. Scartezzini, “Integration of outdoor human comfort in a building energy simulation database using CityGML Energy Ade,” Expand. Boundaries - Syst. Think. Built Environ. - Proc. Sustain. Built Environ. SBE Reg. Conf. Zurich 2016, 2016.

[54] D. Mauree, S. Coccolo, J. Kämpf, and J.-L. Scartezzini, “Multi-scale modelling to assess human comfort in urban canyons,” presented at the Expanding Boundaries - Systems Thinking in the Built Environment - Proceedings of the Sustainable Built Environment (SBE) Regional Conference Zurich 2016.

[55] F. Salamanca, A. Krpo, A. Martilli, and A. Clappier, “A new building energy model coupled with an urban canopy parameterization for urban climate simulations—part I. formulation, verification, and sensitivity analysis of the model,” Theor. Appl. Climatol., vol. 99, no. 3–4, pp. 331–344, Jan. 2010.

[56] D. Mauree, S. Coccolo, J. Kaempf, and J.-L. Scartezzini, “Multi-scale modelling to evaluate building energy consumption at the neighbourhood scale,” PLOS ONE, vol. 12, no. 9, p. e0183437, Sep. 2017.

[57] A. Martilli, A. Clappier, and M. W. Rotach, “An Urban Surface Exchange Parameterisation for Mesoscale Models,” Bound.-Layer Meteorol., vol. 104, no. 2, pp. 261–304, 2002.

[58] A. Krpo, F. Salamanca, A. Martilli, and A. Clappier, “On the Impact of Anthropogenic Heat Fluxes on the Urban Boundary Layer: A Two-Dimensional Numerical Study,” Bound.-Layer Meteorol., vol. 136, no. 1, pp. 105–127, Jul. 2010.

[59] M. Geidl and G. Andersson, “Optimal Power Flow of Multiple Energy Carriers,” IEEE Trans. Power Syst., vol. 22, no. 1, pp. 145–155, Feb. 2007.

[60] M. Mohammadi, Y. Noorollahi, B. Mohammadi-ivatloo, and H. Yousefi, “Energy hub: From a model to a concept – A review,” Renew. Sustain. Energy Rev., vol. 80, no. Supplement C, pp. 1512–1527, Dec. 2017.

[61] A. A. Elmokadem, N. A. Megahed, and D. S. Noaman, “Towards a computer program for building-integrated wind technologies,” Energy Build., vol. 117, no. Supplement C, pp. 230–244, Apr. 2016.

[62] W. Durisch, B. Bitnar, J.-C. Mayor, H. Kiess, K. Lam, and J. Close, “Efficiency model for photovoltaic modules and demonstration of its application to energy yield estimation,” Sol. Energy Mater. Sol. Cells, vol. 91, no. 1, pp. 79–84, Jan. 2007.

[63] A. T. D. Perera, D. M. I. J. Wickremasinghe, D. V. S. Mahindarathna, R. A. Attalage, K. K. C. K. Perera, and E. M. Bartholameuz, “Sensitivity of internal combustion generator capacity in standalone hybrid energy systems,” Energy, vol. 39, no. 1, pp. 403–411, Mar. 2012.

[64] A. T. D. Perera, R. A. Attalage, K. K. C. K. Perera, and V. P. C. Dassanayake, “Designing standalone hybrid energy systems minimizing initial investment, life cycle cost and pollutant emission,” Energy, vol. 54, pp. 220–230, Jun. 2013.

[65] K. Deb, “An efficient constraint handling method for genetic algorithms,” Comput. Methods Appl. Mech. Eng., vol. 186, no. 2–4, pp. 311–338, Jun. 2000.

[66] A. T. D. Perera, R. A. Attalage, K. K. C. K. Perera, and V. P. C. Dassanayake, “Converting existing Internal Combustion Generator (ICG) systems into HESs in standalone applications,” Energy Convers. Manag., vol. 74, pp. 237–248, Oct. 2013.

[67] S. Coccolo, J. Kaempf, D. Mauree, and J.-L. Scartezzini, “Cooling potential of greening in the urban environment, a step further towards practice,” Sustain. Cities Soc., Jan. 2018.

Chapter 9

[1] #Envision2030: 17 goals to transform the world for persons with disabilities | United Nations Enable, (n.d.). https://www.un.org/development/desa/disabilities/envision2030.html (accessed May 24, 2018).

[2] Energy in architecture : the European passive solar handbook / edited by John R. Goulding, J. Owen Lewis, Theo C. Steemers., London: B.T. Batsford for the Commission of the European Communities, Directorate General XII for Science, Research and Development, 1992.

[3] J. Keirstead, M. Jennings, A. Sivakumar, A review of urban energy system models: Approaches, challenges and opportunities, Renew. Sustain. Energy Rev. 16 (2012) 3847–3866. doi:10.1016/j.rser.2012.02.047.

[4] S.C.M. Hui, Low energy building design in high density urban cities, Renew. Energy. 24 (2001) 627–640. doi:10.1016/S0960-1481(01)00049-0.

[5] C.F. Reinhart, C. Cerezo Davila, Urban building energy modeling – A review of a nascent field, Build. Environ. 97 (2016) 196–202. doi:10.1016/j.buildenv.2015.12.001.

[6] A.T.D. Perera, V.M. Nik, D. Mauree, J.-L. Scartezzini, Electrical hubs: An effective way to integrate non-dispatchable renewable energy sources with minimum impact to the grid, Appl. Energy. 190 (2017) 232–248. doi:10.1016/j.apenergy.2016.12.127.

[7] S. Fazlollahi, G. Becker, A. Ashouri, F. Maréchal, Multi-objective, multi-period optimization of district energy systems: IV – A case study, Energy. 84 (2015) 365–381. doi:10.1016/j.energy.2015.03.003.

[8] S. Fazlollahi, G. Becker, F. Maréchal, Multi-objectives, multi-period optimization of district energy systems: III. Distribution networks, Comput. Chem. Eng. 66 (2014) 82–97. doi:10.1016/j.compchemeng.2014.02.018.

[9] J.A. Fonseca, A. Schlueter, Integrated model for characterization of spatiotemporal building energy consumption patterns in neighborhoods and city districts, Appl. Energy. 142 (2015) 247–265. doi:10.1016/j.apenergy.2014.12.068.

[10] J.A. Fonseca, T.-A. Nguyen, A. Schlueter, F. Marechal, City Energy Analyst (CEA): Integrated framework for analysis and optimization of building energy systems in neighborhoods and city districts, Energy Build. 113 (2016) 202–226. doi:10.1016/j.enbuild.2015.11.055.

[11] M. Le Guen, L. Mosca, A.T.D. Perera, S. Coccolo, N. Mohajeri, J.-L. Scartezzini, Improving the energy sustainability of a Swiss village through building renovation and renewable energy integration, Energy Build. 158 (2017) 906–923. doi:10.1016/j.enbuild.2017.10.057.

[12] R. Wu, G. Mavromatidis, K. Orehounig, J. Carmeliet, Multiobjective optimisation of energy systems and building envelope retrofit in a residential community, Appl. Energy. 190 (2017) 634–649. doi:10.1016/j.apenergy.2016.12.161.

[13] A.T.D. Perera, S. Coccolo, J.-L. Scartezzini, D. Mauree, Quantifying the impact of urban climate by extending the boundaries of urban energy system modeling, Appl. Energy. 222 (2018) 847–860. doi:10.1016/j.apenergy.2018.04.004.

[14] S. Salat, Energy loads, CO2 emissions and building stocks: morphologies, typologies, energy systems and behaviour, Build. Res. Inf. 37 (2009) 598–609. doi:10.1080/09613210903162126.

[15] E. Holden, I.T. Norland, Three challenges for the compact city as a sustainable urban form: Household consumption of energy and transport in eight residential areas in the Greater, Urban Stud. 42 (2005) 2145. doi:10.1080/00420980500332064.

[16] W.P. Anderson, S.K. Pavlos, J.M. Eric, Urban Form , Energy and the Environm ent : A Review of Issues , Evidence and Policy, 33 (1996) 7–35.

[17] P. Moonen, T. Defraeye, V. Dorer, B. Blocken, J. Carmeliet, Urban Physics: Effect of the micro-climate on comfort, health and energy demand, Front. Archit. Res. 1 (2012) 197–228. doi:10.1016/j.foar.2012.05.002.

[18] C. Ratti, N. Baker, K. Steemers, Energy consumption and urban texture, Energy Build. 37 (2005) 762–776. doi:10.1016/j.enbuild.2004.10.010.

[19] J. Liu, M. Heidarinejad, S. Gracik, J. Srebric, The impact of exterior surface convective heat transfer coefficients on the building energy consumption in urban neighborhoods with different plan area densities, Energy Build. 86 (2015) 449–463. doi:10.1016/j.enbuild.2014.10.062.

[20] A. Okeil, A holistic approach to energy efficient building forms, Energy Build. 42 (2010) 1437–1444. doi:10.1016/j.enbuild.2010.03.013.

[21] H. Sanaieian, M. Tenpierik, K. van den Linden, F. Mehdizadeh Seraj, S.M. Mofidi Shemrani, Review of the impact of urban block form on thermal performance, solar access and ventilation, Renew. Sustain. Energy Rev. 38 (2014) 551–560. doi:10.1016/j.rser.2014.06.007.

[22] M. Taleghani, L. Kleerekoper, M. Tenpierik, A. van den Dobbelsteen, Outdoor thermal comfort within five different urban forms in the Netherlands, Build. Environ. 83 (2015) 65–78. doi:10.1016/j.buildenv.2014.03.014.

[23] C. Ratti, D. Raydan, K. Steemers, Building form and environmental performance: archetypes, analysis and an arid climate, Energy Build. 35 (2003) 49–59. doi:10.1016/S0378-7788(02)00079-8.

[24] K. Steemers, Energy and the city : density , buildings and transport, 35 (2003) 3–14.

[25] I.D. Watson, G.T. Johnson, Graphical estimation of sky view-factors in urban environments, Int. J. Climatol. 7 (1987) 193–197.

[26] C. Ratti, D. Raydan, K. Steemers, Building Form and Environmental Performance : Archetypes , Analysis and an Arid Climate, Energy Build. 35 (2003) 49–59.

[27] M. Carozza, G. Mutani, S. Coccolo, J.H. Kaempf, Introducing a hybrid energy-use model at the urban scale: the case study of Turin (IT), in: 3rd Build. Simul. Appl. Conf. BSA 2017 Bolzano Italy, 2017.

[28] D. Thomas, C. Miller, J. Kämpf, A. Schlueter, Multiscale co-simulation of EnergyPlus and CitySim models derived from a Building Information Model, Bausim 2014 Fifth Ger.-Austrian IBPSA Conf. (2014) 469–476. doi:10.13140/2.1.4639.1040.

[29] E. Walter, J. Kämpf, A verification of CitySim results using the BESTEST and monitored consumption values, in: Build. Simul. Appl. BSA 2015, 2015.

[30] S. Coccolo, J. Kaempf, J.-L. Scartezzini, The EPFL campus in Lausanne: New energy strategies for 2050, in: Energy Procedia, 2015. doi:10.1016/j.egypro.2015.11.776.

[31] C. Dorsaz, Application d ' un logiciel de simulation de système urbain à un bâtiment de Martigny, Lausanne, 2010.

[32] Lesosai, Lesosai 7.0, (2017).

[33] SIA, SIA 2024 Conditions d'utilisation standard pour l'énergie et les installations du bâtiment, 2006.

[34] Autodesk, Equipment and Lighting Loads, (2017).

[35] J. Remund, S. Müller, S. Kunz, Meteonorm. Global metereological database. Version 7, (2015).

[36] M.C. Peel, B.L. Finlayson, T.A. Mcmahon, Updated world map of the Koeppen-Geiger climate classification, (2007) 1633–1644.

[37] A.T.D. Perera, D.M.I.J. Wickremasinghe, D.V.S. Mahindarathna, R.A. Attalage, K.K.C.K. Perera, E.M. Bartholameuz, Sensitivity of internal combustion generator capacity in standalone hybrid energy systems, Energy. 39 (2012) 403–411. doi:10.1016/j.energy.2011.12.039.

[38] A.T.D. Perera, V.M. Nik, D. Mauree, J.-L. Scartezzini, An integrated approach to design site specific distributed electrical hubs combining optimization, multi-criterion assessment and decision making, Energy. 134 (2017) 103–120. doi:10.1016/j.energy.2017.06.002.

Chapter 10

[1] F. Ueckerdt, L. Hirth, G. Luderer, and O. Edenhofer, “System LCOE: What are the costs of variable renewables?,” Energy, vol. 63, pp. 61–75, Dec. 2013.

[2] F. Ueckerdt, R. Brecha, G. Luderer, P. Sullivan, E. Schmid, N. Bauer, D. Böttger, and R. Pietzcker, “Representing power sector variability and the integration of variable renewables in long-term energy-economy models using residual load duration curves,” Energy, vol. 90, Part 2, pp. 1799–1814, Oct. 2015.

[3] K. Hassan Youssef, “Optimal management of unbalanced smart microgrids for scheduled and unscheduled multiple transitions between grid-connected and islanded modes,” Electr. Power Syst. Res., vol. 141, pp. 104–113, Dec. 2016.

[4] R. Rigo-Mariani, B. Sareni, X. Roboam, and C. Turpin, “Optimal power dispatching strategies in smart-microgrids with storage,” Renew. Sustain. Energy Rev., vol. 40, pp. 649–658, Dec. 2014.

[5] V. Mohan, J. G. Singh, W. Ongsakul, N. Madhu M., and R. S. M.P., “Economic and network feasible online power management for renewable energy integrated smart microgrid,” Sustain. Energy Grids Netw., vol. 7, pp. 13–24, Sep. 2016.

[6] A. G. Zamani, A. Zakariazadeh, and S. Jadid, “Day-ahead resource scheduling of a renewable energy based virtual power plant,” Appl. Energy, vol. 169, pp. 324–340, May 2016.

[7] A. G. Zamani, A. Zakariazadeh, S. Jadid, and A. Kazemi, “Stochastic operational scheduling of distributed energy resources in a large scale virtual power plant,” Int. J. Electr. Power Energy Syst., vol. 82, pp. 608–620, Nov. 2016.

[8] J. Zapata Riveros, K. Bruninx, K. Poncelet, and W. D’haeseleer, “Bidding strategies for virtual power plants considering CHPs and intermittent renewables,” Energy Convers. Manag., vol. 103, pp. 408–418, Oct. 2015.

[9] A. H. Fathima and K. Palanisamy, “Optimization in microgrids with hybrid energy systems – A review,” Renew. Sustain. Energy Rev., vol. 45, pp. 431–446, May 2015.

[10] A. T. D. Perera, R. A. Attalage, K. K. C. K. Perera, and V. P. C. Dassanayake, “Converting existing Internal Combustion Generator (ICG) systems into HESs in standalone applications,” Energy Convers. Manag., vol. 74, pp. 237–248, Oct. 2013.

[11] A. T. D. Perera, D. M. I. J. Wickremasinghe, D. V. S. Mahindarathna, R. A. Attalage, K. K. C. K. Perera, and E. M. Bartholameuz, “Sensitivity of internal combustion generator capacity in standalone hybrid energy systems,” Energy, vol. 39, no. 1, pp. 403–411, Mar. 2012.

[12] M. Fadaee and M. A. M. Radzi, “Multi-objective optimization of a stand-alone hybrid renewable energy system by using evolutionary algorithms: A review,” Renew. Sustain. Energy Rev., vol. 16, no. 5, pp. 3364–3369, Jun. 2012.

[13] D. P. Kaundinya, P. Balachandra, and N. H. Ravindranath, “Grid-connected versus stand-alone energy systems for decentralized power—A review of literature,” Renew. Sustain. Energy Rev., vol. 13, no. 8, pp. 2041–2050, Oct. 2009.

[14] D. Connolly, H. Lund, B. V. Mathiesen, and M. Leahy, “A review of computer tools for analysing the integration of renewable energy into various energy systems,” Appl. Energy, vol. 87, no. 4, pp. 1059–1082, Apr. 2010.

[15] R. Luna-Rubio, M. Trejo-Perea, D. Vargas-Vázquez, and G. J. Ríos-Moreno, “Optimal sizing of renewable hybrids energy systems: A review of methodologies,” Sol. Energy, vol. 86, no. 4, pp. 1077–1088, Apr. 2012.

[16] F. F. Yanine and E. E. Sauma, “Review of grid-tie micro-generation systems without energy storage: Towards a new approach to sustainable hybrid energy systems linked to energy efficiency,” Renew. Sustain. Energy Rev., vol. 26, pp. 60–95, Oct. 2013.

[17] R. Evins, “Multi-level optimization of building design, energy system sizing and operation,” Energy.

[18] S. Fazlollahi, S. L. Bungener, P. Mandel, G. Becker, and F. Maréchal, “Multi-objectives, multi-period optimization of district energy systems: I. Selection of typical operating periods,” Comput. Chem. Eng., vol. 65, pp. 54–66, Jun. 2014.

[19] A. T. D. Perera, R. A. Attalage, K. K. C. K. Perera, and V. P. C. Dassanayake, “Designing standalone hybrid energy systems minimizing initial investment, life cycle cost and pollutant emission,” Energy, vol. 54, pp. 220–230, Jun. 2013.

[20] J.-H. Shi, X.-J. Zhu, and G.-Y. Cao, “Design and techno-economical optimization for stand-alone hybrid power systems with multi-objective evolutionary algorithms,” Int. J. Energy Res., vol. 31, no. 3, pp. 315–328, Mar. 2007.

[21] A. Kamjoo, A. Maheri, A. M. Dizqah, and G. A. Putrus, “Multi-objective design under uncertainties of hybrid renewable energy system using NSGA-II and chance constrained programming,” Int. J. Electr. Power Energy Syst., vol. 74, pp. 187–194, Jan. 2016.

[22] J. L. Bernal-Agustín and R. Dufo-López, “Multi-objective design and control of hybrid systems minimizing costs and unmet load,” Electr. Power Syst. Res., vol. 79, no. 1, pp. 170–180, Jan. 2009.

[23] R. Dufo-López, I. R. Cristóbal-Monreal, and J. M. Yusta, “Optimisation of PV-wind-diesel-battery stand-alone systems to minimise cost and maximise human development index and job creation,” Renew. Energy, vol. 94, pp. 280–293, Aug. 2016.

[24] H. Sayyaadi, M. Babaie, and M. R. Farmani, “Implementing of the multi-objective particle swarm optimizer and fuzzy decision-maker in exergetic, exergoeconomic and environmental optimization of a benchmark cogeneration system,” Energy, vol. 36, no. 8, pp. 4777–4789, Aug. 2011.

[25] W.-S. Tan, M. Y. Hassan, M. S. Majid, and H. Abdul Rahman, “Optimal distributed renewable generation planning: A review of different approaches,” Renew. Sustain. Energy Rev., vol. 18, pp. 626–645, Feb. 2013.

[26] S. C. Bhattacharyya, “Review of alternative methodologies for analysing off-grid electricity supply,” Renew. Sustain. Energy Rev., vol. 16, no. 1, pp. 677–694, Jan. 2012.

[27] D. A. Haralambopoulos and H. Polatidis, “Renewable energy projects: structuring a multi-criteria group decision-making framework,” Renew. Energy, vol. 28, no. 6, pp. 961–973, May 2003.

[28] J.-J. Wang, Y.-Y. Jing, C.-F. Zhang, and J.-H. Zhao, “Review on multi-criteria decision analysis aid in sustainable energy decision-making,” Renew. Sustain. Energy Rev., vol. 13, no. 9, pp. 2263–2278, Dec. 2009.

[29] W. Yunna and S. Geng, “Multi-criteria decision making on selection of solar–wind hybrid power station location: A case of China,” Energy Convers. Manag., vol. 81, pp. 527–533, May 2014.

[30] M. Tahri, M. Hakdaoui, and M. Maanan, “The evaluation of solar farm locations applying Geographic Information System and Multi-Criteria Decision-Making methods: Case study in southern Morocco,” Renew. Sustain. Energy Rev., vol. 51, pp. 1354–1362, Nov. 2015.

[31] M. Vafaeipour, S. Hashemkhani Zolfani, M. H. Morshed Varzandeh, A. Derakhti, and M. Keshavarz Eshkalag, “Assessment of regions priority for implementation of solar projects in Iran: New application of a hybrid multi-criteria decision making approach,” Energy Convers. Manag., vol. 86, pp. 653–663, Oct. 2014.

[32] B. Wang, I. Nistor, T. Murty, and Y.-M. Wei, “Efficiency assessment of hydroelectric power plants in Canada: A multi criteria decision making approach,” Energy Econ., vol. 46, pp. 112–121, Nov. 2014.

[33] J. Ren, A. Fedele, M. Mason, A. Manzardo, and A. Scipioni, “Fuzzy Multi-actor Multi-criteria Decision Making for sustainability assessment of biomass-based technologies for hydrogen production,” Int. J. Hydrog. Energy, vol. 38, no. 22, pp. 9111–9120, Jul. 2013.

[34] M. Kabak, E. Köse, O. Kırılmaz, and S. Burmaoğlu, “A fuzzy multi-criteria decision making approach to assess building energy performance,” Energy Build., vol. 72, pp. 382–389, Apr. 2014.

[35] M. Grujić, D. Ivezić, and M. Živković, “Application of multi-criteria decision-making model for choice of the optimal solution for meeting heat demand in the centralized supply system in Belgrade,” Energy, vol. 67, pp. 341–350, Apr. 2014.

[36] M. Ebrahimi and A. Keshavarz, “Prime mover selection for a residential micro-CCHP by using two multi-criteria decision-making methods,” Energy Build., vol. 55, pp. 322–331, Dec. 2012.

[37] D. Georgiou, E. S. Mohammed, and S. Rozakis, “Multi-criteria decision making on the energy supply configuration of autonomous desalination units,” Renew. Energy, vol. 75, pp. 459–467, Mar. 2015.

[38] E. Khorasaninejad, A. Fetanat, and H. Hajabdollahi, “Prime mover selection in thermal power plant integrated with organic Rankine cycle for waste heat recovery using a novel multi criteria decision making approach,” Appl. Therm. Eng., vol. 102, pp. 1262–1279, Jun. 2016.

[39] A. T. D. Perera, R. A. Attalage, K. K. C. K. Perera, and V. P. C. Dassanayake, “A hybrid tool to combine multi-objective optimization and multi-criterion decision making in designing standalone hybrid energy systems,” Appl. Energy, vol. 107, pp. 412–425, Jul. 2013.

[40] A. Mazza, G. Chicco, and A. Russo, “Optimal multi-objective distribution system reconfiguration with multi criteria decision making-based solution ranking and enhanced genetic operators,” Int. J. Electr. Power Energy Syst., vol. 54, pp. 255–267, Jan. 2014.

[41] W. Durisch, B. Bitnar, J.-C. Mayor, H. Kiess, K. Lam, and J. Close, “Efficiency model for photovoltaic modules and demonstration of its application to energy yield estimation,” Sol. Energy Mater. Sol. Cells, vol. 91, no. 1, pp. 79–84, Jan. 2007.

[42] G. Notton, V. Lazarov, and L. Stoyanov, “Optimal sizing of a grid-connected PV system for various PV module technologies and inclinations, inverter efficiency characteristics and locations,” Renew. Energy, vol. 35, no. 2, pp. 541–554, Feb. 2010.

[43] S. Diaf, D. Diaf, M. Belhamel, M. Haddadi, and A. Louche, “A methodology for optimal sizing of autonomous hybrid PV/wind system,” Energy Policy, vol. 35, no. 11, pp. 5708–5718, Nov. 2007.

[44] M. S. Ismail, M. Moghavvemi, T. M. I. Mahlia, K. M. Muttaqi, and S. Moghavvemi, “Effective utilization of excess energy in standalone hybrid renewable energy systems for improving comfort ability and reducing cost of energy: A review and analysis,” Renew. Sustain. Energy Rev., vol. 42, pp. 726–734, Feb. 2015.

[45] H. Kondziella and T. Bruckner, “Flexibility requirements of renewable energy based electricity systems – a review of research results and methodologies,” Renew. Sustain. Energy Rev., vol. 53, pp. 10–22, Jan. 2016.

[46] * M. I. M. W., “Measuring machine and product mix flexibilities of a manufacturing system,” Int. J. Prod. Res., vol. 43, no. 18, pp. 3773–3786, Sep. 2005.

[47] S. K. Das, “The measurement of flexibility in manufacturing systems,” Int. J. Flex. Manuf. Syst., vol. 8, no. 1, pp. 67–93.

[48] M. Bortolini, M. Gamberi, A. Graziani, and F. Pilati, “Economic and environmental bi-objective design of an off-grid photovoltaic–battery–diesel generator hybrid energy system,” Energy Convers. Manag., vol. 106, pp. 1024–1038, Dec. 2015.

[49] A. Maleki, F. Pourfayaz, and M. A. Rosen, “A novel framework for optimal design of hybrid renewable energy-based autonomous energy systems: A case study for Namin, Iran,” Energy, vol. 98, pp. 168–180, Mar. 2016.

[50] O. Erdinc and M. Uzunoglu, “Optimum design of hybrid renewable energy systems: Overview of different approaches,” Renew. Sustain. Energy Rev., vol. 16, no. 3, pp. 1412–1425, Apr. 2012.

[51] J. L. Bernal-Agustín and R. Dufo-López, “Efficient design of hybrid renewable energy systems using evolutionary algorithms,” Energy Convers. Manag., vol. 50, no. 3, pp. 479–489, Mar. 2009.

Appendix 1

Table A1-1: Parameters for the SPV efficiency model for different solar panel types. Extracted from Ref. [1]

	p	*q*	*r*	*s*	*m*	u	*h*
Monocrystalline	23.62	-0.2983	-0.09307	-0.9795	0.1912	0.9865	0.028
Polycrystalline	15.39	-0.1770	-0.09736	-0.8998	0.0794	0.9324	0.026
Multi Junction	36.02	-0.7576	-0.02863	-1.1432	0.6601	1.0322	0.022

[1] Durisch W, Bitnar B, Mayor J-C, Kiess H, Lam K, Close J. Efficiency model for photovoltaic modules and demonstration of its application to energy yield estimation. Sol Energy Mater Sol Cells 2007;91:79–84. doi:10.1016/j.solmat.2006.05.011

Table A1-2: Acquisition cost of components used for Chapter 2, 5 and 10. This table presents the cost components for both simplified and detailed multi energy hub model. The cost values for different components are collected considering local context for Switzerland (Regression technique presented in Fig. A1-1is used to come up with the cost values.), Sri Lanka, and Sweden. Eurostat [2] is used to convert the cost data for other European cities (considered in Euros) corresponding to other chapters. Here its presented in USD for the sake of uniformity.

Component	Description	Cost($)
Wind Turbine (12 m)		
(20 year life time)	5kW	6000
	10 kW	9000
Solar Panels	(variation plotted below (Fig. A1-1))	
(20 year life time)	Mono-Crystalline (1.22 m^2)	800
	Poly-Crystalline (0.79 m^2)	945
	Amorphous(1.28 m^2)	900
ICG	0.5kVA – 7.5 kVA (single phase) (20000 working hours)	335.5 - 2195
	Hourly O&M	0.16
Cost of fuel	(Diesel 1 liter)	0.8
Battery	12V, 250Ah	380
Inverter	Single phase up to 50kW (four years lifetime)	400-700
Heat pump (ASHP)	300 kW (Max.) A linear variation is assumed	7.95
Cogeneration	300 kW (Max.) A linear variation is assumed	115/kW
Solar thermal	(variation plotted below) Capture area(CA) 50 m^2 for water heating	$4777.4x\ (CA)0^{.421}$

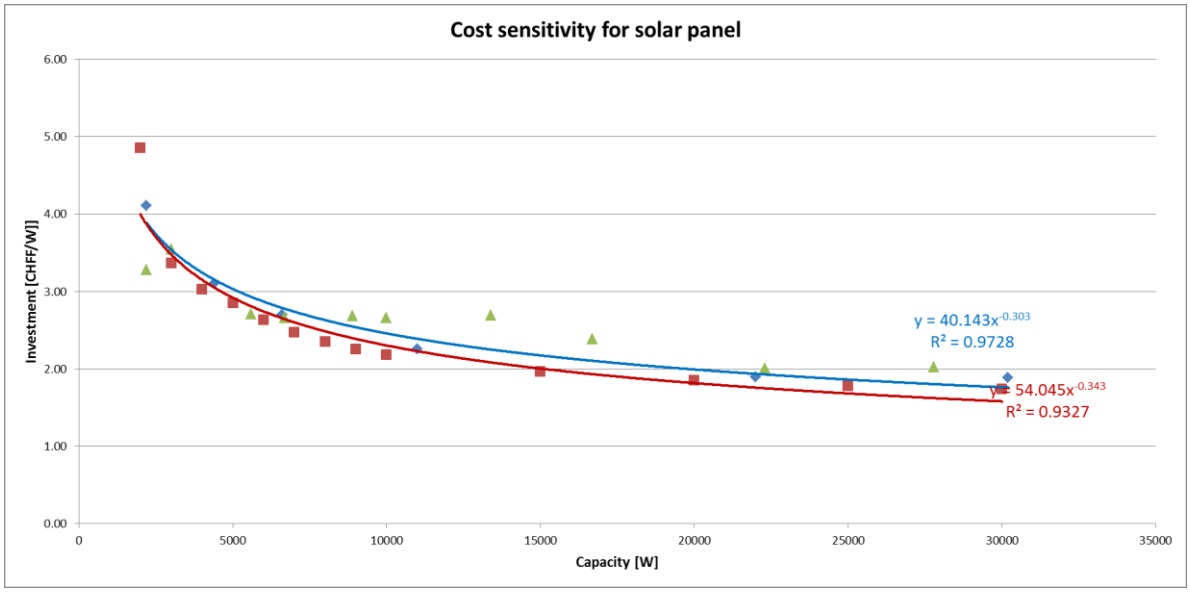

(a)

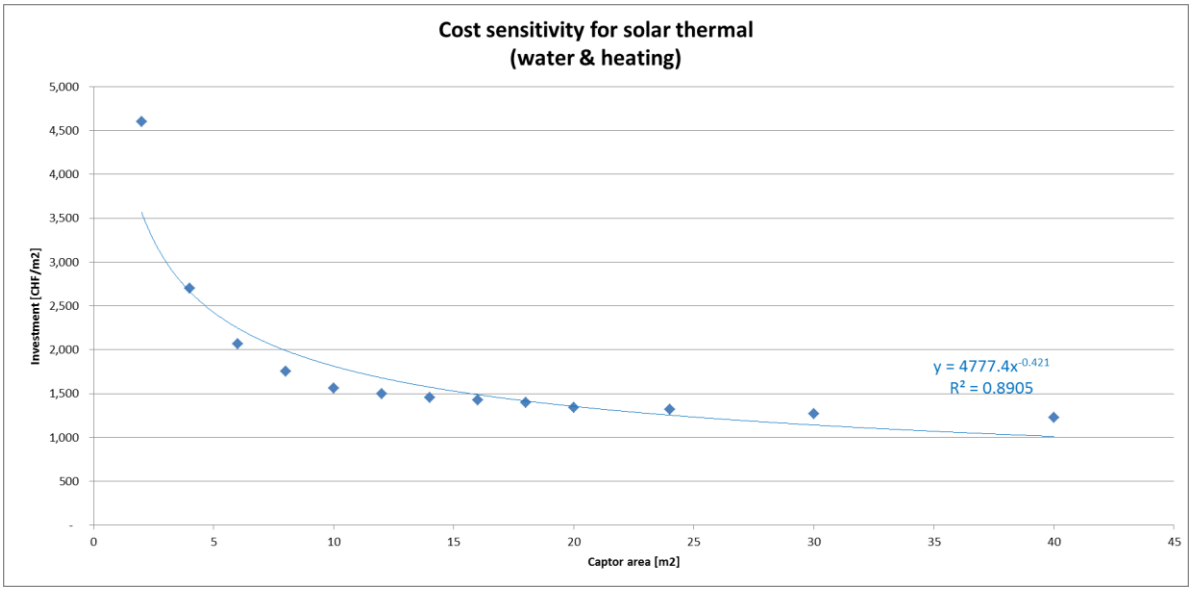

(b)

Fig. A1-1 Fluctuation is (a) solar PV and (b)solar thermal prices with the installed capacity

Table A1-2: Basic parameters of cost model used for Chapter 2, 5 and 10. Eurostat [2] is used to convert the cost data for other European cities corresponding to other chapters.

Parameter	Fraction (%)
SPV Panel & Wind Turbines	
Installation cost as a fraction of acquisition cost	20
Annual O&M as a fraction of acquisition cost	2
ICG Installation cost as a fraction of acquisition cost	5
Local market annual inflation rate	2
Return on Investment	8

Table A1- 3: Specific ranges of the decision space variables

Variable	Lower bound	Upper bound	Interval	Description
SPV Type ($^{NTY\text{-}SPV}$)	0	3	1	Mono-crystaline, Polycrystaline and Amorphous[1]
# SPV Panels N_{SPV}	0	120	1	0-30[1] kW
Type of Turbines ($N^{TY\text{-}W}$)	0	2	1	1, 5 kW
# Wind Turbines	0	15	1	1-75[2] kW
# Battery banks	0	20	1	0-240[3] kWh
ICG Capacity (kVA)	0	15	0.5	0-7.5 kVA
$W_{i,j}$ (weight matrix)	0%	100%	Continuous	
SOC_{Min}	30%	50%	Continuous	
$SOC_{Min,G}$	SOC_{Min}	70%	Continuous	
SOC_{set}	$SOC_{Min,G}$	100%	Continuous	
Lim_{BC}	0%	100%	Continuous	
Lim_{GTB}	0%	Lim_{BC}	Continuous	
Lim_{BD}	0%	100%	Continuous	
Lim_{BTG}	Lim_{BD}	100%	Continuous	

[1] 0.5 kW maximum capacity

[2]Maximum capacity considering component selected with maximum capacity

[3]Each battery bank having 12 kWh capacity

Appendix 2

Operation of the energy hub for the grey box model

Table A2- 1: Brief description about the variables in the dispatch strategy (l ϵ L (L ⊂D))

Acronym used	Description
Lim_{BC}	Critical cost for $GC_{EG}(t)$ above which selling the excess power generated to the grid is economical compared to battery charging
Lim_{BD}	Critical cost for GI_t^{IG} below which purchasing power from grid is economical compared to battery discharging
Lim_{GTB}	Critical cost for GI_t^{IG} below which purchasing power from grid to charge battery bank is economical
Lim_{BTG}	Critical cost for $GC_{EG}(t)$ above which selling stored energy to grid is economical
SOC_{min}	Critical SOC of the battery bank below which discharging is not economical to cater the load mismatch
$SOC_{Min,G}$	Critical SOC of the battery bank below which it is not economical to discharge and/or to sell the stored energy to grid
SOC_{Set}	Maximum state of charged to be reached when charging the battery bank using the grid

Interactions with grid and battery bank (Please refer to the Nomenclature of Chapter 2 for acronyms)

Mode of energy interaction with grid and battery bank need to be determined after calculating the difference between net power generation of the system and the Electricity Load Demand (ELD).A number of factors such as power generation within the energy hub, demand of the energy hub and COE of the Main Transmission Grid (MTG) need to be considered when determining the operating state of the battery bank and level of grid interaction. Ten operating states (main) that system can operate are identified in this study based on aforementioned factors. A detailed description about each state is presented in this section.

State 1: (Power generation is greater than demand, excess directed to MTG)

The dispatch strategy considers $GC_{TG}(t)$ and $GC_{TG}(t)$ of the MTG, maximum limit that can be sell ($TG_{lim}(t)$) and purchased ($FG_{lim}(t)$) from MTG and the SOC of the battery bank when determining the energy flow. State 1 refers to an instance where excess power is generated and COE in MTG is higher enough to sell excess power generated when compared to battery charging. Optimum $GC_{TG}(t)$ (critical point) profitable for selling ($Lim_{Bat,C}$) is computed using the optimization algorithm. System

shifts into to State 1, when $GC_{TG}(t)$ is less than $Lim_{Bat,C}$ and greater than $Lim_{Bat,TG.}$ The excess renewable energy generated should be less than $TG_{lim}(t)$ for this case.

State 2: (Excess generated directed to MTG and discharging battery bank to supply MTG)

With the increase of $GC_{TG}(t)$, there is a critical limit above which it is economical to discharge battery bank and sell electricity to MTG. However, this might lead to instances where energy hub needs to purchase electricity at a higher price from MTG at a later stage. In addition, depth of discharge of the battery bank needs to be considered which reduce the lifetime of the battery bank. Hence, both optimum COE in the MTG for battery discharge (Lim_{BTG}) and minimum SOC for the battery discharging process ($SOC_{Min,G}$) need to be determined. System shifts into State 2, whenever $GC_{TG}(t)$ higher than Lim_{BTG}, SOC of battery bank is higher than $SOC_{Min,G..}$

State 3: (Excess generated directed to battery bank)

When $GC_{TG}(t)$ is less than $Lim_{Bat,C}$, it is economical to direct excess power generated to battery bank. Battery charging from MTG (Lim_{GTB}) is not considered in this state. System shift to State 3 when $GC_{TG}(t)$ is within $Lim_{Bat,C}$ and $Lim_{GTB.}$ However, when SOC of the battery bank is at its maximum level system shift back to State 1 where excess energy will be directed to grid.

State 4: (Excess power generated directed to battery bank and purchasing electricity from MTG)

It is economical to purchasing electricity from grid is economical when the $GC_{FG}(t)$ is low and charge the battery bank. However, charging batteries from the MTG minimize the storage capacity for renewable energy. Therefore, optimum $GC_{TG}(t)$ (Lim_{GTB}) needs to be determined which it is economical to charge batteries from grid whenever COE goes below this value. However, it is important to understand that charging batteries from the grid minimize the storage capacity for renewable energy. Hence, maximum set point of charge $SOC_{Set,G}$ can be set for charging process.

State 5: (Excess generated above storage limits or transfer limits)

Whenever excess energy generated is greater than the maximum that can be transferred, the excess need will be directed to the other option. For example, if excess energy produced by renewable energy sources is higher than $TG_{lim}(t)$ (for State 1) the rest is directed to battery bank. In concise, system moves into State 5 whenever energy interactions in State 1 and State 4 is hindered due to limitations in energy transfer. Whenever, the excess renewable energy generation is higher than sum of both limits it needs to be dumped.

State 6: (Mismatch between demand and generation taken from MTD)

Whenever power generation is not sufficient to supply the demand, mismatch can be taken either from the battery bank, MTG or both. Similar to the State 1, five parameters are used when determining the state of the system. Whenever, $GC_{FG}(t)$ is less it is economical to purchase electricity from MTG instead of using the battery bank. The optimum cost $Lim_{Bat,D}$, is obtained using the optimization algorithm. Battery charging via MTG is not considered in this state (Discussed in detail in State 7). System shifts into to State 6 when $GC_{FG}(t)$ is within $Lim_{Bat,D}$ and greater than $Lim_{GTB.}$ Electricity units purchased from MTG should be less than $FG_{lim}(t)$.

State 7: (Mismatch between demand and generation taken from MTD and battery bank is charged by MTG)

There are instances where $GC_{FG}(t)$ is very low in which it is economical to charge batteries using MTG after delivering the mismatch. Limits related to charge batteries will remain as illustrated in State 4.

State 8: (Mismatch between demand and generation taken from battery bank)

When $GC_{FG}(t)$ is higher than $Lim_{Bat,D}$, it is economical to use battery bank to provide the mismatch. Discharging the battery bank minimize the life time of battery bank. Especially, when reaching lower SOC levels. In order to overcome this problem, minimum SOC level that can be reached in discharging process (SOC_{min}) is optimized using the optimization algorithm. When cost of Grid electricity is higher than $Lim_{Bat,D}$ and battery storage capacity is sufficient to provide the mismatch system switch into State 8.

State 9: (Mismatch is taken from battery bank and battery bank is discharged to sell electricity to MTG)

There are instances where $GC_{TG}(t)$ is notably high. It is economical to discharge battery bank and sell electricity to MTG mean in such instances while providing the mismatch. The critical $GC_{TG}(t)$ price for State 9 is same as State 2 (Lim_{BTG}). System shifts to State 9, whenever $GC_{TG}(t)$ higher than Lim_{BTG}, SOC of battery bank is higher than $SOC_{Min,G.}$ and having excess energy storage after providing the mismatch between demand and power generation.

State 10: (Mismatch between demand and generation taken from battery bank and battery bank is discharged to by MTG)

Whenever, the mismatch between demand and generation is large enough neither MTG nor battery bank alone cannot be used (State 6-9) to provide the mismatch system shifts into State 10. Both MTG and battery bank is used to provide the mismatch in this case. However, there are instances in

which combination of battery bank and MTG cannot provide the mismatch. Loss in power supply will take place in such instances. Loss of load probability is calculated based on this which is taken as a constraint in the optimization algorithm.

Amarasinghage Tharindu Dasun Perera

Doctoral Assistant, EPFL ENAC IIC LESO-PB LE 1 104 (Bâtiment LE),

Station 18, CH-1015 Lausanne, Switzerland.

Phone: +41788570840 Website: http://people.epfl.ch/dasun.perera Email:atdasun@lankamail.com

Education:

2014 Nov to Present	PhD student in **Energy Program** (EDEY), École Polytechnique Fédérale de Lausanne (EPFL), Switzerland. **Thesis Title: Modeling and Assessment of Urban Energy Systems**
2010 Nov to July 2012	MSc by Research in **Mechanical Engineering,** Faculty of Engineering, University of Moratuwa, Sri Lanka**.** **Thesis Title**: **Multi Criterion Decision Making Based on Techno-Economical Optimization of Standalone Hybrid Energy Systems**
2006 June to 2010 Oct	B.Sc Special Honours Degree (4 year) in **Mechanical Engineering** in Faculty of Engineering, University of Moratuwa, Sri Lanka.

Academic/Industrial Positions

2014 November to Present	**Doctoral Assistant,** Solar Energy and Building Physics Laboratory, École Polytechnique Fédérale de Lausanne (EPFL), Switzerland**.**
2018 March	**Visiting researcher** at Building Technology and Urban Systems Division, Lawrence Berkeley National Laboratory, USA
2011 December to 2014 October	**Lecturer,** Department of Mechanical Engineering, Faculty of Engineering, University of Moratuwa, Sri Lanka
2010 October to 2011 November	**Visiting Lecturer/Research Assistant**, Department of Mechanical Engineering, Faculty of Engineering, University of Moratuwa, Sri Lanka
2010 April to 2010 August	**Visiting Instructor**, Department of Mechanical Engineering, Faculty of Engineering, University of Moratuwa, Sri Lanka
2008 October to 2009 March	**Trainee Engineer**, Unilever Sri Lanka (Pvt) limited

Award and recognitions

1. **Outstanding paper award** (out of 800 papers), Applied Energy Conference 2017 (organized by Applied Energy Journal - Elsevier), for the paper titled "Quantifying the impact of urban climate by extending the boundaries of urban energy system modeling"
   Link.
2. Represented EPFL at the **Global Young Scientists Summit** in Singapore 2018 (nominated from EPFL PHD School).
3. **Award for the exceptional contribution** awarded by Dean, School of Architecture, Civil and Environmental Engineering, EPFL (2017)
4. **President's award for Scientific Publications**, awarded by his Excellency the President of Sri Lanka (2015)
5. **National Research Council**- Sri Lanka, **Merit Award** for Scientific Publication (2014)
6. **Postgraduate research scholarship** awarded by EPFL Switzerland (2014)
7. **Postgraduate Research Award[1], Section C** (Engineering, Architecture and Surveying) awarded by **Sri Lanka Association for Advancement of Science (SLAAS), 2013**.
8. **Best undergraduate research project** in Mechanical Engineering, University of Moratuwa, Sri Lanka 2010.

[1] This award is presented to the best postgraduate research project completed in 2012 or 2013 evaluated based on the applicant's publications on his/her postgraduate research. The award is awarded to postgraduate students registered in Sri Lankan Universities or Research Institutes.

Media release

Designing urban energy systems based on the urban climate: featuring in EPFL main website 24/04/2018 (**Link**)

List of Publications

Publications in peer review journals

1. **A.T.D. Perera**, PU Wickramasinghe, V. M. Nik, and J.-L. Scartezzini, "**Energy system optimization using reinforcement learning**" (Manuscript to be submitted)
2. **A.T.D. Perera**, Vahid Nik, Zhengchao Wang, Jean-Louis Scartezzini, "**Towards more interactive energy internet: designing distributed energy systems by using game-theoretic approach**" (Manuscript to be submitted)
3. Dasaraden Mauree , Emanuele Naboni , Silvia Coccolo , **A.T.D. Perera**, Vahid Nik, Jean-Louis Scartezzini "**A review of assessment methods for the urban environment and its energy sustainability to guarantee climate adaptation of future cities** " (Manuscript under review Renewable& Sustainable Energy Reviews)
4. **A.T.D. Perera**, P.U Wickramasinghe, Vahid Nik, Jean-Louis Scartezzini, "**Machine learning methods to assist energy system optimization**" (accepted-Applied Energy)
5. **A.T.D. Perera**, Silvia Coccolo, Jean-Louis Scartezzini, "**Impact of urban form on energy efficiency and renewable energy integration**" (Manuscript in review, Scientific Reports (requested revision))
6. Karni Siraganyan, **A.T.D. Perera**, Dasaraden Mauree, Jean-Louis Scartezzini, **Role of solar PV and storage technologies to make neighborhood more autonomous.** (Revised manuscript to be submitted: Energies (requested revision))
7. **A.T.D. Perera**, Vahid Nik, P.U. Wickramasinghe, Jean-Louis Scartezzini, "**Redefining energy system flexibility for designing distributed energy system"** (Applied Energy: Manuscript requested revision; revised manuscript submitted)
8. Nahid Mohajeri, **A.T.D. Perera**, Silvia Coccolo, Morgane Le Guen, Lucas Mosca, Jean-Louis Scartezzini "**Assessments of sustainable development scenarios for a Swiss village to 2050 through renewable energy integration**." (Manuscript in review: Renewable Energy (requested revision))
9. **A.T.D. Perera**, Silvia Coccolo, Jean-Louis Scartezzini, Dasaraden Mauree, , "**Quantifying the impact of urban climate by extending the boundaries of urban energy system modeling**" Applied Energy 2018 (222), PP. 847–860
10. Dasaraden Mauree, Silvia Coccolo, **A.T.D. Perera** , Vahid Nik, Jean-Louis Scartezzini, Emanuele Naboni, "**A new framework to evaluate urban design using urban microclimatic modelling in future climatic conditions**", Sustainability, 2018, 10(4), 1134
11. Morgane Le Guen, Lucas Mosca, **A.T.D. Perera**, Silvia Coccolo, Nahid Mohajeri, Jean-Louis Scartezzini, "**Improving the energy sustainability of a Swiss village through building renovation and renewable energy integration**", Energy and Buildings, 2018
12. **A.T.D. Perera**, V. M. Nik, D. Mauree, and J.-L. Scartezzini, "**An integrated approach to design site specific distributed electrical hubs combining optimization, multi-criterion assessment and decision making**", Energy 2017 (134), PP. 103-120
13. **A.T.D. Perera**, V. M. Nik, D. Mauree, and J.-L. Scartezzini, "**Electrical hubs: An effective way to integrate non-dispatchable renewable energy sources with minimum impact to the grid**," 2017 (190), pp. 232–248, Applied Energy.
14. **A. T. D. Perera**, A.N. Madusanka, R. A. Attalage, and K.K.C.K. Perera "**A multi-criterion analysis for renewable energy integration process of a standalone hybrid energy system with internal combustion generator**" Journal of Renewable and Sustainable Energy 7, 043128 (2015)
15. **A. T. D. Perera**, R. A. Attalage, K.K.C.K. Perera and V.P.C. Dassanayake "**Converting existing Internal Combustion Generator (ICG) systems into HESs in standalone applications**" 2013 (74) PP. 237-248 Energy Conservation and Management
16. **A.T.D. Perera**, R.A. Attalage, K.K.C.K. Perera and V.P.C. Dassanayake "**Designing standalone hybrid energy systems minimizing initial investment, lifecycle cost and emission**" 2013 (54) PP. 220-230, Energy
17. **A. T. D. Perera**, R. A. Attalage, K.K.C.K. Perera and V.P.C. Dassanayake "**A hybrid tool to combine multi-objective optimization and multi-criterion decision making in designing standalone hybrid energy systems**" 2013 (107) PP. 412-425, Applied Energy

18. **A. T. D. Perera**, D. M. I. J. Wickremasinghe, D. V. S. Mahindarathna, R. A. Attalage, K. K. C. K. Perera, and E. M. Bartholameuz, **"Sensitivity of internal combustion generator capacity in standalone hybrid energy systems**"; 2012 (30) PP. 403-411, Energy

Book Chapters

1. **A. T. D. Perera**, Silvia Coccolo, Pietro Florio, Vahid M. Nik, Dasaraden Mauree and Jean-Louis Scartezzini, **Linking Neighborhoods into Sustainable Energy Systems**, Teodora-Emilia Motoasca (eds.), Avinash Kumar Agarwal (eds.), and Hilde Breesch (eds.), **Energy Sustainability in Built and Urban Environments**, Springer-Nature Publishers

2. Ryan Rienzie, **A.T.D. Perera** and Nadeesh M. Adassooriya , "**Biorecovery of precious metals from e-waste**" M.N.V. Prasad (eds.), Meththika Vithanage (eds.) **Electronic Waste Management and Treatment Technology**, Published by Elsevier.

Publications in Peer Reviewed International Conference Proceedings Indexed in Scopus

1. **A.T.D. Perera,** Wang Zhengchao, P.U. Wickramasinghe, Jean-Louis Scartezzini, **Integrating Vehicles to Grid (V2G) into the urban energy internet** (Abstract submitted to CISBAT)
2. A.T.D. Perera; Kavan Javanroodi, J L Scartezzini ; Vahid Nik, **Urban energy planning by linking urban energy simulation and energy system designing** (Abstract submitted to CISBAT)
3. **A.T.D. Perera,** Silvia Coccolo, Sameh Monna, Jean-Louis Scartezzini and Dasaraden Mauree, **Importance of considering energy system design during the urban planning process,** (Abstract submitted to CISBAT)
4. Delannoy Bruno, Puri Salil **, A.T.D. Perera**, Silvia Coccolo , Dasaraden Mauree and Jean-Louis Scartezzini **Climate impact and energy sustainability of future European neighborhoods.** IEEE-EFEA 2018, Rome-Italy.
5. **A.T.D. Perera**, Vahid Nik and Jean-Louis Scartezzini, **Impacts of extreme climate conditions due to climate change on the energy system design and operation, Applied** Energy Conference 2018, Rhodes-Greece.
6. Salil Puri, **A.T.D. Perera**, Dasaraden Mauree, Silvia Coccolo, Louis Delannoy and Jean-Louis Scartezzini, **The role of distributed energy systems in European energy transition,** Applied Energy Conference, 2018, Rhodes-Greece.
7. **A.T.D. Perera**, Vahid Nik, P.U. Wickramasinghe, Jean-Louis Scartezzini, **Integrating renewable energy technologies into distributed energy systems maintaining system flexibility,** IEEE-EFEA 2018, Rome-Italy.
8. **A.T.D. Perera**, Niko A. Iliadis, Jean-Louis Scartezzini, **Multi stage integration of renewable energy technologies into standalone energy systems.** IEEE-EFEA 2018, Rome-Italy.
9. Wang Zhengchao, **A.T.D. Perera**, **Robust optimization of grids with distributed generation and N-1 security**, Applied Energy Conference -2018 Rhodes Greece.
10. Morgane Le Guen, Lucas Mosca, **A.T.D. Perera**, Silvia Coccolo, Nahid Mohajeri, Jean-Louis Scartezzini, **Achieving energy sustainability in future neighborhoods through building refurbishment and energy hub concept: a case study in Hemberg, Switzerland**, CISBAT 2017, Switzerland
11. **A.T.D. Perera**, Dasaraden Mauree, Jean-Louis Scartezzini, **The energy hub concept applied to a case study of mixed residential and administrative buildings in Switzerland,** CISBAT 2017, Switzerland
12. Karni Siraganyan, Dasaraden Mauree, **A.T.D. Perera**, Jean-Louis Scartezzini, **Evaluating the need for energy storage to enhance autonomy of neighbourhoods,** CISBAT 2017, Switzerland
13. Antoine Kuehner, Nour Mdeihli, Silvia Coccolo, **A.T.D. Perera**, Nahid Mohajeri, Jean-Louis Scartezzini, **Extending building integrated photovoltaics (BiPV) using distributed energy hubs: a case study in Cartigny, Switzerland,** CISBAT 2017, Switzerland
14. Henri Bittel, **A.T.D. Perera**, Dasaraden Mauree, Jean-Louis Scartezzini, **Locating multi energy systems for a neighborhood in Geneva using k-means clustering,** CISBAT 2017, Switzerland
15. **A.T.D. Perera**, Udaranga Wickramasinghe, Vahid Nik, Jean-Louis Scartezzini, **Optimum design of distributed energy hubs using hybrid surrogate models (HSM),** CISBAT 2017, Switzerland

16. Dasaraden Mauree, **A.T.D. Perera**, Jean-Louis Scartezzini, **Influence of Buildings Configuration on the Energy Demand and Sizing of Energy Systems in an Urban Context,** Applied Energy Conference (ICAE), 2017 UK
17. Chatelain Timothée, **A.T.D. Perera**, Dasaraden Mauree, Jean-Louis Scartezzini, **Optimum dispatch of a multi-storage and multi-energy hub with demand response and restricted grid interactions,** Applied Energy Conference (ICAE), 2017 UK
18. C. Athukorala, J. Jayasuriya, **T. D. Perera**, M. P. G. Sirimanna and R. Attalage, **A Techno-Economic Analysis for an Integrated Solar PV/T System for Building Applications**, IEEE-ICIAFS, 2016 Sri Lanka.
19. W.J.A. Jayasuriya, A.U.C.D. Athukorala, S. Ragulageethan, **A.T.D. Perera**, M.P.G. Sirimanna, R.A. Attalage **Performance analysis of photovoltaic thermal (PVT) panels considering thermal parameters,** ASME Power Conference, 2016 USA
20. **A.T.D. Perera**, V.M. Nik, Dasaraden Mauree, J-L Scartezzini. "**Design optimization of Electrical Hubs using hybrid evolutionary algorithm"** ASME Energy Sustainability Conference 2016 USA
21. **A.T.D. Perera**. "**Importance of minimizing waste of renewable energy in designing standalone hybrid energy systems"** ASME Energy Sustainability Conference 2016 USA
22. **A.T.D. Perera**, V.M. Nik, Dasaraden Mauree, J-L Scartezzini **Optimum design and control of grid integrated electrical hubs considering lifecycle cost and emission**, IEEE EnergyCon 2016, Leuven, Belgium
23. **A.T.D. Perera**, V.M. Nik, Dasaraden Mauree, J-L Scartezzini **Sensitivity analysis of the dispatch strategy in designing grid integrated electrical hubs**, IEEE EnergyCon 2016, Leuven, Belgium
24. A.U.C.D. Athukorala, W.J.A. Jayasuriya, S. Ragulageethan, M.P.G. Sirimanna, R.A. Attalage and **A.T.D. Perera**, **A techno-economic analysis for an integrated solar PV/T system with thermal and electrical storage – case study,** MERCon-15, pp. 45-51, 2015 Colombo-Sri Lanka
25. **A. T. D. Perera,** Ashen Wijesiri "**Designing smart hybrid renewable energy systems with V2G**" *7th International Conference on Information and Automation for Sustainability*, 2014, Colombo-Sri Lanka.
26. **A.T. D. Perera,** M.P.G. Sirimanna "**A novel simulation based evolutionary algorithm to optimize building envelope for energy efficient buildings**" *7th International Conference on Information and Automation for Sustainability*, 2014, Colombo-Sri Lanka
27. **A. T. D. Perera,** R. A. Attalage and K. K. C. K. Perera "**An optimal design of a grid connected hybrid electrical energy system using evolutionary computation**" *Eighth International Conference on Industrial and Information Systems (IEEE-ICIIS 2013)* Pp. 12-17, 2013 Sri Lanka
28. **A.T. D. Perera,** A.N. Madusanka and A.A.P. de Alwis "**Techno-economical optimization of a municipal solid waste management system using evolutionary algorithms**" *International Conference on Advances in ICT (IEEE-ICTer 2013)*, 2013 Sri Lanka pp. 92-97
29. M.P.G. Sirimanna**, A. T. D. Perera,** R. A. Attalage "**Numerical estimation of view factors for simple roof enclosures with five surfaces**" *IASTED International Conference on Engineering and Applied Science* pp. 297-302, 2012, Colombo, Sri Lanka
30. Sasiri Gamage, H.A.K. Madhushan**. A. T. D. Perera,** P. Kumarage "**Mathematical modeling and simulation of a standalone solar thermal Organic Rankine Cycle (ORC) with a thermal storage**" *IASTED International Conference on Engineering and Applied Science*, pp. 14-20 2012, Colombo, Sri Lanka
31. **A. T. D. Perera,** M.P.G. Sirimanna, R. A. Attalage K. K. C. K. Perera and VPC Dassanayake"**Multi objective optimization and multi criterion decision making in expanding existing standalone energy systems combining renewable energy sources**" *IASTED International Conference on Engineering and Applied Science* pp. 234-238, 2012, Colombo, Sri Lanka.
32. **A. T. D. Perera,** D.N.S. Kuruppumullage N.A.I.D. Nissanka and A.A.P. de Alwis "**Evolutionary multi objective optimization to optimize waste to energy network**" *International conference on Green technology and Environmental Conservation* (IEEE-GTEC 2011) PP. 45-50, 2011 India
33. **A. T. D. Perera,** P. Kumarage and K. K. C. K. Perera "**Optimal design and control of multiple boiler systems using fuzzy-evolutionary hybrid algorithm**" Sixth International Conference on Industrial and Information systems (IEEE-ICIIS 11), pp. 376-380, 2011 Sri Lanka
34. **A. T. D. Perera,** R. A. Attalage and K. K. C. K. Perera "**Multi objective optimization of lifecycle cost, unmet load and renewable energy capacity for an expansion of existing standalone internal combustion generator systems"** *ASME 2011- 5th International Conference on Energy Sustainability*, PP. 1433-1440, 2011 Washington, DC, USA
35. **A.T.D. Perera**, D.M.I.J. Wickremasinghe, D. Mahindarathna, R. A. Attalage, K. K. C. K. Perera, and E. M. Bartholameuz, "**Novel simulation based evolutionary optimization algorithm to design stand-alone**

hybrid energy systems," 2011 *3rd International Conference on Computer Modeling and Simulation (ICCMS-IEEE 2011)*, V1 pp. 272-275, Mumbai-India: 2011.

36. **A.T.D. Perera**, D.M.I.J. Wickremasinghe, D. Mahindarathna, R.A. Attalage, K.K.C.K. Perera, and E.M. Bartholameuz, "**Determining wind turbine capacity for expansion of off grid Internal Combustion Generators (ICG) system: why it becomes challenging?**," *2nd IEEE International Conference on Sustainable Energy Technologies* , pp. 1-5, Kandy- Sri Lanka: 2010.

Conferences/symposiums: Full paper presented, not indexed in Scopus

1. **A.T.D. Perera**, D.M.I.J. Wickremasinghe, D. Mahindarathna, R.A. Attalage, K.K.C.K. Perera, and E.M. Bartholameuz, " **How does the internal generator capacity and power supply reliability effect hybrid energy system sizing?**" , 16th ERU symposium, Engineering Research Unit, University of Moratuwa-Sri Lanka: 2010,PP. 252-253.
2. **A. T. D. Perera,** D.N.S. Kuruppumullage N.A.I.D. Nissanka and A.A.P. de Alwis **"Multi objective optimization of municipal waste management system to adopt Sri Lankan context.**" Sri Lanka Association for Advancement of Science (SLAAS), 67th Annual session , Section C, PP. 42
3. K.A.E.K. Perera, K.A.L. Kollure, W.A.K.S.S. Prasad, K.K.C.K. Perera and P.A.B.A.R. Perera, **A.T.D. Perera**, "Feasibility Study on Solar Photovoltaic Office Air Conditioning in Sri Lanka" , 17th ERU symposium, Engineering Research Unit, University of Moratuwa-Sri Lanka 2011, PP. 114-116
4. **A.T.D. Perera**, V.M. Nik, Dasaraden Mauree, J-L Scartezzini. "**Evaluating the sensitivity of grid integration level for a multi energy hubs"** CISBAT Conference 2015 Switzerland PP. 505-510
5. W. J. A. Jayasuriya, A. U. C. D. Athukorala, S. Ragulageethan, **A. T. D. Perera**, M. P. G. Sirimanna**. Thermo-economic analysis of a hybrid photovoltaic/thermal (PV/T) system for different configuration settings**. CISBAT 2015, EPFL, Lausanne, September 9-11th, 2015.
6. S.V.R. Gamage, **A.T.D. Perera** and K.K.C.K. Perera, **Design and Analysis of a Cascade Solar Thermal Collector Field for an Organic Rankine Cycle with a Latent Heat Thermal Storage**, **7th *International Conference on Sustainable Built Environment*** ,2016 (ICSBE) , Sri Lanka.
7. Dasaraden Mauree, Silvia Coccolo, Vahid Nik, **Dasun Perera**, et-al. "**Study on the impact climate change on the resilience of the EPFL campus** ";10th International Conference on Urban Climate/14th Symposium on the Urban Environment", 2018, New York, USA

Editorial Assignments (Reviewer)

- **Applied Energy, Solar Energy**, **Applied Soft Computing, Energy Strategy Reviews, Applied Thermal Energy , Energy and Buildings**– Published by Elsvier
- IEEE Transactions on Sustainable Energy
- **Energies** — Published by MDPI, Switzerland
- Invited Reviewer for ASME 2012, 6th International Conference on Energy Sustainability, San Diego, CA, USA
- Editor of ***MECMAG* 09,** local journal published by Department of Mechanical engineering university of Moratuwa (2009-2010)

Teaching and Supervision

Supervised seven master research projects from Mechanical Engineering, Energy Management, Environmental Engineering programs in EPFL

Modules Conducted at École Polytechnique Fédérale de Lausanne (EPFL), Switzerland:

- Building Physics 1 (Assistantship only)
- Building Physics 2 (Assistantship only)

Modules Conducted at Department of Mechanical Engineering, University of Moratuwa, Sri Lanka:

- ME 1822: Basic Engineering Thermodynamics (Lecturer and practical coordinator)
- ME 2032:Thermodynamics of Heat Engines & Work Transfer Devices (Lecturer and module coordinator)
- ME 4242: Energy Technology and Environment (Lecturer and practical coordinator)

Selected Research Work

1. **Urban Energy System Modeling and Assessment** (since 2014)
2. **Mathematical modeling and simulation of a standalone solar thermal Organic Rankine Cycle (ORC) with a thermal energy storage** (2012-2014)
3. **Optimal design and control of multiple boiler systems considering lifecycle cost, exergy loss and pollutant emitted using Fuzzy-Evolutionary hybrid algorithms (**2011-2012)
4. **Designing municipal solid waste management systems, using hierarchical evolutionary algorithms** (Since 2011)
5. **Optimum design and control of standalone Hybrid Energy System** (since 2010)
6. **Impact of building architecture to thermal comfort level; a case study at University of Moratuwa** (Since 2010)

Workshops and PhD schools attended

- One day workshop on Renewable Energy Storage, EMPA-ETH Switzerland-2017.
- Swiss Competence Center for Energy Research (SCCER) PhD School on Energy Transition Engelberg-Switzerland-2017.
- Winter School on Optimization and Operations Research, 2017, Zinal, Switzerland.
- Machine Learning Workshop, 2016, CSEM Neuchâtel, Switzerland.
- EuroTech Winter School on Integrated Approach to Energy Systems winter school/workshop 2015, Switzerland
- PhD summer school on Building physics in urban environments 2015, Torino, Italy

Professional Associations and Societies

- Student Member Institute of Electrical and Electronic Engineers (IEEE)
- Member of ***American Society of Mechanical Engineers*** (ASME)
- Student Member of Sri Lanka Association for Advancement of Science (SLAAS)
- Student member of ***Institute of Engineers Sri Lanka*** (IESL), since March 2009

Academic Related Activities

- Member of EPFY Buddy program for EDEY (Energy PhD program): helping the first year PhD students in EDEY to socialize with other people in the program with the help of experienced PhD students (2016-18)
- A member of organizing committee for Department Industry Collaborative Board (DICB) Meeting 2014, Department of Mechanical Engineering University of Moratuwa.
- Member of the Research Committee, Department of Mechanical Engineering, University of Moratuwa Since January, 2012
- Member of Organizing Committee, Japan SAARC Energy Symposium

References can be forwarded upon request

Ce document a été imprimé au Centre d'impression EPFL,
imprimerie climatiquement neutre, certifiée myClimate.